Gravitational production of matter and radiation during reheating after inflation

Simon Cléry

université PARIS-SACLAY

Gravitational production of matter and radiation during reheating after inflation

Production gravitationnelle de matière et de radiation au cours du reheating après l'inflation

Thèse de doctorat de l'Université Paris-Saclay

École doctorale n° 576, Particules, Hadrons, Energie et Noyau : Instrumentation, Imagerie, Cosmos et Simulation (PHENIICS)
Spécialité de doctorat: Science des Astroparticules et Cosmologie
Graduate School : Physique. Référent : Faculté des sciences d'Orsay.

Thèse préparée dans l'unité de recherche **IJCLab (Université Paris-Saclay, CNRS)**, sous la direction de **Yann MAMBRINI**, Directeur de Recherche.

Thèse soutenue à Paris-Saclay, le 3 Septembre 2024, par

Simon CLERY

Composition du jury

Membres du jury avec voix délibérative

Asmaa ABADA Professeure, IJCLab, Université Paris-Saclay	Présidente
Genevieve BELANGER Directrice de Recherche, LAPTh, Université Savoie Mont Blanc (CNRS).	Rapporteuse & Examinatrice
Michel TYTGAT Directeur de Recherche, Université Libre de Bruxelles (FNRS)	Rapporteur & Examinateur
Valerie DOMCKE Junior Faculty Member, CERN	Examinatrice
Kalliopi PETRAKI Professeure, LPENS, Sorbonne Université	Examinatrice
Joseph SILK Directeur de Recherche, IAP, Sorbonne Université (CNRS)	Examinateur

THESE DE DOCTORAT
NNT : 2024UPASP052

université PARIS-SACLAY

ÉCOLE DOCTORALE
Particules, hadrons, énergie et noyau : instrumentation, imagerie, cosmos et simulation (PHENIICS)

Titre: Production gravitationelle de matière et de radiation au cours du reheating après l'inflation.

Mots clés: Astroparticules, Cosmologie, Inflation, Reheating, Matière Noire, Leptogénèse.

Résumé: L'inflation est actuellement la théorie la plus prometteuse pour décrire les conditions initiales de l'Univers primordial. Dans les modèles les plus simples, un champ scalaire, l'inflaton, parcourt lentement son potentiel avec une forte densité d'énergie, entraînant une expansion accélérée de l'Univers. Les fluctuations quantiques de l'inflaton générées aux petites échelles, peuvent être amplifiées par instabilité gravitationnelle en perturbations cosmologiques, avec un spectre de puissance invariant d'échelle. Ces prédictions des modèles inflationnaires sont en très bon accord avec l'observation des anisotropies du fond diffus cosmologique (CMB) et des structures à grande échelle (LSS). Pour qu'un modèle inflationnaire soit pertinent, il doit également inclure un mécanisme viable de transfert d'énergie de l'inflaton vers les autres champs, produisant ainsi des particules du modèle standard (SM). Ce mécanisme est appelé reheating post-inflationnaire. Le reheating peut également permettre de produire des particules de matière noire, ingrédient fondamental du modèle cosmologique standard, et nécessaire pour expliquer la dynamique des galaxies et des amas de galaxies. Les particules produites après l'inflation doivent d'abord avoir formé un plasma primordial chaud, comme le montrent les données d'observation sur la nucléosynthèse primordiale (BBN) et le CMB. À la fin de l'inflation, l'inflaton se stabilise vers le minimum de potentiel, mettant fin à l'expansion accélérée, et commence à osciller autour de ce minimum. Il peut alors dissiper son énergie et la convertir en particules grâce à son couplage avec d'autres champs. Ce mécanisme est crucial pour comprendre l'évolution de l'Univers primordial avant la BBN. Dans cette thèse, nous explorons la phénoménologie du reheating à travers les désintégrations perturbatives ou les annihilations de l'inflaton vers des particules de différents spins. Nous nous intéressons également à l'influence de l'équation d'état pendant le reheating et à ses implications sur le processus de production de particules. Nous étudions en particulier un potentiel mixte conduisant à une transition de l'équation d'état pendant le reheating et nous montrons qu'il peut modifier de manière significative les prédictions de température de reheating et de fragmentation du condensat d'inflaton. La partie principale de cette thèse se concentre sur la production de particules pendant les oscillations de l'inflaton, via des interactions gravitationnelles. Nous considérons d'abord l'échange de gravitons émergeant d'une description effective de la gravité d'Einstein et nous généralisons ensuite ces résultats à des couplages non-minimaux avec la gravité. Ce cadre théorique est appliqué à la production de particules de matière noire lourdes de différents spins ainsi qu'à la production de particules relativistes du SM. Nous montrons que l'abondance de matière noire observée peut être facilement expliquée par ces interactions gravitationnelles et que la production rapide de particules relativistes peut être fortement influencée par ces effets gravitationnels inévitables. Ensuite, les implications d'un potentiel non-quadratique associé à une équation d'état exotique sont explorées dans le contexte du reheating gravitationnel, conduisant notamment à un signal spécifique dans le spectre des ondes gravitationnelles primordiales, générées pendant l'inflation. Il s'agit d'une signature caractéristique d'un tel scénario, qui pourrait être détectée par de futures expériences d'ondes gravitationnelles. Cette détection mettrait en lumière l'équation d'état et la température de reheating. Nous proposons enfin un scénario minimal dans lequel la matière noire et l'asymétrie matière antimatière sont générées par ces portails gravitationnels pendant le reheating. Nous considérons pour cela la leptogenèse impliquant des neutrinos droits massifs et dérivons des contraintes sur les masses de ces neutrinos dans un tel scénario.

université PARIS-SACLAY

ÉCOLE DOCTORALE
Particules, hadrons, énergie et noyau : instrumentation, imagerie, cosmos et simulation (PHENIICS)

Title: Gravitational production of matter and radiation during reheating after inflation.

Keywords: Astroparticles, Cosmology, Inflation, Reheating, Dark Matter, Leptogenesis.

Abstract: Inflation is currently the most promising theory for depicting the initial conditions in the early Universe. In the simplest models, a scalar field, the inflaton, is slowly rolling down its potential with high energy density, making the Universe exponentially expand. On top of this mechanism of accelerated expansion, quantum fluctuations of the inflaton generated on small scales can be further amplified by gravitational effects and stretched to large-scale cosmological perturbations with a near-scale invariant power spectrum. These predictions of inflationary models are in extremely good agreement with the observation of the Cosmic Microwave Background (CMB) anisotropies and Large Scale Structures (LSS). For an inflationary model to be successful, it also needs to include a viable mechanism to transfer energy from the inflaton to the other fields, producing particles of the Standard Model (SM). We call this mechanism post-inflationary reheating. Reheating can also produce Dark Matter (DM) particles, a necessary ingredient of the standard cosmological model, and to explain the dynamics of galaxies and galaxy clusters. The SM particles produced after inflation must have formed a hot primordial plasma, as highlighted by observational data on the Big Bang Nucleosynthesis (BBN) and CMB measurements. In the standard scenario, the inflaton field falls towards the potential minimum at the end of inflation, ending the accelerated expansion and oscillating around this minimum. It can then dissipate its energy while oscillating and convert it into particles through its coupling to other fields. This mechanism is crucial to understanding the evolution of the early Universe before BBN. This thesis explores the phenomenology of reheating through perturbative decays or scatterings of the inflaton towards particles of different spins. We are also interested in the effect of the equation of state during reheating and its implications on the reheating process. We especially study a mixed potential of the inflaton leading to a transition of the equation of states during reheating, and show that it can significantly alter the predictions of reheating temperature and fragmentation of the inflaton background. The main part of this thesis has been focusing on the production of particles during inflaton oscillations, mediated by Planck-suppressed gravitational interactions. We first consider the graviton portals emerging from an effective description of Einstein's gravity and generalize these results to non-minimal couplings to gravity. This framework is applied to the production of heavy DM particles of different spins as well as the production of relativistic particles of the SM. We show that the right relic abundance of DM could be easily produced through these gravitational portals and that such unavoidable gravitational effects may highly impact the early radiation production from the inflaton. Then, important implications of steep potential associated with a stiff equation of state are explored in the context of gravitational reheating, leading to an interesting signal in the primordial gravitational waves spectrum generated during inflation. This represents a signature of such a scenario and can be probed by future gravitational waves experiments, shedding light on the equation of state and temperature reached during reheating. We finally propose a minimal scenario in which both the DM relic abundance and the asymmetry between baryons and anti-baryons, are generated by gravitational portals during reheating. We rely on the framework of non-thermal leptogenesis involving a Beyond Standard Model scenario with additional heavy right-handed neutrinos. We investigate such a minimal reheating scenario to produce the right relics simultaneously during gravitational reheating, and find constraints on right-handed neutrino masses in this case.

Je dédie ce manuscrit à Rebecca, en souvenir des années passées ensemble à Palaiseau.

"J'ai senti que quelque chose me parlait dans le calme du crépuscule et m'attachait à ce monde encore à découvrir." Hubert Reeves, *Je n'aurai pas le temps : Mémoires.*

Remerciements

Ces trois années de doctorat ont été tout à la fois remplies de joies et de peines. J'ai découvert un milieu qui m'était étranger sous bien des aspects, et j'en ressors grandi. J'ai pu compter sur les personnes qui m'ont accompagné tout au long de ce processus.

Je tiens tout d'abord à remercier Yann Mambrini, mon directeur de thèse, pour la confiance qu'il m'a accordée tout au long de ce projet de thèse de doctorat, et pour ses conseils avisés m'ayant permis d'appréhender au mieux le monde de la recherche en Physique théorique. Je le remercie de m'avoir également enseigné de très nombreuses choses sur des domaines si variés. J'espère continuer notre collaboration fructueuse dans le futur. Je voudrais également remercier chaleureusement tous les membres de mon jury, Asmaa Abada, Genevieve Belanger, Michel Tytgat, Valerie Domcke, Kalliopi Petraki et Joseph Silk, d'être présent.e.s au cours de ma soutenance et pour avoir lu avec attention mon manuscrit de thèse. Leur travail précieux et leur réactivité ont grandement contribué à l'organisation et au bon déroulement des dernières étapes de mon doctorat. J'exprime ma profonde gratitude à tous mes collaborateur·ice·s, sans qui ce travail de recherche n'aurait pas été possible. Tout d'abord, à Keith Olive et Hyun Min Lee, pour leur soutien dans mon parcours de jeune chercheur et leur engagement sans faille dans nos projets et collaborations. Je remercie Alejandro Ibarra de me faire confiance pour la suite de mon parcours, et je suis impatient d'initier notre collaboration scientifique à Munich. Je remercie également Sarunas Verner, Andrey Shkerin, Basabendu Barman, Pascal Anastasopoulos, Nicolas Bernal, Yong Xu, Marcos Garcia, Kunio Kaneta, Debaprasad Maity, Riajul Haque, Ayan Chakraborty, Anish Goshal, et Jean Kimus. Un remerciement particulier à Adriana Menkara, qui m'a accueilli et guidé lors de mon séjour à la CAU, au cœur de Séoul, et avec qui j'ai eu la chance de travailler au cours de ma thèse. Je suis très reconnaissant envers Mathias Pierre, qui a été un second mentor pour moi, notamment au cours de la recherche active de postdocs et durant la phase de rédaction de ce manuscrit. Il m'a été d'une grande aide et m'a soutenu tout au long de cette période angoissante.

Je remercie tous les membres de notre groupe de recherche à l'IJCLab avec qui j'ai pu mener de nombreux travaux et discuter de sujets passionnants dans une ambiance amicale et conviviale. Je remercie tout particulièrement Donald, Jay et Mathieu pour tous ces cafés partagés à se creuser les méninges ! Je passe le flambeau à Mathieu pour la suite de sa thèse,

que j'espère aussi enrichissante que la mienne, et je souhaite le meilleur à Donald et Jay pour la suite de leur parcours. Je remercie également les doctorant · e · s et les postdocs du laboratoire qui ont accompagné mon cheminement à Orsay, en premier lieu Giulia et Florentin, qui m'ont accueilli pendant mon stage de Master 2, ainsi que Nicolas, Kilian, Valentine, Claire, Salva, Teseo, Jordan, et bien d'autres. Je remercie Méril pour ses conseils et son aide précieuse lors des dernières phases de rédaction de ce manuscrit. Je laisse les clés du 108G à mes cobureaux, Panagiotis et Eduardo, qui ont partagé avec moi ces heures de travail au laboratoire dans la bonne humeur et la bienveillance ; prenez soin des plantes, les gars !

Je pense maintenant à mes ami·e·s qui ont été à mes côtés, de près comme de loin, pour me soutenir, me faire rire, me remonter le moral, et enrichir mon existence au cours de ces trois dernières années. Tout d'abord, merci à Gilles, Noémie et Lucas d'avoir été là, dans la même galère, pour notre groupe de parole, et d'avoir rendu quelques moments difficiles plus agréables à traverser. Merci d'avoir supporté le 'rageux' du groupe et d'avoir gardé votre rebeccalme pour me raisonner. Vous allez me manquer à l'autre bout du monde, mais je ne doute pas qu'on se retrouvera vite. Je remercie également Théo qui, malgré la distance, m'a soutenu et rassuré à de multiples reprises sur différents sujets. Désolé de ne pas être venu à ta soutenance, Dr Simon. Ensuite, je remercie mes ami·e·s qui sont là depuis fort longtemps, et qui, malgré l'aspect obscur de cette thèse à leurs yeux, ont fait preuve d'intérêt pour mon projet et m'ont soutenu. Merci à Lambert, Jules, Louise, Irmalo, Marine, Claire, Kévin, Ninon, et tou·te·s les autres. Et non, malheureusement, je n'ai pas encore trouvé ce que je cherchais... Je remercie également Armel pour tous ces pots de Madame Loïk partagés, ainsi que Louis pour les bons moments passés ensemble. Je n'oublie pas, bien entendu, les autres personnes qui ne figurent pas ici, je connais leur importance à mes yeux.

Je suis profondément reconnaissant envers mes parents et mes sœurs, Alice et Camille, pour leurs encouragements et leur aide, que ce soit dans ce projet de thèse ou dans le reste de ma vie. Je suis désolé de vous imposer cette soutenance rébarbative, et en anglais de surcroît. Je remercie aussi Patrick pour son intérêt envers ce projet de thèse, ainsi que pour son aide durant mes années d'études à Orsay. Je remercie Valérie et Françoise pour leur accueil et leur tendresse. À la fin de la rédaction de cette thèse, j'ai une pensée émue pour Stéphane, qui nous manque profondément à tou·te·s. Nous serons ensemble pour nous serrer les coudes.

Je ne peux enfin remercier assez Rebecca, sans qui je n'aurais pas eu le courage de persévérer dans ce projet, comme dans les autres que nous menons ensemble. Merci à elle d'être là à chaque instant, depuis maintenant presque six ans, pour le réconfort, la joie et la confiance que nous partageons. Je la remercie pour toute l'aide apportée au cours de la préparation de cette thèse, jusqu'à la relecture de ce manuscrit. Ces trois dernières années ont été éprouvantes pour nous deux, mais je sais que nous pouvons compter sur le soutien indéfectible l'un de l'autre. J'ai hâte de voir ce que notre nouvelle vie en Allemagne nous réserve et de vivre tous ces moments ensemble.

Contents

Introduction

Over the past century, the advent of two conceptual revolutions in Physics has opened up the possibility of scientific inquiry into the fundamental nature of matter and the Cosmos, beyond the realms of "classical" Physics.

First of all, the marriage of the intrinsic geometry of space-time with the dynamics of matter has profoundly and durably altered our perception of physical objects and their interactions. Einstein's theories of Special and then General Relativity were breakthroughs that changed the paradigm for discussing dynamics and gravitation. One of the crucial predictions of the theory of General Relativity, the existence of gravitational waves, has been confirmed by their recent detection in different experiments, reinforcing the status of Einstein's theory as the most accurate description of gravitational interactions. In the early days of General Relativity, this new paradigm rapidly led to a growing interest in studying the Universe as a whole. In Einstein's theory, it is no longer a rigid, static theater of events but can be seen as a physical object in its own right, deformable and dynamically evolving. At the onset of this revolution, Cosmology was of theoretical interest for Physicists but did not belong to the established domain of Science, essentially due to a lack of precise observations to confirm any cosmological model. However, since the middle of the 20th century, cosmological data have been accumulating, with the development of a large number of observational tools and experiments, making it possible to open the window back to the origins of the Universe. Recent cosmological measurements allowed the establishment of a standard accepted cosmological model by determining the matter-energy content of the Universe. These various surveys provided surprising outcomes: around 70% of the energy density of the Universe is made of an unknown and exotic component responsible for accelerating space-time expansion, which cosmologists called Dark Energy. 30% is composed of cold matter, but with only 5% of ordinary matter (atoms, nuclei, electrons), the remaining being made of another unknown component called Dark Matter, which hasn't been detected in any particle experiment yet.

Surprisingly enough, around the beginning of the 20th century as well, a fine understanding of matter at the shortest scales has made it possible to understand the other limits of classical Mechanics and the classical theory of light. The first Quantum Mechanics development gradually replaced the concepts of waves, bodies, and trajectories with more conceptual wave

functions, quanta or quantum states, and noncommutative observables. Later developments bringing together Special Relativity and Quantum Mechanics looked at quantum field operators and their excitations, which allowed the prediction of the outcome of experiments with incredible precision. Quantum Field Theory is built to deal with the fundamental interactions, currently describing the strong, weak, and electromagnetic interactions. If we still describe particles in this framework, it has almost abandoned any classical conception of a physical object, and the predictions are probabilities of interactions. From this new framework, the Standard Model of particles, the most successful model for describing matter at a fundamental level, has been developed in the second half of the past century. The last predicted piece, which was still missing, has been added to the Standard Model with the detection of the Higgs boson at the Large Hadron Collider in 2012. The Standard Model provides an accurate description of interactions below the atomic scale, allowing us to predict observables with probably the highest precision ever reached in the history of Science. However, the picture may not be considered complete. Fundamental obstacles prevent us from having a complete quantum description of the gravitational interaction, known as the problem of Quantum Gravity. Moreover, the unknown precise nature of Dark Energy and Dark Matter represents one of the main issues of both Particle Physics and Cosmological models.

Particle Physics and Cosmology are deeply intertwined in their ambition to understand these fundamental constituents of the Universe and the forces governing their interactions. One direction of Astroparticle Physics is trying to bridge the gap between the two fields, investigating cosmological relics from the early Universe, such as Dark Matter. A recent attempt in this perspective of understanding the initial conditions of the Universe is the theory of cosmic inflation. Inflation is a postulated period of extremely rapid exponential expansion of the early Universe, posited to solve several cosmological puzzles. It also naturally provides a mechanism for generating the primordial density perturbations that later evolve into the large-scale structure observed in the Universe today. The current inflationary paradigm is formulated within the framework of Quantum Field Theory, together with General Relativity but without unifying them. Inflationary models make several testable predictions that can be confronted with current and future observations, but despite the successes of the inflationary paradigm, several challenges remain. One major issue is the identification of the microscopic description of inflation with a more fundamental theory. Another challenge is the precise modeling of the post-inflationary era called reheating. Following inflation, the Universe enters a phase where some mechanism should allow the production of particles effectively repopulating the Universe with the matter and radiation necessary for the subsequent hot Big Bang evolution. The study of reheating requires understanding the complex non-equilibrium field dynamics and the interplay between different degrees of freedom in the early Universe. Understanding reheating is crucial for connecting the inflationary phase to the well-established thermal history of the Universe and the further generation of structures. The study of inflation and reheating is at the

forefront of High-Energy Physics, Astroparticle Physics, and Cosmology, linking fundamental Particle Physics and cosmological observations.

In this thesis, we will investigate the production of particles in the very early Universe, at the end of the cosmic inflation era, during the reheating process. The main analysis is done during the oscillations of the inflaton field, the field responsible for inflation. We are especially looking at Planck-suppressed gravitational interactions and consider such a minimal reheating scenario to produce the cosmological relics, finding constraints in the parameter space of interest. The work presented in this thesis manuscript is based on several research projects that I carried out with various collaborators during my PhD[1]:

- **S. Cléry**, Y. Mambrini, K.A. Olive, S. Verner, *Gravitational portals in the early Universe*, **Phys.Rev.D 105 (2022) 7, 075005**, arXiv:2112.15214 [1]
- **S. Cléry**, Y. Mambrini, K.A. Olive, A. Shkkerin, S. Verner, *Gravitational portals with nonminimal couplings*, **Phys.Rev.D 105 (2022) 9, 095042**, arXiv:2203.02004 [2]
- B. Barman, **S. Cléry**, R.T Co, Y. Mambrini, K.A. Olive, *Gravity as a portal to reheating, leptogenesis and dark matter*, **JHEP 12 (2022) 072**, arXiv:2210.05716 [3]
- **S. Cléry**, M. A.G. Garcia, Y. Mambrini, K.A. Olive, *Bare mass effects on the reheating process after inflation*, **Phys.Rev.D 109 (2024) 10, 103540**, arXiv:2402:16958 [4]

In addition to the work presented in this manuscript, I also had the opportunity to participate in other research projects:

- **S. Cléry**, H. M. Lee, A. G. Menkara, *Higgs inflation at the pole*, **JHEP 10 (2023) 144**, arXiv:2306.07767 [5]
- N. Bernal, **S. Cléry**, Y. Mambrini, Y. Xu *Probing reheating with graviton bremsstrahlung*, **JCAP 01 (2024) 065**, arXiv:2311.12694 [6]

Before presenting my research work, in the first chapter of this thesis, we introduce the formalism of modern Cosmology, its main predictions, and their agreement with current cosmological surveys, on which all the work described here is based. Part of it is also subject to open questions in the early evolution of the Universe and the generation of cosmological relics, which is the main subject of this thesis. In particular, in chapter 1 we describe the ingredients of the standard model of Cosmology, the ΛCDM model. We outline the main steps in the history of the early Universe, at the homogeneous and isotropic regime level, and we motivate the introduction of the cosmic inflation paradigm from recent precision cosmological measurements.

[1]The papers are listed chronologically in their date of appearance on the arXiv.

In chapter 2, we describe the framework of cosmic inflation and reheating by first looking at the simplest single-field slow-roll models for inflation. We further derive the main predictions of such models in terms of cosmological perturbations, sourcing anisotropies in the relic radiation observed and providing seeds for the formation of large-scale structures in the Universe. We then introduce the mechanism of reheating after inflation, which is at the core of the work pursued during this thesis. We look at different regimes during the oscillations of the inflaton field and describe the rich phenomenology originating from the couplings of different fields with the inflaton background.

Finally, in chapter 3, we introduce the framework of gravitational particle production. Special attention is paid to the semi-classical process of gravitational particle production from the expansion of space-time, which is closely connected to the results obtained in the main work of this thesis. In the second part, we develop this approach and focus on the production of particles during the stage of inflaton oscillation, relying on gravitational portals. We describe how such portals emerged from an effective description of gravity and how it coupled the different sectors during reheating. We apply this framework to the production of heavy particles during reheating and further generalize these gravitational portals to the case of nonminimal gravitational interactions. Finally, we look at a simple scenario for the simultaneous generation of the cosmological relics during reheating, and investigate the constraints on such a scenario.

Chapter 1

Modern Cosmology

Contents

In this chapter, we introduce the framework of modern Cosmology developed over the past century. Our focus is on providing the essential tools to comprehensively describe our entire Universe, especially in its early days. We begin by highlighting the interconnection between the matter-energy content and the geometric structure, leading to the conclusion that our Universe is expanding.

In the second part of the chapter, we depict the significant stages in the history of the Universe that are already quite well understood. In particular, we discuss how the current cosmological observations confirm the existence of an early hot dense state that has further cooled down, leaving different relics that are the most important probes of the Universe expansion. Two main mechanisms have been described for decades and are currently constrained by our detectors and telescopes: the primordial Nucleosynthesis, also called Big Bang Nucleosynthesis (BBN), and the emission of the Cosmic Microwave Background (CMB). These two mechanisms occurred at different epochs in the far past of the Universe, and their probes and confirmations have led to a coherent description of the early Universe, after the first minutes of its evolution until now.

From the measurements of CMB radiation and various other astrophysical observations, we have to conclude that an important fraction of the matter content of the Universe is exotic, in the form of Dark Matter (DM). In this perspective, we then detail the main mechanism currently studied for the generation of the DM component, to explain its abundance as inferred by observations on various scales.

The problem of DM and its production mechanism is closely related to another issue in modern Physics, that is the apparent asymmetry between baryonic and anti-baryonic matter, the so-called Baryon Asymmetry, in our Universe (BAU) today. We discuss some evidence of this asymmetry, and some current approaches to produce such an excess of baryons on anti-baryons during the early evolution of the Universe. Especially, we will focus on the description of the Leptogenesis mechanism as an explanation for this asymmetric state of the Universe.

Finally, the standard description of modern Cosmology fails to explain the spatial flatness and high level of homogeneity and isotropy on the largest scales of the Universe. A modern theory of cosmic inflation has been developed to cure this lack of predictivity. Furthermore, inflation is a theory that predicts the origin of the observed inhomogeneities in the CMB, which are the seeds of the formation of large cosmological structures, such as galaxies and their clusters, that we observe. This is why it is currently one of the most viable predictive scenarios for the very first instants of the Universe. We study in the last part of this chapter the imprints of the initial perturbations on cosmological scales set by inflation and left in the CMB anisotropies before moving to the next chapter, where we introduce the models of inflation and reheating.

1.1 Expanding Universe

The main discovery of the 20th century about Cosmology is probably that the Universe is in expansion. It was established rigorously during the 1920s from several observations of distant galaxies ("nebulae" at that time) that are fainting away from the observer and appear with a "redshifted" spectrum of emission. Edwin Hubble probably made the most crucial role in this discovery with his first observations of distant nebulae outside the Milky Way, and his measurement of their recession velocity as a function of their distance to our Solar System [7]. The relation between these velocities and their cosmological distance to the observer is known as the Hubble-Lemaître law and is a direct probe of an expanding Universe. This discovery of the Universe expansion has confirmed cosmological models that were established first by physicists George Lemaître and Alexander Friedmann [8, 9]. These models were described within the framework of General Relativity which was mainly developed by Albert Einstein around 1915 [10, 11]. They opened a new window on the relation between the geometry of our Universe and its content in terms of matter and energy. The key feature allowing us to relate cosmological observations with Universe archaeology is this expansion of space, and we will introduce the tools to describe the space-time of such an expanding Universe in this part of the thesis.

1.1.1 Basics of General Relativity

The theory of General Relativity is a theory of gravitation. It relates the geometry of curved space-time to its matter and energy content, and so to the gravitational field. It is a metric theory of space-time where geometry and distances on the space-time sheet are described by a metric field $g_{\mu\nu}(x)$, which is a symmetric tensor, related to the invariant line element

$$ds^2 = g_{\mu\nu} dx^\mu dx^\nu \tag{1.1}$$

where x^μ are 4D space-time coordinates. A physical system that is not subject to any force then follows a geodesic trajectory on this space-time sheet described by the equation

$$\frac{d^2 x^\mu}{d\lambda} + \Gamma^\mu_{\alpha\beta} \frac{dx^\alpha}{d\lambda} \frac{dx^\beta}{d\lambda} = 0 \tag{1.2}$$

where λ is a parameter along the trajectory, while $\Gamma^\mu_{\alpha\beta}$ are the Christoffel symbols representing the affine (Levi-Civita) connection on the space-time manifold. They are related to the derivatives of the metric tensor through the relation

$$\Gamma^\mu_{\alpha\beta} = \frac{1}{2} g^{\mu\sigma} \left(\partial_\alpha g_{\sigma\beta} + \partial_\beta g_{\alpha\sigma} - \partial_\sigma g_{\alpha\beta} \right) . \tag{1.3}$$

It can be shown easily that this geodesic equation is obtained from a variational principle of least action along the line element of the trajectory

$$\mathcal{S} = \int ds \quad \text{and} \quad \delta\mathcal{S} = 0 \implies \text{Eq.(1.2)}\,. \tag{1.4}$$

The equations of motion for the metric field itself are the so-called Einstein equations, which provide the relation between the space-time geometry and its content in terms of matter and energy

$$R_{\mu\nu} - \frac{1}{2}R\ g_{\mu\nu} \equiv G_{\mu\nu} = 8\pi G\ T_{\mu\nu} + \Lambda\ g_{\mu\nu} \tag{1.5}$$

where G is the gravitational constant. We introduced different tensors for the geometry of space-time on the left-hand side of the equation, and the stress-energy tensor of matter and energy $T_{\mu\nu}$ on the right-hand side. Λ is a cosmological constant representing the energy density in the absence of non-gravitational fields. We will come back to the status of this constant in modern Cosmology in the next part of the section. $R_{\mu\nu}$ is the Ricci tensor determined by the metric tensor and its derivatives through the connection $\Gamma^{\alpha}_{\mu\nu}$

$$R_{\mu\nu} = \partial_\alpha\Gamma^{\alpha}_{\mu\nu} - \partial_\nu\Gamma^{\alpha}_{\mu\alpha} + \Gamma^{\alpha}_{\beta\alpha}\Gamma^{\beta}_{\mu\nu} - \Gamma^{\alpha}_{\beta\nu}\Gamma^{\beta}_{\mu\alpha}\,. \tag{1.6}$$

$R \equiv R_{\mu\nu}g^{\mu\nu}$ is the Ricci scalar and these two objects define the Einstein tensor $G_{\mu\nu}$. This set of equations provides the dynamics of the space-time sheet according to the content of matter and energy that is standing there. They can be obtained again through a variational principle of least action, and the appropriate action for space-time is the Einstein-Hilbert action (with cosmological constant)

$$\mathcal{S}_{\text{EH}} = -\frac{1}{16\pi G}\int d^4x\sqrt{-g}(R + 2\Lambda) \tag{1.7}$$

where $g \equiv \det(g_{\mu\nu})$. The action for matter $\mathcal{S}_{\text{matter}}$ allows us to define covariantly the stress-energy tensor

$$T_{\mu\nu} \equiv \frac{2}{\sqrt{-g}}\frac{\delta\mathcal{S}_{\text{matter}}}{\delta g^{\mu\nu}} \tag{1.8}$$

and to recover Einstein field equations via $\frac{\delta\mathcal{S}_{\text{tot}}}{\delta g^{\mu\nu}} = \frac{\delta(\mathcal{S}_{\text{EH}}+\mathcal{S}_{\text{matter}})}{\delta g^{\mu\nu}} = 0 \implies$ Eq.(1.5). More precisely, the matter action is related to the field content, and so Lagrangian densities for all the fundamental fields that make up the Universe in terms of matter and radiation

$$\mathcal{S}_{\text{matter}} = \sum_{\text{fields}}\int d^4x\sqrt{-g}\mathcal{L}_{\text{fields}}\ . \tag{1.9}$$

Due to the symmetries of the metric tensor, the total stress-energy tensor is a diagonal tensor. We will see in the following part that we rely on the hypothesis of a homogeneous and isotropic Universe on cosmological scales, which in turn imposes the equality of the spatial components for the stress-energy tensor of fields. The simplest system that satisfies these constraints on

large scales is a perfect fluid, characterized by its stress-energy

$$T_{\mu\nu} = (\rho + P)u_\mu u_\nu - P g_{\mu\nu} \tag{1.10}$$

where P is the mean pressure of the fluid, ρ its mean energy density, and u_μ the components of its bulk four-velocity in an arbitrary reference frame. We introduce here an important quantity, the equation of state for the perfect fluid w, which relates its pressure to its energy density via $P = w\rho$. Then, for an observer attached to the fluid bulk, that is $u_\mu = (1, 0, 0, 0)$, we have in this frame $g_{\mu\nu} = \eta_{\mu\nu} = \text{diag}(1, -1, -1, -1)$ (the Minkowski metric) and one can rewrite the stress-energy tensor for a perfect fluid as

$$T_{\mu\nu} = \text{diag}(\rho, P, P, P) = \text{diag}(\rho, w\rho, w\rho, w\rho) \tag{1.11}$$

1.1.2 Friedmann-Lemaître-Robertson-Walker metric

The description of a space-time metric for the whole Universe relies on the assumption that it is both homogeneous and isotropic on large scales, which is known as the cosmological principle. It states that there is no preferred observer in the Universe, at least on a cosmological scale, meaning that the physical laws and the results we obtain from our computations and observations should be valid everywhere in the Universe. This principle finds observational justification on scales greater than 100 Mpc, which we can call cosmological scales. The main example of this observation of isotropy and homogeneity on the largest scales is the detection of the CMB radiation, as we will see in section 1.5, which appears to have a high degree of isotropy and very tiny anisotropies of temperature showed in Figure 1.1. We will discuss the explanation for such an important level of isotropy and homogeneity on large scales of our Universe when we deal with inflationary cosmology in section 2.1. However, this observation is made from our specific position in the Universe, and it is impossible to know whether the Universe is also isotropic for all observers. The cosmological principle is the fundamental hypothesis according to which the Universe on very large scales is isotropic for all observers at rest with respect to the CMB radiation, which also implies the homogeneity of the Universe. Despite strong motivations and evidence for such a reasonable hypothesis, modern cosmology depends strongly on this philosophical principle, which has never been demonstrated yet. Still, different observations of large-scale structures (the largest clusters of galaxies on cosmological scales) have shown that the reference frame where the CMB is homogeneous is the same as the frame where the large-scale structure distribution is homogeneous, which is a hint in favor of the cosmological principle.

Consequently, to describe the Universe as a physical system, following the theory of General Relativity, we have to construct a 3D spatial metric that is homogeneous and isotropic, embedded within a 4D space-time manifold. In fact, there is only one possible generic form

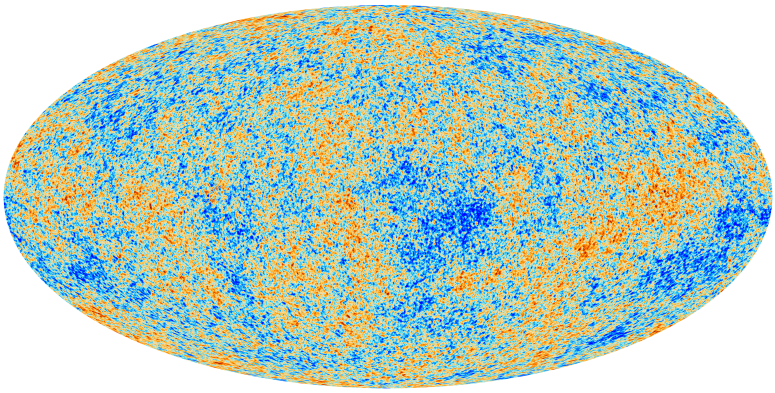

Figure 1.1: *The anisotropies of the CMB temperature as observed by PLANCK satellite (From PLANCK Collaboration). This is a map of the energy of photons received today from all directions in the sky, and emitted after the recombination of protons and electrons in the early Universe. Nearly 380.000 years after the Big Bang, the Universe experienced a transition from an opaque plasma to a transparent medium. It shows tiny temperature fluctuations that correspond to regions of slightly different densities, thought to be the seeds of all future large-scale structures. The temperature contrast is close to* $\Delta T/T_0 \sim 10^{-5}$ *on the whole map, demonstrating a high level of isotropy on such large scales.*

of the metric, compatible with these assumptions implied by the cosmological principle. It was derived and used by different physicists in the the last century, and is now called the Friedmann-Lemaître-Robertson-Walker (FLRW) metric

$$ds^2 = dt^2 - a^2(t)\left(\frac{dr^2}{1-kr^2} + r^2 d\theta^2 + r^2 \sin^2(\theta) d\phi^2\right) \tag{1.12}$$

where $a(t)$ is the scale factor, the dynamical quantity that describes the evolution of the distance due to the expansion between two comoving observers that have no relative velocities between each other. The set (r, θ, ϕ, t) are space-time spherical coordinates referred to as comoving coordinates. We note that in this parametrization, $a(t)$ is dimensionless and we consider r to be the dimensionful radial distance coordinate. In fact, this describes a class of solutions of homogeneous and isotropic Einstein equations, depending on the value of k, which can take the values $-1, 0, +1$, depending on the intrinsic curvature of space of the Universe

$$k = \begin{cases} -1 & \text{a Universe with negative curvature or hyperbolic geometry, infinite and open} \\ 0 & \text{a spatially flat Universe with Euclidean geometry, infinite and open} \\ +1 & \text{a Universe with positive curvature or spherical geometry, closed and finite} \end{cases} \tag{1.13}$$

However, it appears that the current cosmological observations favor an (almost) spatially flat and so Euclidean Universe, i.e. a Universe with $k = 0$ (see sections 1.5). We will come back on an explanation for this fact and the current constraints on spatial curvature in section 2.1 when dealing with inflation. Therefore throughout the rest of this thesis, we will assume, in

general, a spatially flat Universe on cosmological scales and use the FLRW metric with

$$g_{\mu\nu} = \mathrm{diag}(1, -a^2(t), -a^2(t), -a^2(t)) \ . \tag{1.14}$$

The scale factor describes how the distances change on a photon path in an expanding Universe. The wavelength of this photon is subject to the contraction or dilatation of space by a factor $a(t)$, and we define the cosmological redshift of such a photon z, as the ratio of the scale factor at present time t_0 over the scale factor at some past time t

$$1 + z \equiv \frac{\lambda_{\mathrm{obs}}}{\lambda_{\mathrm{emit}}} = \frac{a(t_0)}{a(t)} = \frac{1}{a(t)} \tag{1.15}$$

where by convention we can set $a(t_0) = 1$. The scale factor links the physical distance traveled by a photon $d_H(t)$ separating two objects in the Universe, with the comoving distance $\chi(t)$, the distance that would be traveled if the Universe was not expanding. For a light-like trajectory $ds = 0$ and so

$$d_H(t) = a(t)\chi(t) = a(t) \int_t^{t_0} \frac{dt'}{a(t')} \, . \tag{1.16}$$

It is sometimes also useful to reparametrize the FLRW metric as

$$ds^2 = a^2(t)(d\eta^2 - (d\vec{r})^2) \tag{1.17}$$

defining the conformal time $\eta(t)$, which is the total distance traveled by a light ray since $t = 0$

$$\eta(t) = \int_0^t \frac{dt'}{a(t')} \ . \tag{1.18}$$

With these definitions, it is straightforward to derive the Hubble law for the recession velocity of a galaxy with respect to the observer due to the expansion, assuming it is comoving with the observer (it has no peculiar velocity relative to the observer). By differentiating the relation between proper (physical) distance and comoving distance we obtain

$$v_{\mathrm{rec}}(t) = H(t) \ d_H(t) \tag{1.19}$$

where we introduced the fundamental quantity $H(t)$, the Hubble parameter at a time t, defined as

$$H(t) \equiv \frac{\dot{a}(t)}{a(t)} \ . \tag{1.20}$$

We see that Hubble's law is a direct consequence of the homogeneity and isotropy of the Universe and its dynamical expansion. The Hubble parameter expresses the rate at which the Universe is expanding at a cosmic time t (on a hypersurface of constant cosmic time, to be precise), and it is measured today to be $H(t_0) = H_0 \sim 70 \ \mathrm{km \cdot s^{-1} \cdot Mpc^{-1}}$. It is usually defined through the

dimensionless parameter h as

$$H_0 \equiv 100\ h\ \mathrm{km}\cdot\mathrm{s}^{-1}\cdot\mathrm{Mpc}^{-1} \tag{1.21}$$

We call this quantity the Hubble constant, and it is a fundamental physical quantity of modern Cosmology[1]

1.1.3 Friedmann-Lemaître equations

Cosmology assumes that matter and radiation filling the Universe can be described in terms of fields, looking on large scales as perfect fluids of different species. The stress energy associated with each species is entirely described by the mean energy density of the fluid, ρ_i, and its equation of state parameter w_i as in Eq.(1.11). In addition, the stress-energy tensor has the fundamental property of being conserved under its covariant derivative leading to the continuity equation

$$\nabla_\mu T^\mu_{\ \nu} \equiv \partial_\mu T^\mu_{\ \nu} + \Gamma^\mu_{\alpha\mu} T^\alpha_{\ \nu} - \Gamma^\alpha_{\nu\mu} T^\mu_{\ \alpha} = \frac{\partial \rho_i}{\partial t} + 3(1+w_i) H \rho_i = 0 \tag{1.22}$$

where in the last equality, we have used the computations of the Christoffel symbols from Eq.(1.3) for the FLRW metric Eq.(1.14). The expansion of the Universe is determined by the dynamical evolution of the scale factor $a(t)$ and its derivative through the Hubble parameter $H(t)$, which are solutions of the Einstein equations Eq.(1.5) for the FLRW metric Eq.(1.14). By inserting the FLRW metric and the stress-energy tensors of perfect fluids into the Einstein equations Eq.(1.5), we obtain two equations for the scale factor and its derivatives, the Friedmann-Lemaître equations

$$\left(\frac{\dot{a}}{a}\right)^2 = H^2(t) = \frac{8\pi G}{3}\rho_{\mathrm{tot}} + \frac{\Lambda}{3} \tag{1.23}$$

$$\left(\frac{\ddot{a}}{a}\right) = -\frac{4\pi G}{3}\left(\rho_{\mathrm{tot}} + 3P_{\mathrm{tot}}\right) + \frac{\Lambda}{3}\,. \tag{1.24}$$

These equations are the fundamental equations that govern the evolution of the whole Universe as a space-time sheet, depending on its content in terms of cosmological fluids. Here $\rho_{\mathrm{tot}} = \sum_i \rho_i$ and $P_{\mathrm{tot}} = \sum_i P_i$, the sum of energy densities and pressure for all the species filling the Universe at a cosmic time t. An important observation is that the cosmological constant, Λ, can be absorbed in ρ_{tot} and P_{tot} by defining and associated "vacuum" energy density $\rho_\Lambda = \Lambda/8\pi G$ together with an equation of state for this exotic fluid, $w_\Lambda = -1$. By this definition, we assign an energy density and negative pressure to space-time once it is "empty" or at least not containing any classical field. This cosmological constant energy density and pressure is of great importance

[1] In particular, different cosmological surveys do not agree on the precise value of this quantity, a recent tension in Cosmology that may have to deal with new Physics beyond its current standard description. For a review on the so-called Hubble-tension see [12].

in modern Cosmology and for the inflationary paradigm that is introduced in section 2.1. From the Friedmann-Lemaître equations, once we know how evolve the different components of the Universe on large scales, we can determine the evolution of the whole Universe space-time.

Under the assumption of an adiabatic (smooth) expansion of the Universe between a given $a(t)$ and a_0, with constant equations of state w_i for the perfect fluid, we can solve the continuity equation on cosmological scales, Eq.(1.22), and obtain the generic evolution

$$\rho_i(t) = \rho_{i,0} \left(\frac{a(t)}{a_0} \right)^{-3(1+w_i)} . \tag{1.25}$$

The key parameter that drives the expansion of the Universe is hence the equation of state w_i of the main component energy density, ρ_i, filling the Universe at a cosmic time t. We emphasize the importance of this approximate description in terms of perfect fluids with a constant equation of state, which is the most general form for the stress energy in an FLRW space-time [13], and is remarkably simple to describe various contributions to the matter content filling the Universe at different epochs. It is also convenient to define the critical energy density of the Universe, which is the total energy density today for a spatially flat Universe ($k = 0$), obtained from the first Friedmann-Lemaître equation evaluated today at $a = a_0$,

$$\rho^0_{\rm crit} = \frac{3H_0^2}{8\pi G} . \tag{1.26}$$

The critical density allows us to define the energy density fraction of each component present in a flat Universe by $\Omega_i = \rho_i/\rho^0_{\rm crit}$. Our goal now is to understand the thermodynamics of such perfect fluids to relate pressure and energy density and determine the associated equation of state for the different types of components that can dominate the Universe's evolution.

1.1.4 The Boltzmann equation

The Boltzmann equation allows us to describe the evolution of the distribution function of the particles making up the fields of each "species", $f_i(x, p, t)$, in the phase space (x, p) of positions and momenta of the particles. The distribution function is related to the number of particles $dN_i(x, p, t)$ in an infinitesimal phase-space volume around the point (x, p) at a time t, by [14]

$$dN_i(x, p, t) = f_i(x, p, t) \frac{d^3p \; d^3x}{(2\pi)^3} . \tag{1.27}$$

Hence, the distribution function can be interpreted as the probability density to find the state of the system of particles in the phase-space volume $d^3p \; d^3x$. Then, for a closed system that is not subject to energy exchange or chemical potential with its surrounding environment, we can show the conservation of this probability density along any phase-space trajectory or, equivalently, the conservation of the phase-space volume containing the particles along time.

It is the Liouville theorem stating that the distribution function of each species follows the continuity equation

$$\frac{df_i}{dt} = \frac{\partial f_i}{\partial t} + \frac{\partial f_i}{\partial x^j} \cdot \frac{dx^j}{dt} + \frac{\partial f_i}{\partial p^j} \cdot \frac{dp^j}{dt} = 0 \tag{1.28}$$

where $j = 1, 2, 3$ is a spatial index. We call this equation the collisionless Boltzmann equation, as there is no right-hand side of this equation that can play the role of a source of particles, or momentum transfer between and among species. To solve the Boltzmann equation, we first have to find the expression of $\frac{dp}{dt}$ as a solution to the geodesic equation Eq.(1.2) for a test particle propagating in a given space-time. For homogeneous and isotropic Universe, following the cosmological principle, the distribution function of the cosmological fluids should not depend on x^i and the direction of p^i, but only on the norm of momentum p and cosmic time t as $f(p, t)$. We can consider the FLRW metric to recover a very simple equation for the distribution function of each species

$$\frac{\partial f_i(p,t)}{\partial t} - H(t)p\frac{\partial f_i(p,t)}{\partial p} = 0\,. \tag{1.29}$$

This equation is valid for all particles of all species and is extremely important to understand the behavior of the perfect fluid made up of these particles. We compute the first moment of this probability distribution which is nothing else than the number density of particles in a volume of space at a given cosmic time t,

$$n_i(t) = \int \frac{d^3p}{(2\pi)^3} f_i(p,t) \tag{1.30}$$

as well as the average energy density of the fluid,

$$\rho_i(t) = \int \frac{d^3p}{(2\pi)^3} E f_i(p,t) \tag{1.31}$$

where $E = \sqrt{p^2 + m^2}$ is the energy of the particle of momentum p and mass m. The last thermodynamical quantity to define is the average pressure of the fluid. We can show [14] that it is obtained from the distribution function through the integral

$$P_i(t) = \int \frac{d^3p}{(2\pi)^3} \frac{p^2}{3E} f_i(p,t)\,. \tag{1.32}$$

These expressions for the macroscopic quantities are consistent with the description of the stress-energy tensor of a perfect fluid Eq.(1.11). Indeed, by integrating over momentum $\int \frac{d^3p}{(2\pi^3)}$ the conservation equation Eq.(1.29), we obtain the continuity equation for number density

$$\frac{\partial n(t)}{\partial t} + 3H(t)n(t) = 0 \tag{1.33}$$

which corresponds to the conservation of the number of particles in a comoving volume. In the same way, the integration over momentum after multiplying by the energy of each particle E, leads exactly to the continuity equation for energy density and pressure, which is Eq.(1.22). From the expression of energy density and pressure, we can directly extract the behavior of a gas of relativistic particles of energy $E \sim p \ll m$, and compute the mean equation of state in this case $w_i = P_i/\rho_i = 1/3$. In the same way, for a gas of cold (non-relativistic) particles, $E \sim m \ll p$, we obtain a mean equation of state $w_i \sim \langle p^2 \rangle / m^2 \sim 0$.

Until now, we have described the evolution of distribution functions for species that do not interact with each other. However, in the general case, the number of particles is not conserved in a phase-space volume, due to particle-particle interactions (scattering, pair creation, annihilation, decays, etc). Then, in the Boltzmann equation we have to consider a nonvanishing right-hand side of the equation, introducing the collision term $C[f]$,

$$\frac{\partial f_i(p,t)}{\partial t} - H(t)p\frac{\partial f_i(p,t)}{\partial p} = C[f]\,. \tag{1.34}$$

This collision term is fundamental to track the production of species and their interactions, notably to explain how they can reach a state of maximal entropy at thermal equilibrium, and when they depart from this equilibrium at decoupling (see section 1.2). If one wants to solve the Boltzmann equation, one needs to specify the collision terms of processes that modify the number of particles in the phase space volume. Let us consider a microscopic process described by the following interaction between particles $1, 2, 3, 4$

$$1 + 2 \leftrightarrow 3 + 4\,. \tag{1.35}$$

Then for this specific process, the collision term for particle 1 can be computed as follows

$$\begin{aligned} C[f_1(p_1)] = \frac{1}{2E_1(p_1)} \int d\Pi_2 d\Pi_3 d\Pi_4 (2\pi)^4 \delta^{(4)}(p1 + p2 - p3 - p4) \\ \times \left[-|\overline{\mathcal{M}}_{1+2\to 3+4}|^2 f_1(p_1) f_2(p_2)(1 \pm f_3(p_3))(1 \pm f_4(p_4)) \right. \\ \left. + |\overline{\mathcal{M}}_{1+2\leftarrow 3+4}|^2 f_3(p_3) f_4(p_4)(1 \pm f_1(p_1))(1 \pm f_2(p_2)) \right] \end{aligned} \tag{1.36}$$

where we introduced the Lorentz invariant phase space measure $\Pi_i \equiv \frac{d^3 p_i}{(2\pi)^3 2E_i(p_i)}$. The terms $+, -$, in the parenthesis apply respectively to bosons and fermions statistics, describing either Pauli blocking or Bose enhancement in the production of final state particles. The transition amplitude squared for the process $|\overline{\mathcal{M}}|^2$ is characterized by the specific process, interaction, between the particles. It has to be averaged over initial spin states, summed over final spin states, and divided by symmetry factors accounting for identical initial or final states. To consider all the possible processes affecting $f_1(p_1)$, one has to add to the right-hand side the different transition amplitudes squared involving particle 1 associated with different rates of

interactions.

1.1.5 ΛCDM model

In the precedent parts, we have constructed the main tools required to describe the evolution of the Universe on the largest scales. The success of modern Cosmology relies on the simple and natural assumptions presented above and the accuracy of its main predictions from these simple ingredients. The background dynamics and geometry of the Universe can be fully explained by introducing only five different species described as cosmological perfect fluids. These five components are the core of the so-called ΛCDM model for Cosmology. Among these five species, three of them (baryons, neutrinos, and photons) are already part of the current understanding of particle Physics, which describes standard matter within the Standard Model (SM) (see Appendix A for an overview of the SM of Particle Physics) [2]. Particles that are still relativistic in the Universe today, such as photons that are massless particles, constitute a radiation component with the equation of state $w = 1/3$. In this case from the continuity equation Eq.(1.22) we obtain the evolution of their energy density

$$\rho_R(a) = \rho_R^0 \left(\frac{a}{a_0}\right)^{-4} . \tag{1.37}$$

The main part of the radiation filling the Universe comes from CMB photons, but it represents a very small fraction of the total energy density today [15]

$$\Omega_R^0 \, h^2 \simeq \Omega_\gamma^0 \, h^2 = 2.47 \times 10^{-5} \, h^2 \, . \tag{1.38}$$

where $\Omega_R = \Omega_\gamma + \Omega_\nu$ from photons and neutrinos background relic densities. Baryons correspond to ordinary matter, i.e. atoms (their nuclei as well as electrons). In the ΛCDM paradigm, it is possible to measure the fraction of baryons in terms of energy density from the CMB anisotropies, as we will see in section 1.5. From this measurement [15], it appears that baryons represent only 5% of the energy content of the Universe today. The most precise constraint on this quantity come from the BBN analysis. The abundance of the light nuclei created during BBN depends on the number of baryons present in the Universe at that time, which allows us to determine their abundance today very accurately. Measurements of these light elements' abundances (see 1.2.3), which are independent of CMB measurements, are compatible with the Planck satellite measurement of CMB anisotropies [15]. These measurements establish that the fraction of baryon energy density today is close to

$$\Omega_b^0 \, h^2 = 0.0224 \pm 0.0001 \, . \tag{1.39}$$

[2] We note that the observation of the small masses of neutrinos has a strong impact on Cosmology and has to be accommodated in some extension of the SM, as we will see in section 1.3

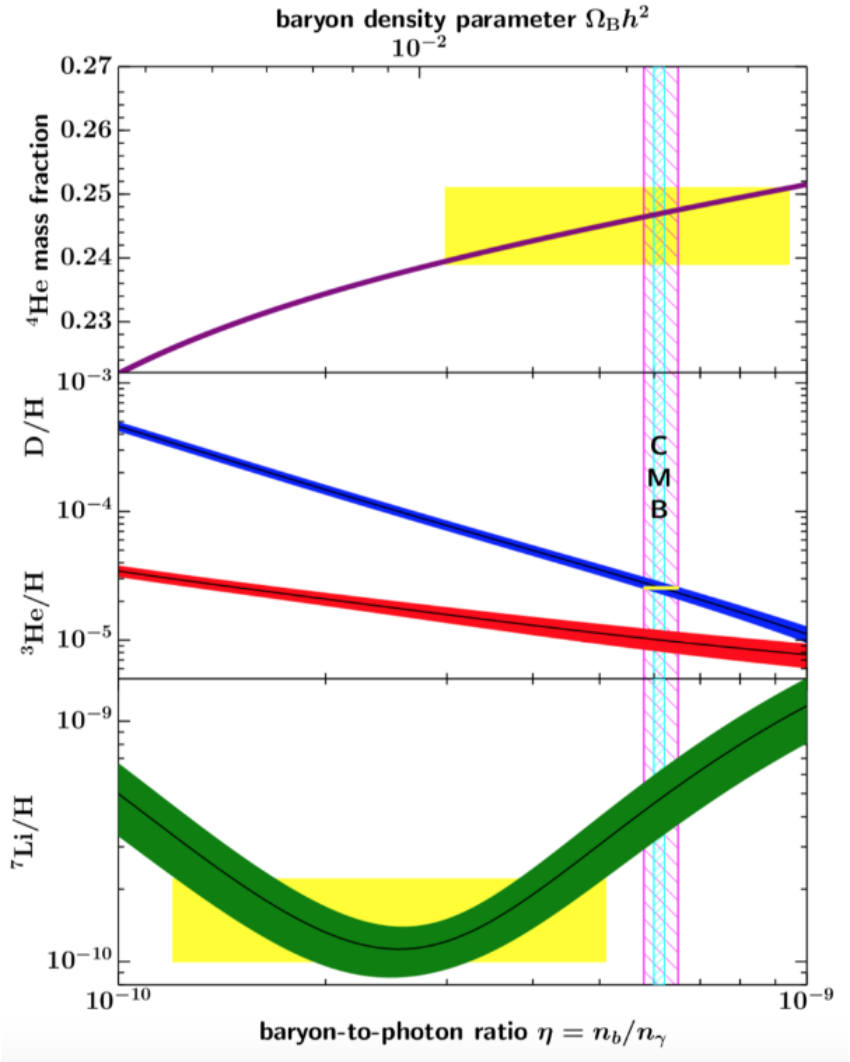

Figure 1.2: *Relative abundance of light elements (see section 1.2.3 for the mechanism of BBN) compared to Hydrogen, as a function of the ordinary matter to photon ratio η_B. Figure taken from [16].*

This compatibility between these two independent probes is one of the main successes of the ΛCDM model. In addition, the other two components of ΛCDM still lack direct detection, and their fundamental description beyond the SM (BSM) in terms of particles and quantum fields is still at the heart of High Energy Physics and Cosmology research goals. The first component is called Cold Dark Matter (CDM) and should be constituted by a non-baryonic and non-relativistic kind of matter. In particular, CDM (as we shall see in section 1.5) is necessary to explain the shape of the CMB anisotropies. The measurement of CMB temperature fluctuations is, therefore, the best way of measuring the current DM fraction. Planck data [15] provide the measurement

$$\Omega^0_{\rm CDM}\, h^2 = 0.119 \pm 0.001\,, \tag{1.40}$$

DM thus makes up about 25% of the energy budget of the Universe today. DM is hence fundamental to explain the expansion of the Universe but is also fundamental to explain the dynamics of gravitationally bound systems such as galaxies and galaxy clusters, meaning that several astrophysical evidence supports its existence. We come back more precisely to the main evidence of its existence while discussing CMB observation in section 1.5 and the main current approaches to explain DM production in section 1.4. Both matter components, baryonic and non-baryonic, constitute a cold non-relativistic fluid in the Universe today. Therefore, matter behaves as a "dust" with the equation of state $w = 0$ leading from the continuity equation Eq.(1.22) to

$$\rho_m(a) = \rho_m^0 \left(\frac{a}{a_0}\right)^{-3} . \tag{1.41}$$

Finally, Cosmology has been led to postulate the existence of a Dark Energy (DE) component in our Universe. In 1998, Riess et al. [17], as well as Perlmutter et al. [18, 19] have shown by measuring the apparent luminosity of Type Ia Supernovae, that the Universe is undergoing an acceleration of its expansion. Besides, the best measurements of large-scale structure and CMB anisotropies indicate that the total amount of matter - both baryonic and DM - accounts for about 30% of the critical density. Therefore, the rest of the Universe's energy content must be something else. The current best explanation for the acceleration of the expansion of the Universe lies in the existence of this DE component, which should have (with current constraint) constant energy density, and that can be associated with the cosmological constant Λ introduced in the Einstein equations Eq.(1.5). The current status of DE is not clear yet, but this fundamental observation of the accelerating expansion in concordance with the other probes from the CMB anisotropies, shows that it should represent the main energy component of our Universe today. The different pieces of evidence for the existence of DE are pushing towards the same amount of DE with about $\sim 68\%$ of the Universe energy budget and a relic density

$$\Omega_\Lambda^0 \; h^2 = 0.316 \pm 0.003 \, . \tag{1.42}$$

Precise measurement of the CMB anisotropies and Type Ia Super Novae distances, assuming a Euclidean (flat) Universe, indicates that this DE component should behave very closely to a cosmological constant, with the equation of state $w_{\rm DE} \simeq 1$. Its associated energy density can be expressed through an equivalent cosmological constant

$$\rho_\Lambda = \frac{\Lambda}{8\pi G} \, . \tag{1.43}$$

corresponding to $\Lambda \sim 10^{-84}$ GeV^2. With all these components, the ΛCDM is built up as a concordance model for Cosmology that can simultaneously explain all the current observations on the largest scale of our Universe. We note additionally that independent constraints from CMB measurements and galaxy surveys strongly indicate the Euclidean nature or very high

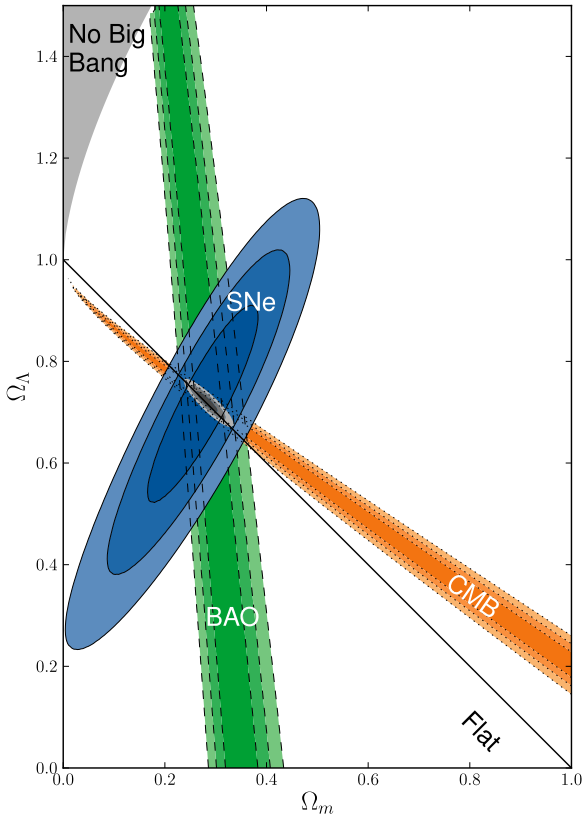

Figure 1.3: *Constraints on the cosmological parameters* $(\Omega_m, \Omega_\Lambda)$ *for the contribution of matter and DE to the total energy budget. Here a curved space is allowed, but the Euclidean flat space line is represented in solid black. Observations of distance-redshift of Type Ia supernovae provide the blue contours, while CMB constraints are in orange. The green curves are coming from observations of the large-scale structures and their matter power spectrum: fluctuations in the density of the visible baryonic matter caused by acoustic density waves result in a statistical signature at the sound horizon scale called Baryonic Acoustic Oscillations (BAO). Figure taken from [20]*

level of flatness of our Universe on the largest scales ($k = 0$). This is also a measure of the consistency of the ΛCDM model, as spatial curvature is related to the critical energy density through

$$\sum_i \Omega_i = \Omega_R + \Omega_m + \Omega_\Lambda \equiv 1 - \Omega_K \quad ; \quad \Omega_K(a) \equiv -\frac{k}{H_0^2 a^2} \tag{1.44}$$

where we recall that $\Omega_R = \Omega_\gamma + \Omega_\nu$ and $\Omega_m = \Omega_b + \Omega_{\rm CDM}$. Current constraints obtained by combining CMB and large-scale structure probes are giving [22]

$$|\Omega_K^0| \lesssim 0.002\,, \tag{1.45}$$

indicating that our Universe is almost perfectly flat. We will discuss the problems introduced by these high levels of flatness, isotropy, and homogeneity when discussing initial conditions of the ΛCDM model, and the current explanation through the inflation paradigm (see section 2.1).

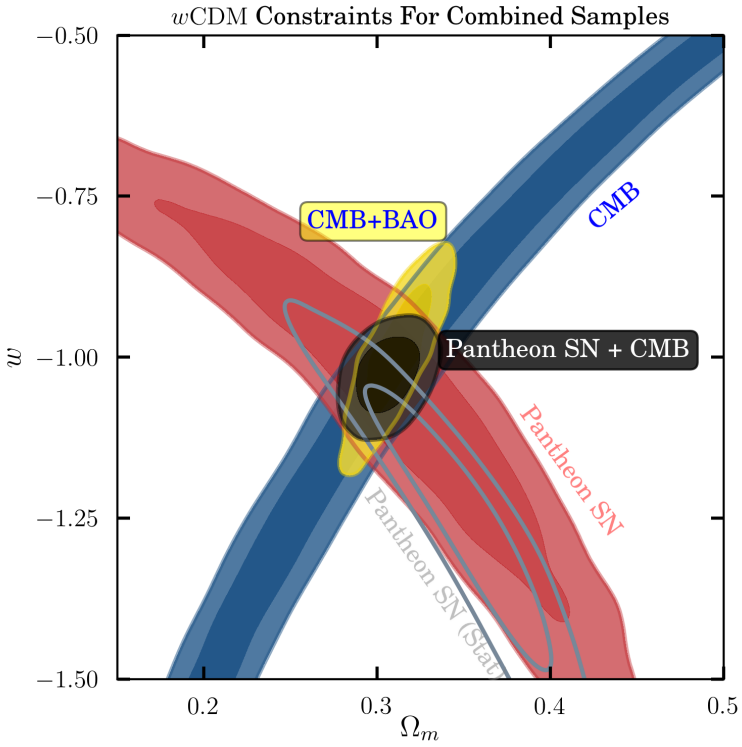

Figure 1.4: *Constraints for* $(\Omega_m, w_{\rm DE})$*, from CMB (blue), CMB+BAO (yellow), and supernovae (red and gray). The combined constraints are in black and indicate that DE has to be close to the behavior of a cosmological constant with* $w_{\rm DE} = -1$*. Figure taken from [21].*

Within the ΛCDM model, we can rewrite the first Friedmann-Lemaître equation for the Hubble parameter as

$$H^2(a(t)) = H_0^2 \left[\Omega_m^0 \left(\frac{a}{a_0} \right)^{-3} + \Omega_R^0 \left(\frac{a}{a_0} \right)^{-4} + \Omega_K^0 \left(\frac{a}{a_0} \right)^{-2} + \Omega_\Lambda^0 \right] \tag{1.46}$$

and solve for the evolution of the scale factor, knowing the abundances of each species today, as constrained by various observations that we discussed above. From the equation, we obtain Figure 1.5, where we see the different trajectories for the relative size of the Universe, the scale factor, as a function of cosmic time, for different energy content and spatial curvature. The current ΛCDM model gathering different observations shows that the trajectory of our Universe is the one with $k = 0$, $\Lambda > 0$ and $\Omega_\Lambda \simeq 0.7$, $\Omega_m \simeq 0.3$.

Finally, the different components in terms of energy density have a different evolution along the expansion, as can be seen from Eqs. (1.41)-(1.37)-(1.43), hence resulting in different relative abundances in the past. In Figure 1.6, we show the past evolution of the different components observed today in the Universe as a function of the scale factor. We clearly see that this indicates three main stages in Universe history: an early domination of radiation energy density, where hot plasma made of relativistic particles dominates the energy budget. Then, this plasma is

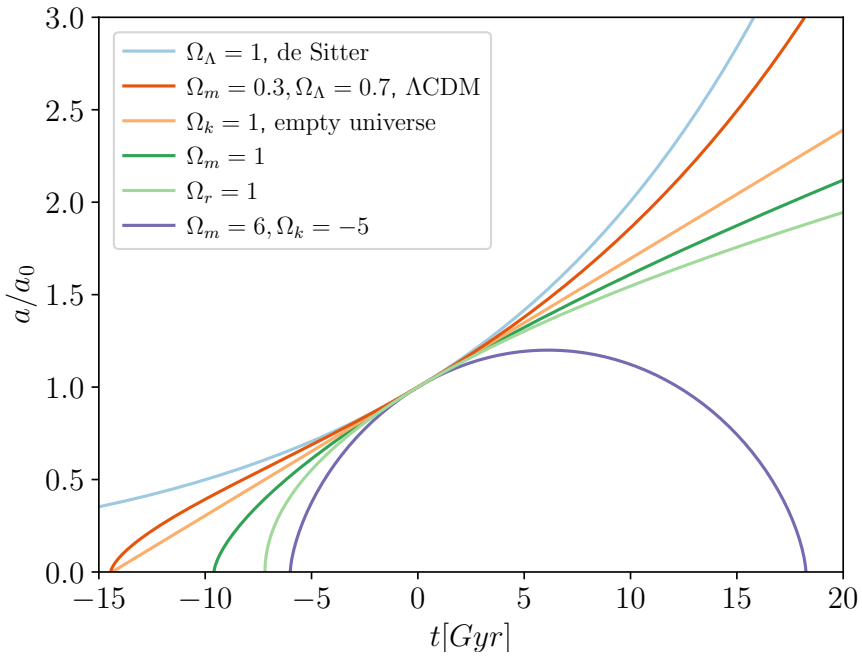

Figure 1.5: *Evolution of the relative size of the Universe (scale factor) as a function of cosmic time in* Gyrs*, for different content of matter-energy. The ΛCDM trajectory corresponds to the red curve, while the other curves are historical cosmological models.*

cooling down while the Universe expands, and non-relativistic matter in the form of DM starts to dominate the expansion at a scale factor $a = a_{\rm eq}$ defined by

$$1 + z_{\rm eq} = \left(\frac{a_0}{a_{\rm eq}}\right) = \frac{\Omega_m^0}{\Omega_R^0} \simeq 3440 \tag{1.47}$$

before reaching a DE domination era of accelerated expansion in the very late Universe.

In the next section, we draw a condensed history of the early days of the Universe by exploring first the radiation-dominated era and the thermal history of the Universe.

1.2 Thermal Universe

After the period of inflation that took place in early times and that we will investigate in section 2.1, the Universe is filled with relativistic particles interacting intensively and forming a thermal bath with a very high energy density of radiation and high temperature T. As the Universe expands, the hot plasma is diluted, and relativistic particles lose their energy through the redshift of their frequencies. The temperature of the plasma drops down, massive particles become non-relativistic and some rates of interaction among the particles of the plasma become suppressed. This will allow for successive depart from thermal equilibrium among the

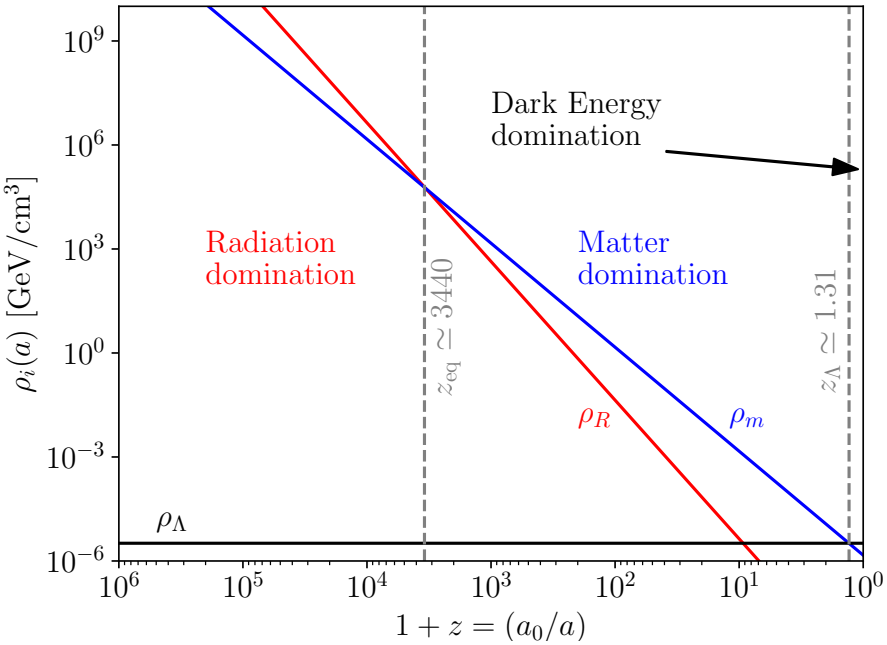

Figure 1.6: *Evolution of the different components of the Universe density as a function of the redshift (scale factor).*

different species of the plasma leading to the generation of thermal relics and further cold relics that are constituting our Universe today. This story of the hot thermal Universe and the different decouplings of species is marked by important events associated with a specific time or temperature [16] :

- $T \lesssim 10^{13}$ GeV $\quad [\mathrm{t} \gtrsim 10^{-30}$ s]: the end of the inflation era and the time of reheating that is the main mechanism studied in this thesis. The early Universe underwent a transition from a quasi-De Sitter era towards a radiation-dominated era, governed by a hot thermal bath at a very high temperature. Grand Unified Theories (GUT) also predict new Physics should occur close to this energy scale (new particles in the spectrum, new interactions with the SM particles, etc).

- $T \lesssim 10^{8} - 10^{11}$ GeV $\quad [\mathrm{t} \gtrsim 10^{-22} - 10^{-28}$ s]: baryogenesis and leptogenesis can occur from out-of-equilibrium processes. Heavy particles, such as DM candidates, can be produced at high temperatures within the thermal bath.

- $T \lesssim 100$ GeV $\quad [\mathrm{t} \gtrsim 10^{-10}$ s]: the Higgs field condensates and exhibits a non-zero vacuum expectation value (VEV), inducing the electroweak symmetry breaking. SM particles acquire masses through their couplings to the Higgs field. Subsequently, weak interactions are mediated by the massive weak bosons and, therefore, are no longer long-ranged. Baryon number (B) violating and lepton number (L) violating (but B-L conserving)

sphalerons are no longer in thermal equilibrium within the bath. Lepton asymmetry can be converted into a baryon asymmetry (see section 1.3).

- $T \lesssim 10 - 100$ GeV [t $\gtrsim 10^{-8} - 10^{-10}$ s]: Weakly Interacting Massive Particle (WIMPs) DM particles (if they exist) initially in thermal equilibrium with the SM particles, decouple from the plasma while being non-relativistic. This freeze-out mechanism explains naturally the relic abundance of DM as it is observed. We will discuss this process in the following part on thermal decoupling and when discussing the mechanisms of DM production in section 1.4.

- $T \lesssim 150$ MeV [t $\gtrsim 10^{-4}$ s]: strong interactions reach non-perturbative regime. The quarks-gluons plasma hadronized as the quarks confine, becoming bound together to form baryons and mesons through non-perturbative processes.

- $T \lesssim 0.1 - 10$ MeV [t $\gtrsim 10^{2} - 10^{-2}$ s]: protons and neutrons fusions form light nuclei through the primordial nucleosynthesis mechanism (BBN) (see bellow 1.2.3). Close to $T \sim 1$MeV, light SM neutrinos do not interact efficiently anymore with electrons and start to decouple from the electron-photons thermal bath, while still being relativistic.

- $T \lesssim 0.1$ eV [t $\gtrsim 380\ 000$ years]: electrons and light nuclei recombine to form neutral atoms (mainly Hydrogen), the Universe becomes transparent to photons. These primordial photons decouple from the bath and freely propagate throughout the Universe in every direction. They form the CMB as it is observed by our telescopes. Before the last scattering of photons ($z \simeq 1100$), the Universe is no longer dominated by radiation from the hot thermal bath, but from non-relativistic matter ($z = z_{\text{eq}} \simeq 3400$). This matter-radiation equality epoch represents the end of the thermal history of the Universe, which is entering its "dark ages" before the formation of stars and galaxies.

In the following part, we describe the several constituents of the thermal bath formed by particles of different species and discuss the notion of thermal equilibrium and thermal decoupling, which are relevant to the rest of the manuscript. In particular, we will discuss slightly the main events taking place during this stage of radiation domination: the BBN and the emission of the CMB photons at recombination, which both constitute the main signatures and observables of the early Universe.

1.2.1 Thermal equilibrium

In early times, the Universe was in a hot dense state, in which particles were highly relativistic and could exchange energy and momentum quite efficiently in a hot plasma at thermal equilibrium. Therefore, we can model the cosmological fluid as a gas of weakly interacting particles and use statistical Physics to describe it. The macroscopic properties of a given gas depend

on the distribution function $f_i(p,t)$, which describes the distribution of states in the phase space. We introduced this distribution in the precedent section when discussing the Boltzmann equation Eq.(1.29).

When particles exchange energy and momentum efficiently, the gas made of one type of particle reaches a state of maximum entropy, called kinetic equilibrium. In an expanding Universe, this state can be reached under the condition that the interaction rates[3], $\Gamma(t)$, between the different particles are more important than the expansion rate or Hubble rate, $\Gamma(t) \gg H(t)$. Indeed, if the expansion rate were too large, particles would not have enough time to interact efficiently before the expansion forbids them to exchange momentum and reach kinetic equilibrium. Kinetic equilibrium between particles can be reached if the interaction rate between them is large enough such that their momenta will be redistributed on all energy scales. This allows us to describe the gas of particles as a single system defined by a macroscopic temperature T. From statistical mechanics, it can be shown that if the kinetic equilibrium condition is satisfied, the phase space distribution $f_i(p,t)$ of the species i is described by a Fermi-Dirac (FD) or Bose-Einstein (BE) distribution depending on the spin of the particles

$$f_i(p,t) = \frac{g_i}{e^{\frac{E(p)-\mu_i}{T(t)}} \pm 1}\,. \tag{1.48}$$

where g_i is the number of degrees of freedom of the species i, $(+)$ and $(-)$ correspond respectively to the FD and BE distributions. The phase space distribution depends only on the momentum norm, satisfying the isotropy condition, and not on position due to homogeneity. It depends on time through the time-evolution of the densities and so temperature as the Universe expands.

Besides, if the gas contains several species in interaction, each species i has its distribution function and its associated chemical potential μ_i, introduced in the FD and BE distributions at equilibrium. The thermodynamical evolution of a complex system composed of multiple species is expressed in terms of the chemical potentials for each of the species. The chemical potential describes the modification of the internal energy state of the system when the number of particles is not conserved. If we consider the interaction between particles A_i producing particles B_i through the reaction

$$\sum_i A_i \longleftrightarrow \sum_i Bi \tag{1.49}$$

the system reaches its chemical equilibrium if

$$\sum_i \mu_{A_i} = \sum_i \mu_{B_i}. \tag{1.50}$$

This condition highlights that the interaction between particles A_i and B_i is at equilibrium,

[3]We come back on the definition and computation of the interaction rates from the collision term of the Boltzmann equation for different models in the parts on DM production section 1.4 and reheating section 2.2

meaning there is as much production of particles B_i as their destruction leading to production of particles A_i. In this state of chemical equilibrium, the relative abundances of each species are time-independent, so their concentration in the plasma does not vary with time. On top of this condition on the chemical potential, there are conservation equations imposed by a conserved charge (electric charge, baryon number, lepton number, etc). For photons, there is no conserved charge, and the number of photons is not conserved as highlighted for instance by the process of double Compton scattering $e^- + \gamma \leftrightarrow e^- + \gamma\gamma$ or Bremsstrahlung. This imposes that $\mu_\gamma = 0$. For particles and anti-particles, carrying opposite conserved charges, the typical process of pair annihilation $e^- + e^+ \leftrightarrow \gamma\gamma$ imposes at equilibrium that $\mu_{e^-} = -\mu_{e^+}$. Such a condition holds for any conserved charge associated with an interaction.

As the system reaches kinetic equilibrium at a maximum entropy state, it is further described by a FD or a BE distribution function. If it is composed of several species interacting, it has reached chemical equilibrium at a maximum entropy state, where the sums of the chemical potentials of the different species on each side of the number-changing reaction equations are equal. Under these conditions, we can say that the system has reached thermal equilibrium. At thermal equilibrium, all the species share the same temperature T in the thermal bath, allowing to rewrite the expressions of the number densities $n_i(T)$, energy densities $\rho_i(T)$ of a species i as a function of the temperature, from equations (1.30), (1.31), (1.48),

$$n_i(T) = \frac{g_i}{(2\pi)^3}\int f_i(p)d^3p = \frac{g_i}{2\pi^2}T^3\int_{x_i}^{\infty} du\frac{u(u^2-x_i^2)^{1/2}}{e^{u-y_i}\pm 1} \tag{1.51}$$

$$\rho_i(T) = \frac{g_i}{(2\pi)^3}\int E(p)f_i(p)d^3p = \frac{g_i}{2\pi^2}T^4\int du\frac{u^2(u^2-x_i^2)^{1/2}}{e^{u-y_i}\pm 1}\,. \tag{1.52}$$

where we defined $x_i \equiv m_i/T$ and $y_i \equiv \mu_i/T$. In the general case, the integrals must be evaluated numerically. However, some limits allow us to understand the Physics taking place in the thermal bath. We first consider negligible chemical potential compared to the temperature of the bath $T \gg \mu_i \implies y_i \ll 1$, which is a good approximation for the primordial thermal bath as the ratio of the baryon to photon is tiny $\eta_b = \frac{n_b}{n_\gamma} \simeq 6\times 10^{-10}$. Then, two limits are useful :

- in the relativistic limit $T \gg m_i \implies x_i \ll 1$, we can compute the integrals analytically from the Euler Γ function and Riemann ζ function,

$$n_i(T) = \left(\frac{3}{4}\right)\frac{\zeta(3)}{\pi^2}g_iT^3 \tag{1.53}$$

$$\rho_i(T) = \left(\frac{7}{8}\right)\frac{\pi^2}{30}g_iT^4 \tag{1.54}$$

  where the fraction in the parenthesis is present only for half-integer spin (fermions) species that have a FD distribution at equilibrium, while this factor is equal to 1 for integer spin (bosons) that follow a BE distribution at equilibrium.

- for non-relativistic species, when $T \lesssim m_i$ and $E \simeq m_i$, the densities at equilibrium are Boltzmann suppressed, making the bosonic and fermionic distribution identical in this limit with

$$n_i(T) = g_i \left(\frac{m_i T}{2\pi}\right)^{3/2} e^{-m_i/T} \tag{1.55}$$

$$\rho_i(T) = g_i m_i \left(\frac{m_i T}{2\pi}\right)^{3/2} e^{-m_i/T} . \tag{1.56}$$

  When the temperature of the plasma evolves below the particle mass, the number density of the species drops exponentially, as massive particles and their anti-particles annihilate while the bath energy is no longer sufficient to compensate by the reverse process of pair production. The energy density is then proportional to the number density, and non-relativistic species behave like a pressureless gas. This is the dominant behavior of the cosmological fluid during the so-called matter-dominated era.

In some cases, it can be useful to derive an analytical solution for densities by considering the Maxwell-Boltzmann distribution function at equilibrium instead of BE or FD distribution. The classical approximation $e^{E/T} \gg 1$ leads to $f_i(T) \simeq g_i e^{-E/T}$ for both bosons and fermions, and to the following approximation for the number density

$$n_i(T) \simeq g_i \frac{m_i^2 T}{2\pi^2} K_2\left(\frac{m_i}{T}\right) . \tag{1.57}$$

where $K_2(x)$ is the modified Bessel function of the second kind. This expression is still valid at the order of 20% for $T \gg E$ [16]. We have treated the different species independently, asking them to follow the same distribution at equilibrium through their interactions between themselves. We can also compute the total energy density of the hot plasma composed of the different particles, some of them still being relativistic and some not. We saw that the energy density in non-relativistic species is Boltzmann suppressed, therefore it is sufficient only to consider relativistic species within the hot thermal bath. The total energy density is

$$\rho_R(T) = g_\rho(T) \frac{\pi^2}{30} T^4 \tag{1.58}$$

where we have to include in $g_\rho(T)$ all relativistic degrees of freedom which are in thermal equilibrium

$$g_\rho(T) = \sum_{i \in \text{bosons}} g_i \left(\frac{T_i}{T}\right)^4 + \left(\frac{7}{8}\right) \sum_{i \in \text{fermions}} g_i \left(\frac{T_i}{T}\right)^4 . \tag{1.59}$$

g_i are the internal degrees of freedom, while T_i is the temperature of the species i in equilibrium among themselves, which can differ after kinetic decoupling from the bath temperature T as we will see in the next part. We come back to the evolution of this effective number of degrees

of freedom in the radiation-dominated Universe after discussing the notion of decoupling of the species.

The primordial plasma is not exactly at equilibrium along the expansion, only a local equilibrium is maintained, and several out-of-equilibrium processes can explain the generation of relics and structures in our Universe today. However, when we can consider that the local equilibrium is maintained, the entropy of the Universe S is conserved, and cosmic expansion can be regarded as an approximate adiabatic process. From the notion of temperature at equilibrium, we can define the notion of entropy S of the Universe using the second principle of Thermodynamics. The following relation is satisfied between the thermodynamic quantities

$$TdS = dU + PdV - \mu dN \tag{1.60}$$

where U and N are respectively the total energy and total number of particles in the system, V the total volume, and P the pressure. We can derive [13] from this relation the following definition of the entropy density per species $s_i = S_i/V$,

$$s_i = \frac{\rho_i + P_i - \mu_i n_i}{T} \tag{1.61}$$

leading at thermal equilibrium (neglecting chemical potentials μ_i) to

$$s_i = g_{i,s}\frac{2\pi^2}{45}T^3\,. \tag{1.62}$$

The total entropy density s is computed from the sum of the contributions of the different relativistic species in thermal equilibrium

$$s = g_s(T)\frac{2\pi^2}{45}T^3 \tag{1.63}$$

where we defined entropy degrees of freedom

$$g_s(T) = \sum_{\text{bosons}} g_i \left(\frac{T_i}{T}\right)^3 + \left(\frac{7}{8}\right) \sum_{\text{fermions}} g_i \left(\frac{T_i}{T}\right)^3 . \tag{1.64}$$

Apart from the case where a species transfers entropy to particles of the thermal bath, all species have the same temperature $T_i = T$, and we have $g_s(T) = g_\rho(T)$. The cubic dependence in T comes from the definition of the entropy density as a function of the energy density and the entropy conservation condition leads to the following relation between T and the scale factor a

$$S = s \times a^3 \propto g_s(T)T^3a^3 = \text{cst} \implies a \propto \frac{1}{T}\,. \tag{1.65}$$

This crucial result allows us to trade time evolution for the evolution of temperature while a hot

plasma in thermal equilibrium dominates the Universe content. Throughout the expansion of the Universe, the equilibrium condition does not hold for all the species, and successive decouplings occur around the state of constant entropy. This means that the particles that decouple from the thermal bath while being non-relativistic transfer their entropy to the relativistic species that are still thermalized and with which they are coupled. Therefore, by looking at the effective numbers of degrees of freedom $g_\rho(T)$, $g_s(T)$ as a function of the temperature, we can follow the history of the successive decouplings by looking at the decreasing value of these numbers of degrees of freedom, and the corresponding increasing value of the thermal bath temperature through

$$g_s^{\text{after}} = g_s^{\text{before}} - g_i \implies T^{\text{after}} = T^{\text{before}} \left(\frac{g_s^{\text{after}}}{g_s^{\text{before}}} \right)^{1/3} \tag{1.66}$$

where we have assumed constant entropy and adiabatic process of decoupling ($g_s T^3 = \text{cst}$). Hence, at each decoupling of a species i, there is a drop in the effective degrees of freedom and a corresponding heating up of the thermal bath. After the decoupling, if the species is still relativistic (being massless or satisfying $m_i \ll T$), it is still having a thermal distribution but with a different temperature T_i unaffected by the entropy injection, evolving further as $T_i \propto \frac{1}{a}$. Hence two different temperatures T, T_i are coexisting and redshifting similarly, one is maintained by the equilibrium condition through interactions, while the other one is just originating from the decoupling of the species. Now that we have described the state of thermal equilibrium among relativistic species during the radiation-dominated era, we are interested in the mechanism of decoupling and how a species departs from its equilibrium with the bath. We will apply it to the generic case of light neutrinos of the SM, before discussing the different successive decoupling that occurred in the early Universe. This will naturally lead us to discuss the mechanism of BBN, recombination, and the emission of CMB photons.

1.2.2 Decoupling

The *chemical* decoupling of a species i in equilibrium with a thermal bath corresponds to the temperature at which the interactions rate $\Gamma(T) = n\langle\sigma v\rangle$ maintaining the chemical equilibrium of this species with particles of the bath become insufficient compared to expansion characterized by the Hubble rate $H(T)$. We have introduced the interaction rate $\Gamma(T)$ computed from the number density n of the particles interacting, v their relative velocity, and σ the associated interaction cross-section. The condition $\Gamma(T) \lesssim H(T)$ is a good approximation that allows determining quite accurately the time of decoupling, although a complete solution relies on solving the Boltzmann equation Eq.(1.34), for the distribution function f_i and through the computation of the collision term associated to number-changing interactions of this species with the bath particles. The chemical decoupling occurs when the number-changing annihilations (or decays) between the bath particles and the species i are no longer in equilibrium due

to the expansion. This can occur because the species is massive and becomes non-relativistic; its number density becomes Boltzmann suppressed as the bath particles do not have sufficiently high energies on average to produce pairs of the species i, and annihilation from the bath starts to be suppressed. Chemical decoupling is finally achieved when self-annihilations (or decays) of the species i are no longer relevant either as number density drops. After this time, no number-changing interactions can take place for the species i, which is "frozen out" of equilibrium. This mechanism of chemical decoupling can, on the other hand, occur while the particle is still relativistic due to a too-small rate of interaction below a certain temperature T, leading also to the decoupling of the species from particles within the bath.

It is important to note that after chemical decoupling, while the number of particles within the species i cannot be modified anymore, the species can still be in *kinetic* equilibrium through scattering processes with relativistic particles in the thermal bath. Indeed, the number density of the relativistic particles in the bath is not suppressed and drops as T^3, so it can maintain a sufficient level to keep the species i in kinetic equilibrium via elastic scattering $\Gamma_{\rm el}(T) \simeq n_{\rm eq}\langle\sigma_{\rm el}\rangle \gtrsim H(T)$. During radiation dominated era, the Friedmann equation Eq.(1.24) indicates that

$$H(T)^2 \sim \frac{T^4}{M_P^2}\,. \tag{1.67}$$

Hence, as the temperature drops, even the elastic scatterings become inefficient $\Gamma_{\rm el}(T) \ll H(T)$ and the species i departs from its kinetic equilibrium. At that time, no process transfers momentum from the bath to the particles of the species i, which is completely frozen. These particles start to propagate freely and their distribution function is keeping the form it had at the moment of the kinetic decoupling[4], energy and momentum of the particles just redshifting afterward. More specifically, when a particle decouples while being relativistic at a temperature $T \gg m_i$, then the distribution function keeps the form

$$f_i(p,t) = \frac{1}{e^{E/T_i} \pm 1} \tag{1.68}$$

with $T_i = T_{\rm dec}\left(\frac{a(t_{\rm dec})}{a(t)}\right)$, the temperature associated to the relativistic species i at a cosmic time t, $T_{\rm dec}$ the temperature at decoupling time. After this decoupling, the number density $n_i(T_i) \propto T_i^3$ as for the equilibrium case, even if $T_i < m_i$. If the decoupling occurs while the particle is non-relativistic i.e $T_{\rm dec} \lesssim m_i$, the distribution function after freeze-out is given by

$$f_i(p,t) = e^{-m_i/T_{\rm dec}} e^{-p^2/2m_iT_i} \tag{1.69}$$

with $T_i = T_{\rm dec}\left(\frac{a(t_{\rm dec})}{a(t)}\right)^2$. So, during the radiation-dominated era, the temperature associated with a decoupled sector which is non-relativistic falls as $T_i \propto a^{-2}$ and not as a^{-1}.

[4]This holds as long as the species i is not coupled to another bath or population of particles that can transfer efficiently momentum.

Neutrino Decoupling

We discuss further in section 1.4 the generation of a cold relic of Weakly Interacting Massive DM particles (WIMPs) from this mechanism of thermal decoupling and freeze-out. But before, we describe an important event occurring in the early Universe, the decoupling of the SM neutrinos from the photon bath. Neutrinos are the only particles of the SM that interact solely through the weak interaction (see appendix A for an overview of the SM of Particle Physics). Due to the weakness of this interaction with the other SM particles, their interaction rates $\Gamma_\nu(T)$ from the scatterings $e\nu \leftrightarrow e\nu$ and annihilation[5] $\nu\nu \leftrightarrow ee$, become smaller than the Hubble rate $H(T)$ at a quite high temperature. We can compute the typical interaction rate between neutrinos and other SM particles from the Fermi theory [16]

$$\sigma \sim (G_F T)^2 \implies \Gamma_\nu = n_\nu \langle \sigma \rangle \sim G_F^2 T^5 \tag{1.70}$$

where $G_F \simeq 10^{-5}$ GeV^{-2} is the Fermi constant, and the rate decreases much more rapidly than $H(T) \propto T^2$. Using the condition $\Gamma_\nu \lesssim H(T)$, we obtain an approximate decoupling temperature of $T_{\rm dec} \sim 1$ MeV, below which neutrinos do not interact anymore with the SM plasma. However, at this temperature neutrinos are still largely relativistic $m_\nu \ll T_{\rm dec} \sim 1$ MeV (see the next section 1.3 where we discuss the SM neutrino mass). After their decoupling, they keep their FD distribution function with a temperature T_ν only affected by the redshift. Even after decoupling $T_\nu = T_\gamma = T$ and neutrinos still participate in the effective relativistic degrees of freedom of the Universe with the same temperature as the photon bath. Shortly after their decoupling, when the temperature of the photon bath drops below $T_\gamma \lesssim m_e = 0.511$ keV, there is not enough energy to efficiently produce electron-positron pairs. Electrons and positrons start to chemically decouple from the bath while becoming non-relativistic and transfer their entropy only to the photons through their annihilation $ee \to \gamma\gamma$ via electromagnetic interactions. In doing so, they reheat partly the photon bath but not the neutrino background as the weak interactions branching ratio $ee \to \nu\nu$ is, in comparison, very suppressed. This has the effect of increasing the photon bath T_γ compared to the neutrino background temperature T_ν, as can be computed from entropy conservation at decoupling

$$\begin{aligned} g_s^\gamma(T > m_e)T^3 &= g_s^\gamma(T_\gamma < m_e)T_\gamma^3 \\ g_s^\nu(T > m_e)T^3 &= g_s^\nu(T_\gamma < m_e)T_\nu^3 \end{aligned} \tag{1.71}$$

[5] Similar processes occur with quarks which around the energy $T \sim 1$ MeV are bounded into protons.

where the effective number of degrees of freedom evaluated at $T > m_e$ and $T_\gamma < m_e$ are given by

$$g_s^\gamma(T > m_e) = \frac{11}{2}, \quad g_s^\nu(T > m_e) = \frac{21}{4}$$
$$g_s^\gamma(T_\gamma < m_e) = 2, \quad g_s^\nu(T_\gamma < m_e) = \frac{21}{4}\,. \tag{1.72}$$

This results after e^+e^- annihilation in a different temperature T_γ and T_ν, respectively in the photon bath and neutrino background, related by the entropy injection of the electrons-positrons in the bath

$$T_\gamma = \left(\frac{11}{4}\right)^{1/3} T_\nu\,. \tag{1.73}$$

Given that the temperature of the CMB as observed today is $T_\gamma^0 \simeq 2.725\ K$, the mechanism of decoupling predicts a neutrino background with a FD distribution[6] at an effective temperature $T_\nu^0 = 1.95\ K$. Nowadays, as neutrinos are massive, they become non-relativistic and their average energy is given by $\langle E\rangle \simeq m_\nu$ while their kinetic energy $\frac{p^2}{2m_\nu}$ is negligible. They constitute a population of background neutrinos with an energy density $\rho_\nu^0 = m_\nu n_\nu^0$, with n_ν^0 computed from the FD distribution function replacing $E \to m_\nu$. This represents a relic density [16]

$$\Omega_\nu^0 h^2 \simeq \frac{m_\nu}{93\ \text{eV}}\,. \tag{1.74}$$

As these non-relativistic neutrinos are part of the matter abundance today, they should not contribute more than $\Omega_m^0 \simeq 0.3$ as obtained within the ΛCDM model. This provides an important upper-bound on the sum of the SM neutrino masses from cosmological origin as first highlighted in [23] by Cowsik and McClelland

$$\sum_\nu m_\nu \lesssim 13.8\ \text{eV} \tag{1.75}$$

where the sum is over the neutrino family within the SM (see appendix A). Due to neutrino-free streaming after their decoupling while being relativistic, they have a strong impact on structure formation in the Universe and the associated matter power spectrum at small scales [24]. CMB data associated with Baryon Acoustic Oscillations (BAO) and Large Scale Structure (LSS) measurements produce very strong upper bounds of the level $\sum_\nu m_\nu \lesssim 0.1$ eV. On the other hand, hot fermionic DM with thermal distribution cannot be too light in order to virialize in gravitating bound systems such as galaxies and dwarf galaxies, due to Pauli exclusion statistics.

[6] As neutrinos are decoupled while being relativistic, exhibiting a FD thermal distribution, this distribution is frozen at the decoupling time and the occupation number is only diluted or redshifted by the expansion, keeping the same shape. This does not mean that neutrinos are in thermal equilibrium among themselves at this temperature.

This provides famous lower limits on neutrino as a DM candidate

$$m_\nu \gtrsim 10 \text{ eV} - 0.1 \text{ keV} \tag{1.76}$$

derived by Tremaine and Gunn [25], which appears to be in contradiction with upper limits on the sum of neutrino masses. These are the main reasons why hot thermal DM such as neutrino is not a viable explanation for the entire DM abundance in our Universe.

Before moving to BBN, we show in Figure 1.7 the evolution of the effective relativistic degrees of freedom as a function of the temperature of the photon thermal bath. At high temperature, well above the electroweak symmetry breaking scale $v_{\text{EW}} \sim 200$ GeV, the SM particles are massless, and the effective number of relativistic degrees of freedom $g_\rho(T) = g_s(T)$ is given by

$$g_\rho^{\text{SM}} = \frac{7}{8}(N_f \times 2) + N_V \times 2 + N_S = \frac{427}{4} = 106.75 \tag{1.77}$$

where $N_f = 45$ is the number of fermionic species (leptons and colored quarks), $N_V = 12$ the number of massless vectors gauged bosons, $N_S = 4$ the number of scalars (Higgs complex $SU(2)$ doublet scalar). $g_\rho(T), g_s(T)$ decrease after the temperature drops below v_{EW} due to the fact

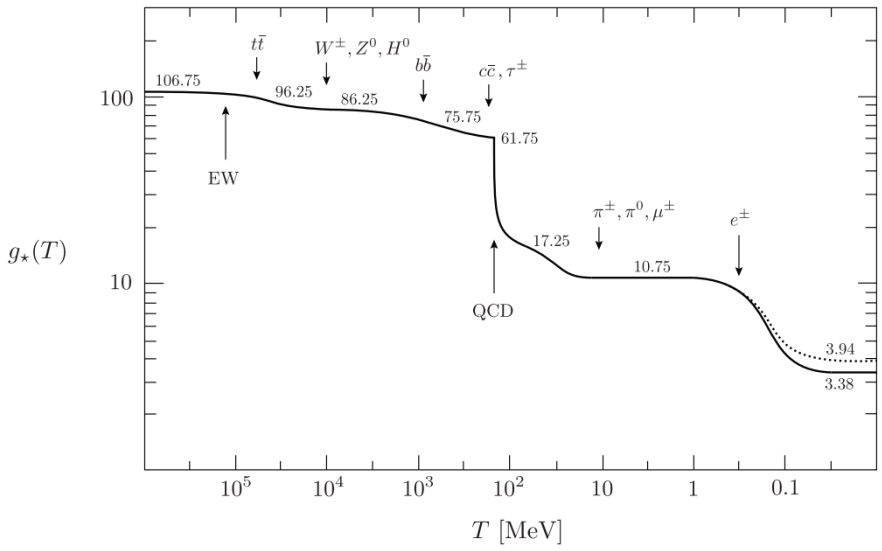

Figure 1.7: *Evolution of relativistic degrees of freedom $g_\rho(T), g_s(T)$ for the Standard Model. The dotted line corresponds to the number of effective degrees of freedom in entropy $g_s(T)$. Figure taken from [26].*

that electroweak masses are generated in the SM through the Brout-Englert-Higgs mechanism (see Appendix A for a description of this mechanism). The Higgs bosons and the top quark are then rapidly Boltzmann suppressed when the temperature becomes smaller than their mass, then it is the turn of bottom quark decoupling, and τ lepton decoupling. Around $T \sim 200$ MeV, $g_\rho(T), g_s(T)$ are importantly suppressed by the QCD phase transition and the hadronization of quarks and gluons through the confinement. Below this temperature, there are composite

states (baryons and mesons) and all the color degrees of freedom are inaccessible. Baryons rapidly become non-relativistic and their density Boltzmann suppressed. A last event occurs around $T \lesssim 1MeV$, as we saw through the electron-positrons annihilation and, at the same time, neutrino decoupling while being relativistic leading soon to a $g_s(T) \neq g_\rho(T)$. Nowadays, at $T = T_\gamma^0$ we can compute that $g_\rho^0 = 3.39$.

1.2.3 Big Bang Nucleosynthesis

We have discussed the decoupling of the neutrinos from the thermal bath which determines their abundance today, and the associated effective temperature of this neutrino background from cosmological origin. In this part, we describe another important event taking place in the early Universe which is the decoupling of baryons from the thermal bath. The case of baryons is much more involved as they are QCD-bound states of quarks and gluons, thus not fundamental particles. The hadronization process itself is still very blurry and the associated QCD phase transition in the early times of the Universe evolution is a very deep subject of active research. However, BBN stands out as one of the most reliable windows into the early Universe, supported by SM Physics. By forecasting the generation and abundance of light elements from Deuterium (D), Helium-3 (^{3}He), Helium-4 (^{4}He), to Lithium-7 (^{7}Li), formed within the initial three minutes, BBN offers a critical test for the standard model of Cosmology and is corroborated by observational data at a very high level of precision. It relies mainly on reactions of light elements and their weak decays which are well understood at this typical energy scale $T \lesssim 1$ MeV. Thus, it is well known that small modifications of the early Universe Physics beyond the SM (BSM), at the time of BBN, should lead to observable deviations in primordial abundances of light elements, putting strong constraints on new Physics scenarios. The onset of BBN took place in the era associated with photon temperatures between $T \simeq$ MeV and $T \simeq$ 10keV. It is the transition from a neutron-proton equilibrium to a Universe with a significant presence of He. BBN produced the main part of the ^{4}He and D present in the Universe, as well as fractions of ^{3}He and ^{7}Li.

The successful BBN mechanism relies on simple ingredients. It is assumed that the particle content at the time of BBN is given by the SM particle spectrum and that QCD phase transitions occurred at a much higher energy scale (confinement of quarks in hadrons). The second important ingredient is that a net baryon asymmetry was already present at the time of BBN and is of the order

$$\frac{n_b - n_{\bar{b}}}{s} \simeq 10^{-10} \,. \tag{1.78}$$

Hence, BBN must have been preceded by a mechanism capable of producing the baryon anti-baryon asymmetry of the Universe, preserved until anti-baryons annihilates with baryons around $T \simeq 1$ MeV injecting entropy in the thermal photon bath. We will discuss the so-called baryogenesis and leptogenesis processes in the next section 1.3. Such mechanisms should pro-

vide a ratio between baryons and photons density η_B which stays frozen out of equilibrium until today

$$\eta_b \equiv \frac{n_b}{n_\gamma}(T < 1 \text{ MeV}) = \frac{n_b^0}{n_\gamma^0} \simeq 6 \times 10^{-10} \tag{1.79}$$

as observed in concordance with BBN in CMB data. As the temperature of the bath is initially well above the mass difference between neutrons and protons $T > \Delta m \equiv m_n - m_p \simeq 1.29$ MeV, and as the neutron lifetime $\tau_n \simeq 886$ s, an almost equal amount of neutrons and protons are in equilibrium at the onset of BBN

$$n_n \simeq n_p(T \gg \Delta m) \simeq \frac{1}{2} n_b \,. \tag{1.80}$$

At a lower temperature, the relative abundance is suppressed by

$$\frac{n_n}{n_p} \sim e^{-\frac{\Delta m}{T}} e^{-\frac{t}{\tau_n}} \tag{1.81}$$

therefore, at the time of baryon freeze-out, the energy density of the Universe is completely dominated by photons, neutrinos, electrons, and positrons. Neutrons and protons represent a negligible fraction of the total energy density. After this decoupling, the number of baryons (anti-baryons) changing interactions are no longer in equilibrium, and successive processes within the baryon sector will allow them to bind together, forming the light elements that will stay out of equilibrium until today.

First, to obtain approximately the abundance of He, we are interested in the freeze-out of the following weak interactions

$$n + \nu \leftrightarrow p + e^- \tag{1.82}$$

which are in thermal equilibrium above $T \gtrsim 1$ MeV, as long as $\Gamma_p(T) = n_\nu \langle \sigma v \rangle \gtrsim H(T)$. This typical weak interaction rate scales as $\Gamma_p(T) \sim G_F^2 T^5$ and we remind that during radiation dominated era, $H(T) = T^2 \left(\frac{g_\rho \pi^2}{90 M_P^2} \right)^{1/2}$. As the Universe cools down, these interaction rates drop below the Hubble rate, and neutron-to-proton transitions slow down. The ratio of their abundance is not anymore in chemical equilibrium and around $T \simeq 0.7$ MeV this relative abundance is frozen-out to $\frac{n_n}{n_p} \simeq e^{-\frac{\Delta m}{T}} \simeq \frac{1}{6}$ [27, 28]. It can be shown that it continues to decrease due to residual interactions and neutron decays down to

$$\left(\frac{n_n}{n_p} \right)_{\text{fo}} \simeq \frac{1}{7} \,. \tag{1.83}$$

at complete freeze-out. The formation of D during this freeze-out of protons and neutrons is prevented by the large density of high-energy photons and the photo-dissociation process that destroys efficiently any bound D, even if the binding energy of Deuterium is quite high $E_D = 2.22$ MeV. Once the temperature drops much below this binding energy, the Boltzmann

suppression of such photons with high energy allows to form an important fraction of D through the nuclear reaction

$$n + p \leftrightarrow D + \gamma \,. \tag{1.84}$$

The resulting Deuterium relative abundance can be expressed as [16]

$$\frac{n_D}{n_p} \sim n_n (m_p T)^{-3/2} e^{E_D/T} \implies \frac{n_D}{n_b} \propto \eta_b \left(\frac{T}{m_p}\right)^{3/2} e^{E_D/T} \tag{1.85}$$

and from the fact that $\eta_b \simeq 10^{-10}$ and $m_p \simeq 1$ GeV, we see that the temperature at which Deuterium is efficiently produced is smaller than $T < 1$ MeV. We can approximately compute that D production occurred when $T \simeq E_D/20$. This also shows that the BBN production process of D production is very sensitive to the baryon to photon ratio η_b, this being a complementary probe of this ratio with CMB observations. We discussed this in the first section of the manuscript, and we showed this agreement between BBN measurements and CMB observations in Fig 1.2. Once this large enough D density is produced, it can initiate other nuclear reactions, in particular neutrons are binding mainly into ^{4}He nuclei that have the highest binding energy per nucleon among light elements [7]. Thus, we obtain quite accurately that the ^{4}He mass fraction in comparison with the total baryon mass is given by [16]

$$Y_p \simeq \frac{4}{2+14} = \frac{1}{4} \,, \tag{1.86}$$

which is the main prediction of the BBN mechanism. This computation is an important achievement of modern Cosmology as it is exactly what is also inferred from various observational probes such as measurements of the interstellar medium composition, as well as the Solar System abundances in the proto-stellar matter, or study of the Lyman-α forest in the spectrum of distant quasars. A more rigorous treatment of the freeze-out and nucleosynthesis mechanism can be obtained by solving numerically the full sets of Boltzmann equations obtained from Eq.(1.34) assuming initial thermal equilibrium of neutrons and protons, for a vanishing initial abundance of the other light elements. In the standard BBN scenario (SBBN), the sets of equations to solve are the following ones

$$\frac{dY_i}{dt} = -H(T) T \frac{dY_i}{dT} = \sum \left(\Gamma_{ij} Y_j + \Gamma_{jkl} Y_k Y_l + ...\right) \tag{1.87}$$

where $Y_i = n_i/s$ are the yields of each element at the time BBN starts. This equation is obtained using $H \equiv \frac{\dot{a}}{a}$ and entropy conservation $T \propto \frac{1}{a} \implies \frac{d}{dt} = -HT\frac{d}{dT}$, as well as calculating the average generalized rates for element interconversion and decay from the right-hand side (collision term) of the Boltzmann equation, associated with the transition amplitude of each process. Many research groups have solved these sets of equations and recent results

[7] A fraction of D remains and a similar fraction of ^{3}He is produced during the process.

[28, 29] are displayed below. These numerical predictions remarkably match the observations

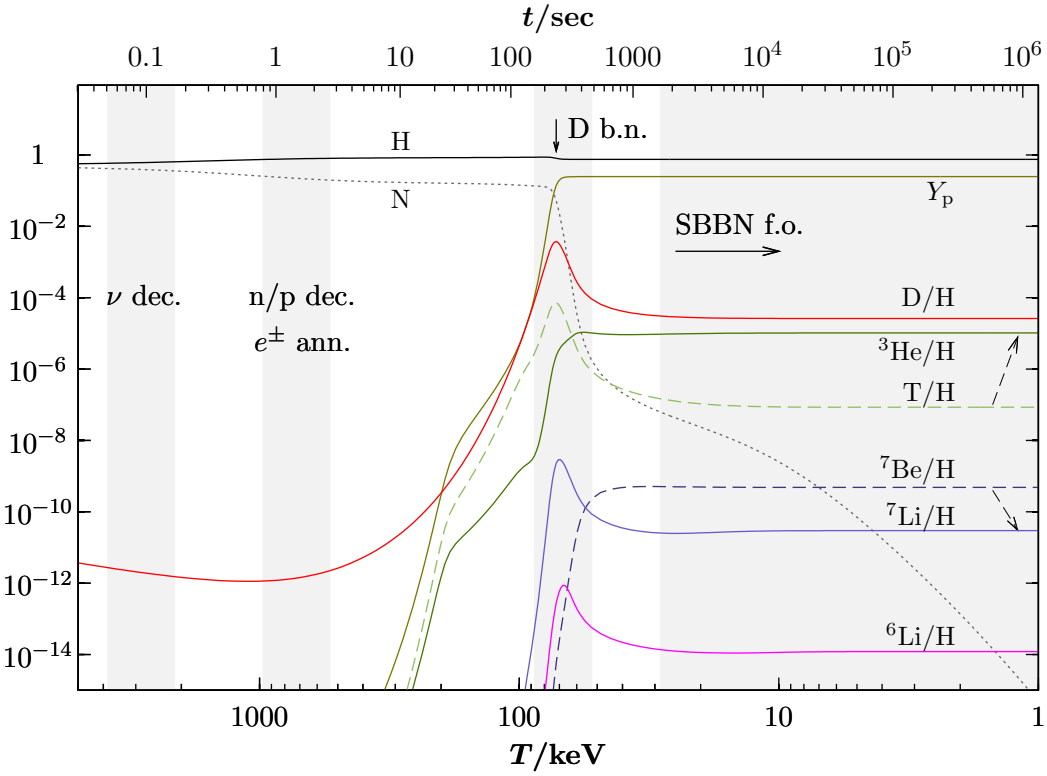

Figure 1.8: *Time and temperature evolution of SBBN light elements abundances. From left to right: neutrino decoupling, electron-positron annihilation, n/p freeze-out,* D *bottleneck, and freeze-out of all nuclear reactions. Protons (H) and neutrons (N) are given relative to* n_b *whereas* Y_p *denotes the* ^{4}He *mass fraction. Figure taken from [28].*

except for the only disagreement in the ^{7}Li abundance, known as the Lithium problem, which is an ongoing active research question.

1.2.4 Dark Radiation

In many extensions of the SM, the existence of additional degrees of freedom in the form of new particles can contribute to a significant modification of the evolution of the effective number of degrees of freedom in the early Universe. Indeed, the radiation content can be expressed in terms of the effective number of relativistic species at a temperature T associated with the temperature of the bath as we introduced in Eqs.(1.58) and (1.59). At the time of BBN the remaining relativistic degrees of freedom in thermal equilibrium in the hot bath are described by the radiation energy density

$$\rho_R = \rho_\gamma + \rho_e + \rho_\nu = \frac{\pi^2}{30}\left(2 + 2\times\frac{7}{4} + N_\nu \times \frac{7}{4}\right) T^4 \tag{1.88}$$

where N_ν is the total number of neutrino flavors (that is 3 within the SM see Appendix A). This has been measured in accelerators to high precision and agrees with SM predictions of $N_\nu = 3$. In the SM, the effective number of neutrino species $N_{\rm eff} = 3.044$ [30] refers to the effective number of thermally excited neutrino species. The difference with $N_\nu = 3$ comes from the heating of neutrinos from small branching fraction $e^+e^- \to \nu\nu$ at electron-positron annihilation and we define $N_{\rm eff}$ though its contribution to the total radiation density

$$\rho_R = \left[1 + N_{\rm eff}\left(\frac{7}{8}\right)\left(\frac{T_\nu}{T_\gamma}\right)^4\right]\rho_\gamma \tag{1.89}$$

which reduces after e^+e^- annihilation to

$$\rho_R = \left[1 + N_{\rm eff}\left(\frac{7}{8}\right)\left(\frac{4}{11}\right)^{4/3}\right]\rho_\gamma\,. \tag{1.90}$$

We can define the associated ΔN_ν via

$$\Delta N_\nu = N_{\rm eff} - N_\nu = N_{\rm eff} - 3 = 0.044\,. \tag{1.91}$$

where the last equality is valid within SM. The presence of any additional relativistic BSM degree of freedom would contribute to the total radiation energy, and its impact can be absorbed in terms of the equivalent number $N_{\rm eff}$ and so ΔN_ν, which can then depart from its SM value. A new relativistic species X will contribute to energy density with an associated effective temperature in this sector T_X,

$$\rho_X(T) = g_X\frac{\pi^2}{30}T_X^4 \tag{1.92}$$

with g_X the number of internal degrees of freedom in the species X. We can relate the density in the new radiation sector, usually called dark radiation as it is not observed yet, to an effective contribution to $N_{\rm eff}$

$$\rho_R = \rho_\gamma + \rho_\nu + \rho_X = \left[1 + N_{\rm eff}\left(\frac{7}{8}\right)\left(\frac{4}{11}\right)^{4/3}\right]\rho_\gamma \tag{1.93}$$

and an associated ΔN_ν^X due to the contribution of X

$$\Delta N_\nu^X = N_{\rm eff} - N_\nu = \frac{4}{7}g_X\left(\frac{11}{4}\right)^{4/3}\left(\frac{T_X}{T_\gamma}\right)^4\,. \tag{1.94}$$

We can notice that for any free streaming relativistic species $\rho_X \propto a^{-4}$, and during radiation-dominated era $\rho_\gamma \propto T^4 \propto a^{-4}$, showing that we can use this contribution to $N_{\rm eff}$ and ΔN_ν for any additional relativistic degrees of freedom around the time of BBN, even if it is not in thermal equilibrium within the new sector. Especially for primordial gravitational radiation

in the form of primordial gravitational waves (GW), we can use this parametrization of this additional contribution to ρ_R as a free streaming dark radiation, to put constraints on the relic density of these primordial GW. Recent Planck measurements of the CMB have become a probe of $N_{\rm eff}$ at the epoch of recombination (see 1.2.5). Planck constraints [15] give at 95% confidence level, $N_{\rm eff} = 2.99 \pm 0.34$. With BAO data included, the measurement becomes more stringent with $N_{\rm eff} = 2.99 \pm 0.17$. Besides, any change in the effective number of relativistic degrees of freedom affects $H(T)$. Hence, an increase in $N_{\rm eff}$ will lead to a larger value for the ^{4}He mass fraction Y_p through the BBN mechanism [31], and so, any BSM Physics (or new cosmological parameters) that affect $H(T)$ alters the light element abundances from BBN. Combining BBN analysis with CMB data, allowing for a variation of $N_{\rm eff}$ as performed in [31], it provides the current best constraint

$$N_{\rm eff} = 2.898 \pm 0.141 \tag{1.95}$$

which in turn provides an upper limit on the additional energy density in the form of dark radiation relic density

$$\Omega_X^0 h^2 \lesssim 1.3 \times 10^{-6}\,. \tag{1.96}$$

As discussed above, a specific example of BSM Physics probed by such measurements of $N_{\rm eff}$ is the generation of GW background, which is a prediction of generic inflation models. After inflation, other processes such as phase transitions or the further evolution of the Hubble expansion during reheating and preheating can source stochastic GW backgrounds or modify the primordial spectrum, as we will discuss in Chapter 3 on gravitational reheating. In all these cases, GW energy density acts as free-streaming dark radiation and thus its impact on BBN and CMB is captured by $N_{\rm eff}$. The limit on GW relic density today from the analysis of its impact on ΔN_ν is given by [31]

$$\Omega_{\rm GW}^0 h^2 \lesssim 1.3 \times 10^{-6} \tag{1.97}$$

for a specific range of frequency of the GW $f \gtrsim 2 \times 10^{-11}$ Hz, as the constraint applies to frequencies above $f > f_{\rm BBN}$ where $f_{\rm BBN}$ is associated to the Hubble scale at BBN time. Indeed, such a constraint applies only to tensor modes with a wavelength smaller than the horizon at the start of BBN.

1.2.5 Recombination and the last scattering surface

At the end of the BBN process, the thermal bath is populated with photons, electrons, and protons in interaction (as well as a smaller fraction of Helium nuclei and traces of the other light elements produced). Neutrinos have already decoupled and the number density of electrons and protons are Boltzmann suppressed as $T \ll m_e, m_p$, while they are still tightly coupled together through Coulomb scatterings $p + e^- \leftrightarrow p + e^-$. After quite a long evolution until $z \sim 1100$ or $t \simeq 380\ 000$ years, the thermal bath (which is not anymore the dominant component of the

Universe since matter equality at $z_{\rm eq} \sim 3000$), attained a temperature of $T \sim 1$ eV. Around this stage the reaction which was in equilibrium

$$p + e^- \leftrightarrow H + \gamma \tag{1.98}$$

starts to become suppressed on one side as the photons do not have enough energy to destroy stable Hydrogen atoms (H) by ionization of the electrons bound to the protons. The binding energy of the neutral Hydrogen atom is $E_H = 13.6$ eV and so it forms naturally from electrons and protons which are in the same abundance (neutrality condition for the Universe $n_e = n_p$) when $T \lesssim E_H$. The number of free electrons and protons starts to become exponentially suppressed and the plasma recombines into neutral Hydrogen gas and photons. To be more precise, before this time the free electron fraction

$$X_e \equiv \frac{n_e}{n_e + n_H} = \frac{n_p}{n_p + n_H} \tag{1.99}$$

follows the Saha equation [14, 16]

$$\frac{X_e^2}{1 - X_e} = \frac{1}{n_e + n_H} \left[\left(\frac{m_e T}{2\pi} \right)^{3/2} e^{E_H/T} \right] \tag{1.100}$$

leading to an exponential increase of the H population around $T \lesssim E_H$. From this simple equation, we can quite accurately compute the recombination time or temperature at which $X_e(T) \lesssim 0.1$, to be $T_{\rm rec} \simeq 0.3$ eV, which is far below the binding energy of the Hydrogen E_H. After the formation of the first neutral atoms begins[8], the mean free path of photons in the bath increases as there are fewer electrons and protons ionized in the plasma on which they can interact[9] through Compton scatterings $\gamma + e^- \leftrightarrow \gamma + e^-$. To accurately predict the decoupling time of the photons associated with their last scattering on the plasma before they free stream, a very accurate treatment of the e^- fraction X_e should be done. There are subtle effects during recombination as the electrons go out of equilibrium, which requires refinement of the Saha equation and a full numerical treatment of the Boltzmann equation for electrons number density [14] in order to predict the decoupling of electrons correctly. The equation to solve is the following

$$\frac{dX_e}{dt} = (1 - X_e) \langle \sigma_T v \rangle \left(\frac{m_e T}{2\pi} \right)^{3/2} e^{-E_H/T} - X_e^2 n_b(T) \langle \sigma^{(c)} v \rangle \tag{1.101}$$

[8] In fact, the binding energy of Helium is higher than the one of Hydrogen, meaning that the fraction of Helium produced through BBN ($\sim 25\%$ in mass) recombines before Hydrogen, increasing the mean free path of photons even before what is naively expected.

[9] Compton scatterings or Thomson scatterings in the low energy limit are more important for electrons than for protons, as the cross-section scales as $\sigma \propto 1/m_i^2$.

where the first term stands for the ionization rate through Compton (Thomson) scatterings, while the second term corresponds to the capture of an electron by a proton to form one excited state of the Hydrogen atom, which further relaxed to its ground state by emitting a photon of energy $E_\gamma < E_H$. However, we can still estimate roughly when the decoupling of photons with electrons occurs by asking

$$n_e(t)\sigma_T \simeq X_e(t) n_b(t)\sigma_T \lesssim H(t) \tag{1.102}$$

where $\sigma_T \simeq 6.65 \times 10^{-25}$ cm^2 is the Thomson cross section of photons on electrons. From the evolution of the Hubble rate, starting in radiation domination, to matter domination (see Eq.(1.46)), we obtain that [14]

$$\frac{n_e\sigma_T}{H}(z) = 123\ X_e \left(\frac{\Omega_b^0 h^2}{0.022}\right)\left(\frac{0.14}{\Omega_m^0 h^2}\right)^{1/2}\left(\frac{1+z}{1000}\right)^{3/2}\left[1+\frac{1+z}{1+z_{\rm eq}}\frac{0.14}{\Omega_m^0 h^2}\right]^{-1/2}. \tag{1.103}$$

This shows that the decoupling of the photons corresponding to the last scattering events occurs when $z \sim 1000$ and when $X_e \lesssim 10^{-2}$. Numerical solutions of $X_e(t)$ show that decoupling of photons occurs while the electrons recombine into neutral Hydrogen, close to $T_{\rm dec} \simeq T_{\rm rec} \simeq 0.2 - 0.3$ eV, hence the process of decoupling is quite fast as recombination begins. After this time, which is called the last scattering surface, primordial photons are no longer interacting and are completely decoupled while being relativistic (they are massless). They start free streaming in all directions keeping the same BE equilibrium distribution function at a temperature $T_{\rm dec}$. As the Universe expands and photons propagate, the temperature of this background radiation cools down to $T_0 \simeq 2.725\ K$, with still a near-perfect BE distribution. They form the CMB radiation as observed by our telescopes. The Hydrogen gas cools down and continues to dilute, except close to overdensity regions of DM and baryons, where the gravitational potential wells lead to the growth of structure. Much later at $z \sim 10$, these overdense regions reheat again due to high density, and future stars allow for re-ionization of the gas, as the Compton scatterings are possible again in these dense regions.

Now that we have introduced the main steps in the evolution of the hot thermal bath made of SM particles, from BBN to CMB emission, we are moving to different aspects of relic density generation, first of baryons that we saw are necessary to explain BBN and CMB measurements, and then of a cold DM component.

1.3 Baryo-Leptogenesis

1.3.1 Evidence for a Baryon Asymmetry

There are several pieces of evidence that our Universe is baryon-antibaryons asymmetric. Cosmic ray detection from galactic and extra-galactic origin indicates that the level of antimatter (mainly anti-protons and positrons) flux compared to the one of the matter is compatible with

the fact that these antimatter cosmic rays are generated from secondary processes taking place at high energy in the galaxies and intergalactic medium, and not originating from primordial origin. Indeed, the observations of cosmic rays provide a significant upper limit $\frac{n_{\bar{b}}}{n_n} \simeq 10^{-4}$ to the antimatter content in cosmic rays [32]. On larger scales, if both matter and anti-matter galaxies exist in the same local clusters, telescopes should be able to detect large amounts of γ-rays photons and pions produced by the annihilation of matter and antimatter. There is no evidence of such a high flux of γ-rays or pions (decaying into lighter particles in flights) in the nearby clusters that contain more than $10^{13} M_\odot$[10], meaning that they are mainly composed of either only baryons or antibaryons. Thus, if anti-matter exists together with matter, it should be highly separated on large scales corresponding to galaxy clusters of masses $M > 10^{13} M_\odot$. This seems to indicate that all visible structures on astrophysical scales, such as stars, and cosmological scales, such as galaxies and clusters, are composed exclusively of matter (baryons and electrons), with negligible amounts of antimatter (antibaryons and positrons) produced by rare events.

However, the main probes of this asymmetry come from the measurement of the light nuclei abundances together with CMB, which highlights the agreement between the hypothesis of BBN and early Universe Cosmology. The precise value of the baryon asymmetry of the Universe is obtained through observations from two independent probes. The first one is via BBN, as discussed in the precedent part, which predicts precisely the abundance of the light elements, D, ^{3}He, ^{4}He, and ^{7}Li. These predictions depend importantly on the baryon to photon ratio η_b, and more specifically, the abundances of D and ^{3}He are very sensitive to this parameter. The primordial abundances of these light elements can be inferred from various observations and give a constraint on η_b, which can accommodate all the relic abundances of these different elements consistently. This in turn provides an accurate estimation of the relic abundance of baryons through

$$\eta_b = 2.74 \times 10^{-8}\ \Omega_b h^2\,. \tag{1.104}$$

The second way to determine Ω_b is from measurements of the CMB anisotropies (see section 1.5). At recombination, when the temperature is sufficiently low for protons and electrons to form neutral H, the cosmological plasma can be described as a photon-baryon fluid in electromagnetic interactions. In the temperature anisotropy power spectrum of the CMB, there are peaks whose spacing and location in Fourier scales are representative of the dynamics of the plasma at the time of photons decoupling. The physical effect of the baryons is to provide an additional density and gravitational pull, which enhances the collapse into potential wells. This translates into an enhancement of the odd peaks in the spectrum known as BAO (see section 1.5). Precise measurement of the location and heights of the peaks constrains the baryon energy density ρ_B at the time of decoupling. In the end, there is an impressive consistency between BBN and CMB estimations depicted in Figure 1.2 of the first section of this manuscript. The most recent

[10] $M_\odot = 1.98 \times 10^{30}$ kg represents one solar mass

of these measurements from PLANCK Collaboration provides the following results for baryon density and asymmetry [15]

$$Y_B = \frac{n_b - n_{\bar{b}}}{s} = (8.72 \pm 0.08) \times 10^{-11}, \qquad \Omega_b h^2 = 0.0224 \pm 0.0001\,. \tag{1.105}$$

These indicate that there must be an asymmetry between SM baryons and SM antibaryons[11] in favor of an asymmetry that should have been generated before BBN and recombination to obtain $\eta_b \simeq 6 \times 10^{-10}$. Given that initial conditions of the Big Bang scenario suggest an equal abundance of baryons and antibaryons from thermal equilibrium at high temperature, the observed baryon asymmetry implies the existence of a dynamical process allowing to depart from this equilibrium between baryons and antibaryons, known as baryogenesis. One might question why we require the baryon asymmetry to be dynamically generated rather than granted by a specific initial condition. Firstly, if the baryon asymmetry were an initial condition, it would necessitate extraordinarily precise fine-tuning to generate such a small value for $\eta_b \simeq 6 \times 10^{-10}$ after decoupling of baryons and annihilation of matter with anti-matter, a level of precision that appears highly improbable. Secondly, many observations support the occurrence of inflation, which would have exponentially diluted any primordial baryon asymmetry rendering this possibility impossible.

Thus, the phenomenon of baryogenesis remains a crucial point in understanding the early Universe composition and evolution and is deeply connected to any attempt to extend the SM of Particle Physics. In the following, we discuss the ingredients of baryogenesis and some of the main scenarios proposed to explain the origin of baryon asymmetry. We specifically look more carefully at the mechanism of leptogenesis which is closely related to neutrino Physics and their mass generation through the Seesaw mechanism. We focus on the framework of non-thermal leptogenesis after inflation which will be used in the third chapter of the manuscript about gravitational leptogenesis during reheating (chapter 3).

1.3.2 Required ingredients

The ingredients required to generate dynamically a baryon asymmetry were originally given by Sakharov in [34] and can be summarized as the following conditions

- *Baryon number violation* is required to generate a net nonzero baryon number (B) starting from a symmetric Universe. In fact, B is conserved at low energy scales within SM but it is not conserved by some processes of the SM at high energy, the so-called sphalerons

[11] We note that we only have evidence of an asymmetry between SM quarks and SM anti-quarks making up SM baryons. However, it may be possible that a dark sector contains also species carrying baryon numbers with portal interactions between the dark sector and the quarks. This allows our Universe to be baryon symmetric and is explored in a recent paper [33].

processes [35, 36]. This anomalous violation in the weak sector of the SM leads to processes that involve 9 left-handed quarks and 3 left-handed leptons. Thus B and lepton number (L) changing processes respecting the condition

$$\Delta B = \Delta L = \pm 3 \tag{1.106}$$

can occur within the SM at high temperatures. We come back to these sphalerons later on.

- *C and CP violation* is required as if C or CP are exact symmetries, the total rate of baryon production is always equal to the process rate which produces an excess of antibaryons. Hence no net production of baryons over antibaryons is possible if C or CP are conserved. The weak interactions of the SM violate C maximally and violate CP (see the introduction of the CKM matrix in appendix A). However, generating the level of baryon asymmetry with such a small amount of CP violation is impossible. Therefore, baryogenesis or leptogenesis requires new sources of CP violation from BSM Physics.
- *Out of equilibrium dynamics* to depart from chemical equilibrium and produce an asymmetry in B or L numbers that are not conserved. In thermal equilibrium, the production rate of baryons is equal to their destruction rate, resulting in no net production. Fortunately, as we saw earlier, the expansion of the Universe provides mechanisms of decoupling leading to out-of-equilibrium dynamics. Within the SM, departure from thermal equilibrium occurs especially at the electroweak phase transition [36]. However, measurements of the Higgs mass and couplings show that this transition is not "strong", as required for successful baryogenesis [37]. Thus, a modification of the electroweak phase transition is required through new Physics and/or considering other out-of-equilibrium processes in another new Physics sector. This new Physics should allow the preservation of the B asymmetry from sphalerons washout.

Many models and scenarios have been proposed to accommodate these conditions in some extension of the SM. Rapidly after exploring gauge unification, GUT baryogenesis in a $SU(5)$ gauge theory has been first explored [38]. It generates the baryon asymmetry in the out-of-equilibrium decays of new heavy bosons. Baryon number violation is natural in such GUT processes since the same representations of the gauge group may contain both quarks and leptons of the SM, making it possible for new scalars or gauge bosons to mediate baryon number-violating interactions among SM fermions. The original GUT baryogenesis scenario has since suffered from the non-observation of proton decay and, more importantly from the fact that $B - L$ is a global symmetry of such models. In this case, the $B + L$ violating SM sphalerons, which are in equilibrium at 100 GeV $<$ T $<$ 10^{12} GeV, washout the baryon asymmetry [36] that is originally produced by out-of-equilibrium decays of the heavy particles. This can be addressed by looking at larger unification gauge groups such as $SO(10)$ in which

a $B-L$ asymmetry may be generated. However, even in these scenarios, the assumptions of producing GUT scale $\Lambda_{\rm GUT} \sim 10^{16}$ GeV states in thermal equilibrium before their decoupling and their decay seem complicated after inflation, given the scale of inflation $H_I \lesssim 10^{14}$ GeV (see section 2.1). Several solutions have been proposed, such as non-perturbative preheating effects and thermalization after inflation, allowing the production of these massive states [39]. We explore the mechanism and some non-perturbative preheating effects in section 2.2. Electroweak baryogenesis is another type of model where the departure from thermal equilibrium takes place during the electroweak phase transition which has to be a strong first-order transition [40] to avoid the washout of the asymmetry from the sphalerons. Thus, a modification of the electroweak scalar potential is required to obtain a successful baryogenesis at electroweak phase transition. One possible extension of the SM with two Higgs doublet (2HDM) [41] in which the Higgs potential has more parameters and violates CP, can accommodate successful baryogenesis.

However, rapidly after the discovery of the sphalerons and the implications for baryogenesis, a very attractive scenario for the generation of the baryon asymmetry has been proposed, based on the production of a lepton asymmetry. This asymmetry from L number violation processes by the out-of-equilibrium decays of heavy SM singlets neutrino was proposed in [42]. These decays of the heavy neutrinos into light leptons and Higgs bosons can violate C and CP leading to the production of an excess of antileptons over leptons. The lepton asymmetry produced can then be converted into a baryon asymmetry by the anomalous electroweak sphalerons, which are in equilibrium at temperatures larger than the electroweak phase transition. This is the so-called leptogenesis process that we discuss in the next part, for a specific scenario of non-thermal leptogenesis.

Electroweak Sphalerons

The SM Lagrangian, invariant under $SU(3)_c \times SU(2)_L \times U(1)_Y$ gauge group (see appendix A) and containing the Higgs field, is invariant under global abelian symmetries that are the baryonic and leptonic symmetries. There are twelve of these global $U(1)$ symmetries associated with the transformations of the left-handed fermion ψ_L,

$$\psi_L(x) \to e^{i\theta}\psi_L(x)\,, \tag{1.107}$$

one for each of the SM left-handed (3 generations of quarks with 3 colors each, and 3 generations of leptons). They are accidental symmetries that prevent any B and L violation for any perturbative process of the SM at the tree level or any order of perturbation theory. 't Hooft proved, however, that nonperturbative effects give rise to processes that violate $B+L$, but not $B-L$ [35]. Indeed, within the SM, a quantum anomaly in the $B+L$ current (a non-conserving $B+L$ process that violates at the quantum level the classical symmetry) arises in the weak

$SU(2)$ gauge interactions, which are chiral (distinguish left and right handed fermion, see appendix A) and non-abelian interactions [43]. The chiral currents associated with left-handed fermions, ψ_L coupled with weak interaction in the SM

$$j_\mu = \overline{\psi_L}\gamma_\mu\psi_L \tag{1.108}$$

are conserved in the classical field theory but are not conserved (anomalous) at the quantum level, related to the triangle loops and renormalization of the theory. The anomaly is given by [44]

$$\partial^\mu j_\mu = \frac{1}{64\pi^2}\epsilon_{\rho\sigma\mu\nu}F_A^{\rho\sigma}F_A^{\mu\nu} = \frac{1}{32\pi^2}F^A_{\mu\nu}\tilde{F}^{\mu\nu A} \tag{1.109}$$

where $\epsilon_{\rho\sigma\mu\nu}$ is the fully anti-symmetric Levi-Civita tensor, F^A the $SU(2)$ field strength for the spin-1 gauge field A and $\tilde{F}^A$ is the dual field strength. The right-hand side source is a topological term called the Chern-Simons term, associated with the gauge field configuration. In four dimensions, the space-time integral of this term can be non-zero for non-abelian gauge fields and lead to a source term for the anomalous current. If there is a field configuration such that this space-time integral is non-zero, with an associated number [37]

$$\Delta Q_{\rm CS} \propto \frac{1}{32\pi^2}\int d^4x F^A_{\mu\nu}\tilde{F}^{\mu\nu A}(x) \tag{1.110}$$

chiral fermions will be created by a non-perturbative process, even though the generation is forbidden for any perturbative process. Hence, changes in the Chern-Simons number result in changes in the baryon number proportional to the number of fermions in the SM. Each of these transitions in the field configuration generates 9 left-handed quarks (3 colors and 3 generations) and 3 left-handed leptons (3 generations). At zero temperature, gauge field configurations that give non-zero $\Delta Q_{\rm CS}$ correspond to instantons which are quantum fluctuations that can experience quantum tunneling between different degenerate minima of the theory, associated with different field configurations [45]. The associated rate of tunneling is highly suppressed and can be estimated to be of the order

$$\Gamma \propto e^{-4\pi/\alpha_W}, \tag{1.111}$$

with $\alpha_W = \frac{g^2}{4\pi}$ the electroweak gauge coupling. Thus, at zero (low) temperature, no $B+L$ violation can be observed. However, at finite high temperatures, thermal fluctuation of the fields could allow efficient transitions called sphalerons (quasi-particles), which violate $B+L$ but preserve the $B-L$ current. The effective dynamics of non-abelian gauge fields at finite temperature studied on the lattice provide the sphaleron transition rates at $T \gg v_{\rm EW}$ to be of the order [46]

$$\Gamma_{\rm sph} \sim \alpha_W^5 T\,. \tag{1.112}$$

This implies that above the electroweak phase transition at temperature $T \gg 100$ GeV, $B+L$ violating rates are in equilibrium in the bath. Thus, sphalerons convert any primordial lepton asymmetry produced before the electroweak phase transition into a baryon asymmetry, as it violates $B+L$ but conserves $B-L$. Therefore, a lepton number violation associated with the generation of a lepton asymmetry at high energies may provide a mechanism for generating more baryons than anti-baryons in the present Universe. This is exactly what models of leptogenesis predict.

1.3.3 Non-thermal Leptogenesis

Several pieces of evidence show that the SM should only be considered as a low-energy effective field theory (EFT) and that there should exist BSM Physics at a higher energy scale. Among the observables signaling the need for BSM Physics, the experimental evidence for SM neutrino masses is particularly appealing. Hence, it is very attractive that a BSM model motivated by the explanation of small SM neutrino masses can also provide a viable mechanism for baryogenesis. Leptogenesis [42] associated with the Seesaw mechanism [47–52] is such a scenario, that has gained increasing interest since its first study.

Neutrino masses and the Seesaw Mechanism

Measurements of the chirality of SM neutrinos have shown for a long time that they have to be left-handed. In the SM, neutrinos are only involved in left-handed current through weak interactions (see appendix A) and right-handed neutrinos (RHN) are not included. Thus, the Higgs mechanism after electroweak symmetry breaking cannot provide a mass to the left-handed neutrinos as it does for the other massive leptons in the SM. Indeed, even a Majorana mass term involving ν_i and its charge conjugate field ν_i^c,

$$\mathcal{L} \supset \frac{1}{2}\overline{\nu_i^c} m_{i,j} \nu_j + \text{h.c.} \tag{1.113}$$

violates lepton number conservation, and such a mass term breaks the $SU(2)_L$ gauge symmetry as a triplet, so this effective operator cannot originate from a Yukawa coupling with the SM Higgs doublet. Yet, long measurements of neutrino fluxes from solar, atmospheric, nuclear reactors, and accelerator sources have highlighted their oscillations, showing that at least two of the SM neutrinos must have small masses (for a recent summary of the measurements and analysis see [53]). More precisely, neutrino oscillation experiments allow us to estimate the mass-squared difference between the neutrino mass eigenstates i, j $\Delta m^2_{ij} = m^2_{\nu_i} - m^2_{\nu_j}$,

$$\text{(Normal)} \quad \Delta m^2_{12} = (7.42 \pm 0.21) \times 10^{-5}\ \text{eV}^2, \quad |\Delta m^2_{32}| \simeq |\Delta m^2_{31}| = (2.510 \pm 0.027) \times 10^{-3}\ \text{eV}^2$$
$$\text{(Inverted)} \quad \Delta m^2_{12} = (7.42 \pm 0.21) \times 10^{-5}\ \text{eV}^2, \quad |\Delta m^2_{23}| \simeq |\Delta m^2_{13}| = (2.490 \pm 0.027) \times 10^{-3}\ \text{eV}^2$$

where the first line corresponds to a hierarchy in mass $m_3 > m_2 \gg m_1$ (Normal) while the second line correspond to $m_2 > m_1 \gg m_3$ (Inverted).

An elegant solution to explain tiny SM neutrino masses is to introduce three generations of RHN, N_i, that are singlets under the SM gauge group. They must also be in heavy states to explain that they haven't been observed in dedicated experiments. With these additional right-handed heavy states, it is possible to construct a Yukawa interaction of RHN and lepton doublets with the Higgs field

$$\mathcal{L} \supset -y_{i\alpha}\overline{N}_i l_\alpha H + \text{h.c.} \tag{1.114}$$

which provides, after electroweak symmetry breaking, a Dirac mass $m_D = y\langle H\rangle = y v_{\text{EW}}$ with $v_{\text{EW}} = 174$ GeV [54] (we remove for clarity flavor indices). However, to generate such small masses for SM neutrinos from the Higgs VEV, the Yukawa couplings $y_{i\alpha}$ have to be extremely small, $y_{i\alpha} \lesssim 10^{-10}$. This fine-tuning of the Yukawa couplings is avoided as one can introduce large Majorana masses M_i for the RHN such that[12]

$$\mathcal{L} \supset -\frac{1}{2}\overline{N_i^c} M_i N_i - y_{i\alpha}\overline{N}_i l_\alpha H + \text{h.c.} \tag{1.115}$$

which is allowed by SM gauge symmetries but implies a lepton-number violation. Indeed, the couplings of RHN to SM lepton doublet, in addition to their Majorana mass term, generate the effective dimension-5 Weinberg operator, $\frac{1}{M_i}\left(\overline{L_L^c} H^*\right)\left(\tilde{H}^\dagger L_L\right)$, at an energy scale $E \ll M_i$. This operator is suppressed by the Majorana mass scale M_i but violates lepton number conservation. By looking at the mass matrix for neutrinos in this model

$$\frac{1}{2}\begin{pmatrix}\bar{\nu} & \overline{N^c}\end{pmatrix}\begin{pmatrix}0 & m_D \\ m_D & M\end{pmatrix}\begin{pmatrix}\nu \\ N^c\end{pmatrix} + \text{h.c.} \tag{1.116}$$

after diagonalization, Majorana mass eigenstates are approximately given by $m_\nu \simeq \frac{m_D^2}{M}$ and $M_N \simeq M$ in the limit $M \gg m_D$. Seesaw models are UV models that induce this hierarchy between the mass scales for heavy RHN and SM active neutrino with $M_N \gg m_\nu$ without asking for very small Yukawa couplings to the Higgs field. The model discussed above is one type of Seesaw mechanism called Type-I, where we have introduced additional singlets fermions (here 3 RHN) to the SM spectrum that effectively explains the Majorana mass term for SM neutrinos with small mass eigenstates originating from a large Majorana mass of the RHN. There are three types of Seesaw models, depending on the new heavy states in interactions with SM neutrinos to explain the mass generation (Type-II with $SU(2)$-triplet heavy scalars and Type III with $SU(2)$-triplets heavy fermions). The minimal Type I Seesaw model requires only two RHN N_i (2RHN model) [55]. It can be obtained as the limit of the three-generation model

[12] We can always work in a basis where the mass matrix for the RHN M is diagonal.

above, where one species decouples because it is either very heavy or has vanishing Yukawa. It can be shown that in this particular limit, only two SM neutrinos acquire a tiny mass, and one remains massless.

Beyond explaining the SM neutrino small masses, such Seesaw models induce a key new ingredient: possible lepton number violation by introducing a Majorana mass term to the RHN. Thus, such models are particularly studied as they can lead to successful leptogenesis in the out-of-equilibrium decay of the heavy RHN N_i. We discuss next one possible simple realization in the context of non-thermal leptogenesis.

Lepton asymmetry from heavy RHN decays

The lepton asymmetry can be produced when the heavy Majorana RHN decays into leptons and Higgs bosons (or their antiparticles) through Yukawa couplings. These decays into light leptons and Higgs bosons can violate CP if the complex Yukawa couplings involved have unremovable phases. This can lead to the production of an asymmetry between leptons and antileptons in the final state. The CP violation is generated by the interference between tree-level decays and the one-loop diagrams from vertex correction and wave function renormalization of the lightest RHN (N_1) decays [42, 56, 57]

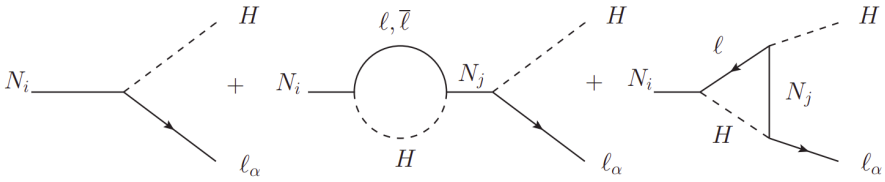

Figure 1.9: *The CP asymmetry in type-I Seesaw results from the interference between tree and 1-loop wave and vertex diagrams. Figure taken from [58].*

$$\begin{aligned} N_1 &\to l_\alpha + H \\ N_1 &\to \bar{l}_\alpha + H^* \,. \end{aligned} \tag{1.117}$$

The CP asymmetry parameter[13] is given by [56, 57]

$$\begin{aligned} \epsilon_{\Delta L} &= \frac{\sum_\alpha [\Gamma(N_1 \to l_\alpha + H) - \Gamma(N_1 \to \bar{l}_\alpha + H^*)]}{\sum_\alpha [\Gamma(N_1 \to l_\alpha + H) + \Gamma(N_1 \to \bar{l}_\alpha + H^*)]} \\ &\simeq -\frac{3}{16} \frac{1}{\mathrm{Im}(yy^\dagger)_{11}} \left[\mathrm{Im}(yy^\dagger)^2_{12} \left(\frac{M_1}{M_2}\right) + \mathrm{Im}(yy^\dagger)^2_{13} \left(\frac{M_1}{M_3}\right) \right] . \end{aligned} \tag{1.118}$$

[13] For the result below we assume a strong hierarchy among RHN masses $M_3, M_2 \gg M_1$.

We can simplify this expression by looking only at the dominant contribution from the Yukawa matrix and using the small neutrino masses parameters from the Seesaw mechanism m_{ν_i}

$$\epsilon_{\Delta L} \simeq -\frac{3\delta_{\text{eff}}}{16\pi}\frac{M_1 m_{\nu,\text{max}}}{v_{\text{EW}}^2} \tag{1.119}$$

where $0 \leq \delta_{\text{eff}} \leq 1$ is the effective CP violating phase in the neutrino mass matrix and $m_{\nu,\text{max}}$ is the heaviest light neutrino mass [54, 59]. At high temperatures, the electroweak sphaleron interactions are in equilibrium and they convert a fraction of a non-zero $B-L$ asymmetry into a baryon asymmetry[60, 61] through

$$Y_B = \frac{8N_f + 4N_H}{22N_f + 13N_H} Y_{\text{B-L}} = \frac{28}{79} Y_{\text{B-L}} \tag{1.120}$$

the baryon yield $Y_B \equiv \frac{n_B}{s}$, and the $B-L$ original asymmetry $Y_{\text{B-L}} \equiv \frac{n_{\text{B-L}}}{s}$, with $N_f = 3$ the number of fermion generations, $N_H = 1$ the number of Higgs doublet. In the context of leptogenesis, there is a generation of a lepton asymmetry and so a $B - L = -L$ asymmetry. Hence, the Seesaw mechanism with RHN requires lepton number violation and provides CP-violating phases in the neutrino Yukawa interactions. From the heavy RHN out-of-equilibrium decay, Sakharov conditions are satisfied for a $B - L = -L$ asymmetry generation, further converted into a baryon asymmetry by electroweak sphalerons.

A natural scenario is a thermal leptogenesis, in which the RHN are produced in thermal equilibrium first, then decay out of equilibrium while decoupling. First, scattering processes in the thermal bath can produce a population of thermal RHN. In this case, the RHN number densities follow the thermal distribution until they start to decouple and decay around $T \sim M$, while their equilibrium number density is Boltzmann suppressed. If the relevant interactions are out-of-equilibrium, the asymmetries survive and the same Yukawa coupling controls the production and decay of the RHN. Usually, this scenario requires a hierarchy in mass scales for the RHN, and in the simplest realization, there are no flavor effects. The initial abundance of N_1 decreases due to scattering, decays, and inverse decays, all of them regrouped in what is called washout processes. The possible importance of flavor effects in leptogenesis is a consequence of the washout, as for inverse decays and washout scatterings it matters to know which leptons are distinguishable from the other due to their different masses and couplings. This leads to interesting effects in the resolution of the relevant Boltzmann equations (see [37] for a review) for the generation of the lepton asymmetries. However, throughout this thesis, we will consider a simple scenario motivated by the paradigm of inflation and reheating, in which RHN are produced by non-thermal processes and stay out of equilibrium before their decay. We refer to this possibility as non-thermal leptogenesis originally introduced in [62], where inflaton decays can source the production of heavy RHN that further decay themselves without ever reaching thermal equilibrium.

For models of non-thermal leptogenesis during reheating, we consider very heavy RHN such that the lightest one satisfies $M_1 > T_{\rm RH}$. In this scenario, at any time during reheating after inflation, no process within the thermal bath is energetic enough to produce RHN[14]. Then, a lepton asymmetry is produced at the decay of the lightest right-handed neutrino when $H \sim M_1$. In this case, the produced asymmetry is computed very simply at the end of reheating from

$$Y_L(T_{\rm RH}) = \epsilon_{\Delta L} \frac{n_{N_1}}{s}(T_{\rm RH}) \rightarrow Y_B(T_{\rm RH}) = \frac{28}{79} \epsilon_{\Delta L} \frac{n_{N_1}}{s}(T_{\rm RH}) \tag{1.121}$$

which is frozen at the time of reheating (see discussion in chapter 3). Constraints on RHN masses can be put in different scenarios to produce the observed baryon asymmetry while considering the Seesaw mechanism generates SM neutrino masses.

After this introduction of non-thermal leptogenesis during reheating, we discuss the production of another cosmological relic density, the production of DM in the early Universe. In fact, it is very intriguing that the DM relic abundance is very close to the one of the baryonic matter ($\Omega^0_{\rm CDM} \simeq 5 \times \Omega^0_b$), probably signaling that similar processes are taking place in the dark sector in the early Universe to generate this relic density. As for the generation of the baryon asymmetry, there are two main approaches to DM production: from thermal processes and a DM species at equilibrium that further freezes out, or through non-thermal production of DM at different stages of the early Universe. We explore these mechanisms for DM production in the following part.

1.4 Dark Matter production

One approach to addressing the generation of a DM relic abundance is to assume that the evolution of the DM component has followed the trajectory of SM species in the hot thermal plasma before decoupling. The mechanism of thermal decoupling, discussed in the preceding section about the thermal Universe, has shown its success at describing very precisely the generation of cosmological relics such as the light elements through BBN, the generation of baryons through thermal baryogenesis or thermal leptogenesis and, as we will see next, the emission of the CMB photons. Hence, it appears natural to look for a similar process at the origin of the DM abundance, considering the particle hypothesis for DM candidate[15], as a thermal relic from the early Universe. This has the advantage of relying only on the microscopic description of the DM model, especially the DM couplings with the SM species, which in turn provides Particle Physics predictions of the DM interactions in DM detection experiments.

[14] To be more precise, one should consider the evolution of the temperature during reheating from a maximum temperature $T_{\rm max}$ to reheating temperature $T_{\rm RH}$ and make sure that no process can destroy the lepton asymmetry.

[15] We note that other possible DM candidates that are not described in BSM models of massive particles are investigated actively such as the Primordial Black Holes (PBH) hypothesis.

In what follows, we will assume the existence of one DM particle χ in interactions with SM particles, such that the interaction rates are in equilibrium at high temperatures and DM follows the thermal equilibrium distribution. Direct and indirect detection experiments put strong constraints on the coupling of DM with SM particles, and these couplings have to be weak enough to explain the lack of detection signal. We first discuss the standard paradigm of WIMPs which are DM particles assumed to be originally in thermal equilibrium and that decoupled from the thermal bath while being non-relativistic. We then explain the current status of the most simple microscopic descriptions of such a scenario before moving to the possibility of producing a DM candidate that never reached thermal equilibrium with non-thermal production of DM.

1.4.1 Thermal freeze-out and the WIMP scenario

We assume here renormalizable interactions between a DM candidate χ and a SM species ψ, which can first produce DM from particles of the bath and then bring χ to its kinetic and chemical equilibrium through $\psi + \psi \leftrightarrow \chi + \chi$ and $\chi + \psi \leftrightarrow \chi + \psi$. Hence, after this state of thermal equilibrium is reached, DM number density depends on the Hubble expansion through the evolution of the temperature and the eventual evolution of the interaction rates. In the standard WIMP scenario, we consider quite naturally that the DM candidate has a typical mass scale $m_\chi \sim$ GeV $-$ TeV close to the electroweak scale within the SM. This is a natural assumption as the Higgs mechanism explains the masses of fundamental particles in the SM around this scale of energy, which can be seen as the effective field theory (EFT) scale of the SM. In addition, we consider weakly interacting particles, with weak couplings and weak cross-sections similar to what is measured for SM neutrino interaction for instance. In this scenario, DM density can be tracked by solving the Boltzmann equation for the processes $\chi\chi \leftrightarrow \psi\psi$. Starting from the simple form of the Boltzmann equation derived in Eq.(1.34) and integrating over the momentum of the DM particles to obtain number density equation, we have[16]

$$\dot{n}_\chi + 3Hn_\chi = -\langle\sigma_{\chi\chi\to\psi\psi}v\rangle\left(n_\chi^2 - n_{\rm eq}^2\right) \tag{1.122}$$

where $\langle\sigma_{\chi\chi\to\psi\psi}v\rangle$ is the thermally averaged cross-section of the process and $n_{\rm eq}$ is the equilibrium density of DM particles within the bath. In the WIMP scenario, an important point is that DM is still in kinetic equilibrium while its chemical decoupling occurs, so we can simplify the computation of the thermally averaged cross-section from the collision term of the Boltzmann equation as [63]

$$\langle\sigma_{\chi\chi\to\psi\psi}v\rangle = \frac{\int d^3p_1 d^3p_2\ \sigma v f_\chi^{\rm eq}(p_1) f_\chi^{\rm eq}(p_2)}{\int d^3p_1 d^3p_2\ f_\chi^{\rm eq}(p_1) f_\chi^{\rm eq}(p_2)} = \frac{\int d^3p_1 d^3p_2\ \frac{|\overline{\mathcal{M}}|^2}{128\pi^3 E_1 E_2} d\Omega f_\chi^{\rm eq}(p_1) f_\chi^{\rm eq}(p_2)}{\int d^3p_1 d^3p_2\ f_\chi^{\rm eq}(p_1) f_\chi^{\rm eq}(p_2)}\,. \tag{1.123}$$

[16] For a pedagogical derivation of the Boltzmann equation relevant for freeze-out DM, we refer to [63].

where $f_\chi^{\rm eq}(p)$ is the distribution function of DM particles at equilibrium. In the last equality, we neglected the mass of particles in the thermal bath in front of the energy in the collision $\sqrt{s} \sim T \gg m_3, m_4$ and use[17]

$$\frac{d\sigma}{d\Omega} \simeq \frac{|\overline{\mathcal{M}}|^2}{128\pi^3 E_1 E_2}\,. \tag{1.124}$$

As discussed in section 1.2, we usually consider the equilibrium distribution of massive particles to be a classical Maxwell-Boltzmann distribution $f_\chi^{\rm eq}(p) = e^{-E(p)/T}$, which is valid for the non-relativistic regime but is still a good approximation in the relativistic limit leading to an analytical equilibrium number density given by Eq.(1.30) $n_\chi(T) = \frac{g_\chi m_\chi^2 T}{2\pi^2} K_2\left(\frac{m_\chi}{T}\right)$. In this case, the computation of the thermally averaged cross section can be done from the integral [63]

$$\langle\sigma v\rangle = \frac{1}{256\pi^2 m_\chi^4 K_2^2\left(\frac{m_\chi}{T}\right)} \int_{4m_\chi^2}^{\infty} \sqrt{s-4m_\chi^2}\,|\overline{\mathcal{M}}|^2 K_1\left(\frac{\sqrt{s}}{T}\right) ds d\Omega\,. \tag{1.125}$$

The right-hand side of the Boltzmann equation leads to the thermal equilibrium between DM and SM particles and constrains the DM density to follow its thermal distribution, which at high temperature $T \gg m_\chi$ gives $n_\chi(T) \propto T^3$. However, below $T \lesssim m_\chi$, in the non-relativistic regime of the WIMP, the production rate is $\propto n_{\rm eq}^2$ thus becomes smaller than the Hubble rate $H(T)$, and results in the suppression of the DM density $n_\chi^{\rm eq}(T) \propto T^{3/2} e^{-m_\chi/T}$, as DM annihilates without being produced anymore. Rapidly after, the DM density freezes out of equilibrium and is further only diluted by the expansion of the Universe. The Boltzmann equation can be expressed using the DM yield $Y_\chi \equiv \frac{n_\chi}{s}$, and as the entropy of the Universe during the radiation-dominated era is conserved $sa^3 = \text{cst}$, the DM yield is equivalent to its comoving number density $Y_\chi \propto \frac{n_\chi}{a^3}$. Neglecting the variation of the effective number of degrees of freedom $g_\rho(T) = g_s(T) \simeq g_*$ during the DM decoupling, and introducing the mass temperature ratio $x \equiv \frac{m_\chi}{T}$, the equation to solve reduces to [16]

$$\frac{dY_\chi}{dx} = \frac{g_* 2\pi}{15}\sqrt{\frac{10}{g_*}}\frac{m_\chi M_P}{x^2}\langle\sigma_{\chi\chi\to\psi\psi} v\rangle \left(Y_{\chi,\rm eq}^2 - Y_\chi^2\right) \tag{1.126}$$

which after integration along the evolution of temperature provides the relic DM yield [64, 65]

$$Y(T_0) \simeq \sqrt{\frac{\pi}{45}} M_P \left[\int_{T_0}^{T_f} g_*^{1/2}\langle\sigma v\rangle dT\right]^{-1}\,. \tag{1.127}$$

T_f is the temperature of the bath at which the DM relic is frozen out. Therefore, this result shows that the DM relic yield in the standard freeze-out mechanism depends only on the thermally averaged cross-section $\langle\sigma v\rangle$. Further, the DM abundance is determined by the values of the cross-section at $T_0 < T < T_f \sim m_\chi$, showing that the thermal production of DM is a low-energy mechanism that can be tackled through the use of EFT for the WIMP. In the

[17] $s = (p_1 + p_2)^2$ is the Mandelstam variable, and $d\Omega$ is the solid angle between outgoing particles 3, 4

generic case, this integral cannot be computed analytically and precise solutions of the DM relic density and freeze-out temperature T_f at which DM decouples are obtained numerically for specific microscopic models of DM interactions. Publicly available numerical packages such as `micrOMEGAs` [66–69] are computing the DM relic for generic models of WIMPs (and Feebly Interacting Massive Particles or FIMPs as well). It is possible to provide an analytical approximation using the non-relativistic[18] velocity expansion of the cross-section (see [16, 63]). For simple models of s-wave annihilation, $\langle\sigma v\rangle$ is independent of T and we can obtain the well-known result for the DM number density evolution shown in Figure 1.10 We can estimate

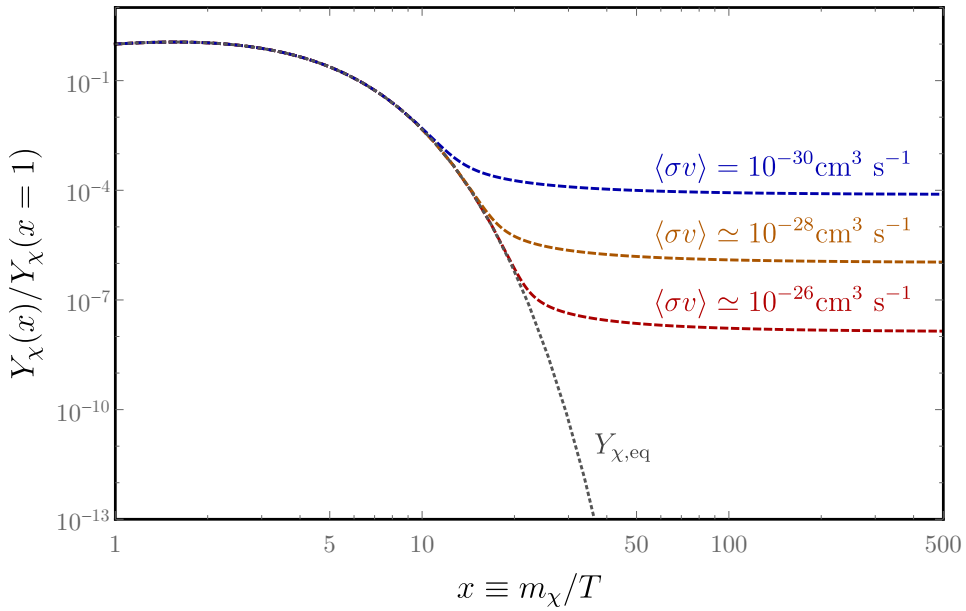

Figure 1.10: *Evolution of the DM yield Y_χ as a function of x. The colored lines are numerical solutions of Eq.(1.126) for different values of $\langle\sigma v\rangle = \text{cst}$ and the dotted black line is the thermal distribution. We see that $T_f \sim 20 m_\chi$ at decoupling time. Figure taken from [70].*

analytically the DM relic for the s-wave annihilation cross section by noticing that for $T \lesssim m_\chi$, the equilibrium density is Boltzmann suppressed and $Y_\chi \gg Y_{\text{eq}}(T)$, leading to

$$\frac{dY}{dx} \simeq -\frac{g_* 2\pi}{15x^2}\sqrt{\frac{10}{g_\star}} m_\chi M_P \langle\sigma v\rangle\ Y_\chi^2 \tag{1.128}$$

which after integration on $x > x_f$ admits the solution

$$\frac{1}{Y_0} - \frac{1}{Y_f} = \frac{g_* 2\pi}{15}\sqrt{\frac{10}{g_\star}} m_\chi M_P \left(\frac{1}{x_f} - \frac{1}{x_0}\right) \implies Y_0 \simeq \frac{15 x_f}{2\pi g_* m_\chi M_P \langle\sigma v\rangle}\sqrt{\frac{g_*}{10}}\,. \tag{1.129}$$

The value of decoupling temperature x_f is approximately the instant when the expansion rate

[18] The non-relativistic limit is valid for WIMP freeze-out as it decouples while being non-relativistic at $T \lesssim m_\chi$, implying $v \ll c$ while DM particles annihilate

becomes of the order of the DM annihilation rate at equilibrium [16]

$$H(x_f) = n_{\rm eq}(x_f)\langle\sigma v\rangle \tag{1.130}$$

and for typical WIMP mass $m_\chi \sim 100$ GeV and weak cross section $\langle\sigma v\rangle \simeq 10^{-26}$ cm^3 s^{-1} we can find $x_f \simeq 20$, which is close to a more precise numerical solution $x_f \simeq 23$. This freeze-out time shows that the WIMP decouples while being non-relativistic, and these results are almost independent of the WIMP mass and cross-section. Computing the relic abundance of WIMP as DM

$$\Omega^0_{\rm CDM}h^2 = \frac{m_\chi Y_0 s_0}{\rho^0_{\rm crit}} \simeq 0.12\left(\frac{m_\chi}{100\ \text{GeV}}\right)\left(\frac{2.5\times10^{-26}\ \text{cm}^3\ \text{s}^{-1}}{\langle\sigma v\rangle}\right) \tag{1.131}$$

shows how the cosmological relic depends on the Particle Physics model of WIMP through $\langle\sigma v\rangle$ and m_χ. We see also that a DM mass of the order of the electroweak scale $m_\chi \sim 100$ GeV and a typical electroweak[19] cross-section $\sigma \sim 10^{-9}$ GeV$^{-2} \simeq 10^{-26}$ cm^3 s^{-1} provide the right relic abundance of DM. This "miracle" has motivated the development of relativistic WIMP models [70] to explain the observed DM relic density from the standard freeze-out scenario. Especially, the simplicity of the freeze-out mechanism is that it does not depend on the DM initial conditions before thermalization, but it occurs only if DM thermalizes at some point during the radiation-dominated era.

It is also important to emphasize that the relic density of DM depends precisely on the value of its cross-section with SM particles. A smaller cross-section induces a too-large DM relic, while a bigger cross-section means more annihilation before decoupling and a smaller relic (see Figure 1.10). Moreover, similar cross-sections are also expected for DM annihilation within our galaxy and for elastic scattering of WIMP particles with SM particles on earth, from particles of DM which are expected to surround our local environment in the Solar System. This fact has led to important investigations for DM in dedicated experiments[20] of direct [71–75] and indirect detection [76–78]. The absence of any experimental signal has strongly constrained the simplest WIMP models [65] as can be seen in Figure 1.11 where constraints on the DM parameters σ and m_χ are reported, from direct detection experiments on the left, and indirect detections on the right. To face these strong constraints from experiments, many models involving more parameters or other assumptions for DM particles in thermal equilibrium have been investigated, such as self-interacting and Strongly Interacting Massive Particles (SIMP) [79] or co-annihilating DM. This current status of DM searches has also led to the exploration of another possibility by relaxing one hypothesis on the evolution of DM in the early Universe: the fact that it has reached thermal equilibrium with the hot thermal bath made of SM particles. Models of very feeble interactions of DM with SM (FIMPs) have been explored since [80],

[19] We can estimate weak annihilation cross section from the s-channel exchange of weak gauge boson leading to $\sigma \sim g^4 m_\chi^2/m_Z^4 \sim 10^{-9}$GeV^{-2}

[20] For a review on DM detection experiments looking for WIMP DM and their constraints on microscopic models see [64, 65, 70]

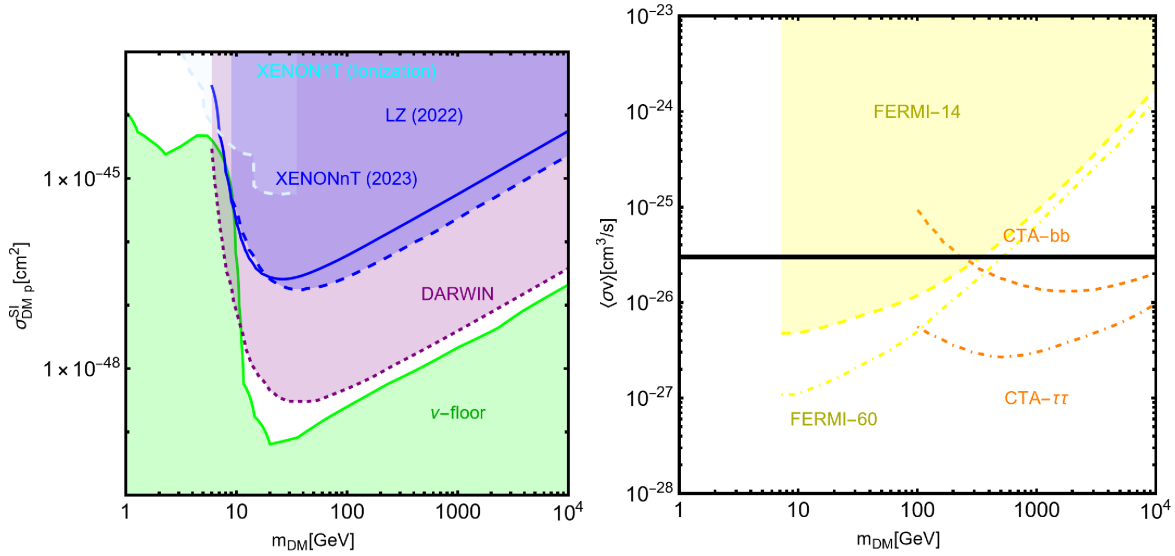

Figure 1.11: *WIMP DM constraints (current in solid lines, projected in dashed). The left panel shows the direct detection limits on m_χ and the spin-independent DM-proton cross-section $\sigma_p^{\rm SI}$, while the right panel refers to the indirect detection constraints on m_χ and $\langle\sigma v\rangle$. Figure taken from [65], see the reference for more details.*

in which DM is not thermal but is still produced by the hot thermal bath. We discuss this possibility in the next part, together with the possible production of even much heavier DM particles in the very early Universe before the radiation-dominated era, during reheating. This will also allow us in chapter 3 to connect the DM puzzle with the Physics of inflation, as the inflaton can also produce DM during reheating from non-thermal processes.

1.4.2 Non-thermal production

When DM particles are so feebly interacting, they may never reach thermal equilibrium in the early Universe. DM production can then be still achieved through the freeze-in mechanism [80–82], from the scattering or decays of particles in the thermal bath. In this scenario, the DM particle interacts with the SM so feebly that it never enters chemical or kinetic equilibrium. Instead, the DM particles are produced from the visible sector until the production stops due to the cooling of the bath temperature. This can be due to two different mechanisms described below.

IR Freeze-in and FIMP

We can consider feeble renormalizable interactions between DM and the visible SM sector, and as the temperature drops below the relevant mass scale of DM particles, or below the mass scale of the particle that decays to DM, the production of DM stops. In this case, decoupling occurs either while the DM particles produced are becoming non-relativistic and the bath does not have sufficiently high energy to produce DM anymore, or when the particle decaying to DM

disappears. In both cases, it is usually referred to as infrared freeze-in because, in that case, the relic density of DM depends solely on the DM mass scale and DM couplings (we suppose the initial abundance of DM to be negligible). This kind of scenario requires renormalizable couplings between DM and the visible sector that are very small $\lesssim O(10^{-7})$ [83] to prevent the dark sector from thermalizing with the bath and still generate the correct relic abundance. To illustrate the standard IR freeze-in scenario, we consider two scenarios, one of a portal interaction mediated by weak bosons with a feeble coupling (a typical example is a Higgs-portal [84, 85]) and the second scenario is the decay of a heavy particle into DM.

In the case of $2 \to 2$ processes, assuming no initial abundance of DM during radiation dominated era, we can neglect the DM yield at the beginning of the process in the Boltzmann equation Eq.(1.126) to solve [16, 83]

$$\frac{dY_\chi}{dx} \simeq \frac{g_* 2\pi}{15}\sqrt{\frac{10}{g_*}} m_\chi M_P \frac{\langle\sigma v\rangle}{x^2} Y_{\rm eq}^2 = \frac{270\sqrt{10}}{16\pi g_*^{3/2}} \frac{M_P}{m_\chi} \frac{1}{(2\pi)^8} \int_{2x}^{\infty} z\sqrt{z^2-4x^2} K_1(z) |\overline{\mathcal{M}}|^2 dz d\Omega \tag{1.132}$$

where we used in the last equality the expression of the equilibrium entropy density $s = \frac{2\pi^2}{45} g_* T^3$, and the equilibrium DM density together with Eq.(1.125), with $z \equiv \frac{\sqrt{s}}{T}$. Typical examples of interactions involve the exchange of weak mediators such as the Higgs bosons exchange mediating the interaction between the DM sector and the visible sector. In this case, for sufficiently high energy when the production of DM occurs at $\sqrt{s} \sim T \gg m_H$ (the mass of the mediator) and $T \gg m_\chi$, we can estimate the amplitude of the process to be of the order

$$|\overline{\mathcal{M}}|^2 \sim \frac{y_\chi^2 y_\psi^2 s^2}{(s-m_H^2)^2} \simeq y_\psi^2 y_\chi^2 \tag{1.133}$$

where y_ψ is a generic Yukawa-like coupling between the Higgs and the SM, while y_χ is another generic Yukawa-like coupling between the Higgs and the DM candidate χ (a Dirac fermion in this case)[21]. Thus we have to solve the equation

$$\frac{dY_\chi}{dx} = \frac{270\sqrt{10}}{4\pi g_*^{3/2}} \frac{M_P}{m_\chi} \frac{1}{(2\pi)^7} y_\chi^2 y_\psi^2 \implies Y(T) \propto \frac{y_\chi^2 y_\psi^2}{T} \tag{1.134}$$

First, we note that this solution is independent of the DM mass, which is a generic feature of IR freeze-in scenarios, and it increases as $\propto 1/T$, which is also a common behavior for most of the FIMP models. Besides, for too large values of the unknown coupling y_χ, the initial production of DM may be very efficient, and it can quickly bring it to its equilibrium number density, meaning that DM can easily reach thermal equilibrium from such portal interactions [16]. However, this may not be the case for feeble couplings, and when $T \simeq m_\chi$ the production stops before the DM sector reaches its thermal abundance. In fact, the value of the coupling required to generate

[21] This discussion is model dependent and other types of microscopic models are explored in [83]. However, the main conclusions reached from this computation are the same in many IR freeze-in models.

the right relic abundance has to be tuned such that when the DM production ceased[22] around $T \sim 20\ m_\chi$, the DM yield is precisely the one that matches current observation of DM density

$$Y_\chi(T \sim 20 m_\chi) = Y_0 \implies y_\chi^2 \simeq 3 \times 10^{-20} \left(\frac{\Omega^0_{\rm CDM} h^2}{0.12}\right) \tag{1.135}$$

where we assumed for illustration purposes that $y_\psi \sim 1$ for simplicity of the argument. Thus, typical FIMP renormalizable portal coupling is of the order $y\chi = y_{\rm FIMP} \sim 10^{-10}$ to provide the correct DM relic through the freeze-in mechanism.

In the case where the main process is the decay of a heavy particle $\sigma \to \chi\chi$ with similar coupling y_χ, we can rewrite the Boltzmann equation in a simpler form [16, 83]

$$\frac{dY_\chi}{dx} = Y_\sigma \frac{\langle\Gamma_\sigma\rangle}{H(x)x} = \frac{M_\sigma^3 \Gamma_\sigma}{2\pi^2 H(x) s(x) x^2} K_1(x) \tag{1.136}$$

where $\langle\Gamma_\sigma\rangle$ is the thermally averaged decay rate of the heavy particle σ which decays preferentially to DM with $\Gamma_\sigma = \frac{y_\chi{}^2 M_\sigma}{8\pi}$. In the last term of the equation we assumed that the initial particles are in thermal equilibrium at the time of their decays, and so accurately described with a Maxwell-Boltzmann distribution. After integration we obtain

$$Y_0 = \frac{y_\chi^2 270\sqrt{10}}{g_*^{3/2} 64\pi^6} \frac{M_P}{M_\sigma} \int_{\frac{M_\sigma}{T_{\rm RH}}}^{\infty} x^3 K_1(x) dx \tag{1.137}$$

where $T_{\rm RH}$ is the reheating temperature, indicating the beginning of the radiation-dominated era (see section 2.2). Assuming that $M_\sigma < T_{\rm RH}$ the value of the Yukawa like coupling y_χ to generate the right DM relic is then

$$y_\chi^2 \simeq 10^{-24} \times \left(\frac{\Omega^0_{\rm CDM} h^2}{0.12}\right) \left(\frac{m_\chi}{100\ {\rm GeV}}\right) \left(\frac{1\ {\rm TeV}}{M_\sigma}\right) \tag{1.138}$$

Again, we see that in this case, we need a very feeble coupling of the order $y_\chi = y_{\rm FIMP} \simeq 10^{-13} - 10^{-11}$ for a 100 GeV DM candidate to satisfy the right relic abundance. We, therefore, arrive at similar generic conclusions for IR freeze-in DM production in both scenarios.

UV Freeze-in

The above calculations assume that the initial abundance of DM is negligible and irrelevant for further production of DM during the radiation era. Nonetheless, in the freeze-in scenario we assumed that DM particles are not in thermal equilibrium with the visible sector thus the production mechanism can be sensitive to UV Physics originating from new Physics at high

[22] This is not occurring at the freeze-out temperature but the Boltzmann suppression factor is the same for the process of DM production and for the process of DM annihilation, leading to very similar temperature of freeze-in in the simplest scenario.

energy scales, or to the initial conditions set during reheating after inflation (see section 2.2 for a first discussion of reheating). In particular, the effect of non-renormalizable couplings in the EFT can be the main source of DM production from higher dimension operators related to some UV new Physics scale $\Lambda_{\rm UV}$. This is in opposition to the thermal DM scenario associated with the freeze-out mechanism, where DM reaches thermal equilibrium erasing effects from initial conditions or UV Physics. This important feature of the UV freeze-in mechanism can be used to constrain different UV models of feebly interacting DM. In such scenarios, it can occur that the annihilation cross-section (or decaying rate) generating DM becomes smaller than the Hubble rate very rapidly after reheating at the beginning of the radiation-dominated era [80, 86]. In this case, the relic density of DM is sensitive to the UV scale $\Lambda_{\rm UV}$ as well as to the reheating temperature $T_{\rm RH}$ after inflation.

We consider a toy model example to understand the typical parametric dependence of the DM relic in UV freeze-in scenarios (for a seminal study, see [86]). DM interacts with the visible sector within the thermal bath through portals interaction mediated by heavy mediator $M_\sigma \gg T_{\rm RH}$. Hence, during a radiation-dominated era and $\sqrt{s} \sim T \ll T_{\rm RH}$, this heavy state can be integrated out of the EFT and generate effective operators between DM and the visible sector suppressed by the UV scale $\Lambda_{\rm UV} \sim M_\sigma$. The associated s-channel amplitude matrix element is typically given by

$$|\overline{\mathcal{M}}|^2 \sim \frac{y_\psi^2 y_\chi^2 s^2}{\Lambda_{\rm UV}^4} \tag{1.139}$$

where we consider Yukawa-like coupling between SM fermions, fermionic DM, and a heavy scalar σ, leading to the Boltzmann equation for the DM yield [16]

$$\frac{dY_\chi}{dx} = \frac{12960\sqrt{10} y_\chi^2 y_\psi^2}{(2\pi)^7} \frac{g_*^{3/2} M_P m_\chi^3}{\Lambda_{\rm UV}^4 x^4 \pi} \implies Y_\chi(T) \simeq \frac{8640\sqrt{10}}{g_*^{3/2}(2\pi)^8} \frac{M_P}{\Lambda_{\rm UV}^4} y_\chi^2 y_\psi^2 \left(T_{\rm RH}^3 - T^3\right) . \tag{1.140}$$

The first thing to emphasize is that it does not depend on the DM mass m_χ and secondly, as $T \lesssim T_{\rm RH}$ during the radiation-dominated era, the production process is active only very close to reheating time, meaning that it occurs at high energy in the bath. Very rapidly, the DM production rate decreases and becomes suppressed importantly by the UV scale $\Lambda_{\rm UV}$, dropping below the Hubble scale. This feature is generic for all UV freeze-in models. Such models depend on two parameters: the couplings on one side and the UV scale (or mass of the heavy mediator here) on the other. One can play on both these parameters to reproduce the right relic of DM but we can give a lower bound on the couplings asking that the UV scale is at least $\Lambda_{\rm UV} > T_{\rm RH}$ and still producing the right DM relic

$$y_\chi^2 y_\psi^2 \gtrsim 10^{-26} \times \left(\frac{\Omega_{\rm CDM}^0 h^2}{0.12}\right) \left(\frac{100\ \text{GeV}}{m_\chi}\right) \left(\frac{T_{\rm RH}}{10^{10}\ \text{GeV}}\right) \tag{1.141}$$

leading to $y_\chi \gtrsim y_{\rm FIMP} \simeq 10^{-7}$ assuming $y_\chi \sim y_\psi$ and $T_{\rm RH} = 10^{10}$ GeV, $m_\chi = 100$ GeV. A

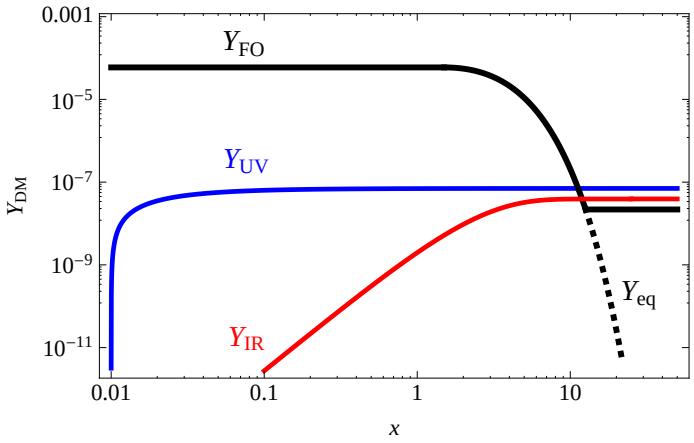

Figure 1.12: *A summary of the evolution of the DM yield $Y = n_{\rm DM}/s$, as a function of $x = m_{\rm DM}/T$, for the freeze-out ($\rm Y_{FO}$), the IR freeze-in ($\rm Y_{IR}$) and the UV freeze-in ($\rm Y_{UV}$) scenarios. Figure taken from [86].*

generalization of such a model has been widely explored in literature and we can show [86] that a UV-induced effective operator of the form

$$|\overline{\mathcal{M}}|^2 \propto \frac{1}{\Lambda_{\rm UV}^{2n}} \tag{1.142}$$

for an integer power n, results in a DM yield depending parametrically on $T_{\rm RH}$, and $\Lambda_{\rm UV}$

$$Y_\chi(T_0) \propto \frac{M_P T_{\rm RH}^{2n-2}}{\Lambda_{\rm UV}^{2n}} \,. \tag{1.143}$$

To conclude this part on DM production, we depict in Figure 1.12 the different mechanisms described above for DM production from processes taking place in the hot thermal.

We emphasize that one goal of this PhD thesis is to explore further the DM production during the reheating phase. This can occur through non-perturbative processes while the inflaton oscillates around its minimum and is coupled to daughter fields, or through perturbative decays and annihilation as we will discuss in section 2.2. Then, as reheating is not an instantaneous process after inflation, there is a complex story for the production of the thermal bath and the dark sector(s) during this stage. Especially there are contributions from the inflaton as well as from SM particles already produced and thermalizing, with a nonstandard evolution of energy densities due to the entropy injection during this stage [87]. The evolution of the inflaton background and the entropy injection in the visible sector induce interesting effects on DM relic density generation. In the last chapter, we describe a new mechanism for DM production, involving the very feeble gravitational interaction during reheating.

1.5 CMB anisotropies

Until now, we discussed early Universe Cosmology, assuming homogeneity and isotropy of the physical conditions on the largest scales. All the events taking place along the expansion history described in this first chapter happened (almost) simultaneously in all places of the Universe. Yet, we also clearly observe that our Universe is not homogeneous and isotropic on smaller scales, and we observe structures such as galaxies and clusters or even smaller objects at very small scales that are not in a diffuse and homogeneous state. Structure formation is impossible in a state of perfect homogeneity and isotropy, as was first assumed in studying the evolution of the Universe from the radiation-dominated era until the late accelerated expansion. We understand that one should also consider small deviations from homogeneity and isotropy which could allow for a dynamical structure formation process to start from small seeds made of inhomogeneities and anisotropies in the physical fields.

All the structures in the Universe and their variety originate from similar initial fluctuations in the density of the different species, further amplified by gravitational instability and their collapse. Then, to explain the presence of large structures that we can see in the Universe, these initial fluctuations must also be present in the very early days at the time of CMB photons emission. Such inhomogeneities in the density of the different species should leave important imprints on the recombination process and the last scatterings of CMB photons, as well as further effects on their path toward our detectors. Thus, measuring and understanding CMB anisotropies has been the first and most important probe of such initial fluctuations in the Universe components.

We introduce in this part some of the main effects affecting the CMB temperature anisotropies power spectrum, their size and distribution, and how this leads to the most precise evaluation of the Cosmological parameters in the ΛCDM paradigm. We briefly discuss the impact of DM and baryons on photons at the time of recombination and decoupling, as well as the measurements of spatial curvature and DE. This will lead us to describe two of the main issues established in the standard Cosmology scenario while measuring the CMB temperature anisotropies and their distribution, issues that are commonly solved by introducing the inflation paradigm. In the next chapter, we will see how inflation succeeds in explaining the initial conditions that have led to CMB anisotropies as they are observed.

1.5.1 Cosmological perturbations in a nutshell

Locally the Universe is not perfectly homogeneous and isotropic, but density fluctuations in the components are small. They are theoretically well described in the linear cosmological perturbation theory[23] at least averaging on sufficiently large scales to avoid the small scales

[23] A full description of perturbed Einstein-Boltzmann equations is beyond the scope of this chapter of the thesis, and we refer to [14, 88] for more details.

non-linearities. We can show that the general form of the linearly perturbed FLRW metric (introduced in section 1.1) is given after gauge fixing[24]

$$ds^2 = (1+2\Psi)dt^2 - a^2(t)\left[(1-2\Phi)\delta_{ij} + 2h_{ij}\right]dx^i dx^j \tag{1.144}$$

introducing two scalar potentials Φ and Ψ called Bardeen potentials, and $h_{\rm ij}$ the transverse traceless part of the metric perturbations describing quadrupolar tensor perturbations associated with primordial GW. We introduce as well the curvature (or scalar) perturbation $\mathcal{R}$ defined as

$$\mathcal{R} = -\frac{2}{3(1+\overline{w})}\left(\Psi + \frac{\dot{\Phi}}{H}\right) + \Phi \tag{1.145}$$

which is directly proportional to the perturbation of the Riemann curvature of the perturbed FLRW space-time in the comoving gauge. For perfect fluids, the two potentials are equal and correspond to the gravitational potential generated by energy-matter over densities through the perturbed Einstein equations. Thus, we introduce perturbation in the stress-energy of the different species through[25]

$$\rho_i(x,t) = \bar{\rho}_i(t) + \delta\rho_i(x,t) = \bar{\rho}_i(t)(1+\delta_i(x,t)) \tag{1.146}$$

$$\delta P_i = c_s^2\ \delta\rho_i(x,t) \tag{1.147}$$

with $\bar{\rho}_i(t)$ the homogeneous component of the energy density of species i, $\delta_i(x,t)$ the density contrast describing the overdensities as a function of time and position, and c_s denoting the sound speed in the plasma made of baryons, electrons, photons in interaction at the time of recombination. We also consider a bulk velocity $\vec{u}_i(x,t)$ for all the species allowing them to have a proper motion in the frame we are considering relative to the bulk of CMB photons. At linear order in perturbation theory, we can work in the Fourier space where Fourier modes of the perturbations are then independent variables

$$\delta_i(k,t) = \int d^3x\ e^{-i\vec{k}.\vec{x}}\delta_i(x,t) \tag{1.148}$$

with k the Fourier scale. We consider only adiabatic perturbations, as no isocurvature perturbations are seen in the CMB data. Adiabatic perturbations mean that the energy densities of each of the species at a certain point and an instant t are the same as that of the background at an instant $t+\delta t(x)$, and $\delta t(x)$ is the same for all species. This is equivalent to saying that local overdensities of each of the species come from the same background state. As we will see, this is naturally the kind of perturbation predicted by single field inflation models where one degree of freedom (the inflaton) is at the origin of the perturbations in the different species. In

[24] This is done in the longitudinal gauge for cosmological perturbations, see [14].

[25] Here we omit the introduction of the anisotropic stress, which is the traceless part of the perturbed stress-energy tensor. It can be the source of GW perturbations of the metric.

particular, this implies that adiabatic perturbations satisfy

$$\delta t(x) = \frac{\delta_i}{(1+w_i)} = \frac{\delta_j}{(1+w_j)} \tag{1.149}$$

for different species i, j at a given time and a given position in the Universe. In the case of adiabatic fluctuations initially in thermal equilibrium and assuming homogeneously and isotropically distribution throughout space with Gaussian statistics, all the statistical properties of the perturbations are described by the initial scalar (here dimensionless) power spectrum $\mathcal{P}_\mathcal{R}(k)$

$$k^3\langle\mathcal{R}(\vec{k})\mathcal{R}^*(\vec{k'})\rangle = (2\pi)^3\delta^{(3)}(\vec{k}-\vec{k'})2\pi^2\mathcal{P}_\mathcal{R}(k) \tag{1.150}$$

with $\delta^{(3)}$ the Dirac delta. $\mathcal{R}(\vec{k})$ is the Fourier transform of the primordial curvature perturbation for some scale $\vec{k}$, set by initial conditions. The primordial curvature power spectrum is parametrized as

$$\mathcal{P}_\mathcal{R}(k) = \mathcal{A}_S\left(\frac{k}{k_*}\right)^{n_s-1} \tag{1.151}$$

with $\mathcal{A}_S$ the amplitude of the scalar power spectrum, n_s the spectral index or scalar tilt and k_* an arbitrary pivot scale. Then, the power spectrum associated with some perturbations $\delta_i(k,t)$ is given by the equal time two-point correlation function

$$k^3\langle\delta_i(\vec{k},t)\delta_i^*(\vec{k'},t)\rangle = (2\pi)^3\delta^{(3)}(\vec{k}-\vec{k'})2\pi^2\mathcal{P}_{\delta_i}(k) \tag{1.152}$$

and it is related to the primordial curvature power spectrum through the transfer function of each species,

$$\mathcal{P}_{\delta_i}(k,t) = \Theta^2_{\delta_i}(k,t)\mathcal{P}_\mathcal{R}(k) \tag{1.153}$$

which depends only on the Universe's content at cosmic time t. For scales such that $k < aH(t)$ at a time t (super-horizon modes), the curvature perturbation and gravitational potentials remain constant. For sub-horizon scales $k > aH(t)$, in a radiation-dominated era, density fluctuations oscillate while the gravitational potentials exhibit dumped oscillations [88]. In a matter-dominated Universe, gravitational potentials are constant while matter density fluctuations grow due to gravitational instability as $\delta_m \propto a$ but in the late accelerated Universe, curvature and density fluctuations decay. This is all that we need to discuss the CMB anisotropies.

1.5.2 CMB spectrum and influence of species

At the time of decoupling, photons start to free stream in the Universe. The CMB spectrum is, to a high degree of precision, a black body spectrum related to a BE distribution for photons, frozen at the time of their last scattering. The intensity of the CMB signal as a function of the

photon frequency ν, is nowadays given by

$$I(\nu) = 4\pi\nu^3 \frac{1}{e^{2\pi\nu/T_0} - 1} \tag{1.154}$$

where the temperature of CMB today is accurately measured to be $T_0 = 2.72548 \pm 0.00057$ K [89]. Very stringent limits can be put on any spectral distortion (mainly due to photons passing through a hot plasma after or during recombination, the so-called Sunyaev–Zeldovich effect) of the CMB black body spectrum. The CMB photons come from all directions, and the frequency spectrum measured is very isotropic, signaling very homogenous conditions at the time of photon decoupling. The first anisotropy in the reception of the CMB photons that have been predicted and then measured is the CMB dipole. This effect comes from the peculiar velocity of the Earth inside the (quasi)-homogeneous radiation bath from CMB. There are combined effects of the proper velocity of Earth within the Solar system, of the Solar system in the galaxy, and of our galaxy in the local group. This peculiar velocity induces a frequency shift of the photons in the observation frame compared to their frequency at emission in the CMB comoving frame, $\nu' = \gamma\nu(1 + \vec{n} \cdot \vec{v})$, $\gamma = \frac{1}{\sqrt{1-v^2}}$ the associated Lorentz factor, p is the photon momentum in CMB comoving frame, $\vec{n}$ its incoming direction and $\vec{v}$ the proper velocity of the observer with respect to the CMB comoving frame. The velocity of the barycenter of the solar system with respect to CMB $v \simeq 370$ km/s, therefore induces a dipole temperature anisotropy in the intensity spectrum

$$\left(\frac{\Delta T}{T_0}\right)_{\text{dipole}} \sim 10^{-3}\,. \tag{1.155}$$

Beyond the astrophysical effects induced by structures on the path of the photons (lensing, inverse Compton scatterings, etc.), smaller amplitude anisotropies of the temperature projected on the CMB map have been observed first by COBE and WMAP and very precisely recently by PLANCK, at the level of $\Delta T/T_0 \sim 10^{-5}$. The anisotropy in a given direction $\hat{n}$ can be understood from several combined effects [88] along the photon geodesic after its decoupling from electrons. The combination of these effects is given by the general relation

$$\frac{\Delta T}{T_0}(\hat{n}) = \left[\frac{1}{4}\delta_\gamma + (\Psi + \Phi) + \vec{u}_b.\hat{n}\right](t_{\text{dec}}, x_{\text{dec}}) + \int_{t_{\text{dec}}}^{t_0} \partial_t \left(\Psi\left(t, x(t)\right) + \Phi\left(t, x(t)\right)\right) dt \tag{1.156}$$

with $\vec{u}_b$ the bulk velocity of baryons (electrons) at decoupling of the photon coming from direction $\hat{n}$. The first two terms in the bracket constitute the Sachs-Wolfe effect corresponding to the gravitational redshift of photons escaping gravitational potential wells given locally by the Bardeen potentials. We can show that for adiabatic perturbations it provides $\Delta T/T_0 = 1/3\Psi(t_{\text{dec}}, x_{\text{dec}})$ depending only on the Newtonian potential at decoupling time on the last scattering surface. The integral corresponds to the integrated Sachs-Wolfe effects when photons propagate in a time-varying gravitational potential that induces a redshift when leaving a potential well different from the blueshift caused when entering. This affects the largest

modes that feel the most the expansion of space-time and, therefore time dependence on the gravitational potentials. Finally, before recombination, baryons and photons are tightly coupled in the plasma. Any baryonic overdensity fluctuation is amplified by gravitational collapse in a patch of size given by the Jeans instability length, but is simultaneously repelled by the radiation pressure of photon overdensity coupled to the baryon overdensity. The interplay of the two effects generates acoustic oscillations (BAO) in the plasma, propagating at the speed of sound c_s. We can relate c_s to the background densities of photons and baryons via

$$c_s^2 = \frac{\rho_\gamma}{3\rho_\gamma + 4\rho_b} \tag{1.157}$$

showing that CMB anisotropies are sensitive to the ratio of baryons to photons η_B at the time of decoupling. The effect of the drag force of baryons on photons through the last term in the bracket above induces oscillations in the photon bath as well.

To project the temperature anisotropies map into a single observable, we expand the direction dependence $\hat{n}$ of the temperature field in spherical harmonics $Y_{lm}(\hat{n})$ given by

$$T(x,t,\vec{n}) = \bar{T}(t) \sum_l \sum_{m=-l}^{l} a_{lm}(x,t) Y_{lm}(\hat{n}) \tag{1.158}$$

where a_{lm} are complex valued functions. We can define the angular power spectrum $C_l(t)$

$$\langle a_{lm}(x,t) a^*_{l'm'}(x,t) \rangle = \delta_{ll'}\delta_{mm'} C_l(t)\,. \tag{1.159}$$

related to the two-point correlation function of CMB anisotropies between two angular directions in the sky via

$$\frac{1}{T_0^2}\langle \Delta T(\hat{n}) \Delta T(\hat{n'}) \rangle = \frac{1}{2\pi} \sum_l (2l+1) C_l P_l(\hat{n}\cdot\hat{n'}) \tag{1.160}$$

with $P_l(x)$ the Legendre polynomials. For a given primordial curvature power spectrum $\mathcal{P}_\mathcal{R}$, one can derive the transfer function, $\Theta_T^2(k,l,t)$, for the photon temperature fluctuations today and relate the angular power spectrum of temperature anisotropies with the primordial curvature power spectrum

$$\mathcal{D}_l(t_0) = \frac{l(l+1)C_l(t_0)}{2\pi} = \int \frac{dk}{k} \Theta_T^2(k,l,t_0) \mathcal{P}_\mathcal{R}(k)\,. \tag{1.161}$$

This angular power spectrum is the main observable extracted from CMB data and provided by Planck collaboration [90] in Figure 1.13.

This function depends on cosmological evolution after recombination through the transfer function and on the primordial Universe through the initial conditions for perturbations via $\mathcal{P}_\mathcal{R}(k)$. The value of the angular separation θ between two points in the CMB anisotropy map

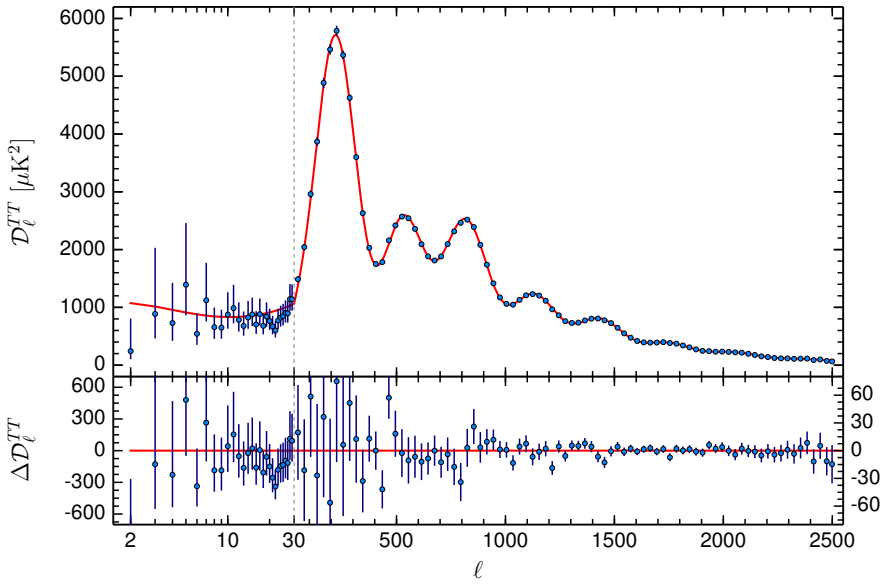

Figure 1.13: *Angular power spectrum of the CMB temperature anisotropy map from Planck Collaboration. In solid red line, the best fit to the spectrum in ΛCDM Cosmology. Figure taken from [90].*

such that $\hat{n} \cdot \hat{n'} = \cos\theta$ is related to $l \sim \pi/\theta$. On large scales (low l), temperature fluctuations from adiabatic perturbations lead through the ordinary Sachs-Wolfe effect to a near-scale-invariant power spectrum related to the amplitude of the primordial curvature power spectrum

$$\mathcal{D}_l \simeq \frac{1}{25}\mathcal{A}_S\,, \tag{1.162}$$

$\mathcal{A}_S \simeq 2\times10^{-9}$ from the Planck analysis[26]. Hence the temperature anisotropy power spectrum is a probe of the primordial power spectrum. For increasing l we see oscillations, the BAO peaks. The acoustic waves propagate in the plasma until the Compton scattering between baryons and photons stops, then photons propagate freely but keep the imprint of the BAO on a sphere of radius given by the sound horizon, $r_s(\tau)$ at a given time τ

$$r_s(\tau) = a(\tau)\int_0^\tau \frac{c_s dt}{a(t)}\,. \tag{1.163}$$

This distance r_s corresponds today in the CMB map to an angular size associated with the first amplified peak in the spectrum. On the other hand, DM distribution is unaffected by photons or baryons drag force and collapses in potential wells, further attracting the baryons. Hence, it can still be seen as imprinted on large-scale structures in distributions of galaxies and galaxy clusters through the measurement of the matter power spectrum [91]. Finally, we see an overall damping of the CMB power spectrum, known as Silk-damping [92]. This effect is due to photon

[26]The spectral index n_s is also constrained from low l CMB spectrum [15], $n_s = 0.9603 \pm 0.0073$.

diffusion at small distances in the baryon-photon plasma that washes out overdensities on the shortest distances and leading to an exponential damping of the spectrum for larger and larger values of l.

Impact of the different components

The CMB power spectrum allows a precise estimate of the ΛCDM parameters. Indeed, the angle on which a given perturbation scale in the CMB is projected depends on the distance from the observer to the last scattering surface. This cosmological angular distance is strongly affected by the content of the Universe throughout its history via

$$d_A(z) = \frac{1}{z+1}\int_0^z \frac{dz'}{H(z')}\,. \tag{1.164}$$

From Eq. (1.46), we clearly see that this angular distance depends strongly on Ω_m^0, Ω_Λ^0 and H_0. The position of the first acoustic peak is given by

$$\theta_* = \frac{r_s}{d_A(z_*)} \simeq 1^\circ \tag{1.165}$$

which is also dependent on the sound speed and so ultimately related to Ω_b^0 or η_b, allowing to infer $\Omega_{\rm CDM}^0$. We can show [88] that increasing the value of $\Omega_{\rm CDM}^0$ while keeping fixed the other abundances induces a shift of the peaks towards larger scales (smaller l, on the left) while at the same time reducing the height of the acoustic peaks, especially of the first one. This important effect of DM on the CMB power spectrum is due to the gravitational pulling of DM on baryons. On the contrary, keeping Ω_m^0 fixed but increasing Ω_b^0 (so decreasing $\Omega_{\rm CDM}^0$) results in a shift towards higher multiples l (smaller scales), and an enhancement of the peaks due to the modification of the sound speed and increase drag force of baryons on photons. A precise measurement of the CMB anisotropies shows the necessity of the presence of a DM component that does not interact substantially with photons at the time of recombination and decoupling. Furthermore, the presence of DM allows for the occurrence of the matter-dominated era before CMB, which leads to an early growth of structure in DM potential wells, with a strong gravitational effect on the baryon and photons later on. All these are strong cosmological evidence for the existence of a DM component dominating the matter content of the Universe.

Finally, using Friedmann equations (1.24), there is a fundamental relation between Ω_Λ^0, H_0 and the spatial curvature of the Universe

$$\Omega_K^0 = 1 - \Omega_\Lambda^0 - \Omega_m^0 \tag{1.166}$$

showing that the contribution of Ω_Λ to the power spectrum is related to the value of H_0 and to the spatial curvature $\Omega_K^0 = -k^2/H_0^2$. In fact, the angular distance is also very sensitive to

the spatial curvature $\Omega_K^0 = -k^2/H_0^2$ (see section 1.1) and CMB analysis combined with other measurements of lensing and BAO analysis in large scale structures provide [15]

$$\Omega_K^0 = -0.0005 \pm 0.0066 \tag{1.167}$$

which is compatible with flat Universe to a high degree of precision. Hence, one can infer the value of Ω_Λ^0 using the concordance equation of ΛCDM paradigm, as it is illustrated in Figure 1.3, where different measurements are combined. The CMB observation is probably the main evidence of DM and DE and the power spectrum analysis allows for a rigorous test of the ΛCDM concordance model, while strongly constraining other alternative scenarios.

1.5.3 Evidences of inflation

We saw how successful and accurate is the explanation of the CMB data within the ΛCDM paradigm. However, it relies on assumptions for the initial state of the perturbations of the different species. They have to be adiabatic, with Gaussian statistics and the specific shape of the primordial curvature power spectrum $\mathcal{P}_\mathcal{R}$ is not predicted by the standard Cosmology scenario. Beyond this, the level of primordial anisotropy and so inhomogeneity is very small $\Delta T/T_0 \simeq 10^{-5}$, while the typical size of the causally connected regions (the causal horizon) on the last scattering surface is relatively small compared to the size of the horizon today. We can estimate from the size of the horizon today $d_H(t_0) \simeq 10^{26}\ m$ that at recombination, there were more than 1000 disconnected patches, but with almost exactly the same state of equilibrium, which seems highly improbable. We also arrive at the conclusion from CMB analysis that the Universe today is spatially flat to a very high degree of precision $\Omega_0 \simeq 0$. Yet we also show that $\Omega_K(a) \propto k^2/a^2$ whereas radiation scales as $\Omega_R(a) \propto a^{-4}$, meaning that in the early Universe, starting from small curvature today, it should have been tremendously smaller than radiation density in the far past. We can compute that assuming an initial thermal Universe starting at Planck scale (quantum gravity regime) the curvature has to be $\lesssim 10^{-64}$ times smaller than radiation energy density at that time [16]. This represents a problematic fine-tuning of the initial conditions for the Universe.

These problems correspond to the fact that the expansion can only be decelerated in standard Cosmological scenarios in the early Universe (at least for low DE energy density). Regarding these apparent issues of the initial conditions in a hot thermal bath, simple scenarios were proposed [93–95] that modify the very first instants of cosmological evolution to assume instead a stage with an accelerated expansion that precedes the thermal Universe. They are now described within the paradigm of cosmic inflation. We introduce inflationary models in more detail in the next chapter, but it can be first described as a stage where a kind of cosmological constant fluid with an energy density Ω_Λ but a negative equation of state $w_\Lambda < -1/3$ dominates

the energy budget in the early Universe. As we saw from Eq (1.24), this results in

$$H^2 \simeq \frac{8\pi G}{3}\rho_\Lambda = \text{cst} \tag{1.168}$$

$$\frac{\ddot{a}}{a} = \rho_\Lambda > 0\,. \tag{1.169}$$

These conditions mean that $\dot{a} = aH$ increases during inflation and the comoving Hubble radius $(aH)^{-1}$ decreases. Since the quantity a^2H^2 increases during inflation, $\Omega_K(a)$ is rapidly driven towards zero during this stage. After the inflationary era, the evolution of the universe is followed by the conventional radiation domination phase, and $\Omega_K/\Omega_R(a)$ begins to increase again, but if inflation lasts sufficiently long, it can achieve a very small initial spatial curvature for our observable Universe today, leading to its measured value today. We can recast this condition on the duration of inflation between an initial scale factor a_i to the end of inflation at $a_{\rm end}$ as

$$\frac{a_i}{a_{\rm end}} \lesssim \frac{a_{\rm end}}{a_0} \tag{1.170}$$

or through the number of *e-folds* during inflation defined as

$$N = \ln\frac{a_{\rm end}}{a_i} \gtrsim \ln\frac{a_0}{a_{\rm end}}\,. \tag{1.171}$$

During inflation, the physical wavelength $a\lambda$ grows faster than the Hubble radius H^{-1}. Therefore, physical wavelengths are stretched outside the Hubble radius during inflation and perturbations on these scales are frozen until reentering the Hubble radius later on. This is illustrated in Figure 1.14, where we show the evolution of the comoving Hubble horizon and the crossing of comoving scales during inflation, followed by their reentry in the subsequent history of the Universe. Thus, causally connected regions can be much larger than the Hubble radius after inflation. After inflation ends, during radiation and matter-domination eras, the Hubble radius grows faster than the physical scales. To solve the horizon problem at CMB decoupling time, the following conditions should hold

$$\int_{t_*}^{t_{\rm dec}} \frac{dt}{a(t)} \gg \int_{t_{\rm dec}}^{t^0} \frac{dt}{a(t)} \tag{1.172}$$

where t_* is the time of the Hubble exit for the perturbations with the comoving pivot scale k_*. This condition means that the comoving distance traveled by photons before decoupling needs to be much larger than the one after the decoupling. Solving this condition leads approximately to the same condition as Eq.(1.171), roughly satisfied for $N \gtrsim 50 - 60$ e $-$ folds.

However, more than just solving these issues of the standard Big Bang scenario, inflation models are predicting the generation of adiabatic cosmological perturbations originating from quantum fluctuations of the inflaton field [97, 98]. These tiny quantum fluctuations also expand

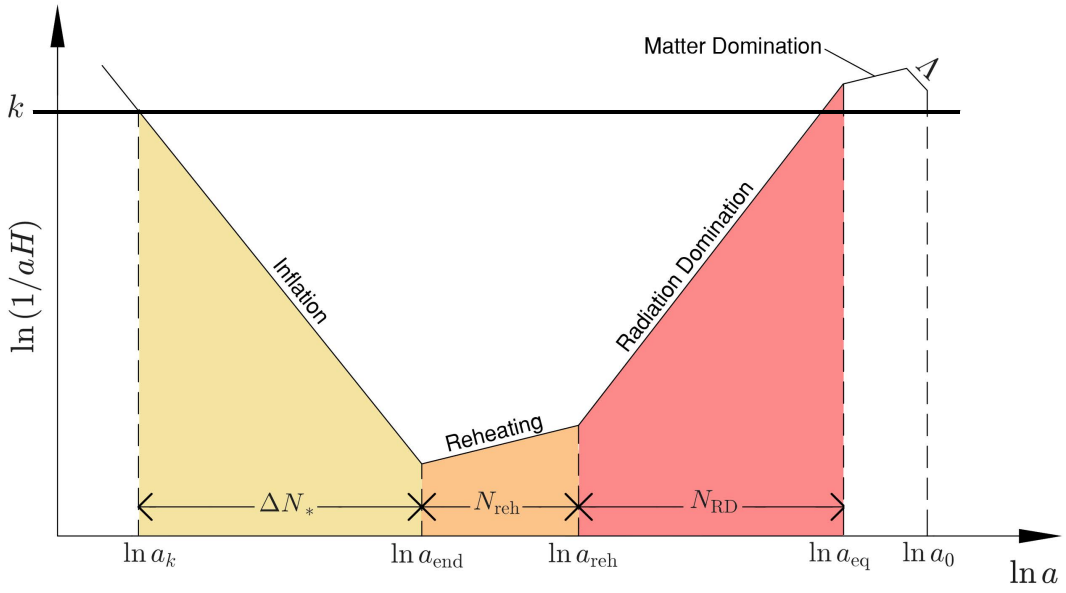

Figure 1.14: *Evolution of the comoving horizon (black thin solid line) during and after inflation. Different comoving scales labeled by k cross the horizon at different times during inflation and reenter the horizon later on. An intermediate time between inflation and the radiation-dominated era, the reheating stage, is represented in orange. Figure taken from [96].*

and freeze on super-horizon scales before reentering the Hubble radius after inflation ends, as shown in Figure 1.14. The simplest inflationary models predict a near scale-invariant curvature power spectrum from inflaton fluctuations, as we will see in section 2.1, that exactly matches the required initial conditions for the perturbations at the origin of the observed CMB anisotropies. On top of these curvature perturbations naturally predicted by inflationary models, quantum fluctuations of the free gravitational field (tensor modes) are also expected to be excited during inflation and stretched through the same mechanism under accelerated expansion. This should result in the generation of a stochastic background of primordial GWs with an associated tensor power spectrum, expected to be also scale invariant and related to the Hubble scale during inflation H_I. The ratio of the amplitude of the tensor to scalar power spectra

$$r = \frac{\mathcal{A}_T}{\mathcal{A}_S} \tag{1.173}$$

is one of the main predictions of slow-roll inflationary models. The re-entry of tensor modes excitations inside the Hubble radius before recombination induces a small quadrupolar anisotropy in the radiation bath through the small metric perturbations it induces, which can polarize the photons as they scatter close to recombination. The so-called B-polarization pattern is a unique signal in CMB photons of tensor modes perturbations on large scales at decoupling [27]. The

[27] Lensing of E polarization modes also induces B polarization, hence it is difficult to subtract this irreducible contribution to the polarization of CMB photons to observe the only tensor mode perturbations, especially on small scales.

current generation of CMB experiments has not yet observed such polarization of the CMB photons from primordial origin. Future CMB experiments such as *LiteBird* will constrain the spectrum of polarized CMB photons looking for a signal from inflation and will at least put an upper bound as small as $r < 0.002$ [99].

The predictions and mechanisms introduced here are the main motivations for studying the inflationary paradigm and explaining the first instants of the Universe's evolution. In the context of an inflationary Universe, we must also understand the transition between inflation and a radiation-dominated Universe, which is the reheating mechanism, the core of this thesis. We introduce and discuss these mechanisms in the next chapter of the thesis.

Chapter 2

Inflation and Reheating

Contents

Inflation was introduced in different works [93–95] as a simple solution to the cosmological problems that we discussed at the end of the precedent chapter. It is now a very general paradigm based on semi-classical Physics and Quantum Field Theory (QFT) in curved spacetime, that has provided a framework to link cosmological observations to quantum effects taking place in the very early Universe. Inflation can be viewed and modeled in many different phenomenological ways. The most common approach is to consider that an inflationary phase occurs thanks to the dynamics of a scalar field, which can be studied through some extension of the SM in the UV such as Higgs-inflation [100] Supersymmetry (SUSY), Supergravity (SUGRA), String Theory or GUT. In such extensions of the SM, we can use inflation as a way to understand both features of quantum gravity or BSM Particle Physics at high energy scales. The inflationary paradigm not only provides an excellent way to solve the standard flatness and horizon problems of Cosmology but also predicts the existence of density perturbations as seeds for large-scale structures. Quantum fluctuations of the inflaton field are stretched on large scales by the accelerated expansion and frozen when leaving the Hubble radius, before reentering the horizon after the end of inflation providing the initial conditions for CMB anisotropies and the growth of structures. An important prediction of single-field inflation is that density perturbations are adiabatic and exhibit a nearly scale-invariant power spectrum. This prediction is directly probed by the measurement of the temperature anisotropies in the CMB from high-precision observations, as we discussed in section 1.5.

In the first part of this chapter, we introduce the main paradigm of single-field slow-roll inflation, which is a broad phenomenological framework allowing for cosmological predictions and observational tests, and that is a natural and successful theory for setting the initial conditions of the Big Bang Cosmology. We first discuss the semi-classical approach to follow the inflaton dynamics during its slow roll, resulting in a quasi-de Sitter phase of accelerated expansion, before looking at the generation of cosmological perturbations from quantum fluctuations during this regime. Furthermore, we describe a specific example of large-field inflationary models motivated by SM UV completion and quantum gravity, which accommodates the current CMB data and belongs to a class of attractor solutions called α-attractor T-models.

In the second part, we are naturally led to the question of the transition from a Universe dominated by vacuum energy of a single scalar field towards the early stage of the radiation domination, where a hot thermal plasma of relativistic SM particles has been produced and is further described in section 1.2. This transition is called reheating after inflation, and it is the main subject of the work done in this thesis. We introduce in this part the dynamics of the inflaton after the stage of slow-roll in large field models once it starts to fall towards the minimum of its potential and oscillates coherently. We further investigate the possible perturbative couplings between the inflaton and matter (as well as DM) that allow for the transfer of energy from the inflaton towards the other degrees of freedom. We also discuss non-perturbative effects in this system of coupled fields through the non-linear dynamics triggering

instabilities and resonances, as well as the fast evolution of the occupation number of the fields coupled to the inflaton background. We finally present the effect of different shapes of the inflaton potential near the minimum, especially by looking at a mixed potential where a transition of the equation of state occurs during reheating.

2.1 Inflation and initial conditions

In this section, we review the framework of inflationary models in their simplest scenario of single scalar field dynamics. Inflation is a simple phenomenological idea that the Universe should grow exponentially under accelerated expansion in its very first instants. In Einstein's gravity, this requires a negative pressure cosmological fluid or, equivalently, a nearly constant energy density throughout the expansion. From Friedmann equations Eq. (1.24) we understand that an accelerating expansion phase requires

$$\frac{\ddot{a}}{a} > 0 \Leftrightarrow (\rho + 3P) < 0\,. \tag{2.1}$$

Hence, an accelerating period is achieved only if the overall pressure P of the cosmological fluid is negative $P < -\rho/3$ or equivalently if the equation of state is $w < -1/3$. Neither a relativistic gas nor a cold matter dust for which $P = \rho/3$ or $P = 0$ respectively can satisfy such a condition. We will see how a scalar field evolving in a specific potential can reproduce such a vacuum energy density with negative pressure. In order to study the properties of the period of inflation, we can assume the extreme condition $P = -\rho$ which is the equation of state of a cosmological constant dominating the Universe evolution. A Universe for which the main component satisfies $P = -\rho$ is called de Sitter Universe. The Friedmann equations (1.24) together with the continuity equation (1.22) for the cosmological constant fluid gives during the de Sitter phase $\rho = \text{cst}$ and so a constant Hubble rate of expansion $H = \text{cst}$. As a result, we obtain the exponential evolution of the scale factor during the de Sitter phase

$$a(t) = a_i e^{H_I(t-ti)} \tag{2.2}$$

where t_i is the time at which de Sitter inflation starts. In this section, we describe the physics of a single scalar field that can achieve such conditions of quasi-de Sitter Universe while dominating the Universe in the early times.

2.1.1 Single-field inflation and the slow-roll regime

The simplest models of inflation involve a single scalar field ϕ, which is called the inflaton. The dynamics of a scalar field minimally coupled to gravity are governed by the action

$$\mathcal{S} = \mathcal{S}_{\rm EH} + \mathcal{S}_\phi = \int d^4x\sqrt{-g}\left[-\frac{M_P^2}{2}R + \frac{1}{2}\partial_\mu\phi\partial^\mu\phi - V(\phi)\right] \tag{2.3}$$

which is the sum of the Einstein-Hilbert action of minimal gravity Eq.(1.7) with the action of a scalar field evolving in the potential $V(\phi)$, which can lead to the accelerated expansion of the Universe. We first consider models minimally coupled to gravity, with canonical kinetic terms for the scalar field[1]. From the Euler-Lagrange equations we obtain the classical Klein-Gordon equation of motion of the scalar field

$$\frac{\delta\mathcal{S}_\phi}{\delta\phi} = 0 \implies \ddot{\phi} + 3H\dot{\phi} - \frac{\nabla^2\phi}{a^2} + V'(\phi) = 0 \tag{2.4}$$

where the term $3H\dot{\phi}$ is a dissipation term due to the expansion of the Universe. The variation of the inflaton action under a metric transformation $\delta g^{\mu\nu}$ allows us to define the scalar field stress-energy tensor (the source of the gravitational field) from Eq.(1.8)

$$T^\phi_{\mu\nu} \equiv \frac{2}{\sqrt{-g}}\frac{\delta\mathcal{S}_\phi}{\delta g^{\mu\nu}} = \partial_\mu\phi\partial_\nu\phi - g_{\mu\nu}\mathcal{L}_\phi\,. \tag{2.5}$$

The corresponding energy density of the inflaton and its pressure density are

$$\rho_\phi \equiv T_{00} = \frac{1}{2}\dot{\phi}^2 + V(\phi) + \frac{1}{2}\frac{(\nabla\phi)^2}{a^2} \tag{2.6}$$

$$P_\phi \equiv \frac{1}{3}T^i{}_i = \frac{1}{2}\dot{\phi}^2 - V(\phi) - \frac{1}{6}\frac{(\nabla\phi)^2}{a^2}\,. \tag{2.7}$$

However, isotropy and homogeneity conditions for the background dominant component of the Universe require that the background component of the scalar field depends only on t. We are naturally led to split the inflaton field in

$$\phi(x,t) = \bar{\phi}(t) + \delta\phi(x,t) \tag{2.8}$$

where $\bar{\phi}(t)$ is the VEV of the inflaton field seen as a quantum field in the isotropic and homogeneous vacuum of FLRW space-time. This physical state can be seen as a Bose-Einstein condensation of the system into the lowest energy state (the zero mode state of infinite wavelength), which can be treated quite as a classical field. On the other hand, $\delta\phi(x,t)$ represents the

[1] We consider in chapter 3 how non-minimal couplings to gravity can be redefined using a conformal transformation of the metric, into a modification of the kinetic term or a modification of the potential of the scalar field.

fluctuations of the inflaton field around its VEV, which have to be quantized in a proper QFT treatment of the inflaton field. As usual, we consider these perturbations to be of small wavelength and small amplitude, not destabilizing the classical trajectory of the scalar inflaton field on large scales such that we treat them as small perturbations on top of the background. For inflationary dynamics, we are mainly concerned with the evolution of the classical background field $\bar{\phi}(t)$, which we will call $\phi(t)$ for simplicity from now on. This scalar condensate provides the classical background configuration sourcing the Einstein-Friedmann equations during inflation, and that evolves in the effective potential[2] given by $V(\phi)$. For a homogeneous classical scalar field, we have to drop the gradient terms, and the Klein-Gordon equation reduces to

$$\ddot{\phi} + 3H\dot{\phi} + V'(\phi) = 0 \tag{2.9}$$

while the density and pressure are given only by

$$\rho_\phi = \frac{1}{2}\dot{\phi}^2 + V(\phi) \tag{2.10}$$

$$P_\phi = \frac{1}{2}\dot{\phi}^2 - V(\phi)\,. \tag{2.11}$$

Thus, we obtain that the equation of state of the Universe dominated by the inflaton is given by the ratio

$$w_\phi \equiv P_\phi/\rho_\phi = \frac{\frac{1}{2}\dot{\phi}^2 - V(\phi)}{\frac{1}{2}\dot{\phi}^2 + V(\phi)}\,. \tag{2.12}$$

Accelerated expansion requires $\ddot{a} > 0$ which implies $w < -1/3$, and we see that it can be achieved if $\dot{\phi}^2 < V(\phi)$. Especially, if we can neglect the kinetic energy of the scalar field dominated by its potential energy, we have $P_\phi \simeq -\rho_\phi \simeq V(\phi)$. Therefore, a scalar field stuck into a region of the field space of non-zero potential mimics the effect of a cosmological constant in terms of density and pressure, resulting in a quasi-de Sitter phase.

If we require that $\dot{\phi}^2 \ll V(\phi)$, the scalar field starting in such a region of the field space is slowly rolling down its potential. This phase of slow-roll is naturally satisfied if the potential is sufficiently flat, ensuring that the rolling of the field is slow due to dissipation from the expansion. For a slow-roll inflation duration sufficiently long to solve classical cosmological problems (see section 1.5), we demand that the kinetic energy remain small, and so the change of $\dot{\phi}$ during expansion should satisfy $|\ddot{\phi}/\dot{\phi}| \ll H$. Hence we impose the *slow-roll conditions* $\dot{\phi}^2 \ll V(\phi)$ and $|\ddot{\phi}| \ll |3H\dot{\phi}|$ such that the new equation of motion becomes

$$3H\dot{\phi} \simeq -V'(\phi)\,. \tag{2.13}$$

[2]We note that quantum effects that renormalize the potential at high energies have to be coherently included into the effective potential, and we consider here the effective theory of a classical field fully specified by the effective potential.

The slow roll conditions also impose that

$$\frac{V'(\phi)^2}{V(\phi)} \ll H^2(\phi) \tag{2.14}$$

$$|V''(\phi)| \ll H^2(\phi) \tag{2.15}$$

which gives the flatness conditions on the inflaton potential that must be satisfied during slow-roll inflation. To describe generically this slow-roll regime, we define dimensionless potential parameters

$$\epsilon_V \equiv \frac{M_P^2}{2}\left(\frac{V'(\phi)}{V(\phi)}\right)^2 \tag{2.16}$$

$$\eta_V \equiv M_P^2\left(\frac{V''(\phi)}{V(\phi)}\right) \tag{2.17}$$

which have to satisfy $\epsilon_V \ll 1$, $|\eta_V| \ll 1$ during slow-roll. Equivalently, noticing that $\ddot{a} = a(\dot{H} + H^2)$, the accelerating expansion condition induces that

$$\epsilon_H \equiv -\frac{\dot{H}}{H^2} = -\frac{d\ln H}{dN} < 1 \tag{2.18}$$

where we also define the first slow-roll parameter ϵ_H, as the first logarithmic derivative of the Hubble rate with respect to the number of e-folds $N \equiv \ln a/a_i$. To achieve sufficiently many e-folds of inflation (see section 1.5), we need ϵ_H to be much less than 1 for long enough. The second slow-roll parameter quantifies the rate of change of ϵ_H

$$\eta_H \equiv \frac{\dot{\epsilon}_H}{H\epsilon_H} = \frac{d\ln\epsilon_H}{dN} \tag{2.19}$$

and has also to satisfy $\eta_H < 1$. We can show that for successful slow-roll inflation, the conditions on potential parameters $\epsilon_V \ll 1$, $|\eta_V| \ll 1$ are equivalent to $\epsilon_H \ll 1$ and $|\eta_H| \ll 1$ and the slow-roll parameters are related via

$$\epsilon_H \simeq \epsilon_V \tag{2.20}$$

$$\eta_H \simeq 4\epsilon_V - 2\eta_V\,. \tag{2.21}$$

Within the slow-roll approximation, the expansion during the domination of the inflaton energy

density is exponential

$$e^{N_{\rm end}} = \frac{a_{\rm end}}{a_i} = \exp\left[\int_{t_i}^{t_{\rm end}} H(t')dt'\right] \simeq \exp\left[\int_{\phi_i}^{\phi_{\rm end}} -\frac{1}{M_P^2}\frac{V(\phi)}{V'(\phi)}d\phi\right] \simeq \exp\left[\int_{\phi_{\rm end}}^{\phi_i} \frac{1}{\sqrt{2\epsilon_V}}\frac{d\phi}{M_P}\right] \tag{2.22}$$

where we use the subscript $\phi_{\rm end}$ to refer to the field value at the end of inflation and ϕ_i at the beginning of inflation, assuming $0 < V(\phi_{\rm end}) < V(\phi_i)$ and $\phi_{\rm end} < \phi_i$. If the value of the inflaton changes on a range larger than $\Delta\phi \sim M_P$, we can obtain large e-foldings solving the flatness and isotropy issues[3]. The fluctuations observed at the CMB pivot scale k_* are created about N_* e-folds before the end of inflation

$$N_* \simeq \int_{\phi_{\rm end}}^{\phi_*} \frac{d\phi}{\sqrt{2\epsilon_V^*}} \simeq 40 - 60\,. \tag{2.23}$$

Hence, to solve the horizon and flatness problems, we require that the total number of e-folds exceeds about 50. The precise value depends on the energy scale of inflation and on the details of reheating after inflation, as we discuss in section 2.3.

So far, we haven't specified the form of the inflaton potential. Since the first models of inflation (some of them have been ruled out by CMB constraints or by the problem of inflation ending) many varieties of inflationary models have been proposed. The different kinds of single-field inflationary models can be classified into three types, depending on the trajectory of the field and the shape of the potential. The first class consists of the "large field" models, in which the initial value of the inflaton is displaced from its minimum by a large (superplanckian $\phi_i > M_P$) value, and it slowly rolls down toward the potential minimum while decreasing. For the rest of this thesis, we will consider such a scenario associated with a specific type of potential introduced in the last part of this section. The second class consists of the "small field" models, in which the inflaton field is initially small (subplanckian $\phi_i < M_P$) and slowly evolves toward the potential minimum at larger values of the field. It seems more complicated for such scenarios to easily accommodate the CMB constraints on the scalar tilt n_s and the tensor-to-scalar ratio r (see section 1.5). We illustrate the two kinds of potential shapes for the large field and small field models, respectively, in Figure 2.1. The third class consists of the hybrid inflation models, in which inflation typically ends through the combined dynamics of a second scalar field which can trigger a phase transition that leads to inflation exit.

[3]We note that large field values $\phi > M_P$ do not mean that quantum gravity corrections become important to follow the inflaton trajectory. This would happen if the energy density (potential) of the scalar condensate is $\sim M_P^4$. This can be avoided with sufficiently small self-coupling of the inflaton.

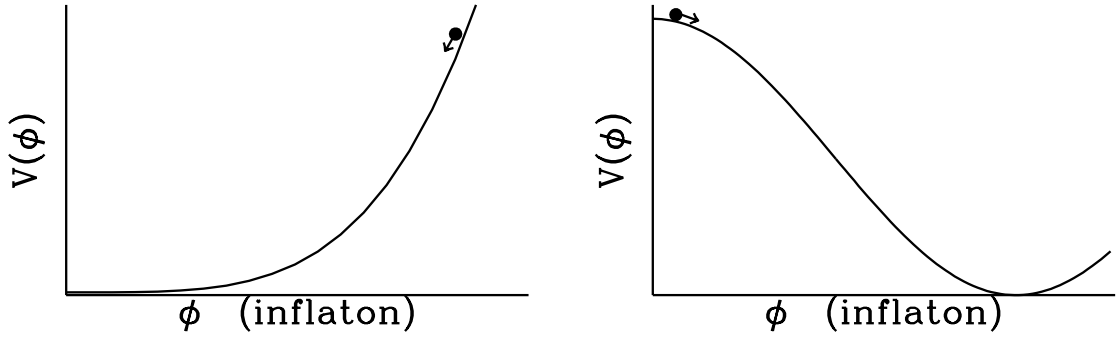

Figure 2.1: *The large field inflation models (Left) versus small field inflation models (Right), while the inflaton is falling towards the minimum of its potential energy. Figure taken from [101].*

Now that we have discussed how the dynamics of a homogeneous scalar condensate slowly rolling down its flat potential can explain the accelerated expansion of the Universe, we succinctly present the main predictions of such kind of models at the level of quantum fluctuations and the resulting cosmological perturbations.

2.1.2 Cosmological perturbations from inflation

We now look at the small perturbations of the scalar field $\delta\phi(x,t)$ around its VEV that will lead to the generation of cosmological perturbations, enabling us to distinguish between different inflation models in their predictions for such seeds of structures on large scales. As we already mentioned in section 1.5, the tiny anisotropies measured in the CMB can be explained within the inflationary paradigm as originating from quantum fluctuations stretched to cosmic sizes during inflation, and that persist long after inflation ends due to their freezing outside the Hubble radius. The generation of adiabatic perturbations, or equivalently curvature perturbations, is a generic prediction of inflation models. It can be easily understood from the presence of a single field ϕ, the inflaton, that sources such perturbations of curvature during inflation. Secondly, the distribution among scales of such primordial perturbations is expected to be near-scale invariant from slow-roll inflation, with Gaussian statistics. Let us describe in more detail where it comes from.

Scalar perturbations

We start with the classical equation of motion for the inflaton perturbations during inflation. Developing the inflaton field as Eq.(2.8) and injecting this decomposition in the Klein-Gordon equation for the inflaton field, we find that the perturbations of the inflaton evolve as [14]

$$\delta\phi'' + 2aH\delta\phi' + \left(k^2 + a^2V''(\phi) - 6\epsilon_H a^2H^2\right)\delta\phi = 0 \tag{2.24}$$

where the derivatives are conformal time derivatives $\frac{d}{d\eta}$, such that $dt = ad\eta$, and k is the comoving momentum associated with the dispersion relation for the inflaton perturbation. Defining the field $X \equiv a\delta\phi$, we can rewrite this equation as a harmonic oscillator but with time-dependent frequency due to expansion,

$$X'' + \left(k^2 + a^2 m_\phi^2 - 6\epsilon_H a^2 H^2 - \frac{a''}{a}\right) X = 0 \tag{2.25}$$

where we define $m_\phi^2 \equiv V''(\phi)$. The time-dependent frequency for each mode is $\omega_k^2 = k^2 + a^2 m_\phi^2 - 6\epsilon_H a^2 H^2 - a''/a$. We canonically quantize such fluctuations introducing the associated modes function $v(k,\eta)$

$$\hat{X}(\vec{k},\eta) = v(k,\eta)\hat{a}_{\vec{k}} + v^*(k,\eta)\hat{a}^\dagger_{\vec{k}} \tag{2.26}$$

where $\hat{a}^\dagger_{\vec{k}}$, $\hat{a}_{\vec{k}}$ are the creation and annihilation operators associated to the field $\hat{X}$. They obey the canonical commutation relations such that

$$\langle \hat{X}(\vec{k},\eta)\hat{X}(\vec{k}',\eta)\rangle = |v(k,\eta)|^2 (2\pi)^3 \delta^{(3)}(\vec{k}-\vec{k}') \tag{2.27}$$

and the mode functions satisfy the following equation of motion

$$v'' + \omega_k(\eta)^2 v = 0\,. \tag{2.28}$$

To solve this equation and obtain the evolution of the mode functions as a function of conformal time η, we have to first solve Friedmann equations during the quasi-de Sitter phase of inflation to express the scale factor evolution. From the definition of the slow roll parameter $\epsilon_H = -\frac{\dot{H}}{H^2}$, one can show that during slow roll $a''/a \sim \eta^{-2}(2+3\epsilon_H)$ [102]. Besides, $\eta_V \ll 1$ during slow-roll, so we have necessarily $m_\phi^2 \ll H^2$ implying for sub-Hubble scales $k^2 \gg a''/a \sim a^2H^2$ that the frequency is approximately constant $\omega_k^2 \sim k^2$. Thus, we find that UV fluctuations with wavelength well within the horizon oscillate as in flat space-time, with plane wave solutions for the mode equation

$$v(k \gg aH, \eta) = \frac{e^{-ik\eta}}{\sqrt{2k}}\,. \tag{2.29}$$

We call such a solution the Bunch-Davies vacuum solution with the proper normalization of the modes. In the generic case Eq.(2.28) can be written as [102]

$$v'' + \left(k^2 - \frac{1}{\eta^2}\left(\nu_\phi^2 - \frac{1}{4}\right)\right) v = 0 \tag{2.30}$$

with $\nu_\phi \simeq \frac{3}{2} + 3\epsilon_V - \eta_V$, using $3\eta_V = m_\phi^2/H^2$ and $\epsilon_H \simeq \epsilon_V$. The generic solution for this differential equation is given by

$$v(k,\eta) = \sqrt{-\eta} A(k) H^{(1)}_{\nu_\phi}(-k\eta) + \sqrt{-\eta} B(k) H^{(2)}_{\nu_\phi}(-k\eta) \tag{2.31}$$

with $H_\nu(x)^{(1)}$ and $H_\nu(x)^{(2)}$ the Hankel's functions of the first and second kind, $A(k)$ and $B(k)$ being integration constants. We impose Bunch-Davies boundary conditions at early times for each mode $-k\eta \gg 1$, corresponding to modes well within the horizon, and obtain the later evolution

$$v(k,\eta) = \frac{\sqrt{\pi}}{2} e^{i(\nu_\phi+1/2)\frac{\pi}{2}} \sqrt{-\eta} H^{(1)}_{\nu_\phi}(-k\eta) \implies \lim_{k\ll aH} v(k,\eta) \propto \frac{1}{\sqrt{2k}} (-k\eta)^{\frac{1}{2}-\nu_\phi} \tag{2.32}$$

where we expressed at the end the limit for super-horizon modes. As a consequence, going back to the perturbations of the inflaton field, we obtain

$$|\delta\phi_k| \simeq \frac{H}{\sqrt{2k^3}} \left(\frac{k}{aH}\right)^{3/2-\nu_\phi} \qquad (k \ll aH) \tag{2.33}$$

which is the main result of the evolution of perturbations of the inflaton on super-horizon scales. This result shows that we can neglect the time evolution of the perturbation once it crosses the horizon, and a near-constant amplitude of the quantum perturbations on super-horizon scales leads rapidly to a large occupation number of the modes, for which the classical treatment of such perturbations becomes accurate. Defining the (dimensionless) power spectrum of the inflaton perturbations, $\mathcal{P}_\phi$, as

$$\langle 0|\delta\phi_k \delta\phi_{k'}|0\rangle = (2\pi)^3 \delta^{(3)}\left(\vec{k}-\vec{k'}\right) |\delta\phi_k|^2 \equiv (2\pi)^3 \delta^{(3)}\left(\vec{k}-\vec{k'}\right) \frac{2\pi^2}{k^3} \mathcal{P}_\phi \,. \tag{2.34}$$

we can compute it on scales $k \ll aH$,

$$\mathcal{P}_\phi \equiv \frac{k^3}{2\pi^2} |\delta\phi_k|^2 = \left(\frac{H}{2\pi}\right)^2 \left(\frac{k}{aH}\right)^{3-2\nu_\phi} \qquad (k \ll aH)\,. \tag{2.35}$$

The power spectrum of fluctuations of the scalar field $\delta\phi$ is nearly independent of the scale k: the amplitude of the fluctuation on super-Hubble scales does not depend on the time at which the fluctuations cross the Hubble radius. There is still a mild scale dependence coming from the small evolution of the Hubble rate during inflation

$$\frac{d\mathcal{P}_\phi}{d\ln k} \equiv n_s - 1 = 3 - 2\nu_\phi = 2\eta_V - 6\epsilon_V \tag{2.36}$$

which defines n_s the scalar tilt for perturbations, related to slow-roll parameters. It is useful to consider, instead of the scalar field perturbations, the gauge-invariant comoving curvature perturbation related to the gravitational potential as introduced in CMB analysis (see section 1.5), which describes adiabatic perturbations of energy densities. During inflation we can show that it is related to the scalar field perturbation as [14]

$$\mathcal{R} = -\frac{aH}{\bar{\phi}'} \delta\phi \tag{2.37}$$

and this quantity is conserved on the super-horizon scales after inflation until the reentry of the corresponding mode within the horizon [14]. When a mode leaves the horizon during inflation, it will reenter the horizon later on, carrying the frozen information coming directly from the time it exited the horizon during inflation. Finally, the initial conditions for the comoving curvature perturbation, sourcing CMB anisotropies, are characterized by the comoving curvature power spectrum (see section 1.5)

$$\mathcal{P}_{\mathcal{R}} = \left(\frac{aH}{\bar{\phi}'}\right)^2 \mathcal{P}_\phi \simeq \frac{1}{2M_P^2\epsilon_V}\mathcal{P}_\phi \,. \tag{2.38}$$

Therefore, single-field slow-roll inflation predicts near-scale-invariant adiabatic perturbations, characterized by the comoving curvature power spectrum. It is usually parametrized considering the exit of the CMB pivot scale k_*, through Eq.(1.151)

$$\mathcal{P}_{\mathcal{R}} = \mathcal{A}_S \left(\frac{k}{k_*}\right)^{n_s-1} \tag{2.39}$$

with A_S the scalar power spectrum amplitude. We can relate the amplitude to the potential

$$\mathcal{A}_S \simeq \frac{V(\phi_*)}{24\pi^2 M_P^4 \epsilon_{V*}} \tag{2.40}$$

where the quantities with subscript $*$ are defined at pivot scale horizon crossing $k_* = aH$.

Primordial Gravitational Waves

The metric perturbations can be split into scalar, vector, and tensor parts according to their transformation properties in space, on hypersurfaces of constant time. The *decomposition theorem* proves that the Einstein equations for the scalar, vector, and tensor parts of the perturbed metric are decoupled in linear perturbation theory. We saw how scalar perturbations of the metric, the curvature perturbation, are sourced by the perturbed scalar inflaton field during inflation. We can show that no vector perturbation is sourced during single-field inflation. Hence, we are left with independent tensor perturbations that can be excited during the quasi-de Sitter phase. They correspond initially to quantum fluctuations $|\tilde{h}_{ij}^{TT}| \ll 1$ in the metric field, which are transverse and traceless (massless tensor modes)

$$ds^2 = a^2(\eta)\left[d\eta^2 - (\delta_{ij} + \tilde{h}_{ij}^{TT})dx^i dx^j\right] . \tag{2.41}$$

We first normalize these tensor modes to $h_{ij} = \frac{M_P}{2}\tilde{h}_{ij} \ll M_P$, which correspond to the canonically normalized gravitons propagating in Minkowski flat space-time. The two transverse traceless tensor degrees of freedom can be represented by the two polarization modes $h_+(k,\eta)$ and $h_\times(k,\eta)$. They both follow the equation of motion derived from perturbed Einstein equations

[14]

$$h'' + 2\frac{a'}{a}h' + k^2 h = 0 \quad (h = h_+,\ h_\times) \tag{2.42}$$

which is the equation of motion of a massless scalar field during inflation. We follow the procedure done for scalar perturbations in the precedent part, introducing the rescaled field $X = ah$, to obtain the mode equation for each polarization

$$v'' + \left(k^2 - \frac{a''}{a}\right) v = 0\,. \tag{2.43}$$

Once they enter the classical regime, these tensor perturbations can be seen as primordial gravitational waves (GW) generated during inflation. From the analysis done for the scalar perturbations, we obtain the corresponding dimensionless tensor power spectrum on super-horizon scales

$$\mathcal{P}_T \equiv \sum_{+,\times} \frac{k^3}{2\pi^2}|\tilde{h}|^2 = 8\left(\frac{H}{2\pi}\right)^2 \left(\frac{k}{aH}\right)^{3-2\nu_T} \qquad (k \ll aH) \tag{2.44}$$

with $\nu_T \simeq 3/2 - \epsilon_V$ for slow-roll inflation. The tensor spectral index n_T is given by

$$n_T \equiv \frac{d\ln \mathcal{P}_T}{d\ln k} = 3 - 2\nu_T \simeq -2\epsilon_V \tag{2.45}$$

where the last relation is called the slow-roll consistency relation. We can show [14] that the tensor perturbations are also frozen when they leave the horizon during inflation, before reentering the horizon later on. Thus, slow-roll inflation also predicts primordial gravitational waves, independent of the curvature perturbation (at linear order), with a near-scale invariant power spectrum as initial conditions. As for comoving curvature perturbations we parametrized the initial tensor power spectrum at the horizon crossing of the CMB pivot scale

$$\mathcal{P}_T = \mathcal{A}_T \left(\frac{k}{k_*}\right)^{n_T}\,. \tag{2.46}$$

where $\mathcal{A}_T = \frac{V(\phi_*)}{24\pi^2 M_P^4}$. We understand that the amplitude of the tensor power spectrum is, this time, independent of the slow-roll parameters and is a direct probe of the scale of inflation H_I. We can define the ratio of the amplitudes of tensor to scalar power spectra as in Eq.(1.173) and obtain

$$r \equiv \frac{\mathcal{A}_T}{\mathcal{A}_S} = 16\epsilon_{V*}\,. \tag{2.47}$$

These are the main predictions of the inflationary paradigm that can be constrained by CMB observations, as we discussed in section 1.5.

2.1.3 A specific class of potential: α attractor T-models

We discuss one specific class of models that are well motivated by UV Physics in the realization of noscale supergravity and that predict inflation observable in agreement with CMB data. The measurements of the tilt of the primordial scalar power spectrum $n_s = 0.9649 \pm 0.0042$, and the strong constraints from the absence of signal of primordial tensor modes by the Planck Collaboration [103], $r < 0.056$, favor a large field inflation model with a very flat potential as a large field plateau, and a quite low energy density $H_I \lesssim 6 \times 10^{13}$ GeV $\Leftrightarrow$ V($\phi \gg$ M$_{\rm P}$) $\lesssim$ $(1.6 \times 10^{16}$ GeV$)^4$. In this perspective, interest is growing for inflation models belonging to a class of solutions, including the Starobinsky model [93], that predict low tensor to scalar ratio and converge to the slow-roll attractor predictions

$$n_s \simeq 1 - 6\epsilon_{V*} + 2\eta_{V*} \simeq 1 - \frac{2}{N_*} - \frac{3}{2N_*^2} \tag{2.48}$$

$$r \simeq 16\epsilon_{V*} \simeq \frac{12}{N_*^2}\,. \tag{2.49}$$

where N_* is the number of e-folds between the horizon crossing of the pivot scale k_* used in CMB data analysis and the end of inflation. We first describe the original Starobinsky model and then show how it can be embedded into a more general class of potential resulting from noscale supergravity construction.

Starobinsky Inflation

Starobinski proposed in [93] a modification of the Einstein-Hilbert action Eq.(1.7), in order to capture UV quantum gravity effects into an effective higher dimension operator proportional to the squared of the Ricci scalar,

$$\mathcal{S} = \int d^4x\sqrt{-g}\left[-\frac{M_P^2}{2}R + \frac{\xi}{12}R^2\right]\,. \tag{2.50}$$

The theory is, in fact, conformally equivalent to Einstein's gravity but with an additional dynamical scalar field ϕ evolving in an exponentially flat potential. Indeed, this can be seen by introducing the auxiliary (non-dynamical) field, χ, with the following action [16]

$$\mathcal{S} = \int d^4x\sqrt{-g}\left[-\frac{M_P^2}{2}R\left(1 + \xi\frac{\chi^2}{M_P^2}\right) - \frac{\beta}{4}\xi\chi^4\right] \tag{2.51}$$

where χ satisfies the Lagrange constraints

$$\chi^2 = -\frac{\xi}{\beta}R \tag{2.52}$$

leading to the original theory for $\beta = 3\xi$. As we have introduced a modification of the effective Planck scale in the action expressed in the Jordan frame, it is useful to perform a Weyl (conformal) redefinition of the metric

$$\tilde{g}_{\mu\nu} = \Omega^2 g_{\mu\nu} \tag{2.53}$$

$$\Omega^2 \equiv 1 + \xi \frac{\chi^2}{M_P^2} \tag{2.54}$$

to look at the theory in the new frame called the Einstein frame, associated with the redefinition of the coordinates. We can show that transforming $R \to \tilde{R}$ through the conformal transformation of the metric, and defining the new scalar degree of freedom as $\phi = \sqrt{\frac{3}{2}} \ln\left(1 + \xi \frac{\chi^2}{M_P^2}\right)$, we obtain the Einstein frame action,

$$\mathcal{S} = \int d^4x \sqrt{-\tilde{g}} \left[-\frac{M_P^2}{2} \tilde{R} + \frac{1}{2} \tilde{g}^{\mu\nu} \partial_\mu \phi \partial^\mu \phi - V(\phi) \right] \tag{2.55}$$

with

$$V(\phi) = \frac{3}{4} m_\phi^2 M_P^2 \left(1 - e^{-\sqrt{\frac{2}{3}} \frac{\phi}{M_P}}\right)^2 \tag{2.56}$$

which is the Starobinsky potential, where $m_\phi^2 = \frac{M_P^2}{\xi}$ [93]. This potential is flat at large field values $\phi \gg M_P$ with $V(\phi) \simeq \frac{3}{4} m_\phi^2 M_P^2$, while it is at leading order in $\phi \ll M_P$, quadratic near its minimum $V(\phi) \simeq \frac{1}{2} m_\phi^2 \phi^2$. This potential provides the slow roll parameters and inflationary predictions given above Eq.(2.49).

Generalizing Starobinsky model: α-attractor T-models

A class of models that generalize the Starobinsky effective potential can be constructed within the framework of noscale supergravity [104, 105]. We do not give any details of the supergravity construction which is far beyond the scope of this thesis, but we review the ingredients necessary to lead to the T-models potential for the effective scalar inflaton, following [87]. In $N = 1$ supergravity, the scalar sector can be described by a superpotential W, and the Kähler potential K, for which we consider the form

$$K = -3 \ln\left(T + \overline{T} - \frac{|\chi|^2}{3}\right) \tag{2.57}$$

where T is a volume modulus and χ is a matter field [87, 104]. We can find the scalar effective potential considering the Wess-Zumino-like superpotential[4]

$$W = M \left(\frac{\chi^2}{2} - \frac{\chi^3}{3\sqrt{3}}\right) \tag{2.58}$$

[4]We work in units of M_P here, but we reintroduce the Planck scale later on.

is given by

$$V(\chi) = \frac{|\frac{\partial W}{\partial \chi}|^2}{(T+\overline{T}-\frac{|\chi|^2}{3})^2} \to V(\phi) = \frac{3}{4}M^2\left(1-e^{-\sqrt{\frac{2}{3}}\phi}\right)^2 \tag{2.59}$$

where we used the field redefinition $\chi = \sqrt{3}\tanh\left(\frac{\phi}{\sqrt{6}}\right)$ and considered that the modulus is stabilized at $\langle T\rangle = 1/2$ [87, 104]. This shows that the effective Starobinsky potential can arise from such a supergravity construction for simple superpotential. A generalization of the effective scalar potential with the same attractor predictions Eq.(2.49) can be derived from the generic superpotential [87]

$$W = 2^{\frac{k}{4}+1}\sqrt{\lambda}\left(\frac{\chi^{\frac{k}{2}+1}}{k+2} - \frac{\chi^{\frac{k}{2}+2}}{3(k+6)}\right) \tag{2.60}$$

leading for ϕ to the effective inflaton potential

$$V(\phi) = \lambda M_P^4\left[\sqrt{6}\tanh\left(\frac{\phi}{\sqrt{6}M_P}\right)\right]^k \tag{2.61}$$

where we restored the Planck mass dimension for clarity of the result. This reduces to the Starobinsky model for $k = 2$ and a suitable choice of λ, but still provides similar plateau potential at large field values for all k. More precisely, it generates the same inflationary predictions from slow-roll parameters (with a very mild dependence on the free parameter k). However, for $\phi \ll M_P$ and $k > 2$, different leading order monomial terms dominate the shape of the potential near the minimum as $V(\phi \ll M_P) \simeq \lambda M_P^4\left(\frac{\phi}{M_P}\right)^k$. We provide in Figure 2.2 the shape of the potential for T-attractor models with different values of k. For such potential

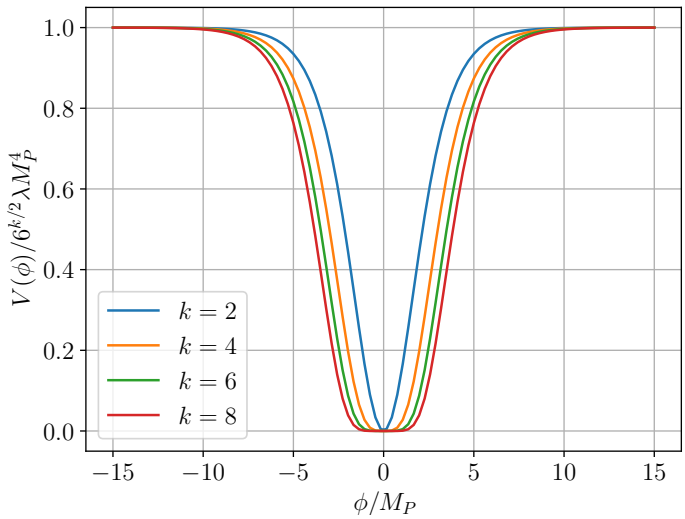

Figure 2.2: *Inflaton potential for T-models Eq.(2.61), for different values of k.*

of the inflaton, in the slow-roll approximation, the number of e-folds Eq.(2.23)

$$N_* \simeq \int_{\phi_{\rm end}}^{\phi_*} \frac{1}{\sqrt{2\epsilon}} \frac{d\phi}{M_P} \simeq \frac{3}{2k} \cosh\left(\sqrt{\frac{2}{3}} \frac{\phi_*}{M_P}\right) \tag{2.62}$$

and the amplitude of the curvature primordial power spectrum is related to the potential via

$$A_{S*} \simeq \frac{V(\phi_*)}{24\pi^2 \epsilon_* M_P^4} \tag{2.63}$$

giving approximately [106] the normalization of λ

$$\lambda \simeq \frac{18\pi^2 A_{S*}}{6^{k/2} N_*^2} \,. \tag{2.64}$$

We remind the Planck pivot scale value $k_* = 0.05$ Mpc^{-1}, and the amplitude of the scalar power spectrum is measured to be $\ln(10^{10} A_{S*}) = 3.044$ [103]. In the next section, we will be interested in the late-time dynamics of the inflaton ϕ as inflation ends, and one must find the inflaton field value at the end of inflation when $\ddot{a} = 0 \Leftrightarrow \dot{\phi}^2 = V(\phi)$. An approximate solution for this condition gives [106]

$$\phi_{\rm end} \simeq \sqrt{\frac{3}{8}} M_P \ln\left[\frac{1}{2} + \frac{k}{3}\left(k + \sqrt{k^2+3}\right)\right] \tag{2.65}$$

for the T-models potential considered above.

Throughout the work done in this thesis, we adopt the T-models as a benchmark model to the effective potential for the inflaton field, and we consider different values of the free parameter k. This leads to interesting phenomenology during the coherent oscillations of the inflaton after inflation, during reheating.

2.2 Post-inflationary reheating

Inflation is a very successful and predictive theory for the initial conditions of Big Bang Cosmology. However, a complete inflationary model requires in addition a mechanism for ending the quasi-de Sitter era and explaining the transition towards the thermal Universe. Indeed, the period of exponential expansion must end with an efficient transfer of the energy stored in the inflaton condensate during inflation, into the different components of a thermal bath filling the Universe in its further evolution. Inflation ends when the potential energy associated with the inflaton field becomes smaller than its kinetic energy, making the slow-roll regime end. This is possible as the scalar inflaton field falls towards the minimum of its potential and when its motion leads to reaching the condition $\epsilon_H = 1$ and $\eta_H = 1$, ending the accelerated expan-

sion of the Universe. In the standard approach it is considered that the homogeneous inflaton condensate begins to oscillate about the minimum of its potential after this time. Within the inflationary paradigm, all elementary particles populating the Universe must be generated after inflation. Therefore the cold inflaton condensate must decay into matter and radiation made of particles of the SM and potentially of dark sectors. The matter and radiation produced must also reach afterward a thermal equilibrium at a temperature greater than $T \gtrsim 1$ MeV to allow for the standard BBN mechanism to proceed (see section 1.2.3). The crucial transition from the state of inflaton condensate domination at the end of inflation to the hot thermal bath is called reheating.

This reheating process is completed when almost all the energy of the scalar inflaton field is transferred to relativistic particles. At this stage, the effective temperature (more precisely, the associated energy density of relativistic particles) of the Universe is called the reheating temperature $T_{\rm RH}$, which is the main prediction of reheating models. We underline that the main challenge of reheating models is to deal with a system of coupled fields in a semi-classical regime of large occupation numbers, but still with important consequences of quantum effects. This has led to two kinds of approach: an analytical approximation under the assumption of perturbative analysis, using Hartree approximation to tackle backreactions in the quantum evolution of coupled fields as well as time-dependent effective masses; on the other hand, solving the full set of coupled equations of motion to follow the non-linear and non-perturbative dynamics of the system in a classical regime. This usually requires dedicated numerical tools, especially modern Lattice simulations. Moreover, the assumptions of single-field slow-roll inflation and the predictions of cosmological observables associated with this simplest model may be impacted by the stage of non-linear dynamics of coupled fields towards the end of inflation. More precisely, the departure from the single-field approximation in coupled systems may lead to non-Gaussianities in the statistics of cosmological perturbations (for reviews, see [107–109]) and a signal of non-linearities in the perturbation spectrum. The study of primordial non-Gaussianities generated during inflation or from reheating dynamics is far beyond this thesis's work, and we will not investigate these constraints further in the following.

In this section we introduce the standard treatment of energy transfer from the inflaton condensate to the coupled fields. We begin with the perturbative approach to reheating which is valid in the small couplings limit. This is the main framework followed throughout this thesis, as we will consider very feeble coupling in the main part of this work along chapter 3. Still, we show the importance of non-perturbative effects in some preheating models originating from the coherent state of the inflaton condensate while it oscillates. These effects include parametric resonances which lead to exponential growth of the occupation numbers of the coupled fields.

2.2.1 Inflaton oscillations

Let us focus on the inflaton potential given in Eq.(2.61) for T-models. At the end of inflation, when $\ddot{a} = 0$, the scalar inflaton condensate starts to oscillate around the minimum of its potential. Around this minimum, the potential can be expanded at small field values as

$$V(\phi \ll M_P) \simeq \lambda M_P^4 \left(\frac{\phi}{M_P}\right)^k \tag{2.66}$$

which is quite generic for other inflationary potentials. For example, Starobinsky inflation corresponds to $k = 2$ for which the inflaton has a constant mass scale. We define the effective mass of the inflaton field as it oscillates through

$$m_\phi^2(t) \equiv V''(\phi) = k(k-1)\lambda M_P^2 \left(\frac{\phi}{M_P}\right)^{k-2} . \tag{2.67}$$

In a quadratic potential, $k = 2$, the inflaton oscillates coherently with a constant mass $m_\phi^2 = \lambda M_P^2$, and for $k > 2$, the oscillations are non-harmonic for the classical field. Ignoring for now interactions with other fields, the inflaton experiences damped oscillations due to expansion

$$\ddot{\phi} + 3H\dot{\phi} + V'(\phi) = 0 . \tag{2.68}$$

From the homogeneous energy density ρ_ϕ and pressure P_ϕ of the inflaton, we obtain the continuity equation Eq.(1.22) as

$$\dot{\rho}_\phi + 3H(\rho_\phi + P_\phi) = 0 . \tag{2.69}$$

In these dynamics, we separate the short time scale of oscillations related to the effective potential of the inflaton field from the longer time scale of damping due to Hubble expansion H. Multiplying the equation of motion Eq.(2.69) by ϕ and averaging each term over one oscillation, it leads to the following useful relation $\langle \dot{\phi}^2 \rangle \simeq \langle \phi V'(\phi) \rangle$, where we have neglected the friction term over one oscillation, and we have as well

$$\langle \rho_\phi \rangle \simeq \frac{k+2}{2} \langle V(\phi) \rangle \tag{2.70}$$

$$\langle P_\phi \rangle \simeq \frac{k-2}{2} \langle V(\phi) \rangle . \tag{2.71}$$

These results show that the average equation of state of the inflaton during the oscillations regime in the potential $V(\phi) \propto \phi^k$ is given by

$$w_\phi = \frac{k-2}{k+2} . \tag{2.72}$$

During the oscillations of the scalar condensate, the homogeneous inflaton background behaves as a cold matter dust if $k = 2$ (quadratic potential) with a constant effective mass m_ϕ^2. However,

for $k > 2$, this is not the case anymore, and it behaves effectively as a radiation for $k = 4$ with a mass that redshifts as $m_\phi \propto 1/a$. In general, the continuity equation for the average energy density of the inflation background implies

$$\dot{\rho}_\phi + 3H(1 + w_\phi)\rho \simeq 0 \implies \rho_\phi(a) = \rho_{\rm end} \left(\frac{a}{a_{\rm end}}\right)^{-\frac{6k}{k+2}} \tag{2.73}$$

if we neglect the interactions. We introduced the energy density at the end of inflation related to the potential $\rho_{\rm end} = \frac{3}{2}V(\phi_{\rm end})$.

The separation of oscillations time scale and expansion time scale allows us to approximately parametrize the solution of the equation of motion as

$$\phi(t) = \phi_0(t) \cdot \mathcal{P}(t) \tag{2.74}$$

where $\phi_0(t)$ is the dumped amplitude of the oscillations while $\mathcal{P}(t)$ is the quasi-periodic function describing the oscillations of the inflaton. We can set the normalization of $\phi_0(t)$ such that $V(\phi_0) = \langle\rho_\phi\rangle$. For a quadratic potential and harmonic oscillations, $\mathcal{P}(t) = \cos((m_\phi(t))$ and in this case, we can also exactly solve the dumping of the oscillations and find the envelope $\phi_0(t) \propto 1/m_\phi t$ [16]. Looking at the inflaton evolution on short time scales, we can consider the

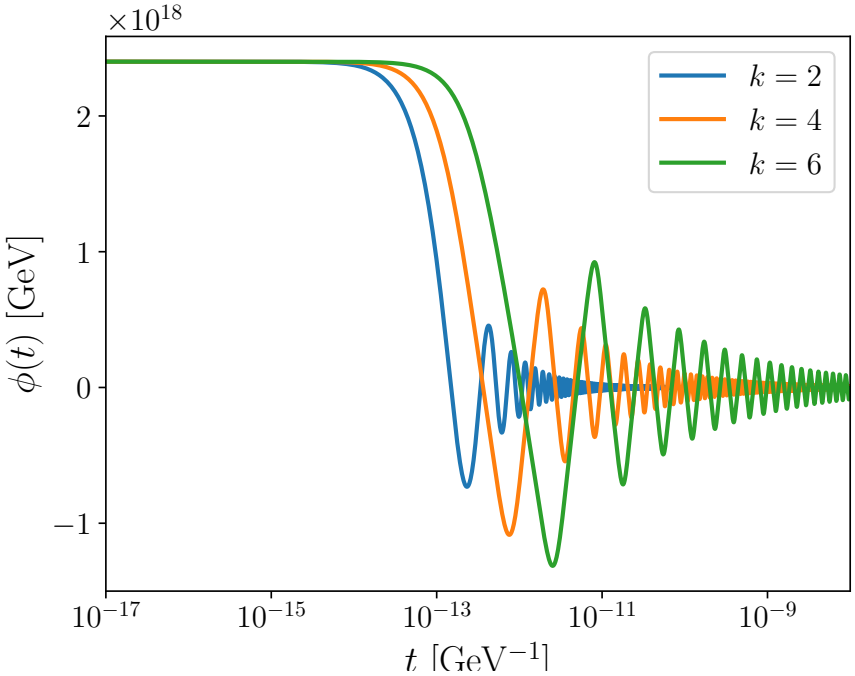

Figure 2.3: *Evolution of the inflaton condensate after inflation in α-attractor T-model potential for different value of $k = 2, 4, 6$. We start the evolution at $\phi(t_{\rm init}) = M_P$.*

amplitude of the field approximately constant, and from the definition of the energy density

$$\rho_\phi = \frac{1}{2}\dot{\phi}^2 + V(\phi) \implies \dot{\mathcal{P}}^2 \simeq \frac{2\rho_\phi}{\phi_0^2}\left(1-\mathcal{P}^k\right) \tag{2.75}$$

integrate this equation to find the frequency of the oscillations

$$\omega = m_\phi \sqrt{\frac{\pi k}{2(k-1)}} \frac{\Gamma\left(\frac{1}{2}+\frac{1}{k}\right)}{\Gamma\left(\frac{1}{k}\right)}\,. \tag{2.76}$$

In the generic potential, the oscillations are anharmonic, and we can develop the periodic function in a Fourier series in terms of the oscillation frequency

$$\mathcal{P} = \sum_{n=-\infty}^{+\infty} \mathcal{P}_n e^{-in\omega t} \tag{2.77}$$

where $\mathcal{P}_n$ are the Fourier modes of the corresponding periodic function $\mathcal{P}(t)$. Each Fourier mode can be seen as an independent classical oscillator with an energy $E_n = n\omega$. All these modes contribute to the inflaton condensate and can be determined numerically by solving the oscillatory behavior of the inflaton in the appropriate potential.

2.2.2 Perturbative treatment

To take into account the interactions of the inflaton condensate with the other fields, we have to solve the Boltzmann equations Eq.(1.34) for both the inflaton distribution function and for the products of its interactions. The interactions of the condensate induce dissipation while it oscillates and we can effectively follow this effect through

$$\ddot{\phi} + (3H + \Gamma_\phi)\dot{\phi} + V'(\phi) = 0 \tag{2.78}$$

where Γ_ϕ is the inflaton background dissipation rate. Under the assumption that the interactions of the inflaton are small perturbations on top of its background evolution, the phase space distribution for the homogeneous inflaton condensate can be written as [106, 110]

$$f_\phi(k,t) = (2\pi)^3 n_\phi(t)\delta^{(3)}(k) \tag{2.79}$$

corresponding to a density of bosonic modes $n_\phi(t)$ all in the zero momentum state of lowest energy (Bose condensation). We underline that no process can inject inflaton quanta into the condensate, however, the production of inflaton fluctuations (particle states), as well as quanta of the other fields, can further backreact on the classical evolution of the background. This is especially important for strong couplings of the fields with the background inflaton (or strong self-interactions), and it can be tackled through some mean field approximation

(Hartree). These methods usually require the use of numerical solvers to track the evolution of distribution functions. However, if the number of occupations of the produced quanta does not grow too fast towards high values, we can neglect backreactions and rescatterings to solve the Boltzmann equations analytically. We consider the process $\phi \to AB$, where A, B are two particles, for which the integrated Boltzmann equation related to the inflaton condensate number density is given by [106]

$$\dot{n}_\phi + 3Hn_\phi = -\sum_{n=\infty}^{+\infty} \int \frac{d^3p_A}{(2\pi)^3 2E_A} \frac{d^3p_B}{(2\pi)^3 2E_B} (2\pi)^4 \delta^{(3)}(p_A + p_B)\delta(n\omega - E_A - E_B)|\mathcal{M}_n|^2 \,. \quad (2.80)$$

We have assumed a large occupation number for the inflaton condensate $1 + f_\phi \simeq f_\phi$ and (at least initially) a low occupation number for the produced quanta, such that Bose-enhancement or Pauli-blocking factors can be ignored. We have to sum over the contribution of each inflaton oscillation mode of energy $E_n = n\omega$ to compute the production rate. The associated transition amplitude from the coherent state to the final states $|\phi\rangle \to |AB\rangle$ is given by $\mathcal{M}_n$ for each mode n, and we underline that this matrix element effectively contains the condensate amplitude of oscillations. Physically, the production of quanta from the inflaton field corresponds to an extraction from a classical background state, and the inflaton field can be treated in this case as a classical time-dependent parameter from which it is possible to extract energy from each Fourier mode. We can, therefore, interpret the amplitude $\mathcal{M}_n$ as a probability of extracting from the vacuum state $|0\rangle$ two quanta of momenta (p_A, p_B), through the interactions given by a Lagrangian density $\mathcal{L}$,

$$\mathcal{M}_n \equiv \int d^4x \langle p_A\ p_B | i\mathcal{L}\left[\phi_0(t)\mathcal{P}_n e^{-in\omega t}, \hat{X_A}, \hat{X_B}\right]|0\rangle \,. \quad (2.81)$$

The energy transfer ΔE per space-time volume is given by

$$\Delta E \equiv \sum_{n=\infty}^{+\infty} \int \frac{d^3p_A}{(2\pi)^3 2E_A} \frac{d^3p_B}{(2\pi)^3 2E_B} (E_A + E_B)(2\pi)^4 \delta^{(3)}(p_A + p_B)\delta(n\omega - E_A - E_B)|\mathcal{M}_n|^2 \,. \quad (2.82)$$

We can define an effective rate for the transfer of energy density [5] through the process $\phi \to AB$, which after integrating the 2-body phase space integrals gives [106]

$$(1 + w_\phi)\Gamma_\phi \rho_\phi \equiv \frac{\Delta E}{\mathrm{Vol}_4} = \frac{1}{8\pi} \sum_{n=1}^{+\infty} |\mathcal{M}_n|^2(n\omega)\beta_n(m_A, m_B) \quad (2.83)$$

with the kinematic factor

$$\beta_n(m_A, m_B) \equiv \sqrt{\left(1 - \frac{(m_A + m_B)^2}{(n\omega)^2}\right)\left(1 - \frac{(m_A - m_B)^2}{(n\omega)^2}\right)} \,. \quad (2.84)$$

[5] We underline that this rate differs from the decay or dissipation rate Γ_ϕ by a factor $(1 + w_\phi)\rho_\phi$.

We are interested in the evolution of the averaged inflaton energy density (the zeroth mode homogeneous condensate) for which we have $\rho_\phi = m_\phi n_\phi$ as the zeroth mode has no momentum. Taking the time derivative, one can show that we obtain

$$\dot{\rho}_\phi + 3H(1+w_\phi)\rho_\phi = -(1+w_\phi)\Gamma_\phi \rho_\phi \,. \tag{2.85}$$

We call it the Boltzmann equation for the energy density of the inflaton condensate. As long as we can neglect the right-hand side of this equation, we recover the adiabatic evolution of the inflaton background as in Eq.(2.73).

The last ingredient to follow the reheating process in this perturbative framework is the evolution of the density of produced quanta through the process $\phi \to AB$. Following the same procedure as what has been done for the inflaton density, we obtain the number density of the produced quanta $n_{i=A,B}$

$$\dot{n}_i + 3Hn_i = R(t) \tag{2.86}$$

where we introduce the production rate as

$$R(t) = (1+w_\phi)\frac{\rho_\phi}{m_\phi}\Gamma_\phi = 2 \times \frac{1}{8\pi}\sum_{n=1}^{\infty}|\mathcal{M}_n|^2\beta_n \tag{2.87}$$

in which factor 2 is taking care of the two quanta produced per interaction. At the production time, kinematics impose $m_i \lesssim E_n$ while $p_i \sim E_n$. Thus, we are following the evolution of relativistic quanta during production. Similarly, using the energy density transfer rate Eq.(2.83), we can follow the evolution of their energy density, ρ_R, called radiation density by solving

$$\dot{\rho}_R + 4H\rho_R = (1+w_\phi)\Gamma_\phi\rho_\phi \,. \tag{2.88}$$

Once the quanta become non-relativistic, their energy density is approximately given by $\rho_i = m_i n_i$. The sets of equations we have to solve during reheating are these Boltzmann equations together with the Friedmann equation for the expansion rate

$$H^2 = \frac{\rho_\phi + \rho_R}{3M_P^2} \,. \tag{2.89}$$

Several simplifications have been made in the description above. First, we haven't considered statistical effects: if these effects become important, a better treatment of the Boltzmann equation is required. It can be done by solving the Boltzmann equation for the "classical" distribution function $f_i^c(t)$, without Bose-enhancement or Pauli blocking, and then deducing the correct distribution function through the relation [111]

$$f_i(k,t) = \frac{1}{2}\left(e^{2f_i^c(k,t)} \pm 1\right) \,. \tag{2.90}$$

From this distribution function, number densities can be computed using the Boltzmann equation taking statistical effects into account.

As stated earlier, when the occupation number becomes too large, backreactions of the produced quanta on the inflaton background are important. These can be approximately taken into account by introducing effective mean field potential for the evolution of the background [112, 113]. As an example, for a quartic coupling interaction with a field χ of the form $\sigma\phi^2\chi^2$, the mean-field approach gives

$$\ddot{\phi} + 3H\dot{\phi} + V'(\phi) + \sigma\langle\chi^2\rangle\phi = 0 \tag{2.91}$$

which is a Hartree approximation. Coherent solutions of the equation of motion and density equations in the regime of strong backreaction usually necessitate numerical integration. We have also neglected the effect of rescatterings mediated by the inflaton or self-interactions, which can contribute to redistributing momentum in the UV [113]. However, we expect all these effects to be small for feeble perturbative couplings, which we consider in this work.

Beyond these non-linear dynamics, non-perturbative effects are expected to occur during reheating and initiate, in some cases, rapid growth of the number of occupations in the fields. We discuss these effects in the last part of the section.

2.2.3 Decays and annihilation of the inflaton condensate

We consider the following generic contributions to the Lagrangian[6] leading to decay or annihilation of the inflaton [106]

$$\mathcal{L} \supset \begin{cases} y\phi\bar{f}f & (\phi \to \bar{f}f) \\ \mu\phi b^2 & (\phi \to bb) \\ \sigma\phi^2 b^2 & (\phi\phi \to bb) \end{cases} \tag{2.92}$$

with f a fermionic field and b a bosonic final state. The Yukawa-like coupling y, and the four-point coupling σ, are dimensionless, while μ is an effective dimensionful coupling. We consider for simplicity that the produced quanta have vanishing bare masses, but the results can be adapted to the case of non-zero masses straightforwardly. Using the development of the inflaton field in Fourier modes Eq.(2.77), we can compute the transition amplitudes for each mode through the different couplings [106]

$$\mathcal{M}_n = y\phi_0\mathcal{P}_n\bar{u}(p_A)v(p_B) \qquad (\phi \to \bar{f}f) \tag{2.93}$$

$$\mathcal{M}_n = \mu\phi_0\mathcal{P}_n \qquad (\phi \to bb) \tag{2.94}$$

$$\mathcal{M}_n = 2\sigma\phi_0^2(\mathcal{P}^2)_n \qquad (\phi \to bb) \tag{2.95}$$

[6] Recently, this analysis has been extended to the case of couplings to vector fields in [114].

In this computation, the initial state is the asymptotic vacuum since no inflaton quanta are produced from the condensate. Instead, we treat the condensate as a time-dependent coefficient of the interaction, and the inflaton is regarded as the homogeneously oscillating classical field. Therefore, in the case of inflation "annihilation" from the coupling $\sigma\phi^2 b^2$, this field square must be expanded in Fourier modes to compute the transition amplitude. We call the associated Fourier coefficients $(\mathcal{P}^2)_n$, but we underline that they are different from the square of the coefficients $\mathcal{P}_n$. The rates for energy density production can be directly computed from these amplitudes and Eq.(2.83). For the different channels, the authors of [106] derived the following expressions

$$\Gamma_{\phi\to\bar{f}f} = \frac{y^2\omega}{8\pi}(k+2)(k-1)\left(\frac{\omega}{m_\phi}\right)^2\sum_{n=1}^{\infty} n^3|\mathcal{P}_n|^2\left(1-\left(\frac{2m_f}{n\omega}\right)^2\right)^{3/2} \tag{2.96}$$

$$\Gamma_{\phi\to bb} = \frac{\mu^2}{8\pi\omega}(k+2)(k-1)\left(\frac{\omega}{m_\phi}\right)^2\sum_{n=1}^{\infty} n|\mathcal{P}_n|^2\left(1-\left(\frac{2m_b}{n\omega}\right)^2\right)^{1/2} \tag{2.97}$$

$$\Gamma_{\phi\phi\to bb} = \frac{\sigma^2\rho_\phi}{8\pi\omega^3}k(k+2)(k-1)^2\left(\frac{\omega}{m_\phi}\right)^4\sum_{n=1}^{\infty} n|(\mathcal{P}^2)_n|^2\left(1-\left(\frac{2m_b}{n\omega}\right)^2\right)^{1/2} \tag{2.98}$$

where we use Eq.(2.76) and Eq.(2.67) to relate the amplitude ϕ_0 to the inflaton effective mass and oscillation frequency, and $\rho_\phi = V(\phi_0)$.

We are considering massless particles, yet the tree-level couplings to the inflaton background induce a time-dependent effective mass for the fields

$$m^2_{\rm eff}(t) = \begin{cases} y^2\phi^2 & (\phi\to\bar{f}f) \\ \mu\phi & (\phi\to bb) \\ 2\sigma\phi^2 & (\phi\phi\to bb) \end{cases} \tag{2.99}$$

and the effect of this time-dependent effective mass can be determined by averaging the effective decay rate over the oscillations. The parameter which drives the associated kinematic effect is the ratio $\mathcal{R} \equiv (2m_{\rm eff}/\omega)^2$, as it can be seen in the expression of the transfer rates. For $\mathcal{R} \ll 1$, the rates at $m_{\rm eff} = 0$ can be used. The regime when $\mathcal{R} \gtrsim 1$ depends on the magnitude of the coupling and the inflaton potential, driving the redshift of the inflaton field $\phi_0(t)$. We introduce effective couplings that take into account such kinematic effects and the influence of

the potential shape such that we can rewrite the effective decay rates as

$$\Gamma_{\phi\to\bar{f}f} = \frac{y_{\rm eff}^2 m_\phi(t)}{8\pi} \tag{2.100}$$

$$\Gamma_{\phi\to bb} = \frac{\mu_{\rm eff}^2}{8\pi m_\phi(t)} \tag{2.101}$$

$$\Gamma_{\phi\phi\to bb} = \frac{\sigma_{\rm eff}^2}{8\pi}\frac{\rho_\phi(t)}{m_\phi^3(t)} \tag{2.102}$$

where for $k = 2$ and $m_{\rm eff} \to 0$, $y_{\rm eff} = y$, $\mu_{\rm eff} = \mu$, $\sigma_{\rm eff} = \sigma$. For $k > 2$ and $m_{\rm eff} \neq 0$, these effective couplings have to be estimated numerically during the oscillations of the background inflaton. The resulting effect when $\mathcal{R} \gtrsim 1$ is also strongly dependent on the spin of the final state particles. For fermionic decays and bosonic scatterings, the authors of [106] determined that

$$\Gamma_\phi(\mathcal{R} \gg 1) \simeq \Gamma_\phi(\mathcal{R} = 0) \times \mathcal{R}(t)^{-1/2} \tag{2.103}$$

leading to less efficient production due to kinematic blocking. On the contrary, the case of decay towards bosons leads to an enhancement of the production rate in the strong kinematic limit,

$$\Gamma_\phi(\mathcal{R} \gg 1) \simeq \Gamma_\phi(\mathcal{R} = 0) \times \mathcal{R}^{1/2}\,, \tag{2.104}$$

signaling the breakdown of perturbativity. This occurs due to the linear dependence on $\phi_0(t)$ of the effective mass for the bosons and shows that the non-perturbative tachyonic instability should be considered rigorously.

We can compute analytically the evolution of the energy densities by solving their Boltzmann equations Eq.(2.85), Eq.(2.88) with the effective transfer rates determined above. To do so, it is useful to parameterize generically the decay rates through

$$\Gamma_\phi(t) = \gamma_\phi \left(\frac{\rho_\phi}{M_P^4}\right)^l \tag{2.105}$$

where the exponent l depends on the channel of production

$$l = \begin{cases} \frac{1}{2} - \frac{1}{k} & (\phi \to \bar{f}f) \\ \frac{1}{k} - \frac{1}{2} & (\phi \to bb) \\ \frac{3}{k} - \frac{1}{2} & (\phi\phi \to bb) \end{cases} \tag{2.106}$$

and

$$\gamma_\phi = \begin{cases} \sqrt{k(k-1)}\lambda^{1/k} M_P \dfrac{y_{\rm eff}^2}{8\pi}\,, & (\phi \to \bar{f} f)\,, \\ \dfrac{\mu_{\rm eff}^2}{8\pi\sqrt{k(k-1)}\lambda^{1/k} M_P}\,, & (\phi \to bb)\,, \\ \dfrac{\sigma_{\rm eff}^2 M_P}{8\pi[k(k-1)]^{3/2}\lambda^{3/k}}\,, & (\phi\phi \to bb)\,. \end{cases} \tag{2.107}$$

The integration of the equation for radiation energy density provides the generic solution [106]

$$\rho_R(a) = \frac{2k}{k+8-6kl}\frac{\gamma_\phi}{H_{\rm end}}\frac{\rho_{\rm end}^{l+1}}{M_P^{4l}}\left(\frac{a_{\rm end}}{a}\right)^4\left[\left(\frac{a}{a_{\rm end}}\right)^{\frac{k+8-6kl}{k+2}} - 1\right] \tag{2.108}$$

where for now we have neglected the effective masses of final states products ($\mathcal{R} \ll 1$) in this result (see section 2.3 for further details on the treatment of these effects). As decays of the condensate begin, the decay products are assumed to thermalize quickly and produce a thermal bath with an associated temperature $\rho_R = \frac{g_*\pi^2}{30}T^4$. We represent such evolution for arbitrary magnitudes of the couplings considered in Figure 2.4. The bath temperature reaches a maximum equivalent temperature $T_{\rm max}$ rapidly, and afterward, as inflaton decays, the temperature falls but not adiabatically. Instead, the temperature decreases more slowly as entropy is injected in the thermal bath from the condensate through continuing decays. The different slopes for the different channels and potential parameter k can be directly computed from Eq.(2.108) and are summarized in [106]. The reheating temperature is defined when the energy density in the radiation bath equals the energy density of the inflaton condensate $\rho_R(a_{\rm RH}) = \rho_\phi(a_{\rm RH})$. When $\mathcal{R} < 1$ and approximating ρ_ϕ as in Eq.(2.73) until the end of the reheating mechanism, it is easy to determine the reheating temperature from Eq.(2.108). The generic solution for the reheating temperature $T(a_{\rm RH}) \equiv T_{\rm RH}$

$$T_{\rm RH} = \left(\frac{30}{g_*\pi^2}\right)^{\frac{1}{4}}\left[\frac{2k}{8+k-6kl}\frac{\sqrt{3}\gamma_\phi}{M_P^{4l-1}}\right]^{\frac{1}{2-4l}} \tag{2.109}$$

when $8+k-6kl > 0$ whereas for $8+k-6kl < 0$ and $k > 4$ we obtain

$$T_{\rm RH} = \left(\frac{30}{g_*\pi^2}\right)^{\frac{1}{4}}\left[\frac{2k}{6kl-k-8}\frac{\sqrt{3}\gamma_\phi}{M_P^{4l-1}}\rho_{\rm end}^{\frac{6kl-k-8}{6k}}\right]^{\frac{3k}{4k-16}}\,. \tag{2.110}$$

In the first case, it is important to note that the reheating temperature is independent of $\rho_{\rm end}$ and entirely determined by the potential parameter k together with the coupling constant for the process considered. On the other hand, there is a dependence on the initial energy density of the inflaton in the second case. Furthermore, in the second case, there is no reheating possible if $k \leq 4$ as the inflaton energy density decreases faster than the radiation energy density produced

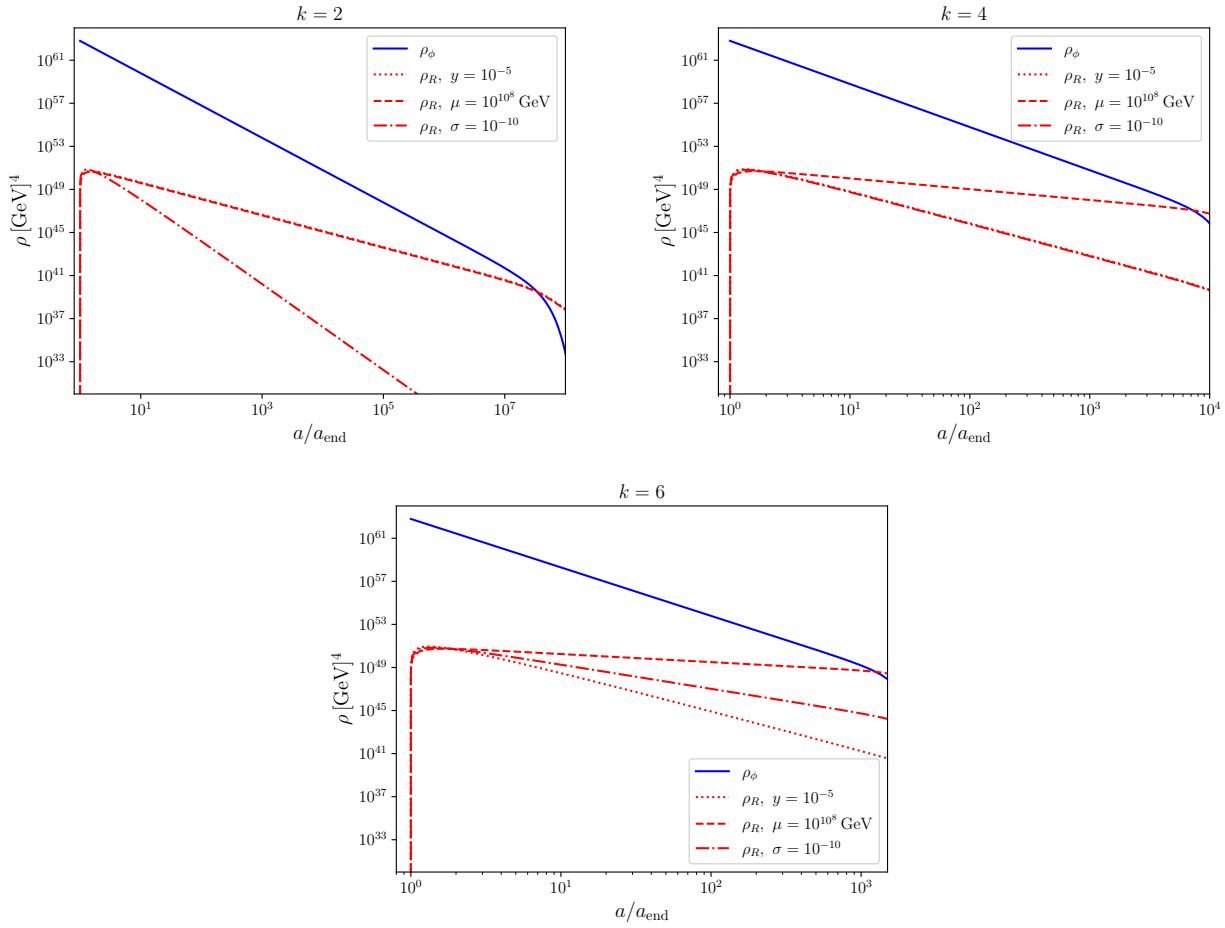

Figure 2.4: *Evolution of energy densities as a function of the scale factor after inflation. Boltzmann equations are integrated numerically. In blue is the inflaton energy density, and in red is the radiation energy density, for different production channels labeled by the associated coupling constant. We do not consider effective masses of the produced quanta in this plot. Top Left:* $k = 2$*, Top Right:* $k = 4$*, Bottom:* $k = 6$*.*

as can be seen for inflaton annihilation and $k = 2$ in Figure 2.4.

The non-standard temperature evolution during the reheating phase directly affects DM production after inflation for the UV freeze-in scenario (see section 1.4). In this case, DM production depends on the higher dimension effective operator that connects DM to the visible sector in the thermal bath. During the freeze-in production, the DM production rate from out-of-equilibrium scatterings can be parametrized the following way [86, 87]

$$R(T) = \frac{T^{n+6}}{\Lambda_{\mathrm{UV}}^{n+2}} \Leftrightarrow \langle \sigma v \rangle \propto \frac{T^n}{\Lambda_{\mathrm{UV}}^{n+2}} \tag{2.111}$$

which is a valid EFT description of the freeze-in production during reheating for $\Lambda_{\mathrm{UV}} > T_{\mathrm{max}}$. It leads to rich phenomenology depending on the dimension n of the EFT operator driving the production process and the DM relic density may depend on either the maximum temperature,

$T_{\max}$, the reheating temperature $T_{\rm RH}$, or both. Thus, the evolution of the temperature during reheating is extremely important for such scenarios [87, 106]. The evolution of energy densities during reheating also plays a crucial role in DM production directly from the inflaton [115–117]. The main goal of this thesis is to investigate a natural and minimal scenario of UV freeze-in during reheating through gravitational-mediated effective operators, including the production of particles from the inflaton. It is described in very detail throughout chapter 3.

2.2.4 Non-perturbative effects

We now discuss non-perturbative effects in the excitation of the fields coupled to the inflaton background while it oscillates. More precisely, we consider the effect of parametric resonances that trigger instability in the evolution of the mode functions for the coupled fields. We usually refer to such effects as preheating compared to a perturbative limit of reheating, as they are expected to occur at the beginning of the oscillations of the inflaton and lead quite rapidly to an enhancement of the occupation numbers of the fields. They further leave a classical state of high occupation numbers for the fields, but perturbative decays of the inflaton are usually still required to deplete its energy density efficiently at the end of the reheating process. We will consider as an example of such early non-perturbative evolution, the case of a massless scalar field χ, coupled to the inflaton through the renormalizable coupling

$$\mathcal{L} \supset \frac{1}{2} m_\phi^2 \phi^2 + \sigma \phi^2 \chi^2 \,. \tag{2.112}$$

This field can account for one degree of freedom of the SM or as a DM field excited during preheating. Such description can be generalized to any spin state and different renormalizable couplings [113, 118, 119], but the evolution of fields through the non-perturbative effects of preheating is usually model-dependent (couplings, spins, potential of the inflaton). Non-perturbative effects come from the short-time driven oscillations in the effective mass of the coupled field χ. For the purpose of this analysis, we consider that the inflaton oscillates in a quadratic potential after inflation ($k = 2$) with a constant effective mass $m_\phi^2 = \lambda M_P^2$ (where we consider the T-models potential as a benchmark). In this case, the equation of motion for the daughter fields is well known to be of the Mathieu type [113], with unstable solutions for the mode functions of the fields. Similar solutions can be found in a quartic potential $k = 4$; however, numerical tools are usually necessary for steeper potential $k > 4$ to study the evolution of the mode functions of coupled fields in such oscillating background.

Parametric resonances and preheating

We consider that the inflaton oscillates about a quadratic minimum with $V(\phi) \simeq \frac{1}{2}m_\phi^2\phi^2$ such that

$$\phi(t) = \phi_0(t) \cdot \cos(m_\phi t)\,. \tag{2.113}$$

$$\phi_0(t) \simeq \frac{\phi_{\rm end}}{m_\phi t} \tag{2.114}$$

and we assume that the normalization of λ is set by CMB anisotropies (see section 2.1) to be $\lambda \sim 10^{-11}$. If the amplitude of inflaton oscillations, $\phi_0(t)$, or the coupling constant σ, become large $\sigma\phi_0(t)^2 > m_\phi^2$, high-order Feynman diagrams can give comparable predictions to the lowest-order ones, signaling the failure of perturbative analysis. Non-perturbative effects can lead to exponential growth of the occupation number of the field and can be seen for a generic class of couplings as a parametric resonance mechanism. To understand this, we start with the equation of motion for the field χ

$$\left(\frac{d^2}{dt^2} - \frac{\nabla^2}{a^2} + 3H\frac{d}{dt} + m_\chi^2(t)\right)\chi = 0 \tag{2.115}$$

where $m_\chi^2(t) = 2\sigma\phi^2(t)$ is the time-varying mass of the field χ due to its quartic coupling to the inflaton background. On average, in this case, $\langle w_\phi\rangle \simeq 0$ and so the scale factor evolution is the same as during the matter-dominated era with

$$a(t) \simeq a_{\rm end}\left(\frac{t}{t_{\rm end}}\right)^{2/3}\,. \tag{2.116}$$

Using the field redefinition $x = a^{3/2}\chi$, we can rewrite the equation of motion for the Fourier modes of the field x as

$$\ddot{x}_p(t) + w_p^2(t)x_p = 0 \tag{2.117}$$

where

$$w_p^2(t) = \frac{p^2}{a^2} + \sigma\phi_0^2(t)\cos^2(m_\phi t) + \frac{9}{4}w_\phi(t)H^2(t)\,. \tag{2.118}$$

We work here in cosmic time t and comoving momentum p, and we do not average over the oscillations, as the small time scale dynamics are responsible for the transfer of energy through non-perturbative effects. We understand from this equation that after a few oscillations of the condensate, $w_\phi(t) \to 0$ and $\phi_0(t)$ is dumped, leading quite rapidly to stable harmonic oscillations of the modes and thus no instability. Thus, non-perturbative effects are expected to be important solely during the first few oscillations of the inflaton. They end after quite a few oscillations and are followed by any perturbative effects that can occur on top of the stable evolution of the modes, as we discussed in the preceding part.

There is a competition between two effects in the evolution of the mode function during the first oscillations: the expansion and dumping from the term $\propto H^2$, and the driving force due to the background through the coupling $\sigma\phi^2(t)$. At the end of inflation, we have on average $V(\phi_0) = \rho_\phi \implies H^2(t) \sim m_\phi^2\phi_0^2(t)/M_P^2$. Thus the ratio of the friction term to the driving term is approximately constant in magnitude during the oscillations

$$\frac{w_\phi H^2}{\sigma\phi^2} \sim \frac{w_\phi m_\phi^2}{\sigma M_P^2} \sim \frac{w_\phi \lambda}{\sigma} \tag{2.119}$$

and is negligible in the case of large couplings $\sigma \gg \lambda$. Especially at the end of inflation $H_{\rm end}^2 \simeq V(\phi_{\rm end})/M_P^2$, we find that in the very first oscillations, we can safely neglect the expansion in the limit of large couplings. In the regime $\sigma \ll \lambda$, we usually can treat the evolution with a good approximation using the perturbative analysis to compute the number densities [7].

In this perspective and to obtain analytical estimates, we first neglect completely the expansion of the Universe during the first oscillations. It is then useful to introduce the following variables

$$z \equiv m_\phi t, \quad A_p \equiv \frac{p^2}{m_\phi^2 a^2} + 2q, \quad q \equiv \frac{\sigma\phi_0^2}{2m_\phi^2} \sim \frac{\sigma}{\lambda} \tag{2.120}$$

where ϕ_0 is considered constant, A_p is the energy in the comoving mode p divided by the inflaton mass, while q is interpreted as the normalized coupling of the mode to the background, also called the resonance parameter. Under this parameterization, the mode equation takes the well-known form of a Mathieu equation

$$\frac{d^2x_p}{dz^2} + \left(A_p - 2q\cos\left(2z\right)\right)x_p = 0\,. \tag{2.121}$$

The Mathieu equation is known to exhibit unstable solutions for some specific values of the parameters q, A_p, called parametric resonances. This unstable evolution of the modes can be understood from its stability/instability chart, illustrated in Fig. 2.5. The white regions correspond to unstable regions, where the mode solutions grow exponentially as $x_p \propto \exp\left(\mu_p z\right)$, the characteristic exponent, μ_p, being called Floquet's exponent for the mode and can be computed by applying Floquet's theory of dynamical systems driven by periodic forces [113, 118]. A real positive Floquet's exponent triggers unstable exponential growth, while it induces oscillation when it is imaginary. The comoving particle occupation number in the mode p is given by [113]

$$n_p = \frac{\omega_p}{2}\left(\frac{|\dot{x}_p|^2}{\omega_p^2} + |x_p|^2\right) - \frac{1}{2} \tag{2.122}$$

[7] We note that in the regime $\sigma \simeq \lambda$ numerical analysis [119] show that the friction can importantly reduce the early production of particles compared to the perturbative analysis predictions

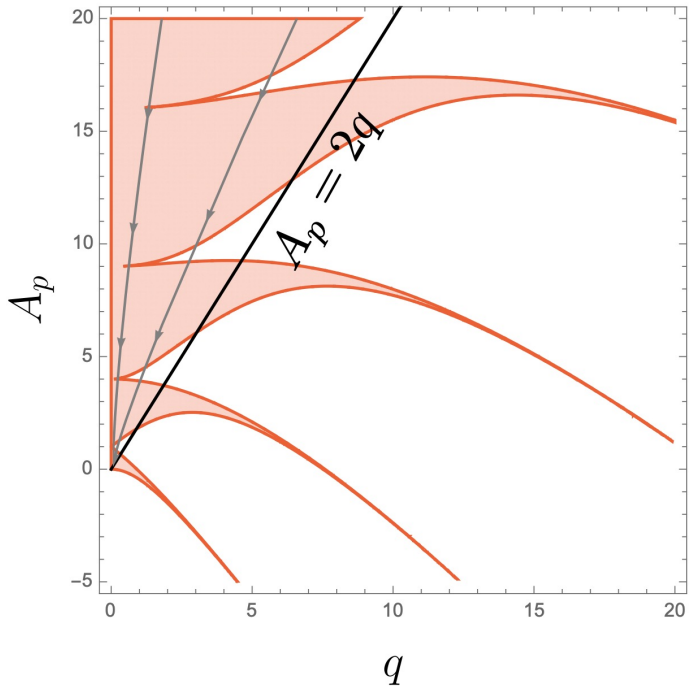

Figure 2.5: *Mathieu stability chart. The white regions correspond to instability bands, where the mode grows exponentially. The red regions correspond to stable regions, where the mode oscillates. The two grey lines correspond to the flow lines of two modes with different p. Figure taken from [119].*

and thus, as the mode functions exponentially grow, the associated occupation number grows as $n_p(t) \propto \exp(2\mu_p t)$, signaling non-perturbative productions of particles. $q \lesssim 1$ corresponds to the regime of "narrow resonance" which can be seen from Figure 2.5. The resonant particle production occurs mainly near the first instability band $A_p \sim 1 \pm q$ in this regime [113]. Yet, one can show that in this regime of narrow resonance the explosive particle production ends rapidly because of the expansion. Indeed, we have considered constant physical momenta p/a in the stability analysis; however, the redshifts drive the modes outside the narrow bands quite rapidly, as can be seen on the trajectory of a specific mode in the stability chart. In addition, the decrease of the amplitude $\phi_0(t)$ cannot be completely neglected when $q < 1$, even from the onset of the oscillations. The band becomes more and more narrow as $\phi_0(t)$ decreases and the combined effects result in a completely ineffective resonant process in the limit $q \ll 1$. In this limit, the perturbative analysis is valid [119].

Therefore, significant non-perturbative production in an expanding universe occurs mainly for $q \gtrsim 1$, called broad resonance regime. It corresponds to a highly non-perturbative regime where the resonance occurs still above the line $A_p = 2q$ in the stability chart. Occupation numbers grow exponentially until they are so large that the back-reaction effects become important. Because the inflaton amplitude decreases, each oscillation mode goes through lower amounts of bands and evolves toward the origin of the stability chart gradually. On the way, each mode has its own history of stability and instability, crossing different bands. In such models

with large q, the expansion of the Universe makes preheating occur as a stochastic resonance mechanism [113] depicted in Figure 2.6. At the end of the process, all the modes reach the limit

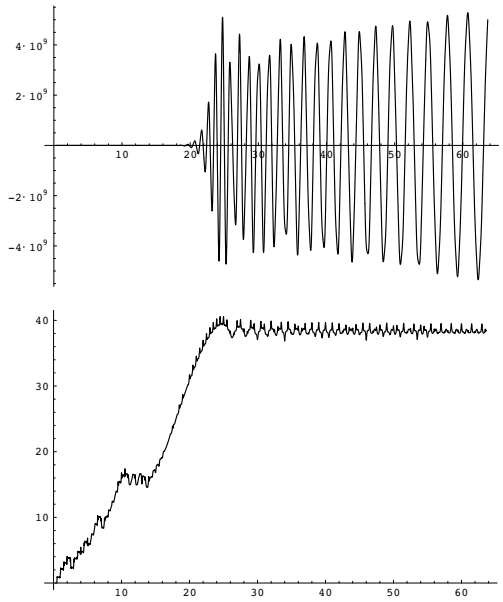

Figure 2.6: *Early stages of parametric resonance, showing the stochastic evolution of a specific mode function x_p (Top) and the associated evolution of the occupation number $n_p(t)$ (Bottom). Figure taken from [113]*

$q \simeq 1$ and enter the inefficient narrow resonance regime, ending the non-perturbative evolution. To summarize, using the kinematic parameter $\mathcal{R} = 4m_\chi^2(t)/m_\phi^2(t)$ introduced before, we have that non-perturbative effects become important when $\mathcal{R} \gg 1$ whereas in the limit $\mathcal{R} \lesssim 1$, perturbative analysis should give appropriate results [119]. In chapter 3, as we consider feeble gravitational couplings, we rely solely on perturbative analysis.

Backreactions and Inflaton fragmentation

Along this preheating stage, the produced particles with high occupation numbers can backreact on the inflaton background. In this case, non-linear interactions become important. The energy density of χ is smaller than the one of the inflaton during reheating, but for a sufficiently large coupling σ, the two can become comparable due to the enhancement of non-perturbative effects. This strong backreaction regime can be tackled by resolving the effect of the field χ in the motion of the background. One can use the Hartree approximation but accounting for these non-linear effects is usually tackled in classical numerical simulations. At large occupation numbers for a sufficiently large coupling, the quantum fields and their perturbations can be approximated as classical and hence studied by solving the classical system of equations of motion without the need to track each mode function separately. Modern numerical tools have been developed to track the evolution of classical fields and their inhomogeneities in the non-linear regime and in an expanding background. The main approach relies on discretizing space-time on a

spatial lattice to solve the non-linear partial differential equations of motions on each lattice site. Public codes such as `CosmoLattice` [120] are the main tools available. Figure 2.7 shows the results of [119] where the authors used `CosmoLattice`, to follow the evolution of the energy densities as a function of time during reheating. We see that for small couplings, the stochastic

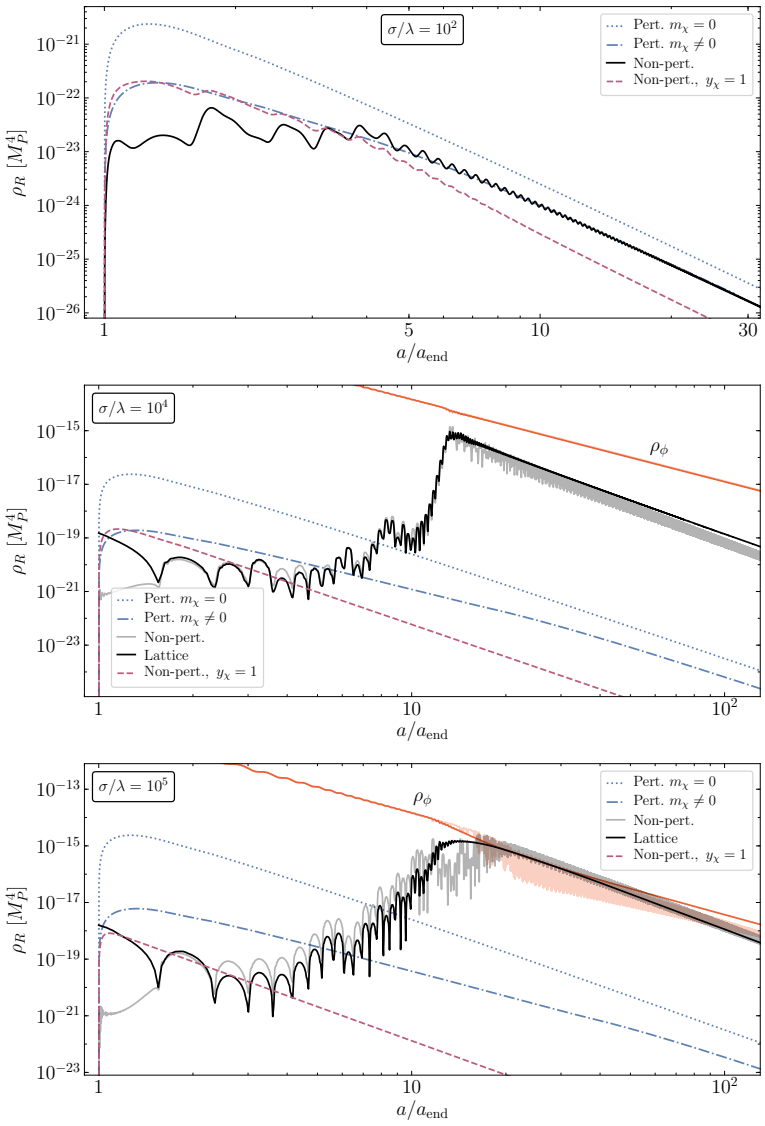

Figure 2.7: *Energy density in relativistic bosons ρ_χ during reheating as a function of the scale factor, for different values of the ratio σ/λ. Results are from perturbative computation when effective mass is ignored (dotted blue) and accounted for (in dashed-dotted blue), computed non-perturbatively in the Hartree approximation (transparent black) using* `CosmoLattice` *(solid black). Figure taken from [119].*

resonances end quite rapidly and provide results similar to those of perturbative computations. For larger and larger couplings, the enhancement of energy density is more and more important, potentially leading to a stage of strong backreactions requiring this numerical analysis.

The effect of rescatterings of produced particles on the background can lead to the disruption of the coherency of the inflaton condensate. This can be seen as a production of inflaton quanta

from interactions, that are not in the lowest energy state and it can significantly alter the further evolution of the universe. Interestingly, in a non-quadratic potential $k > 2$, inflaton exhibits self-interactions which transfer the energy of the coherent homogeneous condensate into inhomogeneous fluctuations $\delta\phi(x,t)$ [118, 121–123]. This can occur even without interactions of the inflaton with other fields. The equation of motion of the inflaton perturbations in a potential $V(\phi) \simeq \lambda M_P^4 \left(\frac{\phi}{M_P}\right)^k$ (with $k > 2$) is given by

$$\delta\ddot{\phi} + 3H\delta\dot{\phi} - \frac{\nabla^2\delta\phi}{a^2} + k(k-1)\lambda M_P^2 \left(\frac{\phi(t)}{M_P}\right)^{k-2} \delta\phi = 0 \tag{2.123}$$

where the perturbations originate initially from quantum fluctuations given by the Bunch-Davies vacuum. The growth of these inhomogeneities can be described with parametric resonances and an exponential growth of the occupation number in inflaton perturbations is expected. Redefining the field $X = a\delta\phi$ and making the change of time variable to conformal time $ad\eta = dt$, the mode equation for inflaton quanta is given by

$$X'' + w_p^2 X_p = 0 \tag{2.124}$$

with (see section 2.1)

$$w_p^2 = \frac{p^2}{a^2} - \frac{a''}{a} + a^2 m_\phi^2(a)\,. \tag{2.125}$$

The driving term that leads to fragmentation through parametric resonance is thus given by $a^2 m_\phi^2(a)$. The resonance structure associated with this equation of motion varies with time for $k > 4$ but is time-independent for $k = 4$, as $m_\phi(a) \propto 1/a$ [122, 123], this fact originating from the conformal invariance of the ϕ^4 theory. In Figures 2.8, the authors of [123] show the evolution of the energy density in inflaton perturbations using `CosmoLattice` for different shapes of the inflaton potential $k = 4, 6, 8$. In this evolution, the early growth of perturbation is approximately following the parametric resonances regime until backreactions on the inflaton background become important. Afterward, the inflaton sector can be considered to be dominated by its perturbations as a gas of relativistic particles in a highly non-linear turbulent regime [118]. The condensate does not disappear completely and the relic condensate generates a mass term for the inflaton particles which allows them to decay further and complete reheating if their decay width dominates the expansion rate $\Gamma_{\delta\phi} \gtrsim H$. The impact of fragmentation of the condensate on the reheating process at late time is explored widely in [119], for different couplings and values of k.

An important effect of the fragmentation of the background is that it gradually leads to a different equation of state for the Universe during reheating, as the condensate is destroyed and replaced by a turbulent gas of inflation quanta. From $\langle w \rangle = \frac{k-2}{k+2}$ it is attracted to a radiation-like equation of state $\langle w \rangle \to 1/3$ as we see in the bottom panels of Figure 2.8. However, taking

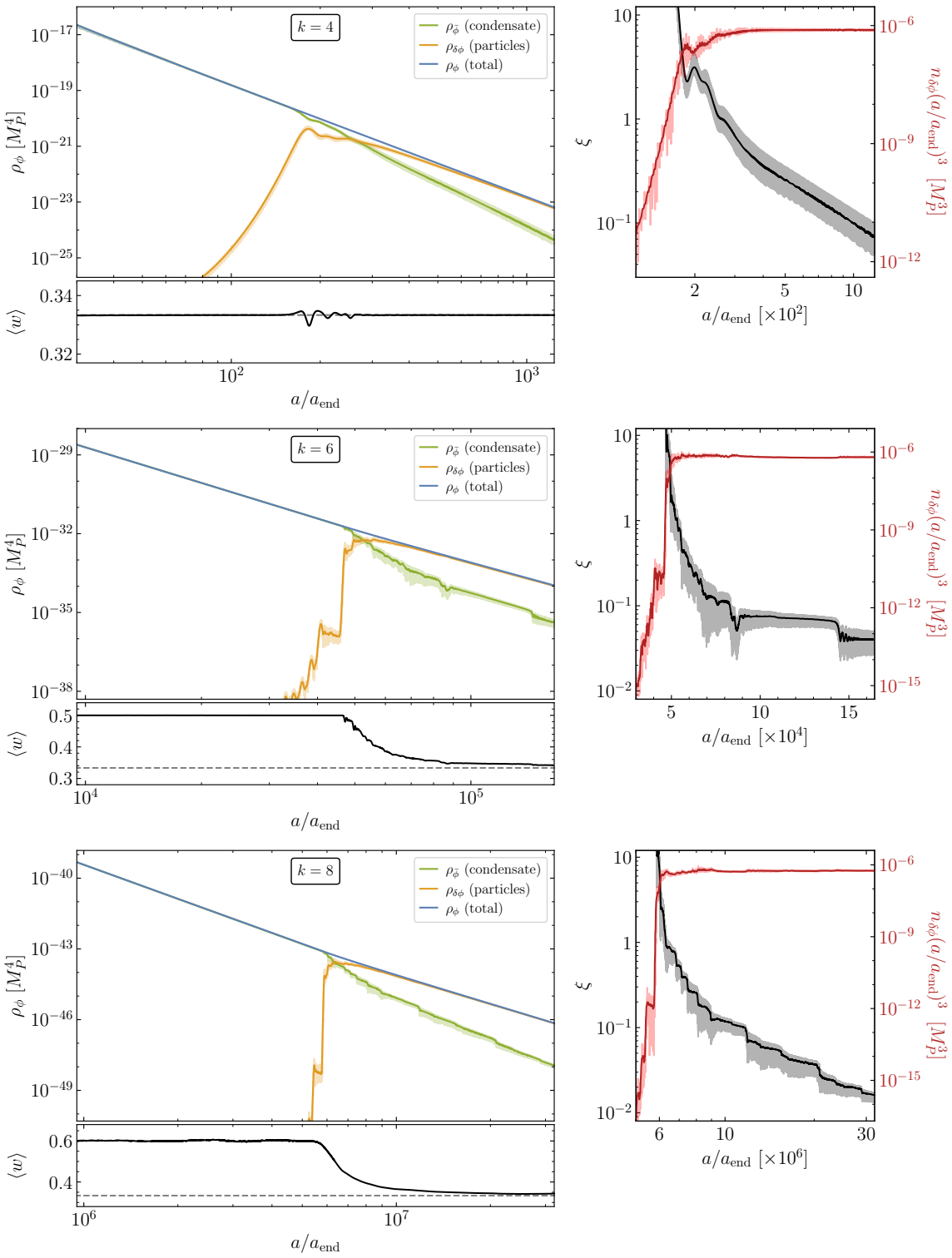

Figure 2.8: *Left: Inflaton energy density in the classical condensate (green), in inflaton particles (yellow), and the sum of both (blue), as functions of the scale factor. Right: Ratio of the energy densities in condensate over particles ξ (black) and comoving number density of inflaton particles $n^3_{\delta\phi}$ (red), during and after fragmentation. Bottom panels: the averaged equation of state during and after fragmentation. Figures taken from [123].*

the expansion into account, due to the faster redshift of the effective mass term $m_\phi^2(t)$, together with the time dependence of the resonance structure, the fragmentation process is expected to be less efficient for steeper potential and to occur on a larger time scale for increasing k [118, 119]. In chapter 3, we explore the possibility of purely gravitational reheating which, as we will see, requires looking at steep inflaton potential with $k > 6$ (high value of the equation of state). Therefore, we expect the effect of self-resonances and fragmentation to be less efficient, allowing us to consider the inflaton condensate as the main component driving the evolution during reheating in this case.

2.3 Reheating in a mixed potential: bare mass effects

This section is based on: **S. Cléry**, M. A.G. Garcia, Y. Mambrini, K.A. Olive, *Bare mass effects on the reheating process after inflation*, **Phys.Rev.D 109 (2024) 10, 103540**, arXiv:2402:16958 [4]

Motivation

The process of transferring the energy stored in inflation oscillations to the SM particles is not instantaneous, as seen in section 2.2. An oscillating inflaton condensate can decay or scatter progressively, producing a bath of relativistic particles. The efficiency of the reheating process depends on the rate of the energy transfer as well as on the shape of the inflaton potential, $V(\phi)$, about its minimum. Even if the exact shape of the potential at the end of inflation is unknown it can often be approximated about its minimum by a polynomial function of ϕ. In many models of inflation, the inflaton potential can be approximated about its minimum by a quadratic term, $V(\phi) = \frac{1}{2}m_\phi^2\phi^2$. The Starobinsky model [93] is one example. In this case, only one Fourier mode of the inflaton oscillation contributes to the reheating process. For a potential whose expansion about its minimum is $V(\phi) = \lambda\phi^k$, with $k \geq 4$, the exercise is more subtle and requires a more involved analysis as detailed in section 2.2. The reheating process will, in general, depend on the spin of the final state particles in either inflaton decays or scatterings, and in some cases, reheating does not occur. However, we cannot exclude the presence of a bare mass term $\frac{1}{2}m_\phi^2\phi^2$, which may be subdominant at the end of inflation, and during the early phases of the oscillations, but which becomes dominant when ϕ has redshifted. The presence of this term, even if it is small, would then modify the reheating mechanisms. In this section, we consider the effects of a bare mass term for the inflaton, when the inflationary potential takes the form $V(\phi) = \lambda\phi^k$ about its minimum with $k \geq 4$. We concentrate on $k = 4$, but discuss general cases as well. We study the impact of such a mass term on reheating processes, as the equation of state of the inflaton condensate changes from $w_\phi = \frac{1}{3}$ to $w_\phi = 0$. We compute the effects on the reheating temperature for cases where reheating is due to inflaton decay (to fermions, scalars, or vectors) or to inflaton scattering (to scalars or vectors). For scattering

to scalars and in the absence of a decay, there is always a residual inflaton background which acts as cold dark matter. We also briefly consider the effect of the bare mass term on the fragmentation of the inflaton condensate.

2.3.1 The transition, $\phi^4 \to \phi^2$

We begin by supposing that the dominant contribution in a series expansion of the inflaton potential about its minimum is the quartic term and that at the end of inflation, this dominates over a quadratic mass term, so that

$$\lambda\phi_{\rm end}^4 \gg \frac{1}{2}m_\phi^2\phi_{\rm end}^2\,. \tag{2.126}$$

For $a > a_{\rm end}$, the evolution of the energy density of ϕ is governed by the Boltzmann equation for ρ_ϕ Eq.(2.85)

$$\frac{d\rho_\phi}{dt} + 3(1+w)H\rho_\phi \simeq 0\,. \tag{2.127}$$

For $k = 4$, Eq. (2.127) gives

$$\rho_\phi = \rho_{\rm end}\left(\frac{a_{\rm end}}{a}\right)^4\,, \tag{2.128}$$

where $\rho_{\rm end}$ is the value of the density of energy of the inflaton at the end of inflation, $\rho_{\rm end} = \frac{3}{2}V(\phi_{\rm end})$. For the T-models with potential given in Eq. (2.61) we have,

$$\phi_{\rm end} \simeq \sqrt{\frac{3}{8}}\,M_P \ln\left[\frac{1}{2} + \frac{k}{3}\left(k + \sqrt{k^2+3}\right)\right]\,. \tag{2.129}$$

The parameter λ in Eq. (2.61) is determined from the normalization of the CMB anisotropies [15]. The normalization of the potential for different values of k can be approximated by Eq.(2.64) where $A_{S*} \simeq 2.1 \times 10^{-9}$ is the amplitude of the curvature power spectrum. For $N_* = 56$ e-folds we find $\lambda = 3.3 \times 10^{-12}$, and $\rho_{\rm end}^{\frac{1}{4}} = 4.8 \times 10^{15}$ GeV (when $k = 4$).

We solve the equation of motion for the inflaton as in Eq.(2.74), introducing $\mathcal{P}(t)$ a quasiperiodic function encoding the (an)harmonicity of short-timescale oscillations in the potential and ϕ_0 the envelope of the oscillations. As ϕ_0 decreases, eventually the evolution of the condensate will be governed by the quadratic term. This occurs at $a = a_{\rm m}$ when

$$\frac{1}{2}m_\phi^2\phi_0^2(a_{\rm m}) = \lambda\phi_0^4(a_{\rm m})\,. \tag{2.130}$$

Using $\phi_0^4(a) = (\rho_{\rm end}/\lambda)(\frac{a_{\rm end}}{a})^4$ for $a_{\rm end} < a < a_{\rm m}$ gives

$$\frac{a_{\rm m}}{a_{\rm end}} = \left(\frac{4\lambda\rho_{\rm end}}{m_\phi^4}\right)^{1/4} \simeq 9.1 \times 10^3\left(\frac{10^9\ {\rm GeV}}{m_\phi}\right)\,. \tag{2.131}$$

In deriving (2.131), we note that the envelope function ϕ_0 is determined by the average energy density $\langle\rho_\phi\rangle = V(\phi_0)$. Thus unless reheating occurs rapidly, the quadratic term will dominate the reheating process even if the quartic dominates after when oscillations begin. This will have huge consequences on the reheating temperature, as well as on the Physics of fragmentation as we will see.

Indeed, if reheating occurs at $a = a_{\rm RH} > a_{\rm m}$, the process is affected by the bare mass term. For $a > a_{\rm m}$, the equation of state changes from $w = 1/3$ (for $k = 4$) to $w = 0$ (for $k = 2$) and the solution for $a \gg a_m$ to the Friedmann equation becomes

$$\rho_\phi = \frac{1}{2}\rho_\phi(a_{\rm m})\left(\frac{a_{\rm m}}{a}\right)^3 = \rho_{\rm end}\left(\frac{a_{\rm end}}{a_{\rm m}}\right)^4\left(\frac{a_{\rm m}}{a}\right)^3 . \tag{2.132}$$

Furthermore,

$$\rho_{\rm m} \equiv \rho_\phi(a_{\rm m}) = 2\rho_{\rm end}\left(\frac{a_{\rm end}}{a_{\rm m}}\right)^4 = \frac{m_\phi^4}{2\lambda} . \tag{2.133}$$

Combining Eqs. (2.131) and (2.132) we obtain

$$\rho_\phi|_{a>a_{\rm m}} = \frac{m_\phi \rho_{\rm end}^{\frac{3}{4}}}{(4\lambda)^{\frac{1}{4}}}\left(\frac{a_{\rm end}}{a}\right)^3 . \tag{2.134}$$

This form for ρ_ϕ dominates the energy density until reheating when $\rho_\phi(a_{\rm RH}) = \rho_{\rm R}(a_{\rm RH})$. Here, $\rho_{\rm R}$ is the energy density transferred to the thermal bath via the Boltzmann equation

$$\frac{d\rho_R}{dt} + 4H\rho_R = (1+w)\Gamma_\phi\rho_\phi . \tag{2.135}$$

From the above, we can determine the reheating temperature for a given mass, m_ϕ for which the bare mass affects the reheating process, and therefore modifies the calculation of $T_{\rm RH}$. The condition $a_{\rm m} < a_{\rm RH}$ implies that $\rho_{\rm m} > \rho_\phi(a_{\rm RH})$ and thus the condition for the quadratic part to dominate the reheating process is given by

$$\rho_{\rm m} \gtrsim \rho_{\rm RH} \quad \Rightarrow \quad \rho_{\rm RH} \lesssim \frac{m_\phi^4}{2\lambda} , \tag{2.136}$$

from Eq.(2.133). Using $\rho_{\rm RH} = \alpha T_{\rm RH}^4$ with $\alpha = \frac{g_{\rm RH}\pi^2}{30}$ for $g_{\rm RH}$ relativistic degrees of freedom at $a_{\rm RH}$, we obtain

$$T_{\rm RH} \lesssim \frac{m_\phi}{(2\alpha\lambda)^{\frac{1}{4}}} \simeq 250\ m_\phi , \tag{2.137}$$

which means that if the energy transfer between the condensate and the thermal bath is slow and the reheating temperature $T_{\rm RH}$ lower than the limit obtained in the equation (2.137), we must take into account the quadratic term to determine $T_{\rm RH}$ when $a_{\rm RH} > a_{\rm m}$.

2.3.2 Limits on the inflaton bare mass

As noted earlier, the CMB observables impose an upper limit to m_ϕ. Planck [15] has determined with relatively high precision, the value for the tilt of the CMB anisotropy spectrum, $n_s = 0.9649 \pm 0.0042$ (68% CL). In addition, the tensor-to-scalar ratio, $r < 0.036$ is constrained by BICEP/Keck observations [124, 125]. To translate these limits to an upper limit on m_ϕ, we use the T-model in Eq. (2.61) as an example. Recall that the conventional slow-roll parameters for a single-field inflationary model are given by

$$\epsilon_V \equiv \frac{1}{2} M_P^2 \left(\frac{V'}{V}\right)^2 , \qquad \eta_V \equiv M_P^2 \left(\frac{V''}{V}\right) , \tag{2.138}$$

the scalar tilt and tensor-to-scalar ratio can be expressed in terms of the slow roll parameters as (see section 2.1)

$$n_s \simeq 1 - 6\epsilon_{V*} + 2\eta_{V*} , \tag{2.139}$$

$$r \simeq 16\epsilon_{V*} . \tag{2.140}$$

In a more precise model determination of N_*, and n_s, there is some dependence on the reheating temperature and equation of state [126, 127]. The computation is based on the self-consistent solution of the relation between N_* and its corresponding pivot scale k_*,

$$\begin{aligned} N_* = & \ln\left[\frac{1}{\sqrt{3}}\left(\frac{\pi^2}{30}\right)^{1/4}\left(\frac{43}{11}\right)^{1/3}\frac{T_0}{H_0}\right] - \ln\left(\frac{k_*}{a_0 H_0}\right) \\ & - \frac{1}{12}\ln g_{\rm RH} + \frac{1}{4}\ln\left(\frac{V(\phi_*)^2}{M_P^4 \rho_{\rm end}}\right) \\ & + \ln\left[\frac{a_{\rm end}}{a_{\rm RH}}\left(\frac{\rho_{\rm end}}{\rho_{\rm RH}}\right)^{1/4}\right] , \end{aligned} \tag{2.141}$$

where the present Hubble parameter and photon temperature are given by $H_0 = 67.36\,\mathrm{km.s^{-1}.Mpc^{-1}}$ [15] and $T_0 = 2.7255$ K [128]. For the T-models dominated by a quadratic term, agreement with Planck/BICEP/Keck data requires N_* between roughly 42 - 56 [129].

In the absence of a mass, $m_\phi = 0$, $N_* \simeq 56$ with $\phi_* = 6.96 M_P$ and $(n_s, r) = (0.964, 0.0034)$, independently of the efficiency of reheating [106, 122]. Therefore, to set limits on a possible mass term for $k = 4$, we set $N_* = 56$. For non-zero masses both n_s and r increase, but the limit on m_ϕ is determined mainly from n_s. Figs. 2.9 and 2.10 show the numerically computed CMB observables n_s and r for a variety of bare masses and inflaton-matter couplings. As is customary, the *Planck* ($k_* = 0.05\,\mathrm{Mpc^{-1}}$) and WMAP ($k_* = 0.002\,\mathrm{Mpc^{-1}}$) pivot scales are chosen for n_s and r, respectively. For $m_\phi \neq 0$, the effective equation-of-state parameter evolves as $w = -1/3 \to 1/3 \to 0 \to 1/3$ from the end of inflation to the end of reheating. The

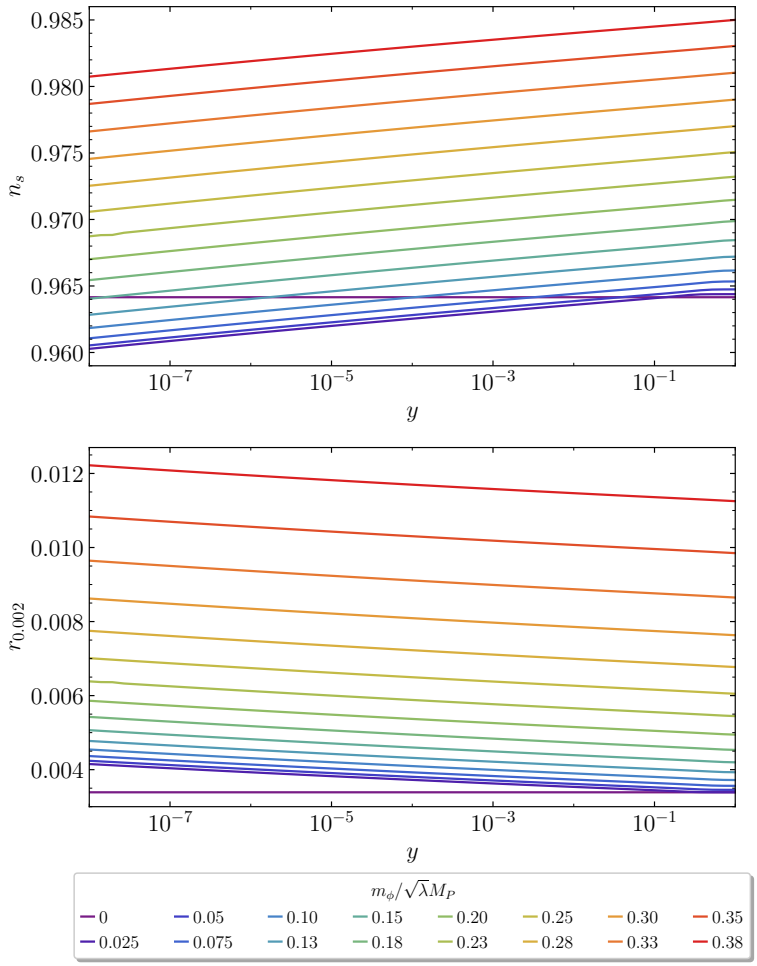

Figure 2.9: *Scalar tilt n_s (top) and tensor-to-scalar ratio r (bottom) as functions of the Yukawa coupling y (2.143), for a selection of bare masses m_ϕ and $k = 4$.*

dependence of N_* on the instantaneous equation-of-state parameter can be made evident by rewriting the last term of (2.141) as

$$\ln\left[\frac{a_{\rm end}}{a_{\rm RH}}\left(\frac{\rho_{\rm end}}{\rho_{\rm RH}}\right)^{1/4}\right] = \frac{1-3w_{\rm int}}{12(1+w_{\rm int})}\ln\left(\frac{\rho_{\rm RH}}{\rho_{\rm end}}\right), \tag{2.142}$$

where $w_{\rm int}$ denotes the e-fold average of the equation of state parameter during reheating [127]. The top panel of Fig. 2.9 depicts the bare mass dependence of the scalar tilt, as a function of an inflaton-matter Yukawa coupling (see Eq. (2.143)). For $m_\phi = 0$, $N_* \simeq 56$ for any y, leading to the purple horizontal line. For $m_\phi = 0.025\sqrt{\lambda}M_P$, the smallest non-zero mass in the Figure, the resulting curve presents two regimes. At $y \gtrsim 10^{-1}$, n_s is independent of y since reheating is completed before matter domination, $a_{\rm RH} < a_{\rm m}$. However, for $y \lesssim 10^{-1}$, reheating is completed by the dissipation of the quadratic, harmonic oscillations of ϕ. A dependence of n_s on y is induced, since now the last term of (2.141) is relevant for the determination of N_*. For smaller y reheating is delayed, resulting in a smaller N_* and as a consequence n_s. In the case of larger

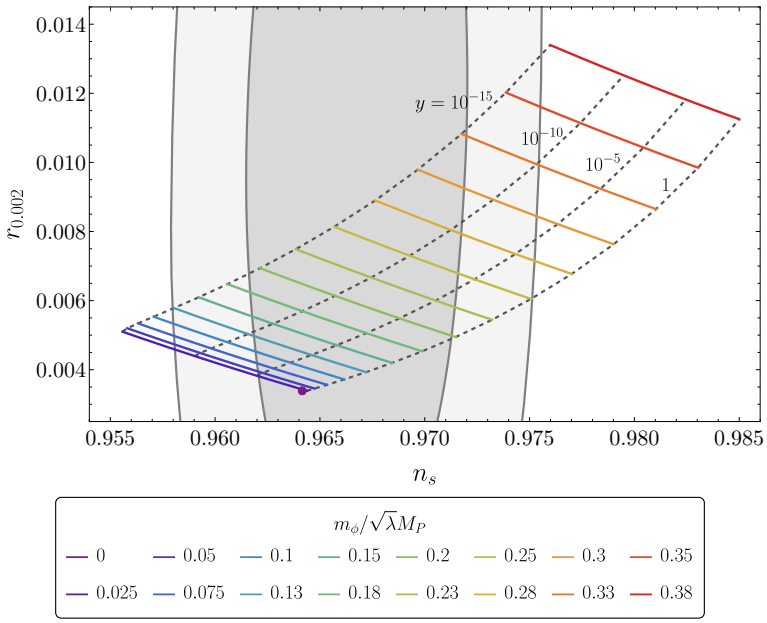

Figure 2.10: *Same as Fig. 2.9 shown in the (n_s, r) plane. The gray (light gray) shaded regions correspond to the 68% (95%) C.L. Planck+BK18 regions [124].*

masses, the pure quartic regime is reduced, or outright lost, and the relation of n_s and y is determined by the duration of reheating in the matter dominated era, and the modification of the slow roll dynamics due to the presence of the large bare mass. Analogous conclusions can be drawn from the bottom panel of Fig. 2.9. In this case the addition of the bare mass increases the value of the tensor-to-scalar ratio, both from the modified inflation dynamics, and from the dependence on y of the number of e-folds N_*.

Fig. 2.10 compares the corresponding (n_s, r) curves against the *Planck*+BK18 constraints [124]. Here the range of couplings spans reheating temperatures from $T_{\rm RH} \sim 2 \times 10^{14}$ GeV for $y = 1$, to $T_{\rm RH} \sim \mathcal{O}(10)$ MeV for $y = 10^{-15}$. We note that for the smallest bare masses high reheating temperatures are favored by the CMB data. On the other hand, for the largest masses considered, lower $T_{\rm RH}$ are preferred. At the nominal $N_* = 56$, corresponding to $y \approx 1$ in the figure, we find that $m_\phi < 0.2\sqrt{\lambda}M_P \simeq 8.8 \times 10^{11}$ GeV at 68% CL with $(n_s, r) = (0.971, 0.0050)$ and $m_\phi < 0.25\sqrt{\lambda}M_P \simeq 1.1 \times 10^{12}$ GeV at 95% CL with $(n_s, r) = (0.975, 0.0061)$. Above these masses, the values of n_s and r rise very quickly and agreement with data is lost. Applying this limit on m_ϕ in Eq. (2.137) gives $T_{\rm RH} \lesssim 2.8 \times 10^{14}$ GeV. In other words, for larger reheating temperatures, the energy transfer is sufficiently efficient to avoid any interference of a possible quadratic interaction without violating the CMB data. Allowing for the full range in coupling y or equivalently $T_{\rm RH}$ and expanding the range in N_*, we see from Fig. 2.10, that the 68% CL upper limit is $m_\phi < 0.33\sqrt{\lambda}M_P = 1.4 \times 10^{12}$ GeV (for $y \geq 10^{-15}$ and a 95% CL upper limit of $m_\phi \lesssim 0.38\sqrt{\lambda}M_P = 1.6 \times 10^{12}$ GeV. For larger masses it becomes impossible to simultaneously satisfy the *Planck* constraints to 2σ and the BBN bound $T_{\rm RH} \gtrsim$ MeV.

In addition to an upper bound to m_ϕ, we expect that radiative corrections to the potential will provide finite mass, which, unless fine-tuned away, will determine a lower bound on the inflaton mass. Since the inflaton must (at some level) be coupled to SM particles, loops involving SM particles with weak scale masses will contibute radiatively to the inflaton mass. Therefore, we expect that the coupling of the inflaton to either fermions or scalars would lead to a mass term proportional to ym_f or μ (see Eqs. (2.143) and (2.156) for couplings to fermions and scalars respectively. While loops involving SM fermions are probably no larger than the weak scale, the coupling to scalars could generate a significant contribution to m_ϕ. Furthermore, in a supersymmetric theory we would also expect contributions to the scalar mass of order the supersymmetry breaking scale. However, as noted, any lower limit to the inflaton mass would be subject to the degree of fine-tuning by canceling a bare mass term with any 1-loop corrections. Therefore unlike the upper limit discussed above, we do not apply a firm lower limit its mass, but recognize that it should not be surprising to generate weak scale masses, even in theories with the potential given in Eq. (2.61) for $k \geq 4$.

2.3.3 Consequences of the inflaton coupling to matter

Reheating to create a thermal bath of Standard Model particles requires some coupling of the inflaton to the Standard Model. The relation between this coupling and the reheating temperature is dependent not only on the shape of the inflaton potential about its minimum, but also on whether the reheating is produced by inflaton decay (in to either fermions, scalars or vectors) or scattering. As in [87, 106] we will study the three possible cases: fermion decay, scalar decay and scalar scattering, adding the vectorial final states (decay and scattering) analyzed in [114].

Inflaton decay to fermions

Given a Yukawa-like coupling of the inflaton to fermions,

$$\mathcal{L}_{\phi ff} = y\phi \bar{f} f \,, \tag{2.143}$$

the inflaton decay rate is

$$\Gamma_\phi = \frac{y_{\rm eff}^2}{8\pi} m_\phi \,. \tag{2.144}$$

Here, the effective Yukawa coupling $y_{\rm eff}(k) \neq y$ is defined by averaging over an oscillation. In general for $k \neq 2$, the effective coupling must be calculated numerically [106, 130, 131]. The general expressions for the reheating temperature, defined by $\rho_\phi(a_{\rm RH}) = \rho_{\rm R}(a_{\rm RH})$ and $\alpha T_{\rm RH}^4 = \rho_{\rm R}(a_{\rm RH})$, are given in section 2.2. $T_{\rm RH}$ depends strongly on the spin of the final state

decay products, and for decays to fermions, Eq. (2.109) gives with $l = 1/2 - 1/k$ and $k < 7$

$$T_{\rm RH} = \left(\frac{1}{\alpha}\right)^{\frac{1}{4}} \left[\frac{k\sqrt{3k(k-1)}}{7-k}\lambda^{\frac{1}{k}}\frac{y_{\rm eff}^2}{8\pi}\right]^{\frac{k}{4}} M_P\,, \tag{2.145}$$

or

$$T_{\rm RH} = \begin{cases} \left(\frac{\lambda}{\alpha}\right)^{\frac{1}{4}} \frac{y_{\rm eff}^2}{\pi} M_P \simeq 4.2\times 10^{14} y_{\rm eff}^2 \text{ GeV} & k = 4\,, \\ \left(\frac{3}{\alpha}\right)^{\frac{1}{4}} \left(\frac{y_{\rm eff}^2 m_\phi M_P}{20\pi}\right)^{\frac{1}{2}} & \\ \quad \simeq 3.3\times 10^{12} y_{\rm eff}\sqrt{\frac{m_\phi}{10^9 \text{GeV}}} \text{ GeV} & k = 2\,. \end{cases} \tag{2.146}$$

Notable in Eq. (2.146) is that $T_{\rm RH}$ exhibits a different dependence on the coupling and mass of the inflaton. In particular, $T_{\rm RH} \propto y_{\rm eff}^2$ in the case $a_{\rm m} > a_{\rm RH}$, $T_{\rm RH} \propto y_{\rm eff}\sqrt{m_\phi}$ if $a_{\rm m} < a_{\rm RH}$. We will see that for sufficiently low coupling, the quadratic term can dominate the reheating process leading to a higher reheating temperature.

When the limit in Eq. (2.137) is satisfied, reheating is sufficiently late to be determined by the quadratic term ($k = 2$ in Eq. (2.146)) and that can be translated into a limit on the coupling $y_{\rm eff}$,

$$y_{\rm eff} \lesssim y_{\rm eff}^{\rm m} = 0.02\sqrt{\frac{m_\phi}{10^9 \text{ GeV}}}\,. \tag{2.147}$$

We show in Fig. 2.11 the value of the reheating temperature as function of $y_{\rm eff}$ for different values of the inflaton bare mass $m_\phi = 10^3$, 10^9 and 10^{11} GeV, neglecting the effects of an effective final state mass (see below) and thus $y_{\rm eff} = y$. To obtain the figure, we solved numerically the complete set of Friedmann equations for ρ_R and ρ_ϕ, taking the full potential $V(\phi) = \frac{1}{2}m_\phi^2\phi^2 + \lambda\phi^4$. We also show for comparison with dashed lines, the analytical value of $T_{\rm RH}$ obtained in Eqs. (2.146). We clearly see the change of behavior $T_{\rm RH} = f(y_{\rm eff})$ below the limiting value in Eq. (2.147) where the bare mass term controls the final reheating temperature. For $y_{\rm eff} \lesssim y_{\rm eff}^{\rm m}$, $T_{\rm RH} \propto y_{\rm eff}$, whereas for larger values of $y_{\rm eff}$, when the reheating is dominated by the quartic part of the potential, the reheating temperature $\propto y_{\rm eff}^2$ and is independent of m_ϕ.

A background field value for ϕ, however, induces an effective mass for the fermion, f, $m_{\rm eff} = y\phi$, and the rates for producing the fermions are suppressed by $\mathcal{R}^{-1/2}$ where $\mathcal{R} \propto m_{\rm eff}^2/m_\phi^2 \propto y^2(\phi_0/M_P)^{4-k}/\lambda$ [106].[8] The mass of the inflaton is defined by

$$m_\phi^2(t) \;\equiv\; V''(\phi_0(t))\,. \tag{2.148}$$

When $\mathcal{R} \gg 1$, there is a significant suppression in the decay rate and $y_{\rm eff} \ll y$. Note that in the case of a quartic potential, $m_\phi \propto \phi$. As $m_{\rm eff} \propto \phi$ also, $\mathcal{R}$ is constant, $\mathcal{R} \simeq 1.4y^2/\lambda \simeq 4.2\times 10^{11} y^2$.

[8] Collective effects can additionally become important for sufficiently large couplings y, resulting in a further Pauli suppression for the efficiency of the decays. For $k = 2$, these preheating effects become relevant for $y \gtrsim 10^{-5}$ [119].

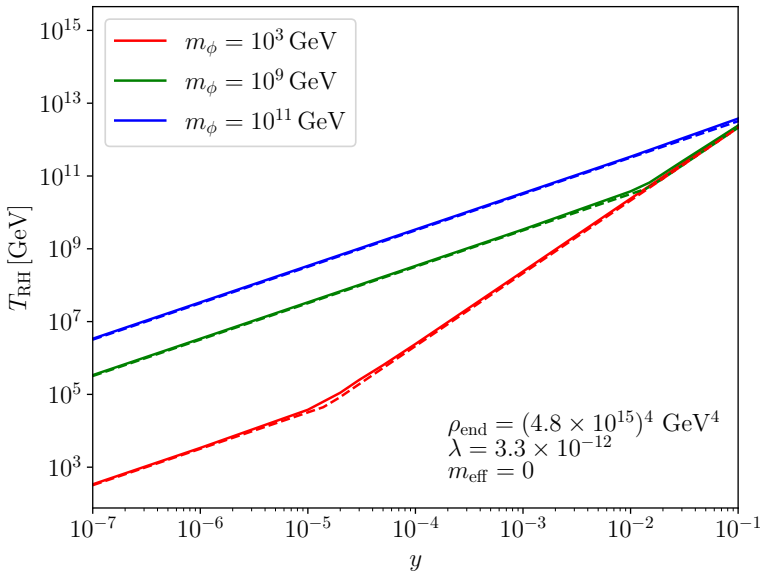

Figure 2.11: *Reheating temperature as a function of the Yukawa coupling y when a bare mass term is added to a quartic potential ($k = 4$). Solid lines are obtained by solving numerically the Boltzmann equations for energy densities, while dashed lines are given by the analytical approximations in Eqs. (2.146) Here we neglect the effective mass of the final state fermion, $\mathcal{R} = 0$ and $y_{\rm eff} = y$.*

In other words, the effect of $\mathcal{R}$ results in a suppression of the reheating efficiency by a constant factor $\mathcal{R}^{-\frac{1}{2}} \simeq 1.5 \times 10^{-6}/y$ throughout the reheating process. This suppression begins to be efficient ($\mathcal{R} \gtrsim 1$) for $y \gtrsim 1.5 \times 10^{-6}$ [106]. On the other hand, for a quadratic potential, $\mathcal{R} = 4(\phi_0/m_\phi)^2 y^2$ *decreases* with time, redshifting as $a^{-\frac{3}{2}}$. Which means that if there is no suppression during the quartic dominated era ($a < a_{\rm m}$), there is no suppression in the quadratic era ($a > a_{\rm m}$).

The kinematic suppression in the effective coupling $y_{\rm eff}$ for $\mathcal{R} \gg 1$ can be parametrized as [106]

$$y_{\rm eff}^2 \simeq c_k \mathcal{R}^{-1/2} (\omega/m_\phi) y^2 \tag{2.149}$$

where c_k is a k-dependent constant[9] and ω is the oscillation frequency. For $k = 4$, $c_4 \simeq 0.5$ and $\omega \simeq 0.49 m_\phi$. This leads to

$$y_{\rm eff} \simeq \frac{1}{2} \times \frac{y}{\mathcal{R}^{\frac{1}{4}}} \simeq 6 \times 10^{-4} \sqrt{y} \qquad (k = 4)\,. \tag{2.150}$$

We note that only when $\mathcal{R} \sim 0.1$, do we recover $y_{\rm eff} = y$. Note also that unless $y_{\rm eff}$ is relatively small, $y_{\rm eff} \lesssim 2 \times 10^{-3}$, the Lagrangian coupling, y, is non-perturbative [106, 123], where this perturbativity limit on $y_{\rm eff}$ assumes $y \lesssim \sqrt{4\pi}$.

For $k = 2$, $c_2 \simeq 0.38$ and $\omega = m_\phi$. At the end of reheating, $\rho_{\rm RH} = \frac{1}{2} m_\phi^2 \phi_0^2 (a_{\rm RH}) = \alpha T_{\rm RH}^4$, so

[9] There is an additional dependence of $y_{\rm eff}$ on the sum of the Fourier modes associated with the inflaton oscillations in the potential $V(\phi) \sim \phi^k$, for each value of k. However, this additional dependence is $\mathcal{O}(1)$, as shown in [106].

that

$$\phi_0(a_{\rm RH}) = \sqrt{2\alpha}\frac{T_{\rm RH}^2}{m_\phi}\,. \tag{2.151}$$

Then, for $\mathcal{R} \gg 1$, we can write

$$y_{\rm eff} \simeq 0.15(m_\phi/T_{\rm RH})\sqrt{y} \qquad (k=2)\,, \tag{2.152}$$

and using Eq. (2.146) for $T_{\rm RH}$ in terms of $y_{\rm eff}$ we have

$$y_{\rm eff} = 6.7\times 10^{-3}\left(\frac{m_\phi}{10^9\ {\rm GeV}}\right)^{\frac{1}{4}} y^{\frac{1}{4}} \qquad (k=2)\,. \tag{2.153}$$

In this case, non- perturbativity sets in unless $y_{\rm eff} \lesssim 1.5(m_\phi/\phi_0)^{\frac{1}{2}}$, assuming that $y_{\rm eff} < y$. Note that for $k > 4$ the limit becomes more severe as $\mathcal{R}$ is larger and increases in time.

Because of the suppression in the decay rate, the relation between $T_{\rm RH}$ and the decay coupling y shown in Fig. 2.11 needs to be reassessed. Indeed, when $y \gtrsim 1.5\times 10^{-6}$, $\mathcal{R} \gtrsim 1$ and the suppression effect should be taken into account. The relation between $T_{\rm RH}$ and y when the effects of kinematic suppression are included is shown in Fig. 2.12. At very low values of y, $\mathcal{R} \ll 1$ and the suppression effects can be ignored. In this case, the relation between $T_{\rm RH}$ and y is unaffected. However, when $y_{\rm eff} \leq y$ the relation is altered. From Eq. (2.153), this occurs when $y > 1.3\times 10^{-6}(m_\phi/{\rm GeV})^{\frac{1}{3}}$, or when $y > 1.3\times 10^{-5}(1.3\times 10^{-3})(6\times 10^{-3})$ when $m_\phi = 10^3$ (10^9) (10^{11}) GeV. These values are seen in Fig. 2.12 when the solid curves begin to deviate from the dashed curves. The dashed curves show the relation in Fig. 2.11 when suppression effects are ignored. The expression for $y_{\rm eff}$ in Eq. (2.153) can be inserted in Eq. (2.146) to obtain the relation between $T_{\rm RH}$ and y for when suppression effects are included and reheating is governed by the quadratic term,

$$T_{\rm RH} = 2.2\times 10^{10}\ {\rm GeV}\left(\frac{m_\phi}{10^9{\rm GeV}}\right)^{\frac{3}{4}} y^{\frac{1}{4}} \qquad (k=2)\,. \tag{2.154}$$

We saw previously in Eq. (2.137) that the reheating temperature is determined by the quartic term only if $T_{\rm RH} \gtrsim 250 m_\phi$. When the kinematic suppression effects are ignored ($y = y_{\rm eff}$), this occurs when y does not satisfy Eq. (2.147). In this case, we can use Eq. (2.150) to determine the relation between $T_{\rm RH}$ and y,

$$T_{\rm RH} = 1.5\times 10^8 y\ {\rm GeV} \qquad (k=4)\,, \tag{2.155}$$

and thus we expect that reheating is determined by the quartic term when $y > 1.7\times 10^{-6} m_\phi/{\rm GeV}$. This occurs at $y = 1.7\times 10^{-3}$ for $m_\phi = 10^3$ GeV as can be seen in Fig. 2.12. For the larger masses shown, we see that the transition would only occur in the non-perturbative regime (with $y \gg 1$) and so for the two higher masses, the reheating temperature is always determined by

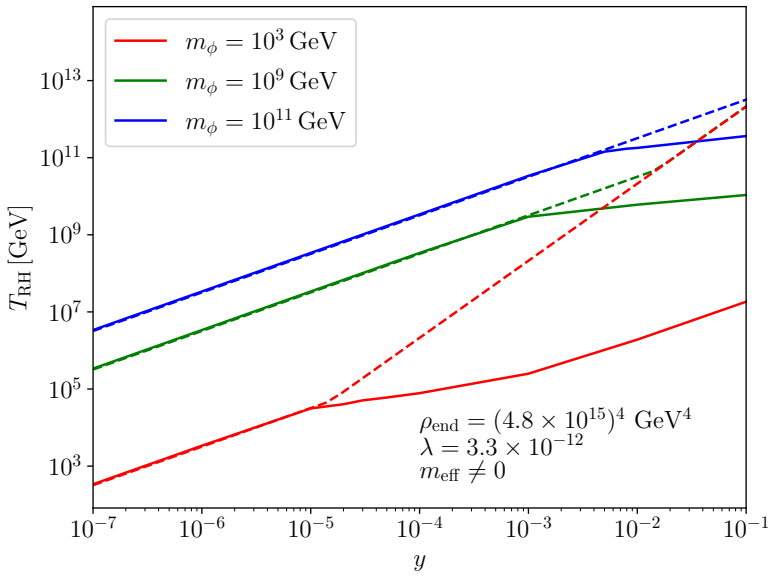

Figure 2.12: *As in Fig. 2.11, the reheating temperature as function of the yukawa coupling y for different values of the inflaton bare mass $m_\phi = 10^3$ GeV (red-dotted), 10^9 GeV (green-dashed) and 10^{11} GeV (full-blue). Here we consider the effective mass of produced fermion, $\mathcal{R} = (2y\phi_0/\omega)^2$.*

the quadratic mass term.

Decay to scalars

Another possibility is that reheating occurs predominantly through inflaton decay to scalars, through the coupling

$$\mathcal{L}_{\phi b^2} = \mu \phi b^2 \tag{2.156}$$

where b is a real scalar field. As was the case for the fermion decay, there is also an effect from the effective mass of the scalar field, and we parameterize it by considering an effective coupling $\mu_{\rm eff}$. We note that $\mu_{\rm eff}$ is now a dimensionful parameter and is *enhanced* (and not reduced) by $\mathcal{R}^{1/2}$ [106]. The associated decay rate is given by

$$\Gamma_{\phi b^2} = \frac{\mu_{\rm eff}^2}{8\pi m_\phi} \,. \tag{2.157}$$

For $k = 2$ this effective coupling reduces to the Lagrangian coupling μ but is different for $k > 2$. It is important to note that in this case, as m_ϕ decreases with time, the decay rate *increases* with time.

For decays to scalars, $l = 1/k - 1/2$, and using the appropriate expression found in the Appendix for γ_ϕ, we have

$$T_{\rm RH} = \left(\frac{1}{\alpha}\right)^{\frac{1}{4}} \left[\frac{2k\sqrt{3}}{(4k+2)\sqrt{k(k-1)}} \lambda^{-\frac{1}{k}} \frac{\mu_{\rm eff}^2}{8\pi M_P^2}\right]^{\frac{k}{4(k-1)}} M_P \,, \tag{2.158}$$

or

$$T_{\rm RH} \;=\; \begin{cases} \left(\frac{1}{\alpha}\right)^{\frac{1}{4}} \left(\frac{\mu_{\rm eff}^2}{36\pi M_P^2}\right)^{\frac{1}{3}} \lambda^{-\frac{1}{12}} M_P \\ \qquad \simeq 1.8\times 10^{18} \left(\frac{\mu_{\rm eff}}{M_P}\right)^{\frac{2}{3}} \text{GeV} \qquad k=4\,, \\ \left(\frac{3}{\alpha}\right)^{\frac{1}{4}} \left(\frac{M_P}{20\pi m_\phi}\right)^{\frac{1}{2}} \mu_{\rm eff} \\ \qquad \simeq 3.3\times 10^3 \mu_{\rm eff} \sqrt{\frac{10^9\,\text{GeV}}{m_\phi}} \qquad k=2\,, \end{cases} \tag{2.159}$$

We show in Fig. 2.13 the evolution of $T_{\rm RH}$ as function of μ for the same set of masses $m_\phi = 10^3$, 10^9 and 10^{11} GeV, in the simplified case with $m_{\rm eff} = 0$. We clearly recognize the dependence $T_{\rm RH} \propto \mu$ for the smaller values of μ and $T_{\rm RH} \propto \mu^{2/3}$ for the larger values, when reheating is dominated by the quartic part of the potential. The value of μ for which reheating is dominated by the quadratic term obtained from Eq. (2.159) with $k = 4$ is

$$\mu \lesssim 1.3\times 10^8 \left(\frac{m_\phi}{10^9\ \text{GeV}}\right)^{\frac{3}{2}}\ \text{GeV}\,, \tag{2.160}$$

which is effectively what is observed in Fig. 2.13. From Eq. (2.160), we see that the reheating temperature for $m_\phi = 10^3$ GeV (red curve) is always due to the quartic term, as the transition from quadratic to quartic occurs at a low value of μ beyond the range shown. For the larger values of m_ϕ, Eq. (2.160) indicates when when the slopes of $T_{\rm RH}$ vs. μ begins to change.

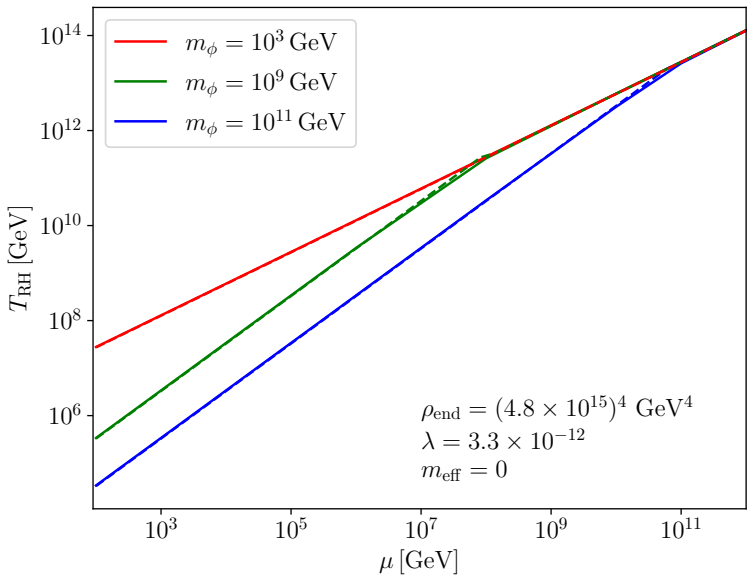

Figure 2.13: *Reheating temperature as function of the bosonic coupling μ, for different values of the inflaton bare mass $m_\phi = 10^3$ GeV (red), 10^9 GeV (green) and 10^{11} GeV (blue). Solid lines are obtained by solving numerically the Boltzmann equations for energy densities, while dashed lines are given by the analytical approximations in Eqs. (2.159). Here we neglect the effective mass of produced bosons, $\mathcal{R} = 0$.*

In order to account for the effective mass $m_{\rm eff}^2 = 2\mu\phi_0$, we need to include an *enhancement* of

the production rate $\propto \mathcal{R}^{\frac{1}{2}}$, with $\mathcal{R} = 8\mu\phi_0/m_\phi^2$ for $k = 2$ and $\mathcal{R} \simeq 2.8\mu/(\lambda\phi_0)$ for $k = 4$. The effective dimensionful coupling[10] when $\mathcal{R} \gg 1$ is [106]

$$\mu_{\rm eff}^2 \simeq \frac{c_k'}{4}(k+2)(k-1)\frac{\omega}{m_\phi}\mathcal{R}^{\frac{1}{2}}\mu^2\,, \tag{2.161}$$

with $c_k' \simeq \{0.38, 0.37, 0.36\}$ for $k = \{2, 4, 6\}$, so that $\mu_{\rm eff} \simeq 0.62(8\phi_0/m_\phi^2)^{\frac{1}{4}}\mu^{\frac{5}{4}}$ for $k = 2$. Then using Eq. (2.151) for ϕ_0 and Eq. (2.159) for $k = 2$ to replace $T_{\rm RH}$, we have

$$\mu_{\rm eff} \simeq 3.3 \times 10^{-10}\ {\rm GeV}\left(\frac{10^9\ {\rm GeV}}{m_\phi}\right)^2\left(\frac{\mu}{\rm GeV}\right)^{\frac{5}{2}}\,. \tag{2.162}$$

Then, the effects of the kinematic enhancement will occur when

$$\mu \gtrsim 2.1 \times 10^6\left(\frac{m_\phi}{10^9\ {\rm GeV}}\right)^{\frac{4}{3}}\ {\rm GeV}\,. \tag{2.163}$$

This can be see seen in Fig. 2.14 for $m_\phi = 10^9$ (10^{11} GeV as the point when the solid curves break away from the dashed curves at $\mu \simeq 2.1\times10^6$ (9.8×10^8) GeV respectively. At lower values of μ, the effects of the kinematic suppression can be ignored. For $m_\phi = 10^3$ GeV, this occurs at a value of μ below the range shown. It must be noted that the enhancement of the particle production rate with $\mathcal{R} \gg 1$ is connected to the (tachyonic) resonant excitation of b. This typically signals the breakdown of the perturbative approximation, requiring the use of lattice codes to capture the bosonic enhancement originated from the short-time preheating effects [132, 133]. We do not consider this effect in the present work, and we take the perturbative rate as a lower bound on the efficiency of the decay process.

In the region when $\mu_{\rm eff} > \mu$ and quadratic reheating dominates, we can insert Eq. (2.162) into Eq. (2.159) to obtain

$$T_{\rm RH} = 1.1 \times 10^{-6}\ {\rm GeV}\ \left(\frac{10^9\ {\rm GeV}}{m_\phi}\right)^{\frac{5}{2}}\mu^{\frac{5}{2}} \qquad (k=2)\,. \tag{2.164}$$

At higher values of μ the transition to quartic reheating occurs and using Eq. (2.161) with the expression for $\mathcal{R}$ for $k = 4$, we find that

$$\mu_{\rm eff} \simeq 2.5\ {\rm GeV}\left(\frac{\mu}{\rm GeV}\right)^{\frac{15}{14}} \tag{2.165}$$

[10] Again, an additional $\mathcal{O}(1)$ dependence of $\mu_{\rm eff}$ on the sum of the Fourier modes associated with the inflaton oscillations for each value of k is neglected here [106]. Note also that the values of c_k' were omitted in [106].

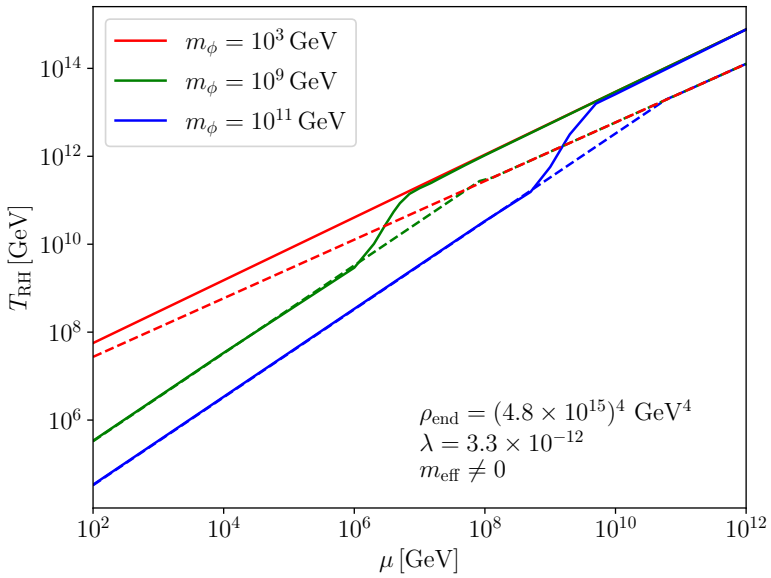

Figure 2.14: *Reheating temperature as function of the bosonic coupling μ, for different values of the inflaton bare mass $m_\phi = 10^3$ GeV (red), 10^9 GeV (green) and 10^{11} GeV (blue). Solid lines are obtained by solving numerically the Boltzmann equations for energy densities, while dashed lines are given by the analytical approximations in Eqs. (2.159). Here we consider the effective mass of produced bosons, $\mathcal{R} = 8\mu\phi_0/\omega^2$.*

which when inserted in Eq. (2.159) gives

$$T_{\rm RH} \simeq 2.5 \times 10^{19}\ {\rm GeV} \left(\frac{\mu}{M_P}\right)^{\frac{5}{7}} \qquad (k=4)\,. \tag{2.166}$$

Decay to Vectors

Recently, we have considered the possibility of inflaton decays to vectors [114] motivated by inflationary models in the context of no-scale supergravity [134] (which easily lend construction of the T-models considered in section 2.1 and here [87]). Often, in such models, the inflaton couplings to matter fermions and scalars are highly suppressed [135–137], and reheating is only possible if the gauge kinetic functions contain inflaton couplings. The inflaton to vector couplings can be parameterized by

$$\mathcal{L} \supset -\frac{g}{4M_P}\phi F_{\mu\nu}F^{\mu\nu} - \frac{\tilde{g}}{4M_P}\phi F_{\mu\nu}\tilde{F}^{\mu\nu}\,, \tag{2.167}$$

From these Lagrangian couplings, we can derive the inflaton decay rate

$$\Gamma_{\phi\to A_\mu A_\mu} \;=\; \frac{\alpha_{\rm eff}^2 m_\phi^3}{M_P^2}\,, \tag{2.168}$$

where $\alpha_{\rm eff}^2 = (g_{\rm eff}^2 + \tilde{g}_{\rm eff}^2)/(64\pi)$. Note the dependence of the width on m_ϕ^3, which is very different

from the decay into fermions ($\propto m_\phi$) and to scalars ($\propto 1/m_\phi$). $\Gamma_{\phi\to A_\mu A_\mu}$ decreases much more rapidly than $\Gamma_{\phi\to ff}$, rendering the reheating much less efficient, even impossible as long as the reheating is dominated by the quartic term.

Indeed, for decay to vectors, $l = 3/2 - 3/k$, and using the appropriate expression for γ_ϕ, we have from Eq. (2.109)

$$T_{\rm RH} = \left(\frac{1}{\alpha}\right)^{\frac{1}{4}} \left[\frac{\sqrt{3}k^{\frac{5}{2}}(k-1)^{\frac{3}{2}}\lambda^{\frac{3}{k}}}{13-4k}\alpha_{\rm eff}^2\right]^{\frac{k}{4(3-k)}} M_P\,. \tag{2.169}$$

This expression is valid so long as $k + 8 - 6kl > 0$, which is the case for $k = 2$, but not for $k \geq 4$. For $k + 8 - 6kl < 0$, the reheating temperature is given by Eq. (2.110) for $k > 4$. For $k = 4$, the radiation density in Eq. (2.108) scales as a^{-4} when $a \gg a_{\rm end}$, as does the inflaton energy density in Eq. (2.73) and we never achieve the condition that $\rho_\phi(a_{\rm RH}) = \rho_R(a_{\rm RH})$ and reheating never occurs. Thus we have

$$T_{\rm RH} \;=\; \begin{cases} \text{no reheating} & k = 4\,, \\ \left(\frac{3}{\alpha}\right)^{\frac{1}{4}}\left(\frac{2m_\phi^3}{5M_P^3}\right)^{\frac{1}{2}}\alpha_{\rm eff}M_P & \\ \qquad \simeq 7.0\times 10^3\alpha_{\rm eff}\left(\frac{m_\phi}{10^9{\rm GeV}}\right)^{\frac{3}{2}}\ {\rm GeV} & k = 2\,, \end{cases} \tag{2.170}$$

Thus for a $k = 4$ inflationary potential, reheating via the decays to vector bosons does not occur in the absence of a bare mass term. The bare mass term is then *necessary* to ensure a successful reheating. However, the bare mass term should ensure $T_{\rm RH} \gtrsim 2$ MeV, which means

$$m_\phi \gtrsim 40\alpha_{\rm eff}^{-\frac{2}{3}}\ {\rm TeV}\,. \tag{2.171}$$

This value is the minimal bare mass necessary to have reheating through decay to vectors for $k = 4$.

Finally we note that there are no kinematic enhancement/suppression effects in this case. Since the inflaton is coupled to F^2 (as opposed to A^2), no mass term is generated. Then $g_{\rm eff} = g$ (and $\tilde{g}_{\rm eff} = \tilde{g}$) for $k = 2$, and for $k = 4$ only differs by a Fourier coefficient in an expansion of $V(\phi)$ [114]. Nevertheless, non-perturbative preheating effects may play a role for large couplings, an effect that we leave for future work [138–140].

Scattering to scalars

We can also consider the case where the inflaton transfers its energy through the coupling

$$\mathcal{L}_{\phi^2 b^2} = \sigma\phi^2 b^2 \tag{2.172}$$

where b is a real scalar field. The associated decay rate is given by [106]

$$\Gamma_{\phi^2 b^2} = \frac{\sigma_{\rm eff}^2}{8\pi}\frac{\rho_\phi}{m_\phi^3} \tag{2.173}$$

where we have introduced the effective coupling $\sigma_{\rm eff}$ obtained, as for $y_{\rm eff}$ and $\mu_{\rm eff}$, after averaging over oscillations of the background inflaton condensate [106]. This effective coupling is equal to the Lagrangian coupling σ for $k = 2$ but is different for $k > 2$ and as in the case of decays to fermions there is a kinematic suppression.

For scattering to scalars, $l = 3/k - 1/2$, and using the appropriate expression found in the Appendix for γ_ϕ, we have from Eq. (2.109) valid when $k \geq 4$,

$$T_{\rm RH} = \left(\frac{1}{\alpha}\right)^{\frac{1}{4}} \left[\frac{\sqrt{3}}{(2k-5)\sqrt{k}(k-1)^{\frac{3}{2}}}\lambda^{-\frac{3}{k}}\frac{\sigma_{\rm eff}^2}{8\pi}\right]^{\frac{k}{4(k-3)}} M_P\,. \tag{2.174}$$

For $k = 2$, $8 + k - 6kl < 0$ and ρ_R redshifts as a^{-4} which is faster than $\rho_\phi \propto a^{-3}$. Thus, in this case, reheating is not possible if the quadratic term becomes dominant before reheating is complete. The reheating temperature can then be written as,

$$T_{\rm RH} = \begin{cases} \left(\frac{1}{\alpha}\right)^{\frac{1}{4}}\left(\frac{\sigma_{\rm eff}^2}{144\pi}\right)\lambda^{-\frac{3}{4}}M_P & \\ \qquad \simeq 8.9\times 10^{23}\sigma_{\rm eff}^2 {\rm GeV} \qquad & k = 4\,, \\ \text{no reheating} \qquad & k = 2\,. \end{cases} \tag{2.175}$$

As one can see, the possibility of reheating through scattering to scalars is opposite the case of decays to vectors. Reheating is *not possible* when the quadratic part of the potential dominates the reheating process. Naively, when we neglect the kinematic suppression effects in $\mathcal{R}$, reheating is therefore only possible if the limit in Eq. (2.137) is violated, namely

$$\sigma_{\rm eff} \gtrsim 5.3\times 10^{-7}\sqrt{\frac{m_\phi}{10^9\ {\rm GeV}}}\,. \tag{2.176}$$

For smaller couplings, the quadratic term will dominate before reheating is complete, and as a result never completes. We note in the expression for $T_{\rm RH}$ in Eq. (2.175), the maximum value for $\sigma_{\rm eff}$ that can be used is determined from $a_{\rm RH} > a_{\rm end}$, which gives

$$\sigma_{\rm eff}^2 < 2.2\times 10^{-9}\,. \tag{2.177}$$

Furthermore, for self-couplings this large, we expect that non-perturbative effects become non-negligible [119]. For larger values, we have a maximum reheating temperature of 2×10^{15} GeV, which is basically determined from $\rho_{\rm end}$.

As previously noted, for inflaton scattering to scalars, there is a kinematic suppression when $\mathcal{R} > 1$. In this case, for $k = 4$, $\mathcal{R} \simeq 2.8\sigma/\lambda$ is a constant and [11]

$$\begin{aligned} \sigma_{\rm eff}^2 &\simeq \frac{c_k''}{8} k(k+2)(k-1)^2 \mathcal{R}^{-1/2} (\omega/m_\phi)\sigma^2 \\ &\simeq 16\mathcal{R}^{-1/2}\sigma^2 \simeq 9.6\sqrt{\lambda}\sigma^{\frac{3}{2}}\,, \end{aligned} \tag{2.178}$$

using $c_4'' = 1.22$. Then the reheating temperature in terms of σ becomes

$$T_{\rm RH} = 1.6 \times 10^{19}\ {\rm GeV}\sigma^{\frac{3}{2}} \qquad (k=4)\,. \tag{2.179}$$

In Fig. 2.15, we compare the reheating temperature as a function of σ when kinematic effects are ignored to the case where they are included. From Eq. (2.178), these effects become important when $\sigma > 3.1 \times 10^{-10}$. The dashed lines correspond to the solution when kinematic effects are ignored. The abrupt increase in $T_{\rm RH}$ occurs when Eq. (2.176) is satisfied (and $\sigma_{\rm eff} = 4\sigma$). In contrast, the solid lines include the kinematic suppression and reheating is possible when Eq. (2.176) is used with Eq. (2.178) or when

$$\sigma \gtrsim 6.4 \times 10^{-6} \left(\frac{m_\phi}{10^9\ {\rm GeV}}\right)^{\frac{2}{3}}\,. \tag{2.180}$$

This limit accounts for the abrupt rise in $T_{\rm RH}$ for the solid lines in Fig. 2.15. At higher coupling, the reheating temperature follows Eq. (2.179) and scales as $\sigma^{\frac{3}{2}}$ as opposed to σ^2 when the suppression effects are ignored. In the latter case, we see the curves flatten at large coupling since $a_{\rm RH}$ is approaching $a_{\rm end}$ and the approximation used in (2.175) breaks down. These curves end when $a_{\rm RH} = a_{\rm end}$, indicated by the vertical gray dotted line. The solid curves would end when $\sigma \simeq 0.002$.

In the absence of a decay term for the inflaton, a bare mass term will eventually lead to a non-zero relic density of inflatons after annihilations freeze out. Indeed, even if $\sigma_{\rm eff}$ is sufficiently large and respects the condition (2.176), the presence of a quadratic term may dominate the energy budget of the Universe. Thus we can derive a limit on a combination of the inflaton mass, $T_{\rm RH}$ and the coupling σ. Saturating the limit leaves us with the inflaton as a cold dark matter candidate! [12]

Indeed, for $\sigma_{\rm eff}$ sufficiently large to ensure reheating with $k = 4$, for $a > a_{\rm RH}$, the evolution of ρ_ϕ is determined from the Boltzmann equation including dissipative effects [106]

$$\frac{d}{da}\left(\rho_\phi a^{\frac{6k}{k+2}}\right) = -\frac{\gamma_\phi}{aH}\frac{2k}{k+2}\frac{\rho_\phi^{l+1}}{M_P^{4l}} a^{\frac{6k}{k+2}}\,. \tag{2.181}$$

[11] We neglect the dependence of $\sigma_{\rm eff}$ on the sum of the Fourier modes associated with the inflaton oscillations for each value of k [106].

[12] The possibility of inflaton dark matter in a similar context was considered in [141] where the conditions for freeze-out of a thermal inflaton given. See also [142–146].

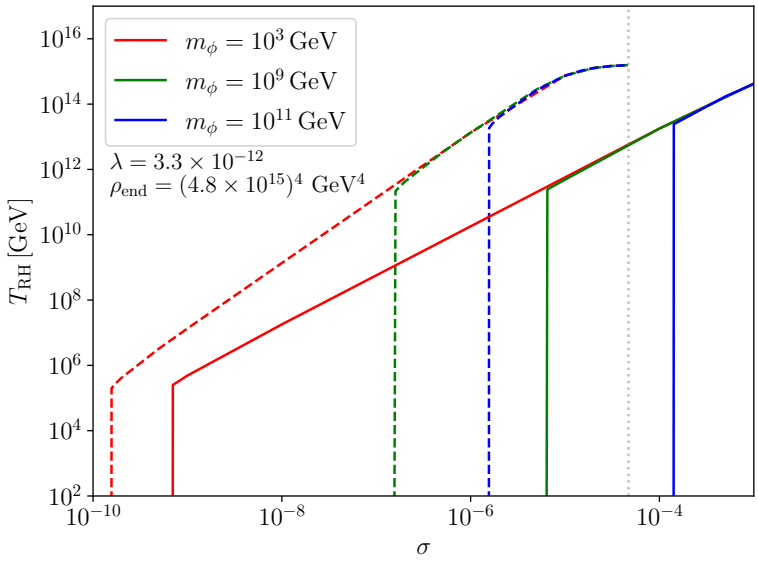

Figure 2.15: *Reheating temperature as function of the scattering coupling σ, for different values of the inflaton bare mass $m_\phi = 10^3$ GeV (red), 10^9 GeV (green) and 10^{11} GeV (blue). Solid lines are obtained by solving numerically the Boltzmann equations for energy densities including the effect of $\mathcal{R}$, while dashed lines neglect the effect of effective masses. The vertical gray dotted line corresponds to the limit Eq.(2.177), when neglecting the effect of $\mathcal{R}$.*

and for $k = 4$, $l = \frac{1}{4}$ and γ_ϕ as given in the Appendix, we find that ρ_ϕ scales as

$$\rho_\phi = 256\rho_{\rm RH}\left(\frac{a_{\rm RH}}{a}\right)^8 . \tag{2.182}$$

Here, we used $H = \sqrt{\rho_R/3M_P^2}$. In the absence of a mass term, since $\Gamma_\phi \propto \gamma_\phi \rho_\phi^{\frac{1}{4}} \propto a^{-2}$ and after reheating, $H \propto \rho_R^{\frac{1}{2}} \propto a^{-2}$, the ratio Γ/H remains constant and the scaling in Eq. (2.182) remains true indefinitely and the density of inflatons becomes negligibly small.

However, when $m_\phi \neq 0$, eventually the mass term dominates over the quartic term (at $a = a_{\rm m}$) and we can determine $a_{\rm m}$, when $\rho_\phi(a_{\rm m}) = \frac{1}{2}m_\phi^2\phi^2(a_{\rm m})$,

$$\frac{a_{\rm m}}{a_{\rm RH}} = \frac{\rho_{\rm RH}^{\frac{1}{8}}\lambda^{\frac{1}{8}}2^{\frac{1}{8}}}{\sqrt{m_\phi}} , \tag{2.183}$$

where the inflaton density is given by

$$\rho_\phi^{\rm m} = \rho_\phi(a_{\rm m}) = \frac{m_\phi^4}{2\lambda} . \tag{2.184}$$

as was previously found in Eq. (2.133).

For $a > a_{\rm m}$, Eq. (2.181) can be solved, now with $k = 2$ and $l = 1$. In the limit that $a \gg a_{\rm m}$,

the residual inflaton density is given by

$$\rho_\phi(a) \simeq \rho_\phi^{\rm m} \left(\frac{a_{\rm m}}{a}\right)^3 , \tag{2.185}$$

so long as $(m_\phi/M_P) \ll (2\lambda)^{\frac{1}{4}}/3^{\frac{1}{3}} \approx .001$, which is always true given the upper limits on m_ϕ discussed in Section 2.3.2. Thus the presence of a mass term in the case where reheating is determined by a quartic coupling of the inflaton to scalars (which requires $k > 2$), leads automatically to cold dark matter candidate.

Given the inflaton density in Eq. (2.185), it is straightforward to compute the relic density today and in effect set a limit on the inflaton bare mass. Today,

$$\rho_\phi = \frac{8 m_\phi^{\frac{5}{2}} \alpha^{\frac{3}{8}} T_0^3}{(2\lambda)^{\frac{5}{8}} T_{\rm RH}^3 2} \xi , \tag{2.186}$$

where $\xi = (43/427)(4/11) \simeq 0.036$ and relative to the critical density we have

$$\Omega_\phi h^2 = 1.6 \left(\frac{m_\phi}{1\ {\rm GeV}}\right)^{\frac{5}{2}} \left(\frac{10^{10}\ {\rm GeV}}{T_{\rm RH}}\right)^{\frac{3}{2}} \tag{2.187}$$

and thus

$$m_\phi < 0.35 \left(\frac{T_{\rm RH}}{10^{10}\ {\rm GeV}}\right)^{\frac{3}{5}}\ {\rm GeV} , \tag{2.188}$$

using $\Omega_\phi h^2 < 0.12$. This is a remarkably strong limit on a bare mass term for the inflaton if it remains stable.

Scattering to Vectors

If the gauge kinetic function is quadratic in the inflaton, then scattering rather decay to vectors occurs. In this case, the inflaton to vector couplings can be parameterized by

$$\mathcal{L} \supset -\frac{\kappa}{4M_P^2}\phi^2 F_{\mu\nu}F^{\mu\nu} - \frac{\tilde{\kappa}}{4M_P^2}\phi^2 F_{\mu\nu}\tilde{F}^{\mu\nu} , \tag{2.189}$$

From these Lagrangian couplings, we can derive the inflaton decay rate

$$\Gamma_{\phi\phi\to A_\mu A_\mu} = \frac{\beta^2 \rho_\phi}{M_P^4} m_\phi , \tag{2.190}$$

where $\beta^2 = (\kappa_{\rm eff}^2 + \tilde{\kappa}_{\rm eff}^2)/(4\pi)$.

For scattering to vectors, $l = 3/2 - 1/k$, and using the appropriate expression for γ_ϕ, we have

from Eq. (2.110)

$$T_{\rm RH} = \left(\frac{1}{\alpha}\right)^{\frac{1}{4}} \left[\frac{\sqrt{3}k}{4k-7}\beta^2(k(k-1))^{\frac{1}{2}}\lambda^{\frac{1}{k}}\right]^{\frac{3k}{4k-16}} \times \left(\frac{\rho_{\rm end}}{M_P^4}\right)^{\frac{4k-7}{4k-16}} M_P\,. \tag{2.191}$$

since $8+k-6kl<0$ for $k\geq 2$. However, Eq. (2.191) is only valid for $k>4$. For $k=2(4)$, $\rho_\phi \propto a^{-3}(a^{-4})$ while $\rho_R \propto a^{-4}$ for all k and reheating is not possible for $k<6$. For these specific cases, we then have

$$T_{\rm RH} = \begin{cases} \text{no reheating} & k=4\,, \\ \text{no reheating} & k=2\,, \end{cases} \tag{2.192}$$

In this case, the presence of a bare mass will not change the lack of reheating through the scattering to vectors.

As a conclusion, whereas in the case of decays to fermions or bosons, the presence of a quadratic term only acts on the *value* of $T_{\rm RH}$, decreasing the reheating temperature in the former case, increasing it in the latter case, the quadratic term when dominant removes the possibility of reheating through scattering to scalars but reopens the possibility of reheating through decay to vectors, but does not allow reheating through the scattering to vectors.

2.3.4 Generalized potentials

The inflationary potential may be dominated by higher order terms if $k>4$. In this section, we generalize some of the arguments made above in the event that the inflationary potential is approximated by

$$\frac{1}{2}m_\phi^2\phi_0^2 + \lambda\phi_0^k M_P^{4-k} \tag{2.193}$$

about its minimum. In this case, the general expression for the scale factor when the mass term dominates is given by

$$\frac{a_{\rm m}}{a_{\rm end}} = \left(\frac{2\lambda^{\frac{2}{k}}M_P^{\frac{2(4-k)}{k}}\rho_{\rm end}^{\frac{k-2}{k}}}{m_\phi^2}\right)^{\frac{k+2}{6k-12}}\,, \tag{2.194}$$

with $\rho_{\rm end}=\frac{3}{2}V(\phi_{\rm end})$ and λ by Eq. (2.64). Then

$$\rho_\phi(a_m) = 2\left(\frac{m_\phi^2}{2}\right)^{\frac{k}{k-2}}\lambda^{\frac{-2}{k-2}}M_P^{\frac{2(k-4)}{k-2}}\,, \tag{2.195}$$

which clearly reduces to Eq. (2.133) for $k = 4$. A parallel derivation leading to Eq. (2.137) implies that

$$\rho_{\rm RH} \lesssim 2 \left(\frac{m_\phi^2}{2}\right)^{\frac{k}{k-2}} \lambda^{\frac{-2}{k-2}} M_P^{\frac{2(k-4)}{k-2}} \tag{2.196}$$

for the mass term to dominate at reheating. In terms of the reheating temperature, this amounts to

$$T_{\rm RH} \lesssim \left(\frac{1}{\alpha}\right)^{\frac{1}{4}} \left(\frac{m_\phi M_P^{\frac{k-4}{k}}}{(2\lambda)^{\frac{1}{k}}}\right)^{\frac{k}{2(k-2)}} . \tag{2.197}$$

For comparison with Eq. (2.137), we have

$$T_{\rm RH} \lesssim \begin{cases} 5.0 \times 10^5 \text{ GeV} \left(\frac{m_\phi}{\rm GeV}\right)^{\frac{3}{4}} & k = 6\,, \\ 6.3 \times 10^6 \text{ GeV} \left(\frac{m_\phi}{\rm GeV}\right)^{\frac{2}{3}} & k = 8\,, \end{cases} \tag{2.198}$$

using $\lambda = 5.7 \times 10^{-13}$ and 9.5×10^{-14} for $k = 6$ and 8, respectively.

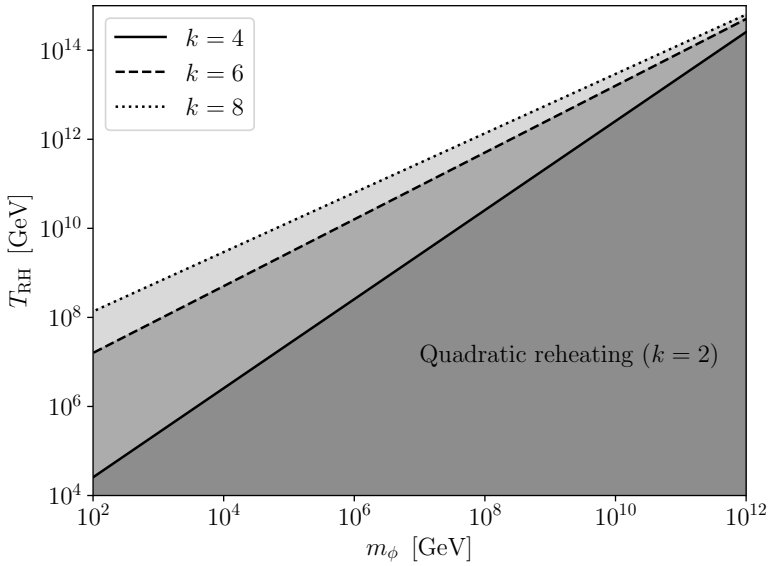

Figure 2.16: *Minimal reheating temperature from Eq.(2.197), below which the inflaton mass term drives the process, as a function of the bare mass m_ϕ and for different values of k, $k = 4$ (solid line), $k = 6$ (dashed), $k = 8$ (dotted). In the different shaded regions, reheating occurs while the inflaton oscillates in a quadratic potential ($k = 2$), given by its bare mass m_ϕ. Above the lines, for different k, reheating occurs while the inflaton oscillates in the potential $V(\phi) \sim \phi^k$.*

2.3.5 Consequence on the inflaton fragmentation

Recently, the authors of [123] and [122] have shown that fragmentation can significantly alter the reheating process. Indeed, the fragmentation of the inflaton condensate results in the population of an inflaton-particle bath, whose very low mass, proportional to the density of

the condensate which remains unfragmented, may not allow reheating temperatures above the BBN bounds for inflaton decays to fermions. This fragmentation is due to the presence of a self-scattering term of type $\lambda\phi^k$, with $k \geq 4$. The inflaton condensate does not fragment in the absence of self-interactions allowing for reheating to occur as discussed above.

However, the study [123] was carried out in the context of a monomial potential of the type $V(\phi) = \lambda\phi^k$. It is then easy to see that the presence of a bare mass term of the type $\frac{1}{2}m_\phi^2\phi^2$ can change the conclusions of this study, in particular if the quadratic term begins to dominate *before* the fragmentation halts. If we define $a_{\rm F}$ as the value of the scale factor at the end of fragmentation, then $a_{\rm F}/a_{\rm end} = 180, 4.5\times10^4, 6\times10^6$ and 7×10^8, for $k = 4, 6, 8$ and 10 respectively [123]. In order for a quadratic term to affect the fragmentation process, we must have $a_{\rm m} \lesssim a_{\rm F}$ and using Eq.(2.131) it becomes easy to compute, for each value of k, the minimal value of m_ϕ necessary to ensure that the quadratic term dominates the potential *before* the end of fragmentation. The problem of a leftover bath of massless inflatons can then be avoided by stopping the fragmentation process.

More precisely, when reheating begins, self interactions can source the growth of the inflaton fluctuations $\delta\phi(t,\boldsymbol{x}) = \phi(t,\boldsymbol{x}) - \bar{\phi}(t)$, where $\bar{\phi}$ denotes the homogeneous condensate. At early times, this growth can be captured by the linear equation of motion

$$\ddot{\delta\phi} + 3H\dot{\delta\phi} - \frac{\nabla^2\delta\phi}{a^2} + V''(\bar{\phi})\,\delta\phi \;=\; 0\,, \tag{2.199}$$

where

$$V''(\bar{\phi}) \;\simeq\; k(k-1)\lambda\bar{\phi}^{k-2}M_P^{4-k} + m_\phi^2\,. \tag{2.200}$$

For $m_\phi = 0$, the oscillating nature of this resulting effective mass term drives the resonant growth of $\delta\phi$ and the eventual fragmentation, $\delta\phi \gg \bar{\phi}$ [121–123, 147–154]. However, if m_ϕ dominates before fragmentation, $V'' \sim$ const., strongly suppressing the oscillatory driving force.[13]

Fig. 2.17 shows the evolution of the total inflaton energy density ρ_ϕ, compared to the energy density in its fluctuations $\rho_{\delta\phi}$, as computed numerically for a T-model of inflation [105] with $k = 4$ and three choices of the bare mass (see [122] for details). The top panel depicts the zero bare mass scenario. In it, the rapid growth of inflaton fluctuations driven by parametric resonance can be appreciated. This growth only stops when $\rho_\phi \simeq \rho_{\delta\phi}$ ($a/a_{\rm end} \simeq 180$), corresponding to the near-complete fragmentation of the inflaton condensate in favor of free ϕ-particles.[14] For the bottom two panels we take $m_\phi > 0$. In both cases, the quartic $\rightarrow$ quadratic transition time has been chosen to be posterior to the complete fragmentation of the inflaton, $a_{\rm m} > a_{\rm F}$. A

[13] For a purely quadratic inflaton potential the growth of fluctuations is still present, albeit not exponentially enhanced, due to the coupling of $\delta\phi$ with the fluctuations of the metric [155–158].

[14] The fragmentation of the inflaton condensate is not total even for $m_\phi = 0$. A small but nonvanishing homogeneous component $\bar{\phi}$ remains, and its presence can induce the decay of the free inflaton quanta $\delta\phi$ [122, 123].

naive estimate from Eq. (2.200) would indicate that the resonant growth of $\delta\phi$ would not stop until

$$\frac{a}{a_{\rm end}} = \frac{\sqrt{12\lambda}\phi_{\rm end}}{m_\phi} \simeq 2.6\,\frac{a_{\rm m}}{a_{\rm end}}\,, \tag{2.201}$$

that is, the field would be fully fragmented before matter domination. However, the full numerical solution of the equation of motion (2.199) shows that the growth of fluctuations is in reality suppressed from $a \lesssim a_{\rm m}/2$, as both panels of Fig. 2.17 demonstrate. Therefore, reaching quadratic dominance is a sufficient condition to avert full fragmentation. Note that for smaller masses than those used in Fig. 2.17, fragmentation would nearly completely destroy the condensate and potentially disrupt the reheating process entirely. On the other hand, for larger masses, the fragmentation process would not be operative at all.

A qualitative depiction of this result for potentials with $k \geq 4$ is shown in Fig. 2.18, where we plot the limit on the mass m_ϕ above which the bare mass term dominates over $\lambda\phi^k$ in the potential as a function of k. We see that for larger value of k, where the fragmentation is less efficient due to the increasing difficulty for the self scattering to occurs for higher modes, even a small bare mass term can be sufficient to stop the fragmentation process and ensure a successful reheating.

To conclude this section, when the inflaton potential is dominated by a quadratic term about its minimum, decays are necessary, as scatterings do not lead to a radiation-dominated universe. However, potentials dominated by higher order interactions, $k > 2$, have anharmonic oscillations and scattering may lead to reheating, though these models may be subject to additional constraints arising from the fragmentation of the inflaton condensate. The details of the reheating process depend on the spin of the final state particles produced.

In models of inflation for which the potential can be expanded about its minimum as $V(\phi) \propto \phi^k$, with $k > 2$, it is quite possible, that a bare mass term in the full scalar potential is also present. We derived upper limits to this mass from CMB observables. The qualitative effect of the mass term also depends on the reheating mechanism (decay or scattering) as well as the spin of the final states. For decays to fermions, the reheating temperature is increased by the presence of mass term, while for scalars, it is decreased. For decays to vectors, reheating does not occur for $k = 4$ in the absence of a mass term and its presence allows for the possibility of reheating in this case. In contrast, if the mass term becomes important before the end of reheating for scattering to scalars, the reheating process is halted. Furthermore, when reheating is accomplished through scattering to scalars with $k \geq 4$, the density of inflatons quickly redshifts (as a^{-8}) until the mass term comes to dominate. In this case, the residual inflaton matter density acts as cold dark matter and a strong limit on the inflaton mass has been derived in Eq. (2.188). Finally, we have seen that for scattering to vectors, reheating with $k = 4$ is not possible ($k \geq 6$ is required), and the mass term does not come to the rescue in this case.

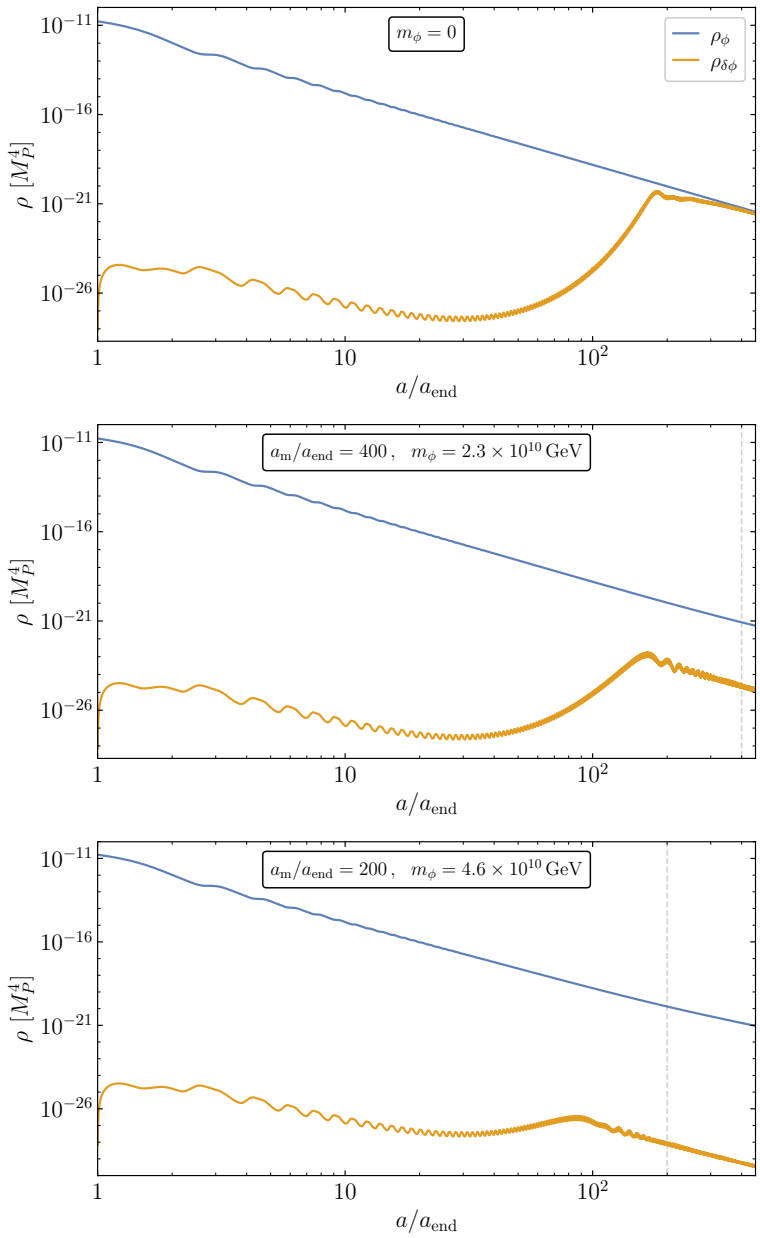

Figure 2.17: *Energy density of the inflaton fluctuations $\rho_{\delta\phi}$ compared to the total energy density ρ_ϕ, for three values of the bare mass, for $k = 4$. The vertical dashed line corresponds to the value of $a_{\rm m}/a_{\rm end}$ when $m_\phi \neq 0$. In both of these cases, although $a_{\rm m} > a_{\rm F}$, the exponential growth of $\delta\phi$ is stopped by the transition to matter-domination.*

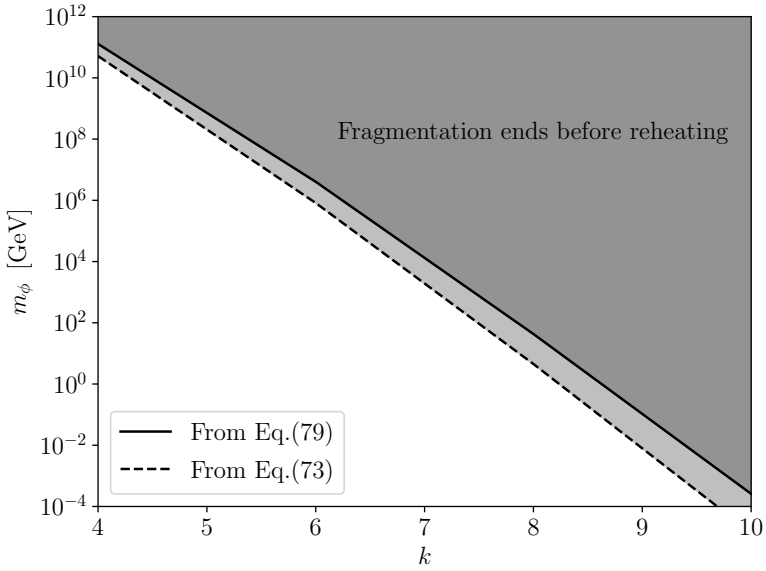

Figure 2.18: *Region in the parameter space where the fragmentation happens after the domination by the bare mass term* $\frac{1}{2}m_\phi^2\phi^2$ *over* $\lambda\phi^k$*, allowing for a quadratic reheating. The dashed line is obtained from Eq.(2.194), while the solid line is obtained from Eq.(2.200).*

Chapter 3

Gravitational particle production

Contents

Production of thermal relics, through the freeze-in or freeze-out mechanisms, requires the temperature of the thermal plasma to be high enough to produce heavy particles. However, DM candidates have not provided any detectable signal through interactions with SM particles in direct detection, indirect detection, or accelerator experiments. The stringent constraints on the magnitude of DM coupling with SM species may suggest that it does not interact other than by gravity. If so, the primordial origin of DM must be explained through gravitational effects, and it is an appealing motivation to study the early-universe production of particles through gravitational interactions.

The first work on gravitational production can be traced back to Schrödinger who studied particle pair creation in the expanding Universe [159]. This seminal work was then pursued by Parker and Ford in [160, 161] and Zel'dovich in [162], where the framework of cosmological gravitational particle production was developed. It is the commonly accepted mechanism to explain the origin of cosmological perturbations from inflation (section 2.1) from the work of Mukhanov and Sasaki [97]. But this mechanism can also naturally explain the generation of relic densities and may play a role in generating the matter-antimatter asymmetry. Cosmological gravitational particle production may produce particles of mass comparable to the scale of inflation, as large as 10^{14} GeV, even if the reheating temperature is much lower after inflation. In addition, as opposed to standard scenarios for the production of cosmological relics, gravitational production occurs inevitably even when the fields do not couple directly to SM particles or the inflaton. In this sense, it is a model-independent mechanism that appears as a minimal extension of SM processes because gravitational production does not depend on any couplings between the different sectors.

The first part of this chapter focuses on gravitational particle production during inflation resulting from the background gravitational field evolution as the Universe expands. It is a semiclassical approach as the gravitational field itself is not quantized, whereas the spectator fields (not coupled but experiencing the expansion) are quantized. We introduce the semiclassical framework of QFT in curved space-time to derive the equations of motion for the Fourier mode of spectator fields during inflation. We see how the expansion induces a mixing of positive and negative-frequency that can be interpreted as a particle production using the Bogoliubov formalism, and how to compute relic number density from it.

In the second part, we develop a novel approach to study particle production originating from gravitational interactions during the inflaton oscillations regime. We adopt a Boltzmann picture computing transition amplitudes and collision terms on short time scales based on QFT in Minkowski space-time and involving effective gravitational operators. The leading order effect is computed from the s-channel gravitons exchange process that we call the (minimal) gravitational portal. It induces a rich phenomenology during reheating depending on the spin of the particle produced and the shape of the inflaton potential around the minimum. We more specifically apply this framework to the production of heavy DM particles during reheating,

looking at the UV freeze-in from the thermal bath mediated by the gravitons, as well as the contribution from the inflaton modes. The effect of these gravitational portals on the production of relativistic quanta of the SM is also studied. In a second section, we further generalize this framework of gravitational portals to the case of nonminimal couplings to gravity for scalar fields. Finally, we consider a simple scenario for the generation of the DM relic abundance and the origin of the baryon asymmetry in the Universe. We look at the gravitational production of heavy RHN during the stage of reheating, which can simultaneously explain the asymmetry from non-thermal leptogenesis as well as provide a proper DM candidate. These RHN are produced from the gravitational portals and stay out-of-equilibrium concerning the hot thermal bath. Such gravitational portals can also produce the relativistic particles of SM that further thermalize into the bath. We investigate the constraints on such a scenario of gravitational reheating involving minimal and nonminimal couplings to gravity.

3.1 Cosmological production

3.1.1 Quantum scalar field in curved space-time

We study a real scalar quantum field $\chi(x)$, evolving in the classical space-time given by the metric $g_{\mu\nu}$ which we consider to be the FLRW background. We write $g_{\mu\nu}(x) = a^2(\eta)\text{diag}\,(1,-1,-1,-1)$ which is related to Minkowski space-time through conformal coordinate transformation, η being the conformal time $ad\eta = dt$. The generic action for the massive scalar field is given by

$$S = \int d^4x\sqrt{-g}\left[-\frac{1}{2}M_P^2(1+\xi)R + \frac{1}{2}\partial_\mu\chi\partial^\mu\chi - \frac{1}{2}m_\chi^2\chi^2\right] \tag{3.1}$$

where ξ is a dimensionless nonminimal coupling to gravity, which directly coupled the scalar field to the Ricci curvature. This specific nonminimal coupling is an expected effective coupling generated in curved space-time by UV processes and is motivated in many cosmological scenarios. However, there can be an additional extension of Einstein gravity with higher dimension operators for gravitational interactions that we do not consider here. To follow the dynamics of such a scalar field during the quasi-de Sitter inflation, we first redefine the field via $X = a\chi$, for which the action becomes [163]

$$\mathcal{S} = \int d^4x\frac{1}{2}\left[(X')^2 - (\nabla X)^2 + \left(\frac{a''}{a}(1+6\xi) - a^2m_\chi^2\right)X^2 - \partial_\eta(aHX^2)\right], \tag{3.2}$$

where we used the relation between the Ricci scalar and the scale factor second derivative in FLRW space-time, $-\frac{1}{6}R(a) = \frac{a''}{a}$. This term in parenthesis in front of X^2 can be interpreted as a time-dependent effective mass of the scalar field due to the expansion of space-time and related to the gravitational coupling. The associated equation of motion can be derived [163]

and is given by

$$X'' - \nabla^2 X + \left(a^2 m_\chi^2 - \frac{a''}{a}(1+6\xi) \right) X = 0\,. \tag{3.3}$$

which is a linear wave equation with a time-dependent effective mass given by the parenthesis. Solutions can be expanded on a basis of mode functions, $\chi_k(\eta)$, given by the Fourier transform of the field $X(x,\eta)$ (on a hypersurface of constant conformal time) labeled by the comoving momentum $\vec{k}$. The field operator is quantized so that each mode is associated with creation and annihilation operators $\hat{a}_k, \hat{a}_k^\dagger$, satisfying canonical commutation relations. The mode functions satisfy the following equation of motion

$$\chi_k''(\eta) + \omega_k(\eta)^2 \chi_k(\eta) = 0 \tag{3.4}$$

for each comoving momentum k, which is a harmonic oscillator equation with a time-dependent comoving frequency

$$\omega_k(\eta)^2 = k^2 + a^2(\eta) m_\chi^2 + \left(\frac{1}{6} + \xi \right) a^2(\eta) R(\eta)\,. \tag{3.5}$$

The set of mode functions forms a complete orthonormal basis of the wave equation solutions and satisfies the so-called Wronskian condition for canonically normalized fields

$$W_k \equiv \chi_k \chi_k'^* - \chi_k^* \chi_k' = i\,. \tag{3.6}$$

In the following, we neglect the backreaction of the field χ on the background metric, as we are looking at a limit of small particle production through gravitational effects. We are mainly interested in solving the mode equation for a quasi-de Sitter space-time during inflation. The origin of the production comes from the time dependence of the frequency of the modes and to understand this mechanism, let us first look at the situation in Minkowski space-time.

If there is no cosmological expansion, the frequency of Fourier modes (computed in the same hypersurface of constant time) is constant for each wave number k. Thus, each mode is a harmonic oscillator, and we have a natural basis for solutions of the wave equation, describing plane waves, for which

$$\chi_k(\eta) = \frac{e^{-i\omega_k \eta}}{\sqrt{2\omega_k}} \tag{3.7}$$

that is the positive-frequency mode function (the negative-frequency mode function is obtained by replacing $\omega_k \to -\omega_k$). The associated creation and annihilation operators act on a unique vacuum state as $\hat{a}_k|0\rangle = 0$ for all Fourier modes, which coincide in all inertial frames. Thus all inertial observers agree on the number of particles that they can define frame-independently through the same operator $\hat{N}_k = \hat{a}_k^\dagger \hat{a}_k$. In this case, the number density of particles in the field

can be computed in a specific state $|\Psi\rangle$ as

$$n = \int \frac{d^3k}{(2\pi)^3} \langle \Psi | \hat{N}_k | \Psi \rangle \, . \tag{3.8}$$

Therefore, if no interactions are considered in the vacuum, we expect no particle to ever be produced and the field to stay throughout its evolution in the non-excited configuration.

For curved space-times, however, it is generally impossible to specify a basis for solutions of positive-frequency modes associated with the dispersion relation above, which holds along space-time dynamics. In this case, inertial observers may decompose the field operator into different mode functions and creation and annihilation operators at different times. Thus, the vacuum state at some time may be an excited state at another time, associated with a nonzero number of particles (quanta) of the fields. The cosmological gravitational particle production results from the mixing of positive and negative-frequency modes in an evolving gravitational background, that induces a time-dependent dispersion relation for the wave equation. We discuss below, in further detail, the formalism of Bogoliubov transformations, which allows to determine this number of particles measured by an observer in an expanding space-time.

One important aspect of the expansion of the Universe is that the FLRW space-time is related to the Minkowski space-time by a time-dependent conformal transformation of the coordinates

$$g_{\mu\nu}^{\mathrm{FLRW}}(\eta) = a^2(\eta)\eta_{\mu\nu} \, . \tag{3.9}$$

Therefore, field theories conformally coupled to gravity do not lead to gravitational production (at least not classically). Indeed, under such a conformal transformation of the metric

$$g_{\mu\nu}(x) \to e^{2\Omega(x)} g_{\mu\nu}(x) \tag{3.10}$$

the action varies as

$$\delta\mathcal{S} = \frac{1}{2} \int d^4x \sqrt{-g} T_{\mu\nu} \delta g^{\mu\nu} = \int d^4x \sqrt{-g} T^{\mu}{}_{\mu} \delta\Omega(x) \tag{3.11}$$

and we understand that if the trace of the stress-energy tensor of a given field vanishes, any conformal variation of the metric coordinates does not modify the action of the field. Therefore, in the case of an expanding (homogenous and isotropic) Universe, it implies that such a field is not experiencing the expansion of the Universe; its equation of motion would be independent of space-time expansion. Thus we expect no gravitational production for a conformal field evolving in an FLRW space-time [1]. One can derive from Eq.(1.8) and the generic action Eq.(3.1) that

[1] Classical conformal symmetry of a field theory may be broken by quantum anomalies, leading to gravitational effect even in an FLRW space-time.

the trace of the stress-energy tensor for a scalar field is given by

$$T^{\mu}{}_{\mu} = (6\xi - 1)\left(g^{\mu\nu}\partial_{\mu}\chi\partial_{\nu}\chi + \chi\right) + m_{\chi}^{2}\chi^{2}\,. \tag{3.12}$$

This shows that (classically) massless scalar field, with a nonminimal coupling to gravity $\xi = -\frac{1}{6}$, are conformally coupled, and no gravitational production is expected in an expanding Universe. Similarly, we can show from the action of a massless vector (spin 1) field, A_{μ}, that it is conformally coupled and that $T^{\mu}{}_{\mu,\,A} = 0$ resulting in no gravitational production of massless spin 1 quanta. Finally, for a spin 1/2 fermion following Dirac action in curved space-time, the trace of the stress-energy tensor $T^{\mu}{}_{\mu,\,1/2} \propto m$. We thus expect a suppressed gravitational production[2] as the mass of the fermion $m \to 0$.

3.1.2 The Bogoliubov transformations

We are interested in computing the gravitational production of particles in FLRW space-time, which describes an early era of inflation close to de Sitter space-time, followed by the classical expansion history of the Universe. In this case, the scale factor $a(\eta)$ grows exponentially fast during inflation and expands further during subsequent cosmological eras. The evolution of the scale factor induces a change in the mode frequency, leading to a fundamental ambiguity in the identification of positive and negative-frequency modes and the notion of excited states. To solve this issue, we consider the in $-$ out formalism of QFT and first, we suppose that at asymptotic times the mode functions are solutions of the free theory in Minkowski background [163],

$$\chi_{k}^{\text{in}}(\eta) \sim \frac{1}{\sqrt{2\omega_{k}^{\text{in}}}} e^{-i\omega_{k}^{\text{in}}\eta} \qquad (\eta \to -\infty) \tag{3.13}$$

$$\chi_{k}^{\text{out}}(\eta) \sim \frac{1}{\sqrt{2\omega_{k}^{\text{out}}}} e^{-i\omega_{k}^{\text{out}}\eta} \qquad (\eta \to +\infty)\,. \tag{3.14}$$

The associated constant frequencies are given at asymptotic far past and far future and are related to two distinct complete sets of operators $\hat{a}_{k}^{\text{in}}, \hat{a}_{k}^{\text{out}}$ to expand the fields. There is at any time a freedom to choose the basis of the mode functions between the in and out to expand the field operators. One can show that, in fact, there is an infinite family of equivalent representations of the fields related by a $SU(1,1)$ transformation [163], that all satisfied the canonical commutation relations, or equivalently, the Wronskian condition for the modes. Such a transformation of modes associated with a transformation of the ladder operators is called a Bogoliubov transformation. It allows to relate the mode functions in the two bases through a

[2] We note that, very recently, gravitationally 1-loop induced effective mass of (chiral) fermions have been investigated in [164]. The authors argue that a gravitational wave background induces a new energy scale that can break the classical conformal invariance of fermionic action and lead to gravitational production. This mechanism may be efficient even for $m \to 0$.

linear combination

$$\chi_k^{\rm in}(\eta) = \alpha_k \chi_k^{\rm out}(\eta) + \beta_k \chi_k^{*\ {\rm out}}(\eta) \tag{3.15}$$

$$\hat{a}_k^{\rm in} = \alpha_k^* \hat{a}_k^{\rm out} - \beta_k^* \hat{a}_{-k}^{\dagger\,{\rm out}} \tag{3.16}$$

where α_k, β_k are called Bogoliubov coefficients. For the new basis modes to follow the same equation of motion and for the new ladder operators to satisfy the canonical commutation relations, it implies that the Bogoliubov coefficients also satisfy $|\alpha_k|^2 - |\beta_k|^2 = 1$. One can check that under this condition on the Bogoliubov coefficients, the new mode functions also satisfy the Wronskian condition. We can easily invert the relation and, using the Wronskian find an expression of the Bogoliubov coefficients as a function of the modes

$$\alpha_k = i\left(\chi_k^{*\,{\rm out}}(\eta)\chi_k'^{\,{\rm in}}(\eta) - \chi_k'^{*\,{\rm out}}(\eta)\chi_k^{\rm in}(\eta)\right) \tag{3.17}$$

$$\beta_k = i\left(\chi_k'^{\,{\rm out}}(\eta)\chi_k^{\rm in}(\eta) - \chi_k^{\rm out}(\eta)\chi_k'^{\,{\rm in}}(\eta)\right)\,. \tag{3.18}$$

We emphasize that the Bogoliubov coefficients themselves are time-independent. In the following, the set of operators $\hat{a}_k^{\rm in}$ define the vacuum state $|0^{\rm in}\rangle$, that we consider to be given by the Bunch-Davies vacuum state. The expected number of particles measured by the $\hat{N}_k^{\ {\rm out}} \equiv \hat{a}_k^{\dagger\,{\rm out}}\hat{a}_k^{\rm out}$ operators may be nonzero in the vacuum state $|0^{\rm in}\rangle$ and the corresponding particle comoving number density is then given by

$$a^3 n = \int \frac{d^3k}{(2\pi)^3}|\beta_k|^2\,. \tag{3.19}$$

We see that if the expansion of space-time induces a mixing of positive and negative-frequency modes, which are solutions of the wave equation, the information is encapsulated in the Bogoliubov coefficients. Gravitational particle production sourced by the classical evolution of the background space-time can be tracked by computing the Bogoliubov coefficient β_k in this in − out formalism.

However, the continuous growth of the scale factor during the expansion shows that space-time is not asymptotically flat in the far past and future and we can associate a continuous change of frequency with a continuous change of the mode functions. Yet, we still can consider that at asymptotic early and late times, the comoving frequency $\omega_k(\eta)$ is slowly varying. The change of frequency is adiabatic as long as

$$\frac{\omega_k'(\eta)}{\omega_k^2(\eta)} \ll 1 \qquad (\eta \to \pm\infty) \tag{3.20}$$

which is generically verified for FLRW space-time expansion, sufficiently far away from any abrupt transition from quasi-de Siter phase to further evolution. For such a case, WKB approximation gives a good definition of in − out asymptotic mode functions (see [163] for further

details on the adiabatic expansion in the WKB method)

$$\chi_k^{\rm in}(\eta) \sim \frac{1}{\sqrt{2\omega_k(\eta)}} e^{-i\int^\eta \omega_k(\tau)d\tau} \qquad (\eta \to -\infty) \tag{3.21}$$

$$\chi_k^{\rm out}(\eta) \sim \frac{1}{\sqrt{2\omega_k(\eta)}} e^{-i\int^\eta \omega_k(\tau)d\tau} \qquad (\eta \to +\infty) \tag{3.22}$$

which defines the positive-frequency mode functions at the leading adiabatic order. This approximation is justified at sufficiently late and early times as higher order terms in the adiabatic expansion are vanishing for $\eta \to \pm\infty$. Thus, the associated ladder operators at asymptotic early times define the adiabatic vacuum state $|0^{\rm in}\rangle$, which we identify with the Bunch-Davies vacuum in the following.

At intermediate times η, we can decompose generically the mode function $\chi_k^{\rm in}(\eta)$ as

$$\chi_k^{\rm in}(\eta) = \tilde{\alpha}_k(\eta)\frac{1}{\sqrt{2\omega_k(\eta)}} e^{-i\int^\eta \omega_k(\tau)d\tau} + \tilde{\beta}_k(\eta)\frac{1}{\sqrt{2\omega_k(\eta)}} e^{i\int^\eta \omega_k(\tau)d\tau} \tag{3.23}$$

where we introduced two generic unknown mode functions $\tilde{\alpha}_k(\eta), \tilde{\beta}_k(\eta)$ which are associated asymptotically in the past to positive, negative-frequency part of the solution to the wave equation such that $\tilde{\alpha}_k(\eta) \to 1$ and $\tilde{\beta}_k(\eta) \to 0$ when $\eta \to -\infty$. With this parametrization of the problem, the game is now to understand the evolution of these two functions as a function of η and try to relate their late-time behavior to the Bogoliubov coefficients associated with the gravitational production mechanism. Asking for $\chi_k^{\rm in}(\eta)$ to solve the equation of motion and using the Wronskian condition $|\tilde{\alpha}_k(\eta)|^2 - |\tilde{\beta}_k(\eta)|^2 = 1$, we can invert the relation defining the unknown function $\tilde{\beta}_k(\eta)$ and compute it as

$$|\tilde{\beta}_k(\eta)|^2 = \frac{\omega_k(\eta)}{2}|\chi_k^{\rm in}(\eta)|^2 + \frac{|\chi_k'^{\rm in}(\eta)|^2}{2\omega_k(\eta)} - \frac{1}{2}\,. \tag{3.24}$$

Furthermore, one can easily show that to solve the equation of motion, these unknown functions are solutions of the following differential equations

$$\tilde{\alpha}_k'(\eta) = \tilde{\beta}_k(\eta)\frac{\omega_k'}{2\omega_k} e^{2i\int^\eta \omega_k(\tau)d\tau} \tag{3.25}$$

$$\tilde{\beta}_k'(\eta) = \tilde{\alpha}_k(\eta)\frac{\omega_k'}{2\omega_k} e^{-2i\int^\eta \omega_k(\tau)d\tau}\,. \tag{3.26}$$

We want to relate the asymptotic behavior of the function $\tilde{\beta}_k(\eta)$ with the coefficient β_k, which is related to the modes via Eq.(3.18). Evaluating this relation at sufficiently late times, one can show that

$$\beta_k = \lim_{\eta\to+\infty} i\left(\chi_k'^{\rm out}(\eta)\chi_k^{\rm in}(\eta) - \chi_k^{\rm out}(\eta)\chi_k'^{\rm in}(\eta)\right) \simeq \lim_{\eta\to+\infty} \tilde{\beta}_k(\eta) \tag{3.27}$$

where we assume that the expansion is adiabatic at late times such that $\frac{\omega_k'}{2\omega_k} \to 0$. It shows that to compute the Bogoliubov coefficient, and so the semi-classical gravitational production, one just needs to evaluate the late time limit of the function $\tilde{\beta}_k(\eta)$. At this point, there are two main approaches. Suppose we can get explicit solutions of the mode function at any time (numerically or under an analytical approximation): in that case, one can compute the function $\tilde{\beta}_k(\eta)$ from Eq.(3.24) and look at its late-time asymptotic value when it should stabilize to the Bogoliubov coefficient β_k. On the other hand, if one has only the solution for the evolution of the time-dependent frequency $\omega_k(\eta)$, one can try to solve the differential equation Eq.(3.26) for $\tilde{\beta}_k(\eta)$ and again evaluate the solution at sufficiently late-time. To do so, a specific situation simplifies the resolution drastically: considering small gravitational production such that $|\tilde{\beta}_k(\eta)| \ll 1$ along the evolution, solving Eq.(3.26) reduces to the evaluation the following integral

$$\tilde{\beta}_k(\eta) \simeq \int^{\eta} d\tau \frac{\omega_k'(\tau)}{2\omega_k(\tau)} e^{-2i\int^{\eta}\omega_k(\tau)d\tau} . \tag{3.28}$$

3.1.3 Production of UV modes from de Sitter phase

We illustrate the generation of a cosmological relic for one simple situation of de Sitter space-time and massless scalar modes, minimally coupled to gravity. This mechanism is particularly important for generating massless gravitons that follow the same dynamics as minimally coupled massless scalars in an expanding Universe. These massless gravitons can be produced from gravitational effects during the quasi-de Sitter inflation, forming a cosmological relic of tensor modes constituting a stochastic background of gravitational waves. The following computation using Bogoliubov transformations is closely related to the one done in the classical limit for the generation of cosmological perturbations during inflation in section 2.1.

The mode equation for massless scalars is simply given by

$$\chi_k''(\eta) + \left(k^2 - \frac{a''}{a}\right)\chi_k(\eta) = 0 \tag{3.29}$$

and during the de Sitter expansion the scale factor grows as

$$a = a_e e^{H_e(t-t_e)} \tag{3.30}$$

where the subscripts t_e and a_e refer to the end of the de Sitter phase. We consider H_e to be the constant Hubble rate for the de Sitter phase, which we can approximately relate to the Hubble rate at the end of inflation. Using the definition of conformal time and Hubble rate $d\eta = \frac{da}{a^2 H}$, we can relate the conformal time to the scale factor as

$$\eta = \int_{a_e}^{a} \frac{da}{a^2 H} \simeq -\frac{1}{aH} \tag{3.31}$$

where in the last equality we used $a \ll a_e$ during de Sitter phase. In particular, it shows that $a''/a \simeq 2/\eta^2$ in de Sitter phase, therefore, the mode equation is reduced to

$$\chi_k''(\eta) + \left(k^2 - \frac{2}{\eta^2}\right)\chi_k(\eta) = 0\,. \tag{3.32}$$

At asymptotic early times, corresponding to $a \ll a_e$ i.e $\eta \to -\infty$, we consider (all) the modes to be in the adiabatic Bunch-Davies vacuum and the solution at a later time can be in this case readily calculated

$$\chi_k(\eta) = \frac{e^{-ik\eta}}{\sqrt{2k}}\left(1 - \frac{i}{k\eta}\right) \tag{3.33}$$

which indeed converges to the plane wave solution at asymptotic times when $k|\eta| \to \infty$. However, at this point, we have to remember that we consider at asymptotic times an adiabatic evolution of the frequency of modes. The adiabatic condition reads

$$\frac{\omega_k'}{2\omega_k^2} \ll 1 \Leftrightarrow k^2\eta^2 \gg 1 \tag{3.34}$$

thus, if the de Sitter phase is eternal, there is no asymptotic time at which the frequency is evolving adiabatically; there is always a break of adiabaticity for any mode at horizon crossing when $k\eta \lesssim 1$. In this perspective, we also have to track the production of modes that exit the horizon in a de Sitter phase. We saw in section 2.1 that such modes are frozen when they leave the horizon and can be rapidly treated in the classical limit. The knowledge of further cosmological evolution is necessary until their reentry inside the horizon, when such modes can source primordial cosmological perturbations as derived in section 2.1. For more details on the Bogoliubov treatment of such IR modes in the various cases of massless or massive fields and non-minimally coupled fields to gravity, see the recent review [163].

For a finite de Sitter phase followed by a further adiabatic expansion, a collection of modes satisfying $k \gg a_e H_e$ are always sub-horizons and remain in the adiabatic limit. Such particle states are well defined in this semi-classical approach, as the curvature does not vary across the spatial extension of such a wavepacket $k \gg aH \sim |1/\eta|$. We can estimate the small generation of excitations for these UV modes from the de Sitter phase. As developed in the preceding part, we have two ways to evaluate gravitational particle production. We have the exact solution of the mode function at any conformal time η during de Sitter so that we can use Eq.(3.24) with

$$|\tilde{\beta}_k(\eta)|^2 = \frac{1}{4k^4\eta^4}\,. \tag{3.35}$$

We obtain the same result by using Eq.(3.28)

$$\tilde{\beta}_k(\eta) = \int^\eta d\tau \frac{\omega_k'}{2\omega_k} e^{-2i\int^\eta \omega_k d\tau} \simeq \int^\eta d\tau \frac{1}{\tau^3 k^2} e^{-2i\int^\eta \omega_k d\tau} \simeq -\frac{1}{2k^2\eta^2}\,. \tag{3.36}$$

Assuming that this function matches the Bogoliubov coefficient at the end of inflation, we obtain the comoving number density generated at the end of de Sitter phase when $\eta_e = -1/a_e H_e$ as

$$a_e^3 n(a_e) = \frac{1}{a_e^3}\int_{a_e H_e}^{+\infty} \frac{d^3k}{(2\pi)^3}|\beta_k|^2 \simeq \frac{1}{a_e^3}\int_{a_e H_e}^{+\infty} \frac{dk}{8\pi^2}\frac{a_e^4 H_e^4}{k^2} \simeq \frac{H_e^3}{8\pi^2}\,. \tag{3.37}$$

As a result, we see that we can expect the generation of particles with large momentum $k \gg a_e H_e$ and a number density at the end of the de Sitter phase given by $n(a_e) \sim H_e^3$, which is further diluted by the expansion. It is close to what was first derived in seminal papers [161, 165] and can be interpreted as a thermal bath of particles with a temperature $T \sim H_{\rm end}$ called the Gibbons-Hawking temperature, associated with the de Sitter cosmological horizon. This is, in fact, the same effect at the origin of the Hawking radiation of black holes considering a Schwarzschild metric or the Unruh effect for accelerated observers.

This simple (and naive) estimate can be refined with several improvements: the number of particles is drastically changed considering massive as well as non-minimally coupled fields. Furthermore, this estimation does not consider the contribution of low momentum modes that are frozen on super-horizon scales, as discussed above. In addition, it is valid for a de Sitter phase with exactly constant Hubble rate $H = H_e$, which is not the case for slow-roll inflation. Finally, it assumes that nothing occurs for these UV modes after de Sitter inflation and that they are frozen during their later evolution. However, as we will see in the next sections, there is an important phenomenology to study the gravitational interactions during the oscillations of the inflaton after inflation, leading to excitations from gravitational interactions of such UV modes. This motivates the work done in this thesis about the gravitational production of particles during reheating within a Boltzmann framework. We underline that the subtle connection between the Bogoliubov approach and the Boltzmann picture for gravitational effects has been investigated for the specific case of Starobinsky inflation in [112, 166, 167], and is under investigation for other inflaton potentials [168].

3.2 Gravitons exchange during reheating

This section is based on: **S. Cléry**, Y. Mambrini, K.A. Olive, S. Verner, *Gravitational portals in the early Universe*, **Phys.Rev.D 105 (2022) 7, 075005**, arXiv:2112.15214 [1]

Motivation

The hypothesis for a WIMP as a dark matter candidate is being challenged by a lack of signal in dedicated direct detection experiments such as XENON1T [169], LUX [72] or PANDAX [170] (see [64] for a detailed review). These experiments exclude a large part of the parameter space in models where dark matter communicates with the Standard Model (SM) via the

Higgs [85, 171–175], the Z [176–179] or even an electroweak extension introducing a massive Z' mediator [180–182]. However, an alternative exists in the form of particles interacting very feebly with the thermal bath, and never having reached thermal equilibrium [80, 183, 184] as introduced in the first chapter for the FIMP scenario (see 1.4). The seclusion can be justified by the weakness of a coupling (gravitational in the case of the gravitino [185–189]) or by the exchange of very heavy mediators (generated by an extra $U(1)$ [190], moduli field [191] or massive spin-2 field [192] as examples). A complete review can be found in [83] as well as related studies in [117, 193–195].

The minimal coupling one can imagine between dark matter and the Standard Model is gravitational mediated through a graviton [196, 197]. As this coupling is unavoidable, any process invoking graviton exchange provides a lower limit on the amount of dark matter produced either via the thermal bath [192, 197–201] or directly through the scattering of the inflaton [202, 203]. The energy available in both cases partly compensates for the strong reduction in coupling by the Planck mass, M_P. This is not too surprising. Indeed, we know that in the case of a FIMP, a coupling of the order of $\sim 10^{-11}$ is needed to produce dark matter in sufficient quantities. This corresponds to an effective coupling of the order of $\frac{E^2}{M_P^2}$, with $E \sim 10^{13}$ GeV representing the available energy in the interaction. This energy corresponds, roughly, to the mass of the inflaton. It is therefore at the end of inflation, during the transition period of reheating, between an inflaton-dominated universe and the radiative universe, that the available energy is sufficient for the efficient gravitational production of dark matter.

The reheating process is not instantaneous [116, 193, 204] and can be sourced by many mechanisms discussed in the section 2.2. The radiation bath may be produced by inflaton decays or scattering which require a coupling of the inflaton to the Standard Model, or as we show below through the gravitational production of radiation. In this case, as the radiation begins to appear the Universe rapidly achieves a maximum temperature, $T_{\rm max}$, and the reheating process continues until radiation domination is achieved at $T_{\rm RH}$. The evolution of the radiation density depends on [87, 106] 1) how it is produced, that is, through decays, or scatterings, 2) the dominant final state particle spin, and 3) the form of the inflaton potential about its minimum. For this analysis we consider that the inflaton oscillates around the minimum of its potential parametrized as $V(\phi) \simeq \lambda \phi^k M_P^{4-k}$. This approximation is appropriate for the Starobinsky model [93] (leading to $k = 2$), as well as more general α-attractor type models [105, 141]. Once the reheating is achieved, $T > T_{\rm RH}$, the inflaton disappears from the energy budget and the temperature evolves isentropically $T \propto a^{-1}$, where a is the scale factor of the Universe. As we show below, the evolution of the radiation density can be modified by the gravitational production of Standard Model quanta which induces a lower bound on the maximum temperature of the Universe. We show that it is of the order of 10^{12} GeV, and is one of the main results of our analysis.

If the production of dark matter occurs during reheating, it is intimately linked to the behavior of the inflaton and the evolution of the thermal bath. Often it is assumed that either the dark matter is directly coupled to the inflaton, in which case, it can be produced directly from inflaton decays [87, 115, 116, 205] or it is coupled to the Standard Model, and thus produced thermal as the gravitino or other super-weakly interacting particles. In the latter case, it has also been shown that radiative decay of the inflaton [206] could be the dominant process to populate the dark Universe.

In the following section, we analyze all processes involving a gravitational interaction, comparing the modes of production via the thermal bath, the scattering of the inflaton, and the gravitational production of particles from the thermal bath that subsequently produce dark matter through gravity as well. In this sense, each of the physical quantities we consider, such as the relic density or maximum temperature, must be considered as *lower bounds*, as the gravitational process we compute is inevitable in any theory based on Einstein's gravity. As a result, these lower bounds must be taken into account in any kind of extension of the Standard Model, and can be thought of as a gravitational "background noise". We do not consider preheating via parametric or stochastic resonances as it has been done in [119], because we want to compute the minimal *unavoidable* amount of dark matter, and thus derive the strongest model-independent constraints on the dark matter mass, supposing that it only couples gravitationally. The only nongravitational coupling we consider is a coupling of the inflaton to SM fields to achieve reheating. Thus, we consider a generic Yukawa-like coupling of the form, $y\phi\bar{f}f$, where f is some Standard Model fermion. We assume rapid thermalization, and these decays are (partially) responsible for the growing thermal bath. However, the production of dark matter from the thermal bath is entirely gravitational.

The framework for our computation is outlined in 3.2.1. We consider both scalar and fermionic dark matter coupled to the Standard Model and the inflaton only through gravity. We compute the rates for the production of dark matter either through thermal scattering (mediated by gravity alone) or from the inflaton condensate. We choose an attractor form for the inflaton potential that, when expanded about its minimum, takes the form ϕ^k. Our results are sensitive to k. Reheating takes place as the inflaton oscillates about this minimum. In 3.2.2 we consider three distinct gravitational processes: the gravitational production of dark matter from the thermal bath, the gravitational production of dark matter from the condensate, and the gravitational production of the thermal bath from the condensate. We then compare each mode in 3.2.3.

3.2.1 The framework

We study universal gravitational interactions that must exist between the inflationary and dark sectors. If the space-time metric is expanded around flat space using $g_{\mu\nu} \simeq \eta_{\mu\nu} + \tilde{h}_{\mu\nu}$ the

gravitational Lagrangian in the transverse-traceless gauge in second order can be written (see Appendix B) as

$$\mathcal{L} = \frac{M_P^2}{2} R \ni \frac{M_P^2}{8} (\partial^\alpha \tilde{h}^{\mu\nu})(\partial_\alpha \tilde{h}_{\mu\nu}) = \frac{1}{2} (\partial^\alpha h^{\mu\nu})(\partial_\alpha h_{\mu\nu}) \tag{3.38}$$

where $h_{\mu\nu} = (M_P/2)\tilde{h}_{\mu\nu}$ is the canonically normalized perturbation and $M_P = (8\pi G)^{-1/2} \simeq 2.4 \times 10^{18}\,\text{GeV}$ is the reduced Planck mass. Gravitational interactions are described by the Lagrangian (see Appendix B)

$$\sqrt{-g}\mathcal{L}_{\text{int}} = -\frac{1}{M_P} h_{\mu\nu} \left(T^{\mu\nu}_{SM} + T^{\mu\nu}_{\phi} + T^{\mu\nu}_{X} \right) . \tag{3.39}$$

Here SM represents Standard Model fields, ϕ is the inflaton and X is a dark matter candidate. The form of the stress-energy tensor $T_i^{\mu\nu}$ depends on the spin of the field, $i = 0,\, 1/2,\, 1$,[3] and is given by

$$T_0^{\mu\nu} = \partial^\mu S \partial^\nu S - g^{\mu\nu} \left[\frac{1}{2} \partial^\alpha S \partial_\alpha S - V(S) \right] , \tag{3.40}$$

$$T_{1/2}^{\mu\nu} = \frac{i}{4} \left[\bar{\chi}\gamma^\mu \overleftrightarrow{\partial^\nu} \chi + \bar{\chi}\gamma^\nu \overleftrightarrow{\partial^\mu} \chi \right] - g^{\mu\nu} \left[\frac{i}{2} \bar{\chi}\gamma^\alpha \overleftrightarrow{\partial_\alpha} \chi - m_\chi \bar{\chi}\chi \right] , \tag{3.41}$$

$$T_1^{\mu\nu} = \frac{1}{2} \left[F^\mu_\alpha F^{\nu\alpha} + F^\nu_\alpha F^{\mu\alpha} - \frac{1}{2} g^{\mu\nu} F^{\alpha\beta} F_{\alpha\beta} \right] , \tag{3.42}$$

where $V(S)$ is the scalar potential for either the scalar dark matter candidate, the SM Higgs boson, or the inflaton, with $S = X, H, \phi$, and $F_{\mu\nu} = \partial_\mu A_\nu - \partial_\nu A_\mu$ is the field strength for a vector field, A_μ. In Fig. 3.1, we show the s-channel exchange of a graviton obtained from the Lagrangian (3.39) for the production of dark matter from either the inflaton condensate or Standard Model fields. In addition, a similar diagram exists for the production of Standard Model fields (during the reheat process) from the inflaton condensate in the initial state.

Although the direct coupling to the massless graviton appears to be feeble due to Planck suppression, the energy available in the thermal bath during the initial stage of reheating is large enough to make the gravitational production rates significant.

The scattering amplitudes related to the production rate of the processes $\phi/\text{SM}^i(p_1) + \phi/\text{SM}^i(p_2) \to \text{SM}^i/X^j(p_3) + \text{SM}^i/X^j(p_4)$ can be parametrized by

$$\mathcal{M}^{ij} \propto M^j_{\mu\nu} \Pi^{\mu\nu\rho\sigma} M^i_{\rho\sigma} , \tag{3.43}$$

where $(i,\, j)$ denotes the spin of the (initial,final) state involved in the scattering process and $i, j = 0, 1/2, 1$. $\Pi^{\mu\nu\rho\sigma}$ is the graviton propagator for the canonical field h with momentum

[3] In this analysis we consider dark matter candidates that are either real scalars or a Dirac fermion.

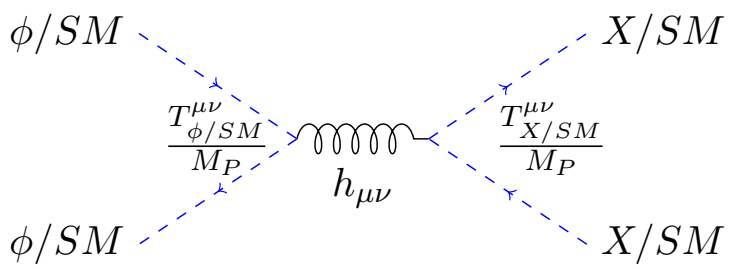

Figure 3.1: *Feynman diagram for the production of dark matter through the gravitational scattering of the Standard Model particle bath or inflaton condensate.*

$k = p_1 + p_2$,

$$\Pi^{\mu\nu\rho\sigma}(k) = \frac{\eta^{\rho\nu}\eta^{\sigma\mu} + \eta^{\rho\mu}\eta^{\sigma\nu} - \eta^{\rho\sigma}\eta^{\mu\nu}}{2k^2} \,. \tag{3.44}$$

The partial amplitudes, $M^i_{\mu\nu}$, are given by

$$M^0_{\mu\nu} = \frac{1}{2}\left[p_{1\mu}p_{2\nu} + p_{1\nu}p_{2\mu} - \eta_{\mu\nu}p_1\cdot p_2 - \eta_{\mu\nu}V''(S)\right] , \tag{3.45}$$

$$M^{1/2}_{\mu\nu} = \frac{1}{4}\bar{v}(p_2)\left[\gamma_\mu(p_1-p_2)_\nu + \gamma_\nu(p_1-p_2)_\mu\right]u(p_1) , \tag{3.46}$$

$$\begin{aligned} M^1_{\mu\nu} = \frac{1}{2}\Big[& \epsilon_2^*\cdot\epsilon_1\left(p_{1\mu}p_{2\nu} + p_{1\nu}p_{2\mu}\right) \\ & - \epsilon_2^*\cdot p_1\left(p_{2\mu}\epsilon_{1\nu} + \epsilon_{1\mu}p_{2\nu}\right) - \epsilon_1\cdot p_2\left(p_{1\nu}\epsilon^*_{2\mu} + p_{1\mu}\epsilon^*_{2\nu}\right) \\ & + p_1\cdot p_2\left(\epsilon_{1\mu}\epsilon^*_{2\nu} + \epsilon_{1\nu}\epsilon^*_{2\mu}\right) \\ & + g_{\mu\nu}\left(\epsilon_2^*\cdot p_1\epsilon_1\cdot p_2 - p_1\cdot p_2\,\epsilon_2^*\cdot\epsilon_1\right)\Big] , \end{aligned} \tag{3.47}$$

with analogous expressions for dark matter in terms of the dark matter momenta, p_3, p_4, and potential $V(X)$, if X is a scalar. For an initial state inflaton with $S = \phi$, we replace $M^0_{\mu\nu}$ with $T^0_{\mu\nu}$ from Eq. (3.40). As we only consider vectors in the Standard Model, their masses have been neglected in Eq. (3.47).

In what follows, we consider three distinct processes based on the diagram in Fig. 3.1: for the production of dark matter, A) SM + SM $\to X + X$, B) $\phi + \phi \to X + X$, where the latter involves the inflaton condensate (zero mode) in the initial state rather than an initial state particle with momentum $p_{1,2}$ (see below for more detail), and C) $\phi + \phi \to$ SM + SM, as a minimal and unavoidable contribution to the reheating process.

The dark matter production rate from SM fields can be readily calculated by assuming that the initial particle states are massless. This assumption can be justified by the fact that the energy associated with the momenta, $p_1\,, p_2$ is extremely large at the end of inflation and

dominates over electroweak scale quantities.

The dark matter production rate $R(T)$ for the SM+SM $\to X + X$ process with amplitude $\mathcal{M}$[4] is

$$R(T) = \frac{2}{1024\pi^6} \times \int f_1 f_2 E_1 \, \mathrm{d}E_1 E_2 \, \mathrm{d}E_2 \, \mathrm{d}\cos\theta_{12} \int |\mathcal{M}|^2 \, \mathrm{d}\Omega_{13} \,, \tag{3.48}$$

where the factor of two accounts for two dark matter particles per scattering, E_i denotes the energy of particle $i = 1, 2, 3, 4$, θ_{13} and θ_{12} are the angles formed by momenta $\mathbf{p}_{1,3}$ and $\mathbf{p}_{1,2}$, respectively, and

$$f_i = \frac{1}{e^{E_i/T} \pm 1} \tag{3.49}$$

represents the assumed thermal distributions of the incoming SM particles.

The total amplitude squared for the gravitational scattering process SM+SM $\to X_j + X_j$ is given by a sum of the three amplitudes associated with different initial state spins,

$$|\mathcal{M}|^2 = 4|\mathcal{M}^0|^2 + 45|\mathcal{M}^{1/2}|^2 + 12|\mathcal{M}^1|^2 \,. \tag{3.50}$$

These were calculated in [192] and it was found that the dark matter production rate is given by

$$R_j^T = R_j(T) = \beta_j \frac{T^8}{M_P^4} \,, \tag{3.51}$$

where j refers to the spin of X (either 0 or 1/2), the constants β_j and details related to the computation of dark matter production rate and the amplitude squared are given in the addendum at the end of the section A.

For the production of dark matter through the scattering of the inflaton condensate we consider the time-dependent oscillation of a classical inflaton field $\phi(t)$. Since our computation depends explicitly on inflaton potential, we consider the α-attractor T-model [105] as a specific example Eq.(2.61),

$$V(\phi) \;=\; \lambda M_P^4 \left| \sqrt{6} \tanh\left(\frac{\phi}{\sqrt{6} M_P} \right) \right|^k \,, \tag{3.52}$$

In this class of models, inflation occurs at large field values ($\phi > M_P$), and after the period of exponential expansion, the inflaton begins to oscillate about the minimum and the process of reheating begins. The potential can be expanded about the minimum as [5]

$$V(\phi) = \lambda \frac{\phi^k}{M_P^{k-4}}, \quad \phi \ll M_P \,. \tag{3.53}$$

[4] It should be noted that we include the symmetry factors associated with identical initial and final states in the squared amplitude, $|\mathcal{M}|^2$.

[5] It should be noted that this discussion is general and not limited to T-models of inflation.

The time-dependent oscillating inflaton field can be parametrized as

$$\phi(t) \;=\; \phi_0(t)\cdot\mathcal{P}(t)\,, \tag{3.54}$$

where $\phi_0(t)$ is the time-dependent amplitude that includes the effects of redshift and $\mathcal{P}(t)$ describes the periodicity of the oscillation.

To calculate the dark matter production rate, we combine the potential (3.53) with Eq. (3.54), which leads to $V(\phi) = V(\phi_0)\cdot\mathcal{P}(t)^k$. We next expand the potential energy in terms of the Fourier modes [106, 131, 207]

$$V(\phi) = V(\phi_0)\sum_{n=-\infty}^{\infty}\mathcal{P}_n^k e^{-in\omega t} = \rho_\phi\sum_{n=-\infty}^{\infty}\mathcal{P}_n^k e^{-in\omega t}\,, \tag{3.55}$$

where ω is the frequency of oscillation of ϕ, given by [106]

$$\omega = m_\phi\sqrt{\frac{\pi k}{2(k-1)}}\frac{\Gamma(\frac{1}{2}+\frac{1}{k})}{\Gamma(\frac{1}{k})}. \tag{3.56}$$

For scalar dark matter, we find that the particle production rate per unit volume and unit time for an arbitrary value of k is given by

$$R_0^{\phi^k} = \frac{2\times\rho_\phi^2}{16\pi M_P^4}\Sigma_0^k\,, \tag{3.57}$$

where the factor of two accounts for the fact we produce two dark matter particles per scattering, with

$$\Sigma_0^k = \sum_{n=1}^{\infty}|\mathcal{P}_n^k|^2\left[1+\frac{2m_X^2}{E_n^2}\right]^2\sqrt{1-\frac{4m_X^2}{E_n^2}}\,, \tag{3.58}$$

where $E_n = n\omega$ is the energy of the n-th inflaton oscillation mode and m_X is the mass of the produced dark matter. A detailed calculation of this rate is presented in the second addendum B.

For the case $k = 2$, we find that the particle production rate is given by

$$R_0^{\phi^2} = \frac{2\times\rho_\phi^2}{256\pi M_P^4}\left(1+\frac{m_X^2}{2m_\phi^2}\right)^2\sqrt{1-\frac{m_X^2}{m_\phi^2}}\,, \tag{3.59}$$

where $m_\phi^2 = V''(\phi_0)$, and since $\sum\mathcal{P}_n^2 e^{-in\omega t} = \cos^2(m_\phi t)$, we find that only the second Fourier mode in the sum contributes, with $\sum|\mathcal{P}_n^2|^2 = \frac{1}{16}$ and $E_2 = 2m_\phi$.[6]

[6]We note that the rate calculated here differs from [202] by a factor of 8, because in the latter the inflaton was treated as a particle and not a condensate resulting in a difference by a factor of 2 in the applied symmetry factors. In addition, the interaction considered there did not use a properly normalized graviton resulting in a

For a fermionic dark matter candidate, we find the following rate

$$R_{1/2}^{\phi^k} = \frac{2 \times \rho_\phi^2}{4\pi M_P^4} \frac{m_X^2}{m_\phi^2} \Sigma_{1/2}^k \,, \tag{3.60}$$

where the factor of two accounts for the sum over the particle and antiparticle final states, with

$$\Sigma_{1/2}^k = \sum_{n=1}^{+\infty} |\mathcal{P}_n^k|^2 \frac{m_\phi^2}{E_n^2} \left[1 - \frac{4m_X^2}{E_n^2}\right]^{3/2} . \tag{3.61}$$

For the case $k = 2$, we obtain

$$R_{1/2}^{\phi^2} \simeq \frac{2 \times \rho_\phi^2}{256\pi M_P^4} \frac{m_X^2}{m_\phi^2} \left[1 - \frac{m_X^2}{m_\phi^2}\right]^{3/2} . \tag{3.62}$$

A detailed discussion related to the dark matter production rates through the inflaton condensate scattering is given in the second addendum B.

For the production of SM fields from inflaton oscillations, we follow the same procedure, but replace the partial amplitude, $M_{\mu\nu}^j$, for dark matter with the appropriate amplitude involving SM fields. Below, we consider only the example of producing Higgs bosons, namely $\phi + \phi \to H + H$.

3.2.2 Gravitational production of quanta

As we discussed above, the graviton can act as a portal between the inflaton, SM fields and a potential dark matter candidate. We here consider three cases in detail:

1. The graviton portal between a thermal bath and dark matter. This is essentially a gravitational freeze-in mechanism for the production of dark matter.

2. The graviton portal between the inflaton and dark matter. In this case, the inflaton directly populates the dark matter without the need of either the thermal bath or a mediator between the SM and the dark matter candidate.

3. The graviton portal between the inflaton and the Standard Model sector to produce a radiative bath at the start of reheating.

3.2.2.1 SM SM $\to h_{\mu\nu} \to$ DM DM

The spin-2 portal for the production of dark matter was considered in [192] for both massive and massless spin-2 fields. Here we restrict our attention to the massless (graviton) portal.

factor of 2 in the vertex and 16 in the rate.

For an inflaton potential with $k = 2$, the scattering cross section between SM fields and dark matter is proportional to T^2/M_P^4, and we expect the resulting dark matter abundance to be primarily sensitive to the reheating temperature (rather than the maximum temperature attained during the reheating process). Sensitivity to $T_{\rm max}$ requires a cross section with a steep dependence on temperature, $\sigma \propto T^n$, with $n \geq 6$. When $k > 2$, sensitivity to $T_{\rm max}$ requires only $n > (10 - 2k)/(k - 1)$ when the primary reheating mechanism is determined by inflaton decays as discussed below. Then, for example, when $k = 4$, when $n > 2/3$, the dark matter abundance becomes sensitive to $T_{\rm max}$. For the graviton portal, then, this occurs when $k \geq 3$.

The gravitational scattering of particles in the primordial plasma can produce massive particles playing the role of a viable dark matter candidate X. Then, the matter density n_X obeys the classical Boltzmann equation[7]

$$\frac{dn_X}{dt} + 3Hn_X = R_X^T \,, \tag{3.63}$$

It is more convenient to work with a as dynamical parameter, rather than t or T. Eq.(3.63) can then be rewritten

$$\frac{dn_X}{da} + 3\frac{n_X}{a} = \frac{R_X^T(a)}{Ha} \,. \tag{3.64}$$

Since the production rate R_X^T is dependent on the initial state energies, i.e., of the temperature of the thermal bath, one needs the expression of $T(a)$ to solve the Boltzmann equation in terms of the scale factor. We explain the functional dependence of R_X^T on a below. Defining the comoving number $Y_X = na^3$, we obtain

$$\frac{dY_X}{da} = \frac{a^2 R_X^i(a)}{H} \,. \tag{3.65}$$

We assume an inflaton potential of the form given in Eq. (3.53). We next apply the expressions for energy conservation for the inflaton density ρ_ϕ and the radiation density ρ_R

$$\frac{d\rho_\phi}{dt} + 3H(1 + w_\phi)\rho_\phi \simeq -(1 + w_\phi)\Gamma_\phi \rho_\phi \tag{3.66}$$

$$\frac{d\rho_R}{dt} + 4H\rho_R \simeq (1 + w_\phi)\Gamma_\phi \rho_\phi \,. \tag{3.67}$$

where $w_\phi = \frac{P_\phi}{\rho_\phi} = \frac{k-2}{k+2}$ [106] is the equation of state parameter. Here we assume that reheating primarily occurs due to the inflaton effective coupling to the Standard Model fermions, given by the Lagrangian

$$\mathcal{L}^y_{\phi - SM} = -y\phi \bar{f} f \,, \tag{3.68}$$

[7]We note that we include the relevant factors of 2 associated with identical initial states in the definition of the particle production rate.

where y is a Yukawa-like coupling and f is a Standard Model fermion. Note that in a gauge invariant theory, the coupling in Eq. (3.68) must originate from a higher dimensional ($D \geq 5$) operator, and thus we view y as an effective coupling. At the renormalizable level, we could also consider a coupling of ϕ to the SM Higgs which for $k = 2$ would lead to an identical evolution during the reheating process.[8] The width of ϕ is easily determined from the coupling (3.68)

$$\Gamma_\phi = \frac{y^2}{8\pi} m_\phi \,. \tag{3.69}$$

Note that for $k > 2$, there is a k-dependent correction and m_ϕ depends on ϕ and hence on the scale factor a. We defined the inflaton energy density and pressure as

$$\rho_\phi = \frac{1}{2}\langle\dot{\phi}^2\rangle + \langle V(\phi)\rangle, \qquad P_\phi = \frac{1}{2}\langle\dot{\phi}^2\rangle - \langle V(\phi)\rangle. \tag{3.70}$$

We can solve Eqs. (3.66, 3.67) and obtain [87, 106]

$$\rho_\phi(a) = \rho_{\rm end}\left(\frac{a_{\rm end}}{a}\right)^{\frac{6k}{k+2}} \tag{3.71}$$

and

$$\rho_R(a) = \rho_{\rm RH}\left(\frac{a_{\rm RH}}{a}\right)^{\frac{6k-6}{k+2}} \frac{1-\left(\frac{a_{\rm end}}{a}\right)^{\frac{14-2k}{k+2}}}{1-\left(\frac{a_{\rm end}}{a_{\rm RH}}\right)^{\frac{14-2k}{k+2}}}\,, \tag{3.72}$$

where these relations hold for $a_{\rm end} \ll a \ll a_{\rm RH}$. $a_{\rm end}$ is a reference point marking the end of inflation. $\rho_\phi(a_{\rm end})$ corresponds to the total energy density (there is virtually no radiation at this point) when the slow-roll parameter $\epsilon = 1$. At this moment, $\rho_{\rm end} = \frac{3}{2}V(\phi_{\rm end})$ [209]. Note that this solution possesses a maximum for $\rho_R(a)$ (at $a = a_{\rm max}$). We have also defined $\rho_{\rm RH}$ and $a_{\rm RH}$ such that $\rho_R(a_{\rm RH}) = \rho_\phi(a_{\rm RH})$. Since

$$\rho_R = \frac{g_T \pi^2}{30} T^4 \equiv \alpha T^4\,, \tag{3.73}$$

where g_T is the number of relativistic degrees of freedom at the temperature, T. Thus, we have $\rho_R(a_{\rm max}) = \alpha T_{\rm max}^4$ and $\rho_R(a_{\rm RH}) = \alpha T_{\rm RH}^4$. The ratio of $a_{\rm max}$ to $a_{\rm end}$ is fixed and depends only on k [87]

$$\frac{a_{\rm max}}{a_{\rm end}} = \left(\frac{2k+4}{3k-3}\right)^{\frac{k+2}{14-2k}}\,. \tag{3.74}$$

Since we can express T as function of the scale factor, a, with Eq. (3.72), we can implement

[8] For other values of k, the relation between T and a is altered for bosonic final states as discussed in detail in [106]. Couplings of the inflaton of the form in Eq. (3.68) as well as couplings to Higgs bosons were discussed in no-scale supergravity inflation models in [208].

that relation in Eq. (3.51) to obtain R_X^T as function of a,

$$R_X^T(a) = \beta_X \frac{\rho_{\rm RH}^2}{\alpha^2 M_P^4} \left(\frac{a_{\rm RH}}{a}\right)^{\frac{12k-12}{k+2}} \left[\frac{1-\left(\frac{a_{\rm end}}{a}\right)^{\frac{14-2k}{k+2}}}{1-\left(\frac{a_{\rm end}}{a_{\rm RH}}\right)^{\frac{14-2k}{k+2}}}\right]^2 . \tag{3.75}$$

Using $H \simeq \frac{\sqrt{\rho_\phi(a)}}{\sqrt{3}M_P}$, which is valid for $a \ll a_{\rm RH}$, Eq. (3.65) becomes

$$\frac{dY_X}{da} = \frac{\sqrt{3}M_P}{\sqrt{\rho_{\rm RH}}} a^2 \left(\frac{a}{a_{\rm RH}}\right)^{\frac{3k}{k+2}} R_X^T(a) . \tag{3.76}$$

The solution to this equation is

$$n_X^T(a_{\rm RH}) = \frac{\beta_X\sqrt{3}}{\alpha^2 M_P^3} \frac{\rho_{\rm RH}^{3/2}}{(1-(a_{\rm end}/a_{\rm RH})^{\frac{14-2k}{k+2}})^2} \begin{cases} \ln\left(\frac{a_{\rm RH}}{a_{\rm end}}\right) - \frac{5}{16}\left(3 - 4\left(\frac{a_{\rm end}}{a_{\rm RH}}\right)^{\frac{8}{5}} + \left(\frac{a_{\rm end}}{a_{\rm RH}}\right)^{\frac{16}{5}}\right) & [k=3] \\ \frac{k+2}{6}\left(\frac{1}{3-k} + \frac{3}{k-1}\left(\frac{a_{\rm end}}{a_{\rm RH}}\right)^{\frac{14-2k}{k+2}}\right. & \\ \left. + \frac{(k-7)^2}{k^3+k^2-17k+15}\left(\frac{a_{\rm end}}{a_{\rm RH}}\right)^{\frac{18-6k}{k+2}} - \frac{3}{k+5}\left(\frac{a_{\rm end}}{a_{\rm RH}}\right)^{\frac{28-4k}{k+2}}\right) & [k\neq 3] \end{cases} \tag{3.77}$$

where we integrated Eq. (3.76) between the values of the scale factor corresponding to the end of inflation, $a_{\rm end}$, and the reheating temperature (reached at $a_{\rm RH}$). Writing the relic abundance [16]

$$\Omega_X h^2 = 1.6 \times 10^8 \frac{g_0}{g_{\rm RH}} \frac{n(T_{\rm RH})}{T_{\rm RH}^3} \frac{m_X}{1\ {\rm GeV}}, \tag{3.78}$$

and inserting Eq. (3.77), we obtain

$$\Omega_X^T h^2 = \Omega_k \times \begin{cases} \frac{5}{18}\ln\left(\frac{\rho_{\rm end}}{\rho_{\rm RH}}\right) - \frac{5}{16}\left(3 - 4\left(\frac{\rho_{\rm RH}}{\rho_{\rm end}}\right)^{\frac{4}{9}} + \left(\frac{\rho_{\rm RH}}{\rho_{\rm end}}\right)^{\frac{8}{9}}\right) & [k=3] \\ \frac{k+2}{6}\left(\frac{1}{3-k} + \frac{3}{k-1}\left(\frac{\rho_{\rm RH}}{\rho_{\rm end}}\right)^{\frac{7-k}{3k}} + \frac{(k-7)^2}{k^3+k^2-17k+15}\left(\frac{\rho_{\rm RH}}{\rho_{\rm end}}\right)^{\frac{3-k}{k}} - \frac{3}{k+5}\left(\frac{\rho_{\rm RH}}{\rho_{\rm end}}\right)^{\frac{14-2k}{3k}}\right) & [k\neq 3] \end{cases} \tag{3.79}$$

with

$$\Omega_k = 1.6 \times 10^8 \frac{g_0}{g_{\rm RH}} \frac{\beta_X\sqrt{3}}{\sqrt{\alpha}} \frac{m_X}{1\ {\rm GeV}} \frac{T_{\rm RH}^3}{M_P^3} \left[1 - \left(\frac{\rho_{\rm RH}}{\rho_{\rm end}}\right)^{\frac{7-k}{3k}}\right]^{-2} , \tag{3.80}$$

where $g_0 = 43/11$ and we take $g_{\rm RH} = 427/4$ as the Standard Model value.

We observe that, for a given reheating temperature, the relic abundance decreases with k.

Furthermore, whereas $\Omega_X^T h^2 \propto T_{\rm RH}^3$ for a quadratic potential, it becomes $\propto T_{\rm RH}^2$ for a quartic potential, and even $\propto T_{\rm RH}$ for $k = 6$. This comes from the fact that the Hubble parameter, dominated by the evolution of the inflaton, has a greater dependence on T for larger values of k, slowing down the production mechanism for large temperatures.

3.2.2.2 $\phi\ \phi \to h_{\mu\nu} \to$ DM DM

As noted earlier, it is also possible that the inflaton condensate can lead to the direct production of dark matter through single graviton exchange [202]. Here, we generalize that result for $k \geq 2$. Having computed the production rate in Eqs. (3.57) and (3.60) for scalar and fermionic dark matter respectively, we can replace R_X^T with the rates in Eq. (3.76). Then integrating

$$\frac{dY_X}{da} = \frac{\sqrt{3}M_P}{\sqrt{\rho_{\rm RH}}} a^2 \left(\frac{a}{a_{\rm RH}}\right)^{\frac{3k}{k+2}} R_X^{\phi^k}(a) \tag{3.81}$$

between $a_{\rm end}$ and $a_{\rm RH}$ gives for scalar dark matter

$$n_0^\phi(a_{\rm RH}) = \frac{\sqrt{3}\rho_{\rm RH}^{3/2}}{8\pi M_P^3} \frac{k+2}{6k-6} \left[\left(\frac{a_{\rm RH}}{a_{\rm end}}\right)^{\frac{6k-6}{k+2}} - 1\right] \Sigma_0^k \tag{3.82}$$

which can be expressed as function of $\rho_{\rm end}$ using Eq. (3.71):

$$n_0^\phi(a_{\rm RH}) \simeq \frac{\sqrt{3}\rho_{\rm RH}^{3/2}}{8\pi M_P^3} \frac{k+2}{6k-6} \left(\frac{\rho_{\rm end}}{\rho_{\rm RH}}\right)^{1-\frac{1}{k}} \Sigma_0^k, \tag{3.83}$$

or

$$\begin{aligned} \frac{\Omega_0^\phi h^2}{0.1} &\simeq \left(\frac{\rho_{\rm end}}{10^{64}{\rm GeV}^4}\right)^{1-\frac{1}{k}} \left(\frac{10^{40}{\rm GeV}^4}{\rho_{\rm RH}}\right)^{\frac{1}{4}-\frac{1}{k}} \left(\frac{k+2}{6k-6}\right) \\ &\times \Sigma_0^k \times \frac{m_X}{2.4 \times 10^{\frac{24}{k}-7}{\rm GeV}} \end{aligned} \tag{3.84}$$

where we assumed $a_{\rm RH} \gg a_{\rm end}$. Note that the dependence on ρ_ϕ used in Eq. (3.81) hides the fact that we considered a decaying inflaton during the reheating.

For fermionic dark matter we obtained

$$\begin{aligned} n_{1/2}^\phi(a_{\rm RH}) &= \frac{m_X^2\sqrt{3}(k+2)\rho_{\rm RH}^{\frac{1}{2}+\frac{2}{k}}}{12\pi k(k-1)\lambda^{\frac{2}{k}} M_P^{1+\frac{8}{k}}} \left[\left(\frac{a_{\rm RH}}{a_{\rm end}}\right)^{\frac{6}{k+2}} - 1\right] \Sigma_{\frac{1}{2}}^k \\ &\simeq \frac{m_X^2\sqrt{3}(k+2)\rho_{\rm RH}^{\frac{1}{2}+\frac{2}{k}}}{12\pi k(k-1)\lambda^{\frac{2}{k}} M_P^{1+\frac{8}{k}}} \left(\frac{\rho_{\rm end}}{\rho_{\rm RH}}\right)^{\frac{1}{k}} \Sigma_{\frac{1}{2}}^k \end{aligned} \tag{3.85}$$

where we used

$$m_\phi^2 = V''(\phi_0) = k(k-1)\lambda^{\frac{2}{k}} M_P^2 \left(\frac{\rho_\phi}{M_P^4}\right)^{1-\frac{2}{k}} . \tag{3.86}$$

We can simplify the expression to write

$$\begin{aligned} \frac{\Omega_{1/2}^{\phi} h^2}{0.1} &= \frac{\Sigma_{1/2}^{k}}{2.4^{\frac{8}{k}}} \frac{k+2}{k(k-1)} \left(\frac{10^{-11}}{\lambda}\right)^{\frac{2}{k}} \left(\frac{10^{40}\mathrm{GeV}^4}{\rho_{\mathrm{RH}}}\right)^{\frac{1}{4}-\frac{1}{k}} \\ &\times \left(\frac{\rho_{\mathrm{end}}}{10^{64}\mathrm{GeV}^4}\right)^{\frac{1}{k}} \left(\frac{m_X}{8.3\times 10^{6+\frac{6}{k}}\mathrm{GeV}}\right)^{3} \end{aligned} \tag{3.87}$$

3.2.2.3 $\phi\ \phi \to h_{\mu\nu} \to$ SM SM

Up until now, we have assumed that the thermal bath was produced via inflaton decays. However, for low reheat temperatures, and hence small values of the Yukawa-like inflaton coupling, y, it is possible that radiation, in the form of Higgs bosons, is produced directly from the condensate via gravitational interactions.

The calculation for the production of SM fields produced by the scattering of the inflaton via gravity is similar to the preceding calculation for dark matter. As was shown in [106, 202], there exists the possibility that the thermal bath is produced not by inflaton decay but rather by inflaton scattering after inflation. This occurs for instance for low values of y. In this case, the maximum temperature is not given by the inflaton width, but by the scattering process, whereas the final reheating (and thus T_{RH}) is still dominated by the decay. This is illustrated in Fig. 3.2 below. In fact, the gravitational scattering $\phi\phi \to h_{\mu\nu} \to HH$ is always present and can never be eliminated. Such a process generates an effective coupling

$$\mathcal{L}_h = \sigma_h \phi^2 H^2 . \tag{3.88}$$

We can write the left-hand side of Eq. (3.67) as [106]

$$(1+w)\Gamma_\phi \rho_\phi = \frac{1}{8\pi}\sum_{n=1}^{\infty} |\mathcal{M}_n|^2 E_n = N\frac{\sigma_h^2}{4\pi}\phi_0^4 \omega \sum_{n=1}^{\infty} n|\mathcal{P}_n^k|^2. \tag{3.89}$$

where we used $\mathcal{M}_n = 2\sigma_h \phi_0^2 \mathcal{P}_n^k$, and $N = 4$ is the number of real scalars in the Standard Model, when we neglect the Higgs mass. Identifying this rate with that in Eq. (3.57), and $(1+w)\Gamma_\phi\rho_\phi = \omega R_0^{\phi^k}$, we deduce that

$$\sigma_h = \frac{\rho_\phi}{2M_P^2\phi_0^2}, \tag{3.90}$$

for each real scalar. Thus for the Standard Model Higgs, and in the case $k = 2$ we have

$$\sigma_h = \frac{m_\phi^2}{4M_P^2} \simeq 3.9 \times 10^{-11} \left(\frac{m_\phi}{3 \times 10^{13}\ \text{GeV}} \right)^2 . \tag{3.91}$$

σ_h can be considered as the lowest possible and inevitable value for a quartic coupling between the inflaton and scalars. This may be important and even dominate the reheating process at its earliest stages. We note that in a theory with additional weak scale scalars such as the minimal supersymmetric Standard Model (MSSM), the gravitational production is increased due to the large number of scalars, $N = 98$ in the MSSM. Note also that there is a minimal gravitational production rate for the production of SM fermions and gauge bosons though this is completely negligible due to the mass suppression (see e.g. Eq. (3.60) for fermions). Thus if we restrict our attention to the Standard Model, we take $N = 4$ corresponding to the four real scalar degrees of freedom.

We now recompute the evolution of the radiation density using Eq. (3.67) and (3.89),

$$\frac{d\rho_R^h}{dt} + 4H\rho_R^h = N \frac{\rho_\phi^2 \omega}{16\pi M_P^4} \sum_{n=1}^{\infty} n |\mathcal{P}_n^k|^2 . \tag{3.92}$$

The solution of (3.92) is

$$\begin{aligned} \rho_R^h &= N \frac{\sqrt{3} M_P^4 \gamma_k \Sigma_k^h}{16\pi} \left(\frac{\rho_e}{M_P^4} \right)^{\frac{2k-1}{k}} \frac{k+2}{8k-14} \\ &\quad \times \left[\left(\frac{a_e}{a} \right)^4 - \left(\frac{a_e}{a} \right)^{\frac{12k-6}{k+2}} \right] \end{aligned} \tag{3.93}$$

with

$$\gamma_k = \sqrt{\frac{\pi}{2}} k \frac{\Gamma(\frac{1}{2} + \frac{1}{k})}{\Gamma(\frac{1}{k})} \lambda^{\frac{1}{k}} \tag{3.94}$$

and

$$\Sigma_k^h = \sum_{n=1}^{\infty} n |\mathcal{P}_n^k|^2 . \tag{3.95}$$

Once again, there is a maximum temperature which can be determined by from the value of a_{end}/a, which maximizes Eq. (3.93),

$$\frac{a_{\text{end}}}{a_{\text{max}}} = \left(\frac{2k+4}{6k-3} \right)^{\frac{k+2}{8k-14}} , \tag{3.96}$$

and hence a maximum radiation density,

$$\rho_{\text{max}}^h = N \frac{\sqrt{3} M_P^4 \gamma_k \Sigma_k^h}{16\pi} \left(\frac{\rho_{\text{end}}}{M_P^4} \right)^{\frac{2k-1}{k}} \frac{k+2}{12k-6} \left(\frac{2k+4}{6k-3} \right)^{\frac{2k+4}{4k-7}} \tag{3.97}$$

For $k = 2$ we have

$$T^h_{\rm max} \simeq 3.1 \times 10^{12} \left(\frac{\rho_{\rm end}}{10^{64}\ {\rm GeV}^4}\right)^{\frac{3}{8}} \left(\frac{m_\phi}{3 \times 10^{13}\ {\rm GeV}}\right)^{\frac{1}{4}} {\rm GeV}\,, \tag{3.98}$$

where we have taken $N = 4$ and scales as $N^{1/4}$. Furthermore, the sum Σ^h_k (3.95) begins at $n = 2$, because 2 modes scatter, and the initial mode has an energy of 2ω, which implies, for $k = 2$,

$$\Sigma^h_2 = 2 \times |\mathcal{P}^2_2|^2 = 2 \times \frac{1}{16} = \frac{1}{8}\,. \tag{3.99}$$

It is important to stress the importance of Eqs. (3.97) and (3.98). These correspond to an absolute *lower bound* on the maximal temperature of the Universe. We have not made any assumption other than the existence of a complex Higgs doublet and the inflaton coupled only through gravity. Our calculation implies that the Universe must have passed through this (or a higher) temperature during the early stages of reheating.

For $k = 2$, the radiation density produced by inflaton scattering as computed above never comes to dominate the energy density and can not lead to reheating. Although scattering can lead to reheating if $k \geq 4$ [106]. Gravitational scattering is less efficient. The "quartic" coupling defined in Eq. (3.90) is only constant if $k = 2$. In general, it scales as ϕ_0^{k-2}. Nevertheless, for $k > 4$ reheating from gravitational scattering is possible, though very inefficient. For example, for $k = 6$, $T_{\rm RH} \lesssim 1$ eV. As a result it is usually necessary to include a decay channel for the inflaton as in Eq. (3.68).[9] We will see in section 3.4 that gravitational reheating can be possible for higher equations of states and which constraints are imposed on this scenario.

For a sufficiently large coupling, y, the radiation produced by decay will always dominate over that produced by scattering as computed above. In addition, the maximum temperature may be greater than the lower bound in Eq. (3.98). However, there is a critical value of y, such that at smaller couplings, the gravitational scattering process (3.89) dominates at some point during the reheating process. This gives us the reheating temperature below which the maximal temperature is fixed by (3.97), and is independent of additional couplings beyond gravity between the inflaton and the standard model sector. To determine the value of this critical coupling (and hence reheating temperature), it is useful to rewrite Eq. (3.72) as

$$\begin{aligned} \rho^y_R &= \frac{\sqrt{3} M_P^4 \gamma_k^3 y^2 \Sigma^y_k}{8\pi} \left(\frac{\rho_{\rm end}}{M_P^4}\right)^{\frac{k-1}{k}} \lambda^{-\frac{2}{k}} \frac{k+2}{7-k} \\ &\quad \times \left[\left(\frac{a_{\rm end}}{a}\right)^{\frac{6k-6}{k+2}} - \left(\frac{a_{\rm end}}{a}\right)^4\right]. \end{aligned} \tag{3.100}$$

[9] Note that even including non-perturbative effects including preheating, does not lead to reheating in the absence of a decay channel for $k = 2$ [119].

We found that the maximum of ρ_R^y when evaluated at $a_{\rm max}$ given by Eq. (3.74) is

$$\begin{aligned}\rho^y_{\rm max} &= \frac{y^2\gamma_k^3\sqrt{3}}{16\pi}\lambda^{\frac{-2}{k}}M_P^4\left(\frac{\rho_{\rm end}}{M_P^4}\right)^{1-\frac{1}{k}}\left(\frac{3k-3}{2k+4}\right)^{\frac{3k-3}{7-k}}\\ &\times\Sigma_k^y\,,\end{aligned} \tag{3.101}$$

where

$$\Sigma_k^y=\sum_{n=1}^{\infty}n^3|\mathcal{P}_n^k|^2\,. \tag{3.102}$$

For $k=2$, the dominant mode is the first mode ($n=1$) which gives

$$\Sigma_2^y=1^3\times|\mathcal{P}_1^2|^2=\frac{1}{4} \tag{3.103}$$

The critical value for y such that the maximum radiation density and temperature are determined from the scattering of the inflaton condensate is given by $\rho^y_{\rm max}<\rho^h_{\rm max}$ which leads to

$$\begin{aligned}y^2 &\lesssim N\frac{\lambda^{\frac{2}{k}}}{\gamma_k^2}\left(\frac{\rho_{\rm end}}{M_P^4}\right)\frac{\Sigma_k^h}{\Sigma_k^y}\\ &\times\left(\frac{k+2}{12k-6}\right)\left(\frac{2k+4}{6k-3}\right)^{\frac{2k+4}{4k-7}}\left(\frac{2k+4}{3k-3}\right)^{\frac{3k-3}{7-k}}\,,\end{aligned} \tag{3.104}$$

which gives for $k=2$ and $N=4$

$$y\lesssim 0.4\sqrt{\frac{\rho_{\rm end}}{M_P^4}}\simeq 6.9\times10^{-6}\left(\frac{\rho_{\rm end}}{10^{64}{\rm GeV}^4}\right)^{\frac{1}{2}} \tag{3.105}$$

or

$$T_{\rm RH}\lesssim 3.0\times10^9\left(\frac{\rho_{\rm end}}{10^{64}{\rm GeV}^4}\right)^{1/2}\left(\frac{\lambda}{2.5\times10^{-11}}\right)^{1/4}{\rm GeV}\,, \tag{3.106}$$

where $T_{\rm RH}$ is defined by [106]

$$\rho_\phi(a_{\rm RH})=\alpha T_{\rm RH}^4=M_P^4\left(\frac{\sqrt{3}\gamma_k^3y^2\Sigma_k^y\lambda^{-\frac{2}{k}}(k+2)}{8\pi(7-k)}\right)^k\,. \tag{3.107}$$

Thus for all models with a reheat temperature due to decays, which is less than that given in Eq. (3.106), the maximum temperature during the reheat process is determined by scattering (mediated by gravity) and thus can not be ignored. Note also that for such small values of y, the kinetic effects due to the effective mass induced by the coupling $y\phi\bar{f}f$ are nonexistent, as shown in [106].

We show in Fig. 3.2 the evolution of the energy densities of the inflaton (blue), the radiation

produced by inflaton decays (orange dashed), the radiation produced by inflaton scattering mediated by gravity (green dashed), and the total radiation density (red) as function of the scaling parameter $a/a_{\rm end}$ for a Yukawa-like coupling $y = 10^{-8}$ with $k = 2$ and $\rho_{\rm end} = 10^{64}$ GeV^4. We clearly see that the beginning of the evolution of the radiation density is dominated by the scattering of the inflaton via graviton exchange (orange line), which determines the maximum temperature. For $k = 2$, the radiation density from scattering falls as a^{-4} [106], whereas the density from decays falls more slowly as $a^{-3/2}$ so that eventually the latter begins to dominate the population of the thermal bath when $a = a_{\rm int}$, until the reheating is complete when $\rho_\phi = \rho_R$ at $a = a_{\rm RH}$. For $a_{\rm int} \gg a_{\rm end}$, we can approximate the crossover point from Eqs. (3.93) and (3.100) using the equality $\rho_R^y = \rho_R^h$. For sufficiently small y and for $k = 2$, we find

$$\frac{a_{\rm int}}{a_{\rm end}} \simeq \left(\frac{8 y^2 \Sigma_2^y}{5 N \Sigma_2^h} \frac{M_P^4}{\rho_{\rm end}} \right)^{-\frac{2}{5}} , \tag{3.108}$$

which gives $a_{\rm int} \simeq 430\ a_{\rm end}$ in good agreement with the numerical solution for the parameter choices used in Fig. 3.2. We stress that the maximum temperature attained $T_{\rm max} \simeq 10^{12}$ GeV is independent of any beyond the Standard Model physics, and is purely gravitational and can not be ignored when production rates are highly dependent on the ratio $T_{\rm max}/T_{\rm RH}$.

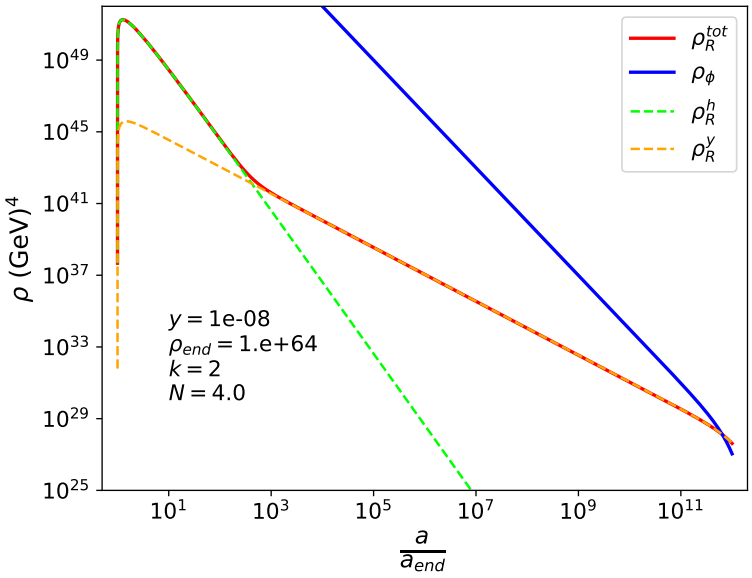

Figure 3.2: *Evolution of the radiation density (red) and inflaton density (blue) as a function of* $a/a_{\rm end}$ *for a Yukawa-like coupling* $y = 10^{-8}$ *with* $\rho_{\rm end} = 10^{64}$ *GeV*^{4} *and* $k = 2$. *This plot is obtained by solving numerically equations (3.66), (3.67) and (3.92). The evolution of the radiation density produced from inflaton decays (orange dashed) and scattering mediated by gravity (green dashed) are also shown.*

We can finally apply our result to the dark matter production through a graviton exchange while the bath is also dominated by the scattering of ϕ through graviton exchange. For $T_{\rm RH} \lesssim 10^9$ GeV, the Boltzmann equation one needs to consider is

$$\frac{dY_X^h}{da} = \frac{\sqrt{3}M_P}{\sqrt{\rho_{\rm end}}} a^2 \left(\frac{a}{a_{\rm end}}\right)^{\frac{3k}{k+2}} R_X^h(a) \tag{3.109}$$

with

$$R_X^h = \beta_X \frac{\rho_{\rm max}^2}{\alpha^2 M_P^4} \left(\frac{a_{\rm max}}{a}\right)^8 . \tag{3.110}$$

The result of the integration gives

$$\begin{aligned} Y_X^h(a_{\rm int}) \quad &= \frac{N^2 3\sqrt{3} M_P^3 \beta_X \gamma_k^2 (\Sigma_k^h)^2}{\alpha^2 65536\pi^2} \left(\frac{k+2}{8k-14}\right)^2 \\ \times \quad &\left(\frac{\rho_{\rm end}}{M_P^4}\right)^{\frac{7k-4}{2k}} a_{\rm end}^3 \left[\left(\frac{k+2}{2k+10}\right)\left(1-\left(\frac{a_{\rm end}}{a_{\rm int}}\right)^{\frac{2k+10}{k+2}}\right)\right. \\ &+ \left(\frac{k+2}{18k-18}\right)\left(1-\left(\frac{a_{\rm end}}{a_{\rm int}}\right)^{\frac{18k-18}{k+2}}\right) \\ &\left. - \left(\frac{k+2}{5k-2}\right)\left(1-\left(\frac{a_{\rm end}}{a_{\rm int}}\right)^{\frac{10k-4}{k+2}}\right)\right] \end{aligned} \tag{3.111}$$

where $a_{\rm int}$ corresponds to the value of the scale factor when the radiation density produced by inflaton decays begins dominate over that produced by gravitational inflaton scattering (this only occurs if y satisfies the bound in Eq. (3.104)). For $a > a_{\rm int}$, the slope of the radiation energy density curve as a function of a changes as seen in Fig. 3.2 and any thermal contribution to the production of dark matter originates from inflaton decay.

For sufficiently small y, $a_{\rm int} \gg a_{\rm end}$, and Eq. (3.111) can be simplified and we see that the dark matter yield does not depend on this intermediate scale factor, but only on $a_{\rm end}$ and $\rho_{\rm end}$. Thus for small y, we can also use Eq. (3.111) to evaluate the dark matter density at $a = a_{\rm RH}$,

$$\begin{aligned} n_X^h(a_{RH}) \quad &\simeq \frac{N^2\sqrt{3}\beta_X\gamma_k^2(\Sigma_k^h)^2 M_P^3}{196608\pi^2\alpha^2}\left(\frac{k+2}{8k-14}\right)^2 \\ &\times \frac{(k+2)(4k-7)^2}{(k-1)(k+5)(5k-2)}\left(\frac{\rho_{\rm end}}{M_P^4}\right)^{\frac{7k-4}{2k}}\left(\frac{\rho_{\rm RH}}{\rho_{\rm end}}\right)^{\frac{k+2}{2k}} \end{aligned} \tag{3.112}$$

and the relic abundance

$$\begin{aligned} \Omega_X^h h^2 \quad &= 1.6\times 10^8 \frac{g_0}{g_{\rm RH}} \frac{m_X}{1\ {\rm GeV}} \frac{\sqrt{3}\beta_X\gamma_k^2(\Sigma_k^h)^2 M_P^3}{196608\pi^2\alpha^2 T_{\rm RH}^3}\left(\frac{k+2}{8k-14}\right)^2 \\ &\times \frac{(k+2)(4k-7)^2}{(k-1)(k+5)(5k-2)}\left(\frac{\rho_{\rm end}}{M_P^4}\right)^{\frac{6k-6}{2k}}\left(\frac{\rho_{\rm RH}}{M_P^4}\right)^{\frac{k+2}{2k}} \end{aligned} \tag{3.113}$$

Because the radiation produced by gravitational scattering dominates near $a_{\rm max}$ only when $T_{\rm RH}$ satisfies Eq. (3.106), the relic density in Eq. (3.113) is suppressed by $(\rho_{\rm RH}/M_P)^{(k+2)/2k}$, and it

never dominates the *gravitational* production of dark matter given in Eq. (3.79), though it can lead to important effects when nongravitational production modes with a strong dependence on temperature are considered.

3.2.3 Results

Given the specific inflaton potential, here the T-models Eq. (3.52) which take the form of Eq. (3.53) when expanded about the origin, we can determine λ from the normalization of the CMB quadrupole anisotropy and $\rho_{\rm end}$ from the condition $\epsilon = 1$, as discussed earlier. Setting $y = 10^{-7}$, for $k = 2$, we have $\lambda = 2.5 \times 10^{-11}$ and $\rho_{\rm end}^{1/4} = 5.2 \times 10^{15}$ GeV[10]. For $k = 4$, $\lambda = 3.3 \times 10^{-12}$ and $\rho_{\rm end}^{1/4} = 4.8 \times 10^{15}$ GeV whereas for $k = 6$, $\lambda = 4.6 \times 10^{-13}$ and $\rho_{\rm end}^{1/4} = 4.6 \times 10^{15}$ GeV. For more on the determination of these parameters, see section 2.1.

Given these (model-dependent) parameter values for $k = 2, 4, 6$, we list in Table 3.1, the values for $T_{\rm max}$ which we obtain from $\rho_{\rm max}^h$ in Eq. (3.97); the maximum coupling y from Eq. (3.104) for which the gravitational produced radiation with temperature $T_{\rm max}$ dominates over that produced by decays; and the corresponding reheating temperature, $T_{\rm RHmax}$ obtained when $y = y_{\rm max}$ using Eq. (3.107) for $\rho_{\rm RH}$. $T_{\rm max} \propto \lambda^{1/4k}$ depends weakly on the inflaton coupling, and thus varies little for different values of k. The coupling $y_{\rm max}$ is independent of λ and also varies little with k. However, the final reheat temperature (which is not a result of purely gravitational interactions) is very sensitive to k as it scales as $y^{k/2}$, resulting in very small reheating temperatures when $k = 4$ or 6 for the small values of y considered.

	$k = 2$	$k = 4$	$k = 6$
$T_{\rm max}$	1.0×10^{12} GeV	7.5×10^{11} GeV	6.5×10^{11} GeV
$y_{\rm max}$	1.8×10^{-6}	1.4×10^{-6}	1.1×10^{-6}
$T_{\rm RHmax}$	7.9×10^{8} GeV	470 GeV	9.7×10^{-4} GeV

Table 3.1: Lower bound on $T_{\rm max}$ generated by the process $\phi\phi \to h_{\mu\nu} \to HH$ for different values of k. The radiation from this gravitational scattering dominates when $y < y_{\rm max}$ and we also list the corresponding reheating temperature $T_{\rm RH}$ when $y = y_{\rm max}$.

We show in Figs.(3.3) and (3.4) (for scalar and fermionic dark matter, respectively) the region in the parameter space defined by the (m_X, $T_{\rm RH}$) plane for which we can obtain a relic abundance consistent with the Planck CMB determination of the cold dark matter density, $\Omega_X h^2 = 0.12$ [22]. We combine the dark matter density originating from thermal production as given in Eq. (3.79) with that from scattering of the condensate to scalars given in Eq. (3.84) or fermions in Eq. (3.87).

For scalar dark matter, scattering in the condensate dominates the production of dark matter and we see from Eq. (3.84) that an isodensity contour should obey a simple power law,

[10]Different values of y give differences (at most) of 20% on λ, and 5% on $\rho_{\rm end}^{1/4}$.

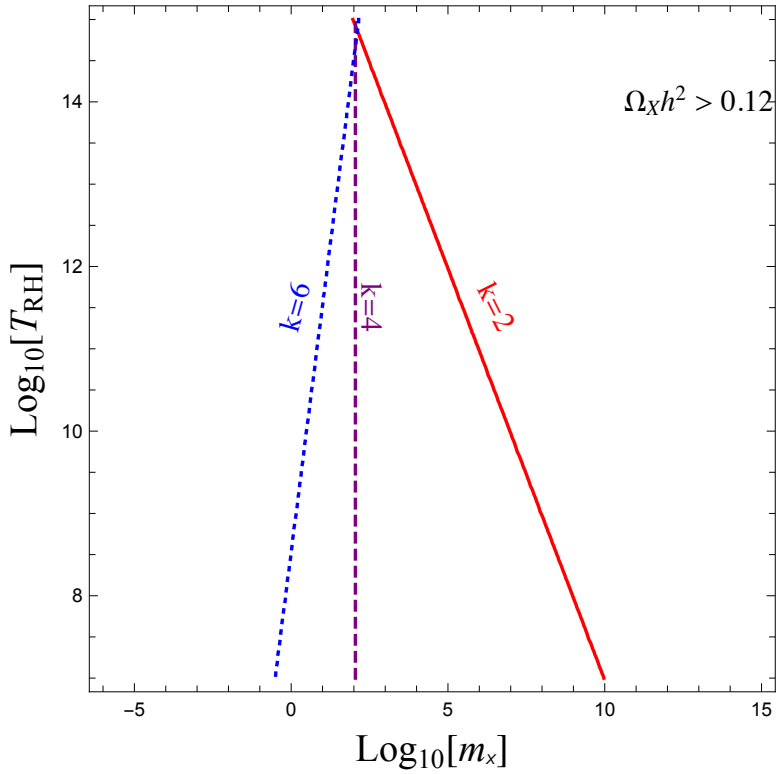

Figure 3.3: *Points respecting Planck constraint* $\Omega h^2 = 0.12$ *in the case of a scalar dark matter, in the plane* (m_X, T_{RH}) *for different values of* k.

corresponding to $m_X \propto (T_{\mathrm{RH}})^{\frac{4}{k}-1}$. Indeed, thermal production is not an efficient mechanism for the scalar dark matter, and the unique mechanism which populates the dark matter density is inflaton scattering (barring any beyond the Standard Model contribution). To better understand this, we can compute the ratio of the rates when $a = a_{\mathrm{max}}$, where the thermal production is maximum. Comparing the rates in Eqs. (3.57) and (3.75)

$$\begin{aligned} \frac{R_0^{\phi^k}(a_{\mathrm{max}})}{R_0^T(a_{\mathrm{max}})} &= \frac{\alpha^2 \Sigma_0^k}{8\pi\beta_0}\left(\frac{3k-3}{2k+4}\right)^{\frac{6}{7-k}}\left(\frac{\rho_{\mathrm{end}}}{\rho_{\mathrm{RH}}}\right)^{\frac{2}{k}} \\ &= g_{\mathrm{max}}^2 \frac{5760\Sigma_0^k}{3997}\left(\frac{3k-3}{2k+4}\right)^{\frac{6}{7-k}}\left(\frac{\rho_{\mathrm{end}}}{\rho_{\mathrm{RH}}}\right)^{\frac{2}{k}} \gg 1\,, \end{aligned} \tag{3.114}$$

where $g_{\mathrm{max}} = 427/4$ is the number of degrees of freedom at a_{max} in the Standard Model. Since $\rho_{\mathrm{end}} \gg \rho_{\mathrm{RH}}$, we clearly see that the ratio is much greater than one. This implies that the gravitational production is always dominated by the scattering of the inflaton zero modes.

Restricting our attention to Eq. (3.84) for the production of dark matter scalars, we see that, for $k = 4$, something interesting happens. The relic abundance is independent of the reheating process, and depends only on the energy density at the end of inflation. This comes from the fact that, for increasing values of k, the production of dark matter is less efficient, and, from

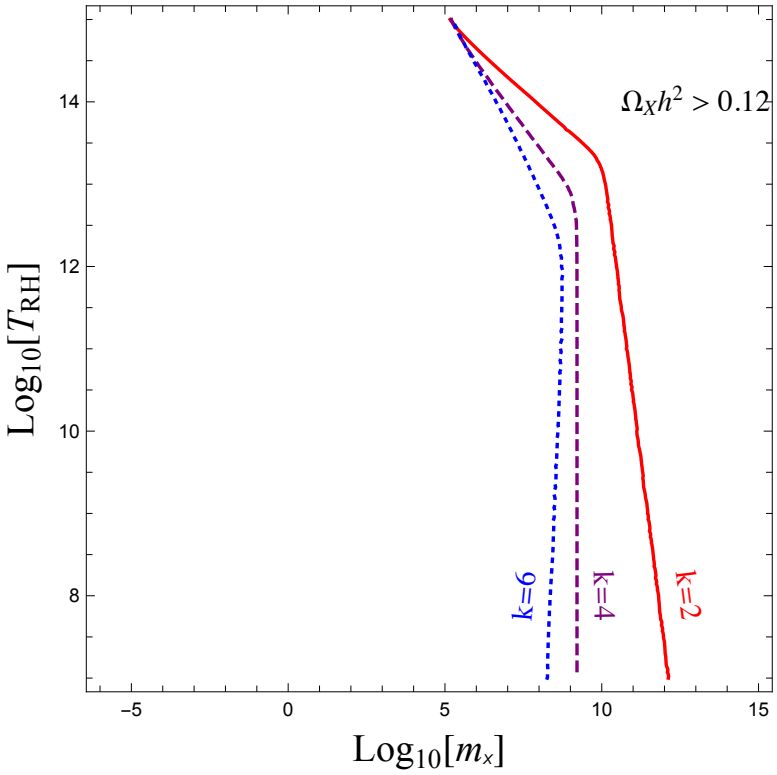

Figure 3.4: *Points respecting Planck constraint* $\Omega h^2 = 0.12$ *in the case of a fermionic dark matter, in the plane* $(m_X,\ T_{\mathrm{RH}})$ *for different values of* k.

Eq. (3.83), we see that $n_0^\phi \propto T_{\mathrm{RH}}^3$ for $k = 4$. Dilution effects thus render the present abundance independent of T_{RH} and there is a unique universal limit of $m_X \lesssim 120$ GeV for scalar dark matter and $\lesssim 1.7 \times 10^9$ GeV for fermionic dark matter (when inflaton scattering dominates). For $k > 4$, the slope of T_{RH} vs m_X changes sign, and the required reheating temperature grows with the dark matter mass. In this case, even sub-GeV dark matter candidates are allowed for low reheating temperatures, whereas for $k = 2$ and $k = 4$ the production process is too weak to produce MeV dark matter in sufficient quantities to account for the cold dark matter density as determined by Planck [22].

The $(m_X,\ T_{\mathrm{RH}})$ plane for fermionic dark matter is shown in Fig. 3.4. In this case both the scattering from a condensate and thermal gravitational contributions must be considered. Notice that there is a change in slope between the required reheating temperature and dark matter mass. For higher masses, the scattering from the condensate dominates as in the case of scalar dark matter and we require $m_X \propto T_{\mathrm{RH}}^{\frac{(k-4)}{3k}}$ as can be seen from Eq. (3.87). However, at lower masses, because of the mass suppression in the rate in Eq. (3.60) and hence the abundance of dark matter in Eq.(3.85), there is a region where the thermal production dominates over $\phi-\phi$ scattering. In this case, $m_X \propto T_{\mathrm{RH}}^{-3}, T_{\mathrm{RH}}^{-2}, T_{\mathrm{RH}}^{-1}$, for $k = 2, 4$ and 6, respectively, as can be seen from Eq. (3.79). The origin of this suppression is simply a helicity argument; the scattering

of two scalars generates rates where a spin-flip is required making it proportional to the mass of the fermion in the final state. Thus the rate vanishes for a massless fermion. This is not the case for thermal production, because Standard Model particles in the thermal bath are relativistic and then can still produce fermionic dark matter through scattering without being affected by a helicity suppression. To be more quantitative, we again compare the production rates in Eqs. (3.60) and (3.75) at $a = a_{\rm max}$

$$\begin{aligned}\frac{R^{\phi^k}_{1/2}(a_{\rm max})}{R^{T}_{1/2}(a_{\rm max})} &= \frac{\alpha^2\Sigma^k_{1/2}}{2\pi\beta_{1/2}}\frac{m_X^2}{m_\phi^2}\left(\frac{3k-3}{2k+4}\right)^{\frac{6}{7-k}}\left(\frac{\rho_{\rm end}}{\rho_{\rm RH}}\right)^{\frac{2}{k}} \\ &= g^2_{\rm RH}\frac{11520\ \Sigma^k_{1/2}}{11351}\frac{m_X^2}{m_\phi^2}\left(\frac{3k-3}{2k+4}\right)^{\frac{6}{7-k}}\left(\frac{\rho_{\rm end}}{\rho_{\rm RH}}\right)^{\frac{2}{k}}\,. \end{aligned} \tag{3.115}$$

In contrast to the scalar case, we see that there exists a value of $m_X \lesssim (.13, .050, .036)(\rho_{\rm RH}/\rho_{\rm end})^{1/k} m_\phi$, for $k = 2, 4$ and 6, respectively, for which the relic abundance is dominated by the thermal production.

3.2.4 Conclusions

We have considered in this section the production of matter and radiation interacting only gravitationally with the inflaton through the exchange of a graviton $h_{\mu\nu}$. We compared the production of dark matter from inflaton scattering and from the thermal bath (mediated only by gravity). The former tends to dominate the production in a large part of the parameter space. However, we noticed a notable difference in the case of fermionic dark matter, because the production through $\phi\phi$ scattering is suppressed by a mass flip proportional to the dark matter mass m_X^2. We have also seen that it is possible to produce radiation from inflaton scattering in the condensate during the earlier stages of reheating. As a result, we have derived a *lower bound* on the maximal temperature is expected from $\phi\phi \to h_{\mu\nu} \to HH$ of the order of 10^{12} GeV for a typical chaotic or $\alpha-$attractor scenario. This lower gravitational bound becomes the effective maximal temperature for $T_{\rm RH} \lesssim 10^9$ GeV (for $k = 2$).

A major challenge for gravitational particle production as well as all mechanisms of reheating is experimental verification. As the processes we have discussed are all minimal, in the sense that they arise simply from Einstein's gravity, they are contained in all models which include models beyond the Standard Model. In that sense, there is nothing unique to the specific processes we have described. Most important is the search for a signature for the maximum temperature attained. Thus, gravitational effects give lower bounds on maximal temperature and relic abundance that cannot be neglected and should be considered as the minimal ingredients to add to any nonminimal extension of the Standard Model. A similar analysis has been pursued in [210]. The results obtained are largely in agreement with our own.

Addenda

A Thermal production

In this addendum, we describe our calculation of the production rate for scalar and fermionic dark matter, and include the amplitude squared for the relevant processes. If we ignore the masses of Standard Model particles, the rate $R(T)$ for the processes $\mathrm{SM} + \mathrm{SM} \to \mathrm{DM}_j + \mathrm{DM}_j$ can be computed from

$$\begin{aligned} R_j^T = \sum_{i=0,1/2,1} N_i R_{ij} &= 2 \times \sum_{i=0,1/2,1} \frac{N_i}{1024\pi^6} \int f_i(E_1) f_i(E_2) E_1 \,\mathrm{d}E_1 E_2 \,\mathrm{d}E_2 \,\mathrm{d}\cos\theta_{12} \int |\mathcal{M}^{ij}|^2 \,\mathrm{d}\Omega_{13} \\ &= \left(4R_{0j} + 45R_{\frac{1}{2}j} + 12R_{1j}\right) , \end{aligned} \tag{3.116}$$

where the factor of two accounts for two dark matter particles per scattering, N_i denotes the number of each SM species of spin i: $N_0 = 4$ for 1 complex Higgs doublet, $N_1 = 12$ for 8 gluons and 4 electroweak bosons, and $N_{1/2} = 45$ for 6 (anti)quarks with 3 colors, 3 (anti)charged leptons and 3 neutrinos, c.f., Eq. (3.50). The infinitesimal solid angle is defined as

$$\mathrm{d}\Omega_{13} = 2\pi \,\mathrm{d}\cos\theta_{13} \,, \tag{3.117}$$

with θ_{13} and θ_{12} being the angle formed by momenta $\mathbf{p}_{1,3}$ and $\mathbf{p}_{1,2}$, respectively. In the massless limit, one can express the amplitude squared in terms of Mandelstam variables, s and t, which are related to the angles θ_{13} and θ_{12} by the expressions

$$t = \frac{s}{2}\left(\cos\theta_{13} - 1\right) , \tag{3.118}$$

$$s = 2E_1E_2\left(1 - \cos\theta_{12}\right) . \tag{3.119}$$

The amplitudes and rates for scalar and fermionic dark matter are given in the following subsections.

Scalar dark matter

We note that we include the symmetry factors of the initial and final states in the squared amplitudes, and indicate it with an overbar:

$$|\overline{\mathcal{M}}^{00}|^2 = \frac{1}{4M_P^4}\frac{t^2(s+t)^2}{s^2} , \tag{3.120}$$

$$|\overline{\mathcal{M}}^{\frac{1}{2}0}|^2 = \frac{1}{4M_P^4}\frac{(-t(s+t))(s+2t)^2}{s^2} , \tag{3.121}$$

$$|\overline{\mathcal{M}}^{10}|^2 = \frac{1}{2M_P^4}\frac{t^2(s+t)^2}{s^2} . \tag{3.122}$$

Using these amplitudes in Eq. (3.116), we obtain [192]

$$R_0^T = \frac{3997\pi^3}{20736000}\frac{T^8}{M_P^4} \equiv \beta_0 \frac{T^8}{M_P^4}\,. \tag{3.123}$$

Fermionic dark matter

The corresponding amplitudes for fermionic dark matter are given by:

$$|\overline{\mathcal{M}}^{0\frac{1}{2}}|^2 = \frac{(-t(s+t))(s+2t)^2}{4M_P^4 s^2}\,, \tag{3.124}$$

$$|\overline{\mathcal{M}}^{\frac{1}{2}\frac{1}{2}}|^2 = \frac{s^4+10s^3t+42s^2t^2+64st^3+32t^4}{8M_P^4 s^2}\,, \tag{3.125}$$

$$|\overline{\mathcal{M}}^{1\frac{1}{2}}|^2 = \frac{(-t(s+t))(s^2+2t(s+t))}{M_P^4 s^2}\,, \tag{3.126}$$

which leads to the following rate [192]

$$R_{\frac{1}{2}}^T = \frac{11351\pi^3}{10368000}\frac{T^8}{M_P^4} \equiv \beta_{\frac{1}{2}} \frac{T^8}{M_P^4}\,. \tag{3.127}$$

B Production from the Inflaton condensate

In this second addendum, we describe our calculation of the particle production rate of dark matter from the scattering of the inflaton condensate. If we consider the gravitational scattering process $\phi(p_1)+\phi(p_2)\to X^i(p_3)+X^i(p_4)$, with $i=0,1/2$, illustrated by the Feynman diagram in Fig. 3.1, then the Boltzmann equation for the number density of produced dark matter particles is given by [106, 110]

$$\frac{dn_X}{dt} + 3Hn_X \;=\; R_i^{\phi^k}\,, \tag{3.128}$$

where the rate is given by

$$\begin{aligned} R_i^{\phi^k} \;&\equiv\; g_X \int d\Psi_{1,2,3,4}(2\pi)^4\delta^{(4)}\left(p_1+p_2-p_3-p_4\right) \\ &\times \left[|\mathcal{M}|^2_{12\to34} f_1 f_2 (1\pm f_3)\,(1\pm f_4) - (34\leftrightarrow 12)\right] \end{aligned} \tag{3.129}$$

where $d\Psi_{1,2,3,4} = \Pi_{i=1}^4 d^3\mathbf{p}_i/\left((2\pi^3)2p_i^0\right)$ denotes the phase space distribution of particles $1,2,3$ and 4, $\mathcal{M}$ is the transition amplitude, f_i is the phase space density of species i, and g_X denotes the number of produced dark matter particles. If we ignore the Bose enhancement and Pauli blocking effects, then the above rate can be approximated as

$$\begin{aligned} R_i^{\phi^k} \;&=\; g_X \int \frac{d^3\mathbf{p}_3}{(2\pi)^3 2p_3^0}\frac{d^3\mathbf{p}_4}{(2\pi)^3 2p_4^0} \\ &\times\; (2\pi)^4\delta^{(4)}\left(p_1+p_2-p_3-p_4\right)|\mathcal{M}|^2_{12\to34}\,. \end{aligned} \tag{3.130}$$

For the inflaton condensate we can use the transition amplitude $\mathcal{M}_n$ for each oscillating field mode of ϕ. In this case, the four-momentum of the n-th oscillation mode is given by $p_1 + p_2 = p_n = \sqrt{s} = (E_n, \mathbf{0})$ with E_n the energy of the n-th oscillation mode. Since the transition amplitude $\mathcal{M}_n$ of the n-th oscillation does not depend on the final particle momenta $\mathbf{p}_{3,4}$, we can approximate the rate as

$$R_i^{\phi^k} = \frac{g_X}{l!}\frac{1}{8\pi}\sum_{n=1}^{\infty}|\mathcal{M}_n|^2\sqrt{1-\frac{4m_X^2}{s}} \tag{3.131}$$

where l is associated with the number of identical particles in the final state.

For the production of scalar dark matter, we find that the scattering amplitude squared is given by

$$|\mathcal{M}_n^{0\phi^k}|^2 = \frac{\rho_\phi^2}{M_P^4}\left[1+\frac{2m_X^2}{s}\right]^2|(\mathcal{P}^k)_n|^2\,, \tag{3.132}$$

where $s = E_n^2 = n^2\omega^2$, and we used $\rho_\phi = \frac{\lambda\phi^k}{M_P^{k-4}}$. We find that the inflaton scattering rate is given by

$$R_0^{\phi^k} = \frac{2\times\rho_\phi^2}{16\pi M_P^4}\sum_{n=1}^{\infty}\left[1+\frac{2m_X^2}{E_n^2}\right]^2|(\mathcal{P}^k)_n|^2\langle\beta_n\left(m_X\,,m_X\right)\rangle\,, \tag{3.133}$$

where

$$\beta_n\left(m_A,m_B\right) \equiv \sqrt{\left(1-\frac{\left(m_A+m_B\right)^2}{E_n^2}\right)\left(1-\frac{\left(m_A-m_B\right)^2}{E_n^2}\right)}\,, \tag{3.134}$$

and we used $g_X = 2$. For the case $k = 2$, we find that the rate is given by Eq. (3.59).

Similarly, for fermionic dark matter, we find that the scattering amplitude squared is,

$$|\mathcal{M}_n^{1/2\,\phi^k}|^2 = \frac{2\rho_\phi^2}{M_P^4}\frac{m_X^2}{s}\left[1-\frac{4m_X^2}{s}\right]|(\mathcal{P}^k)_n|^2\,, \tag{3.135}$$

and the rate is given by Eq. (3.61). The rates as defined in the text depend on various summations over the Fourier modes of the periodicity function $\mathcal{P}(t)$. In Table 3.2, the numerical values of these quantities are given for $k = 2, 4, 6$. Values are given in the limit of vanishing dark matter mass.

	$k=2$	$k=4$	$k=6$
Σ_0^k (Eq. (3.58))	$\frac{1}{16}$	0.063	0.056
$\Sigma_{1/2}^k$ (Eq. (3.61))	$\frac{1}{64}$	0.061	0.101
Σ_k^h (Eq. (3.95))	$\frac{1}{8}$	0.141	0.146
Σ_k^y (Eq. (3.102))	$\frac{1}{4}$	0.241	0.244

Table 3.2: *Numerical values of the various summations of the Fourier modes of the periodicity functions used in the text. The dark matter mass has been neglected in producing the numerical values.*

3.3 Non-minimal couplings to gravity

This section is based on: **S. Cléry**, Y. Mambrini, K.A. Olive, A. Shkkerin and S. Verner, *Gravitational portals with nonminimal couplings*, **Phys.Rev.D 105 (2022) 9, 095042**, arXiv:2203.02004 [2]

Motivation

In the precedent section, we saw that promoting a field theory Lagrangian from a Lorentz-invariant one to a generally covariant one necessarily leads to an interaction between the fields of the theory and the gravitational field. In the case of a scalar field, S, the natural generalization of this minimal interaction scenario is to introduce a non-minimal coupling term of the form

$$\propto \xi_S S^2 R \,. \tag{3.136}$$

Here R is the Ricci scalar and ξ_S is a non-minimal coupling constant. This non-minimal coupling to gravity proved to be useful in many applications to cosmology. Examples include Higgs inflation [100, 211], where S is associated with the Higgs field degree of freedom h — the only scalar degree of freedom in the Standard Model, preheating [212], where S is associated with the inflaton field ϕ, and non-perturbative production of dark matter [213–215], where S represents the scalar dark matter particle X.

We showed in the precedent section that the interaction between the dark and visible sectors induced by gravity leads to unavoidable contributions to reheating and dark matter production, in the thermal bath or via the scattering of the inflaton condensate, through the graviton exchange processes shown in Fig. 3.1. Thus, gravity is strong enough to mediate perturbative channels of reheating and dark matter production. It is therefore important to compare the minimal gravitational particle production to similar processes obtained with non-minimal couplings.

The purpose of this part is to study how the inclusion of the non-minimal coupling terms of the form (3.136) affect the gravitational production of dark matter and radiation during re-

heating. Note that the presence of these terms is unavoidable: if there were no such couplings at the tree level, they would still be generated by quantum corrections [216]. We consider the effects of non-minimal couplings to curvature, for three types of scalars: the Higgs boson, the inflaton, and a scalar dark matter candidate. We study particle production in the processes $hh \to XX$, $\phi\phi \to hh$, and $\phi\phi \to XX$ which are induced by the non-minimal couplings. We compute the abundance of dark matter produced by these non-minimal couplings to gravity as well as the contribution to the production of the radiation bath during reheating.

Here ϕ represents the inflaton background oscillating around its minimum after the end of inflation [160, 161]. Since the scalar fields couple directly to the curvature scalar R, the oscillating background causes the effective masses of the fields to change non-adiabatically and leads to particle production. This regime of particle creation has been considered in several different contexts, including gravitational production of scalar [196, 217–227], fermion [228, 229], and vector dark matter [230–234].

Our main interest is to compare the (dark) matter production channels induced by the non-minimal couplings with the production via the s-channel graviton exchange that sets minimal possible production rates. We will see for which values of the couplings the rates are enhanced, and what are the consequences on the dark matter density or the temperature attained during reheating. We adopt in this section the Starobinsky inflationary potential [93], although our results are largely independent of the particular form of the potential. As for the potentials for the fields h and X, we take them to be renormalizable polynomials. We also assume no direct interaction between ϕ, h, and X.

Working in the perturbative regime implies that the non-minimal couplings must satisfy $|\xi_S| \ll M_P^2/\langle S\rangle^2$, where $\langle S\rangle$ is the vacuum expectation value of $S = \phi, h, X$. The value of ξ_h is constrained from collider experiments as $|\xi_h| \lesssim 10^{15}$ [235, 236].[11] Furthermore, the lower bound on ξ_h comes from the fact that the Standard Model electroweak vacuum may not be absolutely stable [237–243]. To prevent the vacuum decay due to quantum fluctuations during inflation [244–250], the effective mass of the Higgs field induced by the non-minimal coupling must be large enough; this gives $\xi_h \gtrsim 10^{-1}$ [251–253] (see also [254]).[12]

The section is organized as follows: we discuss non-minimal gravitational couplings of the inflaton, the Higgs boson, and a dark matter scalar in detail. We calculate the dark matter production rates either from scattering in the thermal bath or from oscillations in the inflaton condensate. We compare similar processes obtained from the minimal gravitational particle production. We choose the Starobinsky model of inflation and discuss the reheating epoch when the inflaton begins oscillating. In 3.3.3 we discuss the resulting abundance of dark matter

[11] Note that in the case of Higgs inflation, ξ_h is fixed from CMB measurements [100].

[12] This estimate assumes no new physics interfering the RG running of the Higgs self-coupling constant until inflationary energy scales.

produced from the thermal bath and directly from scattering of the inflaton condensate. We also compute the effects of the non-minimal couplings on the maximum temperature attained during reheating. We then compare different processes in 3.3.4, before summarizing our results in 3.3.5.

3.3.1 Scalar-gravity Lagrangian

The theory we consider comprises 3 scalar fields non-minimally coupled to gravity: the inflaton ϕ, the Higgs field[13] H, for which we adopt the Unitary gauge, $H = (0, h)^T/\sqrt{2}$, and the dark matter candidate X. The relevant part of the action takes the form

$$\mathcal{S} \;=\; \int d^4x\sqrt{-\tilde{g}}\left[-\frac{M_P^2}{2}\Omega^2\tilde{R} + \widetilde{\mathcal{L}_\phi} + \widetilde{\mathcal{L}_h} + \widetilde{\mathcal{L}_X}\right] \tag{3.137}$$

with the conformal factor Ω^2 given by

$$\Omega^2 \;\equiv\; 1 + \frac{\xi_\phi\phi^2}{M_P^2} + \frac{\xi_h h^2}{M_P^2} + \frac{\xi_X X^2}{M_P^2}\,. \tag{3.138}$$

Here the tilde used in Eq. (3.137) indicates that the theory is considered in the Jordan frame. For the scalar field Lagrangians we have

$$\widetilde{\mathcal{L}_S} \;= \frac{1}{2}\tilde{g}^{\mu\nu}\partial_\mu S\partial_\nu S - V_S\,, \quad S = \phi, h, X\,. \tag{3.139}$$

Next, we specify the scalar field potentials. For a model of inflation, we choose the well-motivated Starobinsky model for which [93] (see section 2.1)

$$V_\phi \;=\; \frac{3}{4}m_\phi^2 M_P^2\left(1 - e^{-\sqrt{\frac{2}{3}}\frac{\phi}{M_P}}\right)^2\,. \tag{3.140}$$

The Starobinsky potential is equivalent to the T-alpha attractor potential introduced in 2.61, giving similar inflationary predictions at high field value, in the specific case $k = 2$. In what follows, we work in the perturbative regime with $\phi \ll M_P$, hence the potential is approximated as

$$V_\phi \;\simeq\; \frac{1}{2}m_\phi^2\phi^2\,. \tag{3.141}$$

The inflaton mass, m_ϕ, is fixed by the amplitude of scalar perturbations inferred from CMB measurements [22]; for the potential (3.140) this gives $m_\phi = 3\times10^{13}$ GeV [134].

The potential for the Higgs field is taken as follows

$$V_h \;=\; \frac{1}{2}m_h^2h^2 + \frac{1}{4}\lambda_h h^4\,. \tag{3.142}$$

[13] We consider the Higgs boson as a surrogate for any additional scalars with Standard Model couplings.

Here m_h and λ_h are the Higgs mass and quartic coupling, correspondingly. Note that both parameters undergo the renormalization group (RG) running. In what follows we take a weak scale mass, which is a good approximation at the time of reheating and our results are insensitive to λ_h. Finally, the dark matter potential is simply given by

$$V_X \;=\; \frac{1}{2}m_X^2 X^2\,. \tag{3.143}$$

To study the reheating in the theory (3.137), it is convenient to remove the non-minimal couplings by performing the redefinition of the metric field. Leaving the details to the addendum A that follows this section, we write the action (3.137) in the Einstein frame,

$$\begin{aligned}\mathcal{S} \;=\; \int d^4x\sqrt{-g}\,\Bigg[-\frac{M_P^2}{2}R + \frac{1}{2}K^{ij}g^{\mu\nu}\partial_\mu S_i\partial_\nu S_j \\ -\frac{V_\phi + V_h + V_X}{\Omega^4}\Bigg]\,.\end{aligned} \tag{3.144}$$

Here the indices i,j enumerate the fields ϕ, h, X, and the kinetic function is given by

$$K^{ij} \;=\; 6\frac{\partial\log\Omega}{\partial S_i}\frac{\partial\log\Omega}{\partial S_j} + \frac{\delta^{ij}}{\Omega^2}\,. \tag{3.145}$$

Note that the scalar field kinetic term is not canonical. In general, it is impossible to make a field redefinition that would bring it to the canonical form, unless all three non-minimal couplings vanish.[14] For the theory (3.144) to be well-defined, the kinetic function (3.145) must be positive-definite. Computing the eigenvalues, one arrives at the condition

$$\Omega^2 > 0\,, \tag{3.146}$$

which is satisfied automatically for positive values of the couplings. Note that the negative couplings are also allowed for certain scalar field magnitudes.

In what follows, we will be interested in the small-field limit

$$\frac{|\xi_\phi|\phi^2}{M_P^2}\,,\quad \frac{|\xi_h|h^2}{M_P^2}\,,\quad \frac{|\xi_X|X^2}{M_P^2} \ll 1\,. \tag{3.147}$$

We can expand the kinetic and potential terms in the action (3.144) in powers of M_P^{-2}. We obtain a canonical kinetic term for the scalar fields and deduce the leading-order interactions induced by the non-minimal couplings. The latter can be brought to the form

$$\mathcal{L}_{\rm non-min.} \;=\; -\sigma^\xi_{hX}h^2X^2 - \sigma^\xi_{\phi X}\phi^2X^2 - \sigma^\xi_{\phi h}\phi^2h^2\,, \tag{3.148}$$

[14] Such a redefinition exists if the three-dimensional manifold spanned by the fields ϕ, h and X is flat. One can show that it is not the case if at least one of the couplings is non-zero.

where the σ_{ij}^{ξ} are functions of the couplings ξ_i, ξ_j, the masses m_i, m_j, and the Mandelstam variables; see the addendum A for details.

The small-field approximation (3.147) implies the bound $\sqrt{|\xi_S|} \lesssim M_P/\langle S\rangle$ with $S = \phi, h, X$. Since the inflaton value at the end of inflation is $\phi_{\rm end} \sim M_P$ and afterwards $\langle\phi^2\rangle \sim a^{-3}$, where a is the cosmological scale factor, then $|\xi_\phi| \lesssim (a/a_{\rm end})^3$. In particular, at the onset of inflaton oscillations

$$|\xi_\phi| \lesssim 1\,. \tag{3.149}$$

Note that since our calculations involve the effective couplings $\sigma_{\phi X}^{\xi}$ ($\sigma_{\phi h}^{\xi}$), which depend both on ξ_ϕ and ξ_X (ξ_h), the relatively small value of $|\xi_\phi|$ can, in principle, be compensated by a large value of the other couplings.

In Fig. 3.5, we show the scattering processes obtained from the Lagrangian (3.148). These contribute to reheating (when h is in the final state) and dark matter production (when X is in the final state).

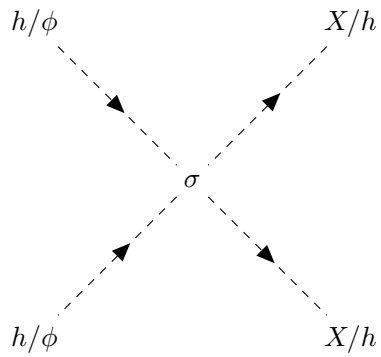

Figure 3.5: *Feynman diagram for the 4-point interactions between the inflaton ϕ, the dark matter scalar candidate X, and the Higgs boson h, given by the Lagrangian (3.148).*

Finally, in evaluating the cosmological parameters, it is important to stay within the validity of the low-energy theory. The cutoff of the theory can be estimated as (see, e.g., [255–257])

$$\Lambda \sim \frac{M_P}{\max_i |\xi_i|}\,. \tag{3.150}$$

In particular, the temperature of reheating must not exceed Λ.

3.3.2 Production rates

In this section, we consider again three processes:

1. The production of dark matter from the scattering of thermal Higgs bosons (assuming reheating is produced by inflaton decay). In this case, the dark matter is populated via a freeze-in mechanism throughout the reheating period.

2. The production of dark matter from direct excitations of the inflaton condensate. This process, which can be viewed as gravitational inflaton scattering, is independent of the presence of a thermal bath.

3. The creation of a radiative bath at the start of reheating arising from the Higgs boson production through gravitational inflaton scattering. Since such a process is unavoidable in minimally coupled gravity, it is interesting to know when such a process becomes dominant in the model with non-minimal couplings ξ_i.

The thermal dark matter production rate $R(T)$ for the process $hh \to XX$ can be calculated from[15] [115, 258]

$$R(T) = \frac{2 \times N_h}{1024\pi^6} \int f_1 f_2 E_1 \, \mathrm{d}E_1 E_2 \, \mathrm{d}E_2 \, \mathrm{d}\cos\theta_{12} \int |\overline{\mathcal{M}}|^2 \, \mathrm{d}\Omega_{13} \,, \tag{3.151}$$

$N_h = 4$ is the number of internal degrees of freedom for 1 complex Higgs doublet, $|\overline{\mathcal{M}}|^2$ is the matrix amplitude squared with all symmetry factors included. This accounts for the explicit factor of 2 in the numerator of Eq. (3.151). The thermal distribution function of the incoming Higgs particles is given by the Bose-Einstein distribution.

The rate for minimal gravitational interactions from Eq. (3.39) was derived in the precedent section. The rate we use here differs in two respects. As noted earlier, we only include Higgs scalars in the initial state whereas in [1, 192], all Standard Model particle initial states were included. Secondly, we keep terms depending on the dark matter mass which had not previously been taken into account. This allows us to consider dark matter masses approaching the inflaton mass and/or the reheating temperature.

For minimal (non-minimal) gravitational interactions, we find that the thermal dark matter production rate can be expressed as

$$R_X^{T,\,(\xi)}(T) = \beta_1^{(\xi)} \frac{T^8}{M_P^4} + \beta_2^{(\xi)} \frac{m_X^2 T^6}{M_P^4} + \beta_3^{(\xi)} \frac{m_X^4 T^4}{M_P^4} \,, \tag{3.152}$$

where the coefficients $\beta_{1,\,2,\,3}^{(\xi)}$ are given in the second addendum B by Eqs. (3.199-3.201) for minimal-gravitational production, and by Eqs. (3.195-3.197) for the non-minimal coupling contribution. The ratio of the non-minimal to minimal rate is shown in Fig. 3.6. However, we note that when $\xi_i \sim \mathcal{O}(1)$ both rates are comparable and interference effects become significant. The full coefficients $\beta_{1,\,2,\,3}$ including interference are given by Eqs. (3.202-3.201) from the second addendum B. We will discuss below the comparison of the effects on dark matter production from the two rates.

[15] We include the symmetry factors associated with identical initial and final states in the definition of $|\overline{\mathcal{M}}|^2$, and a factor of 2 is explicitly included in the definition of the rate to account for the production of 2 identical particles.

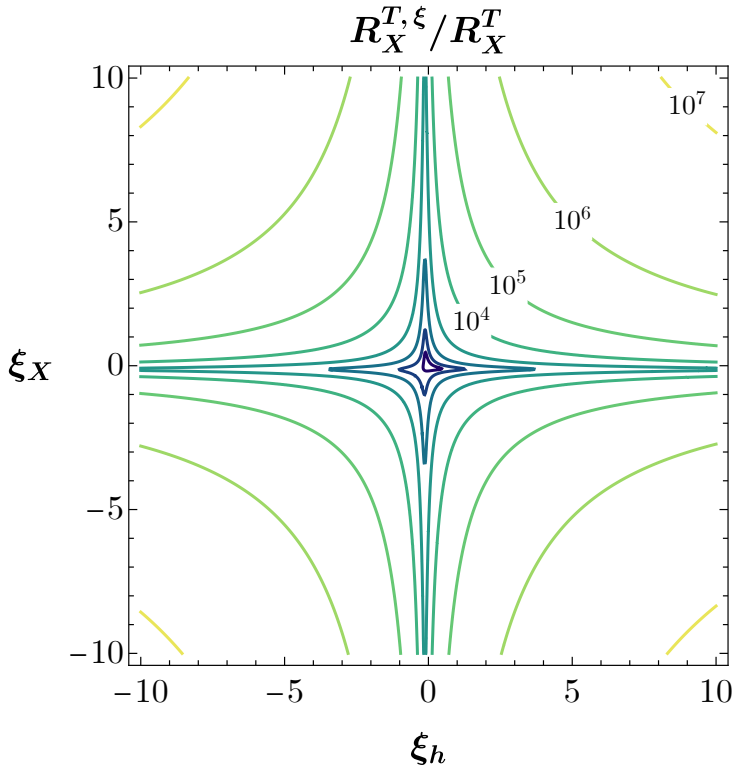

Figure 3.6: *Contours of the ratio of the dark matter production rates from the thermal bath based on non-minimal gravitational interactions to those based on minimal interactions. The ratio is displayed in the* (ξ_h, ξ_X) *plane. Note that as discussed in the Introduction, negative values of* ξ_h *may require new physics (such as supersymmetry) to stabilize the Higgs vacuum.*

The rate for dark matter produced from inflaton oscillations of the inflaton condensate for a potential of the form $V = \lambda\phi^k$ were considered in detail in [1, 106]. The time-dependent inflaton can be written as $\phi(t) = \phi_0(t)\mathcal{P}(t)$, where $\phi_0(t)$ is the time-dependent amplitude that includes the effects of redshift and $\mathcal{P}(t)$ describes the periodicity of the oscillation. The dark matter production rate is calculated by writing the potential in terms of the Fourier modes of the oscillations [1, 106, 131, 207] as introduced in section 3.2. For $k = 2$ (the only case considered here), the frequency of oscillation is simply, $\omega = m_\phi$. The rate generated by non-minimal couplings can be readily calculated using the Lagrangian (3.148), which leads to

$$R_X^{\phi,\xi} = \frac{2 \times \sigma_{\phi X}^{\xi\ 2}}{\pi} \frac{\rho_\phi^2}{m_\phi^4} \Sigma_0^k \,, \tag{3.153}$$

where Σ_0^k is the same coefficient introduced in Eq.(3.95), while $E_n = n\omega$ is the energy of the n-th inflaton oscillation mode. For $k = 2$, only the second Fourier mode in the sum contributes,

with $\sum |\mathcal{P}_n^2|^2 = \frac{1}{16}$. Thus, the rate becomes

$$R_X^{\phi,\xi} \;=\; \frac{2\times {\sigma_{\phi X}^{\xi}}^2}{16\pi}\frac{\rho_\phi^2}{m_\phi^4}\sqrt{1-\frac{m_X^2}{m_\phi^2}}\,, \tag{3.154}$$

where ρ_ϕ is the energy density of the inflaton and the interaction term $\sigma_{\phi X}^{\xi}$ is given in the addendum A by Eq. (3.190).

It was shown in section 3.2.1 that the dark matter production rate through the exchange of a graviton, is given by Eq.(3.59) which can be written in the same form as (3.154) by defining an effective coupling $\sigma_{\phi X}$

$$\sigma_{\phi X} \;=\; -\frac{m_\phi^2}{4M_P^2}\left(1+\frac{m_X^2}{2m_\phi^2}\right)\,. \tag{3.155}$$

A comparison of the non-minimal to minimal rates for the production of dark matter from inflaton scattering is shown in Fig. 3.7. For the production of Higgs bosons through inflaton

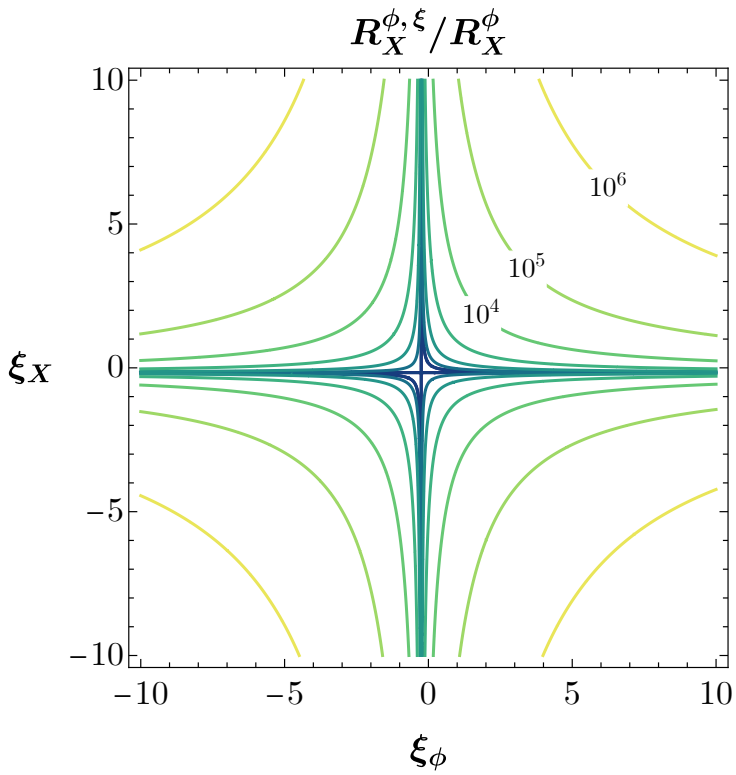

Figure 3.7: *Contours of the ratio of the dark matter production rates from oscillations in the inflaton condensate based on non-minimal gravitational interactions to those based on minimal interactions. The ratio is displayed in the* (ξ_ϕ, ξ_X) *plane.*

condensate scattering, we follow a similar procedure, and from the Lagrangian (3.148) we find

$$R_h^{\phi,\xi} \simeq N_h \frac{2 \times {\sigma_{\phi h}^{\xi}}^2}{16\pi} \frac{\rho_\phi^2}{m_\phi^4}\,, \tag{3.156}$$

where we assumed that $m_h \ll m_\phi$, $N_h = 4$ is the number of internal degrees of freedom for 1 complex Higgs doublet, and $\sigma_{\phi h}^{\xi}$ is given in the addendum A by Eq. (3.191). On the other hand, it was argued in Section 3.2.2 that the scattering $\phi\phi \to hh$ through the graviton exchange can also be parameterized by an effective coupling

$$\mathcal{L}_h = -\sigma_{\phi h}\phi^2 h^2\,, \tag{3.157}$$

with

$$\sigma_{\phi h} = -\frac{m_\phi^2}{4M_P^2}\,, \tag{3.158}$$

and the rate R_h^ϕ is given by the analogous expression to (3.156) with $\sigma_{\phi h}^{\xi}$ replaced by $\sigma_{\phi h}$.

The full four-point coupling of course is given by the sum $\sigma_{\phi h/X}^{\xi} + \sigma_{\phi h/X}$. However, except for values where the two are similar, which occurs when $12\xi^2 + 5\xi \simeq \frac{1}{2}$ (assuming $m_X \ll m_\phi$ and taking the ξ_i to be equal to ξ), either the minimal or the non-minimal contribution dominates. Thus, for the most part, we will consider separately the minimal and non-minimal contributions. Note that for two values of ξ ($\xi \sim -1/2$ and $1/12$) destructive interference could occur causing the entire rate to vanish (at the tree level).

3.3.3 Particle Production with a Non-Minimal Coupling

Given the rates R_i^j calculated in the previous part, we compute the evolution for the gravitational (minimal and non-minimal) contribution to the reheating processes and the dark matter density for the three reactions outlined above.

3.3.3.1 $h\ h \to DM\ DM$

The gravitational scattering of thermal Higgs bosons leads to the production of massive scalar dark matter particles X. The dark matter number density n_X can be calculated from the classical Boltzmann equation Eq.(3.63) We proceed similarly to what we did in the section 3.2.2 by introducing the comoving number density $Y_X = na^3$ and rewriting the Boltzmann equation. Since the production rate (3.152) is a function of the temperature of the thermal bath, it is necessary to determine the relation between T and a to solve the Boltzmann equation as a function of the scale factor a. For the Starobinsky potential in Eq. (3.140), at the end of inflation, the inflaton starts oscillating about a quadratic minimum[16]. We remind the reader

[16]For the inflaton scattering with $V(\phi) \sim \phi^k$, where $k > 2$, see [87, 106, 119, 194, 210, 259, 260].

that for a quadratic minimum, we can set the equation of state parameter $w_\phi = \frac{P_\phi}{\rho_\phi} \simeq 0$. Hence, we can solve Eq.(3.66,3.67) for this specific value of w_ϕ. We assume here that reheating occurs due to the effective inflaton coupling to the Standard Model fermions, given by the interaction Lagrangian Eq.(3.68). We find [87, 106]

$$\rho_\phi(a) = \rho_{\rm end}\left(\frac{a_{\rm end}}{a}\right)^3 \tag{3.159}$$

and

$$\rho_R(a) = \rho_{\rm RH}\left(\frac{a_{\rm RH}}{a}\right)^{\frac{3}{2}} \frac{1-\left(\frac{a_{\rm end}}{a}\right)^{\frac{5}{2}}}{1-\left(\frac{a_{\rm end}}{a_{\rm RH}}\right)^{\frac{5}{2}}}\,, \tag{3.160}$$

in agreement with the generic case for an arbitrary k found in Eq.(3.71, 3.72). We emphasize again that these equations are strictly valid for $a_{\rm end} \ll a \ll a_{\rm RH}$. For the Starobinsky potential, $\rho_{\rm end} \simeq 0.175 m_\phi^2 M_P^2$ [209]. The maximum temperature (or radiation energy density) is attained when the radiation energy density reaches its peak at $\rho_R(a_{\rm max}) = \alpha T_{\rm max}^4$, as described in section 3.2.2.

Using Eq. (3.160) we can then express the production rate from gravitational scattering of thermal particles (3.152) as a function of the scale factor a

$$R_X^{T,(\xi)}(a) \simeq \beta_1^{(\xi)} \frac{\rho_{\rm RH}^2}{\alpha^2 M_P^4}\left(\frac{a_{\rm RH}}{a}\right)^3 \left[\frac{1-\left(\frac{a_{\rm end}}{a}\right)^{\frac{5}{2}}}{1-\left(\frac{a_{\rm end}}{a_{\rm RH}}\right)^{\frac{5}{2}}}\right]^2\,, \tag{3.161}$$

where we assumed that $m_X \ll m_\phi, T$, and thus neglected the terms $\beta_{2,3}^{(\xi)}$. We find that the solution to the DM Boltzmann equation from thermal production is

$$n_X^{T,\xi}(a_{\rm RH}) = \frac{2\beta_1^\xi}{\sqrt{3}\alpha^2 M_P^3}\frac{\rho_{\rm RH}^{3/2}}{(1-(a_{\rm end}/a_{\rm RH})^{\frac{5}{2}})^2}\times \left(1+3\left(\frac{a_{\rm end}}{a_{\rm RH}}\right)^{\frac{5}{2}} - \frac{25}{7}\left(\frac{a_{\rm end}}{a_{\rm RH}}\right)^{\frac{3}{2}} - \frac{3}{7}\left(\frac{a_{\rm end}}{a_{\rm RH}}\right)^5\right)\,, \tag{3.162}$$

where we integrated Eq. (3.76) in the interval $a_{\rm end} < a < a_{\rm RH}$ using the rate above. The relic abundance is then given by

$$\Omega_X^{T,(\xi)}h^2 \;=\; \frac{2}{3}\Omega_k^{(\xi)} \qquad \left[1+3\left(\frac{\rho_{\rm RH}}{\rho_{\rm end}}\right)^{\frac{5}{6}} - \frac{25}{7}\left(\frac{\rho_{\rm RH}}{\rho_{\rm end}}\right)^{\frac{1}{2}} - \frac{3}{7}\left(\frac{\rho_{\rm RH}}{\rho_{\rm end}}\right)^{\frac{5}{3}}\right]\,, \tag{3.163}$$

with

$$\Omega_k^{(\xi)} = 1.6\times 10^8 \frac{g_0}{g_{\rm RH}}\frac{\beta_1^{(\xi)}\sqrt{3}}{\sqrt{\alpha}}\frac{m_X}{1\ {\rm GeV}}\frac{T_{\rm RH}^3}{M_P^3}\left[1-\left(\frac{\rho_{\rm RH}}{\rho_{\rm end}}\right)^{\frac{5}{6}}\right]^{-2}\,, \tag{3.164}$$

where $g_0 = 43/11$ and we use the Standard Model value $g_{\rm RH} = 427/4$. We observe that $\Omega_X^{T,\xi} \propto \beta_1^\xi T_{\rm RH}^3$. Therefore large values of the couplings ξ_h and ξ_X would require a decrease in the reheating temperature. In part 3.3.4 we compare the scattering rates and the dark matter abundances with the minimally coupled case.

3.3.3.2 $\phi\ \phi \to X\ X$

Another mode of dark matter production is through the scattering of the inflaton itself. Whereas the graviton exchange channel was treated with care in section 3.2.2, in the case of non-minimal coupling it suffices to replace $R_X^{T,\xi}$ in Eq. (3.76) with the production rate Eq.(3.154), and to integrate between $a_{\rm end}$ and $a_{\rm RH}$, which leads to

$$n_X^{\phi,\xi}(a_{\rm RH}) = \frac{\sigma_{\phi X}^{\xi\ 2}\rho_{\rm RH}^{3/2}M_P}{4\sqrt{3}\pi m_\phi^4}\left[\left(\frac{a_{\rm RH}}{a_{\rm end}}\right)^{\frac{3}{2}} - 1\right]\sqrt{1-\frac{m_X^2}{m_\phi^2}}\,. \tag{3.165}$$

For $a_{\rm RH} \gg a_{\rm end}$, using Eq. (3.159) we can express $n_X^{\phi,\xi}$ as a function of $\rho_{\rm end}$:

$$n_X^{\phi,\xi}(a_{\rm RH}) \simeq \frac{\sigma_{\phi X}^{\xi\ 2}\rho_{\rm RH}\sqrt{\rho_{\rm end}}M_P}{4\sqrt{3}\pi m_\phi^4}\sqrt{1-\frac{m_X^2}{m_\phi^2}}\,, \tag{3.166}$$

and we find

$$\frac{\Omega_X^{\phi,\xi}h^2}{0.12} \simeq \frac{1.3\times 10^7\sigma_{\phi X}^{\xi\ 2}\rho_{\rm RH}^{1/4}M_P^2}{m_\phi^3}\frac{m_X}{1\,{\rm GeV}}\sqrt{1-\frac{m_X^2}{m_\phi^2}}\,, \tag{3.167}$$

where we assumed the Starobinsky value for $\rho_{\rm end}$. The analogous expression for models with minimally coupled gravity is found by replacing $\sigma_{\phi X}^\xi \to \sigma_{\phi X}$.

Up to this point, we have assumed that the radiation is produced via the direct inflaton decay to a fermion pair. In the next part, we discuss the unavoidable radiation production channel when the inflaton condensate scattering produces Higgs bosons and compare the models with minimal and non-minimal coupling to gravity.

3.3.3.3 $\phi\ \phi \to h\ h$

Gravitational processes that produce dark matter can also populate the thermal bath in the same way. Even if this Planck-suppressed production mechanism does not dominate throughout the entire reheating process, it was shown in precedent section 3.2.2 that for $T_{\rm RH} \lesssim 10^9$ GeV it is graviton exchange that dominates the production of the thermal bath at the very beginning of the reheating, when $\rho_\phi \sim \rho_{\rm end}$. The maximal temperature reached, $T_{\rm max}$, (which can be considered as an absolute lower bound on $T_{\rm max}$) is $T_{\rm max} \sim 10^{12}$ GeV. It is therefore natural to

determine the value of the couplings (ξ_ϕ, ξ_h), for which non-minimal gravitational processes generate the thermal bath at early times, and the maximal temperature which can be attained by these processes.

We compute the radiation energy density produced by gravitational couplings by considering the rate $R_h^{\phi,\xi}$ (3.156) into the Boltzmann equation (3.67)

$$\frac{d\rho_R}{dt} + 4H\rho_R \simeq N_h \frac{\sigma_{\phi h}^{\xi\ 2}}{8\pi} \frac{\rho_\phi^2}{m_\phi^3}\,, \tag{3.168}$$

where we took into account that each scattering corresponds to an energy transfer of $2m_\phi$.[17] The solution to this equation is

$$\rho_R = N_h \frac{\sqrt{3}\sigma_{\phi h}^{\xi\ 2}}{4\pi} \frac{\rho_{\rm end}^{3/2} M_P}{m_\phi^3} \left[\left(\frac{a_{\rm end}}{a}\right)^4 - \left(\frac{a_{\rm end}}{a}\right)^{\frac{9}{2}} \right]. \tag{3.169}$$

Note that the dependence on the scale factor a is very different from that found in Eq. (3.160) due to inflaton decay. Indeed, the Higgs bosons produced by gravitational scattering (minimal as well as non-minimal) are redshifted to a greater extent because of the high dependence of the rate on their energy due to the form of the energy-momentum tensor $T^0_{\mu\nu}$. Since $\rho_R \propto a^{-4}$ in Eq. (3.169) (at large a) and $\rho_\phi \propto a^{-3}$ in Eq. (3.159), reheating through this process does not occur (i.e., ρ_R never comes to dominate the total energy at late times) and inflaton decay is necessary.[18]

However, as in the case of the reheating from the inflaton decay, the energy density in Eq. (3.169) exhibits a maximum when $a = a_{\rm max} = (81/64)a_{\rm end}$. The maximum radiation density is then,

$$\rho_{\rm max}^\xi \simeq N_h \frac{\sigma_{\phi h}^{\xi\ 2}}{12\sqrt{3}\pi} \frac{\rho_{\rm end}^{3/2} M_P}{m_\phi^3} \left(\frac{8}{9}\right)^8, \tag{3.170}$$

and from this expression we find that the maximum temperature produced by gravitational interactions is given by

$$\begin{aligned} T_{\rm max}^\xi &\simeq 6.5\times 10^{11} \left(\frac{|\sigma_{\phi h}^\xi|}{10^{-11}}\right)^{\frac{1}{2}} {\rm GeV} \\ &\simeq 1.8\times 10^{12} \sqrt{|\xi|}\,(|5+12\xi|)^{\frac{1}{2}} \left(\frac{m_\phi}{3\times 10^{13}\,{\rm GeV}}\right) {\rm GeV}\,, \end{aligned} \tag{3.171}$$

where we took $\xi_\phi = \xi_h = \xi$ in the last equality. The analogous expression for models with minimally coupled gravity is found by replacing $\sigma_{\phi h}^\xi \to \sigma_{\phi h}$. To compare the maximum temper-

[17] Or equivalently that each Higgs quanta carries an energy m_ϕ.

[18] This conclusion is avoided if the inflaton potential about minimum is approximated by ϕ^k with a higher power of $k > 4$ [1, 259].

ature obtained by non-minimal interactions with respect to minimal gravitational interactions, we can rewrite Eq. (3.171) (now including minimal interactions in $T^{\xi}_{\rm max}$) as

$$T^{\xi}_{\rm max} \simeq 1.3 \times 10^{12} \left(\frac{|\sigma^{\xi}_{\phi h} + \sigma_{\phi h}|}{\sigma_{\phi h}} \right)^{\frac{1}{2}} \text{GeV} \,. \tag{3.172}$$

The value of ξ for which the maximum temperature generated by the non-minimal coupling surpasses the one from graviton exchange is shown in Fig. 3.8 and is determined using

$$\sqrt{\frac{|\sigma^{\xi}_{\phi h}|}{|\sigma_{\phi h}|}} = \sqrt{2|\xi|}\,(|5 + 12\xi|)^{\frac{1}{2}} > 1 \tag{3.173}$$

which is satisfied when $\xi > 1/12$ or $\xi < -1/2$, as discussed earlier. As noted above and discussed

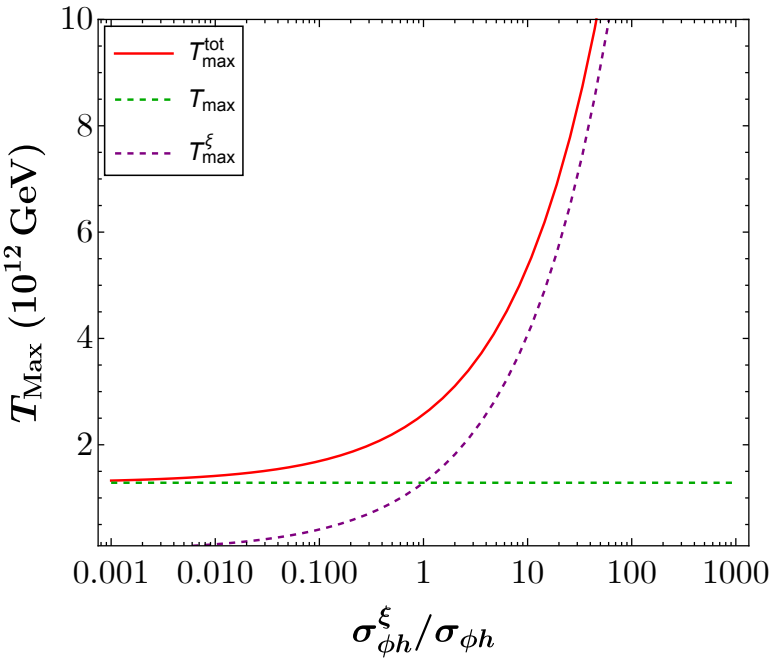

Figure 3.8: *The maximum temperature during reheating generated separately by minimal and non-minimal gravitational scattering of Higgs bosons in the thermal bath.*

in section 3.2.2, minimal (and non-minimal) gravitational interactions for a quadratic inflaton potential do not lead to the completion of the reheating process, thus requiring additional inflaton interactions for decay. Although radiation density produced in scattering falls off faster than that from decay, at early times, the radiation density may dominate and determine $T_{\rm max}$. To determine when the $\phi\,\phi \to h\,h$ process leads to the maximum temperature, we rewrite Eq. (3.160) as:

$$\rho^{y}_{R} \;=\; \frac{\sqrt{3} y^2 m_\phi M_P^3}{20\pi} \left(\frac{\rho_{\rm end}}{M_P^4} \right)^{\frac{1}{2}} \left[\left(\frac{a_{\rm end}}{a} \right)^{\frac{3}{2}} - \left(\frac{a_{\rm end}}{a} \right)^{4} \right] . \tag{3.174}$$

Using Eq. (3.74), we find that the maximum radiation density produced by the inflaton decay

is given by

$$\rho^{y}_{\rm max} = \frac{\sqrt{3}y^2 m_\phi M_P^3}{32\pi}\left(\frac{\rho_{\rm end}}{M_P^4}\right)^{\frac{1}{2}}\left(\frac{3}{8}\right)^{\frac{3}{5}} . \tag{3.175}$$

The maximum temperature is therefore determined by (non-minimal) gravitational interactions when

$$y^2 \lesssim N_h \frac{8\rho_{\rm end}{\sigma^{\xi}_{\phi h}}^2}{9m_\phi^4}\left(\frac{8}{9}\right)^8\left(\frac{8}{3}\right)^{\frac{3}{5}} \tag{3.176}$$

or

$$y \lesssim 1.6\ \sigma^{\xi}_{\phi h}\sqrt{\frac{\rho_{\rm end}}{m_\phi^4}} \simeq 5.4\times 10^4\ \sigma^{\xi}_{\phi h}\left(\frac{3\times 10^{13}\,{\rm GeV}}{m_\phi}\right) . \tag{3.177}$$

This leads to the following reheating temperature:

$$\begin{aligned} T_{\rm RH} &\lesssim 3.1\times 10^{19}\sigma^{\xi}_{\phi h}\left(\frac{m_\phi}{3\times 10^{13}\,{\rm GeV}}\right)^{-1/2}{\rm GeV} \\ &\lesssim 2.4\times 10^9\left(\frac{m_\phi}{3\times 10^{13}}\right)^{\frac{3}{2}}\xi(5+12\xi)\ {\rm GeV} \end{aligned} \tag{3.178}$$

where $T_{\rm RH}$ is given by [106]

$$\rho_\phi(a_{\rm RH}) = \alpha T_{\rm RH}^4 = \frac{12}{25}\Gamma_\phi^2 M_P^2 = \frac{3y^4 m_\phi^2 M_P^2}{400\pi^2} , \tag{3.179}$$

when the reheating temperature is determined by inflaton decay. The primary effect of the gravitational scattering processes on reheating is the augmentation of $T_{\rm max}$ for sufficiently small inflaton decay coupling, y. This can be seen in Fig. 3.9 where we show the evolution of the energy density of radiation from scattering and decay as well as the energy density of the inflaton as a function of $a/a_{\rm end}$ for $\sigma^{\xi}_{\phi h} = 0$ and $\sigma^{\xi}_{\phi h}/\sigma_{\phi h} = 100$, respectively.

As we saw in Eq. (3.173), minimal gravitational interactions dominate over non-minimal interactions when $\sigma^{\xi}_{\phi h} < \sigma_{\phi h}$ or when

$$12\xi_\phi\xi_h + 3\xi_h + 2\xi_\phi < \frac{1}{2} , \tag{3.180}$$

when we neglect contributions proportional to the Higgs mass. In this case, the maximum temperature is determined by gravitational interactions when $y \lesssim 2.1\times 10^{-6}$ from Eq. (3.177) using $\sigma_{\phi h}$ from Eq. (3.158). The evolution of the energy densities in this case is shown in Fig. 3.9 with $y = 10^{-8}$. However as the energy density of radiation after the maximum falls faster than ρ_ϕ, reheating in the Universe is determined by the inflaton decay. For a sufficiently small coupling y, the energy density from the decay dominates the radiation density at $a > a_{\rm int}$, where

$$\frac{a_{\rm int}}{a_{\rm end}} \simeq \left(\frac{5\sigma_{\phi h}^2 N_h \rho_{\rm end}}{y^2 m_\phi^4}\right)^{2/5} \simeq 1.6\left(\frac{\sigma_{\phi h} M_P}{y m_\phi}\right)^{4/5} . \tag{3.181}$$

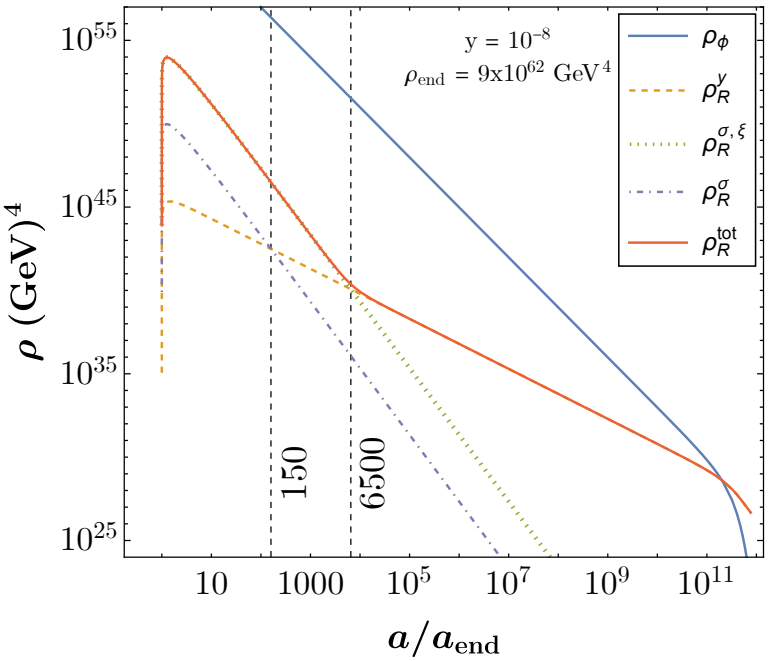

Figure 3.9: *Evolution of the inflaton density (blue) and the total radiation density (red), with radiation density produced from inflaton decays (dashed orange) and $\phi\ \phi \to h\ h$ scattering processes $\rho_R^{\sigma,\xi}$ (dotted green) and ρ_R^{σ} (dash-dotted purple) with $\sigma_{\phi h}^{\xi}/\sigma_{\phi h} = 100$ (or $\xi_\phi = \xi_h = \xi \simeq -2.3$ or 1.8), as a function of $a/a_{\rm end}$ for a Yukawa-like coupling $y = 10^{-8}$ and $\rho_{\rm end} \simeq 0.175\, m_\phi^2 M_P^2 \simeq 9 \times 10^{62}\,{\rm GeV}^4$. The black dashed lines corresponds to the ratios $a_{\rm int}/a_{\rm end} \simeq 150$ and 6500, which agrees with Eq. (3.181). The numerical solutions are obtained from Eqs. (3.66), (3.67), and (3.168).*

For $\sigma_{\phi h} = 3.8 \times 10^{-11}$, $m_\phi = 3 \times 10^{13}$ GeV, and $y = 10^{-8}$ we have $a_{\rm int} \approx 160 a_{\rm end}$, as seen in the figure. When Eq. (3.180) is not satisfied, non-minimal interactions may dominate as shown in the bottom panel of Fig. 3.9, for $\sigma_{\phi h}^{\xi} = 100\sigma_{\phi h}$ and $y = 10^{-8}$. The cross-over can be determined from Eq. (3.181) with the replacement $\sigma_{\phi h} \to \sigma_{\phi h}^{\xi}$. In this example, $a_{\rm int} \approx 6500 a_{\rm end}$.

3.3.4 Results

We now turn to some general results that may be obtained from the framework of described above. Concerning the gravitational production of dark matter from the thermal bath, the difficulty of populating the Universe via the exchange of a graviton was already discussed in section 3.2.2. Summing the minimal and non-minimal contributions in Eq. (3.163), we find for $\rho_{\rm RH} \ll \rho_{\rm end}$

$$\begin{aligned}\frac{\Omega_X^T}{0.12} &\simeq [1 + 30 f(\xi_h, \xi_X)] \left(\frac{T_{\rm RH}}{10^{14}\ {\rm GeV}}\right)^3 \left(\frac{m_X}{4.0 \times 10^9\ {\rm GeV}}\right) \\ &= \left[1 + 120\xi^2(1 + 6\xi + 12\xi^2)\right] \\ &\quad \times \left(\frac{T_{\rm RH}}{10^{14}\ {\rm GeV}}\right)^3 \left(\frac{m_X}{4.0 \times 10^9\ {\rm GeV}}\right) \end{aligned} \tag{3.182}$$

with

$$f(\xi_h, \xi_X) = \xi_h^2 + 2\xi_h\xi_X + \xi_X^2 + 12\xi_h\xi_X\,(\xi_h + \xi_X + 4\xi_h\xi_X)$$

where we assumed $\xi_h = \xi_X = \xi$ in the last equality, for simplicity. It is clear that if we set $\xi = 0$, i.e. if we consider only graviton exchange, the reheating temperature necessary to obtain a reasonable density respecting the data [22] is dangerously close to the mass of the inflaton, even for extremely large dark matter masses. This problem had already been raised in [192] and resolved in [1, 202] by considering the dark matter produced from the (minimal) gravitational inflaton scattering.

On the other hand, from Eq. (3.182) we see that there is another solution to this tension if one allows for non-minimal gravitational couplings. Indeed, it is easy to see that for values of $\xi_i \gtrsim 0.1$ ($f(\xi_h, \xi_X) \gtrsim \frac{1}{30}$), non-minimal gravitational production dominates over graviton exchange. In this case, it becomes easier to obtain the correct dark matter density for more reasonable values of $T_{\rm RH}$ and/or m_X. For example, for a common value $\xi = \xi_h = \xi_X = 1$, a temperature of $T_{\rm RH} \sim 1.2 \times 10^{13}$ GeV, thus slightly below the inflaton mass, is sufficient to produce an EeV dark matter candidate, whereas for $\xi = 1000$, $T_{\rm RH} \sim 10^{11}$ GeV will saturate the relic density for a 2.6 TeV dark matter mass. We show this result in Fig. 3.10 where we plot the reheating temperature needed to satisfy the relic density constraint as function of m_X for different value of ξ. For each value of ξ, the relic density exceeds $\Omega_X h^2 = 0.12$ above the corresponding curve. As one can see, the line for $\xi = 0$ is in the upper corner of the figure at high values of $T_{\rm RH}$ and m_X and these drop significantly at higher values of ξ.

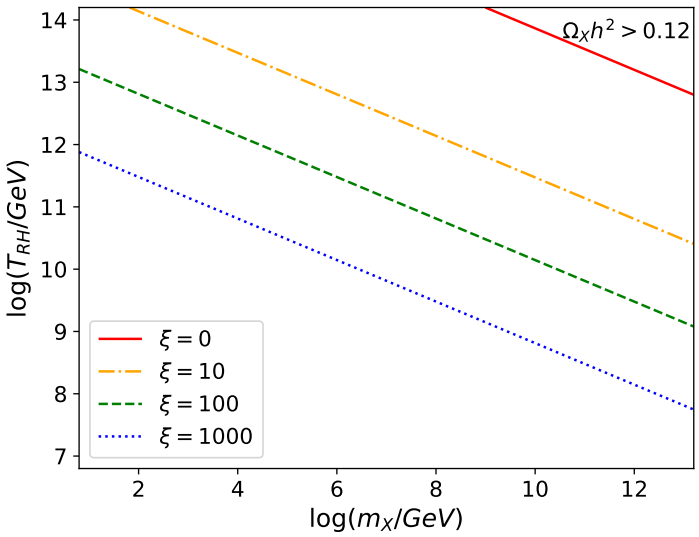

Figure 3.10: *Region of parameter space respecting the relic density constraint* $\Omega_X h^2 = 0.12$ *in the plane* (m_X,$T_{\rm RH}$) *for different values of* $\xi = \xi_h = \xi_X$ *and* $\rho_{\rm end} \simeq 0.175\, m_\phi^2 M_P^2$ *in the case of gravitational production from the thermal bath* $h\ h \to X\ X$. *Both minimal and non-minimal contributions are taken into account.*

As was shown in secton 3.2.2, another possibility to avoid the necessity of high reheating temperatures and/or dark matter masses is the production of matter from the oscillations within the inflaton condensate when the energy stored in the condensate is much larger than the reheating temperature. A simple comparison between Eqs. (3.163) and (3.167) shows that the production of dark matter via inflaton scattering when $\xi_i \neq 0$ generally dominates over the production of dark matter from the thermal bath:

$$\begin{aligned}\frac{\Omega_X^{\phi,\xi}}{\Omega_X^{T,\xi}} &\simeq 34\frac{(\sigma_{\phi X}^{\xi})^2}{\beta_1^{\xi}}\frac{M_P^5}{T_{\rm RH}^2 m_\phi^3} \\ &\simeq 185\frac{M_P m_\phi}{T_{\rm RH}^2}\frac{(5+12\xi)^2}{1+6\xi+12\xi^2} \gg 1\,,\end{aligned} \tag{3.183}$$

where we took $\xi = \xi_\phi = \xi_h = \xi_X$ and $m_X \ll m_\phi$ in the last equality. We are therefore able to state that the relic density of dark matter generated by the non-minimal gravitational scattering of the inflaton is always much more abundant than that produced by the thermal bath.

Dark matter production from inflaton scattering via minimal graviton exchange also dominates over minimal gravitational thermal production (3.2.2). This state of affairs is anything but surprising. Indeed, the energy available in the inflaton condensate at the onset of oscillations is much greater than that available in the thermal bath during the reheating process. As the scattering cross-sections are themselves highly dependent on the energies through the energy-momentum tensor, it is quite normal that inflaton scattering is the dominant process for both minimal and non-minimal gravitational couplings. Since inflaton scattering dominates in both the minimal and non-minimal gravitational interactions we can compare the two. We obtain

$$\frac{\Omega_X^{\phi,\xi}}{\Omega_X^{\phi}} = \frac{\sigma_{\phi X}^{\xi\ 2}}{\sigma_{\phi X}^2} \simeq 4\xi^2(5+12\xi)^2\,, \tag{3.184}$$

and we see again that non-minimal interactions dominate when $\xi > 1/12$ or $< -1/2$.

We show in Fig. 3.11 the region of the parameter space in the $(m_X, T_{\rm RH})$ plane allowed by the relic density constraint, adding all of the minimal and non-minimal gravitational contributions, from inflaton scattering and as well as Higgs scattering from the thermal bath taking $\xi_\phi = \xi_h = \xi_X = \xi$. As expected, for $\xi = 0$ we recover the result found in section 3.2.2. As one can see, the difficulty in the gravitational production from the thermal bath is indeed alleviated as a reheating temperature $T_{\rm RH} \simeq 10^{11}$ GeV allows for the production of a PeV scale dark matter candidate. If in addition we introduce the non-minimal couplings ξ, the necessary reheating temperature to fit the Planck data may be as low as the electroweak scale for a GeV candidate if $\xi \gtrsim 1000$. Finally, we note that given the dark matter mass and reheating temperature (if that sector of beyond the Standard Model physics were known), the contours in Fig. 3.11 allow

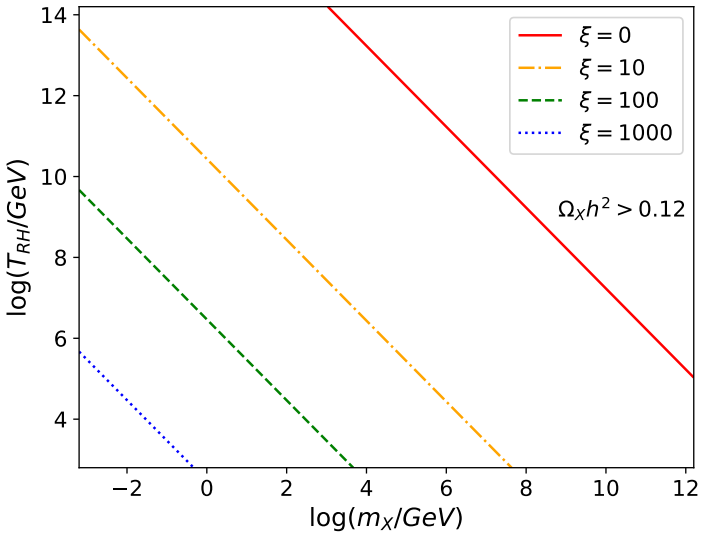

Figure 3.11: *Region of parameter space respecting the relic density constraint* $\Omega_X h^2 = 0.12$ *in the plane* (m_X,$T_{\rm RH}$) *for different values of* $\xi_\phi = \xi_h = \xi_X = \xi$ *and* $\rho_{\rm end} \simeq 0.175\, m_\phi^2 M_P^2$ *in the case of production from gravitational inflaton scattering* $\phi\ \phi \to X\ X$. *Both minimal and non-minimal contributions are taken into account.*

us to place an upper bound on the non-minimal couplings, ξ.We can rewrite Eq. (3.167) as

$$\begin{aligned}\frac{\Omega_X h^2}{0.12} &= 4.1\times 10^{-7}(12\xi^2+5\xi+\frac{1}{2})^2\left(\frac{T_{\rm RH}}{10^{10}{\rm GeV}}\right)\\ &\times\left(\frac{m_X}{1{\rm GeV}}\right)\left(\frac{m_\phi}{3\times 10^{13}{\rm GeV}}\right),\end{aligned} \tag{3.185}$$

when $m_X \ll m_\phi$ and $\xi = \xi_\phi = \xi_X$. Then, for example, if $m_X = 1$ TeV, and $T_{\rm RH} = 10^9$ GeV, we obtain an upper limit of $|\xi| \lesssim 4$.

3.3.5 Conclusions

In this section, we have generalized the *minimal* gravitational interactions in the early Universe, i.e., the s-channel exchange of a graviton, to include *non-minimal* couplings of all scalars to the Ricci curvature R. We consider a scalar sector S_i consisting of the inflaton condensate ϕ, the Higgs field H and a dark matter candidate X, and we have analyzed the impact of couplings of the type $\xi_i S_i^2 R$ on the reheating process and dark matter production. The latter can be generated by the thermal Higgs scattering or excitations of the inflaton, both through minimal and non-minimal gravitational couplings. Whereas the Higgs scattering through the exchange of a graviton necessitates a very large reheating temperature and/or dark matter mass in order to fulfill Planck CMB constraints ($T_{\rm RH} \simeq 10^{14}$ GeV with $m_X \simeq 10^9$ GeV), for $\xi \gtrsim 0.1$, the non-minimal coupling dominates the process and alleviates the tension. For $\xi \simeq 1000$, a dark matter mass of ~ 1 PeV with $T_{\rm RH} \simeq 10^{10}$ GeV will satisfy the constraint, see Fig. 3.10.

However, thermal production is not the sole source of dark matter production through gravity. When we include the contribution (necessarily present) of the inflaton scattering, we showed that the energy stored in the condensate at the end of inflation compensates largely the reduced gravitational Planck coupling. These processes yield the correct relic abundance through minimal graviton exchange for a dark matter mass of $\sim 10^8$ GeV with $T_{\rm RH} \simeq 10^{10}$ GeV, and the constraint is satisfied for a dark matter mass of ~ 100 GeV and $T_{\rm RH} \gtrsim 10^4$ GeV if one adds non-minimal couplings of the order $\xi \simeq 100$ as we show in Fig. 3.11. Gravitational inflaton scattering also affects the reheating process, producing a maximum temperature $\simeq 10^{12}$ GeV with minimal couplings, reaching as large as $T^{\xi}_{\rm max} \simeq 5|\xi| T_{\rm max} \simeq 10^{14}$ GeV for $\xi = 100$ as one can see in Fig. 3.8. This result can be re-expressed as an upper limit to $|\xi|$ given values of m_X and $T_{\rm RH}$.

We can not over-emphasize that all these results are unavoidable, in the sense that they are purely gravitational and do not rely on physics beyond the Standard Model. The relic density of Dark Matter and maximum temperature of the thermal bath computed here should be considered as lower bounds, that should be implemented in any extension of the Standard Model, whatever is its nature.

Addenda

A Leading order interactions

The full Jordan frame action we consider is given by Eq. (3.137). The conformal transformation to the Einstein frame is given by

$$g_{\mu\nu} \;=\; \Omega^2 \tilde{g}_{\mu\nu}\,, \tag{3.186}$$

where $g_{\mu\nu}$ is the Einstein frame space-time metric and the conformal factor is expressed by Eq. (3.138). It can readily be shown that the scalar curvature transforms as (see, e.g., [261])

$$\tilde{R} = \Omega^2 \left[R + 6 g^{\mu\nu} \nabla_\mu \nabla_\nu \ln\Omega - 6 g^{\mu\nu} \left(\nabla_\mu \ln\Omega\right) \left(\nabla_\nu \ln\Omega\right) \right] . \tag{3.187}$$

After eliminating the total divergence term, we find the Einstein frame action (3.144). To find the effective interaction terms we assume the small field limit (3.147) and expand the conformal

factors in the Einstein frame action. We find the following effective interaction Lagrangian:

$$\begin{aligned}\mathcal{L}_{\rm eff} &= -\frac{1}{2}\left(\frac{\xi_\phi\phi^2}{M_P^2}+\frac{\xi_X X^2}{M_P^2}\right)\partial^\mu h\partial_\mu h - \frac{1}{2}\left(\frac{\xi_h h^2}{M_P^2}+\frac{\xi_X X^2}{M_P^2}\right)\partial^\mu\phi\partial_\mu\phi - \frac{1}{2}\left(\frac{\xi_\phi\phi^2}{M_P^2}+\frac{\xi_h h^2}{M_P^2}\right)\partial^\mu X\partial_\mu X \\ &+ \frac{6\xi_h\xi_X hX}{M_P^2}\partial^\mu h\partial_\mu X + \frac{6\xi_h\xi_\phi h\phi}{M_P^2}\partial^\mu h\partial_\mu\phi + \frac{6\xi_\phi\xi_X\phi X}{M_P^2}\partial^\mu\phi\partial_\mu X + m_X^2X^2\left(\frac{\xi_\phi\phi^2}{M_P^2}+\frac{\xi_h h^2}{M_P^2}\right) \\ &+ m_\phi^2\phi^2M_P^2\left(\frac{\xi_X X^2}{M_P^2}+\frac{\xi_h h^2}{M_P^2}\right) + m_h^2h^2\left(\frac{\xi_\phi\phi^2}{M_P^2}+\frac{\xi_X X^2}{M_P^2}\right), \end{aligned} \tag{3.188}$$

and we can rewrite the above Lagrangian in terms of the effective couplings as Eq. (3.148), with

$$\begin{aligned}\sigma_{hX}^{\xi} &= \frac{1}{4M_P^2}\left[\xi_h(2m_X^2+s)+\xi_X(2m_h^2+s)\right. \\ &+ \left.\left(12\xi_X\xi_h(m_h^2+m_X^2-t)\right)\right], \end{aligned} \tag{3.189}$$

$$\sigma_{\phi X}^{\xi} = \frac{1}{2M_P^2}\left[\xi_\phi m_X^2+12\xi_\phi\xi_X m_\phi^2+3\xi_X m_\phi^2+2\xi_\phi m_\phi^2\right], \tag{3.190}$$

$$\sigma_{\phi h}^{\xi} = \frac{1}{2M_P^2}\left[\xi_\phi m_h^2+12\xi_\phi\xi_h m_\phi^2+3\xi_h m_\phi^2+2\xi_\phi m_\phi^2\right], \tag{3.191}$$

where s,t are the Mandelstam variables. The latter couplings assume an inflaton condensate in the initial state rather than a thermal Higgs in the initial state accounting for the lack of symmetry in the three couplings.

B Thermal production with non-minimal couplings

In this addendum, we calculate the thermal dark matter production rate $R_X^{T,\xi}(T)$ arising from the effective four-point interaction $\sigma_{hX}h^2X^2$, where σ_{hX} is given by Eq. (3.189). We also calculate the production rate $R_X^T(T)$ for the thermal scattering processes mediated by gravity alone, SM SM $\to X\ X$, that are unavoidable in models with a minimal coupling to gravity ($\xi_{\phi,h,X}=0$) [1, 192], and compare the two results. The production rate $R_X^{T,\xi}(T)$ can be computed from Eq. (3.151). The matrix element squared is given by

$$|\overline{\mathcal{M}}^{hX,\xi}|^2 = 4\sigma_{hX}^{\xi\ 2}, \tag{3.192}$$

where in the limit where the Higgs boson mass is neglected, the Mandelstam variables s and t are given by

$$t = \frac{s}{2}\left(\sqrt{1-\frac{4m_X^2}{s}}\cos\theta_{13}-1\right)+m_X^2, \tag{3.193}$$

$$s = 2E_1E_2\left(1-\cos\theta_{12}\right). \tag{3.194}$$

We find the following coefficients for Eq. (3.152)

$$\beta_1^\xi = \frac{\pi^3}{2700}\left[\xi_h^2 + 2\xi_h\xi_X + \xi_X^2 + 12\xi_h\xi_X\left(\xi_h + \xi_X + 4\xi_h\xi_X\right)\right], \tag{3.195}$$

$$\beta_2^\xi = \frac{\zeta(3)^2\xi_h}{2\pi^5}\left[\xi_h + \xi_X + 6\xi_h\xi_X - 12\xi_h\xi_X^2\right], \tag{3.196}$$

$$\beta_3^\xi = \frac{\xi_h^2}{576\pi}. \tag{3.197}$$

Similarly, we find the matrix element squared for minimally coupled gravity:

$$|\overline{\mathcal{M}}^{hX}|^2 = \frac{1}{4M_P^4}\frac{\left(t(s+t) - 2m_X^2 t + m_X^4\right)^2}{s^2}, \tag{3.198}$$

where we have neglected the Higgs field mass. We find the coefficients:

$$\beta_1 = \frac{\pi^3}{81000}, \tag{3.199}$$

$$\beta_2 = -\frac{\zeta(3)^2}{30\pi^5}, \tag{3.200}$$

$$\beta_3 = \frac{1}{4320\pi}. \tag{3.201}$$

where we have neglected the Higgs field mass. Note that when both contributions are kept, and we neglect $m_h \ll m_X$, the full coefficients (including interference) are given by

$$\begin{aligned}\beta_1^\xi = \frac{\pi^3}{81000}&\left[30\xi_h^2\left(12\xi_X(4\xi_X+1)+1\right)\right.\\ &\left.+10\xi_h(6\xi_X+1)^2 + 10\xi_X(3\xi_X+1)+1\right],\end{aligned} \tag{3.202}$$

$$\begin{aligned}\beta_2^\xi = -\frac{\zeta(3)^2}{60\pi^5}&\left[2+10\xi_X\right.\\ &\left.+5\xi_h\left(1+6\xi_X+6\xi_h\left(6\xi_X(2\xi_X-1)-1\right)\right)\right],\end{aligned} \tag{3.203}$$

$$\beta_3^\xi = \frac{1}{8640\pi}\left[2+5\xi_h\left(32\xi_h-2\right)\right]. \tag{3.204}$$

which reduces to Eqs. (3.199-3.201) when all $\xi_i = 0$.

3.4 Gravity as a portal to Reheating, Leptogenesis and Dark Matter

This section is based on: B. Barman, **S. Cléry**, R.T Co, Y. Mambrini, K.A. Olive, *Gravity as a portal to reheating, leptogenesis and dark matter*, **JHEP 12 (2022) 072**, arXiv:2210.05716 [3]

Motivation

Dark Matter and inflation require an extension to the Standard Model of particle physics, but it is not the only reason why an extension is necessary. As discussed in section 1.3, the visible or baryonic matter content of the Universe is asymmetric. One interesting mechanism to produce the baryon asymmetry of the Universe (BAU) via the lepton sector physics through leptogenesis [42] where, instead of creating a baryon asymmetry directly, a lepton asymmetry is generated first and subsequently gets converted into baryon asymmetry by the $(B+L)$-violating electroweak sphaleron transitions [36]. In thermal leptogenesis [262–265], the decaying particles, typically right-handed neutrinos (RHNs), are produced thermally from the SM bath. However, the lower bound on the RHN mass in such scenarios (known as the Davidson-Ibarra bound), leads to a lower bound on the reheating temperature $T_{\rm RH} \gtrsim 10^{10}$ GeV [266] so that the RHNs can be produced from the thermal bath. One simpler alternative is the non-thermal production of RHNs [62, 267–270] originating from the decay of inflaton. This interaction is necessarily model dependent as it depends on the Yukawa interaction between the inflaton and the RHNs.

In addition to providing the DM abundance, gravitational interactions can also be the source of baryogenesis. As shown in [59], it is possible to have a model-independent theory of non-thermal production of RHNs from inflation, once the inflaton potential is specified. The abundance of RHNs is calculated in the same manner as the dark matter abundance and can lead to observed BAU from the out-of-equilibrium CP violating decay of the RHNs, produced during the reheating epoch.

In this section of the thesis, we derive a simultaneous solution for the DM abundance, the baryon asymmetry, and the origin of the thermal bath from purely gravitational interactions. In this sense, our scenario can be considered as the most minimal possible, since we do not introduce any new interactions for any process beyond the SM, except for gravity. The only new fields required are the dark matter candidate and the RHNs (which are anyway needed for the generation of neutrino masses). Our only model dependence comes from the choice of the particular inflaton potential. However, we are mostly sensitive to the shape of the potential near the minimum, after inflation. But, as will be shown in the following section, even this dependence proves to be weak when it comes to combining the constraints of reheating, baryo-

genesis, and the dark matter relic density. We will further show that the present framework can give rise to a detectable inflationary Gravitational Waves (GW) background, to probe this scenario for $T_{\rm RH} \lesssim 5 \times 10^6$ GeV in future GW experiments, such as BBO, DECIGO, CE, and ET. That in turn already excludes the minimal gravitational reheating scenario which leads to an excess of the present-day GW energy density, in conflict with the BBN prediction. However, a large part of the parameter space remains within the reach of several futuristic GW detection facilities.

We first review the gravitational production of RHN and SM particles from inflaton scattering and the thermal bath in Sec. 3.4.1, where we also discuss the effect of non-minimal gravitational interactions. We then derive the set of parameters (dark matter mass, RHN mass, and reheating temperature, $T_{\rm RH}$, which simultaneously provide the correct relic density and BAU in Sec. 3.4.5. If the dark matter is not absolutely stable, we are able to propose an explanation for the PeV events observed at IceCube in the case of a long-lived candidate. Finally, we propose a novel scenario where the gravitational production is a two-step process passing through a scalar singlet that couples with the RHN sector in Sec. 3.4.6.

3.4.1 Gravitational production of RHNs

The minimal gravitational interactions are described by the Lagrangian [271, 272]

$$\sqrt{-g}\,\mathcal{L}_{\rm int} = -\frac{1}{M_P}\,h_{\mu\nu}\,\left(T^{\mu\nu}_{\rm SM} + T^{\mu\nu}_{\phi} + T^{\mu\nu}_{X}\right)\,, \tag{3.205}$$

as introduced in 3.2.1 in Eq.(3.39) where ϕ is the inflaton and X is a particle that does not belong to the SM. In the context of this section, we consider X to be a spin 1/2 Majorana fermion which can be associated with DM or a Right-Handed Neutrino (RHN). The form of the stress-energy tensor $T^{\mu\nu}_i$ for Majorana spin-1/2 fermions, takes the form

$$T^{\mu\nu}_{1/2} = \frac{i}{8}\left[\bar{\chi}\gamma^\mu \overleftrightarrow{\partial^\nu}\chi + \bar{\chi}\gamma^\nu \overleftrightarrow{\partial^\mu}\chi\right] - g^{\mu\nu}\left[\frac{i}{4}\bar{\chi}\gamma^\alpha \overleftrightarrow{\partial_\alpha}\chi - \frac{m_\chi}{2}\,\overline{\chi^c}\chi\right]. \tag{3.206}$$

Without loss of generality, we will assume that the inflaton potential $V(\phi)$ is among the class of α-attractor T-models described in Eq.(3.52) which can be expanded about the origin[19]

$$V(\phi) = \lambda\frac{\phi^k}{M_P^{k-4}}\,; \quad \phi \ll M_P. \tag{3.207}$$

[19]Our discussion is general and not limited to T-models of inflation as the way we express the minimum of the potential is generic.

The end of inflation may be defined when $\ddot{a} = 0$ where a is the cosmological scale factor. The inflaton field value in this potential at that time is given by [106, 209]

$$\phi_{\rm end} \simeq \sqrt{\frac{3}{8}} M_P \ln\left[\frac{1}{2} + \frac{k}{3}\left(k + \sqrt{k^2+3}\right)\right]. \tag{3.208}$$

and the inflaton energy density at $\phi_{\rm end}$ is $\rho_{\rm end} = \frac{3}{2}V(\phi_{\rm end})$. The overall scale of the potential parameterized by the coupling λ, is determined from the amplitude of the CMB power spectrum A_S, as in Eq.(2.64). In our analysis, we use $\ln(10^{10}A_S) = 3.044$ [103] and set $N = 55$. This leads to an inflaton mass of $m_\phi \simeq 1.2 \times 10^{13}$ GeV for $k = 2$. More generically, $m_\phi \simeq 1.2 \times 10^{13}$ is also the inflaton mass at the end of inflation for any larger k when the full potential in Eq. (3.52) is used. While $N = 55$ is appropriate for reheating temperatures of order 10^{12} GeV, for lower reheating temperatures (between $10 - 10^7$ GeV) $N = 45 - 50$ [273]. However, we have checked that our results are very insensitive to the value of N.

In addition to the inflationary sector and the SM, neutrino masses and mixing require at least two (heavy) right-handed neutrino states for the seesaw mechanism [49–52, 274, 275]. One of these, if produced and remaining out-of-equilibrium until its decay, can produce a lepton asymmetry. In order to account for the dark matter in a most economic way, we assume three RHNs, N_i, where for now, the lightest of these, N_1 is decoupled from the other two and has a vanishing Yukawa coupling. Aside from the Yukawa couplings, the only couplings we consider between the SM, the RHNs, and the inflaton are gravitational of the form in Eq. (3.205). Needless to say, such interactions are unavoidable, and must be taken into account in any extensions beyond the SM. As a concrete example, we consider the renormalizable interaction Lagrangian between the Majorana RHNs and the SM

$$\mathcal{L} \supset -\frac{1}{2} M_{N_i} \overline{N_i^c} N_i - (y_N)_{ij} \overline{N}_i \widetilde{H}^\dagger L_j + \text{h.c.}\,. \tag{3.209}$$

Here H and L are the SM Higgs and lepton doublet respectively. Lepton number is clearly violated in this Lagrangian.[20] For now, we assume that $(y_N)_{1i} = 0$ for all i and that N_1 is stable. As a result, N_1 is a viable DM candidate. Later, we will relax this condition and consider a metastable DM candidate with $(y_N)_{1i} \neq 0$, allowing for N_1 to decay into neutrinos that could be observed at IceCube. The preservation of the lepton asymmetry will provide a limit on $(y_N)_{1i}/M_{N_1}$. The other two RHNs, namely $N_{2,3}$ are assumed to be heavier and they participate in leptogenesis.

We would like to remind the readers that there are three types of seesaw models, which differ by the properties of the exchanged heavy particles, e.g.,

[20] We consider the RHNs to be mass diagonal.

(i) Type-I: SM gauge fermion singlets

(ii) Type-II: SM $SU(2)_L$ scalar triplets

(iii) Type-III: SM $SU(2)_L$ fermion triplets.

In the present case we are considering the Type-I scenario, which is evident from the Lagrangian in Eq. (3.205). The Type-I seesaw mechanism can indeed be realized with only two active RHN [55, 276–278]. In this context, only the normal ($m_1 < m_2 < m_3$) and inverted ($m_3 < m_2 < m_1$) hierarchies are relevant, where m_i are the light neutrino masses. With only two RHN playing a role in the seesaw mechanism, we expect $m_1 = 0$ or $m_3 = 0$, depending on the hierarchy. Indeed, due to the reduced rank of the mass matrices (a 3×2 Dirac matrix and a 2×2 Majorana matrix) one neutrino remains massless, while the others acquire their light mass through the usual seesaw suppression of the order $m_i \sim \frac{(y_N)^2_{ii}\langle H\rangle^2}{M_{N_i}}$.

We further assume the absence of any direct coupling between the inflaton ϕ and the RHNs, such that there is no perturbative decay of the inflaton into the RHN final state; in other words, we do not attribute a lepton number to the inflaton. Thus, the *only* possible production of the RHNs is the 2-to-2 gravitational scattering of the inflatons and of the particles in the radiation bath. As we will show, these production channels dominate in different regions of the parameter space. In Fig. 3.12, we show the s-channel exchange of a graviton obtained from the Lagrangian in Eq. (3.205) for the production of RHNs from the inflaton condensate, to which we can add a similar diagram for the production of SM fields during the reheating process as described in section 3.2.1. Despite the a priori Planck reduced interactions, we will show that this framework is perfectly capable of simultaneously explaining the dark matter relic abundance and the observed baryon asymmetry, while also reheating the Universe. The Planck suppression due to graviton exchange is indeed partially compensated by the energy available in the inflaton condensate at the end of inflation.

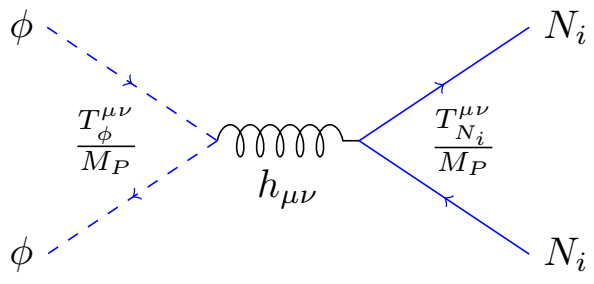

Figure 3.12: *Feynman diagram for the production of RHN through the gravitational scattering of the inflaton condensate. A similar diagram also exists with Standard Model particles in the initial state.*

In this part, we compute the gravitational interactions and resulting abundances of the DM candidate, N_1 as well as the abundance of the RHN neutrino responsible for leptogenesis. We

consider the interactions of the type in Fig. 3.12 between the inflaton and the N_i. In addition, we are interested in the gravitational interactions between the inflaton and SM particles that make up the thermal bath. We will show that it is possible to produce the thermal bath assuming the absence of any inflaton decay mode leading to reheating. We will quantify how such interactions can give rise to reasonable relic density and baryon asymmetry. The DM candidate N_1 can be produced during reheating from inflaton scattering $\phi\phi \to N_1 N_1$ as well as from the thermal bath (mediated by a massless graviton in both cases). For $(y_N)_{1i} = 0$, N_1 couples only gravitationally, and the SM processes will not lead to its production. On the other hand, for the generation of the baryon asymmetry, we will cater to non-thermal leptogenesis, where the RHNs $N_{2,3}$ are too weakly coupled to reach thermal equilibrium. Hence they are predominantly produced only during reheating from gravitational inflaton scattering. To summarize, we consider the following production via graviton exchange

- $\phi\,\phi \to N_1\,N_1$, SM SM $\to N_1\,N_1$ for production of the DM candidate N_1.
- $\phi\,\phi \to N_{2,3}\,N_{2,3}$ for production of $N_{2,3}$ that will lead to non-thermal leptogenesis. (Contributions from SM SM $\to N_{2,3}\,N_{2,3}$ are negligibly small.)
- $\phi\phi \to$ SM SM for the reheating process.

3.4.1.1 Gravitational dark matter

We start by computing the DM number density via 2-to-2 scattering of the bath particles, mediated by graviton exchange. In this case the interaction rate is given by [1, 192, 201, 203]

$$R^T_{N_i} = \frac{1}{2} \times \beta_{1/2}\,\frac{T^8}{M_P^4}\,, \tag{3.210}$$

where we have computed in precedent section, $\beta_{1/2} = 11351\pi^3/10368000 \simeq 3.4 \times 10^{-2}$ in Eq (3.127), the explicit factor of $\frac{1}{2}$ accounting for the Majorana nature of N_i. The evolution of RHN number density n_{N_i} (with $i = 1, 2, 3$) is governed by the Boltzmann equation

$$\frac{dn_{N_i}}{dt} + 3\,H\,n_{N_i} = R^T_{N_i}\,, \tag{3.211}$$

Defining the comoving number density as $Y_{N_i} = n_{N_i}\,a^3$ we can re-cast the Boltzmann equation as

$$\frac{dY^T_{N_i}}{da} = \frac{a^2}{H}\,R^T_{N_i}\,, \tag{3.212}$$

where $i = 1$ for DM production, and the superscript T refer to the thermal source of production. To properly capture the evolution of the inflaton and radiation energy density (and hence temperature) we solve the set of coupled equations (3.67-3.66), for a generic equation of state

of the inflaton fluid w_ϕ. We recall that in our framework the potential $V(\phi)$ is proportional to ϕ^k, Eq. (3.207). During reheating, the total energy density is dominated by the inflaton and we can approximate the Hubble parameter by $H^2 \simeq \rho_\phi/3\,M_P^2$. In this case, we obtain Eq.(3.71)

$$\rho_\phi(a) = \rho_{\rm end}\left(\frac{a_{\rm end}}{a}\right)^{\frac{6k}{k+2}} . \tag{3.213}$$

Recall that we are assuming that the radiation bath is produced *gravitationally* through inflaton scattering; namely, we do not rely on a specific decay channel $\phi \to$ SM particles for reheating. In this case, due to helicity conservation, the production of SM fermions from inflaton scattering is strongly suppressed by the mass of the fermions, whereas massless vectors are not produced because of the antisymmetry of $F_{\mu\nu}$. However, scattering into scalars, especially Higgs scalars, is always allowed and dominates the production rate. In [106], the inflaton dissipation rate was parameterized as $\Gamma_\phi \propto \rho_\phi^l$. For a quartic interaction with constant coupling, $l = (3/k) - (1/2)$. However, for the effective gravitational coupling between the inflaton and SM Higgs, the coupling is proportional to $m_\phi^2 \propto \rho_\phi^{(1-2/k)}$. This leads to $l = (3/2) - (1/k)$. More accurately, expanding the potential energy in terms of the Fourier modes [1, 59, 106, 131, 207, 279] as in Eq.(3.55) the production rate of radiation is given by [1, 2, 59]

$$(1+w_\phi)\,\Gamma_\phi\,\rho_\phi = R_H^{\phi^k} \simeq \frac{N_h\rho_\phi^2}{16\pi M_P^4}\sum_{n=1}^{\infty} 2n\omega|\mathcal{P}_{2n}^k|^2 = \alpha_k M_P^5\left(\frac{\rho_\phi}{M_P^4}\right)^{\frac{5k-2}{2k}} , \tag{3.214}$$

where $N_h = 4$ is the number of internal degrees of freedom for one complex Higgs doublet and we have neglected the Higgs bosons mass. The frequency of oscillations of ϕ is given by Eq.(3.56) [106] and $m_\phi^2 = \frac{\partial^2 V(\phi)}{\partial\phi^2}$ is the inflaton mass squared. The definition of α_k follows the analysis in [59], with the values given in Table 3.3. For $l = (3/2) - (1/k)$ the results of [106] yields for the evolution of the radiation density

$$\rho_R(a) = \rho_{\rm RH}\left(\frac{a_{\rm RH}}{a}\right)^4\left[\frac{1-(a_{\rm end}/a)^{\frac{8k-14}{k+2}}}{1-(a_{\rm end}/a_{\rm RH})^{\frac{8k-14}{k+2}}}\right] , \tag{3.215}$$

which can be obtained by combining (3.213) and (3.214). The evolution in Eq. (3.215) is valid when $a_{\rm end} \ll a \ll a_{\rm RH}$. To obtain Eq. (3.213), we have supposed $H \gg \Gamma_\phi$, which is valid for all a because $\Gamma_\phi < H$ at the end of inflation and Γ_ϕ decreases faster than H for all $k \geq 2$. As a result, we note that gravitational reheating is only possible for $\frac{6k}{k+2} > 4$, *i.e.*, when ρ_ϕ redshifts faster than ρ_R. This limits our parameter space to $k > 4$. It is also important to ensure that a sufficiently large reheating temperature is attained to allow Big Bang Nucleosynthesis (BBN) to occur at $T \sim 1$ MeV as we will discuss in more detail in part 3.4.2. Using Eqs. (3.210) and

k	α_k	α_k^ξ
6	0.000193	$\alpha_k + 0.00766\,\xi_h^2$
8	0.000528	$\alpha_k + 0.0205\,\xi_h^2$
10	0.000966	$\alpha_k + 0.0367\,\xi_h^2$
12	0.00144	$\alpha_k + 0.0537\,\xi_h^2$
14	0.00192	$\alpha_k + 0.0702\,\xi_h^2$
16	0.00239	$\alpha_k + 0.0855\,\xi_h^2$
18	0.00282	$\alpha_k + 0.0995\,\xi_h^2$
20	0.00322	$\alpha_k + 0.112\,\xi_h^2$

Table 3.3: Relevant coefficients for the gravitational reheating [cf. Eq. (3.214) and Eq. (3.251)].

(3.215) and relating T^8 to ρ_R^2, we obtain the thermal rate of DM production

$$R_{N_i}^T = \frac{1}{2} \times \beta_{1/2}\, \frac{\rho_{\rm RH}^2}{c_*^2\, M_P^4} \left(\frac{a_{\rm RH}}{a}\right)^8 \left[\frac{1-(a_{\rm end}/a)^{\frac{8k-14}{k+2}}}{1-(a_{\rm end}/a_{\rm RH})^{\frac{8k-14}{k+2}}}\right]^2 . \tag{3.216}$$

The DM number density at the end of reheating can then be computed by integrating Eq. (3.212), leading to

$$\begin{aligned} n_{N_i}^T(a_{\rm RH}) = {} & \frac{\beta_{1/2}\,(k+2)\,\rho_{\rm RH}^{\frac{3}{2}}}{12\sqrt{3} M_P^3\, c_*^2} \left(\frac{1}{1-r^{\frac{14-8k}{k+2}}}\right)^2 \\ & \times \left[\frac{2(7-4k)^2}{(k+5)(k-1)(5k-2)}\, r^{\frac{10+2k}{k+2}} - \frac{9}{(k+5)} + \frac{18}{(5k-2)}\, r^{\frac{14-8k}{k+2}} - \frac{1}{(k-1)}\, r^{\frac{28-16k}{k+2}}\right] , \end{aligned} \tag{3.217}$$

where $r = a_{\rm RH}/a_{\rm end}$. Since the gravitational reheating temperature is generally quite low as discussed in part 3.4.2, we can consider the limit $r \gg 1$ and the dominant term in the expression above is

$$n_{N_i}^T(a_{\rm RH}) \simeq \frac{\beta_{1/2}\,(k+2)\,\rho_{\rm RH}^{\frac{3}{2}}}{12\sqrt{3} M_P^3\, c_*^2} \frac{2(7-4k)^2}{(k+5)(k-1)(5k-2)}\, r^{\frac{10+2k}{k+2}} . \tag{3.218}$$

The contribution of gravitational scattering of the particles in the primordial plasma to the DM relic abundance can then be determined using [16]

$$\Omega_{N_1}^T\, h^2 = 1.6 \times 10^8\, \frac{g_0}{g_{\rm RH}}\, \frac{n_{N_1}^T(a_{\rm RH})}{T_{\rm RH}^3}\, \frac{M_{N_1}}{\rm GeV} , \tag{3.219}$$

which gives

$$\Omega_{N_1}^T\, h^2 \simeq 1.6 \times 10^8 \times \frac{g_0\,\beta_{1/2}}{g_{\rm RH}} \times \frac{M_{N_1}}{\rm GeV}\, \frac{c_*^{-\frac{5}{6}-\frac{5}{3k}}\,(7-4k)^2\,(k+2)}{6\sqrt{3}\,(k+5)(k-1)(5k-2)} \left(\frac{T_{\rm RH}}{M_P}\right)^{\frac{5k-20}{3k}} \left(\frac{\rho_{\rm end}}{M_P^4}\right)^{\frac{k+5}{3k}} , \tag{3.220}$$

where $g_0 = g_*(T_0) = 43/11$ and $g_{\rm RH} = g_*(T_{\rm RH}) = 427/4$ are the number of relativistic degrees of freedom at present and at the end of reheating respectively. In (3.220), we have used Eq. (3.213) evaluated at $a = a_{\rm RH}$ to relate r, $T_{\rm RH}$, and $\rho_{\rm end}$.

The DM candidate N_1 can also be produced directly from inflaton scattering. As we shall see in the next section, the same process is also involved in the production of the baryon asymmetry. For the production of N_1 through the scattering of the inflaton condensate, we consider the time-dependent oscillations of a classical inflaton field $\phi(t)$. As it has been pointed out in [121, 122, 153, 280], for all potentials steeper than quadratic near the origin, the oscillating inflaton condensate may fragment due to self-interactions and self-resonances. The equation of state, in that case, approaches $w \to 1/3$ at sufficiently late times. If this occurs after $T = T_{\rm RH}$, then this effect is not important since the inflaton energy would already be subdominant. Furthermore, N is predominantly produced at $a_{\rm end}$ so possible fragmentation at later times would not affect the calculation of the baryon asymmetry we considered. Reheating may be affected; however, the exact time when w transitions $1/3$ depends on k and requires dedicated lattice simulations [121–123, 153, 280]. In addition, self-resonance becomes less efficient for larger k as shown by the lattice results for k up to 6 [121, 153, 280] and up to $k = 10$ more recently in [123], while most of our viable results are for $k > 6$. Performing such lattice simulations for larger k is beyond the scope of the present analysis.

Furthermore, we assume a mass hierarchy $M_{N_{1,2,3}} < m_\phi$ such that the s-channel graviton mediated process (as shown in Fig. 3.12) is kinematically allowed. Note that, since N_1 is effectively decoupled from $N_{2,3}$, it does not necessarily need to be the lightest of the three. The production rate for N_i from inflaton scattering mediated by gravity is given[21] by

$$R^{\phi^k}_{N_i} = \frac{\rho_\phi^2}{4\pi M_P^4}\,\frac{M_{N_i}^2}{m_\phi^2}\,\Sigma^k_{N_i}\,, \tag{3.221}$$

where

$$\Sigma^k_{N_i} = \sum_{n=1}^{+\infty} |\mathcal{P}^k_{2n}|^2\,\frac{m_\phi^2}{E_{2n}^2}\left[1 - \frac{4\,M_{N_i}^2}{E_{2n}^2}\right]^{3/2}\,, \tag{3.222}$$

accounts for the sum over the Fourier modes of the inflaton potential, and $m_\phi^2 = \lambda\,k\,(k-1)\,(\rho_\phi/(\lambda\,M_P^4))^{\frac{k-2}{k}}$. Here $E_n = n\omega$ is the energy of the n-th inflaton oscillation mode and M_{N_i} is the mass of the produced RHN. Then, the number density of RHN is obtained by solving a Boltzmann equation analogous to that in Eq. (3.212) as

$$\frac{dY^{\phi^k}_{N_i}}{da} = \frac{\sqrt{3}M_P}{\sqrt{\rho_{\rm RH}}}\,a^2\left(\frac{a}{a_{\rm RH}}\right)^{\frac{3k}{k+2}} R^{\phi^k}_{N_i}(a). \tag{3.223}$$

[21] Note the difference of factor 2 with section 3.2.1, comes from the Majorana nature of the RHNs.

Integration of Eq. (3.223), leads to the following expression for the RHN density [59]

$$n^{\phi^k}_{N_i}(a_{\rm RH}) \simeq \frac{M^2_{N_1}\,\sqrt{3}\,(k+2)\,\rho_{\rm RH}^{\frac{1}{2}+\frac{2}{k}}}{24\,\pi\,k(k-1)\lambda^{\frac{2}{k}}\,M_P^{1+\frac{8}{k}}}\left(\frac{\rho_{\rm end}}{\rho_{\rm RH}}\right)^{\frac{1}{k}}\,\Sigma^k_{N_1}\,, \tag{3.224}$$

evaluated at the end of reheating. To obtain the DM relic abundance, one can again follow Eq. (3.219), but now replacing $n^T_{N_1}(a_{\rm RH})$ with $n^{\phi}_{N_1}(a_{\rm RH})$, and obtain as in section 3.2.1

$$\begin{aligned}\frac{\Omega^{\phi^k}_{N_1}h^2}{0.12} &= \frac{\Sigma^k_{N_1}}{2.4^{\frac{8}{k}}}\frac{k+2}{k(k-1)}\left(\frac{10^{-11}}{\lambda}\right)^{\frac{2}{k}}\left(\frac{10^{40}{\rm GeV}^4}{\rho_{\rm RH}}\right)^{\frac{1}{4}-\frac{1}{k}}\\ &\times\left(\frac{\rho_{\rm end}}{10^{64}{\rm GeV}^4}\right)^{\frac{1}{k}}\left(\frac{M_{N_1}}{1.1\times10^{7+\frac{6}{k}}\,{\rm GeV}}\right)^3\,.\end{aligned} \tag{3.225}$$

The total DM relic abundance is a sum of the gravitational contribution from thermal bath ($\Omega^T_{N_1}\,h^2$) and from inflaton scattering ($\Omega^{\phi^k}_{N_1}\,h^2$).

3.4.1.2 Gravitational leptogenesis

Since N_1 is the stable DM candidate, in the present scenario the lighter of $N_{2,3}$ can undergo out-of-equilibrium decay to SM final states. We denote N_2 to be the lighter of these, and we must require that the mixing of N_1 and N_2 to be sufficiently small so as to prevent the decay of N_2 to N_1. For now, we take this coupling to be absent. The resulting CP asymmetry from the decay of N_2 is of the form [37, 56, 57, 281, 282]

$$\epsilon_{\Delta L} = \frac{\sum_\alpha[\Gamma(N_2\to l_\alpha+H)-\Gamma(N_2\to\bar{l}_\alpha+H^*)]}{\sum_\alpha[\Gamma(N_2\to l_\alpha+H)+\Gamma(N_2\to\bar{l}_\alpha+H^*)]}\,. \tag{3.226}$$

(see section 1.3). The resulting lepton asymmetry depends on the out-of-equilibrium abundance of N_2 as computed in the previous subsection. So long as $M_{N_2}\ll m_\phi$ and any kinematic suppression can be ignored, the number density of N_2 (at $a_{\rm RH}$) will be given by Eq. (3.224) with the substitution $N_1\to N_2$. The CP asymmetry can be expressed as [54, 59, 282]

$$\epsilon_{\Delta L} \simeq \frac{3\delta_{\rm eff}}{16\,\pi}\,\frac{M_{N_2}\,m_{\nu\,,\rm max}}{v^2}\,, \tag{3.227}$$

where $\langle H\rangle\equiv v\approx 174$ GeV is the SM Higgs doublet vacuum expectation value, $\delta_{\rm eff}$ is the effective CP violating phase in the neutrino mass matrix with $0\le\delta_{\rm eff}\le 1$, and, we take $m_{\nu,\rm max}=0.05$ eV as the heaviest light neutrino mass. Here we are interested in non-thermal leptogenesis [267–270, 283–285]. The gravitationally produced N_2 should not be thermalized into the bath for the consistency of the calculation. To check this, we note that the thermalization rate $\Gamma_{\rm th}\simeq y^2_{N_2}T/8\pi$ decreases slower than the Hubble rate $H=\frac{\sqrt{\rho_\phi}}{\sqrt{3}M_P}$ based on Eqs. (3.213) and (3.215). Thermalization is potentially dangerous until $T\simeq M_{N_2}$ when the N_2 out-of-equilibrium decay

rate dominates over the thermalization rate. Using Eq. (3.213), $a_{\rm end}/a \simeq T/T_{\rm max}$ based on Eq. (3.215), and $y_{N_2}^2 \simeq m_\nu M_{N_2}/v^2$, we find that $\Gamma_{\rm th}$ is always less than H at $T = M_{N_2}$ in the parameter space of interest.[22] Thus the resulting lepton asymmetry will not be suppressed by inverse decays.

The produced lepton asymmetry is eventually converted to baryon asymmetry via electroweak sphaleron processes (see section 1.3) leading to

$$Y_B = \frac{n_B}{s} = \frac{28}{79}\epsilon_{\Delta L}\,\frac{n^\phi_{N_2}(T_{\rm RH})}{s}\,, \tag{3.228}$$

where $n^\phi_{N_2}(T_{\rm RH})$ is the number density from Eqs. (3.218) and (3.224) at the end of reheating and $s = 2\pi^2 g_{\rm RH} T_{\rm RH}^3/45$ is the entropy density. The final asymmetry then becomes

$$Y_B \simeq 3.5\times 10^{-4}\,\delta_{\rm eff}\left(\frac{m_{\nu,\rm max}}{0.05\,\text{eV}}\right)\left(\frac{M_{N_2}}{10^{13}\,\text{GeV}}\right)\left.\frac{n^\phi_{N_2}}{s}\right|_{T_{\rm RH}}\,, \tag{3.229}$$

while the observed value, as reported by Planck [22], is $Y_B^{\rm obs} \simeq 8.7\times 10^{-11}$. We note that the lepton asymmetry is not washed out because the lepton-number violating process involving the Yukawa scattering and the electroweak sphaleron processes are never in equilibrium at the same time.

3.4.2 Gravitational reheating temperature

In the precedent part, we computed the energy density in radiation from a purely gravitational process. However, to avoid conflict with the BBN, that requires the reheating temperature $T_{\rm RH} \gtrsim 1$ MeV, one needs to consider $w_\phi \gtrsim 0.65$ [59, 259], or $k = \frac{2\,(1+w_\phi)}{(1-w_\phi)} \gtrsim 9$. This lower bound comes from the fact that, for higher k, the inflaton energy density redshifts faster so the transition to radiation domination is achieved sooner, at a higher temperature. This requirement of having large w_ϕ can be relaxed with non-minimal gravitational couplings as we will discuss in what follows.

The precise bound on $T_{\rm RH}$ is in fact more involved especially for $k \leq 8$ for the following reasons. As noted below Eq. (3.215), the inflaton-dominated era ends when ρ_ϕ redshifts below ρ_R. The difference in the scale factor dependence between ρ_ϕ in Eq. (3.213) and ρ_R in Eq. (3.215) increases with k. In other words, for smaller k, the inflaton energy density does not redshift significantly more than radiation. Thus, $T_{\rm RH}$ for low k needs to be substantially higher than $T_{\rm BBN} \approx 1$ MeV so that the inflaton energy density does not excessively modify the expansion rate of the universe at BBN. We can recast the BBN bound on the extra energy density in the form of $\Delta N_\nu < 0.226$ [31] (see 1.2.4) into a bound on $T_{\rm RH}$ as a function of k using the following

[22] More precisely, $T/T_{\rm max} = a_{\rm max}/a = (a_{\rm max}/a_{\rm end})(a_{\rm end}/a) = ((6k-3)/(2k+4))^{((k+2)/(8k-14))}(a_{\rm end}/a) \approx 3^{1/8}(a_{\rm end}/a)$ for large k see section 3.2.2.

expression

$$1 = \left.\frac{\rho_\phi}{\rho_R}\right|_{T_{\rm RH}} = \left.\frac{\rho_\phi}{\rho_R}\right|_{T_{\rm BBN}} \frac{(a_{\rm BBN}/a_{\rm RH})^{\frac{6k}{k+2}}}{(T_{\rm RH}/T_{\rm BBN})^4}, \tag{3.230}$$

with entropy conservation $g_*(a_{\rm RH})\, T_{\rm RH}^3\, a_{\rm RH}^3 = g_*(a_{\rm BBN})\, T_{\rm BBN}^3\, a_{\rm BBN}^3$ within the SM sector, as well as $\rho_\phi(T_{\rm BBN}) = \frac{7}{8}\left(\frac{4}{11}\right)^{\frac{4}{3}} \Delta N_\nu\, \frac{\pi^2}{30}\, T_{\rm BBN}^4$. The resulting bounds for each k are $T_{\rm RH} \lesssim 40\,{\rm MeV}$ ($k = 6$), $9\,{\rm MeV}$ ($k = 8$), $5\,{\rm MeV}$ ($k = 10$), $4\,{\rm MeV}$ ($k = 12$) and $3\,{\rm MeV}$ ($14 \leq k \leq 20$), which we will show as red-shaded regions in the subsequent figures concerning $T_{\rm RH}$. We note that this estimate is in good agreement with a more rigorous treatment performed in Ref. [286] using a BBN computing package for the case of kination (large k limit).

The reheating temperature can be determined by solving the Boltzmann equation for the radiation energy density produced graitationally. This yields [59]

$$\rho_R(a) \simeq \alpha_k \frac{k+2}{8k-14} \sqrt{3} M_P^4 \left(\frac{\rho_{\rm end}}{M_P^4}\right)^{\frac{2k-1}{k}} \left(\frac{a_{\rm end}}{a}\right)^4, \tag{3.231}$$

and evaluating this at $a_{\rm RH}$ we have

$$T_{\rm RH}^4 = \frac{30}{\pi^2\, g_{\rm RH}}\, M_P^4 \left(\frac{\rho_{\rm end}}{M_P^4}\right)^{\frac{4k-7}{k-4}} \left(\frac{\alpha_k\, \sqrt{3}\, (k+2)}{8k-14}\right)^{\frac{3k}{k-4}}. \tag{3.232}$$

From Eq. (3.232) we find $T_{\rm RH} \simeq 60$ MeV for $k = 10$ and $\rho_{\rm end} \simeq (4.8 \times 10^{15}\,{\rm GeV})^4$. Note that, due to the logarithmic dependence of $\phi_{\rm end}$ on k in Eq. (3.208), $\rho_{\rm end}$ changes very slowly with k and remains approximately fixed to the above value.

In Fig. 3.13, we show in the left panel the reheating temperature for minimal gravitational interactions by the curve labeled $\xi_h = 0$ (other values of ξ_h, non-minimal coupling of the Higgs to the Ricci scalar, are discussed in the next subsection). As one can see, $T_{\rm RH}$ rises to $\simeq 1$ TeV, for $k = 20$. This minimal case with $\xi_h = 0$ is excluded by excessive gravitational waves as dark radiation as will be discussed in part 3.4.4, so a non-minimal coupling is ultimately required.

At the start of the reheating process, the Universe quickly heats to a maximum temperature, $T_{\rm max}$. As discussed in section 3.2.2, the maximum temperature attained through purely gravitational processes is of order 10^{12} GeV, decreasing slightly with k. The maximum radiation density which determines $T_{\rm max}$ was found to be

$$\rho_{\rm max} \simeq \sqrt{3}\, \alpha_k\, M_P^4 \left(\frac{\rho_{\rm end}}{M_P^4}\right)^{\frac{2k-1}{k}} \frac{k+2}{12k-16} \left(\frac{2k+4}{6k-3}\right)^{\frac{2k+4}{4k-7}} \equiv c_*\, T_{\rm max}^4\,. \tag{3.233}$$

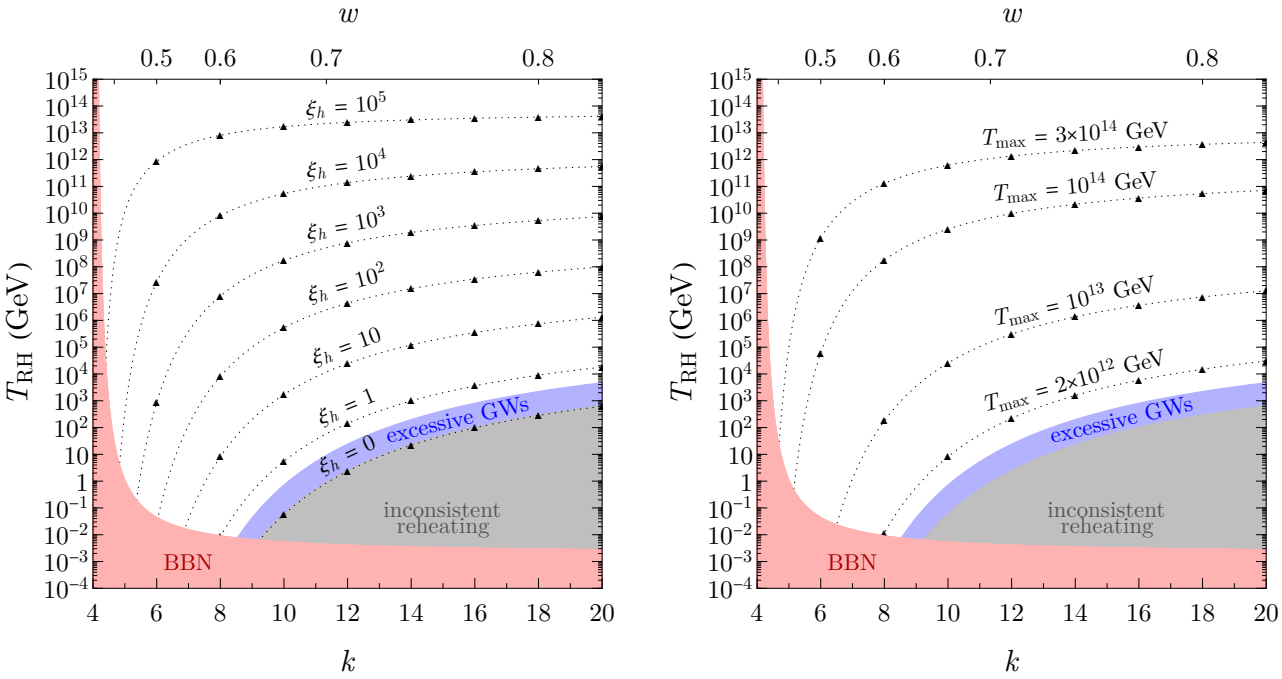

Figure 3.13: *Variation of T_{RH} (left) and T_{max} (right) as a function of k, for different choices of ξ_h. Triangles highlight the physical choices of even k. The red-shaded region is excluded by BBN because low reheating temperatures lead to an excessive inflaton energy density during BBN. The blue-shaded region is similarly excluded by BBN for excessive gravitational waves produced during inflation. The gray-shaded region is excluded as the lowest reheating temperature from gravitational reheating is that from minimal gravity (pure graviton exchange), i.e., $\xi_h = 0$.*

Asymptotically at large k, $T_{\rm max} \approx 8\times10^{11}$ GeV and $\left(\frac{T_{\rm max}}{T_{\rm RH}}\right)_{k\gg4} \sim \left(\frac{1}{\alpha_{k\gg4}}\right)^{1/2}\left(\frac{M_P^4}{\rho_{\rm end}}\right)^{1/2} \gg 1$. This represents a *minimal maximum* temperature, as other processes such as decays (not considered here), may lead to a higher maximum temperature. The value of $T_{\rm max}$ is shown in the right panel of Fig. 3.13. For minimal gravitational interactions, corresponding to the simple exchange of a graviton, $T_{\rm max} \simeq 10^{12}\,$GeV. In fact, as we noted before and will elaborate in part 3.4.4, gravitational reheating with $\xi_h = 0$ (graviton exchange) is already ruled out by the BBN bound on dark radiation in the form of GW. Thus, to account for the reheating mechanism in a gravitational framework, it is necessary to introduce non-minimal couplings of fields to gravity. We compute the reheating and maximum temperatures for non-minimal gravitational interactions in the next subsection. The value of $T_{\rm max}$ will be relevant when we discuss the DM warmness constraint because DM is produced relativistically and predominantly at $T_{\rm max}$.

3.4.3 Non-minimal gravitational production

As pure gravitational particle production can be insufficient, we also consider the possibility that scalar fields have non-minimal couplings to gravity which generate effective couplings between these scalar fields and the RHNs. Thus, we allow both the inflaton ϕ and the Higgs field H to be non-minimally coupled. We denote the complex Higgs doublet as h throughout

the following section. One can then write the action as

$$\mathcal{S}_J = \int d^4x\sqrt{-\tilde{g}}\left[-\frac{M_P^2}{2}\,\Omega^2\,\widetilde{\mathcal{R}} + \widetilde{\mathcal{L}}_\phi + \widetilde{\mathcal{L}}_h + \widetilde{\mathcal{L}}_{N_i}\right], \tag{3.234}$$

where

$$\begin{aligned}
\widetilde{\mathcal{L}}_\phi &= \frac{1}{2}\,\partial_\mu\phi\,\partial^\mu\phi - V(\phi)\\
\widetilde{\mathcal{L}}_h &= \partial_\mu h\,\partial^\mu h^\dagger - V(hh^\dagger)\\
\widetilde{\mathcal{L}}_{N_i} &= \frac{i}{2}\,\overline{\mathcal{N}_i}\overleftrightarrow{\not{\nabla}}\,\mathcal{N}_i - \frac{1}{2}\,M_{N_i}\,\overline{(\mathcal{N})^c}_i\,\mathcal{N}_i + \widetilde{\mathcal{L}}_{\rm yuk}\\
\widetilde{\mathcal{L}}_{\rm yuk} &= -y_{N_i}\,\overline{\mathcal{N}_i}\,\widetilde{h^\dagger}\,\mathbb{L} + \text{h.c.}\,,
\end{aligned} \tag{3.235}$$

and $\mathcal{N}\,,\mathbb{L}$ are the RHN and SM lepton doublet fields in Jordan frame. The conformal factor Ω^2 is given here by

$$\Omega^2 \equiv 1 + \frac{\xi_\phi\,\phi^2}{M_P^2} + \frac{\xi_h\,|h|^2}{M_P^2}\,. \tag{3.236}$$

As in section 3.3.1, it is convenient to remove the non-minimal couplings by performing the usual conformal transformation from the Jordan frame to the Einstein frame,

$$g_{\mu\nu} = \Omega^2\,\tilde{g}_{\mu\nu}\,, \tag{3.237}$$

$$\begin{aligned}
\mathcal{S}_E = \int d^4x\sqrt{-g}\Bigg[&-\frac{M_P^2\,\mathcal{R}}{2} + \frac{K^{ab}}{2}\,g^{\mu\nu}\partial_\mu S_a\,\partial_\nu S_b + \frac{i}{2\,\Omega^3}\,\overline{N_i}\overleftrightarrow{\not{\nabla}}\,N_i - \frac{1}{\Omega^4}\left(\frac{M_{N_i}}{2}\,\overline{N_i^c}\,N_i + \mathcal{L}_{\rm yuk}\right)\\
&- \frac{3i}{4\Omega^4}\,\overline{N_i}\left(\overleftrightarrow{\not{\partial}}\,\Omega\right)N_i - \frac{1}{\Omega^4}\,(V_\phi + V_h)\Bigg]\,,
\end{aligned} \tag{3.238}$$

where we have used

$$\sqrt{-\tilde{g}} \to \frac{\sqrt{-g}}{\Omega^4} \tag{3.239}$$

$$\tilde{\not{\nabla}} \to \Omega\not{\nabla} - \frac{3}{2}\Omega^2(\not{\partial}\Omega)\,, \tag{3.240}$$

and the indices a, b enumerate the fields ϕ, and the real components of h. Then making spinor field redefinition $L \to \Omega^{3/2}L$, $N_i \to \Omega^{3/2}N_i$ and $\overline{N_i} \to \Omega^{3/2}\overline{N_i}$ we recover the following action with canonical kinetic term for the RHN

$$\begin{aligned}
\mathcal{S}_E = \int d^4x\sqrt{-g}\Bigg[&-\frac{M_P^2\,\mathcal{R}}{2} + \frac{K^{ab}}{2}\,g^{\mu\nu}\partial_\mu S_a\,\partial_\nu S_b - \frac{1}{\Omega^4}\,(V_\phi + V_h) + \frac{i}{2}\,\overline{N_i}\overleftrightarrow{\not{\nabla}}\,N_i\\
&- \frac{1}{2\,\Omega}\,M_{N_i}\,\overline{N_i^c}\,N_i + \frac{1}{\Omega}\,\mathcal{L}_{\rm yuk}\Bigg]\,.
\end{aligned} \tag{3.241}$$

where the kinetic function K^{ab} has been introduced in Eq.(3.145). In what follows, consider the small-field limit Eq.(3.147) which constrains $\xi_\phi \ll 1$. However, there is no such constraint on ξ_h which can take relatively large values.

Expanding the kinetic and potential terms in the action in Eq. (3.241) in powers of $1/M_P^2$, we obtain a canonical kinetic term for the scalar fields, and deduce the leading-order interactions between scalars and the RHNs induced by the non-minimal couplings. Note that, the non-minimally coupled Yukawa interaction in Eq. (3.241) gives rise to a 3-to-2 (or 2-to-3) process with RHN in the final state above electroweak symmetry breaking temperature. These processes thus will be kinematically suppressed and have a subdominant contribution to the RHN production. The kinetic terms for the RHNs can be expressed in the form

$$\mathcal{L}_{\rm non-min.} \;=\; -\sigma^{\xi}_{hN_i}\,|h|^2\,\overline{N_i^c}N_i - \sigma^{\xi}_{\phi N_i}\,\phi^2\,\overline{N_i^c}N_i\,, \tag{3.242}$$

with

$$\sigma^{\xi}_{\phi N_i} \;=\; \frac{M_{N_i}}{2M_P^2}\xi_\phi \tag{3.243}$$

$$\sigma^{\xi}_{hN_i} \;=\; \frac{M_{N_i}}{2M_P^2}\xi_h\,. \tag{3.244}$$

These non-minimal interactions open up additional channels

- RHN production from inflaton scattering: $\phi\phi \to N_i\,N_i$
- RHN production from Higgs scattering: $hh^\dagger \to N_i\,N_i$
- Higgs production from inflaton scattering: $\phi\phi \to hh^\dagger$.

Interestingly, as can be seen from the interaction terms, the production of RHNs is systematically proportional to the mass of the fermion. Then, for the thermal production of RHNs, the production rate is

$$R^{T,\xi}_{N_i} \simeq N_h\,\frac{\zeta(3)^2\,\xi_h^2}{32\,\pi^5}\,\frac{M_{N_i}^2\,T^6}{M_P^4}\,, \tag{3.245}$$

where $\zeta(x)$ is the Riemann-zeta function. For both minimal and non-minimal gravitational couplings, the leading term in the production rate for scalar dark matter scales as T^8 [2]. Similarly, the production rate for fermions in minimal gravity also scales as T^8 as seen in Eq. (3.210). However, for non-minimal gravitational interactions, after the conformal rescaling to obtain canonical kinetic terms, there is no non-minimal coupling to the kinetic terms (in contrast to the scalars where this coupling is found in Eq. (3.241)). Instead, we are left with only the mass term coupled to $|h|^2$ and the thermal production rate is proportional only to $\propto M_{N_i}^2 T^6$.

Using the rate in Eq. (3.245) we obtain the number density at the end of reheating due to the non-minimal interaction as

$$n_{N_i}^{T(\xi_h\neq 0)} = \left(\frac{\sqrt{3}\,N_h\,\zeta(3)^2\,\xi_h^2}{32\,\pi^5\,c_*^{3/2}}\,\frac{M_{N_i}^2\,\rho_{\rm RH}}{M_P^3}\right)\frac{(k+2)\left(1-\left(\frac{\rho_{\rm end}}{\rho_{\rm RH}}\right)^{\frac{7}{3\,k}-\frac{4}{3}}\right)^{-3/2}}{72\,(5-4k)\,\Gamma\left(\frac{29-20k}{14-8k}\right)}$$
$$\times\left[9\sqrt{\pi}(5-4k)\left(\frac{\rho_{\rm end}}{\rho_{\rm RH}}\right)^{1/k}\Gamma\left(\frac{4k-4}{4k-7}\right)+4\left(\frac{\rho_{\rm end}}{\rho_{\rm RH}}\right)^{\frac{16k^2+4k+169}{21k-12k^2}}\Gamma\left(\frac{29-20k}{14-8k}\right)\mathcal{G}\right], \quad (3.246)$$

with

$$\mathcal{G}=\left(\frac{\rho_{\rm end}}{\rho_{\rm RH}}\right)^{\frac{4(k+30)}{3k(4k-7)}}\left[3(4k-5)\left(\frac{\rho_{\rm end}}{\rho_{\rm RH}}\right)^{\frac{16k^2+49}{3k(4k-7)}}-6\left(\frac{\rho_{\rm end}}{\rho_{\rm RH}}\right)^{\frac{56}{3(4k-7)}}\right]{}_2F_1(...)\,,$$

where ${}_2F_1\left(-\frac{1}{2},\frac{3}{4k-7},\frac{4k-4}{4k-7},\left(\frac{\rho_{\rm end}}{\rho_{\rm RH}}\right)^{\frac{7}{3k}-\frac{4}{3}}\right)$ is the hypergeometric function. For the inflaton scattering process $\phi\phi\to N_i\,N_i$, on the other hand, we find

$$R_{N_i}^{\phi,\xi} = \frac{M_{N_i}^2\xi_\phi^2\phi_0^4\omega^2}{32\pi M_P^4}\sum_{n=1}^{\infty}(2n)^2|\mathcal{P}_{2n}^{(2)}|^2\times\sqrt{1-\frac{4M_{N_i}^2}{E_{2n}^2}}\,, \quad (3.247)$$

where we define $\phi_0=\left(\frac{\rho_\phi}{\lambda\,M_P^{4-k}}\right)^{\frac{1}{k}}$, $\mathcal{P}_n$ and $\mathcal{P}_n^{(2)}$ by[23]

$$\phi(t)=\phi_0(t)\cdot\mathcal{P}(t)=\phi_0(t)\sum_{n=-\infty}^{\infty}\mathcal{P}_n e^{-in\omega t} \quad (3.248)$$

$$\phi^2(t)=\phi_0^2(t)\cdot\mathcal{P}^2(t)=\phi_0^2(t)\sum_{n=-\infty}^{\infty}\mathcal{P}_n^{(2)} e^{-in\omega t}\,. \quad (3.249)$$

This rate is restricted by the small field limit that imposes a stringent bound $|\xi_\phi|\lesssim 1$. When we compare this rate with the one due to inflaton scattering mediated by minimal gravitational interactions (Eq. (3.221)), we obtain

$$\frac{R_{\phi N_i}^{\phi,\xi}}{R_{N_i}^{\phi^k}}\approx\left[\frac{k\,(k-1)\,\xi_\phi\,(\omega/m_\phi)^2}{\sqrt{8}}\right]^2\frac{\sum_{n=1}^{\infty}(2n)^2|\mathcal{P}_{2n}^{(2)}|^2}{\sum_{n=1}^{\infty}\frac{1}{(2n)^2}\,\left|\mathcal{P}_{2n}^{k}\right|^2}\,. \quad (3.250)$$

This ratio takes values between $\{32\,\xi_\phi^2,\,242\,\xi_\phi^2\}$ for $k\in[6,20]$. Hence, the non-minimal contribution from inflaton scattering dominates over the graviton exchange for $\xi_\phi>\frac{1}{2\sqrt{8}}$ when

[23]Note that we introduce different notations for the Fourier coefficients of the classical fields $\phi(t)$, $\phi^2(t)$ and $V(\phi(t))$.

$k = 6$ and for $\xi_\phi > 0.06$ when $k = 20$. In what follows, we will neglect this contribution as it dominates for values of ξ_ϕ close to the small field limit, making the assumption of canonical kinetic terms of the fields invalid.

The non-minimal coupling of Higgs bosons to gravity provides an additional channel to reheat the Universe through gravitational processes, with the following rate [59]

$$(1+\omega_\phi)\Gamma_\phi = R_H^{\phi,\xi} \simeq \frac{\xi_h^2 N_h}{4\pi M_P^4}\sum_{n=1}^{\infty} 2n\omega \left|2\times\mathcal{P}_{2n}^k\rho_\phi + \frac{(n\omega)^2}{2}\phi_0^2|\mathcal{P}_n|^2\right|^2 = \alpha_k^\xi M_P^5\left(\frac{\rho_\phi}{M_P^4}\right)^{\frac{5k-2}{2k}}, \tag{3.251}$$

where $\mathcal{P}_n$ has been defined in Eq. (3.248) and α_k^ξ is given in Table 3.3. If we solve Eq. (3.67) for ρ_R, the reheating temperature in the presence of the non-minimal coupling is then given by

$$\left(T_{\rm RH}^\xi\right)^4 = \frac{30}{\pi^2 g_{\rm RH}} M_P^4 \left(\frac{\rho_{\rm end}}{M_P^4}\right)^{\frac{4k-7}{k-4}} \left(\frac{\alpha_k^\xi\sqrt{3}\,(k+2)}{8k-14}\right)^{\frac{3k}{k-4}}. \tag{3.252}$$

The reheating temperature as a function of k is shown in the left panel of Fig. 3.13 for several values of ξ_h. The maximum temperature in this case is determined from

$$\rho_{\rm max}^\xi \simeq \sqrt{3}\,\alpha_k^\xi M_P^4\left(\frac{\rho_{\rm end}}{M_P^4}\right)^{\frac{2k-1}{k}} \frac{k+2}{12k-16}\left(\frac{2k+4}{6k-3}\right)^{\frac{2k+4}{4k-7}} \equiv c_*\,(T_{\rm max}^\xi)^4\,. \tag{3.253}$$

Contours of $T_{\rm max}^\xi$ in the $(k, T_{\rm RH})$ plane are shown in the right panel of Fig. 3.13, where the appropriate values of ξ_h taken from the left panel are used to calculate $T_{\rm max}^\xi$.

3.4.4 Gravitational waves generated during inflation

We review here the calculation of gravitational waves (GW) generated by quantum fluctuations during inflation, followed by a cosmological era where the inflaton energy dominates and redshifts faster than radiation. This results in an enhancement of GW, which places a constraint from excessive dark radiation and offers a GW signal with a distinctive spectrum. The ratio of the gravitational wave (GW) energy density to that of the radiation bath is given by [287]

$$\frac{\rho_{\rm GW}}{\rho_R} = \frac{1}{32\pi G\rho_R}\frac{k_{\rm GW}^2}{2}\mathcal{P}_T(k_{\rm GW}) \quad \text{with} \quad \mathcal{P}_T(k_{\rm GW}) \equiv \frac{2H_I^2(k_{\rm GW})}{\pi^2 M_P^2}, \tag{3.254}$$

where $k_{\rm GW}$ is the momentum mode of the GW, $\mathcal{P}_T$ is the primordial tensor power spectrum (see section 2.1), $H_I(k_{\rm GW})$ is the Hubble scale during inflation when the mode $k_{\rm GW}$ exits the horizon, $T_{\rm hc}$ is the horizon-crossing temperature when the mode re-enters the horizon at $k_{\rm GW} = H(T_{\rm hc})$, and the factor of $1/2$ accounts for the time average of the rapidly oscillating metric perturbations. In our case, $\rho_{\rm GW}/\rho_R$ is redshift invariant up to the change of g_* after $T = T_{\rm max}$ because entropy is only efficiently produced at $T = T_{\rm max}$ as discussed in part 3.4.2. Therefore, the final

gravitational wave strength is given by $\Omega_{\rm GW}h^2 = \Omega_\gamma\, h^2\, (\rho_{\rm GW}/\rho_R) \times [g_{*s}^4({\rm eV})/g_*(T_{\rm hc})g_*^3({\rm eV})]^{\frac{1}{3}}$ where $\Omega_\gamma = \rho_{\gamma,0}/\rho_{\rm crit,0}$ is the fraction of the photon energy density today. Here $g_{*s}({\rm eV}) = \left[2 + \frac{7}{8} \times 2 \times 3 \times \left(\frac{4}{11}\right)\right] \simeq 3.91$ and $g_*({\rm eV}) = \left[2 + \frac{7}{8} \times 2 \times 3 \times \left(\frac{4}{11}\right)^{4/3}\right] \simeq 3.36$ denote the effective number of relativistic degrees of freedom relevant for the entropy density and the energy density, respectively.

As one can see, if horizon crossing occurs during radiation domination $k_{\rm GW}^2 = H^2(T_{\rm hc}) = \rho_R/(3M_P^2)$, then the GW spectrum becomes scale invariant. On the other hand, if horizon crossing occurs during the reheating era when the Universe is dominated by inflaton energy density, the GW strength is enhanced by a factor of ρ_ϕ/ρ_R evaluated at $T_{\rm hc}$. As a result, the largest enhancement is for the mode that re-enters the horizon right after inflation at $T_{\rm max}$. For minimal gravitational reheating ($\xi_h = 0$), the enhancement in this mode is $\rho_{\rm end}/\rho_R(T_{\rm max}) \simeq (4{-}6){\times}10^{13}$ for $k \in [6, 20]$, based on Eqs. (3.52) and (3.208). This gives $\Omega_{\rm GW}h^2 \simeq (8{-}10){\times}10^{-6}$, which corresponds to the high frequency points of the blue curves, which fix $\xi_h = 0$, in the left panel of Fig. 3.14. These values are excluded by the BBN bound of $\Omega_{\rm GW}h^2 \simeq 1.3 \times 10^{-6}$ [31] (see 1.2.4), shown by the blue-shaded region at the top. Therefore, the case with minimal gravitational interactions is excluded, which was previously pointed out by Ref. [288]. The constraint is relaxed when $T_{\rm max}$ is increased, e.g., by non-minimal gravitational interactions via ξ_h [cf. Eq. (3.253)], because the GW energy density relative to that of radiation is smaller in this case. The blue region in the right panel of Fig. 3.14 (and subsequent figures) shows the constraint in this non-minimal scenario, which excludes $\xi_h \lesssim 0.5$, as can be seen from the left panel of Fig. 3.13.

In addition to setting a constraint, such enhanced gravitational waves offer an important signature to search for [289]. The amount of enhancement depends on ρ_ϕ/ρ_R at the time of horizon crossing, implying that the GW spectrum depends on the inflaton potential near the minimum and the parameter k. By analyzing modes that re-enter the horizon after $T_{\rm max}$ and using $\rho_\phi \propto a^{-6k/(k+2)}$ from Eq. (3.213), we find the GW spectrum scales with the frequency as $\Omega_{\rm GW}h^2 \propto f^{\frac{k-4}{k-1}}$, which is consistent with Ref. [288]. The enhanced GW spectra are demonstrated in the left panel of Fig. 3.14 for the different values of k in the blue and red curves. The blue (red) curves correspond to the minimal scenario ($T_{\rm RH} = 300\,{\rm TeV}$), and allow for k to vary from 10 (6) to 20 in increments of 2 (for $\xi_h = 0$, $k < 10$ is excluded by BBN for low $T_{\rm RH}$ according to Fig. 3.13.) Here, the frequency is obtained by redshifting the initial momentum mode at $T_{\rm hc}$ to today's photon temperature $T_{\gamma,0}$ as

$$f = \frac{k_{\rm GW}}{2\pi}\frac{T_{\gamma,0}}{T_{\rm hc}}\left(\frac{g_*({\rm eV})}{g_*(T_{\rm hc})}\right)^{\frac{1}{3}}. \tag{3.255}$$

Therefore, by measuring the slope of $\Omega_{\rm GW}h^2$ as a function f, one can determine k and thus reveal the shape of the inflaton potential energy near the minimum. Note that, the end-point frequencies for the red curves are different for different choices of k (and different ξ_h), as for a

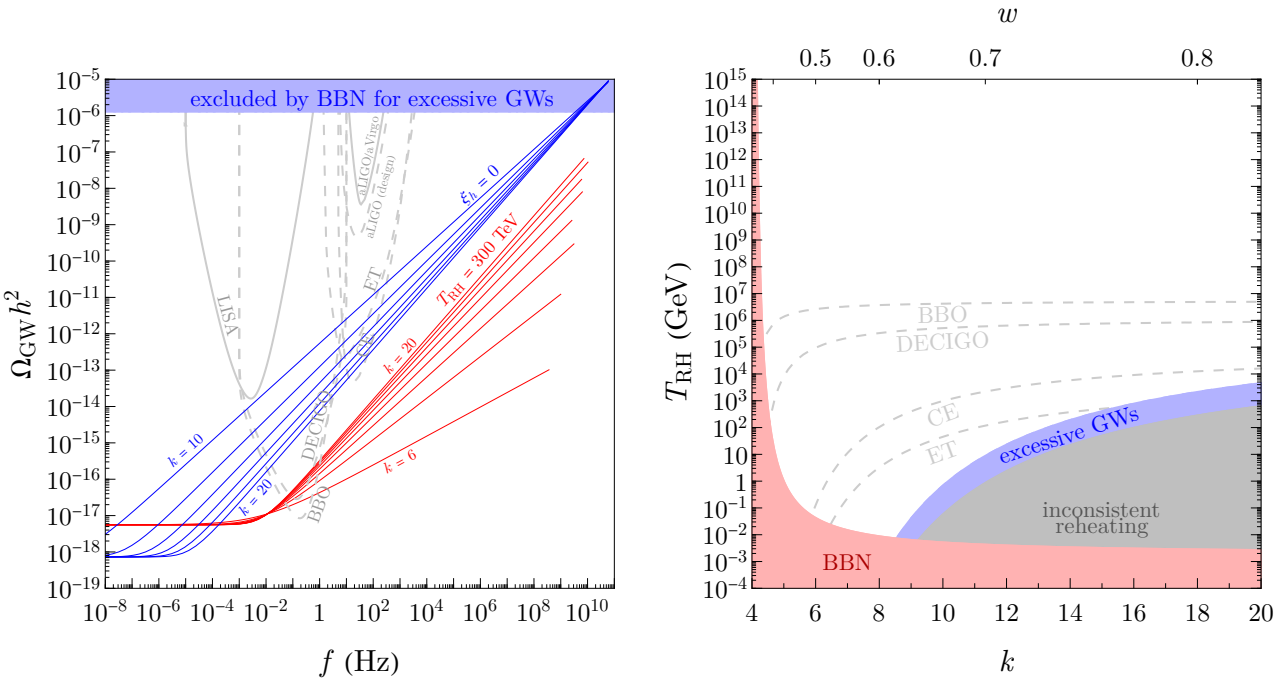

Figure 3.14: *Gravitational wave constraints and future prospects. Left: The blue-shaded region is excluded by BBN for excessive dark radiation. The blue and red curves fix $\xi_h = 0$ and $T_{RH} = 300\,\text{TeV}$, respectively. Various curves of the same color use different values of k as labeled and in increments of 2. The sensitivity of several future experiments as a function of frequency is also shown. Right: The blue region is excluded by BBN for the excessive GW energy as dark radiation. The regions below the gray dashed curves can be probed by the GW experiments as specified.*

given k and $T_{\rm RH}$, the maximum possible frequency is dictated by

$$f_{\rm max} = \frac{H(T_{\rm max})}{2\pi}\,\frac{a_{\rm end}}{a_0}\,, \tag{3.256}$$

which for $\xi_h = 0$ turns out to be $\simeq 7\times 10^{10}$ Hz for all k, while modes with frequencies $f > f_{\rm max}$ are never produced. In the right panel of Fig. 3.14, the regions below the gray dashed curves can be probed by the future gravitational wave observatories—BBO [290–292], DECIGO [293–295], CE [296, 297] and ET [298–301]. Here we use the sensitivity curves derived in Ref. [302]. Since these GW observatories probe frequencies that correspond to modes that exit the horizon early in the inflation period, we use the large-field asymptotic value of $V(\phi)$ in Eq. (3.52) to obtain H_I. In the left panel of Fig. 3.14, we illustrate the GW spectra in the red curves for a fixed $T_{\rm RH} = 300\,\text{TeV}$, which can be detected by DECIGO for $k \geq 8$ and by BBO for all $k \geq 6$. Remarkably, in the right panel, a large region in the parameter space with $T_{\rm RH} < 5\times 10^6\,\text{GeV}$ can be probed by future GW detectors. We emphasize that this potential GW signal is generic for our model and applicable throughout this thesis manuscript, although we do not show these sensitivity curves in all figures for clarity of presentation.

3.4.5 Results and discussion

3.4.5.1 Simultaneous solution: the case of stable DM candidate

As we have seen, for each value of k and ξ_h (in the non-minimal case), there is a unique value for $T_{\rm RH}$ from gravitational portals during reheating. These are shown in the left panel of Fig. 3.13. The gravitational thermal production of DM generally requires reheating temperatures much larger than can be obtained with $\xi_h = 0$. In this part, we will consider $T_{\rm RH}$ and k as free parameters and it should be understood that we are implicitly assuming that $\xi_h \neq 0$ and takes the necessary value to achieve a particular reheating temperature for a given value of k. For the production of DM, both minimal and non-minimal thermal contributions are included, whereas for the generation of a lepton asymmetry, only minimal contributions from inflaton scattering are considered.

The results presented depend on the underlying class of inflationary models. As noted earlier, we consider T-models of inflation [105] for which we have determined λ and $\rho_{\rm end}$ (see section 2.1). As discussed above, there are two contributions to the DM relic density: from gravitational scattering within the newly formed primordial plasma and directly from inflaton scattering. These two contributions are presented separately in the upper two panels of Fig. 3.15. In the upper left panel, we show two contours of the yield, $n_{N_1}/s = 10^{-22}$ and 10^{-24}, for both minimal gravitational interactions (dotted curves) using Eq. (3.217) and non-minimal interactions (dot-dashed curves) using Eq. (3.246). Note the latter yield is proportional to $M_{N_1}^2$ as shown by the contour labels, and we have normalized these contours by choosing $M_{N_1} = 10^8$ GeV. Also note, $M_{N_1} n_{N_1}/s \simeq 0.44$ eV is needed to explain the observed dark matter density, $\Omega_{N_1} h^2 = 0.12$. For $k > 4$ and minimal gravitational interactions, the relic density increases with reheating temperature, $n_{N_1}/s \sim T_{\rm RH}^{\frac{5k-20}{3k}}$. The scaling of n_{N_1}/s for non-minimal interactions is more complicated but also increases with $T_{\rm RH}$.

In the upper right panel of Fig. 3.15, we provide four contours of the yield, n_{N_1}/s, produced from inflaton scattering, which also scales as $M_{N_1}^2$. The gravitational production process from inflaton scattering is complementary to the thermal production process just discussed. Recall that we are assuming ξ_ϕ is small enough that non-minimal scattering processes can be ignored. In this case, from Eq. (3.224), we see that $n_{N_1}/s \sim T_{\rm RH}^{-1+\frac{4}{k}}$ and for $k > 4$, the relic density decreases with increasing $T_{\rm RH}$. As $M_{N_1} n_{N_1}/s \simeq 0.44$ eV is needed to explain the observed DM density, $\Omega_{N_1} h^2 = 0.12$, we find indeed that higher reheating temperatures require *lighter* DM candidates to fit with the relic abundance constraint.

Combining the two constraints shown in the top panels of Fig. 3.15 we see that for a given k and M_{N_1}, there are both upper (from thermal scattering) and lower (from inflaton scattering) limits to $T_{\rm RH}$ so as to avoid exceeding the observed cold DM abundance. The resulting relic density as a function of $T_{\rm RH}$ is shown in the bottom left panel of Fig. 3.15, where we show the total relic abundance $(\Omega_{N_1}^T + \Omega_{N_1}^{\phi^k})\, h^2$ relative to the observed abundance for a fixed $k = 14$ and

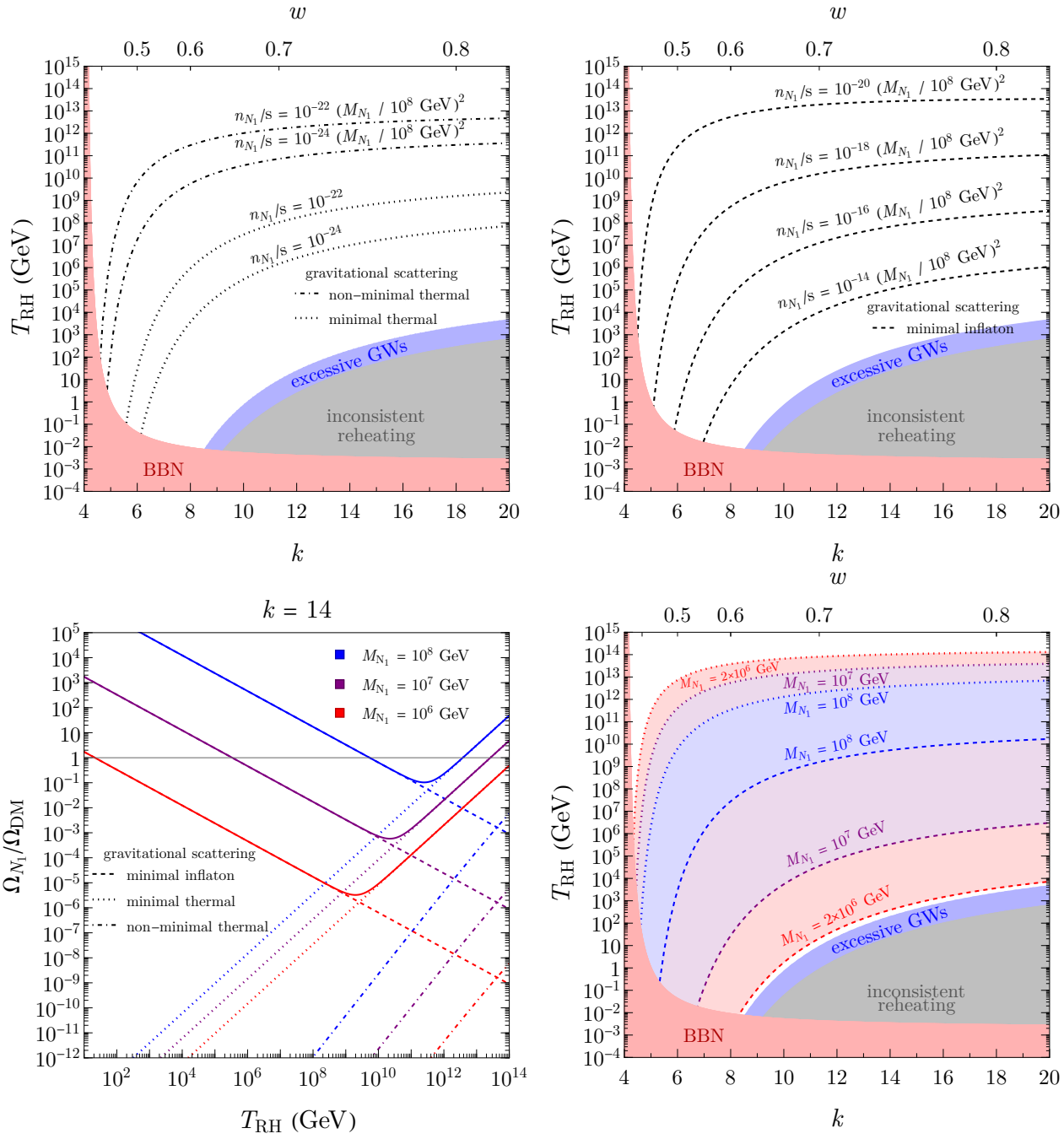

Figure 3.15: *Top left: Contours of fixed comoving number density, $n_{N_1}/s = 10^{-22}$ and 10^{-24} in the (k, T_{RH}) plane. $M_{N_1} n_{N_1}/s \simeq 0.44$ eV is needed to explain the observed dark matter density, $\Omega_{N_1} h^2 = 0.12$. Dotted curves assume DM production solely from minimal gravitational scattering in the thermal bath. Dot-dashed curves correspond to non-minimal gravitational scatterings. The latter are scaled with $M_{N_1}^2$. Top right: Contours of $n_{N_1}/s = 10^{-20}, 10^{-18}, 10^{-16}$ and 10^{-14} each scaled with $M_{N_1}^2$ assuming DM production only from inflaton scattering. In both upper panels, the gray-shaded region is excluded as minimal gravitational interactions necessarily produce larger reheating temperatures. Low reheating temperatures shaded in red (blue) are excluded by BBN for an excessive inflaton (GW) energy. Bottom left: The total relic abundance $(\Omega^T_{N_1} + \Omega^{\phi^k}_{N_1})h^2/0.12$ as a function of reheating temperature for three choices of DM masses $\{10^6, 10^7, 10^8\}$ GeV for fixed $k = 14$. Individual contributions to the dark matter density are distinguished by line types as indicated. Bottom right: Coloured regions correspond to values of (k, T_{RH}) with $(\Omega^T_{N_1} + \Omega^{\phi^k}_{N_1})h^2 \leq 0.12$ for the three choices of M_{N_1} used in the bottom left panel, and the lines styles indicate the dominant contribution.*

three choices of the DM mass $M_{N_1} = \{10^6, 10^7, 10^8\}$ GeV. We clearly see that the desired relic density ($\Omega_{N_1} = 0.12$) is obtained *twice*: (i) at a lower reheating temperature, where inflaton scattering dominates, and (ii) for a higher reheating temperature, when we are in the thermal production regime. The allowed region corresponds to the parameter space at or *below* the line $\Omega h^2/0.12 = 1$ in the bottom left panel of Fig. 3.15. For $M_{N_1} > 3 \times 10^8$ GeV, there are no values of ($T_{\rm RH}$, k) that result in an acceptable density of DM, and the allowed range in $T_{\rm RH}$ is larger with lighter DM. This is understandable as, the thermal relic requiring a *larger upper bound* on $T_{\rm RH}$ for lighter DM, while the inflaton scattering requires a *smaller lower bound* on $T_{\rm RH}$ for lighter DM.

A two-dimensional version of the lower left panel of Fig. 3.15, over a range in k, is shown in the lower right panel. Low values of $T_{\rm RH}$ are excluded by BBN. Once again, the gray-shaded region in the lower right corner of this panel is also excluded since minimal gravitational interactions would produce a reheating temperature larger than the values in that region. Within each shaded band (the color corresponds to a specific choice of M_{N_1}), the total relic density is below the observed DM density. The observed value is reached on the border of the colored bands. For DM of masses very close to 1 PeV, there exists a viable parameter space for $k \geq 9$ (along the boundary of the excessive GW region), requiring $\xi_h \simeq 0.5$. For larger masses, the range in k extends to lower values, and higher reheating temperatures are possible and require larger non-minimal coupling to gravity.

Having identified the regions of the $(k, T_{\rm RH})$ parameter space with a suitable DM density, we turn to the production of the baryon asymmetry through gravitationally induced leptogenesis. This analysis was performed in [59] and therefore we only briefly summarize the results found there. We note, however, Ref. [59] neglected the kinematic suppression in Eq. (3.222) to maintain the model independence of the analysis, though this effect is included in the present work. In Fig. 3.16, we show contours of some benchmark values of the mass of N_2 that reproduce the observed baryon asymmetry $Y_B^{\rm obs}$. We find that the gravitational contribution to the baryon asymmetry is essentially entirely due to inflaton scattering rather than the thermal particles in the SM bath. Since minimal gravitational interactions are excluded by excessive GW, non-minimal interactions are required to produce a sufficiently large thermal bath so that GW fractional energy is consistent with BBN. Leptogenesis via N_2 is therefore possible above the border of the blue-shaded region in Fig. 3.16, indicating a mass $M_{N_2} \gtrsim 3 \times 10^{11}$ GeV is required. Larger values of M_{N_2} can produce the correct asymmetry so long as $\xi_h > 0$. Nonetheless, when $M_{N_2} \gtrsim 3 \times 10^{12}\,\text{GeV}$, the baryon asymmetry starts to become suppressed for the following reason. The inflaton mass obtained from Eqs. (3.52) and (3.208), $m_\phi \simeq 1.2 \times 10^{13}\,\text{GeV}$ across all k values, is no longer much larger than M_{N_2} and the kinematic suppression in Eq. (3.222) becomes important. This explains the existence of the green region as well as why the curve for $M_{N_2} = 10^{13}\,\text{GeV}$ is at a lower $T_{\rm RH}$ than that for $M_{N_2} = 3 \times 10^{12}\,\text{GeV}$. Once again, the bottom red region is forbidden by BBN because of an excessive inflaton energy density during

BBN. In summary, we observe that, saturating the bound on GW from BBN, together with the right DM abundance and successful leptogenesis requires $\xi_h \simeq 0.5$, $M_{N_2} \simeq 3 \times 10^{11}$ GeV and $M_{N_1} \simeq 10^6$ GeV. As discussed above, this parameter space can be extended, allowing larger values $\{M_{N_1}, M_{N_2}\}$ if one considers stronger non-minimal gravitational couplings by $\xi_h \gtrsim 0.5$, thus allowing a larger reheating temperature [cf. Eq. (3.252)].

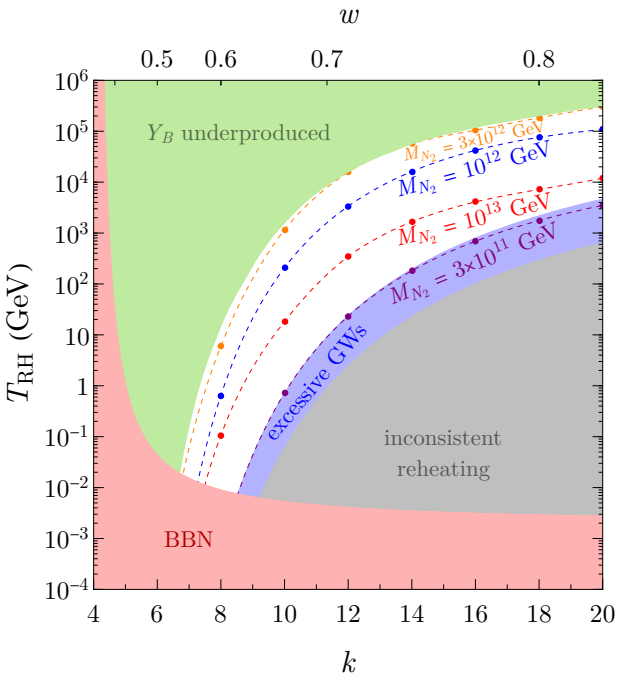

Figure 3.16: *Contours of M_{N_2} corresponding to the observed baryon asymmetry [cf. Eq. (3.229)] in the (k, T_{RH}) plane. The red-shaded region correspond to the lower bound on T_{RH} from BBN, and the green region leads to underproduction of Y_B due to the kinematic suppression in inflaton scattering when M_{N_2} approaches m_ϕ.*

Combining our preceding analyses, it is possible, for a given $V(\phi)$, to constrain the (M_{N_1}, M_{N_2}, ξ_h) parameter space by requiring leptogenesis, DM production and reheating to have a common gravitational origin. Indeed, for a given k and DM mass M_{N_1}, the temperature $T_{\rm RH}$ can be determined by the relic abundance constraint. In turn, $T_{\rm RH}$ determines the value of ξ_h needed to reheat the Universe, as well as the value of M_{N_2} which gives the desired baryon asymmetry through leptogenesis. To illustrate our result, we project the viable parameter space in the (M_{N_1},M_{N_2}) plane in Fig. 3.17 for different values of ξ_h, allowing k to vary within $k \in [6, 20]$. In each coloured line segment, gravitational interactions are responsible for the observed DM relic abundance, the baryon asymmetry and reheating. Different coloured slanted line segments in this figure correspond to different choices of the non-minimal coupling ξ_h, with $\xi_h = 0$ being ruled out from overproduction of GW. The maximum possible value for ξ_h is around 13.5, above which the mass M_{N_2} necessary to reproduce the observed baryon asymmetry gets too close to m_ϕ and kinematic suppression becomes significant, as can be seen from Fig. 3.16. Note that for each ξ_h, the allowed parameter space satisfying all the constraints, is rather restricted.

This is better seen from the right panel figure, where we have zoomed in to the $\xi_h = 1$ case. Interestingly, this shows that the viable parameter space is approximately independent of k, while $k = 6$ and 8 are excluded by BBN as can be seen from the left panel of Fig. 3.13.

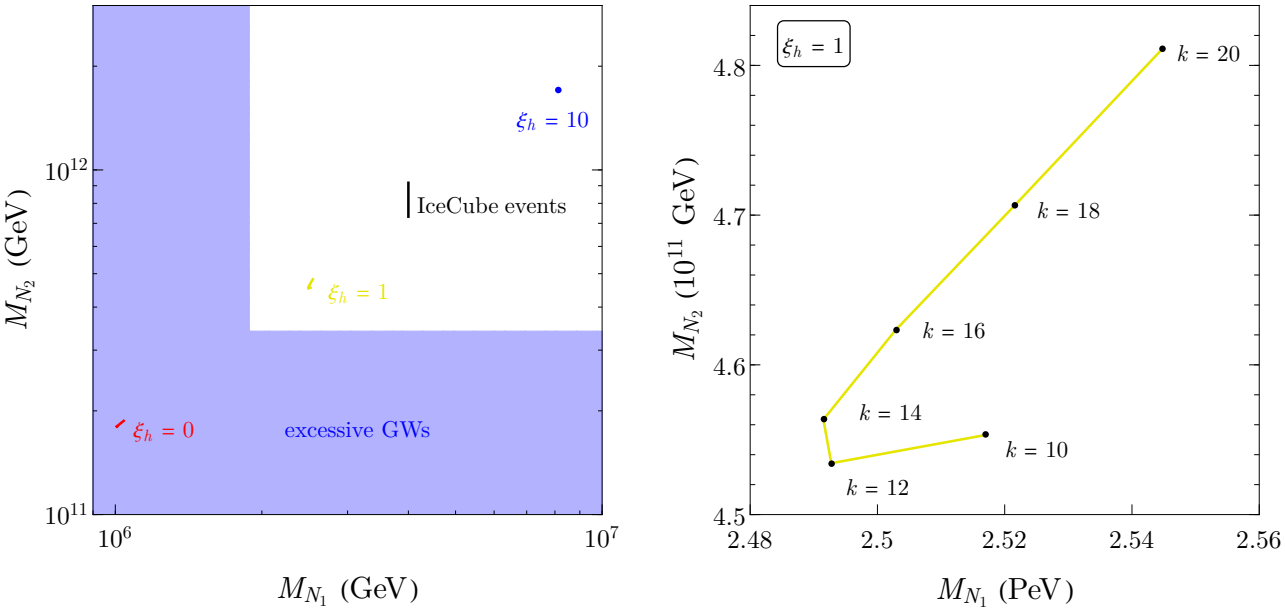

Figure 3.17: *Viable parameter space in the (M_{N_1}, M_{N_2}) plane for which gravitational interactions are responsible for the observed DM relic abundance (in N_1), the baryon asymmetry (produced from N_2 decays), and reheating for $k \in [6, 20]$. In the left panel, different colours correspond to $\xi_h = \{0, 1, 10\}$ diagonally from bottom left (red) to top right (blue). The vertical black segment indicates the range in M_{N_2} for $M_{N_1} = 4$ PeV for the range in k considered, where the connection to the IceCube high-energy neutrino excess will be discussed in the next subsection. In the right panel, we magnify the parameter space for a fixed non-minimal coupling $\xi_h = 1$. The dots correspond to even values of k as indicated.*

3.4.5.2 Simultaneous solution: the case for a decaying DM & IceCube events

Until now, we have assumed that the DM candidate, N_1, is absolutely stable. If it is not, and N_1 has non-zero Yukawa components, y_{1i}, N_1 can decay to SM final states. In this case, one necessary (but not sufficient) constraint on the DM mass and Yukawa coupling arises from the requirement of having a lifetime larger than the age of the Universe $\tau_{N_1} \gtrsim \tau_{\rm univ} \simeq 4.35 \times 10^{17}$ s. On the other hand, the IceCube detector has reported the detection of three PeV neutrinos, a roughly 3σ excess above expected background rates [303–305]. The three highest energy events correspond to deposited energies of 1.04 PeV, 1.14 PeV and 2.0 PeV. Although the origin of these very high energy events is still unclear, it has been shown in Refs. [306–320] that such events could be sourced from the decays of superheavy DM particles. The neutrino energy spectrum presents a high-energy cutoff at $m_{\rm DM}/2$ [307, 308] if two body decays including one neutrino are present. The total excess can be interpreted as high energy neutrinos resulting from the decay of N_1 with $\tau_{N_1} \approx 10^{28}$ s for both normal and inverted hierarchies [307, 321]. Given that the

maximum energy of the IceCube events has been measured to be about 2 PeV, the mass of the DM particle is constrained to be $\simeq 4$ PeV. Moreover, the IceCube spectrum sets a lower bound on the DM lifetime of the order of 10^{28} s [308, 321], which is approximately model-independent and orders of magnitude larger than the lifetime of the Universe. Thus, satisfying this bound automatically makes N_1 a nearly stable relic, and hence a good DM candidate. For $N_1 \to \ell\, H$ decay, we find

$$\tau \equiv \Gamma^{-1}_{N_1 \to \ell\, H} \simeq \left(\frac{y^2_{N_1} M_{N_1}}{8\,\pi}\right)^{-1} \simeq 10^{28}\ \text{s} \left(\frac{4\times 10^{-29}}{y_{N_1}}\right)^2 \left(\frac{1\,\text{PeV}}{M_{N_1}}\right) ; \tag{3.257}$$

that is, the Yukawa coupling y_{N_1} must be highly suppressed. On the other hand, in order to satisfy the observed DM abundance via the freeze-in mechanism in the early Universe through inverse decay $\nu\,, H \to N_1$ involving the same Yukawa, one needs [80, 317]

$$\Omega_{N_1}\, h^2 \simeq 0.12 \left(\frac{y_{N_1}}{1.2\times 10^{-12}}\right)^2 \left(\frac{M_{N_1}}{1\,\text{PeV}}\right) . \tag{3.258}$$

This means that the Yukawa required to interpret the PeV IceCube event from the decay of N_1, $y_{N_1} \sim 10^{-29}$, is far too small for the thermal bath to populate the Universe from the freeze in mechanism. Thus, if we are restricted to dimension-four interactions involving RHN and the SM, it is not possible to simultaneously explain the DM relic density and the IceCube events. Alternatively, we may consider higher dimensional operators [317], modified gravity/cosmology [322] or some different production mechanism for DM [323].

Our minimalistic framework contains a natural avenue to reconcile both the DM abundance and IceCube events, through the gravitational production of decaying PeV neutrinos in the early Universe. However, as discussed in precedent part 3.4.4, the case with minimal gravitational interactions is excluded by BBN for an excessive amount of GW as dark radiation. Thus we then need to go (slightly) beyond the minimal setup and include non-minimal gravitational interactions. We show in Fig. 3.18 contours for $\Omega_{N_1} h^2 = 0.12$ for $M_{N_1} = 4$ PeV in the (k, $T_{\rm RH}$) plane. The orange (dashed, dotted) lines correspond to the two dominant gravitational scattering processes involving the (inflaton, thermal particles) as discussed in the previous subsection. Note however that gravitational thermal production requires a high reheating temperature and is not compatible with the observed baryon asymmetry as can be understood from Fig. 3.16. In contrast, at lower $T_{\rm RH}$, the correct relic density can be produced from inflaton scattering with a lower value of $\xi_h \approx 2.5$. In the left panel of Fig. 3.17, we show, by the black vertical line segment, the range in M_{N_2} obtained from varying k while fixing $M_{N_1} = 4$ PeV. Note that, since N_1 is a long-lived stable relic, it does not contribute to the generation of the baryon asymmetry as its decay takes place below the electroweak phase transition. In addition, because the Yukawa coupling of N_1 is extremely small, its interactions which violate lepton number will not be in equilibrium, and hence will not wash out any of the asymmetry produced

by N_2. We summarize our analysis in the tables presented in the conclusion of the section Tables 3.4 and 3.5.

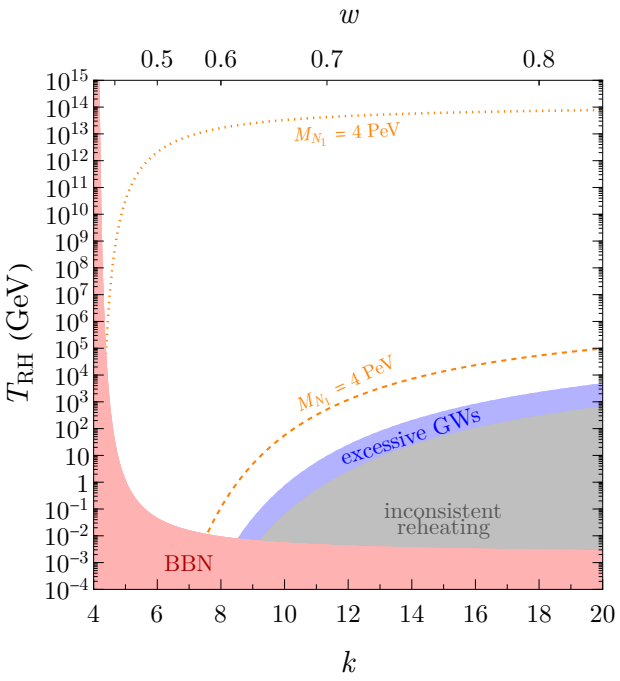

Figure 3.18: *Contours of fixed relic density, $\Omega_{N_1}h^2 = 0.12$ for $M_{N_1} = 4$ PeV. The upper dotted contour corresponds to production from gravitational scattering in the thermal bath (and requires a large value of ξ_h) and the lower dashed contour corresponds to production from inflaton scattering (and requires a relatively low value of ξ_h) Between the two contours $\Omega_{N_1}h^2 < 0.12$ for $M_{N_1} = 4$ PeV.*

3.4.6 Dark matter & leptogenesis with a Majoron

We have seen that our result are particularly constrained because of the strong dependence of the production of the RHN on its mass M_{N_i}, limiting our allowed region to masses above a PeV. In this last part, we consider an alternative mechanism. We include an additional complex scalar field, Φ containing the Majoron [52, 312, 324–331], that acts as an intermediate state in the interactions of the inflaton and RHNs. This interaction is depicted in Fig. 3.19.

The relevant Lagrangian of this extension can be written as

$$\mathcal{L}_\Phi = (-y_R^i\,\Phi\,\overline{N_i^c}\,N_i + \text{h.c.}) + \frac{1}{2}\mu_\Phi^2\,\Phi^2 - \frac{1}{4}\lambda_\Phi\,\Phi^4\,. \tag{3.259}$$

After symmetry breaking, the real part of Φ acquires a non-zero vacuum expectation value, around which one can expand the field as: $\Phi = \frac{1}{\sqrt{2}}(S + v_S)e^{iJ/v_S}$, and J is the Majoron. This expectation value is the origin of the RHN Majorana masses, $M_{N_i} = y_R^i\,v_S/\sqrt{2}$. Then

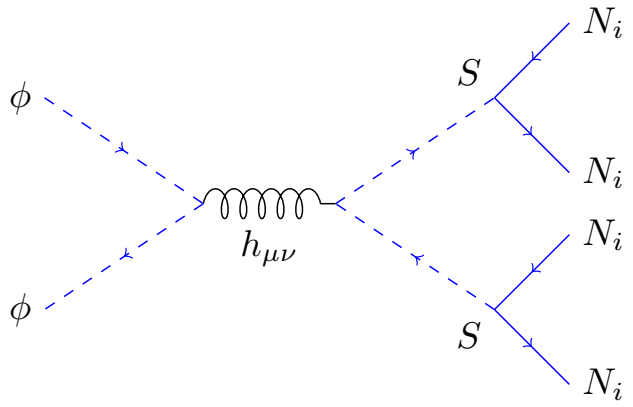

Figure 3.19: *Feynman diagram for the gravitational production of an on-shell scalar S coupled to the heavy neutrinos.*

$m_S = \mu_\Phi < m_\phi$ and the gravitational production rate of the real scalar, S is[24]

$$R_S^{\phi^k} = \frac{2 \times \rho_\phi^2}{16\pi M_P^4} \Sigma_S^k \,, \tag{3.260}$$

where the factor of two accounts for the fact we produce two scalar particles per scattering, with

$$\Sigma_S^k = \sum_{n=1}^{\infty} |\mathcal{P}_{2n}^k|^2 \left[1 + \frac{2\mu_\Phi^2}{E_{2n}^2}\right]^2 \sqrt{1 - \frac{4\mu_\Phi^2}{E_{2n}^2}} \,. \tag{3.261}$$

Since each scalar decays into 2 right-handed neutrinos, we obtain for the density of N_i after integration of the Boltzmann equation,

$$n_{N_i}^{S\phi^k}(a_{\rm RH}) \simeq {\rm Br}_i \times \frac{\sqrt{3}\rho_{\rm RH}^{3/2}}{4\pi M_P^3} \frac{k+2}{6k-6} \left(\frac{\rho_{\rm end}}{\rho_{\rm RH}}\right)^{1-\frac{1}{k}} \Sigma_S^k, \tag{3.262}$$

where we assumed $a_{\rm RH} \gg a_{\rm end}$, and here ${\rm Br}_i = \frac{(y_R^i)^2}{\sum (y_R^i)^2} = \frac{M_{N_i}^2}{M_{N_1}^2 + M_{N_2}^2 + M_{N_3}^2}$ if $N_{1,2,3}$ are all lighter than S. The relic abundance of N_1 is then given by

$$\begin{aligned} \frac{\Omega_{N_1}^{S\phi^k} h^2}{0.12} &\simeq {\rm Br}_1 \times \left(\frac{\rho_{\rm end}}{10^{64}{\rm GeV}^4}\right)^{1-\frac{1}{k}} \left(\frac{10^{40}{\rm GeV}^4}{\rho_{\rm RH}}\right)^{\frac{1}{4}-\frac{1}{k}} \left(\frac{k+2}{6k-6}\right) \\ &\times \Sigma_S^k \times \frac{M_{N_1}}{2.5 \times 10^{\frac{24}{k}-8}{\rm GeV}} \,, \end{aligned} \tag{3.263}$$

whereas the baryon asymmetry follows from Eq. (3.229). Note that so long as $M_{N_i} \ll \mu_\Phi \ll m_\phi$, the resulting dark matter abundance and baryon asymmetry will be independent of m_S. We

[24] As shown in section 3.2.2, and [210], for the case of a scalar field, the gravitational thermal production is always negligible compared to inflaton scattering.

show in Figs. 3.20 and 3.21 respectively, the parameter space allowed by the relic abundance and the baryogenesis constraint in the $(k\,, T_{\rm RH})$ plane. Comparing Fig. 3.20 and the dashed lines (from the inflaton scattering) in the bottom right panel of Fig. 3.15, we notice that the mass of the dark matter respecting Planck constraint is much lower, if the branching fraction to N_1 is large. For $\mathrm{Br}_1 = 1$, the difference is about 8 orders of magnitude, and around 6 orders of magnitude for $\mathrm{Br}_1 = 10^{-2}$. The reason is easy to understand: the production rate through S is boosted in comparison with the direct production, by a factor

$$\frac{R_{N_1}^{S\phi^k}}{R_{N_1}^{\phi^k}} \simeq \mathrm{Br}_1 \frac{m_\phi^2}{M_{N_1}^2}\,. \tag{3.264}$$

For smaller branching fraction, the density of N_1 through this channel is suppressed and the effect is milder and proportional to Br_1, as one can see in Fig. 3.20 right panel.

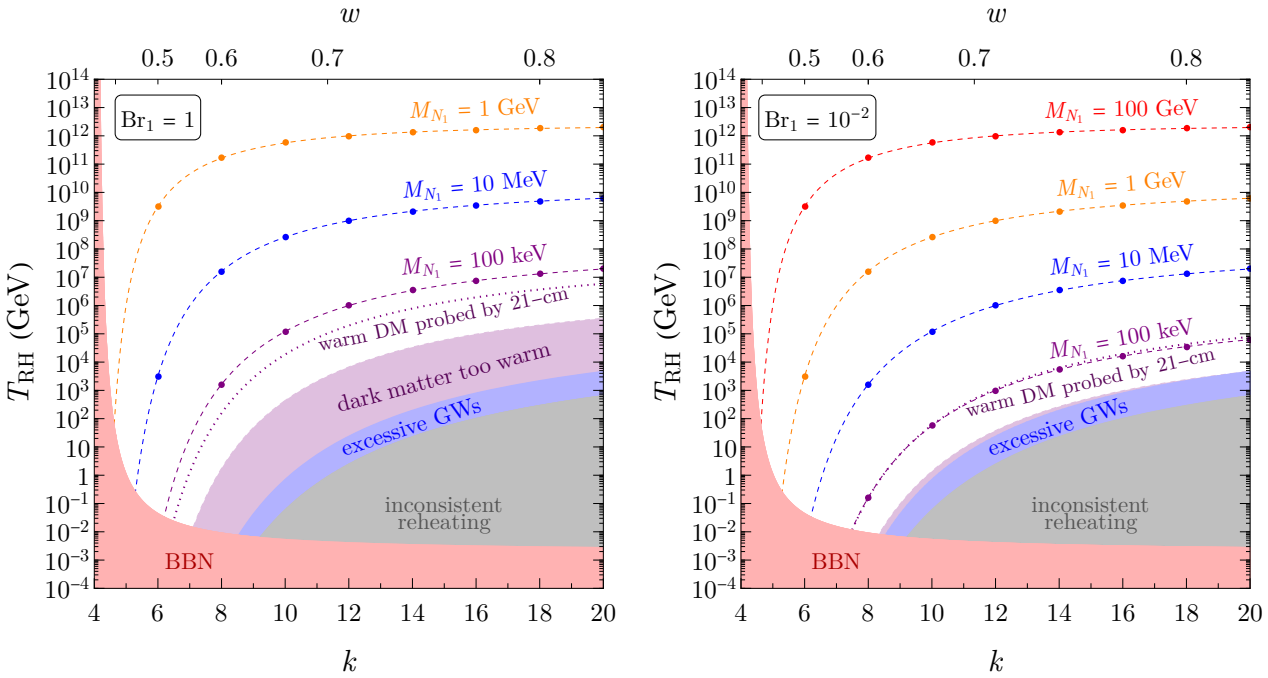

Figure 3.20: *Contours of observed relic abundance assuming $Br_1 = 1$ (left) and $Br_1 = 10^{-2}$ (right) for different choices of the DM mass, considering only Majoron contribution. The purple-shaded region is disallowed from the warm DM limit (see text).*

Given that the required mass, M_{N_1}, can be much lower when we couple the RHNs to the scalar S, and N_1 is produced relativistically, N_1 dark matter may still be warm around the time of CMB decoupling. We derive the warmness constraint by redshifting the N_1 initial momentum of order m_ϕ at $T_{\rm max}$ to the temperature $T \simeq 1$ eV and require that the velocity at $T \simeq 1$ eV is less than 2×10^{-4}. This bound on the velocity is obtained from translating the limit on the warm dark matter mass from the Lyman-α forest [332] in the case where the abundance is generated thermally. The current warmness constraint is shown by the purple

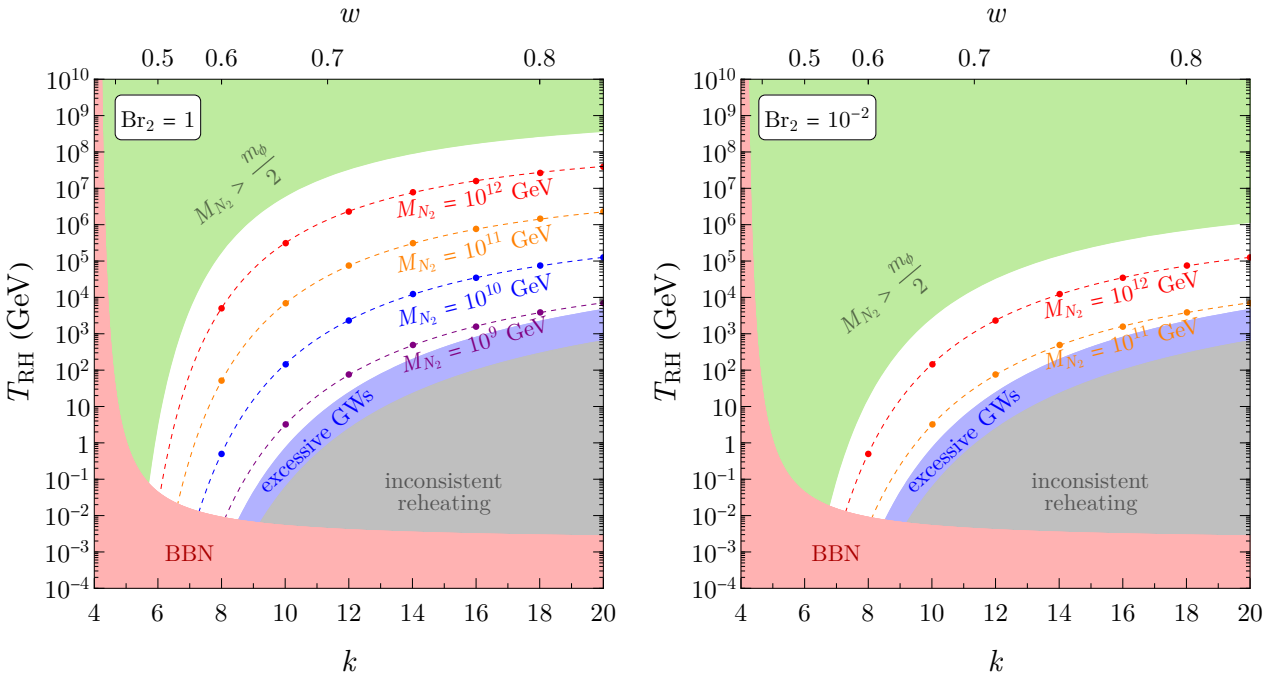

Figure 3.21: *Contours of N_{N_2} corresponding to the observed baryon asymmetry for $Br_2 = 1$ (left) and $Br_2 = 10^{-2}$ (right) in the (k, T_{RH}) plane. Here only the contribution due to the intermediate scalar is included. The green-shaded region is kinematically inaccessible due to $M_{N_2} > m_\phi/2$ [cf. Fig. 3.19].*

region, while the future sensitivity using cosmic 21-cm lines [333] is shown by the purple dotted curve. In summary, this mechanism interestingly allows for electroweak scale fermionic dark matter produced gravitationally, which is not possible by the direct scattering of the inflaton. We show in Fig. 3.21 the parameter space allowed to obtain a sufficient amount of baryon asymmetry for the set of branching ratios $\mathrm{Br}_2 = 1$ and 10^{-2}. Comparing Figs. 3.16 and 3.21 left, we note that for $M_2 = 10^{13}$ GeV the situation is similar to the direct production because no real enhancement $\propto \frac{m_\phi^2}{M_{N_2}^2}$ exists. However, for $M_{N_2} = 10^{11}$ GeV and large values of k, $T_{\rm RH}$ should be about 3 orders of magnitude larger to obtain the same asymmetry. The reason is that for a large value of k, $Y_B \propto \frac{1}{T_{\rm RH}}$ when S is produced (combining Eqs. (3.262) and (3.229)), and $\propto \frac{M_{N_2}^2}{m_\phi^2 T_{\rm RH}}$ when N_2 is produced directly. In other words, $T_{\rm RH}$ should be compensated by a factor $\frac{m_\phi^2}{M_{N_2}^2}$ to avoid an excessive asymmetry. As in the case of dark matter, lowering the branching ratio dilutes the effect as one can see in the right panel of Fig. 3.21.

Finally, we can combine the preceding results on Majoron production, adding the possibility for a gravitational reheating with non-minimal coupling. We illustrate this in Fig. 3.22, which is the analog of Fig. 3.17 but with the scalar S as an intermediate state. For demonstration purposes, here we suppose $M_{N_3} > m_\phi/2$ so that N_3 is not produced by the inflaton or S, resulting in $\mathrm{Br}_2 = 1 - \mathrm{Br}_1 = 1 - (M_{N_1}/M_{N_2})^2 \simeq 1$. As the branching ratios are completely determined by the masses M_{N_1} and M_{N_2}, for a fixed k and a fixed ξ_h, there will be again only one point in the (M_{N_1}, M_{N_2}) plane that could simultaneously obtain the CMB-determined DM

relic abundance and the observed baryon asymmetry. Each color segment in Fig. 3.22 assumes a fixed ξ_h and allows values of $k \in [6, 20]$ that are consistent with the BBN bound on $T_{\rm RH}$. The black dot indicates the $M_{N_{1,2}}$ masses, independent of k, required to explain the IceCube high-energy neutrino excess. The green region is inaccessible because $m_S > M_{N_2} > m_\phi/2$ forbids the production of S via ϕ scattering.[25] Compared to Fig. 3.17, we see that the effect of S as an intermediate state expands the parameter space of allowed dark matter density and baryon asymmetry. Most notably, the parameter space opens up towards lower masses, and allows large values of ξ_h.

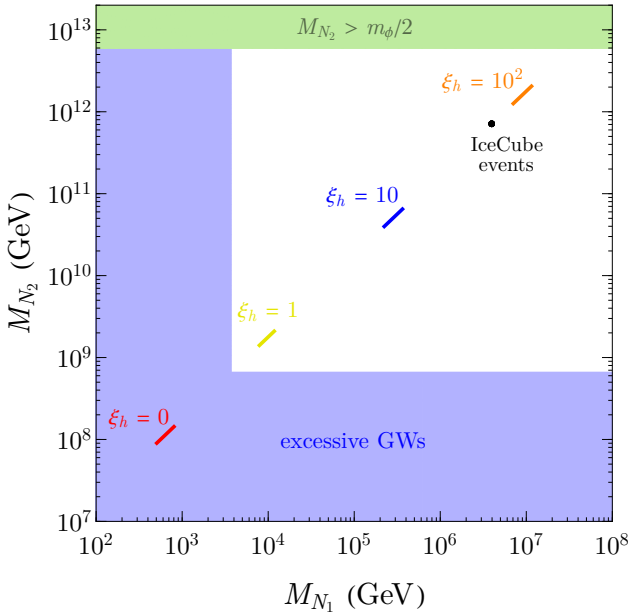

Figure 3.22: *Parameter space satisfying the right dark matter relic abundance and baryon asymmetry, considering the production through S. The line colors correspond to different values of ξ_h, with $\xi_h = \{0, 1, 10, 10^2\}$ from bottom to top, and $\xi_h = 0$ corresponds to minimal graviton exchange. Each colored line segment shows the variation of the predicted masses with $k \in [6, 20]$. The black dot marks the parameter point that can also explain the IceCube high-energy neutrino excess.*

3.4.7 Conclusions

In this section, we have shown the possibility that inflationary reheating, DM, and the BAU can be generated solely by gravitational interactions. The baryon asymmetry is produced through the decay of a RHN M_{N_2}, leading first to a non-zero lepton asymmetry in the leptogenesis framework. For minimal gravitational interactions, $\xi_h = 0$, a large amount of dark radiation is created in the form of gravitational waves and is inconsistent with BBN. Thus, we allow for a non-minimal gravitational coupling $\xi_h R H^2$ where H the Standard Model Higgs field to enhance reheating so that the ratio of GW energy density to the radiation is decreased. The

[25] Note that we have not included the effects of μ_Φ in Σ_S^k. These start to play a role for large $\xi_h \gtrsim 10^2$ when $2M_{N_2}$ becomes close to m_ϕ, since we require $2m_{N_2} < m_S < m_\phi$.

lowest ξ_h consistent with BBN is around 0.5. The range of the parameter space is 2-8 PeV for the dark matter mass M_{N_1} and $0.3 - 1.7 \times 10^{12}$ GeV for the mass of the lepton number violating decaying RHN, M_{N_2}. The range corresponds to a scan over ξ_h. Our solution restricts $0.5 \lesssim \xi_h \lesssim 13.5$ and $T_{\rm RH} < 3 \times 10^5$ GeV, where the maximum reheating temperature is attained with $\xi_h \simeq 4.7$. We summarize our results for fixing different values of ξ_h or M_{N_1} in the upper sections of Table 3.4 and Table 3.5 labeled "Direct gravitational production." Primordial GW generated during inflation allow a large parameter space with $T_{\rm RH} \lesssim 5 \times 10^6$ GeV to be probed in proposed gravitational wave detectors such as BBO, DECIGO, CE and ET.

Direct gravitational production			
ξ_h	$T_{\rm RH}$ [GeV]	M_{N_1} [PeV]	M_{N_2} [GeV]
1	$\{5.6 - 1.8 \times 10^4\}$	$\{2.49 - 2.54\}$	$\{4.5 - 4.8\} \times 10^{11}$
$\{2.5 - 2.7\}$	$\{0.11 - 9.8 \times 10^4\}$	4.0$\star$	$\{7.3 - 9.2\} \times 10^{11}$
10	8.1	8.1	1.7×10^{12}
Gravitational production via S			
ξ_h	$T_{\rm RH}$ [GeV]	M_{N_1}	M_{N_2} [GeV]
1	$\{5.6 - 1.8 \times 10^4\}$	$\{7.9 - 12\}$ TeV	$\{1.4 - 2.1\} \times 10^9$
10	$\{8.1 - 1.3 \times 10^6\}$	$\{220 - 360\}$ TeV	$\{4.0 - 6.5\} \times 10^{10}$
$\{50 - 68\}$	$\{2.6 \times 10^3 - 2.6 \times 10^7\}$	4.0 PeV$\star$	7.1×10^{11}
100	$\{8.1 \times 10^3 - 9.8 \times 10^7\}$	$\{7.1 - 11\}$ PeV	$\{1.3 - 2.0\} \times 10^{12}$

Table 3.4: *Ranges of T_{RH}, DM (M_{N_1}) and RHN (M_{N_2}) masses, over which baryon asymmetry and DM relic abundance are simultaneously satisfied via gravitational yield for different choices of the non-minimal coupling ξ_h; $\xi_h = 0$ corresponds to minimal gravity, which is not shown since it is excluded by BBN for excessive GW. The upper section assumes direction production of $N_{1,2}$, while the lower assumes production via Majoron's CP-even partner S as an intermediate state. Here we allow $k \in [6, 20]$ and omit points whose low T_{RH} values are excluded by BBN. (For the direct gravitational production, a single value of $k = 8$ is allowed for $\xi_h = 10$, while no points are allowed for $\xi_h \gtrsim 13.5$.) The $\star$ entry corresponds to the DM mass that can explain the IceCube high-energy neutrino events.*

Direct gravitational production			
ξ_h	$T_{\rm RH}$ [GeV]	M_{N_1} [PeV]	M_{N_2} [GeV]
1	0.0084 (excluded)	–	–
2.5	0.11	4.0$\star$	7.3×10^{11}
10	8.1	8.1	1.7×10^{12}
Gravitational production via S			
ξ_h	$T_{\rm RH}$ [GeV]	M_{N_1}	M_{N_2} [GeV]
1	0.0084 (excluded)	–	–
10	8.1	220 TeV	4.0×10^{10}
68	2.6×10^3	4.0$\star$	7.1×10^{11}
100	8.1×10^3	7.1 PeV	1.3×10^{12}

Table 3.5: *Same as Table 3.4 but for a fixed $k = 8$ as a benchmark.*

We also showed that N_1, if unstable, can explain the recent IceCube PeV events through its decay into SM neutrinos. In this case, if we want to accommodate simultaneously the correct DM relic abundance, the observed baryon asymmetry, gravitational reheating and the IceCube events, the value of ξ_h is fixed for a given k. We show this result in the second row of the upper section of each table where the assumed value of $m_{N_1} = 4$ PeV is marked by $\star$.

Finally, we proposed a new scenario where the RHN and the DM are produced through an intermediate scalar state S, the CP-even partner of the Majoron. In this case, the gravitational production of the scalar is not helicity suppressed by the mass of the final state fermions. As a result, the mass ranges for N_1 and N_2 are increased. For $0.5 \lesssim \xi_h \lesssim 100$, the mass range for N_1 is 4 TeV to 11 PeV, and the range for N_2 is $7 \times 10^8 - 2 \times 10^{12}$ GeV. Finally, the IceCube events can be explained by appropriate choices of ξ_h and $T_{\rm RH}$ for each k, whereas M_{N_2} is predicted to be 7.1×10^{11} GeV for all k when M_{N_1} is fixed to 4 PeV. We summarize our overall results for fixing different values of ξ_h or M_{N_1} in the lower sections of Table 3.4 and Table 3.5 labeled "Gravitational production via S".

Conclusion

In this thesis, we studied some aspects of particle production in the early Universe, a field of research currently under intense theoretical, phenomenological, and experimental investigations to look for potential probes of new physics. Especially, we have been interested in the reheating process after inflation, a crucial transition between the quasi-de Sitter phase of inflation and the further radiation-dominated Universe. Reheating is fundamental as it has to explain the generation of a hot thermal plasma made of SM particles, as well as the other cosmological relics, such as DM and potentially the baryon asymmetry.

We focused on constructing and using a theoretical framework for gravitational particle production during reheating after inflation. These research works addressed the question of the initial conditions for the thermal Universe as well as the problem of DM production in the scenario where it is completely secluded from the SM sector. The first chapter of this thesis was dedicated to introducing and developing the state of the art of the current understanding of early Universe Cosmology and Astroparticle Physics, while the second and third ones described the paradigm of inflation and reheating, deriving key results on particle production during this stage. In the following, we summarise the main content of each chapter and the important results obtained in this thesis.

In the first part of chapter 1, we presented the basics of General Relativity and the paradigm of modern Cosmology for the homogeneous and isotropic Universe. We summarized the currently accepted ΛCDM concordance model that describes the main components of our Universe and its expansion history. This model is in very precise agreement with the most recent observations of CMB photons and their anisotropies of temperature, the large-scale structure surveys, and the BBN constraints.

In the second part, we depicted the significant stages in the history of the thermal Universe, the condition for thermal equilibrium among the different species to occur, and how successive decoupling can explain the observation of cosmological relics such as CMB photons or DM abundance. The problem of the observed asymmetry between baryons and antibaryons has been addressed by describing baryogenesis constraints and models of non-thermal leptogenesis after inflation. A link with neutrino physics and an explanation for their small masses is

discussed through the Seesaw mechanism involving BSM particles in the form of RHN. We then detailed the main processes currently investigated for the generation of the DM component, involving the WIMP model associated with thermal freeze-out, or the more recent FIMP and UV freeze-in scenarios.

Finally, in the last part of this chapter, we reviewed the cosmological implications of CMB temperature anisotropies measurements. We studied the imprints of the initial cosmological perturbations on the CMB angular power spectrum and which constraints impose the recent and most precise measurements of Planck Collaboration on cosmological models. We explained why the standard description of modern Cosmology fails to explain the spatial flatness and homogeneity and isotropy on the largest scales of the Universe, requiring an extension of the standard hot Big Bang scenario.

In chapter 2, we reviewed the main predictions of the theory of inflation. We presented the most simple scenario of single-field slow-roll inflation, driven by a single scalar field called the inflaton. We showed how the dynamics of such a field can explain the existence of a quasi-de Sitter phase in the first instants of the Universe and how the phenomenological models of inflation are constrained to solve the issues of standard Cosmology. We further introduced the mechanism at play in generating primordial perturbations from the inflaton sector, setting the initial condition for the curvature perturbations that source CMB anisotropies. We discussed the predictions of single-field slow-roll inflationary models in terms of the amplitude of the curvature power spectrum, the scalar tilt, and the tensor-to-scalar ratio, which are the main cosmological parameters related to the inflationary models being constrained by current observations.

In the second part, we introduced the process of reheating after inflation in two kinds of approach: an analytical approximation under the assumption of perturbative analysis, and on the other hand, by solving the full set of coupled equation of motions for the field to follow the non-linear and non-perturbative dynamics of the system in a classical regime. In the first approach, we considered the oscillations of the inflaton around the minimum of its potential and developed its oscillations in Fourier modes. We solved the Boltzmann equation for coupled fields with various couplings and spins as well as different inflaton potentials. Then, we considered the effect of parametric resonances that can trigger instability in the evolution of the mode functions of coupled fields. We derived standard results in the stability analysis for fields coupled to an oscillating background leading in some scenarios to rapid preheating. The effect of inflaton background self-fragmentation has also been discussed.

In the last part, novel results are obtained on the reheating efficiency when the inflaton evolves in a mixed-potential. We considered the effects of a bare mass term for the inflaton, while it oscillates about its minimum but when higher order terms dominate during inflation.

We showed that the presence of a mass term can significantly alter the reheating process, as the equation of state of the inflaton condensate changes when the inflaton amplitude drops due to expansion. We computed the effects on the reheating temperature for cases where reheating is due to inflaton decays or inflaton scatterings. For scattering to scalars and in the absence of decay, we showed that there is always a residual inflaton background that acts as CDM. We derived a strong upper limit for the inflaton bare mass in this case. We also considered the effect of the bare mass term on the inflaton fragmentation.

In chapter 3, we presented the main work conducted during this thesis. First, we reviewed the semi-classical approach to tackle cosmological particle production, involving the study of QFT in curved space-time and the Bogoliubov formalism. This led us to develop a novel framework to compute the production of matter and radiation during reheating interacting only gravitationally through the exchange of a graviton. We compared the production of DM from inflaton scatterings and from the UV-freeze in contribution mediated only by gravity. We showed that the inflaton contribution tends to dominate the production in a large part of the parameter space. We have also seen that it is possible to produce radiation from inflaton scattering in the condensate during the earlier stages of reheating, rapidly reaching an unavoidable high maximal temperature.

We then generalized the minimal gravitational interactions to include non-minimal couplings of scalars to the Ricci curvature R and have analyzed the impact of couplings of the type $\xi_i S_i^2 R$ on the reheating process and DM production. We showed that the non-minimal coupling can dominate the process and alleviate constraints on DM mass to generate the right relic abundance.

Finally, in the last part, we showed the possibility that inflationary reheating, DM, and the baryon symmetry can be generated simultaneously solely by gravitational interactions. We considered a simple BSM scenario involving three generations of RHN where the baryon asymmetry is produced through the decay of a RHN in the non-thermal leptogenesis framework. For minimal gravitational interactions, $\xi_h = 0$, a large amount of dark radiation is created in gravitational waves, putting strong constraints on gravitational reheating scenario. We also allowed for a non-minimal gravitational coupling $\xi_h R H^2$ to enhance reheating so that the ratio of GW energy density to the radiation is decreased. Primordial GW generated during inflation allow a large parameter space for reheating temperature and equation of state to be probed in future gravitational wave experiments such as BBO, DECIGO, CE and ET. We also proposed a new scenario where the RHN and the DM are produced through an intermediate scalar state S, the CP-even partner of the Majoron. In this case, the gravitational production of the scalar is not helicity suppressed by the mass of the final state fermions, resulting in an increased mass range for RHN to produce the baryonic and DM relics simultaneously.

To conclude, this thesis illustrates the crucial importance of reheating after inflation in understanding the generation of cosmological relics and initial conditions for the thermal Universe. It shows the necessity for further investigating the phenomenology of BSM scenarios in the early Universe. We have emphasized the possibility of a minimal scenario where the different sectors interact only through gravitational interactions. We showed that in such a simple case, the generation of cosmological relics can be achieved quite easily. If observational constraints on primordial gravitational waves and the duration of reheating can be put on phenomenological aspects of reheating models, it is necessary to pursue theoretical efforts to link these models to cosmological observables or experimental constraints accurately. The non-linear regime of cosmological perturbations, which could be constrained in future surveys, could shed light on the complex dynamics involving several coupled fields in the early Universe.

Appendix A

The Standard Model: an overview

In Particle Physics, the currently accepted theory is the Standard Model (SM). The SM combines the theory of electroweak interactions and the theory of quantum chromodynamics (QCD), which are QFT and gauge theories. Such QFT rely on local gauge symmetry, which naturally predicts the existence of gauge bosons, mediating interactions between quantum fields. SM predicts which interactions occur among known particles and the probabilities of such interactions. All of the particles in the SM have been experimentally observed, with the final observation being the Higgs boson in 2012 by ATLAS and CMS. It is a renormalizable QFT that allows tree level and any higher order calculations within perturbation theory, and probes quantum effects. The calculations agree with experimental data with high precision. However, the SM does not provide a quantum description of gravity and hence can not be valid up to arbitrary large energies. It is expected that processes taking place around the Planck scale $M_P \simeq 2.5 \times 10^{18}$ GeV, come with significant gravitational corrections that are not tackled within the SM description. Therefore, the Planck scale is a natural UV cutoff of the theory.

SM gauge structure

The SM is a gauge theory defined by its gauge symmetry group, as a direct product of smaller gauge groups

$$\mathcal{G}_{\rm SM} = SU(3)_c \times SU(2)_L \times U(1)_Y \tag{A.1}$$

where $SU(3)_c$ is associated with color charges of quantum fields (QCD), while $SU(2)_L$ is associated with the chiral (left-handed fields) weak-isospin and $U(1)_Y$ to the weak hypercharge, together describing the gauge structure of the electroweak theory. $SU(N)$ gauge groups are non-abelian, meaning gauge transformations are non-commutative. The number of generators required to fully specify $SU(N)$ Lie group is $N^2 - 1$. The generators are elements of the corresponding Lie algebra. In the SM, spin-1 vector fields are the mediators of the gauge interactions

and are spanning the adjoint representation of the associated gauge group. These vector fields A_μ, or gauge bosons, are introduced to ensure gauge invariance and are related to the generators of the group as

$$A_\mu = A_{\mu,a} T^a \tag{A.2}$$

where T^a, $a \in [1, N^2 - 1]$, are the generators, elements of the Lie algebra obeying the following Lie bracket relations

$$[T^a, T^b] = i f^{abc} T^c \tag{A.3}$$

where f^{abc} is the group structure constant associated with the gauge group. For $SU(2)_L$, the generators are given by $T^a = (1/2)\sigma^a$, the three 2×2 Pauli matrices, while for $SU(3)_c$, the generators in the fundamental representation are 3×3 matrices with similar properties called Gell-Mann matrices. The $U(1)_Y$ gauge group is abelian and generated by one field. Therefore, in the SM we have the following vector bosons

$$\begin{aligned} SU(3)_c &: \quad G^a_\mu \quad a = 1, 2, ...8 \quad \text{(gluons)} \\ SU(2)_L &: \quad W^a_\mu \quad a = 1, 2, 3 \quad \text{(weak isospin bosons)} \\ U(1)_Y &: \quad B_\mu \quad \text{(weak hypercharge boson)} \end{aligned}$$

A local gauge transformation acts on quantum fields as

$$\Psi(x) \to e^{ig\theta_a(x)T^a} \Psi(x) \tag{A.4}$$

where the parameter $\theta_a(x)$ depends on space-time. As a consequence, the derivative of a field is no longer gauge invariant. Therefore, gauge covariant derivatives are required, $D_\mu = \partial_\mu - igA^a_\mu T^a$ to maintain gauge invariants of the dynamical theory, where a gauge coupling constant, g, has to be introduced. The vector fields transform as

$$A^a_\mu \to e^{i\theta_a(x)T^a} \left(A^a_\mu + \frac{i}{g}\partial_\mu \right) e^{-i\theta_a(x)T^a} \tag{A.5}$$

such that the covariant derivative remains invariant under gauge gauge transformations. From these fields, we can build a gauge invariant Yang-Mills Lagrangian (generalizing the Maxwell Lagrangian), including kinetic terms and interaction terms for the gauge bosons

$$\mathcal{L}_{\text{gauge}} = -\frac{1}{4} B_{\mu\nu} B^{\mu\nu} - \frac{1}{4} W^a_{\mu\nu} W^{\mu\nu,a} - \frac{1}{4} G^a_{\mu\nu} G^{\mu\nu,a} \tag{A.6}$$

with the following field strength

$$B_{\mu\nu} = \partial_\mu B_\nu - \partial_\nu B_\mu \tag{A.7}$$

$$W^a_{\mu\nu} = \partial_\mu W^a_\nu - \partial_\nu W^a_\mu + g\epsilon^{abc} W^b_\mu W^c_\nu \tag{A.8}$$

$$G^a_{\mu\nu} = \partial_\mu G^a_\nu - \partial_\nu G^a_\mu + g_s f^{abc} G^b_\mu G^c_\nu \tag{A.9}$$

where ϵ^{abc} is the structure constant for $SU(2)$ which is the rank 3 Levi-Civita tensor, and g, g_s the weak gauge coupling for $SU(2)_L$ and the strong gauge coupling for $SU(3)_c$ respectively. Mass for the gauge fields is forbidden by gauge symmetry but the Spontaneous Symmetry Breaking (SSB) of the $SU(2)_L \times U(1)_Y \to U(1)_{\rm EM}$ via the Brout-Englert-Higgs mechanism leads to the mass generation of the weak gauge bosons. A residual $U(1)_{\rm EM}$ gauge symmetry is maintained and associated with Maxwell's theory of electromagnetism such that the photons remain massless. We discuss this mechanism while introducing the Higgs sector.

Higgs sector

The Brout-Englert-Higgs mechanism is the name given to the SSB of the electroweak gauge sector in the SM. This is the process by which matter particles and weak gauge bosons acquire masses. Before SSB, mass terms for particles are forbidden, as they are not gauge invariant. The breaking of the $SU(2)_L \times U(1)_Y$ symmetry at low energy allows for writing renormalizable mass terms for fermions and weak gauge bosons. In such a mechanism, the Lagrangian is still gauge invariant, but the ground state of the system is not invariant under gauge transformation. This is realized by introducing a complex scalar $SU(2)_L$ doublet Φ with Hypercharge $Y = 1/2$, which acquires a non-zero VEV at low energy. This Higgs field can be written as a function of four real degrees of freedom ϕ_i, $(i = 1, ..., 4)$, in the doublet

$$\Phi = \frac{1}{\sqrt{2}} \begin{pmatrix} \phi_1 + i\phi_2 \\ \phi_3 + i\phi_4 \end{pmatrix} . \tag{A.10}$$

This Higgs field has a gauge invariant potential such that the Higgs sector gauge invariant Lagrangian is given by

$$\mathcal{L}_{\rm Higgs} = (D_\mu \Phi)^\dagger (D^\mu \Phi) - V(\Phi) \tag{A.11}$$

with

$$V(\Phi) = -\mu^2 |\Phi|^2 + \lambda |\Phi|^4 \tag{A.12}$$

the Mexican hat potential. The parameter λ is positive, hence the potential is bounded from below, but μ^2 is also positive, leading to a minimum of the potential for a non-vanishing value of the Higgs field (VEV), $v_{\rm EW} = \mu/\sqrt{\lambda}$. It can be seen by an appropriate gauge transformation

of the Higgs field that the vacuum configuration is given by

$$\langle \Phi \rangle = \frac{1}{\sqrt{2}} \begin{pmatrix} 0 \\ v_{\mathrm{EW}} \end{pmatrix} . \tag{A.13}$$

The process is called symmetry breaking because the VEV of the Higgs field breaks the electroweak gauge symmetry as this specific configuration is not invariant under the whole gauge transformation. Thus, the Higgs field spontaneously breaks the symmetry by adopting this ground state. One scalar degree of freedom remains as fluctuations around the electroweak vacuum after SSB, called the Higgs boson h. The Higgs doublet in unitary gauge reduces to

$$\Phi = \frac{1}{\sqrt{2}} \begin{pmatrix} 0 \\ v_{\mathrm{EW}} + h \end{pmatrix} . \tag{A.14}$$

A remaining $U(1)$ symmetry is conserved by this vacuum configuration, as this configuration is invariant under a complex phase rotation. The symmetry-breaking pattern is thus

$$SU(2)_L \times U(1)_Y \to U(1)_{\mathrm{EM}} \tag{A.15}$$

There were four generators for the electroweak gauge group, which reduces to one unbroken generator of the $U(1)_{\mathrm{EM}}$ symmetry after the Higgs field acquires its VEV. The unbroken generator is a linear combination of the generators of $SU(2)_L$ and $U(1)_Y$ identified as the electric charge of electromagnetism

$$Q = \frac{\sigma_3}{2} + \frac{Y}{2}.\mathbb{1} \tag{A.16}$$

with Y the electroweak hypercharge. Each broken generator corresponds to one degree of freedom which is apparently lost in the resulting theory. However, we can show that in this vacuum configuration, electroweak interactions between the Higgs doublet and weak gauge bosons lead to the spontaneous generation of mass terms for the vector fields. From the covariant derivatives in the kinetic terms of the Higgs doublet, it leads to mass terms for three gauge fields $W^{\pm}$ and Z which are the following mass eigenstates

$$\begin{aligned} W_\mu^{\pm} &= \frac{W_\mu^1 \pm W_\mu^2}{\sqrt{2}} \\ \begin{pmatrix} Z_\mu \\ A_\mu \end{pmatrix} &= \begin{pmatrix} \cos\theta_W & -\sin\theta_W \\ \sin\theta_W & \cos\theta_W \end{pmatrix} \cdot \begin{pmatrix} W_\mu^3 \\ B_\mu \end{pmatrix} \end{aligned} \tag{A.17}$$

We see that Z_μ is a mixing of electroweak gauge bosons W_μ^3 and hypercharge B_μ. The mixing angle θ_W is the Weinberg angle defined as $\tan\theta_W \equiv \frac{g'}{g}$, the ratio of $SU(2)_L$ and $U(1)_Y$ gauge

couplings. The masses of the electroweak bosons are given by the VEV and the Weinberg angle

$$m_W = \frac{g v_{\rm EW}}{2}, \quad m_Z = \frac{g v_{\rm EW}}{2\cos\theta_W}, \quad m_A = 0 \tag{A.18}$$

and the photon vector field A_μ remains massless after SSB, which is associated with the remaining $U(1)_{\rm EM}$ gauge symmetry. Hence, three of the four scalar degrees of freedom reduce to massless Goldstone bosons after SSB, which, in a proper gauge, are absorbed in the longitudinal polarization of the gauge fields while generating their masses. Higgs bosons also acquire a mass, generated by Higgs self-interaction after the electroweak SSB

$$m_h = \sqrt{2\lambda} v \tag{A.19}$$

All the masses in the electroweak sector depend only on Higgs potential parameters, which have been measured experimentally.

Quarks and Leptons

The fermionic content of the SM is divided into three generations (flavors) of quarks and leptons. Within each generation $i = 1, 2, 3$, there are $SU(2)_L$ singlets; one up-type quark $u_{R,i}$, one down-type quark $d_{R,i}$, and one lepton $\ell_{R,i}$, that are right-handed Weyl fermions. In addition, within each generation, there are $SU(2)_L$ lepton doublets and quark doublets

$$L_i = \begin{pmatrix} \nu_i \\ \ell_i \end{pmatrix}_L, \quad Q_i = \begin{pmatrix} u_i \\ d_i \end{pmatrix}_L \tag{A.20}$$

that are left-handed Weyl fermions. Hence, SM is a chiral theory distinguishing left-handed and right-handed fermions. The gauge invariant kinetic and gauge interaction terms for the fermions are given by the Dirac Lagrangian

$$\mathcal{L}_{\rm Dirac} = \sum_{\rm leptons} i\overline{L}_i D_\mu \gamma^\mu L_i + \sum_{\rm leptons} i\overline{\ell}_{R,i} D_\mu \gamma^\mu \ell_{R,i} + \sum_{\rm quarks} i\overline{q}_{R,i} D_\mu \gamma^\mu q_{R,i} + \sum_{\rm quarks} i\overline{Q}_i D_\mu \gamma^\mu Q_i \tag{A.21}$$

where the interactions with gauge bosons are provided by the gauge covariant derivatives D_μ introduced above. The associate charges of SM under each gauge group are summarized in Table A.1 below.

Because of the chiral $SU(2)_L$ charges assignment, any mass term in the fermionic sector also breaks gauge symmetry. However, in addition to gauge couplings, fermions in the SM are also coupled to the Higgs doublet through Yukawa interactions. The gauge invariant Yukawa

	$SU(3)_c$	$SU(2)_L$	$U(1)_Y$
Q_L^i	**3**	**2**	$1/6$
u_R^i	**3**	**1**	$2/3$
d_R^i	**3**	**1**	$-1/3$
L_L^i	**1**	**2**	$-1/2$
ℓ_R^i	**1**	**1**	-1
Φ	**1**	**2**	$1/2$

Table A.1: *Fermions and Higgs doublet charges under SM gauge group.*

Lagrangian is given by

$$\mathcal{L}_{\text{Yukawa}} = -(y_\ell)_{ij}\overline{L}_i\Phi\ell_{R,j} - (y_d)_{ij}\overline{Q}_i\Phi d_{R,j} - (y_u)_{ij}\overline{Q}_i\tilde{\Phi}u_{R,j} + \text{h.c.} \tag{A.22}$$

where $\tilde{\Phi} = i\sigma^2\Phi^*$ is the $SU(2)_L$ Higgs doublet conjugate with opposite hypercharge compared to Φ. The Yukawa matrices y_{ij} are 3×3 complex matrices describing the flavor interactions within the SM. After electroweak SSB, in unitary gauge, the Yukawa sector reduces to

$$\mathcal{L}_{\text{Yukawa}} = -\left(\frac{v_{\text{EW}} + h}{\sqrt{2}}\right)\left[(y_\ell)_{ij}\overline{\ell}_{L,i}\ell_{R,j} - (y_d)_{ij}\overline{d}_{L,i}d_{R,j} - (y_u)_{ij}\overline{u}_{L,i}u_{R,j} + \text{h.c.}\right] \tag{A.23}$$

which introduce direct couplings between the Higgs boson and the fermions, as well as flavor non-diagonal mass terms from the non-vanishing VEV of the Higgs field. The leptons mass matrix is assumed diagonal in this basis (mass eigenstates are also flavor eigenstates for leptons) while the quark mass matrices can be diagonalized through the unitarity redefinition of the fields

$$u_{L,i} \to V_u^{ij}u_{L,j}, \quad d_{L,i} \to V_d^{ij}d_{L,j}\,. \tag{A.24}$$

To describe quark oscillations we introduced the CKM matrix $V_{ij}^{\text{CKM}} = (V_u^\dagger V_d)_{ij}$ that is relating flavor quark eigenstates that are interacting under weak interaction, to their free mass eigenstates. This 3×3 complex matrix can be parametrized by three mixing angles θ_{ij} and a non-zero complex phase δ, which induces CP-violation in quarks weak interactions. After the diagonalization of the mass matrix, we are left with the following mass terms for the quarks, as well as for "down-type" leptons

$$m_{q_i} = \frac{y_{ii}v_{\text{EW}}}{\sqrt{2}}, \quad m_{\ell_i} = \frac{y_{ii}v_{\text{EW}}}{\sqrt{2}}\,. \tag{A.25}$$

Due to the chirality of the neutrinos, which are only left-handed Weyl fermions part of the $SU(2)_L$ doublet, no such mass terms are generated for them. No right-handed neutrinos are present within the SM, thus neutrinos remain in massless states. Finally, we see that in the mass basis, fermions of the SM (except neutrinos) interact with the Higgs bosons through the

Yukawa interaction

$$\mathcal{L}_{\text{Yukawa}} \supset -\sum_i \frac{m_{q,i}}{v_{\text{EW}}} h\overline{q}_{L,i} q_{R,i} - \sum_i \frac{m_{\ell,i}}{v_{\text{EW}}} h\overline{\ell}_{L,i} \ell_{R,i} \tag{A.26}$$

showing that couplings between the Higgs boson and SM fermions are proportional to their masses.

To conclude, despite the success of the SM, the theory is challenged by some observations that can not be explained. SM neutrinos are massless within the SM; however, experiments have shown that the neutrinos do have masses, and mixing occurs between them (see section 1.3 for a discussion of some BSM models explaining neutrinos masses). Additionally, there is no particle in the SM that can explain the existence of cold DM. The asymmetry of matter over anti-matter is yet another feature of the observable Universe that can not be explained within the SM (see section 1.3). There exists a hierarchy in the masses of the three generations of quarks and leptons which is not explained. It is, therefore, natural to look for completion of the SM at higher energy scales, but still below the Planck scale.

Appendix B

Weak-Field Gravity and gravitons

In this appendix, we consider gravity as an effective field theory and derive the massless gravitons propagator as well as the leading order gravitational interactions. For this purpose, we look at perturbed Einstein equations, following the procedure presented in [334]. We work in the weak field limit of gravity, assuming that we can expand the local metric field around Minkowski background as

$$g_{\mu\nu} = \eta_{\mu\nu} + \frac{2}{M_P} h_{\mu\nu} \tag{B.1}$$

where $h_{\mu\nu}$ is the massless graviton canonically normalized field. At first order in the perturbation $|h_{\mu\nu}| \ll M_P$, the Ricci tensor and scalar can computed as

$$\begin{aligned} R_{\mu\nu} &= \frac{1}{M_P}\left[\partial_\mu\partial_\lambda h^\lambda_\nu + \partial_\nu\partial_\lambda h^\lambda_\nu - \partial_\mu\partial_\nu h^\lambda_\lambda - \Box h_{\mu\nu}\right] + O(h^2)\,, \\ R &= \frac{2}{M_P}\left[\partial_\mu\partial_\lambda h^{\mu\lambda} - \Box h^\lambda_\lambda\right] + O(h^2)\,. \end{aligned} \tag{B.2}$$

yielding the linearly perturbed Einstein equation through

$$R_{\mu\nu} - \frac{1}{2}\eta_{\mu\nu}R \equiv \frac{\kappa}{2} O_{\mu\nu\alpha\beta} h^{\alpha\beta} = \frac{1}{M_P^2} T_{\mu\nu}\,. \tag{B.3}$$

The differential operator $O_{\mu\nu\alpha\beta}(x)$ has to be gauge–fixed before looking at its associated Green function. Under a general coordinate transformation which leaves the field equations invariant,

$$x^\mu \to x^\mu + \frac{2}{M_P}\xi^\mu(x)\,. \tag{B.4}$$

the metric perturbation transform as

$$h_{\mu\nu} \to h_{\mu\nu} - \partial_\mu\xi_\nu - \partial_\nu\xi_\mu\,. \tag{B.5}$$

Thus, by choosing the appropriate transformation such that

$$\Box\xi_\mu = -(\partial_\mu h^\mu_\nu - \frac{1}{2}\partial_\nu h^\lambda_\lambda) \tag{B.6}$$

we are free to fix the gauge as

$$\partial_\mu h^\mu{}_\nu - \frac{1}{2}\partial_\nu h^\lambda{}_\lambda = 0\,, \tag{B.7}$$

which is called de Donder (harmonic) gauge condition. In this gauge, for the field

$$\bar{h}_{\mu\nu} = h_{\mu\nu} - \frac{1}{2}\eta_{\mu\nu}h^\lambda{}_\lambda\,, \tag{B.8}$$

the equations Eq.(B.3) reduce to the wave equation sourced by stress energy

$$\Box\bar{h}_{\mu\nu} = -\frac{1}{M_P}T_{\mu\nu}\,. \tag{B.9}$$

In this gauge, we can show by expanding the Einstein-Hilbert action Eq.(1.7) $\mathcal{S}_{\rm EH}$ at the second order in the metric perturbation $h_{\mu\nu}$, that the associated Lagrangian density reads [334]

$$\sqrt{-g}\mathcal{L} = \frac{1}{2}\partial_\lambda h_{\mu\nu}\partial^\lambda h^{\mu\nu} - \frac{1}{4}\partial_\lambda h\partial^\lambda h - \frac{1}{M_P}h^{\mu\nu}T_{\mu\nu} \tag{B.10}$$

where we introduced the trace of the metric perturbation $h \equiv h^\mu{}_\mu$ and the leading order coupling to matter is given by the last term involving $T_{\mu\nu}$. This leading order interaction of the graviton field is considered in chapter 3. We can easily rewrite this Lagrangian density and integrate by parts to obtain the form

$$\sqrt{-g}\mathcal{L} = \frac{1}{2}h_{\mu\nu}\Box\left(I^{\mu\nu\alpha\beta} - \frac{1}{2}\eta^{\mu\nu}\eta^{\alpha\beta}\right)h_{\alpha\beta} - \frac{1}{M_P}h^{\mu\nu}T_{\mu\nu}\,. \tag{B.11}$$

where we introduced the identity tensor

$$I^{\mu\nu\alpha\beta} \equiv \frac{1}{2}\left(\eta_{\mu\alpha}\eta_{\nu\beta} + \eta_{\mu\beta}\eta_{\nu\alpha}\right)\,. \tag{B.12}$$

From this effective field theory in the weak-field limit, $|h_{\mu\nu}| \ll M_P$, we quantize the graviton field as the solution of the wave equation Eq.(B.9) in the absence of matter. As the *on-shell* massless photon is described in terms of a spin-one polarization vector $\epsilon_\mu(p)$ which can have helicity projection either $+$ or $-$ along momentum direction, the massless graviton is a spin-2 particle which can have the 2 *on-shell* different helicity projections along its momentum direction. Since $h_{\mu\nu}$ has to be a symmetric tensor, it can be described in terms of a simple

product of spin-1 polarization vectors such as

$$\epsilon_{\mu\nu}^{++} = \epsilon_{\mu}^{+}\epsilon_{\nu}^{+} \tag{B.13}$$

$$\epsilon_{\mu\nu}^{--} = \epsilon_{\mu}^{-}\epsilon_{\nu}^{-} \, . \tag{B.14}$$

These two possible polarizations of the massless tensor field are considered by introducing the polarization tensor $\epsilon_{\mu\nu}$ given by the above products of polarization vectors. We note that the helicity states given are consistent with the harmonic gauge requirement, since they satisfy

$$\eta^{\mu\nu}\epsilon_{\mu\nu} = 0, \text{ and } p^{\mu}\epsilon_{\mu} \tag{B.15}$$

showing that the tensor modes described in that way are *on-shell* transverse-traceless modes. To quantize the graviton field, we use the plane wave decomposition

$$\hat{h}_{\mu\nu}(x) = \sum_{\lambda=++,--} \int \frac{d^3\vec{p}}{(2\pi)^3} \frac{1}{\sqrt{2\omega_p}} \left[\hat{a}_p(\lambda)\epsilon_{\mu\nu}(\lambda)e^{-ip\cdot x} + \hat{a}_p^{\dagger}(\lambda)\epsilon_{\mu\nu}^{*}(\lambda)e^{ip\cdot x}\right] , \tag{B.16}$$

where the ladder operators $\hat{a}_p(\lambda)$ and $\hat{a}_p^{\dagger}(\lambda)$ satisfy the canonical commutation relations

$$[\hat{a}_p(\lambda), \hat{a}_{p'}^{\dagger}(\lambda')] = \delta^{(3)}(\vec{p} - \vec{p'})\delta_{\lambda\lambda'} \, . \tag{B.17}$$

From the Lagrangian density given above, we obtain the equation of motion

$$\left(I^{\mu\nu\alpha\beta} - \frac{1}{2}\eta^{\mu\nu}\eta^{\alpha\beta}\right) \Box D_{\alpha\beta\gamma\delta} = I_{\gamma\delta}^{\mu\nu} \tag{B.18}$$

and one can extract the Green function, corresponding with appropriate initial conditions to the Feynman propagator in momentum space for the massless graviton [334]

$$iD^{\alpha\beta\gamma\delta} = \int \frac{d^4p}{(2\pi)^4} \frac{i}{p^2 + i\epsilon} e^{-q\cdot x} P^{\alpha\beta\gamma\delta} \tag{B.19}$$

with

$$P^{\alpha\beta\gamma\delta} = \frac{1}{2}\left[\eta^{\alpha\gamma}\eta^{\beta\delta} + \eta^{\alpha\delta}\eta^{\beta\gamma} - \eta^{\alpha\beta}\eta^{\gamma\delta}\right] \, . \tag{B.20}$$

The leading order interaction term and the Feynman propagator for massless gravitons are used in chapter 3 to derive transition amplitudes of gravitational portals during reheating.

Synthèse

Modèle cosmologique standard

La Cosmologie moderne, par l'utilisation de la Relativité Générale et de la théorie quantique des champs, ainsi que par l'acquisition de données observationnelles de plus en plus précises, a permis d'élaborer un Modèle Standard pour la composition de notre Univers et son évolution.

L'observation systématique du décalage vers le rouge du spectre lumineux émis par les galaxies lointaines a d'abord permis de mettre en évidence l'expansion de l'espace-temps dans le cadre de la théorie de la relativité générale, fournissant ainsi une histoire de l'Univers dans son ensemble au-delà de celles des objets physiques en son sein. Les principales données ayant permis d'établir le modèle cosmologique proviennent de la détection du fond diffus cosmologique (Cosmic Microwave Background, ou CMB). Cette détection confirme l'expansion de l'Univers à partir d'un état de haute densité d'énergie et de rayonnement, un plasma homogène de particules relativistes en interactions à très haute température. Le spectre de corps noir des photons du CMB résulte d'abord des interactions intenses entre les particules du bain primordial, menant à l'équilibre thermodynamique, puis au découplage progressif des différentes particules à cause de l'expansion, entraînant le refroidissement et la dilution du plasma primordial. Ces photons sont par la suite libres de se propager dans toutes les directions jusqu'à parvenir dans nos détecteurs.

L'étude approfondie du CMB, mais aussi la description du processus de formation des premiers noyaux atomiques (nucléosynthèse primordiale, Big Bang Nucleosynthesis ou BBN) et la mesure de l'abondance des différents éléments chimiques dans l'Univers (voir Figure B.1), ont permis d'aboutir à une description cohérente du contenu de l'Univers en termes de matière et d'énergie. Le modèle cosmologique, appelé modèle ΛCDM, indique que plus de 25% du contenu de l'Univers est une matière noire froide, qui n'est pas baryonique et qui ne produit pas de signal d'interaction avec la matière ordinaire, autre que par son attraction gravitationnelle. Cette matière noire n'a pas encore été détectée directement ou indirectement dans une quelconque expérience cherchant à mettre en évidence ses propriétés d'interaction avec la matière connue. La matière ordinaire ne représente que 5% du contenu de l'Univers en masse-énergie. Enfin, la récente observation du spectre de certaines supernovae (de type Ia), confrontée aux

données issues du CMB, a montré que notre Univers est dans une phase tardive d'expansion accélérée, expliquée par la présence d'une énergie sombre. Les données indiquent que cette énergie sombre devrait représenter près de 70% du contenu énergétique de l'Univers, bien qu'elle n'ait pas encore été détectée directement dans une expérience. Les caractéristiques physiques de cette énergie sombre, déduites des données d'observation, sont compatibles avec l'effet d'une constante cosmologique, notée communément Λ, dans les équations de la relativité générale décrivant l'expansion de l'Univers.

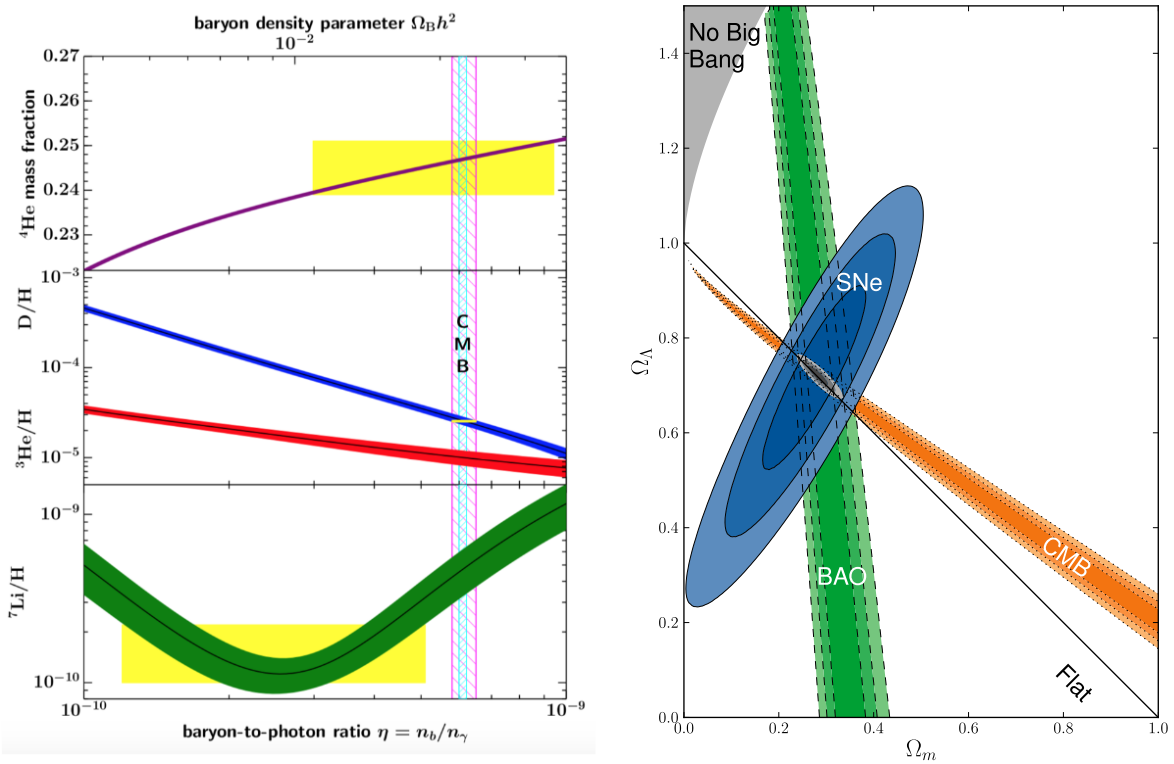

Figure B.1: *Analyse des données d'observation menant au modèle de concordance ΛCDM. A gauche: prédictions de l'abondance des noyaux légers par les modèles de nucléosynthèse primordiale, confronté aux mesures du ratio baryons/photons via l'analyse du CMB. A droite: contraintes sur la densité de matière froide (matière noire et baryonique) et d'énergie sombre, à partir de l'analyse des données du CMB, des structures à grandes échelles et des supernovae. Ces différentes contraintes concordent vers un Univers dominé par l'énergie sombre (70%) et par la matière noire froide (25%), alors que la matière baryonique ne représente que 5% du contenu en masse-énergie.*

A partir de ce modèle du contenu de l'Univers actuel, il est possible de mieux comprendre les phases d'expansion passées (Figure B.2). Le modèle décrit un Univers primordial dominé par un plasma de particules relativistes très énergétiques, qui intéragissent fortement, avec une grande densité d'énergie. L'Univers se refroidit ensuite du fait de l'expansion, menant à la dilution de la densité de particules et à la diminution de leur énergie moyenne. Les particules massives de matière, en premier lieu celles de matière noire, deviennent non-relativistes et finissent par dominer le contenu en énergie. La formation des structures que sont les galaxies, puis les clusters de galaxies, a lieu au cours de cette phase de domination de la matière noire

froide. Enfin, la densité d'énergie de l'énergie sombre, qui n'est pas diluée par l'expansion, finit par dominer le contenu en énergie pour donner lieu à l'accélération de l'expansion de l'Univers.

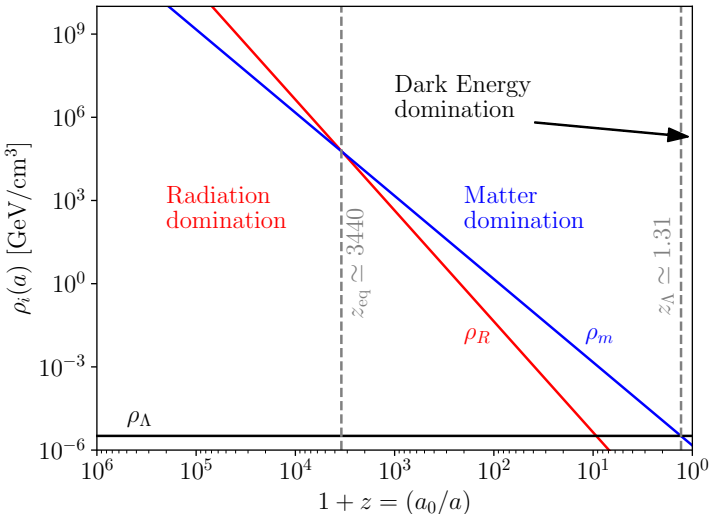

Figure B.2: *Evolution des différentes composantes de l'Univers en terme de densité d'énergie, en fonction du décalage vers le rouge (facteur d'échelle ou taille relative de l'Univers par rapport à sa taille actuelle).*

Histoire thermique de l'Univers et densités reliques

Au cours de l'ère de domination de la radiation, l'Univers primordial est rempli de particules relativistes interagissant intensément et formant un bain à l'équilibre thermique à une température très élevée. À mesure que l'Univers se dilate, le plasma chaud se dilue, et les particules relativistes perdent de l'énergie en raison du décalage vers le rouge relativiste de leurs fréquences. La température du plasma diminue, les particules massives deviennent rapidement non-relativistes, et certains taux d'interaction entre les particules du plasma sont réduits. Cela entraîne un départ progressif hors de l'équilibre thermique des différents types de particules. Le découplage d'un type de particule initialement à l'équilibre correspond au moment où le taux d'interaction, qui maintient l'équilibre de ce type de particules avec les autres au sein du bain thermique, devient insuffisant par rapport à l'expansion caractérisée par le taux d'expansion $H(T)$ (ou Hubble rate).

Les différentes particules du Modèle Standard, mais également les hypothétiques particules des théories au-delà du Modèle Standard, peuvent être initialement à l'équilibre thermique du fait de leus interactions et subir ce découplage par la suite, laissant une densité relique de particules observables aujourd'hui. Certains découplages sont cruciaux pour comprendre l'évolution cosmologique:

- La BBN se distingue comme l'une des fenêtres les plus fiables sur les premiers instants de l'Univers. Le début de la BBN s'est produit à une époque où la température du bain thermique est comprise entre $T \sim 1$ MeV et $T \sim 10$ keV. Il est supposé que le contenu en particules à l'époque de la BBN est donné par le Modèle Standard et que les quarks sont confinés dans les hadrons à ces échelles d'énergie. Le deuxième ingrédient important est qu'une asymétrie baryonique doit déjà présente à l'époque de la BBN, de l'ordre de $\frac{n_b - \bar{n}_b}{s} \sim 10^{-10}$, jusqu'à ce que les anti-baryons s'annihilent avec les baryons autour de $T \sim 1$ MeV, et que la fraction restante se découple du bain thermique. La BBN permet alors d'expliquer la production de la majeure partie de l'hélium-4 et du deutérium présents dans l'Univers, ainsi qu'une fraction de l'hélium-3 et du lithium-7, par des réactions de fusions nucléaires énergétiquement favorisées à ces températures. La BBN offre un test crucial pour le Modèle Standard de la Cosmologie, confirmé par des données observationnelles avec un très haut niveau de précision. Ainsi, il est bien établi que de petites modifications de la Physique de l'Univers primordial au-delà du Modèle Standard, à l'époque de la BBN, devraient entraîner des déviations observables dans les abondances primordiales des éléments légers, imposant donc des contraintes strictes sur les scénarios de nouvelle Physique.

- À la fin du processus de BBN, le bain thermique est peuplé de photons, d'électrons et de protons en interaction, ainsi qu'une fraction de noyaux d'autres éléments légers produits. Les densités d'électrons et de protons sont fortement réduites par le fait que la température du bain thermique décroit sous leur masse (limite non-relativiste), mais les protons et électrons restent couplés par des processus de Coulomb $p + e^- \leftrightarrow p + e^-$. Autour d'un âge de l'Univers de $t \simeq 380\ 000$ ans, le bain thermique atteint une température de $T \sim 1$ eV. À ce stade, la réaction qui était en équilibre $p + e^- \leftrightarrow H + \gamma$ commence à produire plus d'hydrogène, car les photons n'ont plus assez d'énergie pour détruire les atomes d'hydrogène stables par ionisation des électrons liés aux protons. Le plasma se recombine graduellement en un gaz d'hydrogène neutre et en photons libres. Après le début de la formation des premiers atomes neutres, le libre parcours moyen des photons dans le bain thermique augmente, car il y a de moins en moins d'électrons et de protons ionisés dans le plasma avec lesquels ils peuvent interagir par des diffusions Compton $\gamma + e^- \leftrightarrow \gamma + e^-$. Lorsque les photons sont totalement découplés des électrons et protons, ce qu'on appelle la surface de dernière diffusion, les photons du CMB n'interagissent plus tout en restant relativistes et commencent à se propager librement dans toutes les directions, en conservant la même fonction de distribution d'équilibre. À mesure que l'Univers se dilate et que les photons se propagent, la température de ce rayonnement de fond diminue jusqu'à sa valeur actuelle de $T_0 \approx 2,725K$, tout en conservant une distribution de corps noir quasi-parfaite.

Les modèles les plus étudiés pour expliquer la génération d'une densité relique de matière

noire considère que les particules de matière noire ont suivi la même histoire thermique que les particules du Modèle Standard dans le plasma chaud, avant de subir un découplage. Cela présente l'avantage de ne se baser que sur la description microscopique du modèle de matière noire, notamment les couplages avec les particules du Modèle Standard, ce qui permet ensuite de prédire pour les interactions de particules de matière noire dans les expériences de détection en laboratoire. Dans le scénario standard des WIMPs (particules massives interagissant faiblement), les particules de matière noire sont initialement à l'équilibre thermique. Cependant, lorsque la température devient inférieure à la masse de ces WIMPs (régime non-relativiste), le taux de production des particules de matière noire devient rapidement inférieur au taux d'expansion, ce qui entraîne une diminution de la densité de matière noire, la matière noire pouvant s'annihiler sans être produite à nouveau. Dans les modèles de WIMPs, il est naturel de considérer que le candidat de matière noire possède une masse typique $m_\chi \sim \text{GeV} - \text{TeV}$, proche de l'échelle électrofaible au sein du Modèle Standard. Cette hypothèse est naturelle puisque le mécanisme de Higgs explique les masses des particules fondamentales autour de cette échelle d'énergie. Rapidement après, la matière noire se découple complètement du bain thermique et n'est ensuite plus que diluée par l'expansion de l'Univers. La densité relique de matière noire dans ces modèles dépend uniquement de la section efficace d'interaction moyennée $\langle \sigma v \rangle$ (voir Figure B.3). On peut montrer alors qu'une masse de matière noire de l'ordre de l'échelle électrofaible, $m_\chi \sim 100$ GeV et une section efficace électrofaible typique $\sigma \sim 10^{-9}$ GeV$^{-2} \approx 10^{-26}$ cm^3 s^{-1} reproduisent la densité relique observée de matière noire comme inféré par les relevés cosmologiques. Ce « miracle » a motivé le développement de modèles de WIMPs pour expliquer la génération de matière noire. En particulier, la simplicité du mécanisme réside dans le fait qu'il ne dépend pas des conditions initiales avant la thermalisation.

Cependant, malgré des investigations poussées dans des expériences dédiées de détection directe et indirecte de matière noire, l'absence de tout signal expérimental a fortement contraint les modèles de WIMPs les plus simples (voir Figure B.3). Pour faire face à ces fortes contraintes expérimentales, d'autres hypothèses sont étudiées. Ainsi, lorsque les particules de matière noire interagissent très faiblement avec les autres particules, elles peuvent ne jamais atteindre l'équilibre thermique dans l'Univers primordial. La production de matière noire peut alors encore être réalisée par le mécanisme de "freeze-in", à partir des collisions ou des désintégrations de particules, sans atteindre l'équilibre thermique. Parmi ces modèles de freeze-in, une possibilité a en particulier motivé les travaux réalisés au cours de cette thèse. Le mécanisme de production peut être sensible à la Physique modélisant des processus à très hautes énergies (UV), ou à des conditions initiales établies lors des premières phases d'évolution du bain thermique. Cela s'oppose au scénario de matière noire thermique associé au mécanisme de découplage, où la matière noire atteint en premier lieu l'équilibre thermique, effaçant les effets des conditions initiales ou de la Physique UV. Cette caractéristique de sensiblité aux conditons initiales et à la Physique des hautes énergies dans le cas du "freeze-in" peut être utilisée

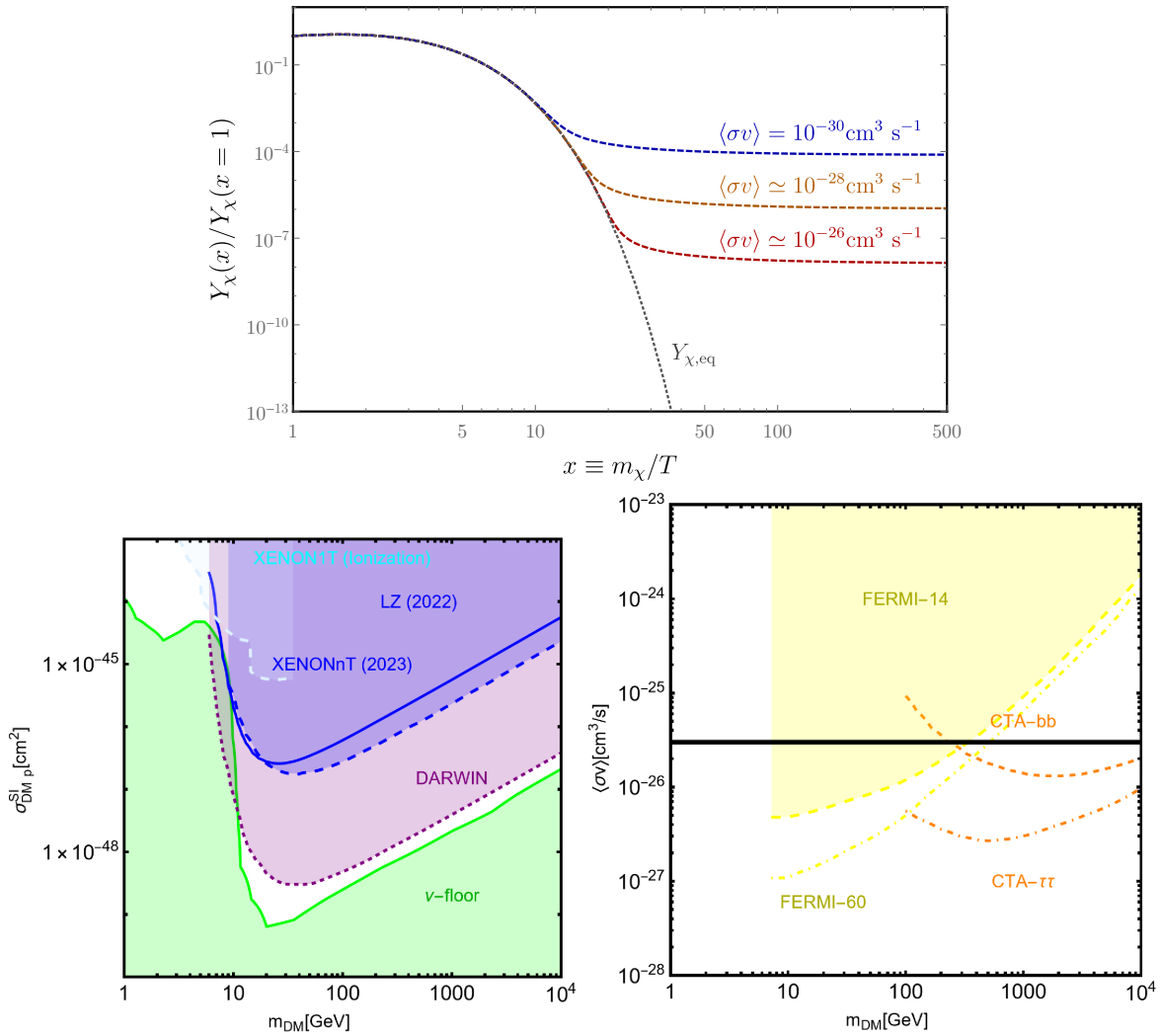

Figure B.3: *Haut: Évolution de la densité de matière noire en fonction de la température, pour une matière noire initialement à l'équilibre avec le bain thermique. Les courbes colorées représentent les solutions numériques de l'équation de Boltzmann dans un modèle de matière noire à l'équilibre thermique, intéragissant faiblement avec les particules du bain thermique (WIMPs), pour différentes valeurs de la section efficace d'interaction $\langle\sigma v\rangle$ = constante. La courbe noire en pointillés correspond à la distribution thermique. Bas: Contraintes sur les WIMPs (actuelles en lignes pleines, projetées en pointillés). Le panneau de gauche montre les limites de détection directe sur m_χ et la section efficace de l'interaction WIMP-proton, tandis que le panneau de droite se réfère aux contraintes de détection indirecte (rayons cosmiques) sur m_χ et $\langle\sigma v\rangle$. Figures tirées de [65, 70].*

pour contraindre différents modèles UV de matière noire intéragissant très faiblement. Un des objectifs de cette thèse de doctorat est la description d'un nouveau mécanisme de production de matière noire, impliquant l'interaction gravitationnelle au cours du reheating après la phase primordiale d'inflation cosmologique.

Enfin, un autre questionnement majeur en Cosmologie et Physique des particules a motivé les travaux réalisés au cours de cette thèse. Différentes observations indiquent que notre Univers est asymétrique en terme d'abondance de baryons et d'antibaryons. La valeur précise

de l'asymétrie est obtenue à partir de deux sources d'observation indépendantes. La première est l'abondance des noyaux légers et la BBN, dont les prédictions dépendent fortement du ratio baryon/photon et donc de l'asymétrie initiale entre baryons et anti-baryons. La seconde méthode repose sur les mesures des anisotropies de température du CMB, également sensible à l'abondance relative de baryons par rapport aux photons. Ces différentes observations indiquent qu'il doit exister une asymétrie entre les baryons et les antibaryons du Modèle Standard avant la BBN et la recombinaison donnant un ratio baryons/photons $\eta_B \simeq 6 \times 10^{-10}$. Étant donné que les conditions initiales du scénario du Big Bang suggèrent une abondance égale de baryons et d'antibaryons en raison de l'équilibre thermique à haute température, l'asymétrie baryonique observée implique l'existence d'un processus dynamique permettant de s'écarter de cet équilibre entre baryons et antibaryons, connu sous le nom de baryogenèse. La baryogenèse ou la leptogenèse nécessite de nouvelles sources de violation de la symétrie CP provenant d'une Physique au-delà du Modèle Standard. Cette nouvelle Physique doit également permettre de préserver l'asymétrie baryonique face aux processus non-perturbatifs appelés sphalérons électrofaibles. Dans cette thèse, nous investiguons un modèle simple de leptogenèse, au cours du reheating après l'inflation. Dans ce cas, l'asymétrie est issue des processus de violation du nombre leptonique par les désintégrations hors équilibre de neutrinos lourds (neutrinos droits). Ces désintégrations des neutrinos lourds en leptons légers et en bosons de Higgs peuvent violer les symétries C et CP, conduisant à la production d'un excès d'antileptons par rapport aux leptons (voir Figure B.4).

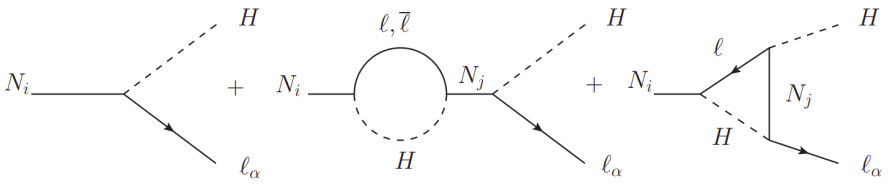

Figure B.4: *L'asymétrie CP dans le modèle Seesaw de type I résulte de l'interférence entre les diagrammes tree-level et les diagrammes à 1-boucle. Figure tirée de [58].*

L'asymétrie des leptons ainsi générée peut ensuite être convertie en asymétrie baryonique par les sphalérons électrofaibles, qui violent $B + L$ (baryons + leptons) mais conservent $B - L$ (baryons - leptons), et sont à l'équilibre à des températures supérieures à la transition de phase électrofaible. Dans cette thèse, nous nous concentrons sur un modèle de leptogenèse non-thermale où les neutrinos droits massifs ne sont pas à l'équilibre dans le bain thermique avant leur désintégration. Nous étudions la production gravitationnelle de tels neutrinos droits massifs pendant le reheating après l'inflation.

Conditions initiales: inflation et reheating

L'Univers n'est pas homogène et isotrope aux petites échelles, et nous observons des structures telles que des galaxies, des amas de galaxies, et des objets à des échelles très réduites. La formation de structures est impossible dans un état de parfaite homogénéité et isotropie. Il faut également considérer de petites fluctuations, permettant à un processus dynamique de formation de structures de débuter à partir de petites "graines" d'inhomogénéités. Il est aujourd'hui bien compris que toutes les structures dans l'Univers proviennent de fluctuations initiales dans la densité des différentes particules, amplifiées ensuite par l'attraction gravitationnelle. Ces fluctuations initiales doivent également être présentes dans les phases primordiales, notamment au moment de l'émission des photons et de la recombinaison des atomes d'hydrogènes, laissant des empreintes visibles dans le CMB. Ainsi, de faibles anisotropies de température du CMB ont été mesurées au 20ème siècle (voir Figure B.5), une observation cruciale pour étudier ces fluctuations initiales dans les composants de l'Univers.

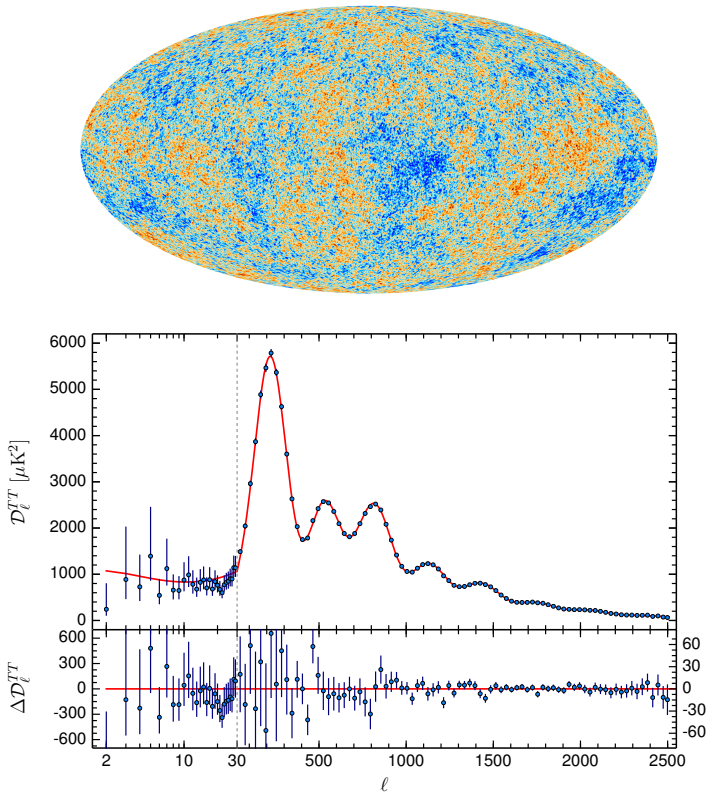

Figure B.5: *Gauche: Les anisotropies de température du CMB telles qu'observées par le satellite PLANCK. Le contraste de température est proche de* $\Delta T/T_0 \sim 10^{-5}$ *sur l'ensemble de la carte. Droite: Spectre de puissance angulaire des anisotropies de température du CMB. En ligne rouge continue, le meilleur ajustement au spectre dans le modèle* ΛCDM*. Figure tirée de [90].*

La forme spécifique du spectre de puissance (Figure B.5) mesurée dans les anisotropies de température du CMB renseigne sur les conditions initiales pour ces perturbations cosmologiques.

Cependant leur existence n'est pas prédite par le modèle cosmologique standard. De plus, le niveau d'anisotropie primordiale est très faible (dans le CMB on mesure un contraste de température de $\Delta T/T_0 \approx 10^{-5}$) tandis que la taille typique des régions causalement connectées (l'horizon causal) est faible au moment de l'émission du CMB, comparée à la taille de l'Univers aujourd'hui (régions d'où nous parviennent les photons aujourd'hui). On peut estimer qu'au moment de l'émission du CMB, il y avait plus de 10^4 zones déconnectées, mais dans le même état d'équilibre thermique, ce qui semble difficilement explicable sans contacte causal. De plus, l'analyse du CMB nous conduit à la conclusion que l'Univers actuel est spatialement plat (euclidien). Pourtant, cette courbure spatiale devrait s'accentuer du fait de l'expansion de l'Univers et aurait dû être extrêmement faible dans le passé: c'est le problème de réglage fin des conditions initiales de courbures et d'inhomogénéité. Ces problèmes correspondent au fait que l'expansion ne peut être que décélérée dans les scénarios cosmologiques standards. C'est pourquoi, une théorie modifiant les tous premiers instants de l'évolution cosmologique a été proposée à la fin du 20ème siècle. Cette théorie suppose l'existence d'une phase d'expansion accélérée précédant l'Univers thermique: c'est l'inflation cosmologique. Elle résout le problème des conditions initiales d'homogénéité et de courbures par la croissance exponentielle de la taille de l'Univers pendant cette phase et fournit un mécanisme pour la formation des structures à grande échelle observées aujourd'hui. Cependant, des défis subsistent, notamment l'identification d'une description microscopique de l'inflation et la modélisation précise de l'ère post-inflationnaire appelée reheating, au cours de laquelle l'univers est repeuplé en matière et en rayonnement.

Les modèles les plus simples d'inflation impliquent un seul champ scalaire ϕ, appelé l'inflaton, couplé minimalement à la gravité et dominant le contenu masse-énergie de l'Univers dans les premières phases d'évolution. En particulier, si l'on peut négliger l'énergie cinétique du champ scalaire, dominée alors par son énergie potentielle, ce champ scalaire imite l'effet d'une constante cosmologique en termes de densité et de pression, résultant en une phase d'expansion accélérée. En imposant les conditions dites de "slow-roll" au potentiel de l'inflaton, le champ scalaire roule lentement vers son minimum de potentiel réalisant la phase d'inflation. Cette phase de slow-roll est naturellement satisfaite si le potentiel est suffisamment plat, garantissant que la descente du champ soit lente en raison de la dissipation causée par l'expansion. En fonction de la trajectoire du champ et de la forme du potentiel, différents modèles peuvent être construits. Dans cette thèse, nous considérons exclusivement des modèles à "grand champ", dans lesquels la valeur initiale de l'inflaton est éloignée de son minimum et prends une grande valeur supérieure à la masse de Planck ($\phi_i > M_P$). En particulier, nous avons basé notre analyse sur une des modèles qui sont bien motivés par la Physique des hautes énergies et la théorie de supergravité, qui prédisent une inflation avec des signatures observables en accord avec les données du CMB (potentiel représenté Figure B.6). Au sein de cette classe de solutions, les modèles convergent vers les mêmes prédictions pour la phase de slow-roll.

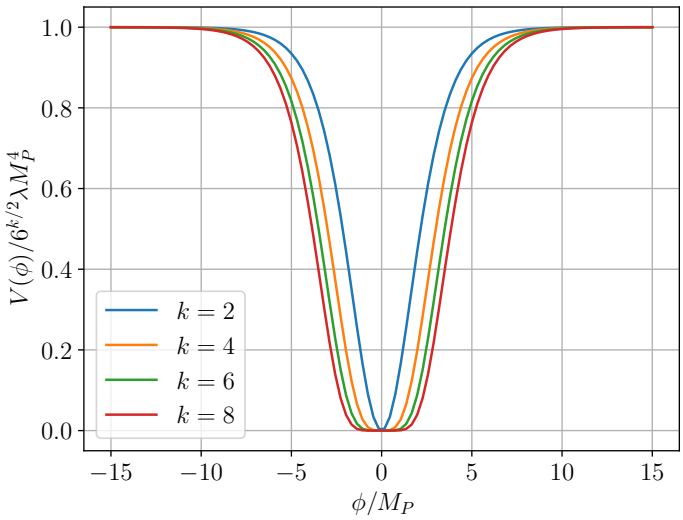

Figure B.6: *Potentiel de l'inflaton pour les modèles issus des théories de supergravité,* $V(\phi) = \lambda M_P^4 \left[\sqrt{6}\tanh\left(\frac{\phi}{\sqrt{6}M_P}\right)\right]^k$*, pour différentes valeurs de* k*.*

Au-delà de résoudre le problème de l'horizon et de l'homogénéité, l'inflation est une théorie prédictive qui explique la génération de perturbations cosmologiques à partir d'effets quantiques. Les petites fluctuations quantiques du champ scalaire $\delta\phi(x,t)$ autour de sa valeur dans le vide (VEV) sont en fait étirées pendant la phase d'expansion accélérée et persistent longtemps après la fin de l'inflation. La génération de perturbations adiabatiques (perturbations de la courbure) est une prédiction générale des modèles d'inflation. De plus, la distribution de ces perturbations primordiales aux différentes échelles physiques est prédite comme étant presque invariante d'échelle en raison du slow-roll. Ceci est en parfait accord avec les observations des anisotropies de température du CMB et les conditions initiales des perturbations cosmologiques.

Un modèle inflationnaire complet nécessite également un mécanisme pour mettre fin à l'ère d'expansion accélérée et expliquer la transition vers l'Univers thermique. En effet, la période d'expansion exponentielle doit se terminer par un transfert efficace de l'énergie stockée dans le condensat d'inflaton durant l'inflation vers les différentes composantes d'un bain thermique domninat ultérieurement l'évolution de l'Univers. L'inflation se termine lorsque l'énergie potentielle associée au champ d'inflaton devient inférieure à son énergie cinétique, mettant fin au régime de slow-roll. Cela se produit lorsque l'inflaton se rapproche du minimum de son potentiel et qu'il commence à osciller autour de ce minimum (voir Figure B.7).

Ce condensat froid oscillant doit se désintégrer en matière et en rayonnement constitués de particules du Modèle Standard et potentiellement de matière noire. La matière et le rayonnement produits doivent ensuite atteindre un équilibre thermique à une température supérieure à $T \gtrsim 1\,\text{MeV}$ pour permettre à la BBN de se dérouler correctement. Cette transition du conden-

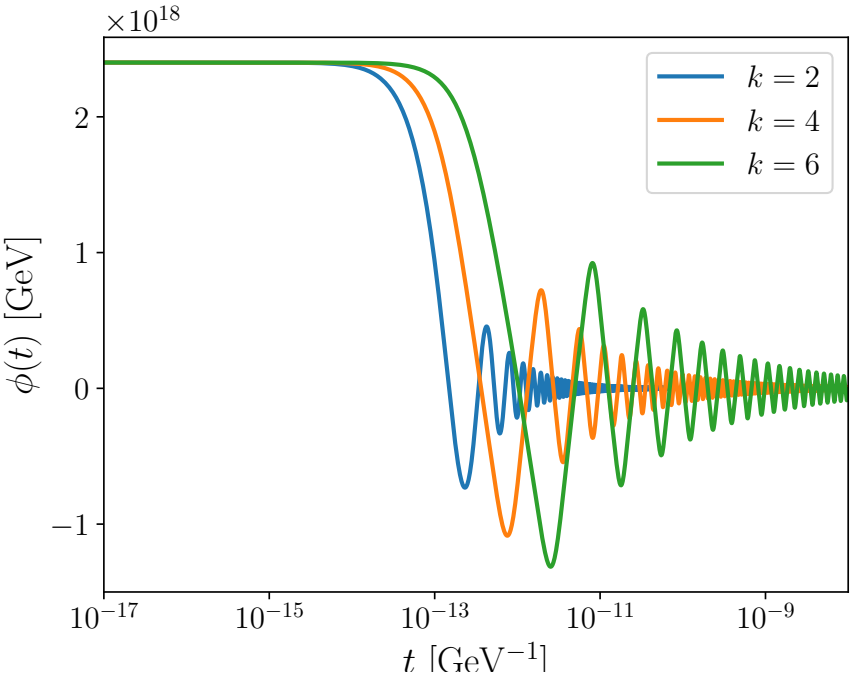

Figure B.7: *Évolution de l'amplitude du condensat d'inflaton après l'inflation dans le potentiel présenté plus haut, pour différentes valeurs de* $k = 2, 4, 6$.

sat vers le bain thermique chaud est appelée reheating. Quand cette tranisition est terminée, la température effective de l'Univers est alors appelée la température de reheating notée T_{RH}. Il est important de souligner que le principal défi des modèles de reheating est la compréhension de la dynamique d'un système de champs couplés dans un régime semi-classique, mais où les effets quantiques jouent encore un rôle important. Deux approches sont adoptées:

- Pour prendre en compte les interactions du condensat d'inflaton avec les autres champs, nous devons résoudre les équations de transport (Boltzmann) pour l'inflaton et pour les produits de ses interactions. Sous l'hypothèse de faibles interactions, on peut négliger les rétroactions des produits sur l'évolution de l'inflaton pendant les oscillations. Si le nombre d'occupation pour les quanta produits reste faible, de sorte que les facteurs d'amplification ou de blocage dû à la statistique quantique peuvent être ignorés, on peut utiliser une approche perturbative pour résoudre l'équation de Boltzmann. Nous devons alors sommer les contributions de chaque mode d'oscillation de l'inflaton pour calculer le taux de production. On peut interpréter l'amplitude de transition comme une probabilité d'extraction de deux quanta à partir du condensat d'inflaton. Nous considérons différents couplages perturbatifs (voir Figure B.8) entre l'inflaton et des champs de différents spins, représentant les degrés de liberté du Modèle Standard.

- Si les couplages sont forts, des effets non perturbatifs dans l'excitation des champs couplés à l'inflaton peuvent intervenir pendant les oscillations. Plus précisément, des résonances

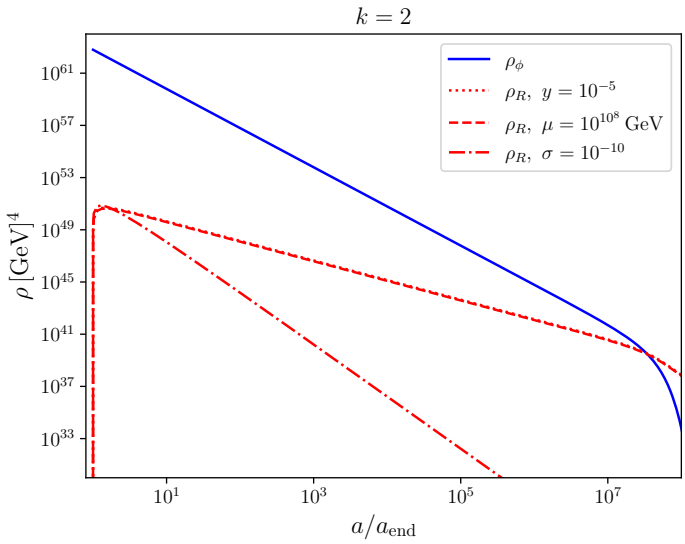

Figure B.8: *Évolution des densités d'énergie en fonction du facteur d'échelle après l'inflation. En bleu, la densité d'énergie de l'inflaton (pour le potentiel tel que $k = 2$), et en rouge, la densité d'énergie de la radiation, pour différents canaux de production étiquetés par la constante de couplage associée.*

paramétriques peuvent déclencher une instabilité dans l'évolution des modes et une explosion de la production de particules avec un nombre d'occupation qui croît exponentiellement. Nous faisons généralement référence à ces effets sous le nom de preheating, car ils se produisent au début de la phase d'oscillations de l'inflaton. Ils laissent ensuite un état classique de haute occupation pour les champs, mais des processus perturbatifs sont généralement toujours nécessaires pour transférer efficacement l'énergie à la fin du processus de reheating.

Dans ce travail de thèse, nous avons considéré principalement une approche perturbative, du fait des couplages faibles entre l'inflaton et les autres champs qui ont été étudiés. Nous avons également analysé l'efficacité du processus en fonction de la forme du potentiel d'inflaton autour du minimum. Même si la forme exacte du potentiel à la fin de l'inflation est inconnue, elle peut souvent être approchée autour de son minimum par une fonction polynomiale de ϕ. Dans de nombreux modèles d'inflation, le potentiel d'inflaton autour de son minimum est dominé par un terme quadratique $V(\phi) = \frac{1}{2}m_\phi^2\phi^2$ (le modèle de Starobinsky en est un exemple). Pour un potentiel dont l'expansion autour de son minimum est $V(\phi) = \lambda\phi^k$ avec $k > 2$, le reheating est plus compliqué à modéliser et nécessite une analyse plus approfondie.

Cependant, nous ne pouvons pas exclure systématiquement la présence d'un terme de masse pour l'inflaton $\frac{1}{2}m_\phi^2\phi^2$, qui peut être initialement négligeable mais qui peut devenir dominant lorsque les oscillations de ϕ sont amorties au cours par l'expansion. La présence de ce terme, même s'il est faible, modifie alors significativement le transfert d'énergie de l'inflaton vers les autres champs. Nous étudions l'impact d'un tel terme de masse sur les processus de reheating,

alors que l'équation d'état du condensat d'inflaton change de $w_\phi = \frac{1}{3}$ à $w_\phi = 0$. Nous calculons les effets sur la température de reheating pour les cas de désintégrations de l'inflaton (vers des fermions, des scalaires ou des vecteurs) ou de l'annihilation de l'inflaton (vers des scalaires ou des vecteurs). Pour les collisions produisant des scalaires et en l'absence de désintégration, il reste toujours une densité résiduelle d'inflaton qui agit comme de la matière noire froide. Nous considérons également brièvement l'effet du terme de masse sur les rétroactions des perturbations d'inflaton produites sur le condensat d'inflaton (fragmentation du condensat).

Production gravitationnelle de particules

Dans cette thèse, nous explorons principalement la production de particules dans l'Univers primordial à la fin de l'inflation, pendant le processus de reheating. Nous étudions plus spécifiquement les interactions gravitationnelles dans un scénario minimal de reheating, produisant les différentes reliques cosmologiques. L'interaction minimale et irréductible qui doit exister entre la matière noire et les particules du Modèle Standard est médiée par les gravitons. L'origine de ce couplage est le couplage effectif, dans le cadre de la relativité générale, entre le tenseur énergie impulsion des différents champs et les perturbations de la métrique (les gravitons) via le Lagrangien effectif $\sqrt{-g}\mathcal{L} \supset -\frac{1}{M_P} h_{\mu\nu} T^{\mu\nu}$. Comme ce couplage est inévitable, il fournit une limite inférieure au nombre de particules produites par le processus d'échange de gravitons (s-channel). À la fin de l'inflation, pendant la période de reheating, l'énergie disponible du champ inflationnaire conduit à une production gravitationnelle significative, qui peut être plus efficace que la production à partir du bain thermique. Nous avons évalué ces contributions et trouvé les contraintes pour obtenir la densité relique observée de matière noire dans l'espace des paramètres donné par la masse des particules de matière noire et la température de reheating (Figure B.9). Nous considérons en premier lieu l'échange d'un graviton, $h_{\mu\nu}$, entre l'inflaton ou des particules du bain thermique et des particules de matière noire (bosoniques, fermioniques).

Les particules relativistes du Modèle Standard peuvent également être produites efficacement par l'inflaton via des effets gravitationnels pendant le reheating, pour atteindre rapidement une densité de radiation très élevée (Figure B.10). Cette production est de fait inévitable et peut mener à des températures très élevées pour le bain thermique juste après l'inflation $T \sim 10^{12}$ GeV. Ce résultat est indépendant du potentiel inflationnaire considéré comme nous l'avons démontré.

Nous avons ensuite étendu cette analyse en introduisant des couplages non minimaux à la gravité via le terme de courbure $\xi_i \mathcal{R} S_i^2$ qui générant des couplages effectifs entre les différents secteurs (S_i pouvant être respectivement l'inflaton, le champ scalaire de matière noire, ou le champ de Higgs). Pour ne pas compromettre l'inflation et maintenir un terme cinétique canonique pour l'inflaton pendant sa phase d'oscillation, nous imposons une limite de faible champ, ce qui contraint le couplage non-minimal $\xi_\phi \ll 1$. Ainsi, le seul couplage non minimal

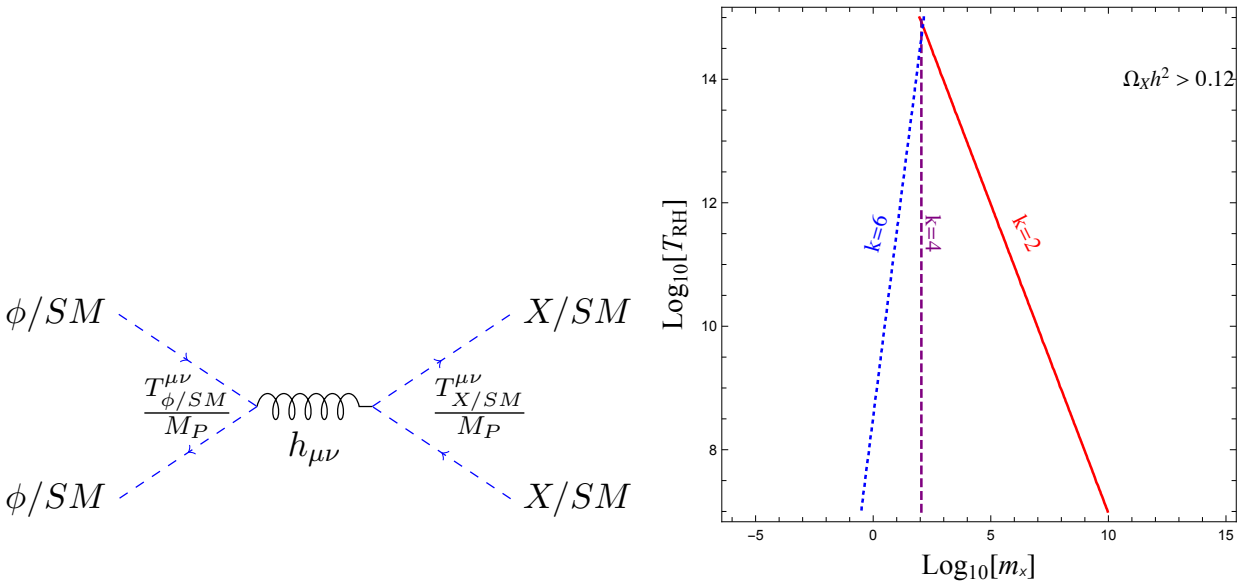

Figure B.9: *Gauche: Diagramme de Feynman pour la production gravitationnelle de particules par échange de gravitons. Droite: Courbes respectant la contrainte de densité relique de matière noire* $\Omega h^2 = 0.12$ *dans le cas d'une matière noire scalaire, en fonction de la masse de la particule* m_χ *et la température de reheating atteinte* T_{RH} *et pour différents potentiels d'inflaton (paramètre* k*).*

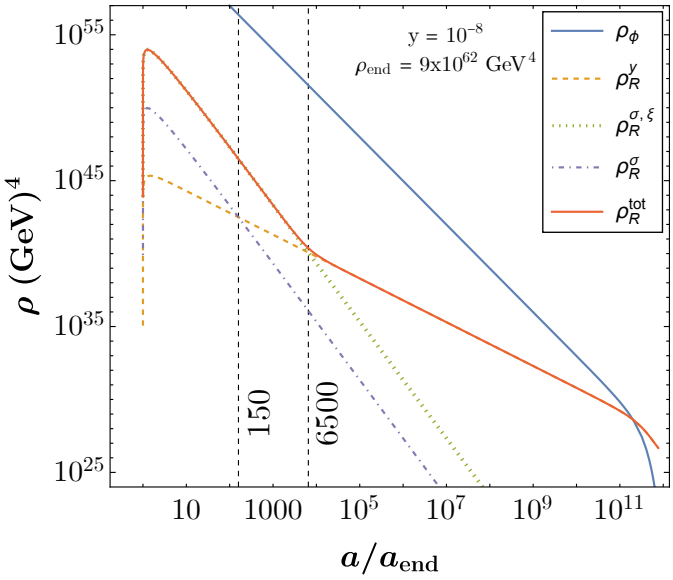

Figure B.10: *Évolution de la densité de l'inflaton (en bleu) et de la densité totale de rayonnement (en rouge), avec la densité de rayonnement produite par les désintégrations de l'inflaton (pointillés orange) et les processus gravitationnels minimaux (pointillés violets) et avec un couplage non-minimal à la gravité (pointillés violets). Le maximum atteint par la production gravitationnelle minimale (courbe violette) correspond à une température équivalente de* $T_{\mathrm{max}} \sim 10^{12}$ GeV.

pertinent considéré est celui du champ de Higgs ξ_h. Il est alors utile de redéfinir le champ métrique via la transformation conforme appropriée pour redéfinir la théorie dans un cadre de gravité usuelle mais avec des couplages effectifs supplémentaires entre les champs. En développant l'action dans la limite de faibles champs, nous obtenons des termes cinétiques

canoniques effectifs et déduisons les interactions au premier ordre induites par le couplage non minimal. Ces nouveaux couplages induisent une production plus efficace de matière noire et de radiation pendant le reheating (voir Figures B.10 et B.11).

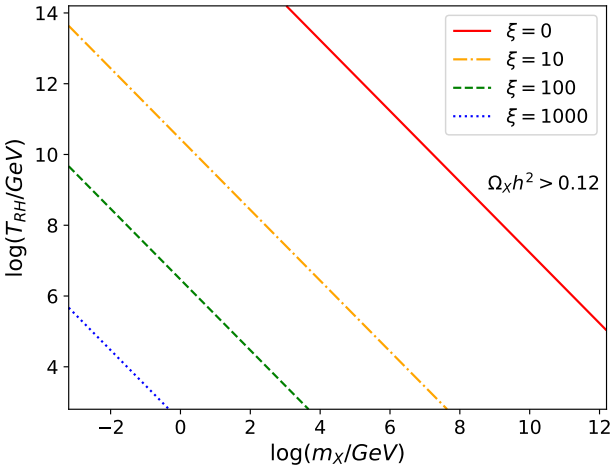

Figure B.11: *Région de l'espace des paramètres respectant la contrainte de densité relique de matière noire* $\Omega_X h^2 = 0.12$ *pour un champ scalaire et différentes valeurs des couplages non-minimaux* $\xi = \xi_h = \xi_X$ *dans le cas de la production gravitationnelle. Les contributions minimales et non minimales sont toutes deux prises en compte. Le potentiel d'inflaton est fixé avec le paramètre* $k = 2$.

Nous avons également montré que le reheating par les seuls processus d'échange de gravitons nécessite un terme $V(\phi) \sim \phi^k$ dans le potentiel pour l'inflaton avec $k > 8$. Ce mécanisme de reheating gravitationnel entraîne également une faible température de reheating (Figure B.12). Cela a pour conséquence une importante amplification du spectre de puissance des modes tensoriels excités pendant l'inflation, les ondes gravitationnelles primordiales (Figure B.12). Ceci est exclu en raison d'une génération excessive de radiation supplémentaire sous forme d'ondes gravitationnelles à l'époque de la BBN. Le spectre présente une amplification distinctive qui dépend de la forme du potentiel de l'inflaton dans lequel il oscille, avec comme densité relique d'ondes gravitationnelles $\Omega_{\rm GW} h^2 \propto f^{\frac{k-4}{k-1}}$. Les contraintes sur les degrés de liberté relativistes effectifs, $\Delta N_{\rm eff}$, au moment de la BBN et du découplage du CMB se traduisent par une contrainte sur les ondes gravitationnelles reliques $\Omega_{\rm GW} h^2 \lesssim 5.6 \times 10^{-6}\, \Delta N_{\rm eff}$. Cette limitation du reheating gravitationnel minimal motive l'introduction, comme une généralisation naturelle, de couplages non minimaux à la gravité, en particulier pour le champ de Higgs du Modèle Standard. Ce couplage non minimal augmente la température de reheating atteinte par ces portails gravitationnels. Au-delà de la contrainte imposée par les ondes gravitationnelles primordiales, cet effet permet d'envisager un test observationnel de tels scénarios de reheating avec de faibles températures pour différentes équations d'état de l'inflaton (différents potentiels). De futurs détecteurs d'ondes gravitationnelles pourraient permettre de contraindre l'espace des paramètres pour le reheating, et ceci de manière indépendante du modèle de couplage de l'inflaton avec la matière (voir Figure B.12).

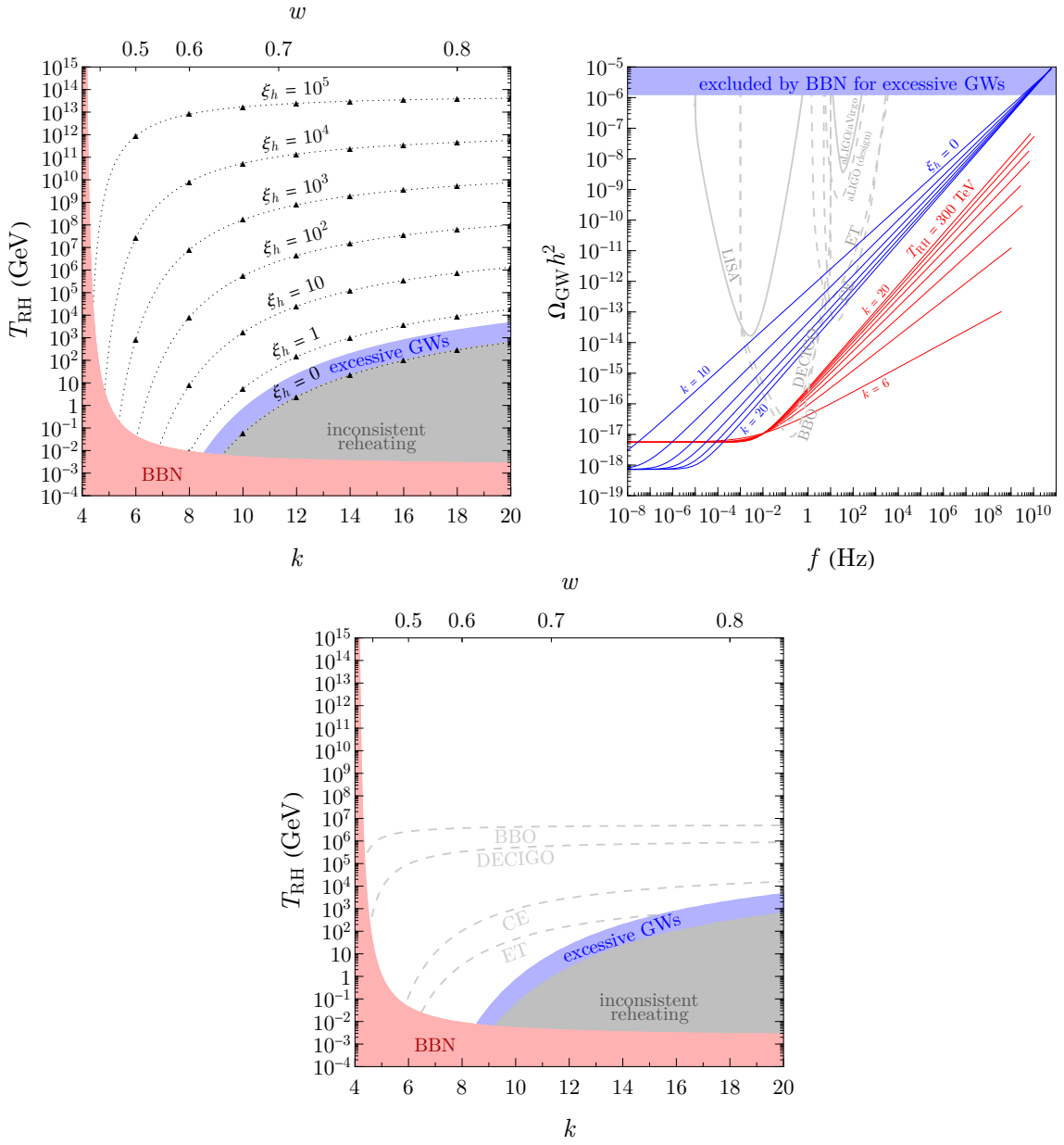

Figure B.12: *Haut gauche: Température de reheating $T_{\rm RH}$ atteinte par la production gravitationnelle incluant la contribution non minimale via le couplage ξ_h. La région rouge est exclue en raison d'une température de réchauffement trop basse pour un succès de la BBN. Haut droite: Densité relique des ondes gravitationnelles primordiales en fonction de la fréquence, pour différents couples (ξ_h, k) en bleu, et pour une $T_{\rm RH}$ fixée avec différents k en rouge. La région bleue est exclue par la BBN du fait de l'excès d'onde gravitationnelle. Les courbes de sensibilité des futurs détecteurs de GWs sont montrées. Bas: Projection des contraintes futures des détecteurs d'ondes gravitationnelles dans l'espace des paramètres $(T_{\rm RH}, k)$. La région bleue est déjà exclue en raison d'un excès de la relique d'ondes gravitationnelles.*

Enfin, nous montrons qu'un scénario minimal utilisant uniquement ces "portails gravitationnels" est capable de générer simultanément la densité relique observée de matière noire ainsi que l'asymétrie baryonique via la leptogenèse non-thermale, tout en produisant un bain thermique suffisamment chaud après l'inflation. Nous montrons qu'il est possible de produire les

neutrinos droits lourds pendant le reheating via les interactions gravitationnelles, à partir du condensat d'inflatons. Cette production peut être alimentée, soit par des bosons de Higgs du Modèle Standard en échangeant des gravitons et en étant médiée par le couplage non minimal à la gravité ξ_h, soit directement à partir de l'inflaton médiée par la gravité. Ces neutrinos droits massifs sont par ailleurs motivés par le mécanisme de "seesaw" pouvant expliquer la faible masse des neutrinos actifs. L'abondance de neutrinos droits peut ensuite conduire à l'asymétrie baryonique observée (Figure B.13) grâce à la désintégration hors équilibre des RHN violant la symétrie CP. Dans cette perspective, nous dérivons une solution simultanée pour l'abondance de matière noire, l'asymétrie baryonique, et l'origine du bain thermique à partir d'interactions purement gravitationnelles (Figure B.13). En combinant les analyses précédentes, il est possible de contraindre, pour un potentiel dans lequel évolue l'inflaton $V(\varphi)$, l'espace des paramètres (M_{N1}, M_{N2}, ξ_h) en exigeant que la leptogenèse non-thermale, la production de matière noire et le reheating aient une origine commune par les interactions gravitationnelles considérées.

Conclusion

Dans cette thèse, nous avons étudié certains aspects de la production de particules dans l'Univers primordial, un domaine de recherche actuellement au centre d'investigations théoriques, phénoménologiques et expérimentales intenses pour rechercher des indices potentiels de nouvelle Physique. En particulier, nous nous sommes intéressés au processus de reheating, une transition cruciale entre la phase d'inflation et la phase de domination de la radiation. Le reheating est fondamental car il doit expliquer la génération d'un plasma thermique chaud composé de particules du Modèle Standard, ainsi que d'autres reliques cosmologiques, comme la matière noire et potentiellement expliquer l'asymétrie baryonique.

Nous nous sommes concentrés dans cette thèse sur la construction et l'utilisation d'un cadre théorique pour la production gravitationnelle de particules pendant le reheating. Cette thèse illustre l'importance cruciale d'approfondir les recherches sur la phénoménologie des scénarios au-delà du Modèle Standard dans l'Univers primordial. Nous avons mis en avant la possibilité d'un scénario minimal où les différents secteurs interagissent uniquement à travers des interactions gravitationnelles effectives. Nous avons montré que, dans un tel cas simple, la génération de reliques cosmologiques peut être réalisée aisément. Si des contraintes observationnelles sur les ondes gravitationnelles primordiales et la durée du reheating peuvent être prises en compte dans les aspects phénoménologiques de ces modèles, il est nécessaire de poursuivre les efforts théoriques pour relier ces prédictions aux observables cosmologiques ou aux contraintes expérimentales avec précision. Le régime non linéaire des perturbations cosmologiques, qui pourrait être contraint dans de futures campagnes d'observations, pourrait apporter un éclairage sur la dynamique complexe impliquant plusieurs champs couplés après l'inflation cosmologique.

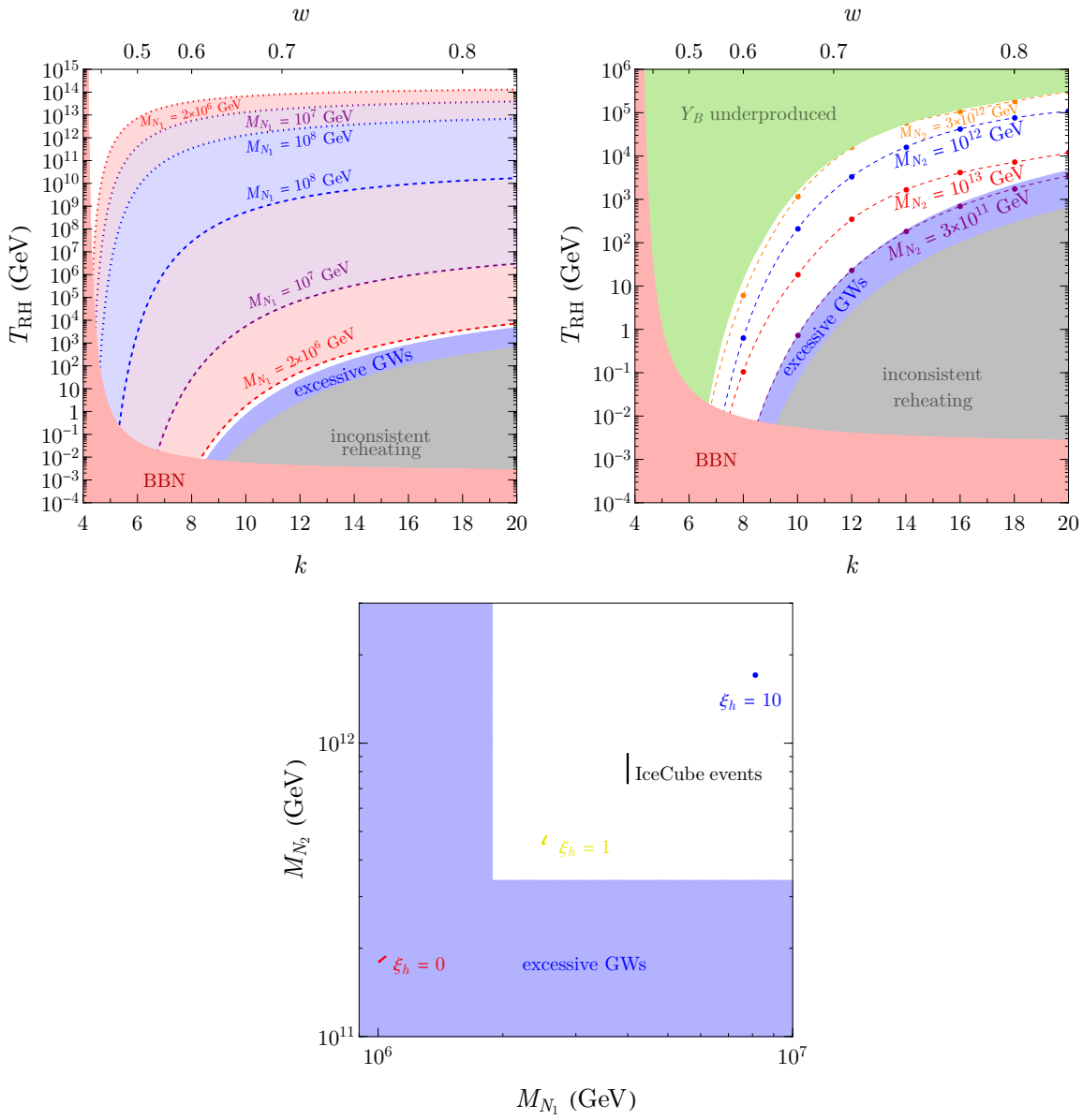

Figure B.13: *Haut gauche: Les régions colorées correspondent aux valeurs de* $(k, T_{\rm RH})$ *avec* $\Omega_{N_1}h^2 \leq 0.12$ *pour trois choix de masse de matière noire* M_{N_1} *(rouge, bleu, violet). Haut droite: Contours de* M_{N_2}*, la masse des neutrinos droits instables qui se désintègrent au cours de la leptogenèse, correspondant à l'abondance baryonique observée dans le plan* $(k, T_{\rm RH})$*. La région verte conduit à une sous-production de baryons en raison de la cinématique de l'interaction lorsque* M_{N_2} *approche de la masse de l'inflaton. Bas: Espace des paramètres viable dans le plan* (M_{N_1}, M_{N_2}) *où les interactions gravitationnelles sont responsables de la densité relique de la matière noire observée, de l'asymmetrie baryonique (produite par les désintégrations de* N_2*) et du reheating, pour* $k \in [6, 20]$*. Les différentes couleurs correspondent à différents* ξ_h*.*

Bibliography

[1] S. Clery, Y. Mambrini, K.A. Olive and S. Verner, *Gravitational portals in the early Universe*, *Phys. Rev. D* **105** (2022) 075005 [2112.15214].

[2] S. Clery, Y. Mambrini, K.A. Olive, A. Shkerin and S. Verner, *Gravitational portals with nonminimal couplings*, *Phys. Rev. D* **105** (2022) 095042 [2203.02004].

[3] B. Barman, S. Cléry, R.T. Co, Y. Mambrini and K.A. Olive, *Gravity as a portal to reheating, leptogenesis and dark matter*, *JHEP* **12** (2022) 072 [2210.05716].

[4] S. Clery, M.A.G. Garcia, Y. Mambrini and K.A. Olive, *Bare mass effects on the reheating process after inflation*, *Phys. Rev. D* **109** (2024) 103540 [2402.16958].

[5] S. Cléry, H.M. Lee and A.G. Menkara, *Higgs inflation at the pole*, *JHEP* **10** (2023) 144 [2306.07767].

[6] N. Bernal, S. Cléry, Y. Mambrini and Y. Xu, *Probing reheating with graviton bremsstrahlung*, *JCAP* **01** (2024) 065 [2311.12694].

[7] E. Hubble, *A relation between distance and radial velocity among extra-galactic nebulae*, *Proc. Nat. Acad. Sci.* **15** (1929) 168.

[8] A. Friedman, *On the Curvature of space*, *Z. Phys.* **10** (1922) 377.

[9] G. Lemaitre, *A Homogeneous Universe of Constant Mass and Growing Radius Accounting for the Radial Velocity of Extragalactic Nebulae*, *Annales Soc. Sci. Bruxelles A* **47** (1927) 49.

[10] A. Einstein, *The Field Equations of Gravitation*, *Sitzungsber. Preuss. Akad. Wiss. Berlin (Math. Phys.)* **1915** (1915) 844.

[11] A. Einstein, *Cosmological Considerations in the General Theory of Relativity*, *Sitzungsber. Preuss. Akad. Wiss. Berlin (Math. Phys.)* **1917** (1917) 142.

[12] E. Di Valentino, O. Mena, S. Pan, L. Visinelli, W. Yang, A. Melchiorri et al., *In the realm of the Hubble tension—a review of solutions*, *Class. Quant. Grav.* **38** (2021) 153001 [2103.01183].

[13] E.W. Kolb and M.S. Turner, *The Early Universe*, *Front. Phys.* **69** (1990) 1.

[14] S. Dodelson, *Modern Cosmology*, Academic Press, Amsterdam (2003).

[15] Planck collaboration, *Planck 2018 results. VI. Cosmological parameters*, *Astron. Astrophys.* **641** (2020) A6 [1807.06209].

[16] Y. Mambrini, *Particles in the dark Universe*, *Springer Ed., ISBN 978-3-030-78139-2* (2021) .

[17] Supernova Search Team collaboration, *Observational evidence from supernovae for an accelerating universe and a cosmological constant*, *Astron. J.* **116** (1998) 1009 [astro-ph/9805201].

[18] Supernova Cosmology Project collaboration, *Measurements of the cosmological parameters Omega and Lambda from the first 7 supernovae at z>=0.35*, *Astrophys. J.* **483** (1997) 565 [astro-ph/9608192].

[19] Supernova Cosmology Project collaboration, *Measurements of* Ω *and* Λ *from 42 High Redshift Supernovae*, *Astrophys. J.* **517** (1999) 565 [astro-ph/9812133].

[20] Supernova Cosmology Project collaboration, *Improved Cosmological Constraints from New, Old and Combined Supernova Datasets*, *Astrophys. J.* **686** (2008) 749 [0804.4142].

[21] Pan-STARRS1 collaboration, *The Complete Light-curve Sample of Spectroscopically Confirmed SNe Ia from Pan-STARRS1 and Cosmological Constraints from the Combined Pantheon Sample*, *Astrophys. J.* **859** (2018) 101 [1710.00845].

[22] Planck collaboration, *Planck 2018 results. VI. Cosmological parameters*, 1807.06209.

[23] R. Cowsik and J. McClelland, *An Upper Limit on the Neutrino Rest Mass*, *Phys. Rev. Lett.* **29** (1972) 669.

[24] S. Roy Choudhury and S. Choubey, *Updated Bounds on Sum of Neutrino Masses in Various Cosmological Scenarios*, *JCAP* **09** (2018) 017 [1806.10832].

[25] S. Tremaine and J.E. Gunn, *Dynamical role of light neutral leptons in cosmology*, *Phys. Rev. Lett.* **42** (1979) 407.

[26] D. Baumann, *Cosmology*, Cambridge University Press (7, 2022), 10.1017/9781108937092.

[27] K. Jedamzik and M. Pospelov, *Big Bang Nucleosynthesis and Particle Dark Matter*, *New J. Phys.* **11** (2009) 105028 [0906.2087].

[28] M. Pospelov and J. Pradler, *Big Bang Nucleosynthesis as a Probe of New Physics*, *Ann. Rev. Nucl. Part. Sci.* **60** (2010) 539 [1011.1054].

[29] K.A. Olive and E.D. Skillman, *A Realistic determination of the error on the primordial helium abundance: Steps toward non-parametric nebular helium abundances*, *Astrophys. J.* **617** (2004) 29 [astro-ph/0405588].

[30] K. Akita and M. Yamaguchi, *A precision calculation of relic neutrino decoupling*, *JCAP* **08** (2020) 012 [2005.07047].

[31] T.-H. Yeh, J. Shelton, K.A. Olive and B.D. Fields, *Probing Physics Beyond the Standard Model: Limits from BBN and the CMB Independently and Combined*, 2207.13133.

[32] G. Steigman, *Observational tests of antimatter cosmologies*, *Ann. Rev. Astron. Astrophys.* **14** (1976) 339.

[33] M. Císcar-Monsalvatje, A. Ibarra and J. Vandecasteele, *Matter-antimatter asymmetry and dark matter stability from baryon number conservation*, *JCAP* **01** (2024) 028 [2307.02592].

[34] A.D. Sakharov, *Violation of CP Invariance, C asymmetry, and baryon asymmetry of the universe*, *Pisma Zh. Eksp. Teor. Fiz.* **5** (1967) 32.

[35] G. 't Hooft, *Symmetry breaking through bell-jackiw anomalies*, *Physical Review Letters* **37** (1976) 8.

[36] V.A. Kuzmin, V.A. Rubakov and M.E. Shaposhnikov, *On the Anomalous Electroweak Baryon Number Nonconservation in the Early Universe*, *Phys. Lett. B* **155** (1985) 36.

[37] S. Davidson, E. Nardi and Y. Nir, *Leptogenesis*, *Phys. Rept.* **466** (2008) 105 [0802.2962].

[38] M. Yoshimura, *Unified Gauge Theories and the Baryon Number of the Universe*, *Phys. Rev. Lett.* **41** (1978) 281.

[39] E.W. Kolb, A.D. Linde and A. Riotto, *GUT baryogenesis after preheating*, *Phys. Rev. Lett.* **77** (1996) 4290 [hep-ph/9606260].

[40] V.A. Rubakov and M.E. Shaposhnikov, *Electroweak baryon number nonconservation in the early universe and in high-energy collisions*, *Usp. Fiz. Nauk* **166** (1996) 493 [hep-ph/9603208].

[41] M. Losada, *High temperature dimensional reduction of the MSSM and other multiscalar models*, *Phys. Rev. D* **56** (1997) 2893 [hep-ph/9605266].

[42] M. Fukugita and T. Yanagida, *Baryogenesis Without Grand Unification*, *Phys. Lett.* **B174** (1986) 45.

[43] S.L. Adler, *Axial-vector vertex in spinor electrodynamics*, *Phys. Rev.* **177** (1969) 2426.

[44] A.M. Polyakov, *Gauge Fields and Strings*, vol. 3 (1987).

[45] A.A. Belavin, A.M. Polyakov, A.S. Schwartz and Y.S. Tyupkin, *Pseudoparticle Solutions of the Yang-Mills Equations*, *Phys. Lett. B* **59** (1975) 85.

[46] Y. Burnier, M. Laine and M. Shaposhnikov, *Baryon and lepton number violation rates*

across the electroweak crossover, *JCAP* **02** (2006) 007 [hep-ph/0511246].

[47] P. Minkowski, $\mu \to e\gamma$ *at a Rate of One Out of* 10^9 *Muon Decays?*, *Phys. Lett. B* **67** (1977) 421.

[48] M. Gell-Mann, P. Ramond and R. Slansky, *Complex Spinors and Unified Theories*, *Conf. Proc. C* **790927** (1979) 315 [1306.4669].

[49] T. Yanagida, *Horizontal gauge symmetry and masses of neutrinos*, *Conf. Proc. C* **7902131** (1979) 95.

[50] R.N. Mohapatra and G. Senjanovic, *Neutrino Mass and Spontaneous Parity Violation*, *Phys. Rev. Lett.* **44** (1980) 912.

[51] J. Schechter and J.W.F. Valle, *Neutrino Masses in SU(2) x U(1) Theories*, *Phys. Rev.* **D22** (1980) 2227.

[52] J. Schechter and J.W.F. Valle, *Neutrino Decay and Spontaneous Violation of Lepton Number*, *Phys. Rev. D* **25** (1982) 774.

[53] M.C. Gonzalez-Garcia, M. Maltoni and T. Schwetz, *NuFIT: Three-Flavour Global Analyses of Neutrino Oscillation Experiments*, *Universe* **7** (2021) 459 [2111.03086].

[54] K. Kaneta, Y. Mambrini, K.A. Olive and S. Verner, *Inflation and Leptogenesis in High-Scale Supersymmetry*, *Phys. Rev. D* **101** (2020) 015002 [1911.02463].

[55] P.H. Frampton, S.L. Glashow and T. Yanagida, *Cosmological sign of neutrino CP violation*, *Phys. Lett. B* **548** (2002) 119 [hep-ph/0208157].

[56] M.A. Luty, *Baryogenesis via leptogenesis*, *Phys. Rev. D* **45** (1992) 455.

[57] L. Covi, E. Roulet and F. Vissani, *CP violating decays in leptogenesis scenarios*, *Phys. Lett. B* **384** (1996) 169 [hep-ph/9605319].

[58] C.S. Fong, E. Nardi and A. Riotto, *Leptogenesis in the Universe*, *Adv. High Energy Phys.* **2012** (2012) 158303 [1301.3062].

[59] R.T. Co, Y. Mambrini and K.A. Olive, *Inflationary gravitational leptogenesis*, *Phys. Rev. D* **106** (2022) 075006 [2205.01689].

[60] S.Y. Khlebnikov and M.E. Shaposhnikov, *The Statistical Theory of Anomalous Fermion Number Nonconservation*, *Nucl. Phys. B* **308** (1988) 885.

[61] J.A. Harvey and M.S. Turner, *Cosmological baryon and lepton number in the presence of electroweak fermion number violation*, *Phys. Rev. D* **42** (1990) 3344.

[62] T. Asaka, K. Hamaguchi, M. Kawasaki and T. Yanagida, *Leptogenesis in inflaton decay*, *Phys. Lett. B* **464** (1999) 12 [hep-ph/9906366].

[63] P. Gondolo and G. Gelmini, *Cosmic abundances of stable particles: Improved analysis*,

Nucl. Phys. **B360** (1991) 145.

[64] G. Arcadi, M. Dutra, P. Ghosh, M. Lindner, Y. Mambrini, M. Pierre et al., *The waning of the WIMP? A review of models, searches, and constraints*, *Eur. Phys. J. C* **78** (2018) 203 [1703.07364].

[65] G. Arcadi, D. Cabo-Almeida, M. Dutra, P. Ghosh, M. Lindner, Y. Mambrini et al., *The Waning of the WIMP: Endgame?*, 2403.15860.

[66] G. Belanger, F. Boudjema, A. Pukhov and A. Semenov, *MicrOMEGAs 2.0: A Program to calculate the relic density of dark matter in a generic model*, *Comput. Phys. Commun.* **176** (2007) 367 [hep-ph/0607059].

[67] G. Belanger, F. Boudjema, A. Pukhov and A. Semenov, *Dark matter direct detection rate in a generic model with micrOMEGAs 2.2*, *Comput. Phys. Commun.* **180** (2009) 747 [0803.2360].

[68] G. Bélanger, F. Boudjema, A. Goudelis, A. Pukhov and B. Zaldivar, *micrOMEGAs5.0 : Freeze-in*, *Comput. Phys. Commun.* **231** (2018) 173 [1801.03509].

[69] G. Alguero, G. Belanger, F. Boudjema, S. Chakraborti, A. Goudelis, S. Kraml et al., *micrOMEGAs 6.0: N-component dark matter*, *Comput. Phys. Commun.* **299** (2024) 109133 [2312.14894].

[70] M.M. Pierre, *Dark Matter phenomenology : from simplified WIMP models to refined alternative solutions*, Ph.D. thesis, U. Paris-Saclay, 2018. 1901.05822.

[71] XENON collaboration, *First Dark Matter Search Results from the XENON1T Experiment*, *Phys. Rev. Lett.* **119** (2017) 181301 [1705.06655].

[72] LUX collaboration, *Results from a search for dark matter in the complete LUX exposure*, *Phys. Rev. Lett.* **118** (2017) 021303 [1608.07648].

[73] PandaX-II collaboration, *Dark Matter Results From 54-Ton-Day Exposure of PandaX-II Experiment*, *Phys. Rev. Lett.* **119** (2017) 181302 [1708.06917].

[74] LZ collaboration, *First Dark Matter Search Results from the LUX-ZEPLIN (LZ) Experiment*, *Phys. Rev. Lett.* **131** (2023) 041002 [2207.03764].

[75] XENON collaboration, *First Dark Matter Search with Nuclear Recoils from the XENONnT Experiment*, *Phys. Rev. Lett.* **131** (2023) 041003 [2303.14729].

[76] H.E.S.S. collaboration, *Search for dark matter annihilations towards the inner Galactic halo from 10 years of observations with H.E.S.S*, *Phys. Rev. Lett.* **117** (2016) 111301 [1607.08142].

[77] HESS collaboration, *Search for γ-Ray Line Signals from Dark Matter Annihilations in the Inner Galactic Halo from 10 Years of Observations with H.E.S.S.*, *Phys. Rev. Lett.*

120 (2018) 201101 [1805.05741].

[78] Fermi-LAT collaboration, *Limits on Dark Matter Annihilation Signals from the Fermi LAT 4-year Measurement of the Isotropic Gamma-Ray Background*, *JCAP* **09** (2015) 008 [1501.05464].

[79] Y. Hochberg, E. Kuflik, T. Volansky and J.G. Wacker, *Mechanism for Thermal Relic Dark Matter of Strongly Interacting Massive Particles*, *Phys. Rev. Lett.* **113** (2014) 171301 [1402.5143].

[80] L.J. Hall, K. Jedamzik, J. March-Russell and S.M. West, *Freeze-In Production of FIMP Dark Matter*, *JHEP* **03** (2010) 080 [0911.1120].

[81] J. McDonald, *Thermally generated gauge singlet scalars as selfinteracting dark matter*, *Phys.Rev.Lett.* **88** (2002) 091304 [hep-ph/0106249].

[82] K. Petraki and A. Kusenko, *Dark-matter sterile neutrinos in models with a gauge singlet in the Higgs sector*, *Phys. Rev. D* **77** (2008) 065014 [0711.4646].

[83] N. Bernal, M. Heikinheimo, T. Tenkanen, K. Tuominen and V. Vaskonen, *The Dawn of FIMP Dark Matter: A Review of Models and Constraints*, *Int. J. Mod. Phys.* **A32** (2017) 1730023 [1706.07442].

[84] J. McDonald, *Gauge singlet scalars as cold dark matter*, *Phys. Rev.* **D50** (1994) 3637 [hep-ph/0702143].

[85] C.P. Burgess, M. Pospelov and T. ter Veldhuis, *The Minimal model of nonbaryonic dark matter: A Singlet scalar*, *Nucl. Phys. B* **619** (2001) 709 [hep-ph/0011335].

[86] F. Elahi, C. Kolda and J. Unwin, *UltraViolet Freeze-in*, *JHEP* **03** (2015) 048 [1410.6157].

[87] M.A.G. Garcia, K. Kaneta, Y. Mambrini and K.A. Olive, *Reheating and Post-inflationary Production of Dark Matter*, *Phys. Rev. D* **101** (2020) 123507 [2004.08404].

[88] R. Durrer, *The Cosmic Microwave Background*, Cambridge University Press, 2 ed. (2020).

[89] D.J. Fixsen, *The temperature of the cosmic microwave background*, *The Astrophysical Journal* **707** (2009) 916–920.

[90] Planck collaboration, *Planck 2015 results. XI. CMB power spectra, likelihoods, and robustness of parameters*, *Astron. Astrophys.* **594** (2016) A11 [1507.02704].

[91] BOSS collaboration, *The clustering of galaxies in the completed SDSS-III Baryon Oscillation Spectroscopic Survey: cosmological analysis of the DR12 galaxy sample*, *Mon. Not. Roy. Astron. Soc.* **470** (2017) 2617 [1607.03155].

[92] J. Silk, *Cosmic black body radiation and galaxy formation*, *Astrophys. J.* **151** (1968) 459.

[93] A.A. Starobinsky, *A New Type of Isotropic Cosmological Models Without Singularity*, *Phys. Lett. B* **91** (1980) 99.

[94] A.H. Guth, *The Inflationary Universe: A Possible Solution to the Horizon and Flatness Problems*, *Phys. Rev. D* **23** (1981) 347.

[95] A.D. Linde, *A New Inflationary Universe Scenario: A Possible Solution of the Horizon, Flatness, Homogeneity, Isotropy and Primordial Monopole Problems*, *Phys. Lett. B* **108** (1982) 389.

[96] I. Khan, A.C. Vincent and G. Worthey, *Preheating and reheating effects of the Kähler moduli inflation I model*, *Phys. Rev. D* **108** (2023) 103546 [2111.11050].

[97] V.F. Mukhanov and G.V. Chibisov, *Quantum Fluctuations and a Nonsingular Universe*, *JETP Lett.* **33** (1981) 532.

[98] H. Kodama and M. Sasaki, *Cosmological Perturbation Theory*, *Prog. Theor. Phys. Suppl.* **78** (1984) 1.

[99] LiteBIRD collaboration, *Probing Cosmic Inflation with the LiteBIRD Cosmic Microwave Background Polarization Survey*, *PTEP* **2023** (2023) 042F01 [2202.02773].

[100] F.L. Bezrukov and M. Shaposhnikov, *The Standard Model Higgs boson as the inflaton*, *Phys. Lett. B* **659** (2008) 703 [0710.3755].

[101] E.W. Kolb, *Dynamics of the inflationary era*, in *Pritzker Symposium and Workshop on the Status of Inflationary Cosmology*, 1, 1999 [hep-ph/9910311].

[102] A. Riotto, *Inflation and the theory of cosmological perturbations*, *ICTP Lect. Notes Ser.* **14** (2003) 317 [hep-ph/0210162].

[103] Planck collaboration, *Planck 2018 results. X. Constraints on inflation*, *Astron. Astrophys.* **641** (2020) A10 [1807.06211].

[104] J. Ellis, D.V. Nanopoulos and K.A. Olive, *No-Scale Supergravity Realization of the Starobinsky Model of Inflation*, *Phys. Rev. Lett.* **111** (2013) 111301 [1305.1247].

[105] R. Kallosh and A. Linde, *Universality Class in Conformal Inflation*, *JCAP* **07** (2013) 002 [1306.5220].

[106] M.A.G. Garcia, K. Kaneta, Y. Mambrini and K.A. Olive, *Inflaton Oscillations and Post-Inflationary Reheating*, *JCAP* **04** (2021) 012 [2012.10756].

[107] N. Bartolo, E. Komatsu, S. Matarrese and A. Riotto, *Non-Gaussianity from inflation: Theory and observations*, *Phys. Rept.* **402** (2004) 103 [astro-ph/0406398].

[108] X. Chen, *Primordial Non-Gaussianities from Inflation Models*, *Adv. Astron.* **2010**

(2010) 638979 [1002.1416].

[109] C.T. Byrnes and K.-Y. Choi, *Review of local non-Gaussianity from multi-field inflation*, *Adv. Astron.* **2010** (2010) 724525 [1002.3110].

[110] S. Nurmi, T. Tenkanen and K. Tuominen, *Inflationary Imprints on Dark Matter*, *JCAP* **11** (2015) 001 [1506.04048].

[111] A. Ghosh and S. Mukhopadhyay, *Momentum distribution of dark matter produced in inflaton decay: Effect of inflaton mediated scatterings*, *Phys. Rev. D* **106** (2022) 043519 [2205.03440].

[112] M.A.G. Garcia, M. Pierre and S. Verner, *Scalar dark matter production from preheating and structure formation constraints*, *Phys. Rev. D* **107** (2023) 043530 [2206.08940].

[113] L. Kofman, A.D. Linde and A.A. Starobinsky, *Towards the theory of reheating after inflation*, *Phys. Rev. D* **56** (1997) 3258 [hep-ph/9704452].

[114] M.A.G. Garcia, K. Kaneta, W. Ke, Y. Mambrini, K.A. Olive and S. Verner, *The Role of Vectors in Reheating*, 2311.14794.

[115] E. Dudas, Y. Mambrini and K. Olive, *Case for an EeV Gravitino*, *Phys. Rev. Lett.* **119** (2017) 051801 [1704.03008].

[116] M.A.G. Garcia, Y. Mambrini, K.A. Olive and M. Peloso, *Enhancement of the Dark Matter Abundance Before Reheating: Applications to Gravitino Dark Matter*, *Phys. Rev. D* **96** (2017) 103510 [1709.01549].

[117] S.-L. Chen and Z. Kang, *On UltraViolet Freeze-in Dark Matter during Reheating*, *JCAP* **05** (2018) 036 [1711.02556].

[118] K.D. Lozanov, *Lectures on Reheating after Inflation*, 1907.04402.

[119] M.A.G. Garcia, K. Kaneta, Y. Mambrini, K.A. Olive and S. Verner, *Freeze-in from preheating*, *JCAP* **03** (2022) 016 [2109.13280].

[120] D.G. Figueroa, A. Florio, F. Torrenti and W. Valkenburg, *CosmoLattice: A modern code for lattice simulations of scalar and gauge field dynamics in an expanding universe*, *Comput. Phys. Commun.* **283** (2023) 108586 [2102.01031].

[121] K.D. Lozanov and M.A. Amin, *Self-resonance after inflation: oscillons, transients and radiation domination*, *Phys. Rev. D* **97** (2018) 023533 [1710.06851].

[122] M.A.G. Garcia and M. Pierre, *Reheating after inflaton fragmentation*, *JCAP* **11** (2023) 004 [2306.08038].

[123] M.A.G. Garcia, M. Gross, Y. Mambrini, K.A. Olive, M. Pierre and J.-H. Yoon, *Effects of fragmentation on post-inflationary reheating*, *JCAP* **12** (2023) 028 [2308.16231].

[124] BICEP, Keck collaboration, *Improved Constraints on Primordial Gravitational Waves using Planck, WMAP, and BICEP/Keck Observations through the 2018 Observing Season*, *Phys. Rev. Lett.* **127** (2021) 151301 [2110.00483].

[125] M. Tristram et al., *Improved limits on the tensor-to-scalar ratio using BICEP and Planck data*, *Phys. Rev. D* **105** (2022) 083524 [2112.07961].

[126] A.R. Liddle and S.M. Leach, *How long before the end of inflation were observable perturbations produced?*, *Phys. Rev. D* **68** (2003) 103503 [astro-ph/0305263].

[127] J. Martin and C. Ringeval, *First CMB Constraints on the Inflationary Reheating Temperature*, *Phys. Rev. D* **82** (2010) 023511 [1004.5525].

[128] D.J. Fixsen, *The Temperature of the Cosmic Microwave Background*, *Astrophys. J.* **707** (2009) 916 [0911.1955].

[129] J. Ellis, M.A.G. Garcia, D.V. Nanopoulos, K.A. Olive and S. Verner, *BICEP/Keck constraints on attractor models of inflation and reheating*, *Phys. Rev. D* **105** (2022) 043504 [2112.04466].

[130] Y. Shtanov, J.H. Traschen and R.H. Brandenberger, *Universe reheating after inflation*, *Phys. Rev. D* **51** (1995) 5438 [hep-ph/9407247].

[131] K. Ichikawa, T. Suyama, T. Takahashi and M. Yamaguchi, *Primordial Curvature Fluctuation and Its Non-Gaussianity in Models with Modulated Reheating*, *Phys. Rev. D* **78** (2008) 063545 [0807.3988].

[132] J.F. Dufaux, G.N. Felder, L. Kofman, M. Peloso and D. Podolsky, *Preheating with trilinear interactions: Tachyonic resonance*, *JCAP* **07** (2006) 006 [hep-ph/0602144].

[133] J. Fan, K.D. Lozanov and Q. Lu, *Spillway Preheating*, *JHEP* **05** (2021) 069 [2101.11008].

[134] J. Ellis, M.A.G. Garcia, N. Nagata, N.D. V., K.A. Olive and S. Verner, *Building models of inflation in no-scale supergravity*, *Int. J. Mod. Phys. D* **29** (2020) 2030011 [2009.01709].

[135] M. Endo, K. Kadota, K.A. Olive, F. Takahashi and T.T. Yanagida, *The Decay of the Inflaton in No-scale Supergravity*, *JCAP* **02** (2007) 018 [hep-ph/0612263].

[136] J. Ellis, M.A.G. Garcia, D.V. Nanopoulos and K.A. Olive, *Phenomenological Aspects of No-Scale Inflation Models*, *JCAP* **10** (2015) 003 [1503.08867].

[137] J. Ellis, D.V. Nanopoulos, K.A. Olive and S. Verner, *Phenomenology and Cosmology of No-Scale Attractor Models of Inflation*, *JCAP* **08** (2020) 037 [2004.00643].

[138] J.T. Deskins, J.T. Giblin and R.R. Caldwell, *Gauge Field Preheating at the End of Inflation*, *Phys. Rev. D* **88** (2013) 063530 [1305.7226].

[139] P. Adshead, J.T. Giblin, T.R. Scully and E.I. Sfakianakis, *Gauge-preheating and the end of axion inflation*, *JCAP* **12** (2015) 034 [1502.06506].

[140] J.R.C. Cuissa and D.G. Figueroa, *Lattice formulation of axion inflation. Application to preheating*, *JCAP* **06** (2019) 002 [1812.03132].

[141] M.A.G. Garcia, Y. Mambrini, K.A. Olive and S. Verner, *On the Realization of WIMPflation*, *JCAP* **10** (2021) 061 [2107.07472].

[142] A.R. Liddle and L.A. Urena-Lopez, *Inflation, dark matter and dark energy in the string landscape*, *Phys. Rev. Lett.* **97** (2006) 161301 [astro-ph/0605205].

[143] A. de la Macorra, *Dark Matter from the Inflaton Field*, *Astropart. Phys.* **35** (2012) 478 [1201.6302].

[144] K. Mukaida and K. Nakayama, *Dark Matter Chaotic Inflation in Light of BICEP2*, *JCAP* **08** (2014) 062 [1404.1880].

[145] L. Ji and M. Kamionkowski, *Reheating constraints to WIMP inflation*, *Phys. Rev. D* **100** (2019) 083519 [1905.05770].

[146] O. Lebedev and J.-H. Yoon, *Challenges for inflaton dark matter*, *Phys. Lett. B* **821** (2021) 136614 [2105.05860].

[147] A.V. Frolov, *Non-linear Dynamics and Primordial Curvature Perturbations from Preheating*, *Class. Quant. Grav.* **27** (2010) 124006 [1004.3559].

[148] P.B. Greene, L. Kofman, A.D. Linde and A.A. Starobinsky, *Structure of resonance in preheating after inflation*, *Phys. Rev. D* **56** (1997) 6175 [hep-ph/9705347].

[149] D.I. Kaiser, *Preheating in an expanding universe: Analytic results for the massless case*, *Phys. Rev. D* **56** (1997) 706 [hep-ph/9702244].

[150] J. Garcia-Bellido, D.G. Figueroa and J. Rubio, *Preheating in the Standard Model with the Higgs-Inflaton coupled to gravity*, *Phys. Rev. D* **79** (2009) 063531 [0812.4624].

[151] M.A. Amin, R. Easther, H. Finkel, R. Flauger and M.P. Hertzberg, *Oscillons After Inflation*, *Phys. Rev. Lett.* **108** (2012) 241302 [1106.3335].

[152] M.P. Hertzberg, J. Karouby, W.G. Spitzer, J.C. Becerra and L. Li, *Theory of self-resonance after inflation. I. Adiabatic and isocurvature Goldstone modes*, *Phys. Rev. D* **90** (2014) 123528 [1408.1396].

[153] K.D. Lozanov and M.A. Amin, *Equation of State and Duration to Radiation Domination after Inflation*, *Phys. Rev. Lett.* **119** (2017) 061301 [1608.01213].

[154] D.G. Figueroa and F. Torrenti, *Parametric resonance in the early Universe—a fitting analysis*, *JCAP* **02** (2017) 001 [1609.05197].

[155] F. Finelli and R.H. Brandenberger, *Parametric amplification of gravitational fluctuations during reheating*, *Phys. Rev. Lett.* **82** (1999) 1362 [hep-ph/9809490].

[156] K. Jedamzik, M. Lemoine and J. Martin, *Collapse of Small-Scale Density Perturbations during Preheating in Single Field Inflation*, *JCAP* **09** (2010) 034 [1002.3039].

[157] J. Martin, T. Papanikolaou and V. Vennin, *Primordial black holes from the preheating instability in single-field inflation*, *JCAP* **01** (2020) 024 [1907.04236].

[158] J. Martin, T. Papanikolaou, L. Pinol and V. Vennin, *Metric preheating and radiative decay in single-field inflation*, *JCAP* **05** (2020) 003 [2002.01820].

[159] E. Schro¨dinger, *The proper vibrations of the expanding universe*, *Physica* **6** (1939) 899.

[160] L. Parker, *Particle creation in expanding universes*, *Phys. Rev. Lett.* **21** (1968) 562.

[161] L.H. Ford, *Gravitational Particle Creation and Inflation*, *Phys. Rev. D* **35** (1987) 2955.

[162] Y.B. Zel'dovich, *Particle Production in Cosmology*, *Soviet Journal of Experimental and Theoretical Physics Letters* **12** (1970) 307.

[163] E.W. Kolb and A.J. Long, *Cosmological gravitational particle production and its implications for cosmological relics*, 2312.09042.

[164] A. Maleknejad and J. Kopp, *Weyl Fermion Creation by Cosmological Gravitational Wave Background at 1-loop*, 2406.01534.

[165] G.W. Gibbons and S.W. Hawking, *Cosmological Event Horizons, Thermodynamics, and Particle Creation*, *Phys. Rev. D* **15** (1977) 2738.

[166] K. Kaneta, S.M. Lee and K.-y. Oda, *Boltzmann or Bogoliubov? Approaches compared in gravitational particle production*, *JCAP* **09** (2022) 018 [2206.10929].

[167] M.A.G. Garcia, M. Pierre and S. Verner, *New window into gravitationally produced scalar dark matter*, *Phys. Rev. D* **108** (2023) 115024 [2305.14446].

[168] A. Chakraborty, S. Cléry, M.R. Haque, D. Maity and Y. Mambrini, *Non-perturbative gravitational production during reheating*, *In preparation* (2024) .

[169] XENON collaboration, *Dark Matter Search Results from a One Ton-Year Exposure of XENON1T*, *Phys. Rev. Lett.* **121** (2018) 111302 [1805.12562].

[170] PandaX-II collaboration, *Results of dark matter search using the full PandaX-II exposure*, *Chin. Phys. C* **44** (2020) 125001 [2007.15469].

[171] Y. Mambrini, *Higgs searches and singlet scalar dark matter: Combined constraints from XENON 100 and the LHC*, *Phys. Rev. D* **84** (2011) 115017 [1108.0671].

[172] O. Lebedev, H.M. Lee and Y. Mambrini, *Vector Higgs-portal dark matter and the invisible Higgs*, *Phys. Lett. B* **707** (2012) 570 [1111.4482].

[173] A. Djouadi, O. Lebedev, Y. Mambrini and J. Quevillon, *Implications of LHC searches for Higgs–portal dark matter*, *Phys. Lett. B* **709** (2012) 65 [1112.3299].

[174] A. Djouadi, A. Falkowski, Y. Mambrini and J. Quevillon, *Direct Detection of Higgs-Portal Dark Matter at the LHC*, *Eur. Phys. J. C* **73** (2013) 2455 [1205.3169].

[175] J.A. Casas, D.G. Cerdeño, J.M. Moreno and J. Quilis, *Reopening the Higgs portal for single scalar dark matter*, *JHEP* **05** (2017) 036 [1701.08134].

[176] G. Arcadi, Y. Mambrini and F. Richard, *Z-portal dark matter*, *JCAP* **03** (2015) 018 [1411.2985].

[177] M. Escudero, A. Berlin, D. Hooper and M.-X. Lin, *Toward (Finally!) Ruling Out Z and Higgs Mediated Dark Matter Models*, *JCAP* **12** (2016) 029 [1609.09079].

[178] J. Kearney, N. Orlofsky and A. Pierce, *Z boson mediated dark matter beyond the effective theory*, *Phys. Rev. D* **95** (2017) 035020 [1611.05048].

[179] J. Ellis, A. Fowlie, L. Marzola and M. Raidal, *Statistical Analyses of Higgs- and Z-Portal Dark Matter Models*, *Phys. Rev. D* **97** (2018) 115014 [1711.09912].

[180] A. Alves, S. Profumo and F.S. Queiroz, *The dark Z' portal: direct, indirect and collider searches*, *JHEP* **04** (2014) 063 [1312.5281].

[181] G. Arcadi, Y. Mambrini, M.H.G. Tytgat and B. Zaldivar, *Invisible Z' and dark matter: LHC vs LUX constraints*, *JHEP* **03** (2014) 134 [1401.0221].

[182] O. Lebedev and Y. Mambrini, *Axial dark matter: The case for an invisible Z'*, *Phys. Lett. B* **734** (2014) 350 [1403.4837].

[183] X. Chu, T. Hambye and M.H.G. Tytgat, *The Four Basic Ways of Creating Dark Matter Through a Portal*, *JCAP* **1205** (2012) 034 [1112.0493].

[184] A. Biswas, D. Borah and A. Dasgupta, *UV complete framework of freeze-in massive particle dark matter*, *Phys. Rev.* **D99** (2019) 015033 [1805.06903].

[185] D.V. Nanopoulos, K.A. Olive and M. Srednicki, *After Primordial Inflation*, *Phys. Lett. B* **127** (1983) 30.

[186] J.R. Ellis, J.S. Hagelin, D.V. Nanopoulos, K.A. Olive and M. Srednicki, *Supersymmetric Relics from the Big Bang*, *Nucl. Phys. B* **238** (1984) 453.

[187] M.Y. Khlopov and A.D. Linde, *Is It Easy to Save the Gravitino?*, *Phys. Lett. B* **138** (1984) 265.

[188] J.R. Ellis, J.E. Kim and D.V. Nanopoulos, *Cosmological Gravitino Regeneration and Decay*, *Phys. Lett. B* **145** (1984) 181.

[189] K.A. Olive, D.N. Schramm and M. Srednicki, *Gravitinos as the Cold Dark Matter in an*

$\Omega = 1$ *Universe*, *Nucl. Phys. B* **255** (1985) 495.

[190] G. Bhattacharyya, M. Dutra, Y. Mambrini and M. Pierre, *Freezing-in dark matter through a heavy invisible Z'*, *Phys. Rev. D* **98** (2018) 035038 [1806.00016].

[191] D. Chowdhury, E. Dudas, M. Dutra and Y. Mambrini, *Moduli Portal Dark Matter*, *Phys. Rev. D* **99** (2019) 095028 [1811.01947].

[192] N. Bernal, M. Dutra, Y. Mambrini, K. Olive, M. Peloso and M. Pierre, *Spin-2 Portal Dark Matter*, *Phys. Rev. D* **97** (2018) 115020 [1803.01866].

[193] N. Bernal, *Boosting Freeze-in through Thermalization*, *JCAP* **10** (2020) 006 [2005.08988].

[194] N. Bernal, F. Elahi, C. Maldonado and J. Unwin, *Ultraviolet Freeze-in and Non-Standard Cosmologies*, *JCAP* **1911** (2019) 026 [1909.07992].

[195] B. Barman, D. Borah and R. Roshan, *Effective Theory of Freeze-in Dark Matter*, 2007.08768.

[196] Y. Ema, R. Jinno, K. Mukaida and K. Nakayama, *Gravitational Effects on Inflaton Decay*, *JCAP* **05** (2015) 038 [1502.02475].

[197] M. Redi, A. Tesi and H. Tillim, *Gravitational Production of a Conformal Dark Sector*, *JHEP* **05** (2021) 010 [2011.10565].

[198] M. Garny, M. Sandora and M.S. Sloth, *Planckian Interacting Massive Particles as Dark Matter*, *Phys. Rev. Lett.* **116** (2016) 101302 [1511.03278].

[199] Y. Tang and Y.-L. Wu, *On Thermal Gravitational Contribution to Particle Production and Dark Matter*, *Phys. Lett. B* **774** (2017) 676 [1708.05138].

[200] M. Chianese, B. Fu and S.F. King, *Impact of Higgs portal on gravity-mediated production of superheavy dark matter*, *JCAP* **06** (2020) 019 [2003.07366].

[201] N. Bernal and C.S. Fong, *Dark matter and leptogenesis from gravitational production*, *JCAP* **06** (2021) 028 [2103.06896].

[202] Y. Mambrini and K.A. Olive, *Gravitational Production of Dark Matter during Reheating*, *Phys. Rev. D* **103** (2021) 115009 [2102.06214].

[203] B. Barman and N. Bernal, *Gravitational SIMPs*, *JCAP* **06** (2021) 011 [2104.10699].

[204] G.F. Giudice, E.W. Kolb and A. Riotto, *Largest temperature of the radiation era and its cosmological implications*, *Phys. Rev. D* **64** (2001) 023508 [hep-ph/0005123].

[205] J. Ellis, M.A.G. Garcia, D.V. Nanopoulos, K.A. Olive and M. Peloso, *Post-Inflationary Gravitino Production Revisited*, *JCAP* **03** (2016) 008 [1512.05701].

[206] K. Kaneta, Y. Mambrini and K.A. Olive, *Radiative production of nonthermal dark*

matter, *Phys. Rev. D* **99** (2019) 063508 [1901.04449].

[207] K. Kainulainen, S. Nurmi, T. Tenkanen, K. Tuominen and V. Vaskonen, *Isocurvature Constraints on Portal Couplings*, *JCAP* **06** (2016) 022 [1601.07733].

[208] J. Ellis, M.A.G. García, D.V. Nanopoulos and K.A. Olive, *Two-Field Analysis of No-Scale Supergravity Inflation*, *JCAP* **01** (2015) 010 [1409.8197].

[209] J. Ellis, M.A.G. Garcia, D.V. Nanopoulos and K.A. Olive, *Calculations of Inflaton Decays and Reheating: with Applications to No-Scale Inflation Models*, *JCAP* **07** (2015) 050 [1505.06986].

[210] M.R. Haque and D. Maity, *Gravitational dark matter: Free streaming and phase space distribution*, *Phys. Rev. D* **106** (2022) 023506 [2112.14668].

[211] O. Lebedev, *The Higgs portal to cosmology*, *Prog. Part. Nucl. Phys.* **120** (2021) 103881 [2104.03342].

[212] Y. Ema, R. Jinno, K. Mukaida and K. Nakayama, *Violent Preheating in Inflation with Nonminimal Coupling*, *JCAP* **02** (2017) 045 [1609.05209].

[213] B.A. Bassett and S. Liberati, *Geometric reheating after inflation*, *Phys. Rev. D* **58** (1998) 021302 [hep-ph/9709417].

[214] S. Tsujikawa, K.-i. Maeda and T. Torii, *Resonant particle production with nonminimally coupled scalar fields in preheating after inflation*, *Phys. Rev. D* **60** (1999) 063515 [hep-ph/9901306].

[215] T. Markkanen and S. Nurmi, *Dark matter from gravitational particle production at reheating*, *JCAP* **02** (2017) 008 [1512.07288].

[216] C.G. Callan, Jr., S.R. Coleman and R. Jackiw, *A New improved energy - momentum tensor*, *Annals Phys.* **59** (1970) 42.

[217] D.J.H. Chung, E.W. Kolb and A. Riotto, *Nonthermal supermassive dark matter*, *Phys. Rev. Lett.* **81** (1998) 4048 [hep-ph/9805473].

[218] S. Hashiba and J. Yokoyama, *Gravitational reheating through conformally coupled superheavy scalar particles*, *JCAP* **01** (2019) 028 [1809.05410].

[219] N. Bernal, A. Chatterjee and A. Paul, *Non-thermal production of Dark Matter after Inflation*, *JCAP* **12** (2018) 020 [1809.02338].

[220] L. Li, T. Nakama, C.M. Sou, Y. Wang and S. Zhou, *Gravitational Production of Superheavy Dark Matter and Associated Cosmological Signatures*, *JHEP* **07** (2019) 067 [1903.08842].

[221] J.A.R. Cembranos, L.J. Garay and J.M. Sánchez Velázquez, *Gravitational production of scalar dark matter*, *JHEP* **06** (2020) 084 [1910.13937].

[222] N. Herring, D. Boyanovsky and A.R. Zentner, *Nonadiabatic cosmological production of ultralight dark matter*, *Phys. Rev. D* **101** (2020) 083516 [1912.10859].

[223] E. Babichev, D. Gorbunov, S. Ramazanov and L. Reverberi, *Gravitational reheating and superheavy Dark Matter creation after inflation with non-minimal coupling*, *JCAP* **09** (2020) 059 [2006.02225].

[224] S. Ling and A.J. Long, *Superheavy scalar dark matter from gravitational particle production in α-attractor models of inflation*, *Phys. Rev. D* **103** (2021) 103532 [2101.11621].

[225] Y. Ema, R. Jinno, K. Mukaida and K. Nakayama, *Gravitational particle production in oscillating backgrounds and its cosmological implications*, *Phys. Rev. D* **94** (2016) 063517 [1604.08898].

[226] Y. Ema, K. Nakayama and Y. Tang, *Production of Purely Gravitational Dark Matter*, *JHEP* **09** (2018) 135 [1804.07471].

[227] Y. Ema, K. Mukaida and K. Nakayama, *Scalar field couplings to quadratic curvature and decay into gravitons*, *JHEP* **05** (2022) 087 [2112.12774].

[228] Y. Ema, K. Nakayama and Y. Tang, *Production of purely gravitational dark matter: the case of fermion and vector boson*, *JHEP* **07** (2019) 060 [1903.10973].

[229] N. Herring and D. Boyanovsky, *Gravitational production of nearly thermal fermionic dark matter*, *Phys. Rev. D* **101** (2020) 123522 [2005.00391].

[230] P.W. Graham, J. Mardon and S. Rajendran, *Vector Dark Matter from Inflationary Fluctuations*, *Phys. Rev. D* **93** (2016) 103520 [1504.02102].

[231] A. Ahmed, B. Grzadkowski and A. Socha, *Gravitational production of vector dark matter*, *JHEP* **08** (2020) 059 [2005.01766].

[232] C. Gross, S. Karamitsos, G. Landini and A. Strumia, *Gravitational Vector Dark Matter*, *JHEP* **03** (2021) 174 [2012.12087].

[233] A. Arvanitaki, S. Dimopoulos, M. Galanis, D. Racco, O. Simon and J.O. Thompson, *Dark QED from inflation*, *JHEP* **11** (2021) 106 [2108.04823].

[234] B. Barman, N. Bernal, A. Das and R. Roshan, *Non-minimally coupled vector boson dark matter*, *JCAP* **01** (2022) 047 [2108.13447].

[235] M. Atkins and X. Calmet, *Bounds on the Nonminimal Coupling of the Higgs Boson to Gravity*, *Phys. Rev. Lett.* **110** (2013) 051301 [1211.0281].

[236] Z.-Z. Xianyu, J. Ren and H.-J. He, *Gravitational Interaction of Higgs Boson and Weak Boson Scattering*, *Phys. Rev. D* **88** (2013) 096013 [1305.0251].

[237] R.A. Flores and M. Sher, *Upper Limits to Fermion Masses in the*

Glashow-Weinberg-Salam Model, *Phys. Rev. D* **27** (1983) 1679.

[238] M. Sher, *Electroweak Higgs Potentials and Vacuum Stability*, *Phys. Rept.* **179** (1989) 273.

[239] G. Isidori, G. Ridolfi and A. Strumia, *On the metastability of the standard model vacuum*, *Nucl. Phys. B* **609** (2001) 387 [hep-ph/0104016].

[240] F. Bezrukov, M.Y. Kalmykov, B.A. Kniehl and M. Shaposhnikov, *Higgs Boson Mass and New Physics*, *JHEP* **10** (2012) 140 [1205.2893].

[241] G. Degrassi, S. Di Vita, J. Elias-Miro, J.R. Espinosa, G.F. Giudice, G. Isidori et al., *Higgs mass and vacuum stability in the Standard Model at NNLO*, *JHEP* **08** (2012) 098 [1205.6497].

[242] D. Buttazzo, G. Degrassi, P.P. Giardino, G.F. Giudice, F. Sala, A. Salvio et al., *Investigating the near-criticality of the Higgs boson*, *JHEP* **12** (2013) 089 [1307.3536].

[243] A.V. Bednyakov, B.A. Kniehl, A.F. Pikelner and O.L. Veretin, *Stability of the Electroweak Vacuum: Gauge Independence and Advanced Precision*, *Phys. Rev. Lett.* **115** (2015) 201802 [1507.08833].

[244] A. Vilenkin, *Gravitational Effects in Guth Cosmology*, *Phys. Lett. B* **115** (1982) 91.

[245] A. Vilenkin and L.H. Ford, *Gravitational Effects upon Cosmological Phase Transitions*, *Phys. Rev. D* **26** (1982) 1231.

[246] A.D. Linde, *Scalar Field Fluctuations in Expanding Universe and the New Inflationary Universe Scenario*, *Phys. Lett. B* **116** (1982) 335.

[247] A.A. Starobinsky, *Dynamics of Phase Transition in the New Inflationary Universe Scenario and Generation of Perturbations*, *Phys. Lett. B* **117** (1982) 175.

[248] A. Vilenkin, *Quantum Fluctuations in the New Inflationary Universe*, *Nucl. Phys. B* **226** (1983) 527.

[249] A.D. Linde, *The New Mechanism of Baryogenesis and the Inflationary Universe*, *Phys. Lett. B* **160** (1985) 243.

[250] K. Enqvist, K.W. Ng and K.A. Olive, *Scalar Field Fluctuations in the Early Universe*, *Nucl. Phys. B* **303** (1988) 713.

[251] J.R. Espinosa, G.F. Giudice and A. Riotto, *Cosmological implications of the Higgs mass measurement*, *JCAP* **05** (2008) 002 [0710.2484].

[252] M. Herranen, T. Markkanen, S. Nurmi and A. Rajantie, *Spacetime curvature and the Higgs stability during inflation*, *Phys. Rev. Lett.* **113** (2014) 211102 [1407.3141].

[253] T. Markkanen, S. Nurmi, A. Rajantie and S. Stopyra, *The 1-loop effective potential for*

the Standard Model in curved spacetime, *JHEP* **06** (2018) 040 [1804.02020].

[254] T. Markkanen, A. Rajantie and S. Stopyra, *Cosmological Aspects of Higgs Vacuum Metastability*, *Front. Astron. Space Sci.* **5** (2018) 40 [1809.06923].

[255] C.P. Burgess, H.M. Lee and M. Trott, *Power-counting and the Validity of the Classical Approximation During Inflation*, *JHEP* **09** (2009) 103 [0902.4465].

[256] J.L.F. Barbon and J.R. Espinosa, *On the Naturalness of Higgs Inflation*, *Phys. Rev. D* **79** (2009) 081302 [0903.0355].

[257] F. Bezrukov, A. Magnin, M. Shaposhnikov and S. Sibiryakov, *Higgs inflation: consistency and generalisations*, *JHEP* **01** (2011) 016 [1008.5157].

[258] K. Benakli, Y. Chen, E. Dudas and Y. Mambrini, *Minimal model of gravitino dark matter*, *Phys. Rev. D* **95** (2017) 095002 [1701.06574].

[259] M.R. Haque and D. Maity, *Gravitational Reheating*, 2201.02348.

[260] A. Ahmed, B. Grzadkowski and A. Socha, *Implications of time-dependent inflaton decay on reheating and dark matter production*, *Phys. Lett. B* **831** (2022) 137201 [2111.06065].

[261] Y. Fujii and K. Maeda, *The scalar-tensor theory of gravitation*, Cambridge Monographs on Mathematical Physics, Cambridge University Press (7, 2007), 10.1017/CBO9780511535093.

[262] W. Buchmuller, P. Di Bari and M. Plumacher, *Cosmic microwave background, matter - antimatter asymmetry and neutrino masses*, *Nucl. Phys. B* **643** (2002) 367 [hep-ph/0205349].

[263] W. Buchmuller, P. Di Bari and M. Plumacher, *The Neutrino mass window for baryogenesis*, *Nucl. Phys. B* **665** (2003) 445 [hep-ph/0302092].

[264] P.H. Chankowski and K. Turzynski, *Limits on T(reh) for thermal leptogenesis with hierarchical neutrino masses*, *Phys. Lett. B* **570** (2003) 198 [hep-ph/0306059].

[265] G. Giudice, A. Notari, M. Raidal, A. Riotto and A. Strumia, *Towards a complete theory of thermal leptogenesis in the SM and MSSM*, *Nucl. Phys. B* **685** (2004) 89 [hep-ph/0310123].

[266] S. Davidson and A. Ibarra, *A Lower bound on the right-handed neutrino mass from leptogenesis*, *Phys. Lett.* **B535** (2002) 25 [hep-ph/0202239].

[267] G. Giudice, M. Peloso, A. Riotto and I. Tkachev, *Production of massive fermions at preheating and leptogenesis*, *JHEP* **08** (1999) 014 [hep-ph/9905242].

[268] G. Lazarides and Q. Shafi, *Origin of matter in the inflationary cosmology*, *Phys. Lett. B* **258** (1991) 305.

[269] B.A. Campbell, S. Davidson and K.A. Olive, *Inflation, neutrino baryogenesis, and (S)neutrino induced baryogenesis*, *Nucl. Phys. B* **399** (1993) 111 [hep-ph/9302223].

[270] F. Hahn-Woernle and M. Plumacher, *Effects of reheating on leptogenesis*, *Nucl. Phys. B* **806** (2009) 68 [0801.3972].

[271] S.Y. Choi, J.S. Shim and H.S. Song, *Factorization and polarization in linearized gravity*, *Phys. Rev. D* **51** (1995) 2751 [hep-th/9411092].

[272] B.R. Holstein, *Graviton Physics*, *Am. J. Phys.* **74** (2006) 1002 [gr-qc/0607045].

[273] J. Ellis, M.A.G. Garcia, D.V. Nanopoulos, K.A. Olive and S. Verner, *BICEP/Keck constraints on attractor models of inflation and reheating*, *Phys. Rev. D* **105** (2022) 043504 [2112.04466].

[274] P. Minkowski, $\mu \to e\gamma$ *at a rate of one out of 109 muon decays?*, *Physics Letters B* **67** (1977) 421.

[275] M. Gell-Mann, P. Ramond and R. Slansky, *Complex Spinors and Unified Theories*, *Conf. Proc.* **C790927** (1979) 315 [1306.4669].

[276] M. Raidal and A. Strumia, *Predictions of the most minimal seesaw model*, *Phys. Lett. B* **553** (2003) 72 [hep-ph/0210021].

[277] A. Ibarra and G.G. Ross, *Neutrino phenomenology: The Case of two right-handed neutrinos*, *Phys. Lett. B* **591** (2004) 285 [hep-ph/0312138].

[278] T. Rink, *Leptonic CP violation in the minimal type-I seesaw model: Bottom-up phenomenology & top-down model building*, Master's thesis, Heidelberg U., 2017.

[279] A. Ahmed, B. Grzadkowski and A. Socha, *Higgs Boson-Induced Reheating and Dark Matter Production*, *Symmetry* **14** (2022) 306.

[280] D. Maity and P. Saha, *(P)reheating after minimal Plateau Inflation and constraints from CMB*, *JCAP* **07** (2019) 018 [1811.11173].

[281] M. Flanz, E.A. Paschos and U. Sarkar, *Baryogenesis from a lepton asymmetric universe*, *Phys. Lett. B* **345** (1995) 248 [hep-ph/9411366].

[282] W. Buchmuller, P. Di Bari and M. Plumacher, *Leptogenesis for pedestrians*, *Annals Phys.* **315** (2005) 305 [hep-ph/0401240].

[283] T. Asaka, H. Nielsen and Y. Takanishi, *Nonthermal leptogenesis from the heavier Majorana neutrinos*, *Nucl. Phys. B* **647** (2002) 252 [hep-ph/0207023].

[284] V.N. Senoguz and Q. Shafi, *GUT scale inflation, nonthermal leptogenesis, and atmospheric neutrino oscillations*, *Phys. Lett. B* **582** (2004) 6 [hep-ph/0309134].

[285] B. Barman, D. Borah and R. Roshan, *Nonthermal leptogenesis and UV freeze-in of dark*

matter: Impact of inflationary reheating, *Phys. Rev. D* **104** (2021) 035022 [2103.01675].

[286] R.T. Co, D. Dunsky, N. Fernandez, A. Ghalsasi, L.J. Hall, K. Harigaya et al., *Gravitational wave and CMB probes of axion kination*, *JHEP* **09** (2022) 116 [2108.09299].

[287] K. Saikawa and S. Shirai, *Primordial gravitational waves, precisely: The role of thermodynamics in the Standard Model*, *JCAP* **05** (2018) 035 [1803.01038].

[288] D.G. Figueroa and E.H. Tanin, *Inconsistency of an inflationary sector coupled only to Einstein gravity*, *JCAP* **10** (2019) 050 [1811.04093].

[289] M. Giovannini, *Gravitational waves constraints on postinflationary phases stiffer than radiation*, *Phys. Rev. D* **58** (1998) 083504 [hep-ph/9806329].

[290] J. Crowder and N.J. Cornish, *Beyond LISA: Exploring future gravitational wave missions*, *Phys. Rev. D* **72** (2005) 083005 [gr-qc/0506015].

[291] V. Corbin and N.J. Cornish, *Detecting the cosmic gravitational wave background with the big bang observer*, *Class. Quant. Grav.* **23** (2006) 2435 [gr-qc/0512039].

[292] G.M. Harry, P. Fritschel, D.A. Shaddock, W. Folkner and E.S. Phinney, *Laser interferometry for the big bang observer*, *Class. Quant. Grav.* **23** (2006) 4887.

[293] N. Seto, S. Kawamura and T. Nakamura, *Possibility of direct measurement of the acceleration of the universe using 0.1-Hz band laser interferometer gravitational wave antenna in space*, *Phys. Rev. Lett.* **87** (2001) 221103 [astro-ph/0108011].

[294] S. Kawamura et al., *The Japanese space gravitational wave antenna DECIGO*, *Class. Quant. Grav.* **23** (2006) S125.

[295] K. Yagi and N. Seto, *Detector configuration of DECIGO/BBO and identification of cosmological neutron-star binaries*, *Phys. Rev. D* **83** (2011) 044011 [1101.3940].

[296] LIGO Scientific collaboration, *Exploring the Sensitivity of Next Generation Gravitational Wave Detectors*, *Class. Quant. Grav.* **34** (2017) 044001 [1607.08697].

[297] D. Reitze et al., *Cosmic Explorer: The U.S. Contribution to Gravitational-Wave Astronomy beyond LIGO*, *Bull. Am. Astron. Soc.* **51** (2019) 035 [1907.04833].

[298] M. Punturo et al., *The Einstein Telescope: A third-generation gravitational wave observatory*, *Class. Quant. Grav.* **27** (2010) 194002.

[299] S. Hild et al., *Sensitivity Studies for Third-Generation Gravitational Wave Observatories*, *Class. Quant. Grav.* **28** (2011) 094013 [1012.0908].

[300] B. Sathyaprakash et al., *Scientific Objectives of Einstein Telescope*, *Class. Quant. Grav.* **29** (2012) 124013 [1206.0331].

[301] M. Maggiore et al., *Science Case for the Einstein Telescope*, *JCAP* **03** (2020) 050 [1912.02622].

[302] K. Schmitz, *New Sensitivity Curves for Gravitational-Wave Experiments*, 2002.04615.

[303] IceCube collaboration, *First observation of PeV-energy neutrinos with IceCube*, *Phys. Rev. Lett.* **111** (2013) 021103 [1304.5356].

[304] IceCube collaboration, *Evidence for High-Energy Extraterrestrial Neutrinos at the IceCube Detector*, *Science* **342** (2013) 1242856 [1311.5238].

[305] IceCube collaboration, *Observation of High-Energy Astrophysical Neutrinos in Three Years of IceCube Data*, *Phys. Rev. Lett.* **113** (2014) 101101 [1405.5303].

[306] Y. Bai, R. Lu and J. Salvado, *Geometric Compatibility of IceCube TeV-PeV Neutrino Excess and its Galactic Dark Matter Origin*, *JHEP* **01** (2016) 161 [1311.5864].

[307] T. Higaki, R. Kitano and R. Sato, *Neutrinoful Universe*, *JHEP* **07** (2014) 044 [1405.0013].

[308] A. Esmaili, S.K. Kang and P.D. Serpico, *IceCube events and decaying dark matter: hints and constraints*, *JCAP* **12** (2014) 054 [1410.5979].

[309] A. Bhattacharya, M.H. Reno and I. Sarcevic, *Reconciling neutrino flux from heavy dark matter decay and recent events at IceCube*, *JHEP* **06** (2014) 110 [1403.1862].

[310] J. Zavala, *Galactic PeV neutrinos from dark matter annihilation*, *Phys. Rev. D* **89** (2014) 123516 [1404.2932].

[311] C. Rott, K. Kohri and S.C. Park, *Superheavy dark matter and IceCube neutrino signals: Bounds on decaying dark matter*, *Phys. Rev. D* **92** (2015) 023529 [1408.4575].

[312] E. Dudas, Y. Mambrini and K.A. Olive, *Monochromatic neutrinos generated by dark matter and the seesaw mechanism*, *Phys. Rev. D* **91** (2015) 075001 [1412.3459].

[313] K. Murase, R. Laha, S. Ando and M. Ahlers, *Testing the Dark Matter Scenario for PeV Neutrinos Observed in IceCube*, *Phys. Rev. Lett.* **115** (2015) 071301 [1503.04663].

[314] L.A. Anchordoqui, V. Barger, H. Goldberg, X. Huang, D. Marfatia, L.H.M. da Silva et al., *IceCube neutrinos, decaying dark matter, and the Hubble constant*, *Phys. Rev. D* **92** (2015) 061301 [1506.08788].

[315] P. Ko and Y. Tang, *IceCube Events from Heavy DM decays through the Right-handed Neutrino Portal*, *Phys. Lett. B* **751** (2015) 81 [1508.02500].

[316] S.B. Roland, B. Shakya and J.D. Wells, *PeV neutrinos and a 3.5 keV x-ray line from a PeV-scale supersymmetric neutrino sector*, *Phys. Rev. D* **92** (2015) 095018 [1506.08195].

[317] M. Chianese and A. Merle, *A Consistent Theory of Decaying Dark Matter Connecting IceCube to the Sesame Street*, *JCAP* **04** (2017) 017 [1607.05283].

[318] M. Re Fiorentin, V. Niro and N. Fornengo, *A consistent model for leptogenesis, dark matter and the IceCube signal*, *JHEP* **11** (2016) 022 [1606.04445].

[319] M.A.G. Garcia, Y. Mambrini, K.A. Olive and S. Verner, *Case for decaying spin- 3/2 dark matter*, *Phys. Rev. D* **102** (2020) 083533 [2006.03325].

[320] E. Dudas, T. Gherghetta, K. Kaneta, Y. Mambrini and K.A. Olive, *Gravitino decay in high scale supersymmetry with R -parity violation*, *Phys. Rev. D* **98** (2018) 015030 [1805.07342].

[321] C.A. Argüelles, D. Delgado, A. Friedlander, A. Kheirandish, I. Safa, A.C. Vincent et al., *Dark Matter decay to neutrinos*, 2210.01303.

[322] P. Jizba and G. Lambiase, *Tsallis cosmology and its applications in dark matter physics with focus on IceCube high-energy neutrino data*, 2206.12910.

[323] M. Ahmadvand, *Filtered asymmetric dark matter during the Peccei-Quinn phase transition*, *JHEP* **10** (2021) 109 [2108.00958].

[324] Y. Chikashige, R.N. Mohapatra and R.D. Peccei, *Are There Real Goldstone Bosons Associated with Broken Lepton Number?*, *Phys. Lett. B* **98** (1981) 265.

[325] V. Berezinsky and J.W.F. Valle, *The KeV majoron as a dark matter particle*, *Phys. Lett. B* **318** (1993) 360 [hep-ph/9309214].

[326] M. Lattanzi and J.W.F. Valle, *Decaying warm dark matter and neutrino masses*, *Phys. Rev. Lett.* **99** (2007) 121301 [0705.2406].

[327] F. Bazzocchi, M. Lattanzi, S. Riemer-Sørensen and J.W.F. Valle, *X-ray photons from late-decaying majoron dark matter*, *JCAP* **08** (2008) 013 [0805.2372].

[328] M. Lattanzi, S. Riemer-Sorensen, M. Tortola and J.W.F. Valle, *Updated CMB and x- and γ-ray constraints on Majoron dark matter*, *Phys. Rev. D* **88** (2013) 063528 [1303.4685].

[329] M. Lattanzi, R.A. Lineros and M. Taoso, *Connecting neutrino physics with dark matter*, *New J. Phys.* **16** (2014) 125012 [1406.0004].

[330] J. Gehrlein and M. Pierre, *A testable hidden-sector model for Dark Matter and neutrino masses*, *JHEP* **02** (2020) 068 [1912.06661].

[331] E. Dudas, L. Heurtier, Y. Mambrini, K.A. Olive and M. Pierre, *Model of metastable EeV dark matter*, *Phys. Rev. D* **101** (2020) 115029 [2003.02846].

[332] V. Iršič et al., *New Constraints on the free-streaming of warm dark matter from intermediate and small scale Lyman-α forest data*, *Phys. Rev. D* **96** (2017) 023522

[1702.01764].

[333] M. Sitwell, A. Mesinger, Y.-Z. Ma and K. Sigurdson, *The Imprint of Warm Dark Matter on the Cosmological 21-cm Signal*, *Mon. Not. Roy. Astron. Soc.* **438** (2014) 2664 [1310.0029].

[334] J.F. Donoghue, M.M. Ivanov and A. Shkerin, *EPFL Lectures on General Relativity as a Quantum Field Theory*, 1702.00319.